Clinical Gated Cardiac SPECT

Second Edition

Edited By

Guido Germano, PhD
Professor of Medicine
UCLA School of Medicine
Director, Artificial Intelligence Program
Cedars-Sinai Medical Center
Los Angeles, CA
USA

Daniel S. Berman, MD
Professor of Medicine
UCLA School of Medicine
Director, Cardiac Imaging
Cedars-Sinai Medical Center
Los Angeles, CA
USA

Blackwell Futura

Clinical Gated Cardiac SPECT
Second Edition

To our wonderful research staff and clinical colleagues, without whom this book would not have been possible.

Guido Germano and Daniel S. Berman

To Claire and Giulia, with love.

Guido Germano

Clinical Gated Cardiac SPECT

Second Edition

Edited By

Guido Germano, PhD
Professor of Medicine
UCLA School of Medicine
Director, Artificial Intelligence Program
Cedars-Sinai Medical Center
Los Angeles, CA
USA

Daniel S. Berman, MD
Professor of Medicine
UCLA School of Medicine
Director, Cardiac Imaging
Cedars-Sinai Medical Center
Los Angeles, CA
USA

Blackwell Futura

Blackwell Futura is an imprint of Blackwell Publishing

Blackwell Publishing, Inc., 350 Main Street, Malden, Massachusetts 02148-5020, USA
Blackwell Publishing Ltd, 9600 Garsington Road, Oxford OX4 2DQ, UK
Blackwell Science Asia Pty Ltd, 550 Swanston Street, Carlton, Victoria 3053, Australia

First published 1999
Second edition 2006

1 2006

ISBN-13: 978-1-4051-3155-1
ISBN-10: 1-4051-3155-1

Library of Congress Cataloging-in-Publication Data

Clinical gated cardiac SPECT / edited by Guido Germano, Daniel S. Berman. – 2nd ed.
p. ; cm.
Includes bibliographical references and index.
ISBN-13: 978-1-4051-3155-1 (alk. paper)
ISBN-10: 1-4051-3155-1 (alk. paper)
1. Heart–Tomography. 2. Coronary heart disease–Tomography. 3. Myocardial infarction–Tomography.
I. Germano, Guido. II. Berman, Daniel S. (Daniel Sholom), 1944–
[DNLM: 1. Heart–radionuclide imaging. 2. Tomography, Emission-Computed, Single-Photon.
3. Coronary Disease–radionuclide imaging. 4. Gated Blood-Pool Imaging. WG 141.5.R3 C641 2006]

RC683.5.T66C55 2006
616.1′207575–dc22

2006009615

A catalogue record for this title is available from the British Library

Acquisitions: Steve Korn and Gina Almond
Production: Simone Dudziak and Beckie Brand
Set in 9.5/12 Palatino and Frutiger by TechBooks, India
Printed and bound in Singapore by Fabulous Printers Pte Ltd

For further information on Blackwell Publishing, visit our website:
www.blackwellcardiology.com

The publisher's policy is to use permanent paper from mills that operate a sustainable forestry policy, and which has been manufactured from pulp processed using acid-free and elementary chlorine-free practices. Furthermore, the publisher ensures that the text paper and cover board used have met acceptable environmental accreditation standards.

Contents

Contributors

Jeroen J. Bax, MD, PhD
Professor of Cardiology
Leiden University Medical Center
Leiden
The Netherlands

Daniel S. Berman, MD
Professor of Medicine
UCLA School of Medicine
Director, Cardiac Imaging
Cedars-Sinai Medical Center
Los Angeles, CA
USA

E. Gordon DePuey, MD
Director of Nuclear Medicine
Professor of Radiology
Columbia University College of Physicians and Surgeons
St. Luke's-Roosevelt Hospital
Division of Nuclear Medicine
New York, NY
USA

David S. Fieno, PhD, MD
Physician-in-Training
Internal Medicine
Research Scientist
Nuclear Medicine and Cardiac Imaging
Cedars-Sinai Medical Center
Los Angeles, CA
USA

Guido Germano, PhD
Professor of Medicine
UCLA School of Medicine
Director, Artificial Intelligence Program
Cedars-Sinai Medical Center
Los Angeles, CA
USA

Rory Hachamovitch, MD, MSc, FACC
Director, Nuclear Cardiology
Los Angeles County-USC Medical Center
Associate Professor of Medicine
Division of Cardiovascular Medicine
Keck School of Medicine
University of Southern California
Los Angeles, CA
USA

Sean W. Hayes, MD
Assistant Director, Nuclear Cardiology
Cedars-Sinai Medical Center
Los Angeles, CA
USA

Fahim H. Jafary, MD, FACC
Associate Professor of Medicine & Consultant Cardiologist
Director, Nuclear Cardiology Services
Aga Khan University Hospital
Karachi
Pakistan

Francis J. Klocke, MD
Professor of Medicine
Director, Feinberg Cardiovascular Research Institute
Feinberg School of Medicine
Nothwestern University
Chicago, IL
USA

Serge D. Van Kriekinge, PhD
Assistant Professor of Medicine
UCLA School of Medicine Research Scientist
Artificial Intelligence Program
Cedars-Sinai Medical Center
Los Angeles, CA
USA

Josef Machac, MD
Professor of Radiology
Director of Nuclear Medicine
Mount Sinai School of Medicine
New York, NY
USA

Don Poldermans, MD
Professor of Medicine
Department of Anesthesiology
Erasmus Medical Centre
Rotterdam
The Netherlands

Alan Rozanski, MD
Director, Nuclear Cardiology
St. Luke's–Roosevelt Hospital Center
Professor of Medicine
Columbia University College of Physicians and Surgeons
New York, NY
USA

Leslee J. Shaw, PhD
Associate Professor of Medicine
Cedars-Sinai Medical Center
Los Angeles, CA
USA

Piotr J. Slomka, PhD, FCCPM
Associate Professor of Medicine
UCLA School of Medicine Research Scientist,
Artificial Intelligence Program
Cedars-Sinai Medical Center
Los Angeles, CA
USA

Louise E. J. Thomson, MBChB, FRACP
Cardiologist and Nuclear Medicine Physician
S. Mark Taper Foundation Imaging Center
Cedars-Sinai Medical Center
Los Angeles, CA
USA

James E. Udelson, MD
Associate Chief, Division of Cardiology
Director, Nuclear Cardiology
Tufts-New England Medical Center
Boston, MA
USA

Preface

Nuclear cardiology has demonstrated continuous dramatic growth for over 30 years, and has now become central to the clinical evaluation of patients with known or suspected coronary artery disease (CAD). Gated myocardial perfusion single-photon emission computed tomography (SPECT) at rest and stress has emerged as the predominant nuclear cardiology modality. The addition of ECG-gating has allowed nuclear cardiology to expand from the assessment of myocardial perfusion alone to the routine assessment of both perfusion and function from a single study.

In 1999, we published the first monographs dedicated to the performance, interpretation, and applications of gated SPECT, with the aim of providing a means for interested physicians, scientists, and technologists to become thoroughly familiar with the gated SPECT technique and its clinical applications.

This second edition, which follows many advances in the field of gated SPECT, updates the various aspects of gated SPECT previously covered, and expands the subjects for which previously there was little supportive data in the literature. Due to growth in cardiac positron emission tomography (PET), magnetic resonance imaging (MRI), and computed tomography (CT), separate chapters dealing with these modalities and their relationship to gated SPECT have been added to this new edition. Cardiologists, radiologists, nuclear medicine physicians, and technologists involved in nuclear cardiology are likely to find this book useful.

The book is composed of 14 chapters by leading physicians and scientists in the field. Chapter 1 describes the physiologic principles involved in the assessment of myocardial perfusion and ventricular function. Chapter 2 provides an understanding of the physics and technical aspects of gated SPECT. Chapter 3 covers the available stress testing and image acquisition protocols. Chapters 4 and 5 address conceptual as well as practical issues concerning the quantitation of myocardial perfusion and ventricular function with gated SPECT. Chapter 6 provides a comprehensive, systematic approach to the interpretation and reporting of both perfusion and function from gated SPECT. Chapter 7 covers artifacts that may be solved by gated SPECT, as well as those that may be associated with its performance. The clinical applications of gated SPECT in chronic and acute CAD, and the assessment of myocardial viability are covered in Chapters 8, 9, and 10. Gated blood pool SPECT is described in Chapter 11. Due to the increased use of cardiac PET, gated PET for assessment of myocardial perfusion and function is presented in Chapter 12. Chapter 13 compares the capabilities of gated SPECT with those of cardiac MRI, and Chapter 14 discusses the emerging field of cardiac CT and the relationship of this modality to nuclear cardiology.

The Editors gratefully acknowledge the expert assistance of Sherry Casanova, and Xing-Ping Kang, MD, in the preparation of the monograph.

Guido Germano, PhD
Daniel S. Berman, MD

Los Angeles, California

1 Perfusion and function in the normal and abnormal heart

Francis J. Klocke

Introduction

This chapter is intended to summarize the salient features of the normal physiology and pathophysiology of the coronary circulation and myocardial function. The intent is to provide physicians and scientists involved in imaging myocardial perfusion and function a basic understanding of the mechanisms involved in these processes.

Balance between myocardial oxygen demand and supply

The continuous work of the heart throughout life requires a high level of supply of nutrients. Because the heart has a limited and short-lived capacity for anaerobic metabolism, the functional adequacy of the coronary circulation depends on its ability to supply sufficient oxygen to meet metabolic requirements over a wide range of ventricular activity [1]. The necessary balance between myocardial oxygen demand and supply is illustrated schematically in Fig. 1.1.

The primary physiologic factors governing myocardial oxygen demand include afterload, heart rate, and contractile state:

1. Afterload, the stress developed by myocardial fibers during shortening, is directly proportional to systolic pressure and the ventricular radius of curvature and inversely proportional to ventricular wall thickness. Systolic arterial pressure is a clinically useful surrogate for afterload, although it cannot account for changes in either ventricular cavity dimension or wall thickness. Wall tension, which takes chamber radius into account but pertains only to thin wall structures, is less frequently substituted for wall stress.
2. The effect of heart rate on myocardial oxygen demand depends primarily on the number of contractions per minute. Positive inotropic effects of increased rate are involved to a lesser degree.
3. Contractile state. Myocardial contractility is an additional important factor related to the strength of contraction. It remains difficult to evaluate quantitatively in humans (as reflected by the numerous indices that have been proposed to evaluate it).
4. Preload. Changes in ventricular volume can alter afterload (via changes in wall thickness) and contractile state (via the Starling effect).

These four parameters normally account for approximately 80% of myocardial oxygen consumption. Stroke volume has a limited independent effect on oxygen usage.

Another important factor when considering the need to balance oxygen demand and supply is the coronary circulation's high degree (70–80%) of oxygen extraction under basal conditions. The heart has only limited ability to adjust to increasing oxygen demand by increasing transmyocardial oxygen extraction. Thus, changes in oxygen demand mandate changes in coronary blood flow on essentially a 1:1 basis.

Because of the ease with which it can be measured, the "double product" of peak systolic blood pressure and heart rate continues to be used frequently as an index of left ventricular oxygen demand [2]. Experimental studies supporting the use of double product have been summarized elsewhere [3]. The index correlates usefully with left ventricular oxygen consumption during exercise [4] and other activities. It also remains valid in the presence of beta blockade [5]. As noted above, limitations may arise during interventions involving substantial changes in ventricular volume.

Factors controlling coronary blood flow

As in other organs, the primary physiologic factors controlling blood flow in the heart are driving pressure and

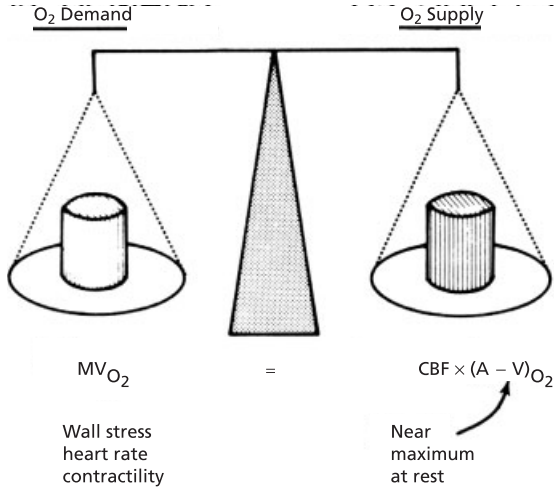

Figure 1.1 Normal balance between myocardial oxygen demand (MV_{O2}) and supply. As discussed in the text, the double product of peak systolic pressure and heart rate is used clinically as a surrogate index of oxygen demand. (Reprinted with permission from [1])

impedance (resistance). However, each of these parameters has unique features in the heart.

Driving pressure

Coronary driving pressure, traditionally considered to be the difference between coronary arterial and coronary venous pressures, is usually calculated as the difference between mean aortic and right atrial pressures. There is now evidence that the effective back pressure in the coronary bed is actually higher than right atrial pressure [6,7]. Often referred to as "zero-flow pressure," this back pressure is at least a few mm Hg higher than right atrial pressure during maximum coronary vasodilation, and substantially higher when microvascular vasomotor tone is operative. Although mechanisms underlying zero-flow pressure remain unsettled, it can be affected substantially by changes in vasomotor tone and increases in ventricular diastolic pressure, and probably varies transmurally.

Impedance (resistance)

Although impedance to flow is often considered only in terms of resistance, it includes capacitive and inertial as well as resistive components. Capacitive effects are prominent in the heart because of its large intravascular volume (6–15% of total heart weight) [8] and fluctuations and redistribution of blood volume during the cardiac cycle. Resistance nonetheless remains the dominant component of impedance.

Coronary resistance – functional components

Coronary vascular resistance can be considered in terms of three functional components (Fig. 1.2).

Conduit artery resistance ("R_1")

General features

The contribution of epicardial arteries to total coronary vascular resistance is trivial under normal conditions. However, epicardial artery diameter is affected by vasoactive substances produced by local endothelium and/or autonomic activation and is subject to coronary spasm. Effects of the vasoactive substances are relevant to normal coronary circulatory control and have increased importance in abnormal states.

Effects of endothelial and autonomic factors

Nitric oxide produced locally in conduit artery endothelium exerts a small tonic vasodilating effect under resting conditions [9,10]. Increases in coronary flow increase local shear stress; if endothelial function is intact, the conduit artery dilates further [11–13]. Increased production of nitric oxide is importantly involved in the additional dilation. However, an endothelium-derived hyperpolarizing factor also plays a role in flow-induced dilation of conduit arteries in experimental animals [14], and seems likely to participate in humans as well.

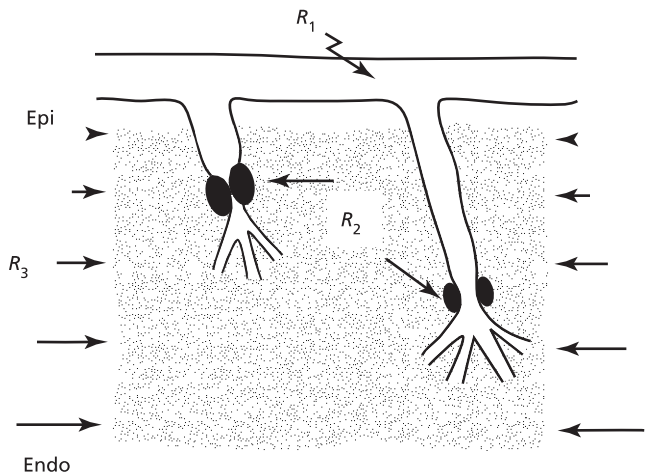

Figure 1.2 Schematic representation of the three functional components of coronary vascular resistance. R_1, conduit artery resistance; R_2, microvascular resistance, i.e., small arteries and arterioles; R_3, compressive resistance. R_3 increases in magnitude from epicardium (Epi) to endocardium (Endo), while R_2 compensates by varying transmurally in a directionally opposite manner. (Reprinted with permission from [1].)

Conduit arteries are subject to α-adrenergic vasoconstrictorand β-adrenergic vasodilator influences. α_1-Adrenergic constriction appears not to be active under resting conditions in normal human epicardial arteries [15] but can become important in pathologic states. α_1-Adrenergic constriction in intramural portions of conduit arteries during exercise may assist in maintaining subendocardial perfusion by reducing to-and-fro oscillation of blood during vigorous myocardial contraction [16]. β-Adrenergic activation contributes to epicardial artery dilation during exercise [17].

Microvascular (autoregulatory) resistance ("R_2")

General features

Coronary vascular resistance resides primarily at the arteriolar and small artery level and relates to both the number of microvessels and their degree of vasodilation. As indicated by Poiseuille's law, resistance in individual vessels is inversely proportional to the fourth power of vessel radius. Under normal conditions, approximately 25% of total resistance is located in vessels greater than 200 μm in diameter, 20% in vessels between 100 and 200 μm, and 55% in vessels less than 100 μm [18]. These size-related values of small vessel resistance become important when evaluating effects of vasoactive stimuli; i.e., different stimuli have predominant effects on different microvessels.

Adjustments in microcirculatory resistance play the dominant role in maintaining a normal balance between myocardial oxygen demand and supply. The process by which resistance adjusts to keep coronary flow constant when coronary artery pressure is reduced is referred to as *autoregulation*.

Major controlling factors

Factors affecting microcirculatory resistance can be summarized under four headings.

Metabolic factors

In view of the tight coupling between coronary flow and myocardial oxygen requirements, it is not surprising that metabolic factors play a major role in coronary flow regulation.

Metabolic vasodilation occurs primarily in arterioles less than 100 μm in diameter [19]. Over the years many products of local metabolism have been proposed as *the* metabolic regulator of resistance. These include adenosine, ATP, local O_2 and/or CO_2 tension, and local tissue pH or lactic acid concentration. Berne and coworkers amassed a large body of evidence supporting the role of adenosine, which is continuously produced by local metabolism and removed by reentry into cardiomyocytes and conversion to other substances [20]. As well known clinically, adenosine has a powerful vasodilating effect on microcirculatory resistance vessels. Its interstitial concentration in the heart varies directly with metabolic activity and importantly modulates the tone of resistance vessels. However, Feigl and colleagues have presented evidence indicating that vasodilation induced by metabolites can occur despite inhibition of adenosine receptors [21].

The vasodilating action of adenosine is mediated through A_{2A} receptors and K_{ATP} channels in humans [22–24] as well as experimental animals [25]. Adenosine acts primarily at the level of small arterioles (<100 m) and its action is generally classified as endothelial-independent vasodilation. Nonetheless, as described below, endothelial function plays a secondary role of further increasing flow during adenosine vasodilation.

Endothelial factors

Vasoactive substances produced locally by coronary endothelium have received increasing attention in recent years. Vasodilation primarily governed by this process is termed endothelial-dependent vasodilation.

Nitric oxide is produced locally by microcirculatory as well as conduit vessels [26]. In vivo microvascular vasodilation mediated by nitric oxide appears to involve primarily vessels greater than 100 μm, i.e., small arteries rather than arterioles [27]. When flow increases, e.g., in response to increased metabolic activity, nitric oxide production increases concurrently. This may be a mechanism responsive to shear stress in small arteries similar to that in conduit arteries. Increased nitric oxide production augments effects of other vasodilating factors and can serve as a "braking" factor on concurrently active vasoconstrictor mechanisms [28].

An endothelium-derived hyperpolarizing factor also plays a role in flow-induced dilation in microvessels. Studies from Gutterman's laboratory indicate that this mechanism is quantitatively important in human coronary arterioles [29], and involves endothelial-release of H_2O_2 [23].

Additional endothelial-derived products of interest include prostacyclins (vasodilators) and endothelins (vasoconstrictors). Although it is not proven, endothelium-derived agents other than nitric oxide may also have their primary effect on microvessels greater than 100 μm.

Neurohumoral factors

Microcirculatory resistance vessels are affected by both the autonomic nervous system and circulating vasoactive substances. The importance of autonomic innervation has become increasingly apparent in recent years. Our understanding of the signaling processes involved, and their various interactions, remains in evolution.

Sympathetic-induced constriction of microvascular smooth muscle is mediated primarily through postsynaptic α_2-adrenergic receptors. α_2-Adrenergic vasoconstriction is not demonstrable under normal resting conditions [30] but can become evident when the normal vasodilating action of endothelium-generated nitric oxide is attenuated.

When evaluating sympathetic-induced microvascular vasodilation, direct neural effects on microvessels must be distinguished from metabolic effects resulting from concurrent myocardial stimulation [31]. Microvascular sympathetic dilation is mediated through two receptor mechanisms.

β_2-Adrenergic receptors

β_2-Adrenergic vasodilation has been demonstrated directly in human coronary arterioles [32]. In addition, the degree of augmentation of myocardial flow during cold pressor testing in cardiac transplant recipients depends on the degree of regional sympathetic reinnervation [33]. The functional importance of neurally induced β-adrenergic vasodilation in ordinary activities is supported by canine studies indicating that this factor accounts for approximately 25% of total coronary vasodilation during exercise [34].

α_2-Adrenergic receptors

α_2-Adrenergic receptors have been reported to be present on microvascular endothelium as well as microvascular smooth muscle [35]. The endothelial receptors may reduce the constrictor effect of the smooth muscle receptors when α_2 agonists are administered. Reduced constriction would apparently depend on increased endothelial production of nitric oxide and, in human coronary microvessels, involve local kinin synthesis as an intermediate step [26].

Autonomic effects on coronary microvascular resistance involve reflex as well as direct stimuli. Parasympathetic activation during baroreceptor and chemoreceptor reflexes produces vasodilation by augmenting local production of nitric oxide [36].

Myogenic factors

Coronary arterioles also exhibit myogenic effects; i.e., increases in intraluminal pressure stimulate smooth muscle vasoconstriction, and decreases cause vasodilation. Myogenic effects may have a particular role in modulating precapillary pressure and therefore tissue exchange.

Overview

The net magnitude of microcirculatory resistance depends on the summated effects of these several, sometimes competing factors. Under basal conditions, metabolic factors predominate. During exercise and other forms of increased activity, endothelial and neurohumoral mechanisms are activated and contribute importantly to maintaining the appropriate balance between oxygen demand and supply. When endothelial and/or neurohumoral mechanisms are not normally active, responses to metabolic stimuli can be blunted.

Compressive resistance ("R_3")

General features

Compressive resistance refers to the effects on coronary blood vessels of local forces within the ventricular wall during individual cardiac cycles. These forces produce the well-known difference in coronary flow between systole and diastole; i.e., left ventricular contraction normally reduces flow into the epicardial arteries during systole to less than one-third of that in diastole.

When superimposed on conduit and microvascular resistance during systole, compressive forces narrow intramural arteries and other vessels substantially, displacing their contained blood retrogradely and antegradely and greatly reducing incoming flow in epicardial arteries. These forces also produce a large gradient in intramyocardial tissue pressure across the ventricular wall. Pressure in the subendocardial myocardium approximates intracavitary ventricular pressure while subepicardial tissue pressure remains close to intrapericardial pressure.

A finite period in early diastole is required for reexpansion and refilling of vessels compressed during systole, thereby delaying early diastolic inner wall perfusion. An inner-to-outer gradient in intramyocardial tissue pressure also occurs in diastole [37]. Although normally much smaller than the systolic gradient, the diastolic gradient is also affected by changes in ventricular diastolic pressure or intrapericardial pressure [38].

Transmural variations in perfusion and resistance

The general principles governing overall left ventricular perfusion require refinement when considering perfusion in different transmural portions of the full-thickness ventricular wall. Compressive effects cause the inner layers of the ventricular wall to be particularly dependent on diastolic perfusion. Increasing epi- to endocardial compressive effects are normally counterbalanced by directionally opposite differences in microcirculatory resistance (Fig. 1.2).

In addition, myocardial oxygen demand can vary transmurally. Myocardial oxygen consumption has been reported to be approximately 20% greater in the subendocardium than the subepicardium [39]. Relative

increases in subendocardial oxygen demand are consistent with models of transmural variations in developed stress [40] and in vivo measurements of transmural variations in diastolic sarcomere length [41]. Increased subendocardial oxygen extraction can reduce but does not negate the need for the full-cycle level of subendocardial flow to at least equal that in the subepicardium. Accordingly, flow per unit weight of myocardium (ml/(min g)) is usually 10–30% greater in the subendocardium than the subepicardium [42].

Since the mechanical effects of ventricular contraction impede systolic perfusion to the greatest extent in the inner layers of the heart, the inner layers are particularly dependent on diastolic perfusion. Transmural differences in driving pressure and microvascular resistance exert opposing effects in order to maintain subendocardial perfusion at the level needed to meet local oxygen demand [3]. The pressure drop in arteries upstream of the microcirculation is greater in arteries supplying the subendocardium than the subepicardium, presumably because of the longer intramural path of the vessels supplying the inner myocardial layers [43]. The back pressure opposing coronary flow is probably also greater in the subendocardium than the subepicardium [37,44]. The resulting reduction in subendocardial driving pressure is potentially counterbalanced by an intrinsically greater subendocardial vasodilatory capacity (i.e., smaller minimum resistance) [45]. Increased microvascular vasodilation successfully maintains the required level of subendocardial flow in most situations in normal hearts. Nonetheless, when demand is high or inflow is restricted by a process such as progressive coronary artery constriction, vasodilator reserve becomes exhausted sooner in the inner layers of the heart than the outer, resulting in subendocardial ischemia [46].

Summary

Coronary vascular resistance at any point in the heart depends on the summated effect of these three functional components. Microvascular resistance normally predominates.

Techniques used clinically to evaluate conduit artery and microvascular resistance

Cold pressor test

The cold pressor test has been used frequently to assess the vasoactivity of epicardial conduit arteries and microcirculatory resistance vessels. When the subject's forearm is immersed in ice water, blood pressure and heart rate rise reflexly as the sympathetic nervous system is activated. Coronary flow normally increases proportionally to the increase in myocardial oxygen demand.

The normal coronary vascular response to cold pressor testing includes dilation of both epicardial arteries and microcirculatory resistance vessels. It involves activation of myocardial β_1 receptors, microvascular α_2- and β_2-adrenergic receptors [47], and endothelial flow-induced dilation [48]. Since dilatory components of the response are reduced when endothelium is dysfunctional, the test is often utilized as a noninvasive probe of endothelium-dependent vasomotion [49]. Reductions in neurally mediated adrenergic vasodilation can participate in the response through reduced stimulation of β_2-receptors in microvascular smooth muscle [32,33] and/or α_2-receptors on microvascular endothelium [26].

Intracoronary acetylcholine

Intracoronary injection of acetylcholine normally causes epicardial artery diameter to increase in a dose-dependent manner [50]. The increase is mediated through increased endothelial synthesis of nitric oxide and is frequently used as a test of conduit artery endothelial function.

Coronary pressure–flow relationships in vivo

Full-thickness myocardium

Functional aspects of coronary circulatory behavior can be illustrated using diagrams depicting steady-state relationships between coronary arterial pressure and coronary flow. These are usually constructed using average values of flow for the full-thickness myocardial wall. Figure 1.3 illustrates four situations in normal individuals.

Transmural differences

As noted previously, myocardial oxygen consumption is frequently greater in the subendocardium than the subepicardium, necessitating a correspondingly greater subendocardial flow. Figure 1.4 is taken from the work of Canty [51,52], who has provided steady-state transmural pressure–flow relationships in conscious chronically instrumented dogs. As coronary artery pressure is reduced at constant myocardial oxygen demand, autoregulatory microvascular dilation maintains flow at the necessary level until vasodilator reserve is exhausted. Because subendocardial flow requirements exceed those in the subepicardium, the pressure "breakpoint" at which flow begins to fall is higher in the subendocardium than the subepicardium (Fig. 1.4a). The "breakpoint" pressure

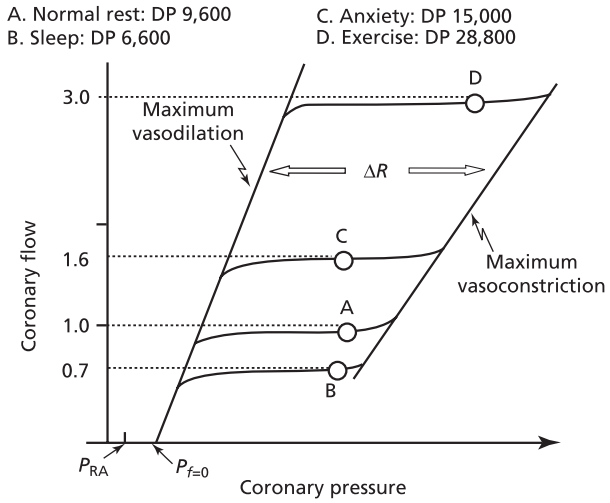

Figure 1.3 Pressure–flow diagrams depicting steady-state relationships between mean coronary artery pressure and coronary flow in the full-thickness myocardial wall in normal individuals. The line depicting the pressure–flow relation during maximum vasodilation intersects the pressure axis at a "zero-flow" pressure ($P_{f=0}$), which is higher than right atrial pressure (P_{RA}). The space between the lines representing maximum vasodilation and maximum constriction is the potential operating range for changes in coronary resistance (ΔR).

1 Normal resting conditions (point A). Typical values of BP (blood pressure) and HR (heart rate) might be 120/70 mmHg (mean 87) and 80 bpm, producing a double product of 9600. The normal resting value of flow is designated 1.0.

2 Sleep (Point B). BP and HR would probably be lower, e.g., 110/70 (mean 83) and 60 with a double product of 6600. The lower double product would require a coronary flow only 69% of that needed at rest when awake.

3 Anxiety-producing situation, with tachycardia and systemic vasodilation (Point C): BP and HR might be 110/70 (mean 83) and 140. The double product of 15,000 is 160% of that under normal resting conditions.

4 Treadmill exercise (Point D): A BP of 180/80 (113) and HR of 160 would represent an increase in double product to 300% of that under resting conditions. The threefold increase would presumably have had to be accompanied by an increase in coronary flow to 300% of its resting value.

(Reprinted, with revision, with permission from [1].)

also varies with changes in flow requirement, and can rise substantially during rapid tachycardia (Fig. 1.4b).

Quantitative measurements of coronary flow

General considerations

When considering absolute values of coronary flow, several points need to be kept in mind. Individual values need to be considered in relation to concomitant myocardial oxygen demand. Because of its practical availability, the "double product" index is most frequently used [53,54].

Quantitative measurements of flow are usually confined to the left ventricle. Measurements employing positron emission tomography (PET) provide values in terms of flow per unit weight, i.e., ml/(min g) [54,55]. Measurements employing an intraarterial Doppler velocity catheter and angiographic measurements of arterial cross-sectional area provide absolute values in ml/min for the area supplied by the artery. Sequential measurements before and following an intervention assume that the area supplied is not altered by the intervention. If only velocity is measured, the intervention is also assumed not to alter arterial cross-sectional area. Gullberg et al. have recently demonstrated that measurements of absolute flow (and flow reserve) can also be obtained by dynamic SPECT [56], although systems with sufficient count sensitivity to allow rapid sequential monitoring of the myocardial and blood concentrations of radioactivity needed for these measurements to date have not become widely available commercially.

All measurement techniques have significant methodological limitations. Since flow normally varies within the ventricle on both macroscopic [57] and microscopic [58,59] levels, an average value for the entire left ventricle represents the mean value of some distribution of flow.

Measurements employing invasive techniques in normal individuals have necessarily been limited in number. Most "normal" measurements have been obtained in patients undergoing cardiac catheterization for clinical indications and proving to have normal or near-normal findings. A frequent example would be individuals with atypical chest pain in whom coronary arteriography is needed to exclude coronary artery disease.

Measurements employing noninvasive techniques have frequently included normal volunteers as well as individuals undergoing cardiac evaluation. PET has played the dominant role in this area. All quantitative measurements involve assumptions concerning blood-tissue tracer exchange and some form of flow modeling. These differ somewhat, depending on both the tracer employed (^{13}N-ammonia, ^{15}O-oxygen) and the laboratory in which the measurement is made. Schelbert has recently provided an excellent review of cardiac PET methodology and findings in normal and disease states [54].

"Normal" values at rest

Measurements employing PET have now been reported in substantial numbers of normal individuals. Schelbert has tabulated measurements in 12 studies involving 214 patients [54, Table 10]. Resting left ventricular flows averaged 0.89 ± 0.15 (SD) ml/(min g). Camici and colleagues have reported resting values averaging 0.99 ± 0.23 ml/(min g)

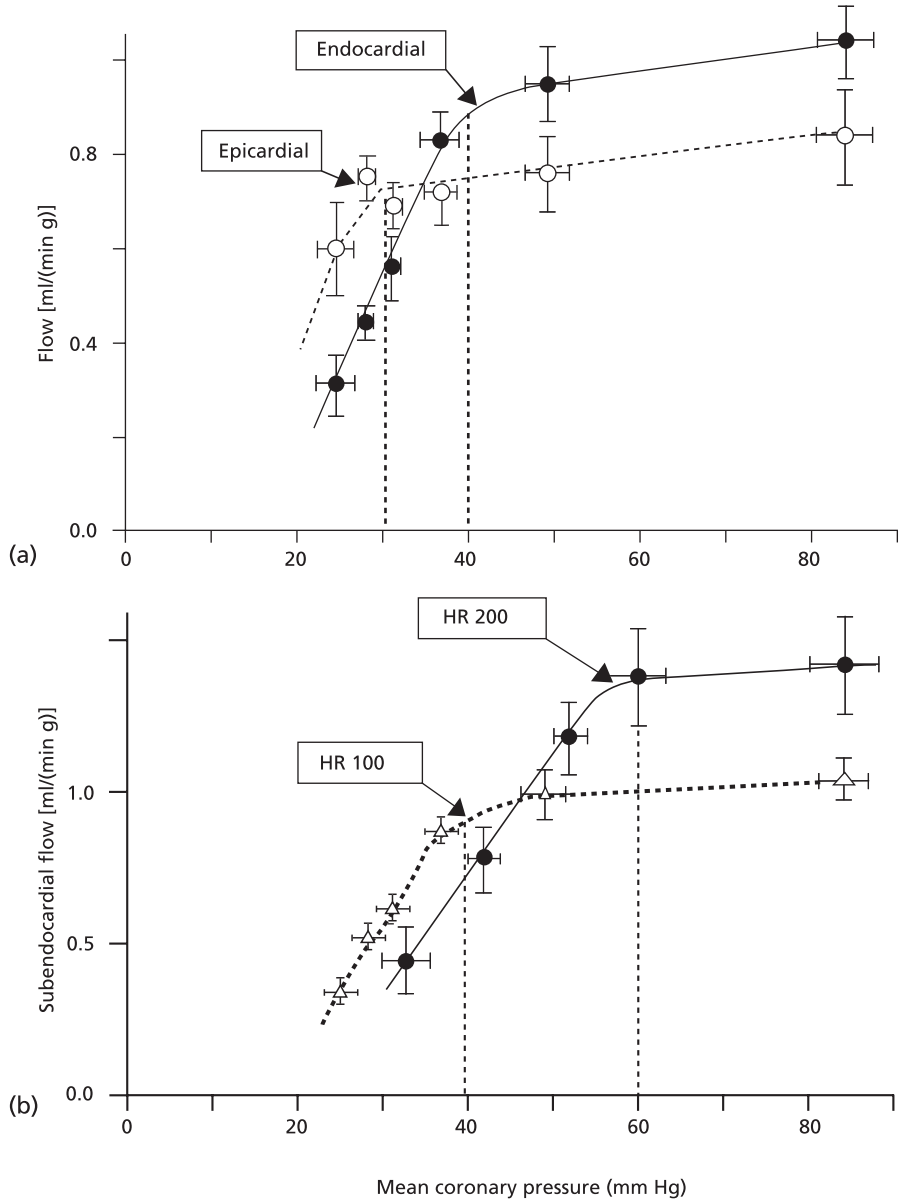

Figure 1.4 (a) Subendocardial and subepicardial pressure–flow relationships in the circumflex bed of conscious chronically instrumented dogs. Data are from Canty [51]. Under control conditions (coronary pressure 84 ± 10 mm Hg), subendocardial flow is 26% higher than subepicardial flow (1.06 ± 0.22 vs. 0.82 ± 0.24 ml/(min g)), reflecting higher oxygen demand in the subendocardial myocardium. When coronary pressure is reduced by progressive circumflex artery constriction, normal autoregulatory mechanisms maintain control flows until circumflex pressure falls below 40 mm Hg. At that "breakpoint" subendocardial flow begins to decrease. Subepicardial flow is maintained until coronary pressure falls below 30 mm Hg, when it too begins to decrease. The subendocardial/subepicardial flow ratio falls progressively when subendocardial flow begins to decrease (Redrawn from [51]). (b) Changes in the subendocardial pressure–flow relationship during tachycardia. Data are again from Canty et al. [52]. When heart rate increases from 100 to 200 bpm, subendocardial flow increases by approximately 40% and the "breakpoint" pressure at which subendocardial flow begins to fall increases from 40 to 60 mm Hg. (Redrawn with permission from [52].)

in 169 normal volunteers in their own studies [60]. Their coefficient of variation (27%) improved only slightly (to 24%) when values were normalized for differences in double product.

The relatively wide range of normal flow values emphasizes the difficulty in classifying an individual measurement in a patient as "normal" or "abnormal." The variability is probably more physiologic than methodologic; e.g., arithmetic mental stress increases resting flow and double product by approximately 30% [61]. Reproducibility of individual measurements in Schelbert's laboratory is approximately 16%, and improves to

approximately 10% when normalized for differences in double product [62].

PET measurements indicate that average resting left ventricular flow increases with age greater than 50, concomitant with age-related increases in double product [53,60]. Resting flow has been reported to be higher in females than males in some [57,63] but not all [53] studies.

Maximum coronary vasodilation

Transient coronary artery occlusion is the most consistent stimulus for producing maximum coronary vasodilation, i.e., for minimizing coronary resistance. In humans, coronary flow normally peaks at four to eight times its resting value during the "reactive" hyperemia, which follows release of a coronary artery occlusion lasting 20 or more seconds [64,65]. The relationship between coronary flow and arterial pressure during maximum vasodilation is depicted by the line on the left in Fig. 1.3.

Because total coronary resistance depends on compressive as well as microcirculatory factors, flow during maximum vasodilation varies with heart rate; i.e., tachycardia can produce a moderate reduction in the slope of the pressure–flow line representing maximum vasodilation. A reduction in slope also occurs when left ventricular preload is elevated or the left ventricle is hypertrophied. Conversely, anemia (reduced blood viscosity) increases the slope of the maximum vasodilation line.

When coronary flow is measured during vasodilation, vasodilation is usually produced pharmacologically. The most commonly employed agent is adenosine, usually given as an intravenous infusion (140 μg/(kg min)) but occasionally injected directly into a coronary artery (12–18 μg) during invasive studies. Dipyridamole (0.56 mg/(kg min) infused intravenously over 4 min) continues to be used by some laboratories. Selective adenosine A_2 receptor agonists which reduce uncomfortable side effects of systemically administered adenosine [66] are likely to become available in the near future. Papaverine, which is injected directly into a coronary artery, can produce ventricular arrhythmias and is now used infrequently.

As noted previously, it is now clear that a portion of the vasodilatory response to pharmacological agents involves the release of endothelium-derived vasodilating factors as flow (and local shear stress) increase in response to the pharmacological agent [25]. In normal individuals studied by Buus et al., adenosine-induced hyperemia decreased by an average of 21% when endogenous nitric oxide synthesis was inhibited [67]. Thus, the total response to a pharmacological vasodilating agent reflects the combined effect of agent-induced relaxation of vascular smooth muscle and endothelium-mediated vasodilation. The distribution of microvascular resistance bears importantly on this response.

As noted previously, metabolic vasodilation occurs primarily in arterioles less than 100 μm in diameter [19]. Adenosine and related compounds also have their primary vasodilating effect on microvessels of this size. Since these vessels represent only 55% of total coronary resistance, microvessels greater than 100 μm are also involved in maximal vasodilatory responses. When flow increases in response to dilation of less than 100-μm-diameter vessels, endothelial shear stress increases in larger microvessels, resulting in increased production of nitric oxide (and perhaps hyperpolarzing and other vasodilatory agents as well). Thus, metabolic or pharmacological dilation of small arterioles leads to dilation of larger resistance vessels and, if endothelial function is compromised, vasodilatory responses to metabolic stimuli and adenosine are reduced.

PET flows during adenosine- or dipyridamole-induced vasodilation averaged 3.71 ± 0.62 ml/(min g) in the tabulation by Schelbert mentioned above [54]. Similar values in the Camici lab's normal volunteers were 3.54 ± 1.01 ml/(min g) (coefficient of variation 29%) [57].

Coronary flow reserve

Coronary flow reserve is defined as the ratio of coronary flow during maximum vasodilation to that immediately preceding vasodilation. The clinical advantage of the flow reserve measurement is that a region is compared to itself, between rest and stress, avoiding the issues of underdetection of regional abnormality in the presence of balanced reduction of flow. Several methodological considerations need to be kept in mind during measurements of flow reserve. Because of variations in individual response, standard doses of adenosine and/or dipyridamole do not always produce maximum reductions in microvascular resistance. Since numerical values of flow reserve depend on flow immediately prior to as well as during vasodilation, basal conditions during the prevasodilation measurement are also important. Increases in heart rate and ventricular preload reduce reserve and need to be considered in interpreting measurements [68,69]. The same is true for adenosine- or dipyridamole-associated reductions in arterial pressure and reflex tachycardia.

"Normal" values of flow reserve also vary more than is sometimes appreciated. Marcus and colleagues pioneered Doppler measurements of coronary flow velocity in humans in the early 1980s. In initial measurements at the time of open heart surgery, ratios of peak to resting velocity were similar in the right and left ventricles and averaged 5.8 ± 2.2 [64]. Wilson et al. subsequently reported values ranging from 3.8 to 7.0 and averaging 5.0 in a small group of individuals with atypical chest pain and normal coronary arteriograms studied in the cardiovascular

laboratory [70]. Using the same approach, McGinn et al. reported values ranging from 3.0 to 7.5 and averaging 4.0 ± 1.1 in 25 cardiac transplant recipients with heart rates of 100 and normal coronary arteries and myocardium [68].

More recent "normal" values obtained using Doppler velocity measurements have varied among laboratories. For example, Kern et al. report values averaging 2.8 ± 0.6 in 85 patients with chest pain syndromes and arteriographically normal arteries and 3.1 ± 0.9 in 108 heart transplant recipients [71], whereas Houghton et al. find values averaging 4.4 ± 2.3 and 4.1 ± 2.0 in 96 African-Americans and Caucasian-Americans [72].

In Schelbert's tabulation of PET data, values of flow reserve in individual studies ranged from 3.0 to 5.4 and averaged 4.0 ± 0.66 [54, Table 10]. In the study of Camici et al., values in normal volunteers ranged from 1.4 to 8.1 and averaged 3.8 ± 1.2 [57]. Spatial heterogeneity of flow reserve was evident regionally. In addition, as reported in animal studies [73], baseline and hyperemic flows in individual myocardial segments did not correlate; i.e, resting and maximal flows were sometimes discordant.

Attempts to define a single "cut-point" separating normal and abnormal values of coronary flow reserve are complicated by the wide range of normal values. There is agreement that flow reserve measured using PET is reduced moderately at ages greater than 50 [53,57]. Gender differences have not been identified [53,57,63]. The variability of normal values can be especially problematic when attempting to classify an individual value as normal or abnormal. Nevertheless, given the potential of flow reserve measurements for adding to the detection of perfusion limitations, continued exploration of clinical applications remains important as detectors, modeling, and computing systems improve over time.

Effects of physical training and deconditioning

Physical training has beneficial effects on both myocardial oxygen demand and the coronary circulation. It is well established that myocardial oxygen requirements for any given level of activity are less in a trained individual. Heart rate is the major factor in this response. The trained individual has a lower resting rate, and achieves any given level of exercise at a lower rate, than the untrained individual [74]. In addition to reducing myocardial oxygen demand, the slower rate increases the duration of diastolic perfusion, thereby augmenting coronary flow reserve. Studies in experimental animals indicate that physical training also increases the diameter of conduit coronary arteries by a few percent, and may increase myocardial capillary density [75]. Small degrees of ventricular hypertrophy have also been reported [76].

Conversely, deconditioning increases myocardial oxygen requirements at any given level of activity [74]. The higher heart rate needed to generate the required cardiac output in the deconditioned individual is the major factor involved. Conduit coronary artery diameter and ventricular mass may diminish slightly [75,76].

Measures of myocardial function in humans

The importance of measurements of cardiac function in clinical decision making underscores the value of assessing chamber size and contractile function concurrently with myocardial perfusion. Parameters of particular interest include left ventricular volumes and ejection fraction, regional wall motion, and myocardial mass. Beller has provided a cogent discussion of the relative clinical strengths and limitations of measurement techniques now used widely [77]. These include echocardiography, angiography, and gated magnetic resonance imaging as well as gated SPECT and equilibrium radionuclide angiography.

Global ventricular function

Global ventricular function is most commonly assessed by measuring ejection fraction (end-diastolic − end-systolic volume/end-diastolic volume). Ejection fraction has proven to have enormous clinical value despite its known variability with loading conditions (particularly afterload) and heart rate, and sometimes challenging measurement issues. Measurements of chamber volume frequently involve an assumed geometric model, e.g., a prolate ellipsoid for the left ventricle and a crescentic solid for the right ventricle [78]. Options for avoiding an assumed geometry include summing data from multiple transverse slices, reconstructing three-dimensional volumes from two-dimensional images, and gated imaging of the ventricular blood pool following labeling with a radionuclide tracer. The latter is particularly useful in right ventricular studies. All volume measurements cannot deal fully with the complex pattern of ventricular motion during contraction (which includes rotational and translational motion as well as transverse and apex-to-base shortening). Accurate definition of endocardial borders can also be problematic. Despite these limitations, the value of ejection fraction as an indicator of prognosis and an important determinant in therapeutic decisions is unquestioned.

M-mode echocardiographic measurements of fractional shortening provide an additional ejection phase index of left ventricular function. Isovolumic phase indices continue to be used occasionally. The rate of change of ventricular pressure (dP/dt) is affected by preload,

i.e., end-diastolic ventricular pressure. More complex parameters, e.g., end-systolic pressure-dimension indices, can provide relatively load-independent estimates of contractility.

Regional ventricular function

Regional contractile performance is usually assessed by evaluating endocardial wall motion or transmural wall thickening. The latter is generally considered preferable. The clinical importance of detecting, and at least semiquantifying, regional contractile abnormalities is well established. An important recent development has been the agreement on "Standardized Myocardial Segmentation and Nomenclature for Tomographic Imaging of the Heart" developed under the auspices of the American Heart Association by the American Society of Echocardiography, American Society of Nuclear Cardiology, North American Society of Cardiac Imaging, Society for Cardiac Angiography and Interventions, and the Society for Cardiovascular Magnetic Resonance [79]. Consensus recommendations are provided for orientation of the heart, names for cardiac planes, number of myocardial segments, selection and thickness of cardiac slices for display and analysis, nomenclature and location of segments, and assignment of segments to coronary arterial territories. The resulting 17-segment system for assessing the myocardium and left ventricular cavity (Fig. 1.5) is suitable for evaluating perfusion as well as function.

Regional myocardial function is usually assessed visually, often with semiquantitative characterization as normal, hypokinetic, akinetic, or dyskinetic. The clinical value of this approach is reflected in its continued widespread usage and acceptance. However, several complexities of regional contractile behavior discussed by Mulhern and Skorton in an earlier edition of this book [78] need to be recognized. The complex and nonuniform nature of ventricular muscle fiber architecture results in some degree of nonuniformity of contraction pattern in even the normal left ventricle. This nonuniformity may underlie some of the nonuniformity of regional blood flow in normal ventricles. Generally accepted criteria for normal endocardial motion or wall thickening in all portions of the ventricle are not available. Estimates of regional contraction can also be confounded by rotational and translational motion during systole which is unrelated to contraction. Approaches for dealing with noncontractile motion include the centerline approach developed by Sheehan and colleagues [80] and floating- and fixed-axis analyses discussed by Force and Parisi [81]. Finally, in slice-based approaches, efforts to image the same portion of myocardium at end-systole and end-diastole are complicated by base-to-apex shortening and/or translational movement during contraction. Techniques such as myocardial tagging with magnetic resonance imaging (MRI) can be helpful in addressing these problems.

Ventricular remodeling

Structural and functional changes in the left ventricle following myocardial infarction or other injury, referred to as remodeling, have received increasing attention in recent years. Myocardial dysfunction involving areas not included in the infarction is of particular concern. Initially compensatory ventricular dilation sometimes progresses to an adverse degree, resulting in deteriorating overall function and ejection fraction. Early measurements of ejection fraction, infarct size and location, and TIMI-grade flow in the infarct-related artery can assist in identifying individuals at high risk of adverse remodeling [82].

Remodeling is ordinarily identified using an imaging technique, most commonly echocardiography. The recent development of delayed contrast-enhanced magnetic resonance imaging [83,84] has added the capability to identify infarcted tissue selectively with high resolution. Thus, it is now possible to define the circumferential, longitudinal, and transmural extent of infarctions, and to identify otherwise unappreciated subendocardial infarctions. Due principally to limitations of resolution, definition of the extent of infarction is currently less precise with most other imaging techniques. Delayed contrast enhancement using multislice computed tomography (CT), however, has shown promise in this regard. With MRI, infarct size can be followed throughout the period of acute injury and subsequent resorption and scar formation. When imaging is performed during the first few days, areas of microvascular obstruction can be identified within the zone of infarction (the "no-reflow" phenomenon) [85–87]. Recent data suggest that this phenomenon is predictive of adverse remodeling. The direct visualization of infarctions with MRI and possibly CT also offers advantages over surrogate measures based on wall motion abnormalities or resting perfusion scans. Wall motion abnormalities related to areas of infarction can be distinguished from those representing viable hypocontractile myocardium, i.e., stunned or hibernating myocardium. Abnormalities in perfusion scans resulting from areas of infarction can be distinguished from those caused by flow reductions in viable myocardium [88]. Theoretically, these distinctions are also possible with radionuclide methods such as rest/redistribution thallium SPECT, but would require improved resolution over that currently available. Hypertrophy of viable noninfarcted muscle can be identified and quantified even when total ventricular mass does not change (because of concurrent reductions in infarct size as necrotic tissue is resorbed and replaced by scar) [89].

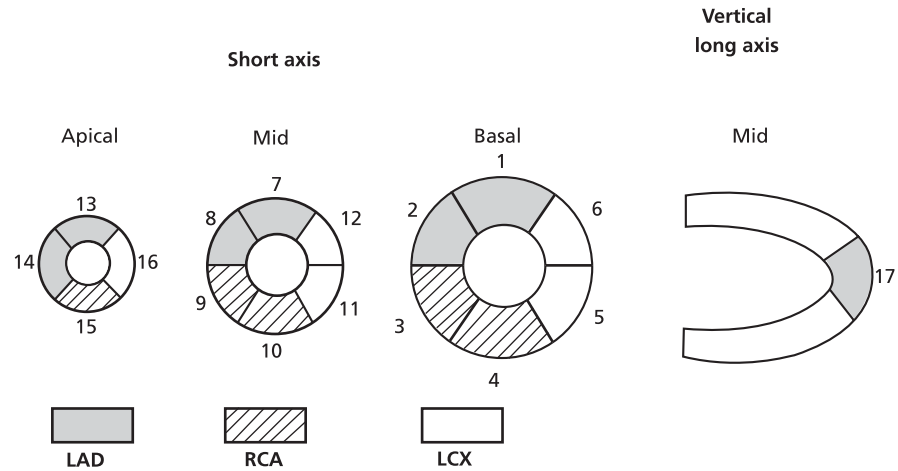

(a)

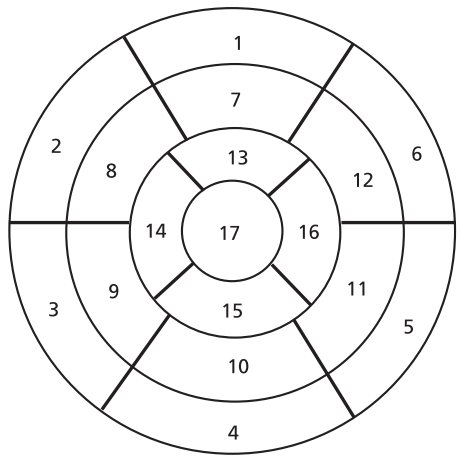

1. Basal anterior
2. Basal anteroseptal
3. Basal inferoseptal
4. Basal inferior
5. Basal inferolateral
6. Basal anterolateral
7. Mid anterior
8. Mid anteroseptal
9. Mid inferoseptal
10. Mid inferior
11. Mid inferolateral
12. Mid anterolateral
13. Apical anterior
14. Apical septal
15. Apical inferior
16. Apical lateral
17. Apex

(b)

Figure 1.5 Recommended 17-segment system for assessing regional ventricular function and/or perfusion (reprinted with permission from [79]). (a) Assignment of the 17 myocardial segments to the territories of the left anterior descending (LAD), right (RCA), and left circumflex (LCX) coronary arteries. (b) Display, on a circumferential polar plot, of the 17 myocardial segments and the recommended nomenclature for tomographic imaging of the heart.

Pathophysiologic alterations in coronary artery disease

Hemodynamics of stenotic lesions

In considering pathophysiologic alterations in coronary artery disease, it is useful to begin by examining effects of stenotic lesions independently of the distal coronary vasculature. Building on Gould's original experimental studies [90–92], several groups have contributed to our current understanding of factors governing energy losses across a stenosis. These are illustrated schematically in Figs. 1.6 and 1.7. As depicted in the figures, small increments in severity of an established stenosis can have important clinical effects [93,94]. Such an increment might represent static progression of the underlying atherosclerotic process but can also result dynamically from local vasomotion, a platelet aggregate or small thrombus, or intramural hemorrhage. Conversely, small

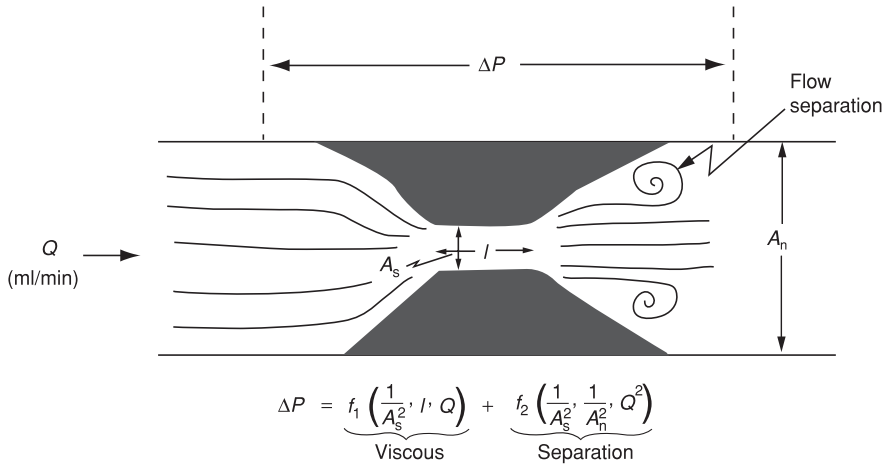

Figure 1.6 Factors governing the pressure drop (ΔP) across a stenosis. Q, flow; l, stenosis length; A_S, minimum cross-sectional area within the stenosis; A_n, cross-sectional area in adjacent section of the artery (reprinted with permission from [93]). The pressure drop across a stenosis varies with flow and is influenced by both frictional (viscous) and separation losses. Four points are noteworthy: (1) Frictional losses are proportional to flow and vary linearly with stenosis length; (2) separation losses are proportional to flow raised to the second power and become increasingly important as flow increases; (3) separation losses also increase nonlinearly with severity of stenosis; (4) for any given level of flow, the most important determinant of stenosis severity is the minimum cross-sectional area within the stenosis, which appears as a second-order term in the expression of both frictional and separation losses.

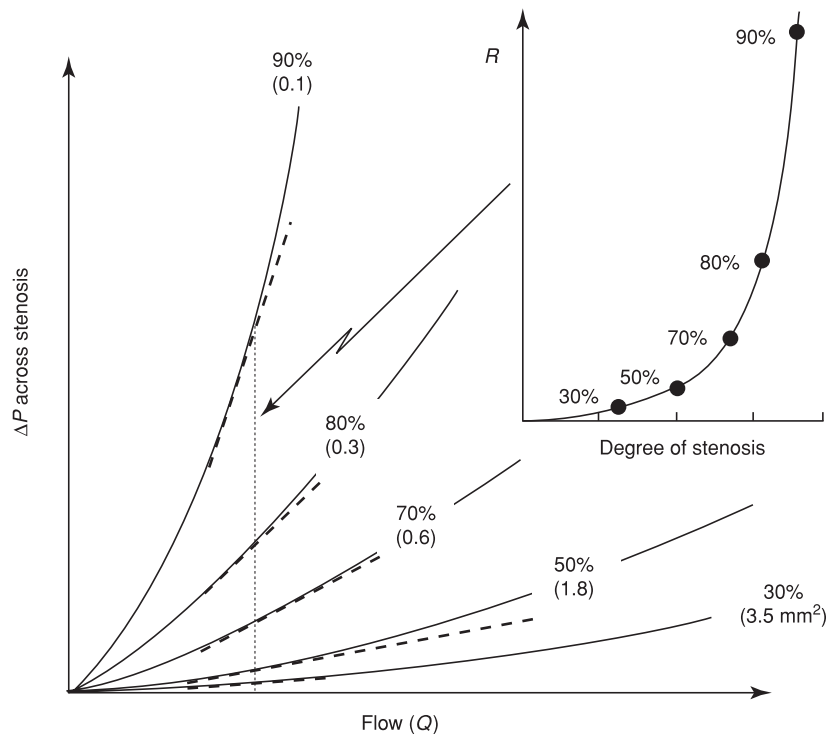

Figure 1.7 Additional features of the relationship between pressure drop across a stenosis (ΔP) and flow (Q) through the stenosis. As usually done clinically, degree of stenosis is expressed as percent diameter narrowing (assuming circular stenosis geometry). The dashed tangent lines represent the resistance (R) offered by individual stenoses at a particular level of flow (vertical dotted line) (Reprinted with permission from [93]). Although the figure has been derived using fluid mechanics equations for steady flow of an incompressible fluid in rigid tubes, it applies in principle to the in vivo coronary circulation. Two points are noteworthy: (1) Because the relationship between pressure drop and flow is alinear, the pressure drop across a stenosis increases progressively more rapidly as flow rises; i.e., the resistance of even a rigid stenosis increases with flow. (2) At any given level of flow, stenosis resistance also increases alinearly and progressively more rapidly with stenosis severity. As shown in the inset, this latter point is especially relevant for greater than 50% diameter stenoses; e.g., stenosis resistance doubles as the degree of narrowing increases from 70 to 80%, and doubles again between 80 and 90%.

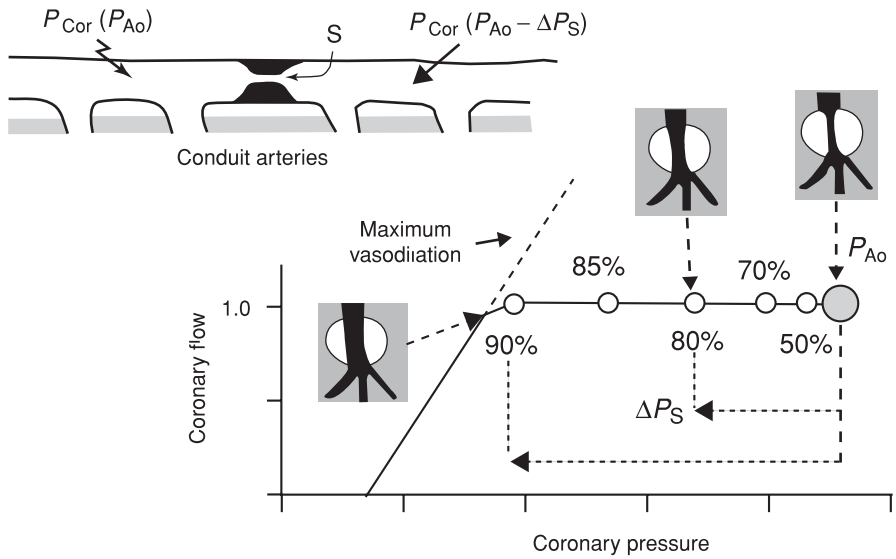

Figure 1.8 Schematic representation of in vivo effects of stenoses (redrawn with permission from [1,94]). (a) Coronary artery pressure (P_{Cor}) is the same as aortic pressure (P_{Ao}) upstream of a stenosis (S) within an epicardial artery but is reduced beyond the stenosis by the transstenotic pressure gradient (ΔP_S). The magnitude of reduction depends on the factors illustrated in Figs. 1.6 and 1.7. (b) Pressure–flow relationships under resting conditions for varying degrees of stenosis. Values of poststenotic pressure corresponding to different degrees of stenoses are shown by open circles. Reductions in poststenotic pressure are modest for less than 70% diameter stenoses but increase rapidly thereafter. Compensatory microcirculatory vasodilation is able to maintain resting flow at its normal level but is almost exhausted at the 90% stenosis level.

decreases in stenosis severity, either static or dynamic, can have important benefit.

Since coronary lesions frequently do not involve the entire circumferential vessel wall, dynamic changes in the severity of atherosclerotic stenoses are expected. Abnormalities in endothelium-mediated vasodilation blunt flow-induced dilatory responses and increase susceptibility to α-adrenergic vasoconstriction, e.g., α-adrenergic activation during exercise can constrict atherosclerotic epicardial arteries [95]. Conversely, reductions in conduit artery caliber can often be counteracted by nitroglycerin.

Stenosis effects in the intact circulation

Effects of coronary stenoses on the resting pressure–flow relationship are depicted schematically in Fig. 1.8. Reductions in poststenotic pressure are modest for less than 70% diameter stenoses but increase rapidly thereafter. Compensatory microcirculatory vasodilation is able to maintain resting flow at its normal level but is almost exhausted at the 90% stenosis level.

Figure 1.9 shows the pressure–flow relationship throughout the full range of coronary vasodilation. Maximum vasodilated flow is reduced by approximately 20% for a 50% stenosis, approximately 40% for a 70% stenosis, and approximately 60% for an 80% stenosis. Flow reserve is essentially absent for stenoses greater than 90%. The additional factor of transmural differences in perfusion is illustrated in Fig. 1.10.

Arterial remodeling and estimates of stenosis severity

The limitations of estimating stenosis severity by comparing an area of arteriographic narrowing to an adjacent area of an artery involved with a diffuse abnormality such as atherosclerosis are well recognized. Because of the eccentric nature of many stenoses, percent diameter narrowing is usually defined as the maximum narrowing observed in views taken from various angles and positions. Complexities of remodeling of the arterial wall [96] also need to be considered. As illustrated in Fig. 1.11, the atherosclerotic process proceeds in an outward as well as inward direction, and frequently involves an increase in external arterial diameter as well as a reduction in luminal diameter. Increases in diameter which precede luminal narrowing can lengthen the asymptomatic phase of developing coronary disease. When evaluating a stenosis arteriographically, the area of luminal narrowing and adjacent "reference" area each represent the result of a process involving both atherosclerotic proliferation and arterial enlargement. The stenosis reflects a relative local difference in the proliferative-enlargement process, the factors governing which remain incompletely understood.

In vivo measurements of transstenotic pressure gradients: fractional flow reserve

The development in recent years of pressure-monitoring guide wires only 0.10–0.15 in. in diameter has enabled

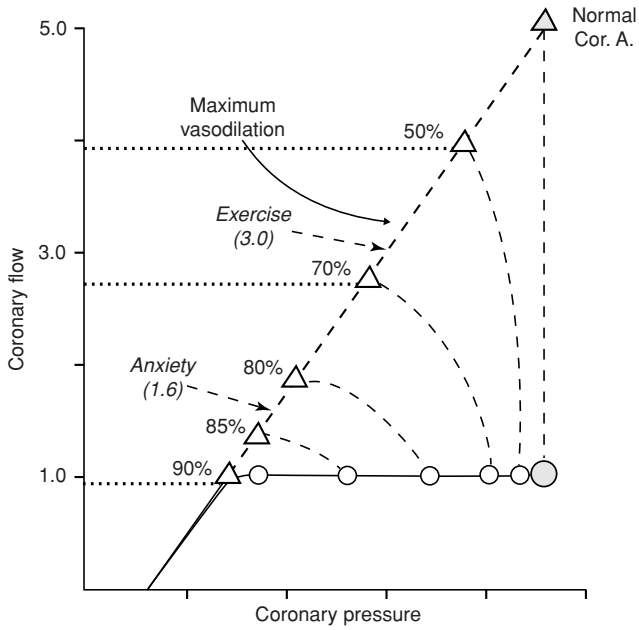

Figure 1.9 In vivo pressure–flow relationship throughout the full range of coronary vasodilation. The heavy line represents flow during maximum vasodilation; i.e., when total coronary resistance ($R_1 + R_2 + R_3$) is minimum. Maximum flow is reduced from 5 to approximately 4 ml/(min g) by a 50% diameter stenosis, and to approximately 2.7, 1.9, 1.4, and 1.1 ml/(min g) by 70, 80, 85, and 90% stenoses, respectively. The dashed lines connecting resting and vasodilated points for individual stenoses are curvilinear because of the curvilinear relationships between pressure gradient and flow in the stenoses. In this schematic illustration, the increases in flow required in the examples for exercise (3.0) and anxiety (1.6) in Fig. 1.3 would fail to be met when stenoses reached 70 and 85%, respectively. (Redrawn with permission from [94].)

pressure gradients across individual stenoses to be measured precisely in coronary patients. In 1993 Pijls and colleagues proposed that stenosis severity could be evaluated in terms of *fractional flow reserve* (FFR), defined as "the maximally achievable flow in the presence of a stenosis divided by the maximum flow expected in the same distribution in the absence of a stenosis" [97]. Using a model modified from Gould's previous studies [98], FFR was calculated by measuring transstenotic gradients during maximum coronary vasodilation and expressing poststenotic pressure as a fraction of prestenotic (aortic) pressure. Application to coronary patients followed quickly [99,100]. The technique appears advantageous in relation to velocity-based measures of reserve [101] and is now utilized in a number of catheterization laboratories. It can evaluate sequential stenoses in a single artery [102] and has demonstrated abnormal pressure drops in arteries of coronary patients not showing focal stenoses arteriographically [103]. A recent commentary by Pijls summarizes additional clinical applications [104].

As discussed subsequently in the section on collateral circulation, the availability of poststenotic pressure measurements offers opportunities for studying the distal coronary bed as well as conduit arteries. However, studies based on the model utilized by Pijls et al. [97] involve additional assumptions concerning coronary back pressure (zero-flow pressure), capacitance, collateral circulation, and effects of compressive resistance. This remains an evolving area of study.

Concurrent abnormalities in conduit artery and microvascular vasodilation

Intrinsic vasodilating mechanisms are noticeably blunted in conduit and resistance vessels in patients with coronary atherosclerosis. As early as 1976 Mudge et al. demonstrated abnormal responses of total coronary resistance during cold pressor testing in patients with coronary disease [105]. The abnormality was subsequently shown to involve both conduit and resistance vessels [12,47] and reflects endothelial dysfunction in both vessel types [106]. The defect in endothelium-mediated vasodilation involves reduced production of nitric oxide and appears to predate the development of clinically evident disease; i.e., it is evident in patients with risk factors for coronary disease who still have angiographically normal coronary arteries [10]. With blunting of normal endothelium-mediated vasodilation, vasoconstrictor mechanisms can become evident [15,30]. As discussed by Heusch et al. [15], α_2-adrenergic microvascular vasoconstriction probably contributes frequently to exercise-induced ischemia.

Collateral circulation

It has long been recognized that a well-developed coronary collateral circulation has a clinically important impact [107,108]. However, the reasons why substantial collaterals develop in only a minority of coronary patients remain unclear. Heterogeneity among individuals involves genetic factors in at least some cases, e.g., collateral development correlates with a particular haptoglobin phenotype in diabetics [109]. It has also been associated with the ability to augment production of vascular endothelial growth factor in response to hypoxia [110].

Coronary collaterals arise from preexisting microvascular interconnections that remodel into functional conductance arteries [111]. Collateralized human hearts show a predominance of collateralization through intramural vessels, with variable additional contributions of larger anastomoses at the epicardial level [112]. Collateral channels connect into the recipient bed primarily at the arteriolar level, i.e., at vessels with diameters of 20–100 μm [113]. Capillary density is not increased after the initial phase of collateral development but increased numbers

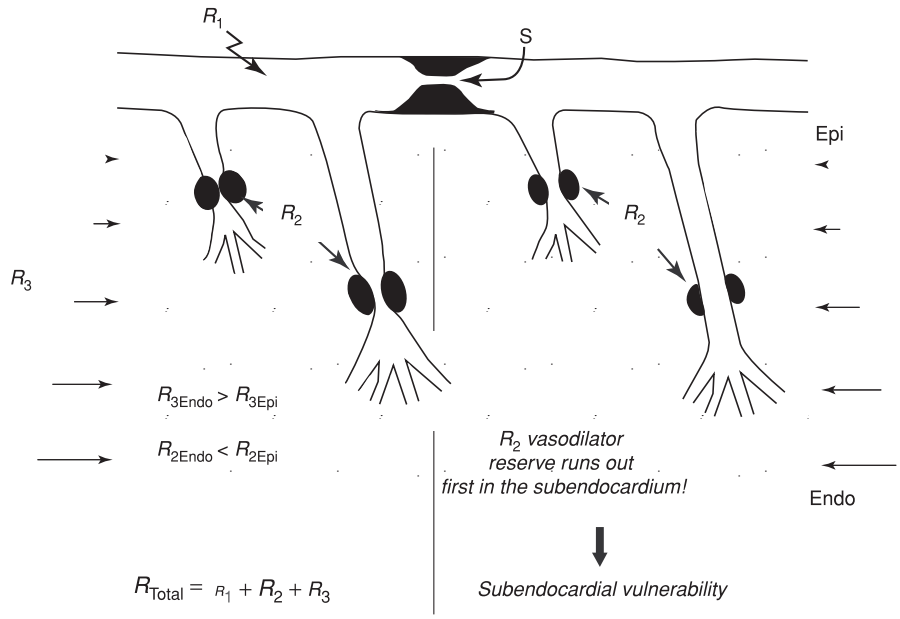

Figure 1.10 Normal transmural differences in perfusion and effects of a coronary stenosis. As discussed previously, microvascular resistance (R_2) is normally less in the inner (Endo) than outer (Epi) layers of the ventricular wall; i.e., subendocardial dilation compensates for the transmural gradient in compressive resistance (R_3). Vasodilator reserve is consequently less in the subendocardium than the subepicardium. Thus, as also illustrated in Fig. 1.4, an inability to maintain the normal balance between myocardial oxygen demand and coronary flow occurs initially in the subendocardium. (Redrawn with permission from [1].)

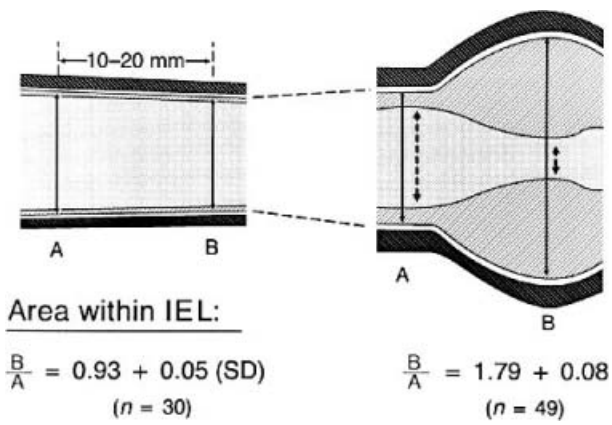

Figure 1.11 Atherosclerotic coronary artery remodeling, illustrated using data from Stiel et al. [95], in human coronary arteries fixed at a normal arterial pressure. The proximal portion of a normal coronary artery is shown on the left and a stenotic atherosclerotic artery on the right. The atherosclerotic process (hatched area) encroaches on luminal area but the degree of encroachment is attenuated by an increase in overall arterial diameter. The local increase in enlargement can be expressed as the ratio of the areas contained within the internal elastic membrane (IEL) at points B and A. In the series of Stiel et al. this ratio averaged 1.79 in diseased arteries, as opposed to 0.93 in nondiseased normally tapering arteries. The percent luminal narrowing that would be calculated arteriographically depends on the relative luminal diameters at points A and B in the atherosclerotic artery. (Reprinted with permission from [94].)

of 20–100 μm distribution vessels persist. Experimental studies indicate that collateral vessels exhibit endothelium-dependent vasodilation [114,115] and are responsive to a variety of vasoactive stimuli. Nitric oxide [116] and prostacyclin [117] appear to have tonic vasodilating activity. Aspirin-induced blockade of cyclooxygenase activity (and presumably prostaglandin production) reduces collateral flow at least transiently but the reduction is reversible with nitroglycerin [118].

Even when coronary collaterals are well developed, the amount of flow that can be provided is limited. The ability to measure distal coronary artery pressure during angioplasty has provided more quantitative estimates of collateral efficacy than can be obtained angiographically. When an artery is occluded distal to a stenosis, the steady-state occlusion pressure represents the inflow pressure generated by collaterals in the artery's distal bed. This pressure exceeded 30 mm Hg in only 26 of 120 patients reported by Pijls et al. in 1995 [119, Fig. 1.3]. Values less than 30 mm Hg have a very limited flow supplying capacity (see Figs. 1.4, 1.8, and 1.9) and usually cannot maintain a normal demand/supply balance under even resting conditions. They may be sufficient if demand is reduced, e.g., in hibernating myocardium [120].

In their original study describing the use of fractional flow reserve to evaluate stenosis severity [97], Pijls and colleagues also proposed a pressure-based collateral flow index based on the relative values of distal coronary pressure

(P_w) and aortic pressure (P_a) during balloon occlusion. The model on which the index is based assumes a coronary back pressure equal to central venous pressure (P_v) and is calculated as $(P_w - P_v)/(P_a - P_v)$. In their 1995 study of 120 coronary patients, an index "cut-point" of 0.24 was felt to be optimal in separating patients with and without ECG signs of ischemia during balloon occlusion [119]. More recently, using an assumed P_v of 5 mm Hg, Seiler and colleagues have reported values averaging 0.17 ± 0.09 in 40 patients with, and 0.44 ± 0.16 in 11 patients without, ECG signs of ischemia during balloon occlusion [121]. This group also calculated a collateral flow index based on Doppler flow velocities in the stenotic artery before and following angioplasty and found it similar to the pressure-based index (average difference $= 0.03 \pm 0.10$, linear $r^2 = 0.64$). They have now extended their experience to 450 patients and confirm that two-thirds of patients do not have sufficient collateral flow to prevent myocardial ischemia during coronary occlusion [122]. Not withstanding these limitations, even a level of collateral flow that cannot prevent ischemia can often reduce its adverse consequences [123]. While collaterals may provide adequate flow to preserve viability, and perhaps even normal resting flow in some patients, collaterals that increase coronary flow sufficiently to prevent ischemia during peak exercise are uncommon, even when they are prominent angiographically.

Clinical importance of regional differences in perfusion

As noted in an earlier section of this chapter, maximum coronary vasodilation involves endothelium-mediated vasodilation as well as direct relaxation of arteriolar smooth muscle. Because of the abnormalities summarized above, coronary flow reserve in patients with coronary artery disease can be decreased moderately throughout the left ventricle independently of the effects of arterial stenoses. Thus, regional differences in perfusion are usually more important than absolute reductions in flow reserve for evaluating the effects of a stenosis during exercise, pharmacological vasodilation, or other stresses.

Because radionuclide approaches for evaluating perfusion depend on assessing the entrance and/or retention of blood-borne tracer in the myocardium, it is important to understand the relationship between flow and transmyocardial extraction of tracer. With the exception of ^{15}O-water, virtually all tracers exhibit a reduction in the proportion extracted during circulation through the myocardium as flow exceeds approximately two times normal. For example, a number of studies have documented that the fractional extractions of ^{201}Tl and ^{99m}Tc-sestamibi or -tetrofosmin decrease as flow increases above approximately 2 ml/(min g) [124,125]. This property is also

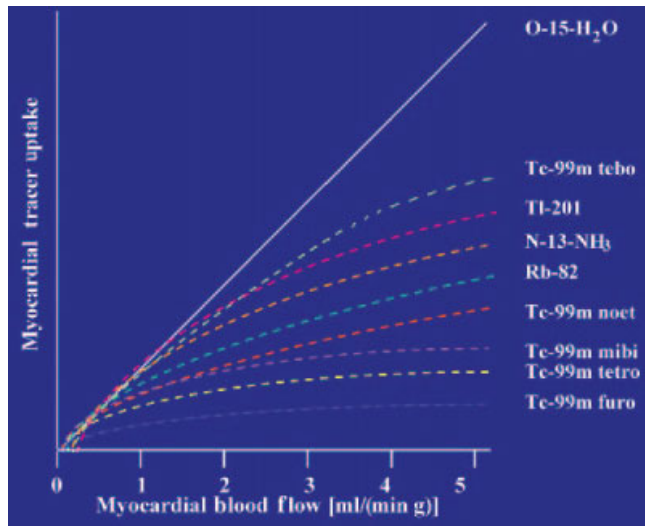

Figure 1.12 Schematic representation of relative extraction fractions of PET and SPECT radiopharmaceuticals.

observed with PET agents such as ^{82}Rb and ^{13}N-ammonia. Since the flow during maximum vasodilation is normally at least 4 ml/(min g), modest reductions in vasodilated flow – as illustrated schematically for a 70% stenosis in Fig. 1.9 – can be difficult to appreciate [126]. While issues of tissue retention through the imaging time are also important, the reduction of extraction fraction with increasing flow is the fundamental limiting variable in detectibility of mild stenoses with the tracer method. ^{99m}Tc-teboroxime, a tracer that was commercially available in the early 1990s in the United States, was reported to have extraction fraction at high flow rates exceeding that of ^{201}Tl, suggesting that in combination with vasodilator stress, this agent might be more sensitive than other radionuclide methods in detecting mild stenoses. Rapid washout of this tracer from the myocardium, and avid accumulation in the liver, resulted in little practical clinical use. The relative extraction fractions of the various PET and SPECT radiopharmaceuticals are schematically illustrated in Fig. 1.12. Quantitative measurements of perfusion using PET and tracers such as $^{13}NH_3$, ^{15}O, and ^{82}Rb involve additional complexities that Schelbert has summarized [54]; those involved in the use of dynamic SPECT have been summarized by Gullberg [56].

Although data addressing the minimal difference in regional flow needed for a defect to be identified are limited, a difference of at least 30% seems a reasonable estimate but depends on the detection system being employed. Transmural differences resulting in full-thickness flow reductions of less than 30% require higher-than-usual resolution with most tracer techniques. Figure 1.13 presents interpretive issues for three situations that might be expected to produce similar defects on perfusion images but would have different clinical implications.

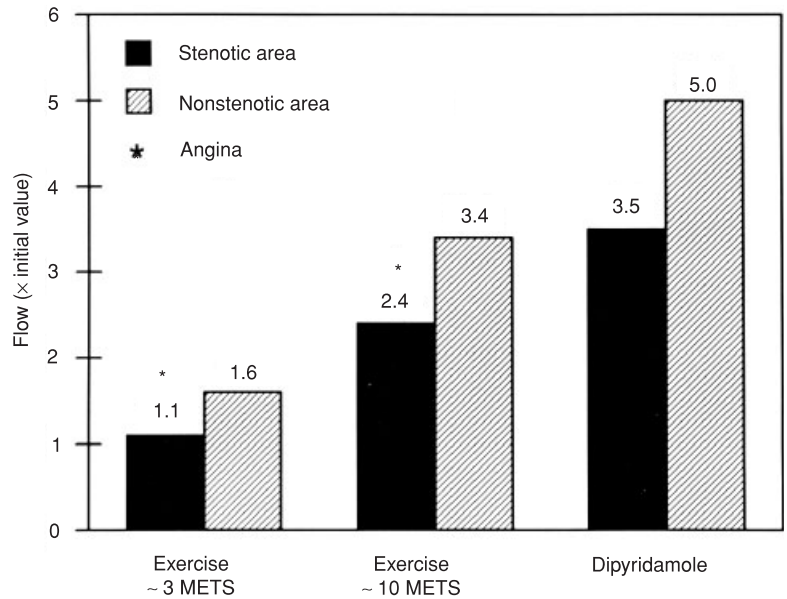

Figure 1.13 Examples of 30% reductions in regional flow having different clinical implications. The paired columns on the left depict exercise with angina at a low work load. Extrapolating from the studies of Kitamura et al. [4], an exercise level of 3 metabolic equivalents (METS) would require an increase to 1.6 times resting flow (1.0). The center columns represent exercise with angina at a high work load (10 METS), requiring a flow of 3.4 times the resting value. Although the relative perfusion deficits are similar, the therapeutic implications of ischemia at 3 and 10 METS differ. The columns on the right represent findings that might occur during maximum pharmacological vasodilation with a 60% stenosis. A 30% regional reduction in flow corresponds to a regional increase to 3.5 (rather than 5.0) times resting flow and occurs without a corresponding increase in myocardial oxygen demand. Thus, the relative perfusion deficit is not associated with ischemia. Although a finding of this type can be diagnostically useful in identifying an asymptomatic stenosis, it may be difficult to discern using tracer techniques in which transmyocardial tracer extraction decreases progressively as flow exceeds twice resting values. (Reprinted with permission from [94].)

Pathophysiologic alterations in microvascular function and conduit artery caliber without apparent coronary artery disease

Information is now available concerning conduit artery and microvascular function in a variety of clinically relevant situations in which coronary artery disease is not apparent. Abnormalities in endothelial-mediated coronary vasomotion have been identified in individuals with coronary risk factors and in the early stages of several disease processes. Four situations are illustrative.

Cigarette smoking

It is well established that cigarette smoking produces acute increases in heart rate, arterial pressure, and myocardial contractility. These are mediated through the sympathetic nervous system and involve both cardiostimulatory (β-adrenergic) and vasoconstrictor (α-adrenergic) influences [127].

Since cigarette smoking acutely increases the double product index, increases in resting coronary flow are expected and do occur in otherwise healthy young adults with relatively short smoking histories (6 ± 3 pack years) [128]. However, flow during dipyridamole-induced vasodilation is reduced in these individuals, resulting in substantial transient decreases in flow reserve. In long-term smokers (27 ± 13 years) without cardiovascular risk factors, expected increases in resting coronary flow during smoking are blunted or reversed [129]. Long-term smokers also show blunted flow responses to cold pressor testing [130,131], which can be normalized by intravenous administration of L-arginine and are therefore felt to reflect sustained endothelial dysfunction [130].

Abnormal responses to smoking are accentuated in individuals with coronary artery disease. It has been known since the 1980s that expected increases in coronary flow accompanying smoking-induced increases in double product are blunted or reversed in coronary patients [132–135]. The abnormal response involves constriction of both epicardial conduit arteries and microcirculatory resistance vessels [136,137]. It can be reversed by nonspecific α-adrenergic blockade [135] and probably involves α_1-adrenergic constriction of conduit arteries and α_2-adrenergic constriction of resistance vessels as well as blunted endothelial-dependent vasodilatory mechanisms.

It can also be prevented by the administration of calcium antagonists or nitroglycerin [138].

Hyperinsulinemia and diabetes mellitus

Indications that hyperinsulinemia is an independent risk factor for developing ischemic heart disease have stimulated a variety of studies of insulin's effects on the coronary circulation. Effects on conduit arteries have been examined using intracoronary acetylcholine or the cold pressor test. Effects on microvascular resistance have been evaluated by responses of coronary flow to cold pressor testing, intravenous adenosine infusion, or intracoronary papaverine injection.

Because insulin increases sympathetic nerve activity, modest increases in basal levels of coronary flow following insulin administration have to be considered in relation to concomitant changes in myocardial oxygen demand [139]. McNulty et al. attempted to circumvent this issue using intracoronary infusion of small doses of insulin in patients undergoing coronary arteriography [140]. They report approximately 20% consistent increases in coronary sinus flow without increases in myocardial oxygen consumption. In addition, Sundell and colleagues find that insulin increases adenosine-stimulated flow and coronary flow reserve in a dose-dependent manner in healthy young subjects [141]. Flow during adenosine infusion increased by an average of 20% during physiological hyperinsulinemia (~65 mU/l), and by an additional 19% when insulin levels were increased to pharmacological levels (~460 mU/l). Thus, insulin appears to have vasodilator as well as hypoglycemic activity.

Insulin-induced dilation of the coronary vasculature involves activation of both the sympathetic nervous system and endothelium-dependent mechanisms. Since insulin-induced increments in coronary flow reserve in healthy young men are not affected by dexamethasone pretreatment, local endothelium-dependent mechanisms (rather than central sympathetic activation) are thought normally to predominate [142]. However, although insulin-induced increments in coronary reserve are initially similar in young men with and without type 1 diabetes, the increments in diabetic patients can be abolished by dexamethasone pretreatment [142]. Central sympathetic activation therefore seems to play an important role in diabetes, possibly by augmenting adrenergic microvascular dilation to compensate for endothelial dysfunction. Studies of Di Carli et al. support this view [33]. Increases in coronary flow in partially reinnervated transplanted hearts during cold pressor testing were greater in regions of the left ventricle showing sympathetic reinnervation (as assessed with ^{11}C-hydroxyephedrine uptake) than in those remaining denervated. In addition, despite similar responses to intravenous adenosine, diabetic patients with autonomic dysfunction showed systematically smaller increases in coronary flow during cold pressor testing than diabetic patients without autonomic neuropathy [143].

Coronary vascular dysfunction can be demonstrated in the early stages of diabetes. Increases in coronary flow during cold pressor testing are blunted in insulin-resistant individuals without glucose intolerance, and the abnormality can be normalized by insulin-sensitizing thiazolidinedione therapy [144]. Abnormal responses to cold pressor testing also occur in approximately one-third of asymptomatic, non-insulin-treated type 2 diabetic patients [145]. As diabetes progresses and becomes evident clinically, abnormal responses to cold pressor testing and reductions in coronary flow reserve become present consistently [143,146–148]. Reduced hyperemic responses to adenosine can, at least in young otherwise healthy type I diabetics, be ameliorated by raising insulin levels to supraphysiologic levels (93 ± 27 mU/l) [149].

Mechanisms possibly underlying abnormal coronary vascular responses in diabetic patients continue to be explored. Miura et al. have demonstrated that K_{ATP} channel-mediated coronary arteriolar dilation is intrinsically impaired [150]. Nitenberg and colleagues report that abnormal responses to cold pressor testing and reductions in flow reserve can be ameliorated by inhibition of oxygen-derived free radical production [151,152]. Johansson et al. find that administration of proinsulin C-peptide, which is cleaved from proinsulin and released into the circulation in amounts equimolar with insulin, can restore reduced levels of adenosine-stimulated coronary flow to those of healthy controls while plasma insulin concentrations remain in the normal physiological range [153]. Hansen et al. have reported similarly beneficial effects of C-peptide using contrast echocardiographic indices of flow [154].

The possibility that occult coronary artery disease in diabetic patients played a role in some of the findings in this section cannot be excluded, particularly in studies of individuals undergoing diagnostic cardiac catheterization who proved to have arteriographically normal or "near normal" coronary arteries. Hemodynamically significant coronary stenoses would no doubt accentuate diabetes-related abnormalities in cold pressor testing and coronary flow reserve. It remains clear, however, that diabetics often have abnormal flow reserve in the absence of epicardial stenoses, probably secondary to endothelial dysfunction.

Lipid abnormalities

Schelbert has summarized several studies indicating systematic reductions in hyperemic flows (~25%) and coronary flow reserve in hypercholesterolemic and hypertriglyceridemic patients without clinically detectible coronary artery disease [54, Table 14]. Reductions in hyperemic flow and coronary reserve probably again reflect

endothelial dysfunction. Responses to cholesterol-lowering therapies indicate that these abnormalities are at least partially reversible [54, Table 15]. Leung and Lau have reported that acetylcholine-induced epicardial artery constriction in hypercholesterolemic patients with angiographically normal coronary arteries can also be reversed by cholesterol lowering [155].

Hypertension and ventricular hypertrophy

Endothelium-dependent coronary vasomotion is frequently abnormal in hypertensive patients. Constriction of conduit arteries to acetylcholine was identified in the early 1990s [156–159]. Coronary flow reserve was subsequently reported to be reduced in hypertensive patients without other coronary risk factors [106,160], and in asymptomatic young men with borderline hypertension and no signs of angina or left ventricular hypertrophy [161]. Microvascular abnormalities have been suggested to underlie anginal chest pain in hypertensive patients without left ventricular hypertrophy [162]. In part, reduced coronary flow reserve is related to increased resting flow levels in these patients; however, there is also a reduced vasomotion component.

When left ventricular hypertrophy becomes demonstrable in hypertensive individuals, coronary flow reserve is reduced consistently. Reductions averaging 33% were reported by Strauer as early as 1979 [163]. This finding was confirmed in the early 1980s [164,165], has been observed consistently in subsequent studies, and has been suggested to underlie angina pectoris in hypertensive patients with hypertrophied ventricles [165]. The degree of reduction in flow reserve in hypertensive disease varies directly with the magnitude of hypertrophy [166] and is greater in African-Americans than Caucasian-Americans [72]. Consistent with the reduction in reserve, Polese et al. have reported that the "breakpoint" pressure at which autoregulatory vasodilation is exhausted (see Fig. 1.4) is increased in hypertensive patients with left ventricular hypertrophy [167]. Experimental studies suggest that increases in coronary back pressure, i.e., "zero-flow pressure," also play a role in the reduced reserve of hypertrophied ventricles [168]. Reductions in reserve can, at least in some cases, involve structural as well as functional changes [169]. Although several groups have demonstrated treatment-induced regression of hypertrophy, information about changes in flow reserve is limited. Studies thus far indicate improvement [170–172].

Reductions in coronary flow reserve also occur regularly in ventricular hypertrophy caused by conditions other than essential hypertension. Early studies in humans with aortic stenosis and volume overload hypertrophy were performed by Marcus and colleagues [65,173,174]. Studies during the past two decades have addressed a number of additional abnormalities [175,176].

References

1. Klocke FJ, Ellis AK. Physiology of the coronary circulation. In Parmley WW, Chatterjee K, eds. Cardiology. Philadelphia: J.B. Lippincott Co.;1990:1–16;Chap. 7.
2. Nelson RR, Gobel FL, Jorgensen CR, Wang K, Wang Y, Taylor HL. Hemodynamic predictors of myocardial oxygen consumption during static and dynamic exercise. Circulation 1974;50:1179–1189.
3. Klocke FJ, Ellis AK. Control of coronary blood flow. In Creger WP, Coggins CH, Hancock EW, eds. Annual Review of Medicine: Selected Topics in the Clinical Sciences. Palo Alto: Annual Reviews, Inc., 1980:489–508.
4. Kitamura K, Jorgensen CR, Gobel FL, Taylor HL, Wang Y. Hemodynamic correlates of myocardial oxygen consumption during upright exercise. Journal of Applied Physiology 1972;32:516–522.
5. Jorgensen CR, Wang K, Wang Y, Gobel FL, Nelson RR, Taylor H. Effect of propranolol on myocardial oxygen consumption and its hemodynamic correlates during upright exercise. Circulation 1973;48:1173–1182.
6. Klocke FJ, Mates RE, Canty JM Jr, Ellis AK. Coronary pressure–flow relationships. Controversial issues and probable implications. Circulation Research 1985;56:310–323.
7. Satoh S, Klocke FJ, Canty JM Jr. Tone-dependent coronary arterial–venous pressure differences at the cessation of venous outflow during long diastoles. Circulation 1993;88: 1238–1244.
8. Marcus ML. The Coronary Circulation in Health and Disease. New York: McGraw-Hill; 1983: 17.
9. Quyyumi AA, Dakak N, Andrews NP, Gilligan DM, Panza JA, Cannon RO III. Contribution of nitric oxide to metabolic coronary vasodilation in the human heart. Circulation 1995;92:320–326.
10. Quyyumi AA, Dakak N, Andrews NP et al. Nitric oxide activity in the human coronary circulation. Impact of risk factors for coronary atherosclerosis. Journal of Clinical Investigation 1995;95:1747–1755.
11. Hintze TH, Vatner SF. Reactive dilation of large coronary arteries in conscious dogs. Circulation Research 1984;54:50–57.
12. Cox DA, Vita JA, Treasure CB, et al. Atherosclerosis impairs flow-mediated dilation of coronary arteries in humans. Circulation 1989;80:458–465.
13. Drexler H, Zeiher AM, Wollschlager H, Meinertz T, Just H, Bonzel T. Flow-dependent coronary artery dilatation in humans. Circulation 1989;80:466–474.
14. Canty JM Jr, Schwartz JS. Nitric oxide mediates flow-dependent epicardial coronary vasodilation to changes in pulse frequency but not mean flow in conscious dogs. Circulation 1994;89:375–384.
15. Heusch G, Baumgart D, Camici P, et al. Alpha-adrenergic coronary vasoconstriction and myocardial ischemia in humans. Circulation 2000;101:689–694.
16. Morita K, Mori H, Tsujioka K, et al. Alpha-adrenergic vasoconstriction reduces systolic retrograde coronary blood flow. American Journal of Physiology 1997;273:H2746–H2755.

17. Okajima M, Takamura M, Vequaud P, Parent R, Lavallee M. Beta-adrenergic receptor blockade impairs NO-dependent dilation of large coronary arteries during exercise. American Journal of Physiology 2003;284:H501–H510.
18. Chilian WM, Eastham CL, Marcus ML. Microvascular distribution of coronary vascular resistance in beating left ventricle. American Journal of Physiology 1986;251:779–788.
19. Komaru T, Lamping KG, Eastham CL, Dellsperger KC. Role of ATP-sensitive potassium channels in coronary microvascular autoregulatory responses. Circulation Research 1991;69:1146–1151.
20. Belardinelli L, Linden J, Berne RM. The cardiac effects of adenosine. Progress in Cardiovascular Diseases 1989;32:73–97.
21. Tune JD, Gorman MW, Feigl EO. Matching coronary blood flow to myocardial oxygen consumption. Journal of Applied Physiology 2004;97:404–415.
22. Farouque HM, Worthley SG, Meredith IT, Skyrme-Jones RA, Zhang MJ. Effect of ATP-sensitive potassium channel inhibition on resting coronary vascular responses in humans. Circulation Research 2002;90:231–236.
23. Miura H, Bosnjak JJ, Ning G, Saito T, Miura M, Gutterman DD. Role for hydrogen peroxide in flow-induced dilation of human coronary arterioles. Circulation Research 2003;92:e31–e40.
24. Farouque HM, Worthley SG, Meredith IT. Effect of ATP-sensitive potassium channel inhibition on coronary metabolic vasodilation in humans. Arteriosclerosis, Thrombosis and Vascular Biology 2004;24:905–910.
25. Davis CA III, Sherman AJ, Yaroshenko Y, et al. Coronary vascular responsiveness to adenosine is impaired additively by blockade of nitric oxide synthesis and a sulfonylurea. Journal of the American College of Cardiology 1998;31:816–822.
26. Kichuk MR, Seyedi N, Zhang X, et al. Regulation of nitric oxide production in human coronary microvessels and the contribution of local kinin formation. Circulation 1996;94:44–51.
27. Stepp DW, Nishikawa Y, Chilian WM. Regulation of shear stress in the canine coronary microcirculation. Circulation 1999;100:1555–1561.
28. Stepp DW, Merkus D, Nishikawa Y, Chilian WM. Nitric oxide limits coronary vasoconstriction by a shear stress-dependent mechanism. American Journal of Physiology 2001;281:H796–H803.
29. Miura H, Wachtel RE, Liu Y, et al. Flow-induced dilation of human coronary arterioles: important role of Ca(2+)-activated K(+) channels. Circulation 2001;103:1992–1998.
30. Indolfi C, Piscione F, Villari B, et al. Role of alpha 2-adrenoceptors in normal and atherosclerotic human coronary circulation. Circulation 1992;86:1116–1124.
31. Klocke FJ, Kaiser GA, Ross J Jr, Braunwald E. An intrinsic adrenergic vasodilator mechanism in the coronary vascular bed of the dog. Circulation Research 1965;16:376–382.
32. Sun D, Huang A, Mital S, et al. Norepinephrine elicits beta2-receptor-mediated dilation of isolated human coronary arterioles. Circulation 2002;106:550–555.
33. Di Carli MF, Tobes MC, Mangner T, et al. Effects of cardiac sympathetic innervation on coronary blood flow. New England Journal of Medicine 1997;336:1208–1215.
34. Tune JD, Richmond KN, Gorman MW, Feigl EO. Control of coronary blood flow during exercise. Experimental Biology and Medicine 2002;227:238–250.
35. Angus JA, Cocks TM, Satoh K. The alpha adrenoceptors on endothelial cells. Federation Proceedings 1986;45:2355–2359.
36. Feigl EO. Neural control of coronary blood flow. Journal of Vascular Research 1998;35:85–92.
37. Rouleau J, Boerboom LE, Surjadhana A, Hoffman JI. The role of autoregulation and tissue diastolic pressures in the transmural distribution of left ventricular blood flow in anesthetized dogs. Circulation Research 1979;45:804–815.
38. Aversano T, Klocke FJ, Mates RE, Canty JM Jr. Preload-induced alterations in capacitance-free diastolic pressure-flow relationship. American Journal of Physiology 1984;246:H410–H417.
39. Weiss HR, Sinha AK. Regional oxygen saturation of small arteries and veins in the canine myocardium. Circulation Research 1978;42:119–126.
40. Mirsky I. Left ventricular stresses in the intact human heart. Biophysical Journal 1969;9:189–208.
41. Yoran C, Covell JW, Ross J Jr. Structural basis for the ascending limb of left ventricular function. Circulation Research 1973;32:297–303.
42. Hoffman JIE, Buckberg GD. Transmural variations in myocardial perfusion. Progress in Cardiology 1976;5:37–89.
43. Chilian WM. Microvascular pressures and resistances in the left ventricular subepicardium and subendocardium. Circulation Research 1991;69:561–570.
44. Ellis AK, Klocke FJ. Effects of preload on the transmural distribution of perfusion and pressure–flow relationships in the canine coronary vascular bed. Circulation Research 1980;46:68–77.
45. Archie JP Jr. Minimum left ventricular coronary vascular resistance in dogs. Journal of Surgical Research 1978;25:21–25.
46. Canty JM Jr, Smith TP Jr. Adenosine-recruitable flow reserve is absent during myocardial ischemia in unanesthetized dogs studied in the basal state. Circulation Research 1995;76:1079–1087.
47. Nabel EG, Ganz P, Gordon JB, Alexander RW, Selwyn AP. Dilation of normal and constriction of atherosclerotic coronary arteries caused by the cold pressor test. Circulation 1988;77:43–52.
48. Zeiher AM, Drexler H, Wollschlager H, Just H. Modulation of coronary vasomotor tone in humans. Progressive endothelial dysfunction with different early stages of coronary atherosclerosis. Circulation 1991;83:391–401.
49. Prior JO, Quinones MJ, Hernandez-Pampaloni M, et al. Coronary circulatory dysfunction in insulin resistance, impaired glucose tolerance, and type 2 diabetes mellitus. Circulation 2005;111:2291–2298.
50. Ludmer PL, Selwyn AP, Shook TL, et al. Paradoxical vasoconstriction induced by acetylcholine in atherosclerotic

coronary arteries. New England Journal of Medicine 1986;315:1046–1051.
51. Canty JMJ. Coronary pressure-function and steady-state pressure–flow relations during autoregulation in the unanesthetized dog. Circulation Research 1988;63:821–836.
52. Canty JMJ, Giglia J, Kandath D. Effect of tachycardia on regional function and transmural myocardial perfusion during graded coronary pressure reduction in conscious dogs. Circulation 1990;82:1815–1825.
53. Czernin J, Muller P, Chan S, et al. Influence of age and hemodynamics on myocardial blood flow and flow reserve. Circulation 1993;88:62–69.
54. Schelbert HR. Positron emission tomography of the heart: methodology, findings in the normal and the diseased heart, and clinical applications. In Phelps ME, ed. PET Molecular Imaging and Its Biological Applications. New York: Springer-Verlag, 2004:389–508.
55. Bergmann SR. Cardiac positron emission tomography. Seminars in Nuclear Medicine 1998;28:320–340.
56. Gullberg GT, Huesman RH, DiBella EVR, Reutter BW. Dynamic cardiac single-photon emission computed tomography using fast data acquisition systems. In: Zaret BL, Beller, GA, eds. Clinical Nuclear Cardiology – State of the Art and Future Directions. 3rd edn. St. Louis: Mosby, Inc.; 2005:117–139;Chap. 8.
57. Chareonthaitawee P, Kaufmann PA, Rimoldi O, Camici PG. Heterogeneity of resting and hyperemic myocardial blood flow in healthy humans. Cardiovascular Research 2001;50:151–161.
58. King RB, Bassingthwaighte JB, Hales JR, Rowell LB. Stability of heterogeneity of myocardial blood flow in normal awake baboons. Circulation Research 1985;57:285–295.
59. Hoffman JIE. Heterogeneity of myocardial blood flow. Basic Research in Cardiology 1995;90:103–111.
60. Camici PG, Rimoldi OE. Myocardial blood flow in patients with hibernating myocardium. Cardiovascular Research 2003;57:302–311.
61. Schoder H, Silverman DH, Campisi R, et al. Regulation of myocardial blood flow response to mental stress in healthy individuals. American Journal of Physiology 2000;278: H360–H366.
62. Nagamachi S, Czernin J, Kim AS, et al. Reproducibility of measurements of regional resting and hyperemic myocardial blood flow assessed with PET. Journal of Nuclear Medicine 1996;37:1626–1631.
63. Duvernoy CS, Meyer C, Seifert-Klauss V, et al. Gender differences in myocardial blood flow dynamics: lipid profile and hemodynamic effects. Journal of the American College of Cardiology 1999;33:463–470.
64. Marcus M, Wright C, Doty D, et al. Measurements of coronary velocity and reactive hyperemia in the coronary circulation of humans. Circulation Research 1981;49:877–891.
65. Marcus ML, Doty DB, Hiratzka LF, Wright CB, Eastham CL. Decreased coronary reserve: a mechanism for angina pectoris in patients with aortic stenosis and normal coronary arteries. New England Journal of Medicine 1982;307:1362–1366.
66. Udelson JE, Heller GV, Wackers FJ, et al. Randomized, controlled dose-ranging study of the selective adenosine A2A receptor agonist binodenoson for pharmacological stress as an adjunct to myocardial perfusion imaging. Circulation 2004;109:457–464.
67. Buus NH, Bottcher M, Hermansen F, Sander M, Nielsen TT, Mulvany MJ. Influence of nitric oxide synthase and adrenergic inhibition on adenosine-induced myocardial hyperemia. Circulation 2001;104:2305–2310.
68. McGinn AL, White CW, Wilson RF. Interstudy variability of coronary flow reserve. Influence of heart rate, arterial pressure, and ventricular preload. Circulation 1990;81:1319–1330.
69. Rossen JD, Winniford MD. Effect of increases in heart rate and arterial pressure on coronary flow reserve in humans. Journal of the American College of Cardiology 1993;21:343–348.
70. Wilson RF, Laughlin DE, Ackell PH, et al. Transluminal, subselective measurement of coronary artery blood flow velocity and vasodilator reserve in man. Circulation 1985;72:82–92.
71. Kern MJ, Bach RG, Mechem CJ, et al. Variations in normal coronary vasodilatory reserve stratified by artery, gender, heart transplantation and coronary artery disease. Journal of the American College of Cardiology 1996;28:1154–1160.
72. Houghton JL, Prisant LM, Carr AA, Flowers NC, Frank MJ. Racial differences in myocardial ischemia and coronary flow reserve in hypertension. Journal of the American College of Cardiology 1994;23:1123–1129.
73. Austin RE Jr, Aldea GS, Coggins DL, Flynn AE, Hoffman JI. Profound spatial heterogeneity of coronary reserve. Discordance between patterns of resting and maximal myocardial blood flow. Circulation Research 1990;67:319–331.
74. Saltin B, Blomqvist G, Mitchell JH, Johnson RL, Wildenthal K, Chapman CB. Response to exercise after bed rest and after training. Circulation (Supplements) 1968;38:VII-1–VII-78.
75. Wyatt HL, Mitchell J. Influences of physical conditioning and deconditioning on coronary vasculature of dogs. Journal of Applied Physiology 1978;45:619–625.
76. Wyatt HL, Mitchell, JH. Influences of physical training on the heart of dogs. Journal of Applied Physiology 1974;45:883–889.
77. Beller GA. Relative merits of cardiovascular diagnostic techniques. In Braunwald E, Zipes DP, Libby P, eds. Heart Disease: A Textbook of Cardiovascular Medicine. 6th edn. Philadelphia: W.B. Saunders; 2001:422–442.
78. Mulhern KM, Skorton DJ. Clinical measurement of regional and global function in the normal and abnormal heart. In Germano G, Berman DS, eds. Clinical Gated Cardiac SPECT. 1st edn. Armonk, NY: Futura Publishing Co.; 1999:73–92.
79. Cerqueira MD, Weissman NJ, Dilsizian V, et al. Standardized myocardial segmentation and nomenclature for tomographic imaging of the heart: a statement for healthcare professionals from the Cardiac Imaging Committee of the Council on Clinical Cardiology of the American Heart Association. Circulation 2002;105:539–542.
80. Sheehan FH, Bolson EL, Dodge HT, Mathey DG, Schofer J, Woo HW. Advantages and applications of the centerline

method for characterizing regional ventricular function. Circulation 1986;74:293–305.
81. Force T, Parisi A. Quantitative methods for analyzing regional systolic function with two-dimensional echocardiography. In Kerber RE, ed. Echocardiography in Coronary Artery Disease. Mt. Kisco, NY: Futura Publishing Co.; 1988:193–219.
82. Gaudron P, Eilles C, Kugler I, Ertl G. Progressive left ventricular dysfunction and remodeling after myocardial infarction. Potential mechanisms and early predictors. Circulation 1993;87:755–763.
83. Kim RJ, Fieno DS, Parrish TB, et al. Relationship of MRI delayed contrast enhancement to irreversible injury, infarct age, and contractile function. Circulation 1999;100:1992–2002.
84. Wu E, Judd RM, Vargas JD, Klocke FJ, Bonow RO, Kim RJ. Visualisation of presence, location, and transmural extent of healed Q-wave and non-Q-wave myocardial infarction. Lancet 2001;357:21–28.
85. Wu KC, Zerhouni EA, Judd RM, Lugo-Olivieri CH, Barouch LA, Schulman SP, Blumenthal RS, Lima, JAC. Prognostic significance of microvascular obstruction by magnetic resonance imaging in patients with acute myocardial infarction. Circulation 1998;97:765–772.
86. Rogers WJ, Kramer CM, Geskin G, et al. Early contrast-enhanced MRI predicts late functional recovery after reperfused myocardial infarction. Circulation 1999;99:744–750.
87. Wu E, Tejedor P, Lee DC, et al. No reflow detected by delayed contrast enhancement predicts ventricular remodeling following an ST-segment elevation myocardial infarction. Circulation 2004;110:III-444.
88. Wagner A, Mahrholdt H, Holly TA, et al. Contrast-enhanced MRI and routine single photon emission computed tomography (SPECT) perfusion imaging for detection of subendocardial myocardial infarcts: an imaging study. Lancet 2003;361:374–379.
89. Fieno DS, Hillenbrand HB, Rehwald WG, et al. Infarct resorption, compensatory hypertrophy, and differing patterns of ventricular remodeling following myocardial infarctions of varying size. Journal of the American College of Cardiology 2004;43:2124–2131.
90. Gould KL, Lipscomb K, Hamilton GW. Physiologic basis for assessing critical coronary stenosis. American Journal of Cardiology 1974;33:87–94.
91. Gould KL. Pressure–flow characteristics of coronary stenoses in unsedated dogs at rest and during coronary vasodilation. Circulation Research 1978;43:242–253.
92. Gould KL. Dynamic coronary stenosis. American Journal of Cardiology 1980;45:286–292.
93. Klocke FJ. Clinical and experimental evaluation of the functional severity of coronary stenoses. Newsletter of the Council on Clinical Cardiology, American Heart Association 1982;7:1–9.
94. Klocke FJ. Cognition in the era of technology: "seeing the shades of gray." Journal of the American College of Cardiology 1990;16:763–769.
95. Julius BK, Vassalli G, Mandinov L, Hess OM. Alpha-adrenoceptor blockade prevents exercise-induced vasoconstriction of stenotic coronary arteries. Journal of the American College of Cardiology 1999;33:1499–1505.
96. Stiel GM, Stiel LSG, Schofer J, Donath K, Mathey DG. Impact of compensatory enlargement of atherosclerotic coronary arteries on angiographic assessment of coronary artery disease. Circulation 1989;80:1603–1609.
97. Pijls NH, van Son JA, Kirkeeide RL, De Bruyne B, Gould KL. Experimental basis of determining maximum coronary, myocardial, and collateral blood flow by pressure measurements for assessing functional stenosis severity before and after percutaneous transluminal coronary angioplasty. Circulation 1993;86:1354–1367.
98. Gould KL. Coronary artery stenosis. New York: Elsevier; 1990.
99. De Bruyne B, Baudhuin T, Melin JA, et al. Coronary flow reserve calculated from pressure measurements in humans. Validation with positron emission tomography. Circulation 1994;89:1013–1022.
100. Pijls NH, De Bruyne B, Peels K, et al. Measurement of fractional flow reserve to assess the functional severity of coronary-artery stenoses. New England Journal of Medicine 1996;334:1703–1708.
101. De Bruyne B, Bartunek J, Sys SU, Pijls NH, Heyndrickx GR, Wijns W. Simultaneous coronary pressure and flow velocity measurements in humans. Feasibility, reproducibility, and hemodynamic dependence of coronary flow velocity reserve, hyperemic flow versus pressure slope index, and fractional flow reserve. Circulation 1996;94:1842–1849.
102. Pijls NH, De Bruyne B, Bech GJ, et al. Coronary pressure measurement to assess the hemodynamic significance of serial stenoses within one coronary artery: validation in humans. Circulation 2000;102:2371–2377.
103. De Bruyne B, Hersbach F, Pijls NH, et al. Abnormal epicardial coronary resistance in patients with diffuse atherosclerosis but "normal" coronary angiography. Circulation 2001;104:2401–2406.
104. Pijls NH. Is it time to measure fractional flow reserve in all patients? Journal of the American College of Cardiology 2003;41:1122–1124.
105. Mudge GH Jr, Grossman W, Mills RM Jr, Lesch M, Braunwald E. Reflex increase in coronary vascular resistance in patients with ischemic heart disease. New England Journal of Medicine 1976;295:1333–1337.
106. Zeiher AM, Drexler H, Saurbier B, Just H. Endothelium-mediated coronary blood flow modulation in humans. Effects of age, atherosclerosis, hypercholesterolemia, and hypertension. Journal of Clinical Investigation 1993;92:652–662.
107. Schwarz F, Flameng W, Ensslen R, Sesto M, Thormann J. Effect of coronary collaterals on left ventricular function at rest and during stress. American Heart Journal 1978;95:570–577.
108. Billinger M, Kloos P, Eberli FR, Windecker S, Meier B, Seiler C. Physiologically assessed coronary collateral flow and adverse cardiac ischemic events: a follow-up study in 403 patients with coronary artery disease. Journal of the American College of Cardiology 2002;40:1545–1550.

109. Hochberg I, Roguin A, Nikolsky E, Chanderashekhar PV, Cohen S, Levy AP. Haptoglobin phenotype and coronary artery collaterals in diabetic patients. Atherosclerosis 2002;161:441–446.
110. Schultz A, Lavie L, Hochberg I, et al. Interindividual heterogeneity in the hypoxic regulation of VEGF: significance for the development of the coronary artery collateral circulation. Circulation 1999;100:547–552.
111. Buschmann I, Schaper W. The pathophysiology of the collateral circulation (arteriogenesis). Journal of Pathology 2000;190:338–342.
112. Schaper W, Sharma HS, Quinkler W, Markert T, Wunsch M, Schaper J. Molecular biologic concepts of coronary anastomoses. Journal of the American College of Cardiology 1990;15:513–518.
113. White FC, Carroll SM, Magnet A, Bloor CM. Coronary collateral development in swine after coronary artery occlusion. Circulation Research 1992;71:1490–1500.
114. Altman J, Dulas D, Pavek T, Laxson DD, Homans DC, Bache RJ. Endothelial function in well-developed canine coronary collateral vessels. American Journal of Physiology 1993;264:H567–H572.
115. Dulas D, Altman JD, Hirata-Dulas C, Bache RJ. Endothelium-dependent vasodilation in well-developed coronary collateral vessels. Journal of Cardiovascular Pharmacology 1996;28:488–493.
116. Frank MW, Harris KR, Ahlin KA, Klocke FJ. Endothelium-derived relaxing factor (nitric oxide) has a tonic vasodilating action on coronary collateral vessels. Journal of the American College of Cardiology 1996;27:658–663.
117. Altman J, Dulas D, Bache RJ. Effect of cyclooxygenase blockade on blood flow through well-developed coronary collateral vessels. Circulation Research 1992;70:1091–1098.
118. Altman JD, Dulas D, Pavek T, Bache RJ. Effect of aspirin on coronary collateral blood flow. Circulation 1993;87:583–589.
119. Pijls NH, Bech GJ, el Gamal MI, et al. Quantification of recruitable coronary collateral blood flow in conscious humans and its potential to predict future ischemic events. Journal of the American College of Cardiology 1995;25:1522–1528.
120. Heusch G, Schulz R. Hibernating myocardium. Circulation Research 2002;91:863–865.
121. Seiler C, Fleisch M, Garachemani A, Meier B. Coronary collateral quantitation in patients with coronary artery disease using intravascular flow velocity or pressure measurements. Journal of the American College of Cardiology 1998;32:1272–1279.
122. Pohl T, Seiler C, Billinger M, et al. Frequency distribution of collateral flow and factors influencing collateral channel development. Functional collateral channel measurement in 450 patients with coronary artery disease. Journal of the American College of Cardiology 2001;38:1872–1878.
123. Heusch G, Schulz R. Perfusion-contraction match and mismatch. Basic Research in Cardiology 2001;96:1–10.
124. Leppo JA, Meerdink DJ. Comparison of the myocardial uptake of a technetium-labeled isonitrile analogue and thallium. Circulation Research 1989;65:632–639.
125. Glover DK, Ruiz M, Edwards NC, et al. Comparison between 201Tl and 99mTc sestamibi uptake during adenosine-induced vasodilation as a function of coronary stenosis severity. Circulation 1995;91:813–820.
126. Lee DC, Simonetti OP, Harris KA, et al. Magnetic resonance versus radionuclide pharmacological stress perfusion imaging for flow-limiting stenoses of varying severity. Circulation 2004;110:58–65.
127. Winniford MD. Smoking and cardiovascular function. Journal of Hypertension 1990;8:S17–S23.
128. Czernin J, Sun K, Brunken R, Bottcher M, Phelps M, Schelbert H. Effect of acute and long-term smoking on myocardial blood flow and flow reserve. Circulation 1995;91:2891–2897.
129. Campisi R, Czernin J, Schoder H, et al. Effects of long-term smoking on myocardial blood flow, coronary vasomotion, and vasodilator capacity. Circulation 1998;98:119–125.
130. Campisi R, Czernin J, Schoder H, Sayre JW, Schelbert HR. L-Arginine normalizes coronary vasomotion in long-term smokers. Circulation 1999;99:491–497.
131. Iwado Y, Yoshinaga K, Furuyama H, et al. Decreased endothelium-dependent coronary vasomotion in healthy young smokers. European Journal of Nuclear Medicine and Molecular Imaging 2002;29:984–990.
132. Nicod P, Rehr R, Winniford MD, Campbell WB, Firth BG, Hillis LD. Acute systemic and coronary hemodynamic and serologic responses to cigarette smoking in long-term smokers with atherosclerotic coronary artery disease. Journal of the American College of Cardiology 1984;4:964–971.
133. Klein LW, Ambrose J, Pichard A, Holt J, Gorlin R, Teichholz LE. Acute coronary hemodynamic response to cigarette smoking in patients with coronary artery disease. Journal of the American College of Cardiology 1984;3:879–886.
134. Deanfield JE, Shea MJ, Wilson RA, Horlock P, de Landsheere CM, Selwyn AP. Direct effects of smoking on the heart: silent ischemic disturbances of coronary flow. American Journal of Cardiology 1986;57:1005–1009.
135. Winniford MD, Wheelan KR, Kremers MS, et al. Smoking-induced coronary vasoconstriction in patients with atherosclerotic coronary artery disease: evidence for adrenergically mediated alterations in coronary artery tone. Circulation 1986;73:662–667.
136. Quillen JE, Rossen JD, Oskarsson HJ, Minor RL Jr, Lopez AG, Winniford MD. Acute effect of cigarette smoking on the coronary circulation: constriction of epicardial and resistance vessels [see comment]. Journal of the American College of Cardiology 1993;22:642–647.
137. Zeiher AM, Schachinger V, Minners J. Long-term cigarette smoking impairs endothelium-dependent coronary arterial vasodilator function. Circulation 1995;92:1094–1100.
138. Winniford MD, Jansen DE, Reynolds GA, Apprill P, Black WH, Hillis LD. Cigarette smoking-induced coronary vasoconstriction in atherosclerotic coronary artery disease and prevention by calcium antagonists and nitroglycerin. American Journal of Cardiology 1987;59:203–207.
139. Iozzo P, Chareonthaitawee P, Di Terlizzi M, Betteridge DJ, Ferrannini E, Camici PG. Regional myocardial blood flow and glucose utilization during fasting and physiological hyperinsulinemia in humans. American Journal of

Physiology – Endocrinology and Metabolism 2002;282: E1163–E1171.
140. McNulty PH, Pfau S, Deckelbaum LI. Effect of plasma insulin level on myocardial blood flow and its mechanism of action. American Journal of Cardiology 2000;85:161–165.
141. Sundell J, Nuutila P, Laine H, et al. Dose-dependent vasodilating effects of insulin on adenosine-stimulated myocardial blood flow. Diabetes 2002;51:1125–1130.
142. Laine H, Nuutila P, Luotolahti M, et al. Insulin-induced increment of coronary flow reserve is not abolished by dexamethasone in healthy young men. Journal of Clinical Endocrinology and Metabolism 2000;85:1868–1873.
143. Di Carli MF, Bianco-Batlles D, Landa ME, et al. Effects of autonomic neuropathy on coronary blood flow in patients with diabetes mellitus. Circulation 1999;100:813–819.
144. Quinones MJ, Hernandez-Pampaloni M, Schelbert H, et al. Coronary vasomotor abnormalities in insulin-resistant individuals. Annals of Internal Medicine 2004;140:700–708.
145. Momose M, Abletshauser C, Neverve J, et al. Dysregulation of coronary microvascular reactivity in asymptomatic patients with type 2 diabetes mellitus. European Journal of Nuclear Medicine and Molecular Imaging 2002;29:1675–1679.
146. Nitenberg A, Valensi P, Sachs R, Dali M, Aptecar E, Attali JR. Impairment of coronary vascular reserve and ACh-induced coronary vasodilation in diabetic patients with angiographically normal coronary arteries and normal left ventricular systolic function. Diabetes 1993;42:1017–1025.
147. Nahser PJ Jr, Brown RE, Oskarsson H, Winniford MD, Rossen JD. Maximal coronary flow reserve and metabolic coronary vasodilation in patients with diabetes mellitus. Circulation 1995;91:635–640.
148. Nitenberg A, Ledoux S, Valensi P, Sachs R, Attali JR, Antony I. Impairment of coronary microvascular dilation in response to cold pressor-induced sympathetic stimulation in type 2 diabetic patients with abnormal stress thallium imaging. Diabetes 2001;50:1180–1185.
149. Sundell J, Laine H, Nuutila P, et al. The effects of insulin and short-term hyperglycaemia on myocardial blood flow in young men with uncomplicated Type I diabetes. Diabetologia 2002;45:775–782.
150. Miura H, Wachtel RE, Loberiza FR Jr. Diabetes mellitus impairs vasodilation to hypoxia in human coronary arterioles: reduced activity of ATP-sensitive potassium channels. Circulation Research 2003;92:151–158.
151. Nitenberg A, Paycha F, Ledoux S, Sachs R, Attali JR, Valensi P. Coronary artery responses to physiological stimuli are improved by deferoxamine but not by L-arginine in non-insulin-dependent diabetic patients with angiographically normal coronary arteries and no other risk factors. Circulation 1998;97:736–743.
152. Nitenberg A, Ledoux S, Valensi P, Sachs R, Antony I. Coronary microvascular adaptation to myocardial metabolic demand can be restored by inhibition of iron-catalyzed formation of oxygen free radicals in type 2 diabetic patients. Diabetes 2002;51:813–818.
153. Johansson BL, Sundell J, Ekberg K, et al. C-peptide improves adenosine-induced myocardial vasodilation in type 1 diabetes patients. American Journal of Physiology 2004;286:E14–E19.
154. Hansen A, Johansson BL, Wahren J, von Bibra H. C-peptide exerts beneficial effects on myocardial blood flow and function in patients with type 1 diabetes. Diabetes 2002;51:3077–3082.
155. Leung W-H, Lau C-P. Beneficial effect of cholesterol-lowering therapy on coronary endothelium-dependent relaxation in hypercholesterolaemic patients. Lancet 1993;341: 1496–1500.
156. Brush JE Jr, Faxon DP, Salmon S, Jacobs AK, Ryan TJ. Abnormal endothelium-dependent coronary vasomotion in hypertensive patients [see comment]. Journal of the American College of Cardiology 1992;19:809–815.
157. Treasure CB, Klein JL, Vita JA, et al. Hypertension and left ventricular hypertrophy are associated with impaired endothelium-mediated relaxation in human coronary resistance vessels. Circulation 1993;87:86–93.
158. Antony I, Lerebours G, Nitenberg A. Loss of flow-dependent coronary artery dilatation in patients with hypertension. Circulation 1995;91:1624–1628.
159. Egashira K, Suzuki S, Hirooka Y, et al. Impaired endothelium-dependent vasodilation of large epicardial and resistance coronary arteries in patients with essential hypertension. Different responses to acetylcholine and substance P. Hypertension 1995;25:201–206.
160. Antony I, Nitenberg A. Coronary vascular reserve is similarly reduced in hypertensive patients without any other coronary risk factors and in normotensive smokers and hypercholesterolemic patients with angiographically normal coronary arteries. American Journal of Hypertension 1997;10:181–188.
161. Laine H, Raitakari OT, Niinikoski H, et al. Early impairment of coronary flow reserve in young men with borderline hypertension. Journal of the American College of Cardiology 1998;32:147–153.
162. Brush J Jr, Cannon RO III, Schenke WH, et al. Angina due to coronary microvascular disease in hypertensive patients without left ventricular hypertrophy. New England Journal of Medicine 1988;319:1302–1307.
163. Strauer BE. Ventricular function and coronary hemodynamics in hypertensive heart disease. American Journal of Cardiology 1979;44:999–1006.
164. Pichard AD, Gorlin R, Smith H, Ambrose J, Meller J. Coronary flow studies in patients with left ventricular hypertrophy of the hypertensive type. Evidence for an impaired coronary vascular reserve. American Journal of Cardiology 1981;47:547–554.
165. Opherk D, Mall G, Zebe H, et al. Reduction of coronary reserve: a mechanism for angina pectoris in patients with arterial hypertension and normal coronary arteries. Circulation 1984;69:1–7.
166. Kozakova M, de Simone G, Morizzo C, Palombo C. Coronary vasodilator capacity and hypertension-induced increase in left ventricular mass. Hypertension 2003;41:224–229.

167. Polese A, De Cesare N, Montorsi P, et al. Upward shift of the lower range of coronary flow autoregulation in hypertensive patients with hypertrophy of the left ventricle. Circulation 1991;83:845–853.
168. Duncker DJ, Zhang J, Bache RJ. Coronary pressure–flow relation in left ventricular hypertrophy. Importance of changes in back pressure versus changes in minimum resistance. Circulation Research 1993;72:579–587.
169. Schwartzkopff B, Motz W, Frenzel H, Vogt M, Knauer S, Strauer BE. Structural and functional alterations of the intramyocardial coronary arterioles in patients with arterial hypertension. Circulation 1993;88:993–1003.
170. Motz W, Strauer BE. Improvement of coronary flow reserve after long-term therapy with enalapril. Hypertension 1996;27:1031–1038.
171. Parodi O, Neglia D, Palombo C, et al. Comparative effects of enalapril and verapamil on myocardial blood flow in systemic hypertension. Circulation 1997;96:864–873.
172. Akinboboye OO, Chou RL, Bergmann SR. Augmentation of myocardial blood flow in hypertensive heart disease by angiotensin antagonists: a comparison of lisinopril and losartan. Journal of the American College of Cardiology 2002;40:703–709.
173. Doty DB, Eastham CL, Hiratzka LF, Wright CB, Marcus ML. Determination of coronary reserve in patients with supravalvular aortic stenosis. Circulation 1982;66:1186–1192.
174. Marcus ML, Harrison DG, Chilian WM, et al. Alterations in the coronary circulation in hypertrophied ventricles. Circulation 1987:I19–I25.
175. Choudhury L, Rosen SD, Patel D, Nihoyannopoulos P, Camici PG. Coronary vasodilator reserve in primary and secondary left ventricular hypertrophy. A study with positron emission tomography. European Heart Journal 1997;18:108–116.
176. Camici PG. Coronary vasodilator reserve in left ventricular hypertrophy. Italian Heart Journal 2001;2:20S–22S.

2 Physics and technical aspects of gated myocardial perfusion SPECT

Guido Germano
Daniel S. Berman

Introduction

Gated myocardial perfusion SPECT has been extensively validated for its ability to provide objective information regarding rest and stress myocardial perfusion and rest and poststress left ventricular function. It has become part of mainstream clinical practice and is predominantly used for the evaluation of patients with known or suspected coronary artery disease. While the final results can be objectively analyzed, their accuracy depends on the technical quality of the study. Furthermore, interpretation of myocardial perfusion SPECT requires an understanding of the physics and technical aspects of the procedure. While planar imaging currently accounts for less than 10% of all nuclear cardiology studies in the United States, planar or projection images still constitute the foundation on which SPECT is built. Figure 2.1 briefly outlines how a projection image is generated by a single-detector gamma camera (also referred to as Anger camera in honor of its inventor, Hal Anger). In this example, a ^{99m}Tc-based radiopharmaceutical is injected into a patient, taken up by his or her myocardial muscle, and radioactivity is emitted in the form of photons (gamma rays) having energy of 140 keV. Some of those photons impinge on a scintillation detector positioned with its plane parallel to the patient's long axis, the "allowed" angle of impact being constrained to be reasonably close to 90° through the use of a collimator. The scintillation detector is made of high-density material such as thallium-activated sodium iodide or NaI(Tl); when radiation penetrates it, energy is dissipated by conversion into light photons, which are in turn converted into electrons and amplified into an electrical current by a set of photomultiplier tubes (PMTs) directly coupled to the scintillating crystal. The current is proportional to the amount of energy dissipated in the detector, which ideally should be equal to that of the original gamma ray, but is considered acceptable if it lies within a 15–20% window about the expected 140 keV value. For each "hit" by a photon, the point of impact (X, Y) on the detector is derived by analysis of the fraction of light photons collected by different PMTs – if the associated energy Z is within the window, energy discrimination circuitry generates a signal that allows the "event" to be accumulated into a computer matrix or "projection image."

The gated SPECT acquisition

In a SPECT acquisition, the camera detector(s) rotates around the long axis of the patient, acquiring one projection image at each of many, evenly spaced angular locations (steps) along the acquisition orbit. If the acquisition is gated, several (8 or 16) projection images are acquired at each projection angle, with each image corresponding to a specific portion of the cardiac cycle termed "interval" or "frame" (Fig. 2.2). All projection images for a given interval can be reconstructed/reoriented into a SPECT or tomographic image volume using filtered backprojection or iterative reconstruction techniques, and volumes relative to the various gated SPECT intervals can be displayed in four-dimensional format (x, y, z, and time), allowing for the assessment of dynamic cardiac function. In addition, summing all individual intervals' projections at each angle before reconstruction produces an "ungated" or "summed gated" SPECT image volume, from which perfusion can be assessed. Thus, one can think of a gated SPECT acquisition as yielding both a standard SPECT data set and a larger gated SPECT data set, as will be discussed in detail later in this chapter. The strong appeal of gated SPECT imaging is a direct consequence of the ease and modest expense with which perfusion assessment is "upgraded" to perfusion + function assessment, and accounts for the phenomenal growth of the technique over the past decade (Fig. 2.3).

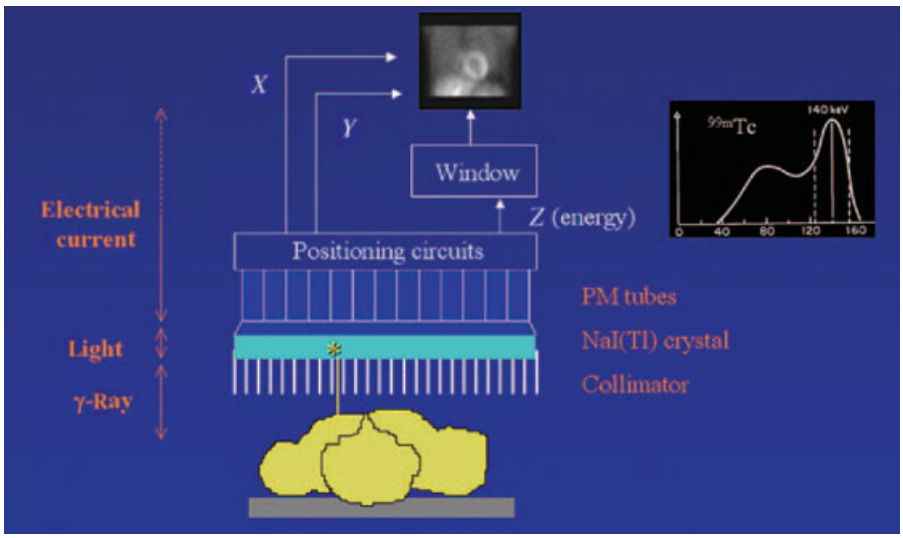

Figure 2.1 Basic functioning of the gamma or Anger camera, on which SPECT imaging is based. *, scintillation with the sodium-iodide crystal. The diagram in the upper left illustrates the energy spectrum of technesium 99m (^{99m}Tc). The dashed vertical lines indicate the 20% energy window surrounding the 140 keV primary photopeak of ^{99m}Tc. Abbreviation: PM, photomultiplier.

Gating choices

The gating of a SPECT acquisition is easily implemented using the QRS complex of the ECG signal, since its principal peak (R wave) corresponds to end-diastole. The gating hardware interfaces with the acquisition computer that controls the gantry, and data corresponding to each frame is automatically sorted by the camera into the appropriate image matrix. For example, counts collected during the nth interval from the occurrence of each R wave trigger (Fig. 2.4) while the detector is at the same projection angle ϑ are assigned to the same image (frame n, angle ϑ). In an ideal world, every cardiac beat would have the same duration, constant during the gated SPECT acquisition, and each of the 8 or 16 gating intervals could be preset to span 1/8 or 1/16 of that cardiac beat duration. The fact that this situation is virtually never verified leads to the need to introduce additional nomenclature and distinguish between multiple gating approaches, some of which are differently implemented on different camera systems.

Fixed temporal resolution gating

In the fixed temporal (FT) resolution gating approach [1–3], all gated SPECT intervals have the same length, and that length is fixed regardless of the actual duration of the cardiac cycle. Let us assume, for ease of argument, that a FT acquisition utilizes eight frames of 100 ms each, and that framing starts immediately upon detection of each R wave ("forward gating"). While an 800 ms distance between consecutive R waves (a 75 bpm heart rate) may have been measured for a patient at the inception of the gated acquisition, it is unreasonable to expect that

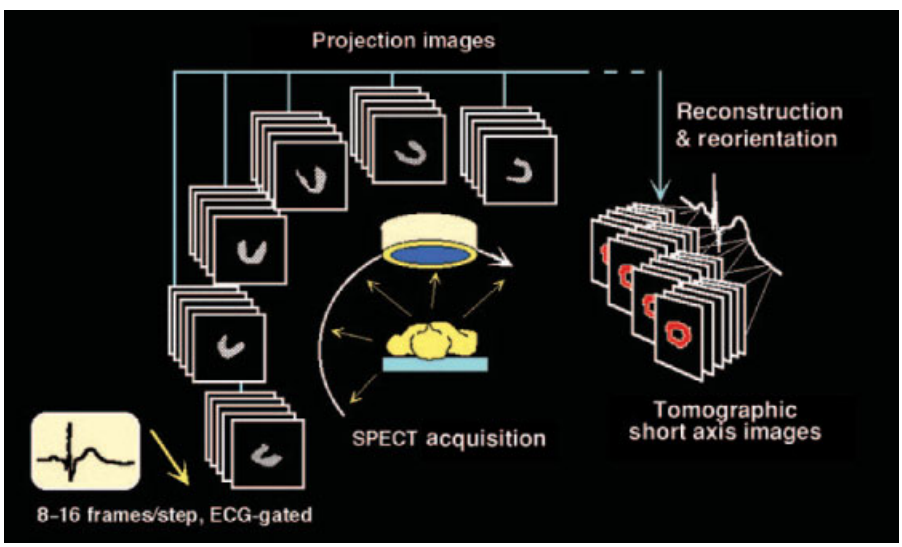

Figure 2.2 Schematic representation of ECG-gated perfusion SPECT acquisition and processing.

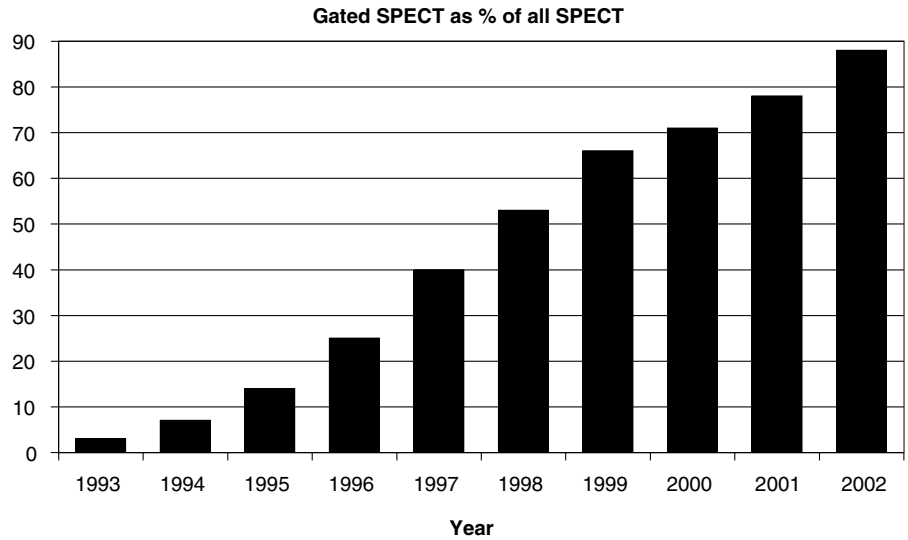

Figure 2.3 Growth in the percentage of all perfusion SPECT studies acquired in the USA using the ECG-gated technique. (Courtesy of IMV Medical Information Division, Des Plaines, IL.)

rate to be perfectly stable during the entire study. In actuality, when the time between two consecutive R-wave triggers is longer than 800 ms (the heart rate is lower than 75 bpm), all incoming data after the first 800 ms would be discarded (Fig. 2.5a). Conversely, when the time between two consecutive R-wave triggers is shorter than 800 ms (the heart rate is higher than 75 bpm), the last frame(s) would not accumulate data (Fig. 2.6a). In order to allow the FT method to adequately sample the end-diastolic phase of "long" cardiac beats, a "backward gating" technique has been developed. In this approach, the gating intervals are synchronizedfrom the R-wave backward (Fig. 2.5b), and applied to the latest heartbeat's data stored in a memory buffer. As backward gating could cause undersampling of the systolic phase of the cardiac cycle, a combination of forward and backward gating is often used (Fig. 2.5c) [5].

Variable temporal resolution gating

In the "variable temporal" (VT) resolution gating approach, all gated SPECT intervals still have the same length, but that length is dynamically adjusted to ensure full and complete coverage of the latest heart cycle(s), as defined by the R–R duration (Figs. 2.5d and 2.6b). The VT method is computationally more intensive than the FT method, requiring the alteration of the intervals' length on a beat-by-beat or angle-by-angle basis [2,6], but current camera systems can readily accomplish this task. The difference between VT and FT is truly conceptual in nature. Given that the goal of gating consists in summing counts from the same portion of the cardiac cycle, the FT approach bases its assessment of systolic function on the physiologic observation that a longer (shorter) beat is due solely to the lengthening (shortening) of its end-diastolic phase. Conversely, the VT approach's underlying assumption is that alterations in the cardiac rhythm uniformly stretch or compress the cardiac cycle as a whole.

List mode acquisition

A sophisticated approach to the problem of nonconstancy of the R–R interval in gated studies is the "(temporal) list mode" acquisition technique [7–9]. In list mode, each individual count is stored in a memory bin, which contains information on the count's location in the *XY* detector plane and on the exact time of its arrival (as determined by the camera's internal clock) relative to the ECG signal. When the acquisition is complete, the cardiac cycle lengths

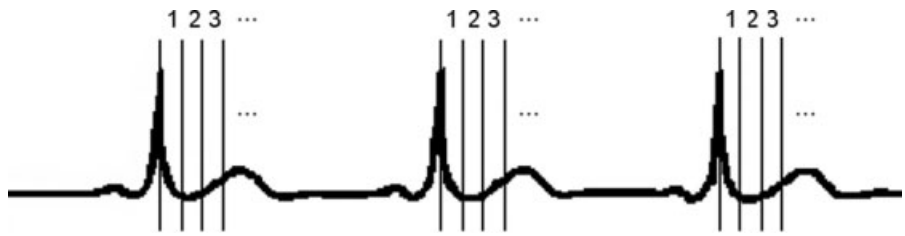

Figure 2.4 ECG gating. Each cardiac beat (defined by two successive R-wave peaks) is divided into a number of temporal intervals or gating frames. Data collected during homologous frames in different beats are summed together, as they refer to the same phase of the cardiac cycle.

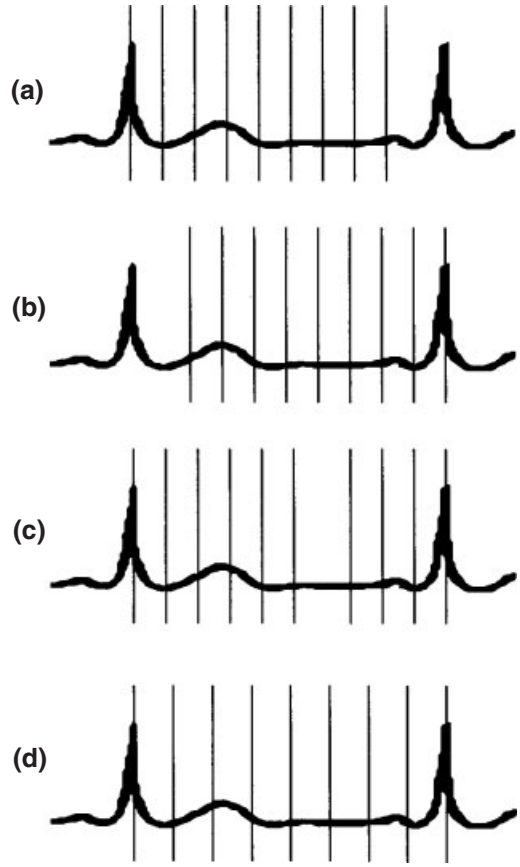

Figure 2.5 Examples of an 8-interval, fixed temporal (a) forward-framed, (b) backward-framed, and (c) forward/backward-framed (two-third of the intervals forward-framed, one-third backward-framed) acquisition, as well as (d) an 8-interval, variable temporal acquisition, all for a cardiac beat of longer than average duration. (Reproduced with permission from [4].)

(R–R durations) can be histogrammed, an acceptance window selected which straddles the histogram's peak, and events occurring during cycles of acceptable length sorted into frames based on the FT resolution or VT resolution method of choice. It is obvious that list mode acquisition requires substantially more memory and more postacquisition processing than standard acquisition. For instance, 200,000 counts accumulated in a projection image in frame mode would occupy $(64)^2 = 4096$ memory locations if a 64×64 pixel^2 matrix is used, as opposed to 200,000 memory locations in temporal list mode. Moreover, the individual memory location in list mode would have to be more expansive, as it must contain the additional timing information. To obviate memory and processing problems, it has been proposed that the processing of list mode data should occur concurrently with its acquisition, i.e., in real time [10]. Nevertheless, we consider it unlikely that list mode acquisition will be widely used in clinical gated SPECT in the future.

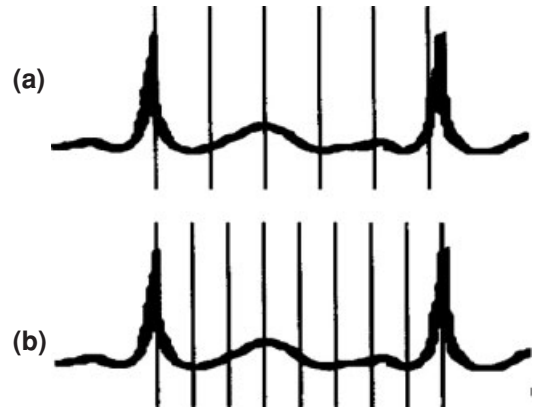

Figure 2.6 Examples of (a) an 8-interval, fixed temporal forward-framed, and (b) an 8-interval, variable temporal acquisition, both for a cardiac beat of shorter than average duration.

The beat length acceptance window

The unavoidable variability of the cardiac beat length during gated acquisitions has led to the building of tolerances in the gating process. The beat length acceptance window aims at eliminating data from beats that are "too short" or "too long," while still accepting a sensible number of them, and it can be seen as analogous to the energy acceptance window that is positioned on the radioisotope's photopeak prior to acquisition (NB: "length" and "duration" are used interchangeably in this section). Let us assume that the expected cardiac beat length, as set in the FT or VT protocol, is 1 s (heart rate = 60 bpm): a beat length acceptance window of 20% will then allow accumulation of data from cardiac beats having a duration within ±10% of the expected duration (in our case, within a 900–1100 ms range). An acceptance window of 100%, somewhat counterintuitively, allows accumulation of data from beats of duration within ±50% of the expected (in our case, within a 500–1500 ms range). This is *not* equivalent to accepting 100% of the beats, which is instead consistent with having a window of infinite width (Fig. 2.7).

When deciding on a setting for the cardiac beat length acceptance window, it is important to remember that, as previously stated and again stressed in Fig. 2.8, a gated SPECT acquisition produces both gated short-axis images (through reconstruction and reorientation of the projection data sets corresponding to the individual gating intervals) and standard short-axis images (through reconstruction and reorientation of the sum of the projection sets across all intervals). While cardiac function is assessed from the former, myocardial perfusion is derived from the latter. If too many beats are rejected by a narrow window in the presence of arrhythmia or gating problems, not only does that make the gated information and the assessment of cardiac function unreliable but perfusion assessment might also be compromised, a situation that the authors

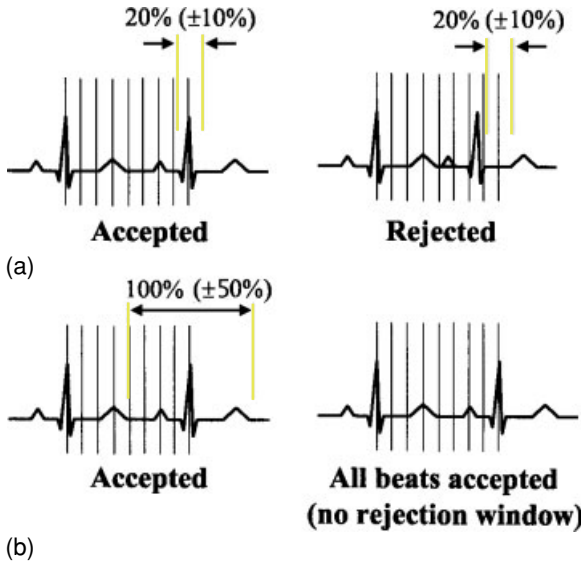

Figure 2.7 Examples of (a) an 8-interval, fixed temporal forward-framed, and (b) an 8-interval, variable temporal acquisition, both for a cardiac beat of shorter than average duration. (Modified and reproduced with permission from [11].)

deem unacceptable in clinical practice. This is not an issue if an "extra frame" (a 9th frame in 8-frame or a 17th frame in 16-frame gated SPECT imaging) exists where all counts rejected by the acceptance window are accumulated, so that they can be summed to those in the individual intervals' projection images before reconstruction – in that case, there will be virtually as many counts in the "summed gated" images as if gating had not been used, and the acceptance window can be set to a narrow value, typically 20–30%. If, on the other hand, no extra frame exists, it would be advisable to open the acceptance window to 100% or infinity, so as to maximize the quality of the images from which perfusion will be assessed (Fig. 2.9).

To summarize, we choose to preserve at all costs the integrity of the SPECT data from which myocardial perfusion is assessed. The downside of this approach is that counts from arrhythmic beats may be allowed into the gated SPECT images, whose reliability must therefore be evaluated with great care. The block diagram in Fig. 2.9 shows our recommended criteria for setting the cardiac beat length acceptance window, as well as the implications of doing so.

1 If a 20–30% beat acceptance window is used in conjunction with the "extra frame" feature, (a) the gated intervals do not contain data from arrhythmic beats, and (b) the extra frame (if accessible by itself) provides a convenient additional tool to assess how many counts were rejected, both globally and on a projection-by-projection basis. In this case, the gated SPECT data set is essentially reliable if it contains enough counts.
2 If a wide open acceptance window is used because no "extra frame" is available, the reliability of the gated SPECT data set must be deduced from "circumstantial evidence": (a) the technologist ought to monitor the ECG during acquisition, and/or a paper strip of the ECG ought to be collected for each study, so that the occurrence of abnormalities in the cardiac rhythm can be noted – some laboratories recommend the exclusion of gated data acquired from patients with more than one premature ventricular contraction (PVC) per six cardiac beats [11]; (b) software can be developed or obtained that aims at detecting gating errors from postacquisition analysis of the relative counts and count patterns in the various gated frames [13,14]; (c) when provided by the camera manufacturer, graphs of accepted counts or heart rate as a function of the projection angle (as well as beat length histograms) can provide an immediate visual pointer to gating abnormalities (Fig. 2.10), and (d) the time–volume curve must be reviewed for potential distortions and abnormalities, as explained in Chapter 5.

Most camera manufacturers do have, or plan to provide the "extra frame" feature in conjunction with gated SPECT

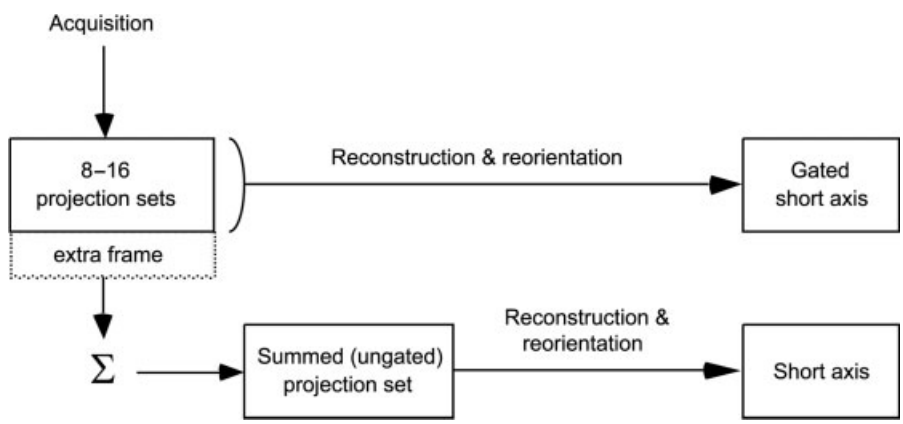

Figure 2.8 Importance of the "extra frame" in gated SPECT acquisitions. (Adapted and reproduced with permission from [12].)

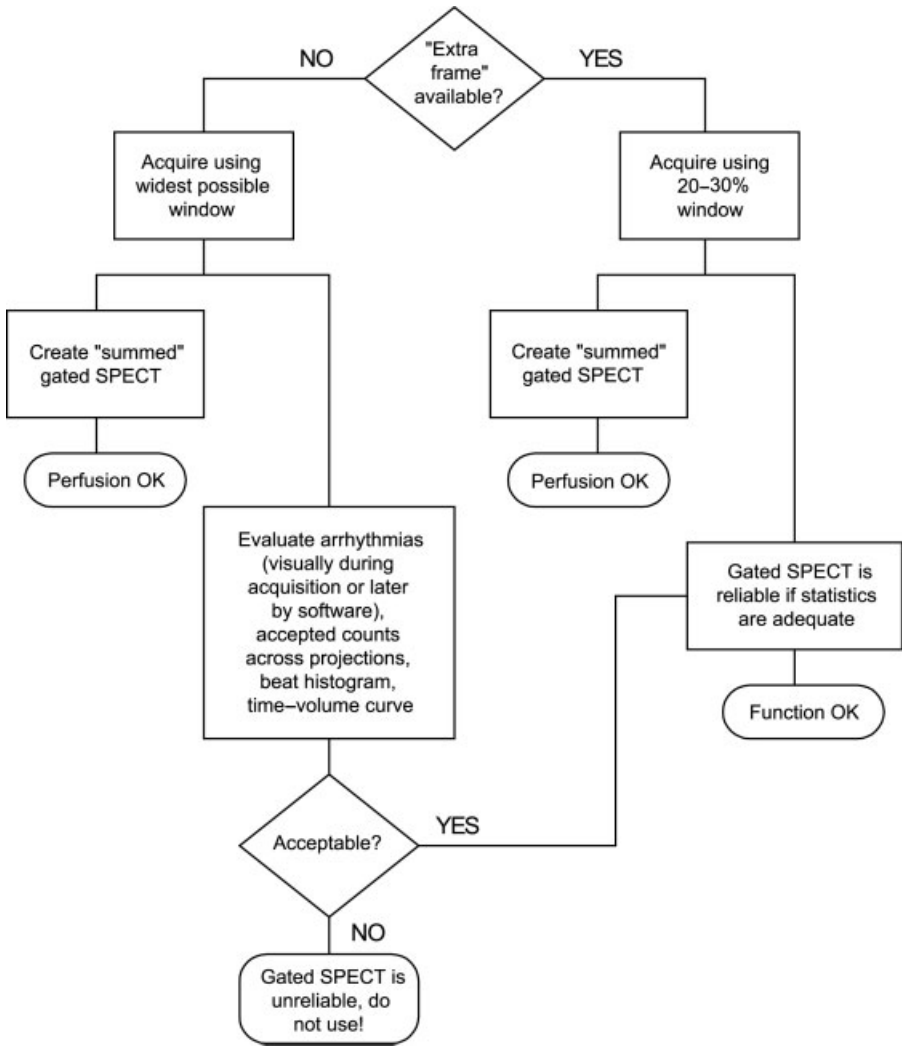

Figure 2.9 Setting the cardiac beat acceptance window.

imaging, following strong recommendations by several academic and professional societies with an interest in nuclear cardiology [15]. Also, independent and simultaneous acquisition of the gated and ungated data sets ("concurrent imaging") has been proposed (Philips Medical Systems, personal communication, 2005), and might emerge as the optimal approach because it allows the use of a narrow window on the gated portion, and no window at all on the ungated portion of the study. That notwithstanding, the lack of standardized, automatic quality control tools for the determination of the reliability of gated SPECT data is currently still an important challenge for this technique [16] and will require more focused targeting by camera manufacturers in the near future.

As a final note, the PVC rejection factor specifies the number of cardiac beats that the camera acquisition software must ignore immediately after a "bad beat" (a beat that has been rejected by the beat length acceptance window). The PVC rejection factor is generally set to 1, meaning the first beat after a bad beat is also rejected, regardless of its own length.

Count drop-off and normalization

We have previously seen that, when the time between two consecutive R wave triggers is shorter than expected by the FT forward-framing mode (but still within the acceptance window), the last gating frame(s) will not accumulate counts (Fig. 2.6a). This phenomenon goes under the name of "count drop-off," and typically results in a visually apparent "flicker" when the gated images are displayed in cinematic fashion. To alleviate this problem, each gating frame at each projection angle can be "time normalized" to the first (or the first few) gating frame(s) of the first projection angle. As shown in Fig. 2.11 for the simplified case of a projection containing data from three cardiac beats, and acquired using eight 100 ms frames in FT forward-framing mode, time normalization would require a scaling factor

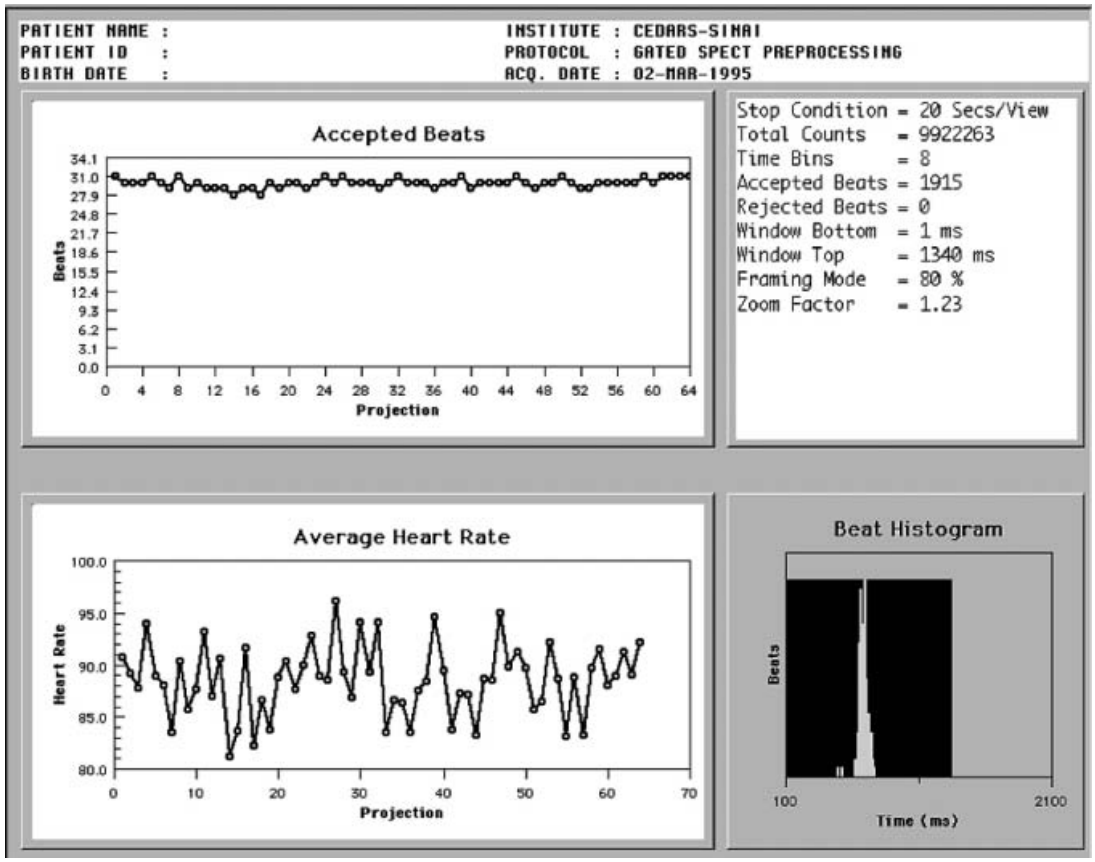

Figure 2.10 Graphs of accepted beats and heart rate as a function of the projection number. Together with the cardiac beat length histogram, these tools are useful to assess the reliability of the gated data sets.

of 2 (300/150) to be applied to every pixel in frame 8 of that projection, since the accepted beats had lengths of 725, 750, and 775 ms. While normalization eliminates image flicker and may make it easier to visually evaluate myocardial wall motion and thickening, it does not improve the statistical quality of the data. In some cases, it may even create additional artifacts. For example, "hot" pixels can be created when normalizing a frame with very poor statistics, which in turn may cause artifactual "streaks" in the reconstructed images. While normalization can provide a useful visual aid, it is not essential to the analysis of gated perfusion SPECT data, and along with beat length acceptance windowing it is a potential source of corruption of the perfusion data.

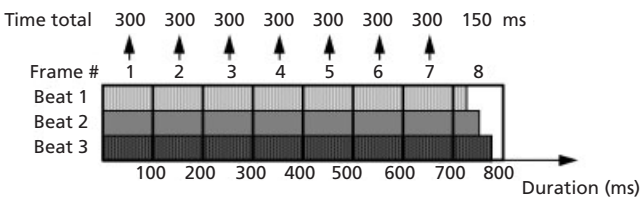

Figure 2.11 Time normalization of gating frames.

Acquisition protocol choices

Isotopes

As further explained in Chapters 3 and 5, it is the authors' belief that, as long as adequate count statistics are achieved, there is no limitation as to the specific perfusion agent that can be imaged with the gated SPECT technique. Regardless of the radiopharmaceutical used, the quality of a gated SPECT study will be closely and directly related to the number of counts in its individual frames. Count statistics are influenced by numerous factors, including injected dose, acquisition time, patient size, camera configuration and sensitivity, collimation, number of frames, and count acceptance criteria. Defining "adequate" count statistics in absolute terms is fraught with peril, because its two most readily available measures, i.e. the total number of counts in a standard projection image or in the entire image volume, are composed of (1) the total number of counts in the myocardium (the quantity we are interested in, but cannot access without some form of myocardial segmentation) and (2) the total number of extracardiac counts, which is a function of protocol choice, patient health, and body habitus. Our own experience with 60-projection acquisitions

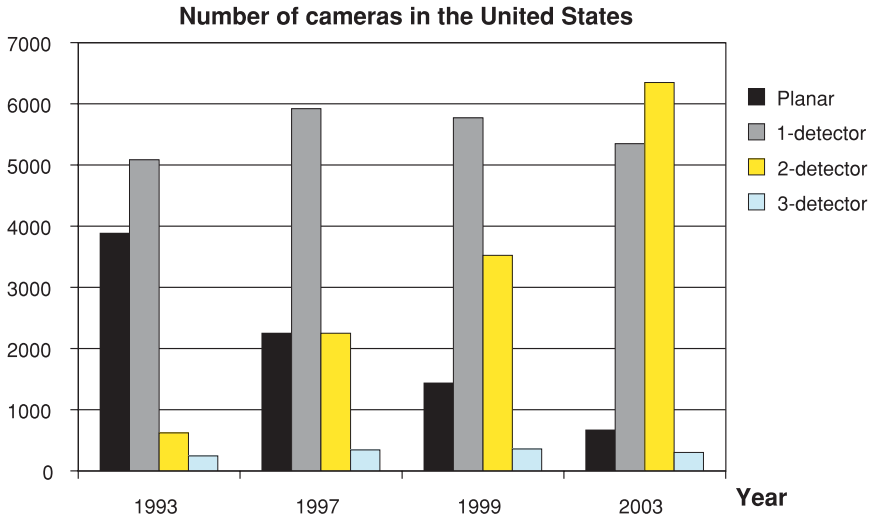

Figure 2.12 Growth trends for planar, single, and multidetector cameras in the United States. (Courtesy of IMV Medical Information Division, Des Plaines, IL.)

over a 180° orbit indicates that if one creates a composite image by adding together the "summed gated" projection images for the seven angles within ±10.5° of LAO (left anterior oblique) 45° and isolates the myocardium in that composite image, the average myocardial counts per pixel (64 by 64 pixel images) is 789 ± 237 for gated ^{99m}Tc-sestamibi, and 306 ± 81 for gated ^{201}Tl, *in the context of our standard gated SPECT acquisition protocols* [17]. Ideally, this number should be greater if in a given individual the target-to-background ratio is lower than usual. More specific criteria for setting up gated SPECT acquisitions in such a way as to achieve adequate image quality are outlined in the following sections of this chapter.

Single-detector vs. multidetector cameras

Multidetector cameras have consistently outsold single-detector systems since 1993, and their increasing diffusion is an important factor supporting the increasing utilization of gated SPECT imaging (Fig. 2.12). In particular, dual-detector cameras with the two detectors positioned at 90° allow completion of 180° SPECT acquisitions in half the time as a single-detector system for the same count level, or collection of twice the counts in the same time, and are therefore highly efficient for gated cardiac SPECT imaging. Various camera configurations are shown in Fig. 2.13, and their comparative performance in completing a 180° and a 360° SPECT acquisition with equal count statistics is shown in Table 2.1.

Length of acquisition

Ideally, the length of acquisition (expressed in seconds per projection) for a gated ^{99m}Tc-based SPECT study need not exceed that traditionally employed for a nongated SPECT study, as it has been suggested that common protocols for the latter may consistently provide more counts than are needed [19]. For gated ^{201}Tl SPECT, however, extending the acquisition time may be necessary, especially in late redistribution analysis. While many other factors are involved, Table 2.2 gives the values currently used at Cedars-Sinai for gated SPECT acquisitions using a variety of cameras, low-energy-high-resolution (LEHR) collimation, 3° projection spacing and 16-frame gating. It is clear that although in principle any type of acquisition can be gated, practical considerations on patient tolerance and avoidance of motion limit some acquisitions

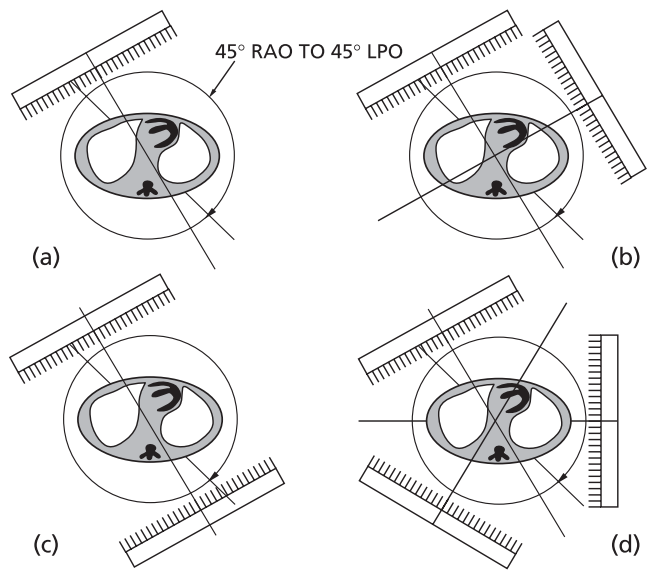

Figure 2.13 Common detector configurations in SPECT cameras: (a) basic single detector camera, (b) dual-detector, 90° configuration camera, (c) dual-detector, 180° configuration camera, and (d) triple-detector camera. (Reproduced with permission from [18].)

Table 2.1 Duration of SPECT studies acquired with single- and multidetector cameras.

	180° acquisition	360° acquisition
1 detector	*T*	2*T*
2 detectors (180° configuration)	*T*	*T*
3 detectors (120° configuration)	(2/3)*T*	(2/3)*T*
2 detectors (90° configuration)	*T*/2	*T*

Note: All cameras rotate at the same speed, continuous or pseudo-continuous rotation is assumed, and the time *T* employed by a single-detector camera for a 180° acquisition is taken as reference.

to multidetector cameras. Also, our approach leaves the acquisition time constant across patients for a given radioisotope and protocol, while the injected dose is varied as indicated in Table 2.3. Other centers acquire a planar ungated image at the beginning of the study, calculate the total counts within the image or (by using a region of interest) in the myocardium, and adjust the acquisition time accordingly. Of course, both approaches aim at ensuring that adequate counts are collected. "Fast" gated acquisitions, although originally reported for ^{99m}Tc-sestamibi and ^{99m}Tc-tetrofosmin in conjunction with multidetector systems [20] and focusing collimators [21,22], are still not widely used in clinical practice, due principally to compromise in perfusion image quality.

Number of frames

While 8-frame gating is still prevalent in gated perfusion SPECT imaging due to processing/analysis times and storage requirements considerations, it is obvious that the cardiac cycle can be more accurately described with more frequent temporal sampling. The authors have adopted 16-frame gating for all routine clinical ^{99m}Tc-based and ^{201}Tl gated SPECT imaging at their institution, although most of the considerations contained in this book relative to acquisition, processing, and quantitation of gated perfusion SPECT data are relatively independent of the number of gating intervals acquired.

Table 2.3 Relationship between injected dose and patient weight for commonly used radiopharmaceuticals.

Patient weight (lbs)	^{99m}Tc-based agents (stress) (mCi)	^{99m}Tc-based agents (rest) (mCi)	^{201}Tl (mCi)
<185	25	10	3
185–225	30	12	3.5
225–250	35	12	4
>250	40	14	4.5

As discussed in Chapter 5, 16-frame gating offers the opportunity to assess diastolic left ventricular function. Sixteen-frame gating leads to quantitative ejection fraction results that are slightly higher than those obtained from 8-frame gating, but the relationship between the two is predictable and quite uniform over a wide ejection fraction range [23]. With the increased number of frames, the 16-frame method allows the end-systolic frame to be obtained at true end-systole.

Detector rotation orbits

While conventional SPECT acquisitions have been performed rotating the detector(s) along circular orbits, recent trends in instrumentation (dual-detector cameras with 90° detectors), protocols (combined emission/transmission), and algorithms (attenuation, scatter, and resolution compensation) are increasingly requiring noncircular orbits, also referred to as elliptical or patient-contoured [24]. The argument in favor of circular orbits is that all projection images have approximately the same resolution, given their fairly constant distance from the imaged heart (source-to-collimator distance is the main determinant of resolution). Conversely, noncircular orbits aim at achieving the best possible resolution at each angle by bringing the detector as close to the patient as practical. Since artifacts may result when these projection images of widely

Table 2.2 Injected dose and total gated perfusion SPECT study duration for different camera/detector configurations and commonly used radiopharmaceuticals.

				Total study duration (min)		
Isotope	Dose (mCi)	No. of projections	Seconds per projection	1-detector, 2-detector @180°	2-detector @90°	3-detector @120°
^{99m}Tc-based (stress)	25–40	60	25	25	12.5	16.7
^{99m}Tc-based (rest)	10–14	60	25	25	12.5	16.7
^{201}Tl (rest)	3–4.5	60	35	35	17.5	23.3
^{201}Tl (4 h)	3–4.5	60	35	35	17.5	23.3
^{201}Tl (24 h)	3–4.5	60	50	50	25	33.3

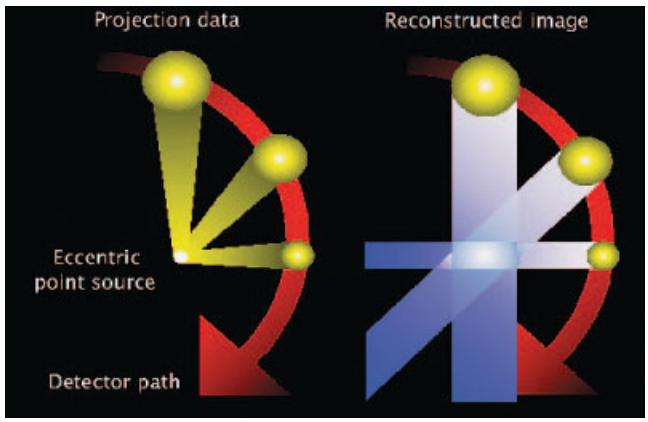

Figure 2.14 Blending projection images with different resolution characteristics in the reconstruction process may cause distortions in the reconstructed object – this is of particular concern with noncircular or eccentric orbits, since resolution is directly related to the source–detector distance. (Courtesy of Jonathan M Links, PhD.)

different resolution are combined in reconstruction [25], as shown in Fig. 2.14, software approaches are being developed to reduce that variability [26–28]. There is currently no evidence that function parameters measured from gated SPECT have substantial dependence on orbit shape.

Projection images need to be distributed over a minimum of 180° in order not to introduce severe artifacts during reconstruction [29], and current clinical practice overwhelmingly favors 180° orbits spanning from the right anterior oblique (RAO) to the left posterior oblique (LPO) view, mainly for the study duration considerations outlined in Table 2.1. Published reports comparing 180° and 360° orbits with respect to image resolution and perfusion defect contrast are not in agreement, describing the former to be superior [30–34], inferior [35–37], or equivalent [38,39] to the latter in clinical studies and phantom experiments. Even less data exist with respect to differences in gated SPECT function parameters, although excellent correlation has been reported between left ventricular ejection fraction and volume quantitative measurements from 180° and 360° data [40].

The traditional detector rotation pattern is called *step-and-shoot*. In this approach, the detector "steps" through a discrete number of views along the orbit, and the camera electronics temporarily stop data collection while the detector advances from one view to the next, causing a "dead time" of a few seconds per view. In a more recent approach, called "continuous" acquisition, the detector rotates continuously and at constant speed around the patient, with data collection enabled at all times. The acquisition orbit is divided in a number of sub-arcs, and data collected along each arc is assigned to a projection image. Pseudo-continuous (also called modified step-and-shoot) acquisition is a hybrid approach: the detector moves as in step-and-shoot, but data collection continues during the stepping period. Since it has been demonstrated that continuous acquisition does not appreciably decrease the resolution of the SPECT image if the spacing between projections is less than or equal to 6° [4,41], acquisitions are preferably performed in the continuous or pseudo-continuous mode, to avoid dead-time-related inefficiencies. The number of projection images acquired over a 180° orbit is not critical because, as long as their angular spacing is constant and less than or equal to 6°, neither perfusion nor function assessment will likely be affected [42]. Of course, utilizing 6° spacing between projections would require doubling the acquisition time per projection (and halving the number of projections) in Table 2.2, if equal statistics are desired. Standard numbers of projections in current camera systems are 30, 32, 60, and 64 for 180° acquisitions.

Acquisition zoom

Setting up a gated or nongated acquisition that "zooms" in on the left ventricle is possible by amplifying the analog position signals generated by the camera front-end electronics. Acquisition zoom can be centered [43] or off-axis [44] with respect to the center of the camera's field of view, and a zoom greater than 1 will improve image resolution by magnifying the image of the LV. Since the dimension of the individual pixels is reduced but the amount of radioactivity in the myocardium does not change, however, a larger number of pixels will be needed to cover the myocardium, and the average number of counts per pixel will decrease, leading to higher image noise. Moreover, in SPECT imaging, a zoom that is too large may cut off portions of the LV at some projection angles. These facts suggest that a compromise must be sought between resolution and noise, and excessive zoom values are to be avoided. Our own experience with nongated SPECT acquisitions have shown acquisition zooms of 1.3–1.4 to yield optimal image quality [45], and it is expected that these findings would be extendable to gated SPECT acquisitions. As noted above, zooming can also be accomplished during reconstruction, but zooming during acquisition is preferred.

Collimators

The standard collimator used in nuclear cardiology is a parallel hole collimator. There is a direct trade-off between resolution and sensitivity with parallel hole collimators, and fine differences can be achieved by varying the number, bore, shape, and length of the holes. Specifically, a parallel hole collimator that favors resolution is the low-energy-high-resolution (LEHR) collimator, while one that favors sensitivity is the low-energy-all-purpose (LEAP) collimator. When acquiring SPECT images using different radiopharmaceuticals (for example, rest ^{201}Tl and

poststress ^{99m}Tc-sestamibi in the separate dual isotope protocol [46]), we have found it desirable to minimize intrinsic resolution differences by using the same collimator, a LEHR. While this approach was developed for perfusion imaging, we do believe that it is also valid for gated SPECT imaging, and much of the published literature on gated ^{201}Tl SPECT is in fact based on the use of a LEHR collimator [17,47–51]. Using a LEAP collimator may be a viable approach for maximizing sensitivity with "^{201}Tl-only" protocols [52,53], especially if implemented on single-detector systems, and it has also been reported to be a potentially superior alternative to LEHR collimation with respect to myocardial recovery coefficient and contrast, when resolution compensation is used [54].

Another way to increase sensitivity is to map the organ of interest (the myocardium) to a larger portion of the detector by exploiting the intrinsic magnification properties of a fan beam or cone beam collimator [55]. These collimators focus to a point (cone beam) or to a line parallel to the axis of rotation of the camera and beyond the patient (fan beam). The increase in sensitivity produced by these collimators is not associated with a loss of resolution; however, the data volume may not be adequately sampled at all angles due to truncation artifacts [56], and fan beam/cone beam collimators are not widely used in clinical practice. Use of "cardiofocal" cone beam collimators has been reported a few years ago in conjunction with gated ^{99m}Tc-tetrofosmin SPECT imaging [21,22], but that report has not been followed by further investigation and validation.

Acquisition by time or counts

The data presented in Table 2.2 reflect gated SPECT acquisitions performed using a fixed number of seconds per projection angle, as nongated SPECT studies would. Due to the additional issues introduced by rejected data, virtually all manufacturers provide a count-based gated acquisition mode, which advances the detector from one projection angle to the next only after a given number of counts have been collected. While this approach has the potential to reduce the effect of arrhythmias, it has the undesirable effect (depending on the acceptance window) of lengthening gated SPECT acquisitions, sometimes beyond a patient's ability to remain still. Since count-based gated SPECT acquisitions also make it difficult to plan clinical throughput (study duration is unpredictable), they are not recommended for use in other than very specific applications.

Image reconstruction and reorientation

Image reconstruction

Figure 2.15 illustrates the practical implementation of SPECT reconstruction by backprojection [29]. The two-dimensional projection images (perpendicular to the plane of the page, as is the patient) yield a series of "activity profiles" (also termed count profiles or scan profiles) for each transaxial plane of interest (Fig. 2.15a). Each profile represents the integrated sum of the activity underneath the detector along a given angle in that particular

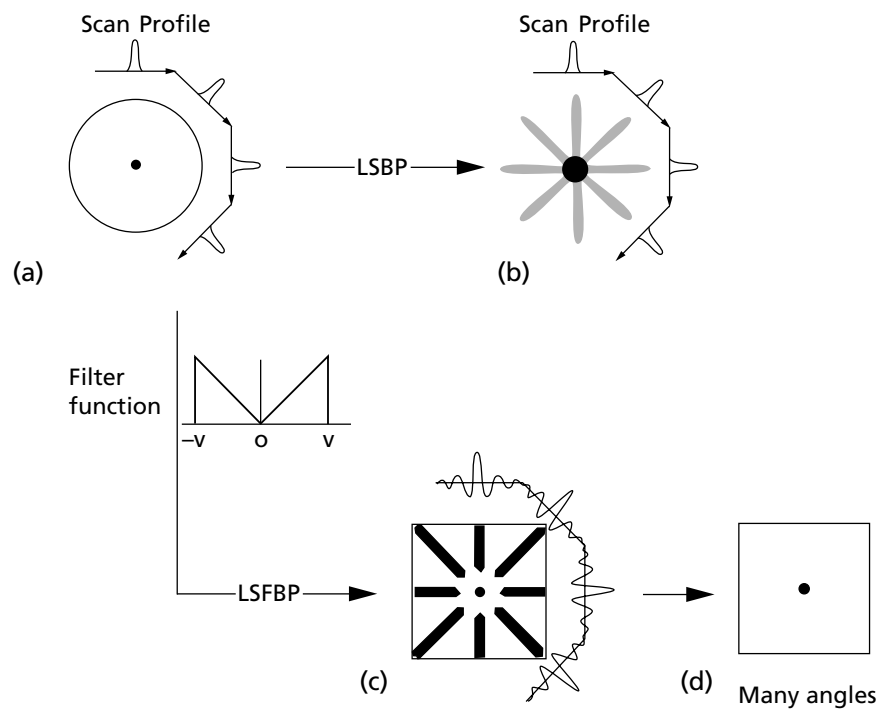

Figure 2.15 Implementation of tomographic reconstruction by linear superimposition of backprojections (LSBP) and linear filtered backprojections (LSFBP). In modern tomography, LSFBP is universally preferred to LSBP. (Reproduced with permission from [29].)

plane, and all profiles are used to "reconstruct" the image representing the activity in that plane (transaxial image). Since no information is available concerning the depth of the activity responsible for a peak in a profile, the simplest assumption to make is that it was uniformly distributed. Thus, the counts in each profile are uniformly redistributed (backprojected) onto the transaxial image, following the linear superimposition of backprojections (LSBP) scheme (Fig. 2.15b). A drawback of this approach is that LSBP results in loss of resolution, loss of contrast, and creation of the characteristic "star artifact." To alleviate this problem, count profiles can be altered (filtered) before reconstruction using an oscillating function which has both positive and negative values, so as to cancel out the star's "rays" (Fig. 2.15c). This latter approach is termed linear superimposition of filtered backprojections (LSFBP), or filtered backprojection (FBP) in short notation, and represents the current standard for reconstruction of gated and ungated tomographic images in nuclear cardiology.

A different reconstruction technique that is gaining wider acceptance, fueled by increases in computer speed and increased use of attenuation/scatter/resolution compensation, is iterative reconstruction [57]. Iterative reconstruction is based on the algebraic reconstruction technique, which sees each count profile as an equation with a number of unknowns equal to the dimension of the image matrix [58]. If enough equations are provided (enough projection images or count profiles are acquired), the system can be solved and the mathematically exact values for all pixels in the transaxial image can be derived, as demonstrated in Fig. 2.16 for a simple 2 × 2 matrix. For the 64 × 64 or 128 × 128 matrixes used in SPECT, system solving is practically always implemented using an iterative process, which starts with an "educated guess" represented by the filtered backprojection output and generally achieves convergence in 10–15 iterations. As discussed in Chapter 5, there is currently no evidence that function parameters measured from gated SPECT depend substantially on whether iterative or filtered backprojection was used as the reconstruction technique of choice.

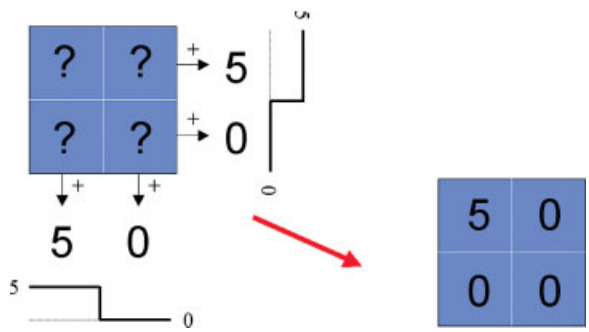

Figure 2.16 Algebraic reconstruction of tomographic images. Each point in each count profile is the sum of a row, a column, or a diagonal distribution of pixels (two profiles are shown here). If enough profiles are acquired, a system of equations can be built and solved for the exact count values in those pixels. (Modified and reproduced with permission from [59].)

Of note, it has been suggested that the individual intervals of a gated SPECT study do not need to be reconstructed separately and independently. Incorporation of temporal filtering within the iterative reconstruction process has reportedly led to a dramatic reduction in image noise, at the cost of a minor systematic error [60]. In a similar approach, taking advantage of the compression and signal decorrelation properties of the Karhunen-Loeve transform when reconstructing gated SPECT projection data sets has been reported to result in less image noise and faster processing times [61].

Filters

The ramp filter used to eliminate the star artifact in filtered backprojection is a "high-pass filter," because it lets high frequencies pass unattenuated while it attenuates low spatial frequencies. The concept of spatial frequency is based on mathematical operators (the Fourier transform) that are rather complex and have been described extensively elsewhere [29,59]. For our purposes, it will suffice to say that low frequencies correspond to large, uniform objects (like the rays of the star artifact), while high frequencies correspond to small objects and sudden variations in radioactivity between adjacent pixels (the "edge" of the myocardium, for example, marks a high-frequency transition area). Therefore, a high-pass filter will "sharpen" an image by attenuating low frequencies, whereby a low-pass filter will "smooth" the image by attenuating high frequencies. Nuclear cardiac images are relatively count-poor, due to limitations in the injected dose, the use of physical collimation and the attenuation introduced by the thorax, and so projection images are affected by random noise. Since noise by definition involves high frequencies, and as such it can be reduced by smoothing, low-pass filters have become the most extensively used filters in nuclear cardiology. The most popular low-pass filters belong to the Butterworth family, with other less widespread options including the Hanning filter and the Metz and Wiener adaptive filters [62]). The Butterworth filter family is described in the frequency domain by the following class of functions:

$$B(f) = \frac{1}{1 + (f/f_c)^{2n}} \quad (1)$$

where f_c is the critical or "cutoff" frequency and n the order of the filter. In essence, n controls the slope of the curve, while f_c is the spatial frequency corresponding to an attenuation of 50% and controls the location of the curve's inflection point, as shown in Fig. 2.17. It is important to

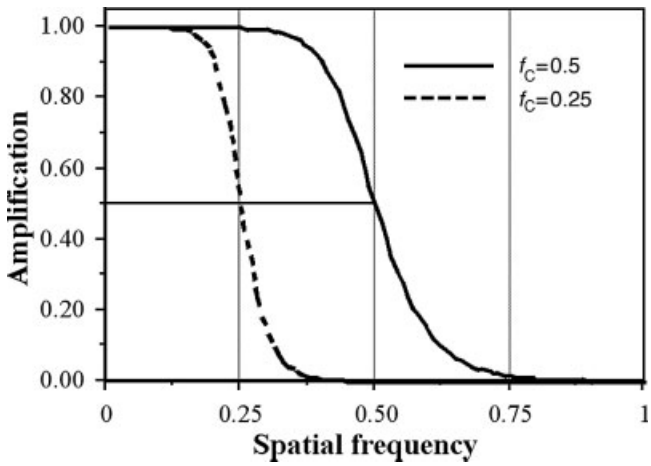

Figure 2.17 Two curves belonging to the family of Butterworth filters of order 5 (f_c is the cutoff frequency). Generally speaking, the smaller the area encompassed by the curve of a filter in the frequency domain, the smoother the resulting image, because more spatial frequencies are attenuated.

be aware of the fact that there is some confusion as to the units of measurement for the cutoff frequency of a Butterworth filter. While some prefer to express it as a 0–1 numeric range (1 being the highest attainable frequency or Nyquist frequency), others point out that the Nyquist frequency is by definition equivalent to 0.5 cycles per pixel, and adopt a 0–0.5 range instead. In other words, the *same* cutoff frequency can be reported as 0.3 or 0.6 on two different camera systems. Whether a cutoff frequency is expressed in cycles per pixel or as a fraction of the Nyquist frequency, it should be clear that any spatial frequency measurement must always be accompanied by a disclosure of the pixel size value. Table 2.4 shows the Butterworth filter parameters currently used at our institution based on the 0–1 cutoff range, a pixel size of 6.5–6.6 mm, and the dual isotope doses and acquisition times already specified in Tables 2.2 and 2.3. As it is sensible to expect, a gated SPECT study needs to be smoothed a bit more than an ungated or summed gated study, due to the lower counts in each of its multiple frames.

Table 2.4 Butterworth filter parameters employed at the authors' institution using the 0–1 cutoff range, a pixel size of 6.5–6.6 mm, and the dual isotope doses and acquisition times described in Tables 2.2 and 2.3.

	Ungated		Gated	
Butterworth	**Order**	**Cutoff**	**Order**	**Cutoff**
^{99m}Tc-based (stress)	5	0.66	5	0.50
^{99m}Tc-based (rest)	5	0.55	5	0.50
^{201}Tl (rest)	10	0.50	10	0.40
^{201}Tl (4 h)	10	0.50	10	0.40
^{201}Tl (24 h)	10	0.40	10	0.40

Low-pass filtering is usually accomplished on the projection images before reconstruction (or during reconstruction, modifying the ramp filter by a "low-pass window"). These approaches should be equivalent to filtering the reconstructed images (two-dimensionally or three-dimensionally), given the theoretical linearity of the process. In practice, however, nonlinearities are introduced by some camera manufacturers by "clipping" negative pixels resulting from filtering, and it is generally accepted that pre-reconstruction filtering is the most desirable way to achieve noise reduction in nuclear cardiology imaging.

Reorientation

The output of filtered backprojection or iterative reconstruction is a set of "transaxial" images, or images perpendicular to the long axis of the patient. Since the orientation of the LV in the thorax is patient-specific, it is customary to "reorient" transaxial images perpendicularly to the long axis of the LV, creating "short-axis" images that have standardized orientation and are therefore more comparable across patients. While tomographic image reorientation has traditionally been accomplished by manually tracing projections of the left ventricular long axis in two midventricular planes, one transaxial and the other sagittal, software is widely available today that automates this tedious process [63–65], at the same time greatly improving its accuracy (most algorithms operate in the three-dimensional space) and reproducibility. An example of automatic reorientation of transaxial images into short- and long-axis images is shown in Fig. 2.18 (right side) for a non-gated SPECT study, together with the filtering and reconstruction that produce the transaxial images themselves (left side).

Reorientation of gated SPECT images is generally performed using one fixed left ventricular long axis, since identifying one axis per gating frame would be made difficult by image noise. It is often convenient to reconstruct and reorient the gated SPECT and the summed gated SPECT data sets at the same time, using the same reconstruction limits and reorientation angles (the filtering parameters are slightly different, as explained above and in Table 2.4). In addition to "zooming in" on the myocardium during data acquisition, it is also possible to perform "zoomed reconstruction" of the projection data (centered or off-axis, the latter being shown in Fig. 2.19). Both acquisition zoom and reconstruction zoom will "blow up" the image of the LV and likely improve the accuracy of volumetric and ejection fraction measurements based on pixel counting (see Chapter 5), although it would be intuitively

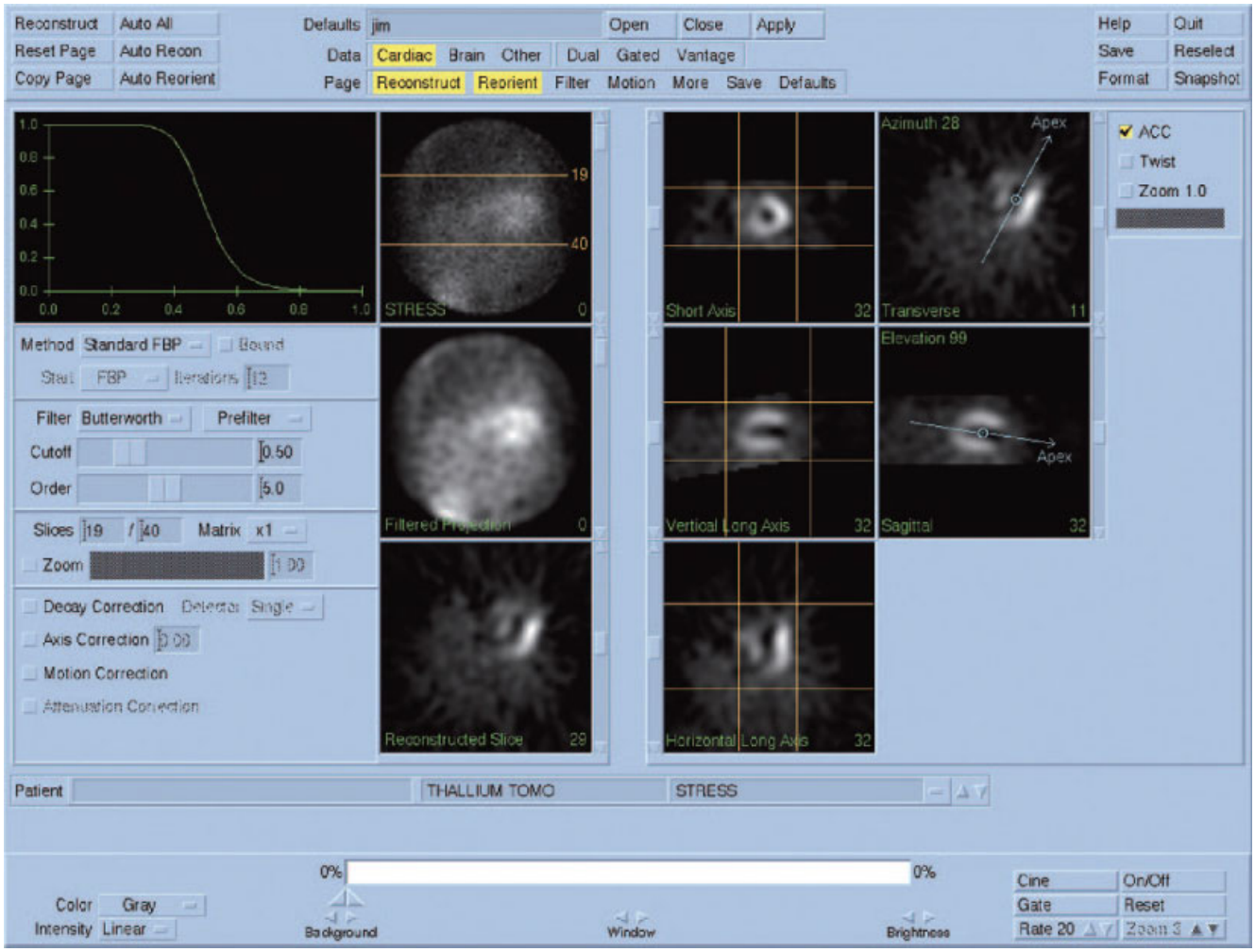

Figure 2.18 Automatic reconstruction/reorientation of SPECT data. Reconstruction limits are determined from the projection data set (middle left, top), which is then filtered (middle left, middle) with a Butterworth filter of preset parameters (left) and reconstructed into a transaxial data set (middle left, bottom). The three-dimensional location of the LV's long axis is determined (right) and the short-axis and vertical and horizontal long-axis data sets (middle right, top to bottom) generated.

expected that zooming during acquisition would lead to superior results.

Attenuation, scatter, variable resolution, and motion

The quality of the reconstructed and reoriented SPECT images depends on that of the projection images from which they are derived. The projection images, in turn, can be compromised by a host of technical and physical factors, including Compton scatter, photon absorption, variable resolution for noncircular acquisition orbits, and patient or organ motion. Figure 2.20 presents a schematic representation of the first two phenomena, particularly important in cardiac imaging because of the heart's close proximity to organs of much different densities.

Attenuation vs. absorption

As exemplified in Fig. 2.20, photons that originate in the myocardium and reach the scintillation detector without prior interaction are called *primary photons*, and are most valuable because they contribute information as to how much radioactivity was taken up at a specific myocardial location. Photons that hit atomic electrons within the patient's body before reaching the detector are said to have undergone "Compton scattering" – their direction is altered and their energy reduced, and even though they may still fall within the energy discrimination window they will carry incorrect positional information. Specifically, myocardial counts may be incorrectly assigned to other areas, reducing the apparent myocardial uptake (case 2a in Fig. 2.20), or extracardiac counts may be likewise interpreted as coming from the myocardium, with consequent

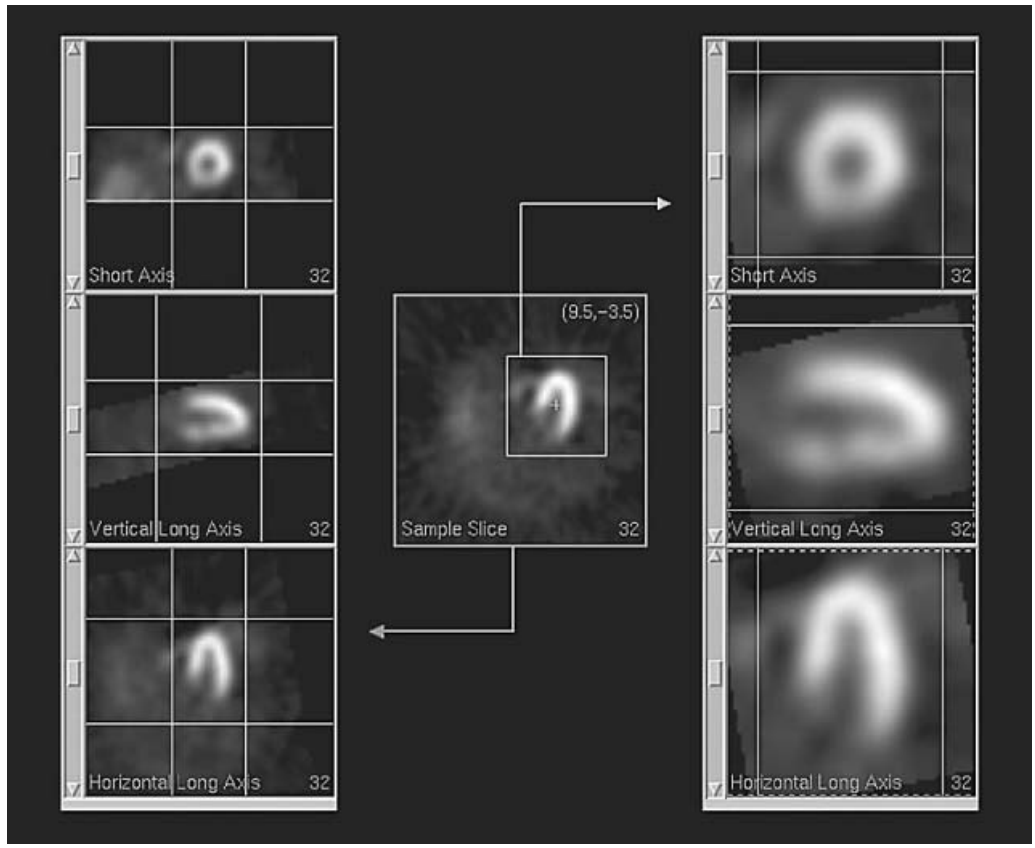

Figure 2.19 Zoomed off-axis reconstruction. Standard nonzoomed reconstruction (left column) results in tomographic images where the myocardium occupies a small portion of the 64 × 64 pixel matrix, while zoomed off-axis reconstruction (right column) maximizes the portion of the 64 × 64 matrix covered by the myocardium. Zoomed reconstruction is not equivalent to zooming the tomographic image after reconstruction, since the latter only involves pixel replication and does not improve resolution.

potential loss of image resolution and defect contrast (case 2b in Fig. 2.20). It is also possible for the energy of photons emitted by the myocardium to be completely absorbed by an atomic electron (case 3 in Fig. 2.20), in which case no counts are accumulated in the projection image. Technically, attenuation accounts for *both* absorbed and Compton-scattered photons – however, in nuclear cardiology literature, attenuation has become virtually synonymous with absorption. Typical artifacts associated with photon attenuation are apparent perfusion defects in the anterior and/or lateral myocardial wall (breast attenuation), and defects in the inferior wall secondary to diaphragmatic attenuation, as will be discussed in detail in Chapter 7.

Motion

Motion is believed to affect as many as 10–20% of all cardiac SPECT studies. Generally speaking, it can be divided into organ motion (upward creep) and patient motion ("bouncing", translations and rotations of the returning or nonreturning type). Upward creep of the heart is often found when imaging is started too soon following exercise stress [66], and reflects the gradual return of the diaphragm to its pre-exercise location in a patient's chest. Bouncing refers to an up-and-down, oscillating pattern of motion caused by breathing or other factors, usually along the vertical direction. Returning and nonreturning translations by the patient may occur along the vertical direction, horizontal direction, or both.

The practical effects of motion on a SPECT acquisition depend on the type and degree of motion, time at which it occurs, and number and configuration of camera detectors employed, as investigated in detail by Matsumoto et al. [67]. Generally speaking, artifacts will range from subtle to severe deformations of the left ventricular cavity (Fig. 2.21), culminating in the well-known "hurricane sign" [68]. Although motion correction software is widely available and reasonably effective in correcting various types of translational motion, its effectiveness is very limited with rotational motion [67,69]; for this and other reasons, it is advisable to use motion compensation techniques only in cases where there is a clear need for it, and not as a matter of routine. The best solution to patient

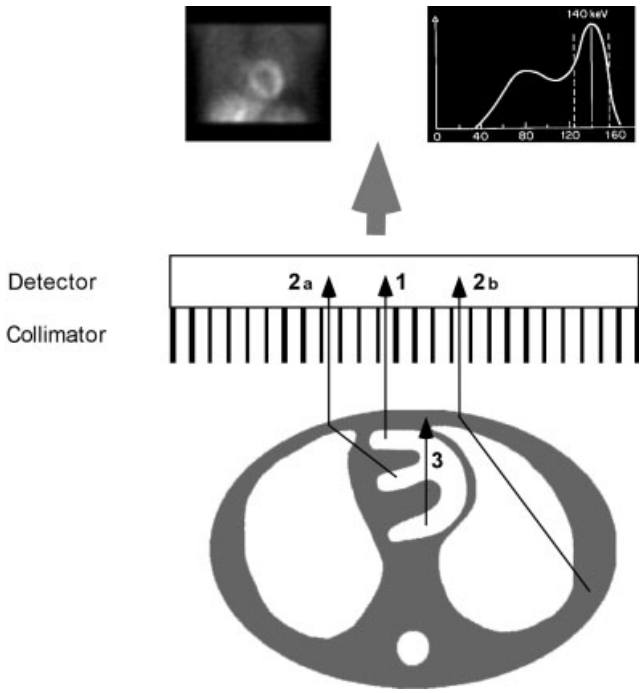

Figure 2.20 Different categories of photons in nuclear imaging: (1) primary photons, which are uncontaminated and account for the photopeak in the energy spectrum (top right); (2a-2b) Compton-scattered photons, which have lower energy and carry incorrect positional information; (3) absorbed photons, which are not collected in forming the projection image (top left). (Modified and reproduced with permission from [59].)

motion is to prevent it during SPECT acquisition – for example, by reducing the total acquisition time, using arm holding devices or imaging the patient in the prone position, the latter approach being also useful to reduce left ventricular inferior wall attenuation [70].

Image storage

Although the cost of electronic storage has declined substantially over the past few years, it still pays to be sensible when storing and archiving gated SPECT data. As previously explained, the various data sets generated by a gated SPECT acquisition and processing sequence comprise the gated "raw" (projection) images, from which the "summed raw" images are generated, the filtered projection images (gated and summed), the transaxial or transverse tomographic images (gated and summed), and the short-axis, vertical long-axis, and horizontal long-axis tomographic images (gated and summed). The hard disk of the computer on which gated processing was performed will likely contain all of these data sets (plus assorted bitmapped images), until it is time to archive that particular patient folder to make space for more recent patients. At that point, a decision must be made as to how many data sets should be preserved on long-term optical or tape storage media. Since all data sets can be generated from the raw gated projection images, a minimalistic approach would only archive the latter, and re-create the former as needed. The authors prefer to also archive the gated and summed gated short-axis images, because it is from them that quantitative measurements were directly derived. Of note, all long-axis images are intrinsically contained in the short-axis images, if the latter are dealt with in three-dimensional fashion. The overall space occupied by summed short-axis plus gated raw and short-axis images should not exceed 8–10 MB for a 16-frame, 64 × 64 matrix acquisition protocol, and can be reduced to little more than 1–2 MB using standard lossless compression techniques. Of note, if attenuation correction hardware and software were to be employed in conjunction with gating, the number of files and their complexity would be greatly increased.

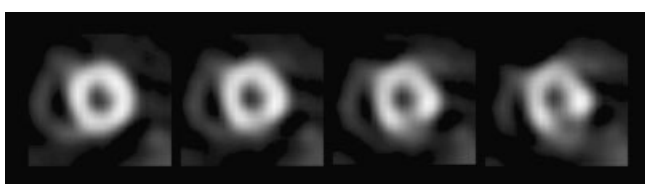

Figure 2.21 Motion artifacts created in a short-axis image by (left to right) zero, one, two, and three pixels vertical shifting of all projections corresponding to the last 7 minutes of a 14-minute, 180° ^{99m}Tc-sestamibi SPECT acquisition. Note the progressive deformation of the ventricular cavity as the degree of motion increases, as well as the artifactual perfusion defect in the inferior myocardial wall. (Reproduced with permission from [59].)

References

1. Bacharach SL, Green MV, Borer JS, et al. A real-time system for multi-image gated cardiac studies. Journal of Nuclear Medicine 1977;18(1):79–84.
2. Bacharach SL, Bonow RO, Green MV. Comparison of fixed and variable temporal resolution methods for creating gated cardiac blood-pool image sequences. Journal of Nuclear Medicine 1990;31(1):38–42.
3. Green MV, Ostrow HG, Douglas MA, et al. High temporal resolution ECG-gated scintigraphic angiocardiography. Journal of Nuclear Medicine 1975;16(1):95–98.
4. Germano G, Van Train K, Kiat H, Berman D. Digital techniques for the acquisition, processing, and analysis of nuclear cardiology images. In Sandler MP, ed. Diagnostic Nuclear Medicine. 3rd edn. Baltimore: Williams & Wilkins; 1995:347–386.
5. Juni JE, Chen CC. Effects of gating modes on the analysis of left ventricular function in the presence of heart rate variation [see comments]. Journal of Nuclear Medicine 1988;29(7):1272–1278.

6. Garcia E, Bateman T, Berman D, Maddahi J. Computer techniques for optimal radionuclide assessment of the heart. In Gottschalk A, ed. Diagnostic Nuclear Medicine. 2nd edn. Baltimore: Williams & Wilkins; 1988:259–290.
7. Bacharach SL, Green MV, Borer JS. Instrumentation and data processing in cardiovascular nuclear medicine: evaluation of ventricular function. Seminars in Nuclear Medicine 1979;9(4):257–274.
8. Jengo JA, Mena I, MacDonald N, Criley JM. Evaluation of left ventricular function (ejection fraction and segmental wall motion) by single pass radioisotope angiography. International Journal of Nuclear Medicine and Biology 1979;6(1):35–44.
9. Case J, Bateman T, Cullom S, McGhie A, O'Keefe J. Evaluation of a post-acquisition list mode rebinning of ECG-gated SPECT myocardial perfusion images [abstract]. Journal of Nuclear Medicine 2000;41(5):170P.
10. Lear JL, Pratt JP. Real-time list-mode processing of gated cardiac blood pool examinations with forward-backward framing. European Journal of Nuclear Medicine 1992;19(3):177–180.
11. Cullom SJ, Case JA, Bateman TM. Electrocardiographically gated myocardial perfusion SPECT: technical principles and quality control considerations. Journal of Nuclear Cardiology 1998;5(4):418–425.
12. Germano G, Berman D. Gated single-photon emission computed tomography. In Iskandrian AE, Verani MS, eds. Nuclear Cardiac Imaging: Principles and Applications. 3rd edn New York: Oxford University Press; 2003:121–136.
13. Nichols K, DePuey E, Dorbala S, Sharma A, Salenski H, Rozanski A. Prevalence of gating errors in myocardial perfusion SPECT data [abstract]. Journal of Nuclear Medicine 1998;39(5):45P.
14. Kasai T, DePuey E, Shah A, Merla V. Gating errors with ECG gated myocardial perfusion SPECT – identification and classification [abstract]. Journal of Nuclear Cardiology 2003;10(1):S17.
15. Bar Harbor Invitation Meeting 2000. Journal of Nuclear Cardiology 2001;8(2):224–316.
16. Nichols K, DePuey E, Yoon J, Merced M, Yao S, Rozanski A. Relative influence of gating errors on myocardial perfusion and function computed by QGS software [abstract]. Journal of Nuclear Medicine 1999;40(5):157P.
17. Germano G, Erel J, Kiat H, Kavanagh PB, Berman DS. Quantitative LVEF and qualitative regional function from gated thallium-201 perfusion SPECT. Journal of Nuclear Medicine 1997;38(5):749–754.
18. Galt J, Germano G. Advances in instrumentation for cardiac SPECT. In DePuey EG, Berman DS, Garcia EV, eds. Cardiac SPECT Imaging. New York: Raven Press; 1995:91–102.
19. DePuey EG, Nichols KJ, Slowikowski JS, et al. Fast stress and rest acquisitions for technetium-99m-sestamibi separate-day SPECT. Journal of Nuclear Medicine 1995;36(4):569–574.
20. Mazzanti M, Germano G, Kiat H, Friedman J, Berman DS. Fast technetium 99m-labeled sestamibi gated single-photon emission computed tomography for evaluation of myocardial function. Journal of Nuclear Cardiology 1996;3(2):143–149.
21. Everaert H, Vanhove C, Hamill JJ, Franken PR. Cardiofocal collimators for gated single-photon emission tomographic myocardial perfusion imaging. European Journal of Nuclear Medicine 1998;25(1):3–7.
22. Everaert H, Vanhove C, Franken PR. Gated SPET myocardial perfusion acquisition within 5 minutes using focussing collimators and a three-head gamma camera. European Journal of Nuclear Medicine 1998;25(6):587–593.
23. Germano G, Kiat H, Kavanagh PB, et al. Automatic quantification of ejection fraction from gated myocardial perfusion SPECT. Journal of Nuclear Medicine 1995;36(11):2138–2147.
24. Todd-Pokropek A. Non-circular orbits for the reduction of uniformity artefacts in SPECT. Physics in Medicine and Biology 1983;28(3):309–313.
25. Maniawski PJ, Morgan HT, Wackers FJ. Orbit-related variation in spatial resolution as a source of artifactual defects in thallium-201 SPECT [see comments]. Journal of Nuclear Medicine 1991;32(5):871–875.
26. Cullom S, Hendel R, Liu L, Garcia E, White M, Berman D. Diagnostic accuracy and image quality of a scatter, attenuation and resolution compensation method for Tc-99m cardiac SPECT: preliminary results [abstract]. Journal of Nuclear Medicine 1996;37(5):81P.
27. Links JM, Becker LC, Rigo P, et al. Combined corrections for attenuation, depth-dependent blur, and motion in cardiac SPECT: a multicenter trial. Journal of Nuclear Cardiology 2000;7(5):414–425.
28. Harel F, Genin R, Daou D, et al. Clinical impact of combination of scatter, attenuation correction, and depth-dependent resolution recovery for Tl-201 studies. Journal of Nuclear Medicine 2001;42(10):1451–1456.
29. Sorenson JA, Phelps ME. Physics in Nuclear Medicine. 2nd edn. Orlando: Grune & Stratton; 1987.
30. Eisner RL, Nowak DJ, Pettigrew R, Fajman W. Fundamentals of 180 degree acquisition and reconstruction in SPECT imaging. Journal of Nuclear Medicine 1986;27(11):1717–1728.
31. Maublant JC, Peycelon P, Kwiatkowski F, Lusson JR, Standke RH, Veyre A. Comparison between 180 degrees and 360 degrees data collection in technetium-99m MIBI SPECT of the myocardium. Journal of Nuclear Medicine 1989;30(3):295–300.
32. Knesaurek K, King MA, Glick SJ, Penney BC. Investigation of causes of geometric distortion in 180 degrees and 360 degrees angular sampling in SPECT. Journal of Nuclear Medicine 1989;30(10):1666–1675.
33. Freeman MR, Konstantinou C, Barr A, Greyson ND. Clinical comparison of 180-degree and 360-degree data collection of technetium 99m sestamibi SPECT for detection of coronary artery disease. Journal of Nuclear Cardiology 1998;5(1):14–18.
34. Chen M, Jaszczak RJ, Gilland DR, Bowsher JE, Metz C. Receiver operating characteristic evaluation of triple-head 360 degree versus dual-head 180 degree myocardial SPECT acquisition [abstract]. Journal of Nuclear Medicine 2002;43(5):53P.
35. Liu YH, Lam PT, Sinusas AJ, Wackers FJT. Differential effect of 180 degrees and 360 degrees acquisition orbits on the accuracy of SPECT imaging: quantitative evaluation in

phantoms. Journal of Nuclear Medicine 2002;43(8):1115–1124.
36. Goris ML, Zhu HJ. Evaluation of the respective value of 360 versus 180 degree and ungated versus end-diastolic imaging in myocardial scintigraphy with Tc-99m agents [abstract]. Journal of Nuclear Medicine 2002;43(5):194P.
37. Ruter R, Hurska C, O'Connor M. Effect of angular rotation and type of orbit on apparent count distribution in SPECT images of a normal myocardium [abstract]. Journal of Nuclear Medicine 2003;44(5):193P.
38. LaCroix KJ, Tsui BM, Hasegawa BH. A comparison of 180 degrees and 360 degrees acquisition for attenuation-compensated thallium-201 SPECT images. Journal of Nuclear Medicine 1998;39(3):562–574.
39. O'Connor MK, Leong LK, Gibbons RJ. Assessment of infarct size and severity by quantitative myocardial SPECT: results from a multicenter study using a cardiac phantom. Journal of Nuclear Medicine 2000;41(8):1383–1390.
40. Vanhove C, Franken PR, Defrise M, Bossuyt A. Comparison of 180 degrees and 360 degrees data acquisition for determination of left ventricular function from gated myocardial perfusion tomography and gated blood pool tomography. European Journal of Nuclear Medicine and Molecular Imaging 2003;30(11):1498–1504.
41. Cao Z, Maunoury C, Chen CC, Holder LE. Comparison of continuous step-and-shoot versus step-and-shoot acquisition SPECT. Journal of Nuclear Medicine 1996;37(12):2037–2040.
42. Germano G, Kavanagh PB, Berman DS. Effect of the number of projections collected on quantitative perfusion and left ventricular ejection fraction measurements from gated myocardial perfusion single-photon emission computed tomographic images. Journal of Nuclear Cardiology 1996;3(5):395–402.
43. Richardson R, Thomas F. An adjustable zoom-mode gain control for computerized gamma-camera systems. Journal of Nuclear Medicine 1979;21(8):790–792.
44. Bellina CR, Benassi A, Riva A, Guzzardi R. An electronic "diaphragm" for the gamma camera, with adjustable zooming and offset. Journal of Nuclear Medicine 1984;25(9):1019–1022.
45. Chua T, Kiat H, Germano G, et al. Rapid back to back adenosine stress/rest technetium-99m teboroxime myocardial perfusion SPECT using a triple-detector camera. Journal of Nuclear Medicine 1993;34(9):1485–1493.
46. Berman DS, Kiat H, Friedman JD, et al. Separate acquisition rest thallium-201/stress technetium-99m sestamibi dual-isotope myocardial perfusion single-photon emission computed tomography: a clinical validation study. Journal of the American College of Cardiology 1993;22(5):1455–1464.
47. Mochizuki T, Murase K, Fujiwara Y, Tanada S, Hamamoto K, Tauxe WN. Assessment of systolic thickening with thallium-201 ECG-gated single-photon emission computed tomography: a parameter for local left ventricular function. Journal of Nuclear Medicine 1991;32(8):1496–1500.
48. Maunoury C, Chen CC, Chua KB, Thompson CJ. Quantification of left ventricular function with thallium-201 and technetium-99m-sestamibi myocardial gated SPECT. Journal of Nuclear Medicine 1997;38(6):958–961.
49. Tadamura E, Kudoh T, Motooka M, et al. Assessment of regional and global left ventricular function by reinjection T1-201 and rest Tc-99m sestamibi ECG-gated SPECT: comparison with three-dimensional magnetic resonance imaging. Journal of the American College of Cardiology 1999;33(4):991–997.
50. Bacher-Stier C, Müller S, Pachinger O, et al. Thallium-201 gated single-photon emission tomography for the assessment of left ventricular ejection fraction and regional wall motion abnormalities in comparison with two-dimensional echocardiography. European Journal of Nuclear Medicine 1999;26(12):1533–1540.
51. Manrique A, Koning R, Cribier A, Véra P. Effect of temporal sampling on evaluation of left ventricular ejection fraction by means of thallium-201 gated SPET: comparison of 16- and 8-interval gating, with reference to equilibrium radionuclide angiography. European Journal of Nuclear Medicine 2000;27(6):694–699.
52. Akinboboye O, El-Khoury Coffin L, Sciacca R, Bergmann S, Blood D, King D. Accuracy of gated SPECT thallium left ventricular volumes and ejection fractions: comparison with three-dimensional echocardiography [abstract]. Journal of the American College of Cardiology 1998;31(2, Suppl A):85A.
53. Bateman T, Magalski A, Barnhart C, O'Keefe J, Jones P. Global left ventricular function assessment using gated SPECT-201: comparison with echocardiography [abstract]. Journal of the American College of Cardiology 1998;31(2, Suppl A):441A.
54. Lau YH, Hutton BF, Beekman FJ. Choice of collimator for cardiac SPET when resolution compensation is included in iterative reconstruction. European Journal of Nuclear Medicine 2001;28(1):39–47.
55. Moore SC, Kouris K, Cullum I. Collimator design for single photon emission tomography. European Journal of Nuclear Medicine 1992;19(2):138–150.
56. Gregoriou GK, Tsui BM, Gullberg GT. Effect of truncated projections on defect detection in attenuation-compensated fanbeam cardiac SPECT. Journal of Nuclear Medicine 1998;39(1):166–175.
57. Brooks RA, Di Chiro G. Theory of image reconstruction in computed tomography. Radiology 1975;117(3, Pt 1):561–572.
58. Herman GT, Meyer LB. Algebraic reconstruction techniques can be made computationally efficient (positron emission tomography application). IEEE Transactions on Medical Imaging 1993;12(3):600–609.
59. Germano G. Technical aspects of myocardial SPECT imaging. Journal of Nuclear Medicine 2001;42(10):1499–1507.
60. Vanhove C, Franken PR, Defrise M, Deconinck F, Bossuyt A. Reconstruction of gated myocardial perfusion SPET incorporating temporal information during iterative reconstruction. European Journal of Nuclear Medicine and Molecular Imaging 2002;29(4):465–472.
61. Narayanan MV, King MA, Wernick MN, Byrne CL, Soares EJ, Pretorius PH. Improved image quality and computation reduction in 4-D reconstruction of cardiac-gated SPECT images. IEEE Transactions on Medical Imaging 2000;19(5):423–433.
62. King MA, Schwinger RB, Doherty PW, Penney BC. Two-dimensional filtering of SPECT images using the Metz and

Wiener filters. Journal of Nuclear Medicine 1984;25(11):1234–1240.
63. Cauvin JC, Boire JY, Maublant JC, Bonny JM, Zanca M, Veyre A. Automatic detection of the left ventricular myocardium long axis and center in thallium-201 single photon emission computed tomography. European Journal of Nuclear Medicine 1992;19(12):1032–1037.
64. Germano G, Kavanagh PB, Su HT, et al. Automatic reorientation of three-dimensional, transaxial myocardial perfusion SPECT images [see comments]. Journal of Nuclear Medicine 1995;36(6):1107–1114.
65. Slomka PJ, Hurwitz GA, Stephenson J, Cradduck T. Automated alignment and sizing of myocardial stress and rest scans to three-dimensional normal templates using an image registration algorithm [see comments]. Journal of Nuclear Medicine 1995;36(6):1115–1122.
66. Friedman J, Van Train K, Maddahi J, et al. "Upward creep" of the heart: a frequent source of false-positive reversible defects during thallium-201 stress-redistribution SPECT. Journal of Nuclear Medicine 1989;30(10):1718–1722.
67. Matsumoto N, Berman DS, Kavanagh PB, et al. Quantitative assessment of motion artifacts and validation of a new motion-correction program for myocardial perfusion SPECT. Journal of Nuclear Medicine 2001;42(5):687–694.
68. Sorrell V, Figueroa B, Hansen CL. The "hurricane sign": evidence of patient motion artifact on cardiac single-photon emission computed tomographic imaging. Journal of Nuclear Cardiology 1996;3(1):86–88.
69. Fitzgerald J, Danias PG. Effect of motion on cardiac SPECT imaging: recognition and motion correction. Journal of Nuclear Cardiology 2001;8(6):701–706.
70. Kiat H, Van Train KF, Friedman JD, et al. Quantitative stress-redistribution thallium-201 SPECT using prone imaging: methodologic development and validation. Journal of Nuclear Medicine 1992;33(8):1509–1515.

3 Stress testing and imaging protocols

Sean W. Hayes
Daniel S. Berman
Guido Germano

Introduction and overview

Since the early 1970s, there has been a sustained growth of nearly 15% per year in the field of nuclear cardiology. The widespread clinical acceptance of the method is based on a large body of evidence. Recent ACC/AHA/ACP-ASIM guidelines have revealed an abundance of data on the clinical incremental value of nuclear cardiology procedures [1–4]. Today, state-of-the-art nuclear cardiology allows for the precise measurement of both myocardial function and relative regional perfusion at rest and stress, providing accurate risk assessment in a wider variety of patient subsets. Gated myocardial perfusion SPECT (MPS) now comprises approximately 95% of the procedures in nuclear cardiology. The gated SPECT procedures can be performed with a variety of different stress methods, radiopharmaceuticals, and imaging protocols. This clinically oriented chapter discusses the radiopharmaceuticals, the stress protocols, and the gated SPECT acquisition protocols that are commonly used or considered in the performance of these studies.

Radiopharmaceuticals

The radiopharmaceuticals used for gated MPS share the characteristic that they are accumulated in the myocardium in proportion to regional myocardial blood flow. The concept that coronary artery disease (CAD) can be detected with this approach is based on the ability to detect a reduction in myocardial perfusion in a region supplied by a stenosed vessel compared to a normal region during hyperemia. The relationship between the degree of coronary artery narrowing and the maximal hyperemic response was first elucidated by Gould in 1974 [5]. Resting myocardial perfusion is normal until the luminal diameter narrowing of a coronary artery exceeds 90–95%. With maximal coronary hyperemia produced by dipyridamole, Gould demonstrated a progressive decrease in the hyperemic response associated with increasing degrees of stenosis greater than 50%; this implies that all forms of stress testing will be insensitive for the detection of coronary atherosclerosis until a hemodynamically significant lesion has developed. This hemodynamically significant lesion could be fixed or dynamic, such that spasm or paradoxical vasoconstriction during stress could result in a reduction of peak hyperemic perfusion even in the absence of a fixed greater than 50% stenosis by angiography.

Thallium-201

Thallium-201 is a cyclotron-generated radionuclide with a half-life of 73 hours, which emits gamma rays at 68 to 80 keV (94% abundant) and at 167 keV (10% abundant). Due to its relatively long half-life, the absorbed radiation dose is such that recommended injected doses are limited to 3–4 mCi. On a millicurie basis, approximately 15 times as much radioactivity can be given with Tc-99m agents as with Tl-201, making the latter less, than ideal from the standpoint of radiation exposure to the patient. However, thallium-201 has excellent physiological properties for myocardial perfusion imaging. Importantly, for stress myocardial perfusion scintigraphy, a linear relationship between blood flow and thallium-201 uptake is maintained during exercise up to very high levels of flow (approximately >3 ml/(min g)) where a "roll-off" in uptake occurs [6,7]. After intravenous injection, thallium-201 is rapidly extracted by various organs, roughly in proportion to the distribution of cardiac output [8]. While the initial myocardial distribution of thallium-201 is proportional to regional myocardial blood flow, the equilibrium myocardial distribution of thallium-201 is proportional to the regional potassium pool, reflecting the amount of viable myocardium. Like potassium, thallium-201 is not bound in the myocardial cell, but equilibrates following the same electrochemical gradient as applied to potassium. Following intravenous injection and initial myocardial uptake,

approximately half of the thallium-201 washes out from the normal myocardium over 5–8 hours [9]. Differential washout between hypoperfused but viable myocardium and normal zones and washin to initially hypoperfused zones are the fundamental mechanisms of thallium-201 redistribution.

The principal factor governing the "washout rate" of thallium-201 is the concentration gradient between the myocardial cell and the blood. There is slower blood clearance of thallium-201 following resting or low-level exercise injection. For this reason, diffuse slow washout of thallium, a common measurement when only planar imaging was performed, may be observed in normal patients who do not achieve adequate levels of stress as well as in patients with diffuse ischemia. Typically, redistribution occurs over a few hours, but this process may be delayed. For example, if the thallium-201 blood levels are low, less thallium-201 is available to be delivered to previously ischemic myocardium in the redistribution phase, leading to an underestimation of viable myocardium. Most commonly, low circulating thallium-201 (and potassium) levels occur secondary to elevated plasma insulin levels following a carbohydrate meal [10]. Since hyperinsulinemic states may thus slow redistribution, fasting is recommended prior to and for 4 hours following thallium-201 injection.

The time to completed redistribution of thallium-201, at which true equilibrium concentration is reached, is variable. In 1978, the phenomenon of late redistribution of thallium-201 and an inverse relationship between the degree of coronary stenosis and subsequent redistribution of thallium-201 were reported [11]. Redistribution may occur early in areas with minor stenoses (where hyperemia postexercise would be expected) and may be late in regions with critical stenoses (in which poststress hyperemia would be unlikely and resting hypoperfusion might slow the delivery of thallium-201 to the region) [12].

Technetium-99m sestamibi and tetrofosmin

Technetium-99m (Tc-99m) is produced from a molybdenum-99m generator, has a half-life of 6 hours, and emits monoenergetic gamma rays at 140 keV. With the commonly used tracers Tc-99m sestamibi and Tc-99m tetrofosmin, the whole-body radiation dose is estimated to be 16 mrad/mCi, in contrast to 240 mrad/mCi associated with thallium-201. Due to this more favorable dosimetry, the usual dose of technetium-99m myocardial perfusion imaging agents is in the range of 30 mCi. Technetium-99m sestamibi belongs to a class of compounds called isonitriles and is a complex organic compound that behaves physiologically as a monovalent cation. Following its extraction from the blood, technetium-99m sestamibi is bound by mitochondria so that a limited amount of technetium-99m sestamibi myocardial washout (or washin) occurs over time [13,14]. As with thallium-201, the initial uptake of technetium-99m sestamibi is a function of myocardial perfusion to viable tissue. There is a linear relationship between intravenously injected dose per gram of myocardium and myocardial blood flow, from the very low range up to approximately 2–2.5 ml/(min g), a flow level generally associated with maximal treadmill exercise [15]. However, thallium-201 has a higher myocardial uptake (as measured by the percent injected dose per gram of myocardium) throughout the range of flow, secondary to a higher extraction fraction, than technetium-99m sestamibi (approximately 85% compared to 65%) [16,17]. At very low levels of flow, extraction of these tracers appears to increase, affecting technetium-99m sestamibi more than thallium-201 [18]. Technetium-99m tetrofosmin is the other commonly used myocardial perfusion imaging agent at the present time. Technetium-99m tetrofosmin is extracted by the myocardium and bound in mitochondria in a manner similar to that observed with technetium-99m sestamibi. The extraction fraction of this agent is slightly lower than that of technetium-99m sestamibi [19]. There is also less hepatic uptake with this tracer than with technetium-99m sestamibi, resulting in early, more favorable heart/liver ratios following resting injection [20,21]. The various acquisition protocols recommended for technetium-99m tetrofosmin are essentially the same as those for sestamibi (see below).

At very high levels of flow, with all of the myocardial perfusion tracers, there is a progressive decline in the degree by which the uptake of radioactivity increases as a function of flow. Since pharmacologic stress testing with adenosine or dipyridamole frequently results in flow rates in the range of 4 ml/(min g) [22], on a theoretical basis one would expect that thallium-201, technetium-99m sestamibi, or technetium-99m tetrofosmin would have difficulties in distinguishing myocardial regions in which the flow increased to 3 ml/(min g) from regions in which flow increased to 4 ml/(min g). In other words, all of these tracers may be limited in detecting mild coronary reductions in peak hyperemia that would be expected from mild, but hemodynamically significant, coronary stenoses.

On theoretical grounds, the implications of extraction fraction differences are that thallium-201 could be more effective in defining mild coronary stenosis and may be associated with a "deeper" defect contrast (more count reduction compared to normal) than technetium-99m sestamibi, while technetium-99m sestamibi may show greater defect contrast and greater ability to detect mild coronary stenosis than technetium-99m tetrofosmin [23]. One commonly quoted study demonstrated that the magnitude of stress-induced reversible defects with technetium-99m tetrofosmin was less than that of technetium-99m sestamibi [24], a

finding previously described comparing technetium-99m sestamibi to thallium-201 [25,26]. On the other hand, from a practical standpoint, both the technetium-99m agents provide greater flexibility than thallium-201, since they do not require that imaging commence soon after the stress injection for maximal sensitivity (due to mitochondrial binding). In contrast, with thallium-201, imaging must be performed soon after stress testing, in order to detect mild, reversible defects. Thus, if soft tissue attenuation or patient motion compromises a study, the benefit of repeating the acquisition is questionable with thallium. With technetium-99m sestamibi or tetrofosmin, on the other hand, stress testing and tracer injection could take place at a location remote from the imaging laboratory, and image acquisition can simply be repeated (e.g., in the prone position) when patient motion, soft tissue attenuation, or other artifact is considered to be responsible for the production of a perfusion defect.

Technetium-99m teboroxime

Technetium-99m teboroxime belongs to another class of neutral lipophilic complexes of boronic acid called BATO compounds. Technetium-99m teboroxine has been reported to have a higher extraction fraction than thallium-201. Additionally, it appears that the high extraction fraction with this agent plateaus at a higher flow rate than with other agents [27,28]. These highly desirable extraction characteristics of teboroxime are counterbalanced by prominent back-diffusion, related to its neutral, lipophilic properties and to the fact that this agent is not bound intracellularly; i.e., teboroxime washes out very rapidly from the myocardium [29]. Although the myocardium can be visualized with this tracer for approximately 20 minutes after injection, the kinetic properties of technetium-99m teboroxime require that initial imaging be completed within the first few minutes after tracer injection in order to reflect blood flow distribution at the time of injection. Single-detector SPECT imaging and gated SPECT imaging are essentially not feasible with this agent; however, with multiple-detector systems, rapid SPECT imaging was demonstrated to be feasible [30]. Due to marked and persistent hepatic uptake of this compound, however, approximately 20% of cases have been found to be uninterpretable, even when very early post-injection imaging was performed with a multicrystal camera [30].

Due to the requirement for very rapid imaging, technetium-99m teboroxime is the most technically demanding of the available myocardial perfusion tracers. On the other hand, its excellent extraction and washout kinetics provide opportunities not present with the other agents. The high extraction across the full range of flow suggests the possibility that this tracer would be more sensitive for detecting mild coronary stenoses than the other available perfusion agents. While not currently in clinical use, technetium-99m teboroxime is an FDA approved radiopharmaceutical with characteristics that could be of great clinical importance if methods to image for a very brief time were available.

Acquisition protocols

Thallium-201 "only" protocols

With thallium-201, a variety of SPECT acquisition protocols are available (Fig. 3.1). When thallium-201 alone is employed as the radiopharmaceutical, acquisition protocols use some combination of stress imaging with redistribution and/or reinjection imaging. Kiat et al. demonstrated that 24-hour redistribution was superior to 4-hour redistribution SPECT in prediction of whether stress defects would improve after revascularization [31]. Reinjection thallium SPECT, as initially described, involved obtaining an additional image in patients with nonreversible ("fixed") perfusion defects following reinjection of one-half of the dose used at stress, with imaging performed immediately thereafter [32]. This protocol has been shown to improve detection of viable myocardium over standard stress/4-hour redistribution imaging [33]. Since it requires three image acquisitions and a decision as to whether the reinjection is needed, a two-acquisition sequence with stress and redistribution/reinjection imaging is commonly performed. If with this approach no fixed defects are noted, further imaging is not required. If, on the other hand, following the 4-hour reinjection/redistribution image, fixed defects are

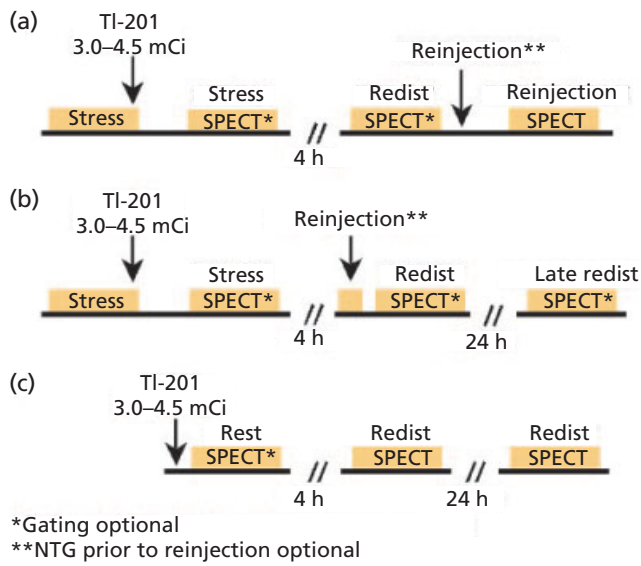

Figure 3.1 Thallium-201 protocols: (a) stress/redistribution (redist), reinjection; (b) stress/reinjection/late redistribution; (c) rest/redistribution.

present, then 24-hour imaging results in a significant improvement in detection of viable myocardium [33]. An alternate protocol that appears to be gaining popularity is to give sublingual nitroglycerin prior to the reinjection of thallium-201. With this approach, the frequency of further improvement at 24-hour imaging may be substantially reduced; i.e., we consider it likely that a stress and nitrate augmented early reinjection protocol will reduce the benefit of, and thus the need for, 24-hour imaging [34]. The other form of thallium-201 imaging in frequent use is the rest/redistribution protocol, considered to be the most effective thallium-201 protocol for the assessment of viable myocardium [35,36]. It has recently been demonstrated with rest injection that 24-hour imaging detects additional regions of myocardial viability compared to 4-hour redistribution imaging alone [37], with a somewhat lower frequency than had been previously shown with exercise injection [38], probably secondary to higher blood levels following resting injection.

From a technical standpoint, several considerations are important. With a thallium-201 only SPECT protocol, all-purpose collimators [39] are commonly employed, although some suggest the use of high-resolution collimators [40,41]. If high-resolution collimators are used, a longer acquisition time would be recommended than for the technetium-99m-based SPECT, so as to provide adequate SPECT count statistics. This lengthening of the acquisition time is particularly important for late redistribution imaging (24-hour), because of the lower count rate due to radioactive decay. In the authors' current 24-hour thallium SPECT protocol, 55 seconds per projection with 32 projections from each detector in a dual-detector system is employed. Clearly, the resultant 30-minute image requires excellent patient cooperation in order to avoid motion artifacts. As noted above, the timing of the initial poststress acquisition is particularly important with thallium-201, since excessive delay could result in decreased sensitivity for detection of CAD, due to early redistribution of the radiopharmaceutical. On the other hand, SPECT acquisition of either thallium-201 or the technetium-99m myocardial perfusion agents should generally not begin less than 10 minutes following exercise injection, owing to the frequent observation of an artifactual perfusion defect due to "upward creep of the heart" [42]. This phenomenon is related to the increased depth of respiration that occurs very early postexercise, which is associated with an average lower position of the diaphragm (and consequently of the heart) in the chest, compared to the normal ventilatory state. This causes the heart to gradually move cephalad during the early portion of SPECT acquisition, resulting in a form of motion artifact in reconstruction. By delaying acquisition until 10–15 minutes after exercise stress, this "upward creep" artifact is avoided. Theoretically, motion correction algorithms could be employed to eliminate the artifact caused by "upward creep," and thus imaging could commence earlier after stress, potentially increasing the frequency of detecting transient, stress-induced wall motion abnormalities in ischemic zones.

Technetium-99m sestamibi or tetrofosmin protocols

Since uptake and radiation dosimetry of these compounds are similar, the recommended acquisition protocols are the same. Due to the absence of clinically significant redistribution, separate rest and stress injections are standard with technetium-99m sestamibi or tetrofosmin SPECT [43,44]. A variety of protocols can be used with these agents, including 2-day stress/rest, same-day rest/stress, same-day stress/rest, and dual isotope. From the standpoint of defect contrast and optimal image quality, the 2-day stress/rest protocol is ideal (Fig. 3.2a). With the 2-day stress/rest protocol, both the stress and rest studies are obtained following the injection of high doses of technetium-99m sestamibi or tetrofosmin, allowing the acquisition of high-quality, high-count images for the accurate assessment of perfusion and function. The principal drawback of this protocol is its requirement for two imaging days, resulting in a delay in the delivery of final information to be used in patient management. The same-day low-dose rest/high-dose stress protocol (Fig. 3.2b) [45], perhaps the most commonly employed technetium-99m sestamibi protocol, has the disadvantage of causing a reduction in stress defect contrast, as approximately 15% of the radioactivity observed at the time of stress imaging comes from

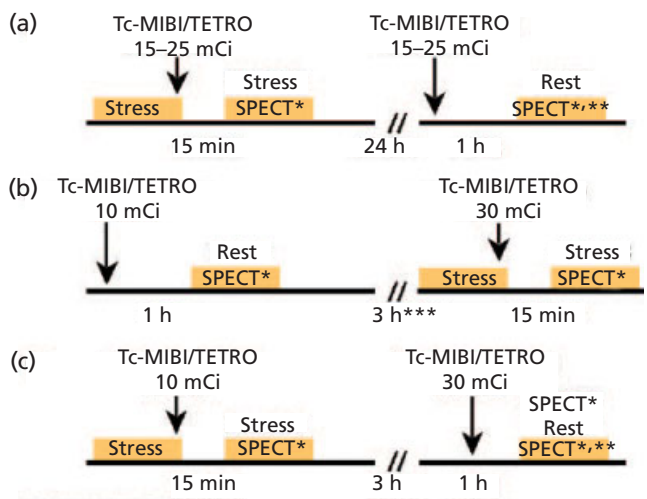

*Gating recommended
**NTG prior to rest injection optional
***Delay time can be reduced by lowering rest dose and increasing stress dose

Figure 3.2 Two-day (a), same-day rest/stress (b), and same-day stress/rest (c), technetium-99m sestamibi or tetrofosmin protocols. Abbreviations: Tc-MIBI/TETRO, technetium-99m sestamibi or tetrofosmin; Tl-201, thallium-201.

the preexisting resting myocardial distribution. The same-day low-dose stress/high-dose rest sequence (Fig. 3.2c) [46,47], on the other hand, has the advantage of requiring image acquisition times essentially identical to those used for thallium-201 imaging, making it easy for a laboratory to alternate between stress/redistribution thallium-201 and stress/rest technetium-99m sestamibi or tetrofosmin protocols. The principal drawback of this approach is that less than ideal count rates are associated with the most important stress image set, and it is difficult to accurately assess defect reversibility [48]. With respect to the assessment of myocardial viability, all stress/rest or rest/stress technetium-99m sestamibi or tetrofosmin imaging protocols have theoretical limitations in separating severely hibernating myocardium from infarction. These constraints do not apply to thallium-201, because of its redistribution properties [49,50]. Viability assessment with technetium-99m sestamibi or tetrofosmin may be improved by the administration of nitroglycerin prior to the rest-injection study [51,52].

Dual-isotope protocols

A common alternative to the standard technetium-99m sestamibi or tetrofosmin protocols is a rest thallium-201/stress technetium-99m sestamibi dual-isotope SPECT. Dual-isotope imaging takes advantage of the Anger camera's ability to collect data in different energy windows. The two fundamental types of dual-isotope protocols are referred to as "simultaneous" or "separate" dual-isotope SPECT (Fig. 3.3).

Simultaneous dual-isotope imaging

Simultaneous dual-isotope imaging (Fig. 3.3a) has many theoretical advantages, compared with conventional stress and rest protocols [50,53]. It halves camera acquisition time and substantially abbreviates the overall study duration for the patient. Furthermore, the inherent registration of stress and rest image sets reduces the frequency of unrecognized artifacts associated with separate stress and rest image acquisitions. This protocol, however, rests on unproven assumptions, the most important being that the effect of radioisotope cross-talk from the higher Tc-99m to the lower Tl-201 energy window is insignificant, or can be accounted for. Kiat et al. demonstrated in a report of patient studies that the downscatter of technetium-99m sestamibi into the thallium-201 acquisition window causes substantial (approximately 20%) reduction in thallium-201 defect contrast, leading to an overestimation of defect reversibility [53]. Interesting data regarding downscatter correction methods have been reported by de Jong et al. [54] as well as by other groups [55]. Also recently, Nakamura et al. had reported excellent clinical results with a simultaneous dual-isotope approach that incorporates a downscatter correction for the technetium-99m into the thallium-201 window [56]. Other authors have reported interesting preliminary data using an approach that markedly reduces the technetium-99m sestamibi dose [57]. This dual-isotope protocol could be performed in the same manner with tetrofosmin as with sestamibi. Until the approaches to downscatter correction are more thoroughly validated clinically, we do not recommend general use of the simultaneous dual-isotope protocol.

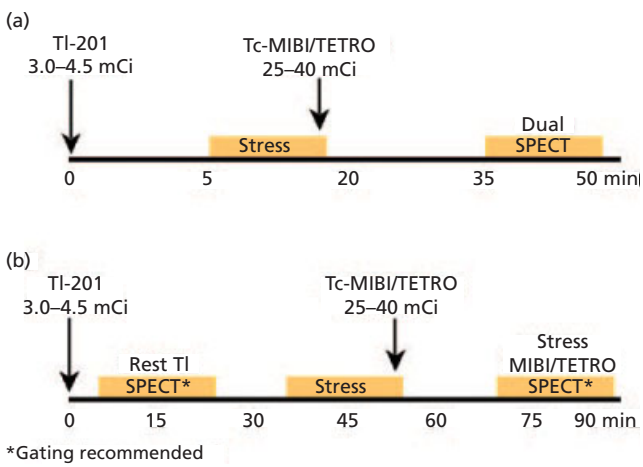

Figure 3.3 Simultaneous (a) and separate acquisition (b) dual-isotope rest thallium-201/stress technetium-99m sestamibi or tetrofosmin SPECT protocols.

Separate dual-isotope imaging

Because of the negligible (2.9%) contribution of thallium-201 into the technetium-99m energy acquisition window [53] and the fact that the thallium-201 image data set is acquired before technetium-99m administration, the separate acquisition approach using rest thallium-201/stress technetium-99m sestamibi or tetrofosmin provides an alternative that does not require correction for cross contamination between the two radioisotopes (Fig. 3.3b). With sestamibi, the sensitivity and specificity of this protocol have been shown to be approximately 90% [58]. Of note, with this protocol, if defects are present on the rest thallium-201 study, redistribution thallium-201 SPECT can be performed before or 24 hours after the technetium-99m sestamibi or tetrofosmin injection (Figs. 3.4 and 3.5).

With the technetium-99m myocardial perfusion imaging agents, the additional ability to perform first pass radionuclide angiography at rest or at peak exercise is present [59]. However, the technique of first pass radionuclide ventriculography as an adjunct to MPS has not become widely utilized due to the expense of the additional equipment needed, the added complexity of routine use of first pass exercise radionuclide ventriculography, and the paucity of data demonstrating the added value of

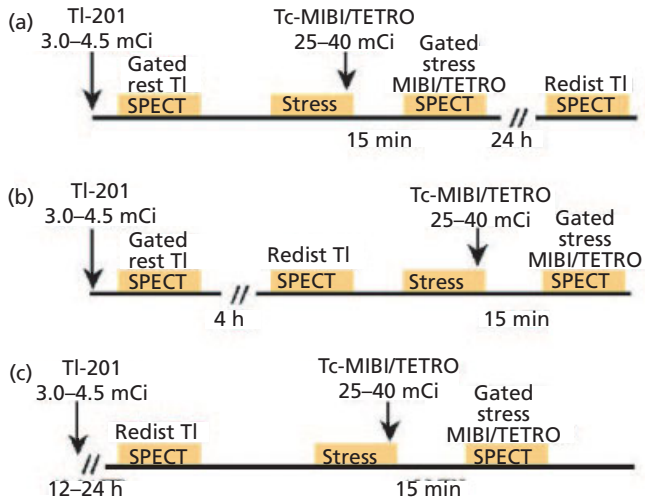

Figure 3.4 Common protocols for combining redistribution thallium-201 imaging with rest thallium-201/stress technetium-99m sestamibi or tetrofosmin SPECT: (a) 24-hour imaging after standard dual-isotope acquisition, (b) 4-hour redistribution imaging prior to stress, and (c) injection the night before with redistribution thallium-201 SPECT as first acquisition sequence.

this approach when ventricular function is measured with gated SPECT.

Gated SPECT

With all of the SPECT protocols, it is currently recommended that ECG gating also be performed [60]. Gating of the poststress acquisition is performed in most laboratories. We and other investigators have also found that there is added value in gating both the rest and the stress acquisitions, providing the added ability to detect poststress stunning from the finding of new region wall motion abnormalities not seen on the resting studies. Gated SPECT can be performed with thallium-201 as well as Tc-99m agents, particularly with multidetector systems. Left ventricular ejection fraction measurement with gated thallium-201 SPECT correlates highly with that of technetium-99m sestamibi SPECT [61]. However, when either thallium-201 or Tc-99m agent acquisitions are performed, the necessity to employ acquisition protocols that provide an adequate total number of myocardial counts in each frame of the gated SPECT study must be emphasized.

Exercise protocols

Exercise stress is the most commonly performed form of stress for MPS. Exercise stress allows assessment of exercise capacity, heart rate and blood pressure responses, and symptoms as well as ST segment response, providing additional clinical information that can be useful in daily clinical decision making. For exercise nuclear imaging, (1) an indwelling intravenous line for injection of the tracer at peak exercise must be inserted prior to stress, (2) injection of the tracer should be performed at maximal stress, and (3) exercise should continue for an additional minute to allow optimal myocardial tracer concentration. For the technetium-99m perfusion tracers, due to the slower blood clearance than thallium-201, we have recommended additional exercise at a lesser workload for an additional 2 minutes.

For patients undergoing treadmill exercise stress, although most are symptom-limited studies, achieving 85% of the maximum predicted heart rate (220 – age) has been the traditional cutoff for an acceptable level of stress. Recently, chronotropic incompetence defined as a low percent of heart rate (HR) reserve achieved equal to (peak HR − rest HR)/(220 − age − rest HR) × 100, with less than 80% considered abnormal, has been shown to be a powerful predictor of cardiac death and all-cause mortality in patients undergoing exercise MPS [62,63]. In a study by Azarbal et al. in 10,021 patients undergoing exercise MPS, the inability to achieve 80% of heart rate reserve was a more powerful predictor of cardiac death than failure to reach 85% of maximal predicted heart rate, and identified more high-risk patients (29.5% vs. 13.3% of patient population) [63]. Even with mild to moderate perfusion defects, patients achieving greater than 80% of heart rate reserve were very low risk for cardiac death. Also, patients with normal MPS but abnormal heart rate reserve achieved were at just as high a risk for overall mortality as patients with abnormal MPS but normal heart rate reserve achieved. Thus, physicians should not be misled that patients with normal stress MPS in the setting of an abnormal heart rate reserve are a low-risk group – they are at substantial risk. These considerations illustrate how the prognostic information of the exercise stress test itself needs to be integrated with the nuclear findings and is a benefit of performing exercise stress over pharmacologic stress, as also discussed in Chapters 6 and 8. It has been suggested that when assessing heart rate response to exercise, the heart rate reserve approach should be used and should replace the traditional percent of age-predicted heart rate achieved [64].

Our current routine clinical protocol is shown in Fig. 3.6. Poststress imaging routinely commences 15 minutes after stress, but because of the absence of significant redistribution can begin hours after stress injection. The advantage of starting imaging earlier is that it increases the opportunity to observe stress-induced stunning during gated SPECT acquisition.

Withholding antiischemic medications

The primary goals of stress MPS are to detect and risk-stratify patients with known or suspected CAD. The ability

of SPECT to reach these goals is related to the estimation of the proportion of the supplied by vessels with hemodynamically significant stenoses. To this end, it is important that the patient achieve an adequate level of stress during the exercise procedure. Patients under the influence of β-blockers or calcium-channel blockers often fail to reach an adequate level of stress during exercise. For this reason, recent guidelines have suggested that patients should be off antianginal medications at the time of testing. In this regard, we recommend withholding β-blockers and calcium blockers for 4–5 half-lives (e.g., 36–48 h) before testing [65], and long-acting nitrates on the day of the study. As with exercise, when the goal is to evaluate the effectiveness of medical therapy or to assess the amount of ischemia on treatment, the patient is not withdrawn from these medications. These recommendations have been incorporated into the recent ACC/AHA/ASNC guidelines [1].

Pharmacologic stress protocols

For patients who cannot achieve an adequate level of stress, pharmacologic stress testing is generally performed. The frequency of pharmacologic testing is increasing, and is currently over one-third of myocardial

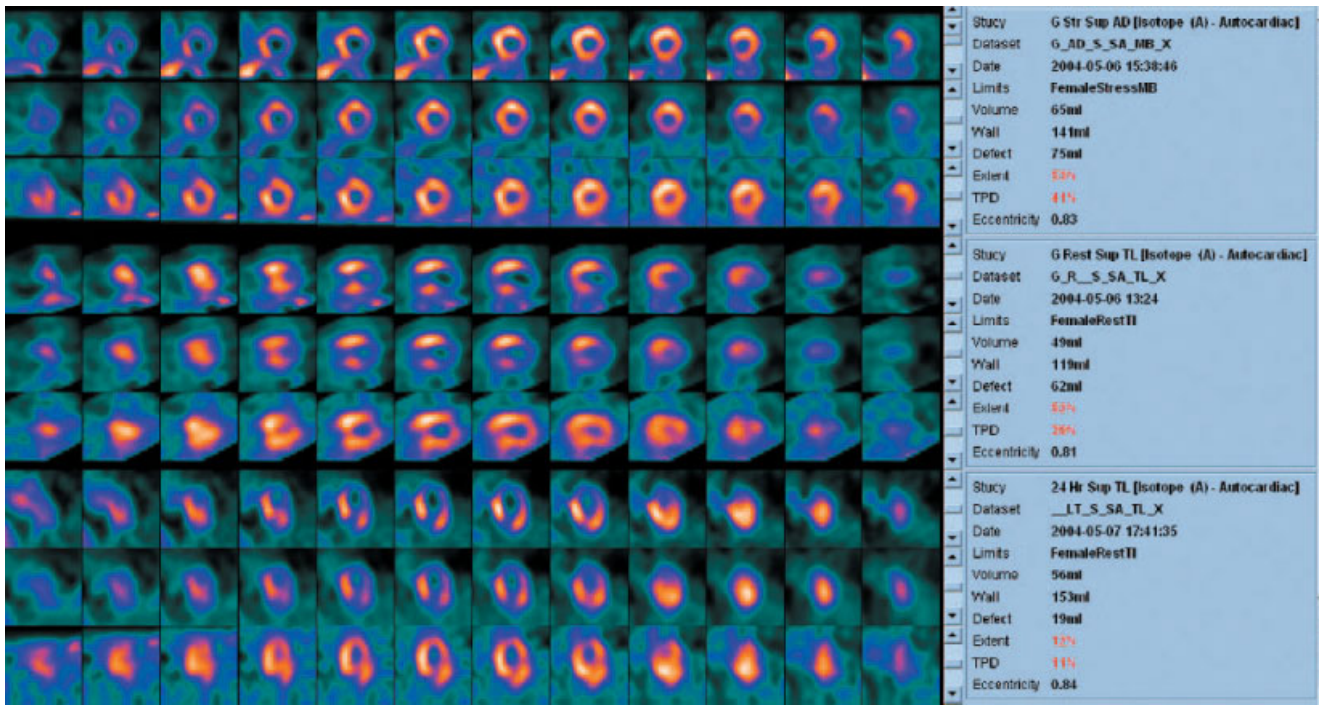

(a)

Figure 3.5 (a) Adenosine stress technetium-99m sestamibi (top), rest thallium-201 (middle), and 24-hour thallium-201 (bottom) SPECT images in a patient with a small acute myocardial infarction with a serum troponin of 6. Given the large fixed perfusion defects in the left anterior descending (LAD) coronary artery territory on rest/stress imaging in the setting of only a small cardiac enzyme leak, 24-hour redistribution imaging was requested. The 24-hour images demonstrate extensive reversibility, consistent with severe resting ischemia (hibernating myocardium) in the LAD distribution. Initial coronary angiography demonstrated a 40% stenosis (by visual inspection) in the proximal LAD, but correlation with the nuclear results led to repeat angiography with intravascular ultrasound, which demonstrated a proximal LAD 80% stenosis. (b) Quantitative perfusion analysis of the rest and stress SPECT images in part (a). The middle column shows the two-dimensional quantitative display of stress defect extent (top), rest defect extent (middle), and defect reversibility (bottom). The right column illustrates the three-dimensional quantitative display. The black regions in the top and middle panels indicate the perfusion defect extent, and the white region in the bottom panel indicates the perfusion defect reversibility. The far-right column indicates quantitative values showing stress defect extent of 53% and rest defect extent of 52%. Additionally, computer derived, visually verified 17-segment scores are illustrated in the lower right. The scores indicate stress (Str), rest (Rst), and reversibility (Rev) values. The summed stress score (SSS) is 21, the summed rest score (SRS) is 21, and the summed difference score (SDS) is 0. The rest/stress images indicate the presence of a large nonreversible defect of the entire distal left ventricle. (c) Quantitative perfusion SPECT display of the rest and 24-hour (late) redistribution thallium images from the same patient illustrated in parts (b) and (c). Note that by 24-hour imaging, the perfusion defect has become mostly reversible with a summed rest score (SRS) of 21, a summed late score (SLS) of 7, and a summed rest-late difference score (SDS) of 14. Quantitative analysis confirms the visual observation of extensive defect reversibility by 24-hour redistribution thallium-201 imaging. The findings suggest severe resting ischemia (hibernating myocardium) in the left anterior descending coronary artery territory.

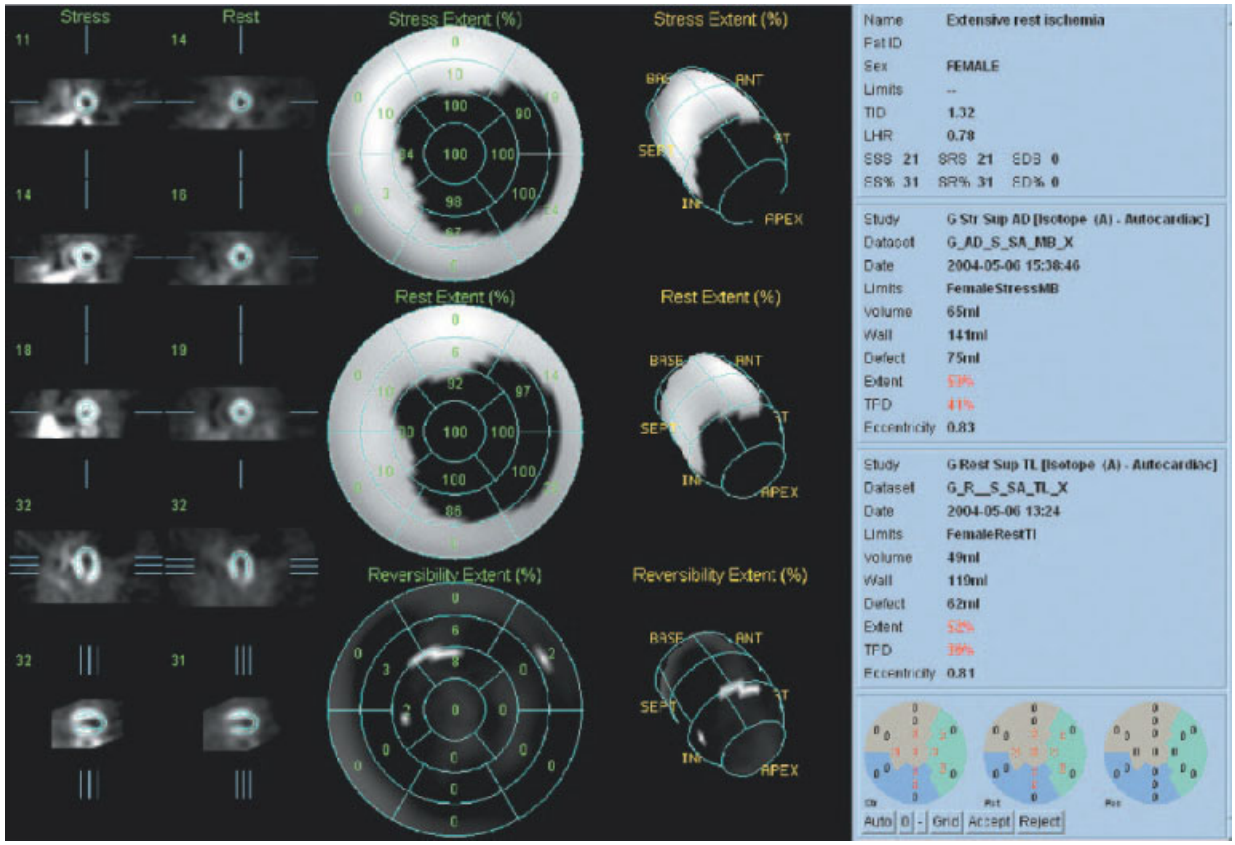

(b)

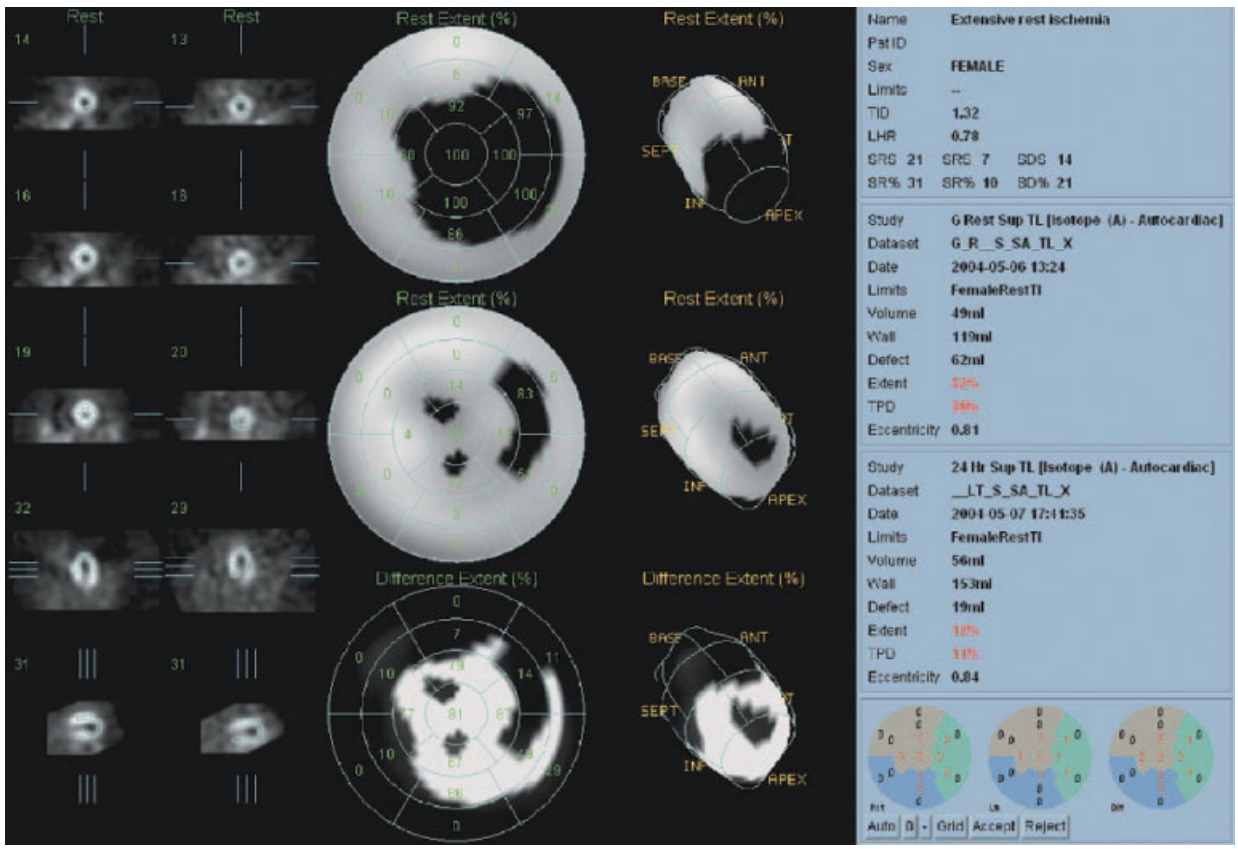

(c)

Figure 3.5 (*Continued*)

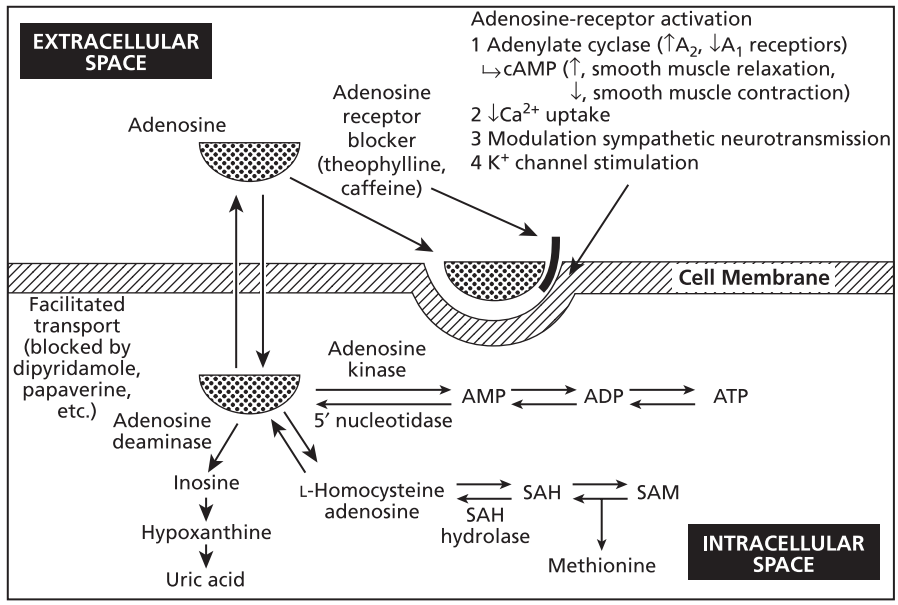

Figure 3.6 Adenosine production, transport, receptor activation, and metabolism. (Reproduced with permission from [66].)

perfusion scintigraphy, and in our laboratories, performing both in-patient and out-patient studies now constitute over 50% of the stress procedures for use with gated SPECT.

Vasodilator stress

The preferred form of pharmacologic stress for MPS is the use of coronary vasodilators – dipyridamole or adenosine. The action mechanism of these agents is shown in Fig. 3.7 [66]. Dipyridamole blocks the cellular reuptake of adenosine, increasing the extracellular adenosine concentration. Increased extracellular adenosine, either with adenosine infusion or with dipyridamole, causes coronary vasodilation. In CAD, the agents generally produce a perfusion heterogeneity without ischemia, but in the presence of severe CAD, ischemia may occur, often associated with a coronary steal [67].

Figure 3.8 illustrates the comparative effects of the vasodilators, exercise, and dobutamine [68].

In general, diagnostic accuracy for myocardial perfusion scintigraphy using pharmacologic stress is equivalent to exercise, despite the observation that vasodilators increase coronary flow to a greater degree than exercise [69]. The failure of vasodilator stress to increase the sensitivity of MPS for coronary disease detection over exercise may be due to a variety of factors. As described above, the "roll-off" in tracer uptake at high coronary flow rates results in the failure of available radiopharmaceuticals to differentiate the fourfold increase in flow associated with vasodilator stress from the threefold increases in coronary flow associated with exercise. With vasodilator stress, ischemia (as opposed to flow heterogeneity) is less commonly

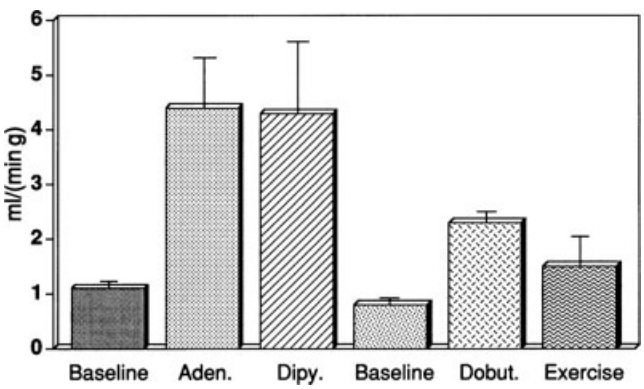

Figure 3.7 Coronary blood flow at baseline, exercise, dobutamine (Dobut.), adenosine (Aden.), and dipyridamole (Dipy.) stress measured with ^{13}N-labeled ammonia. Baseline results are listed twice because of slight differences in absolute results. (Reproduced with permission from [68].)

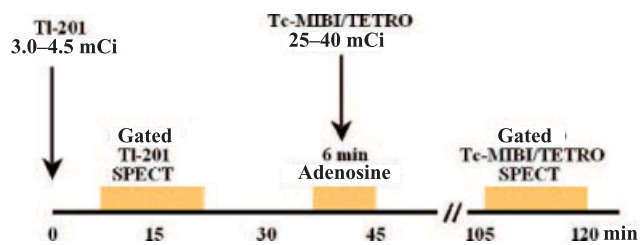

Figure 3.8 A standard separate acquisition rest thallium-201/adenosine stress technetium-99m sestamibi or tetrofosmin SPECT acquisition protocol. Abbreviations: Tc-MIBI/TETRO, technetium-99m sestamibi or tetrofosmin; Tl-201, thallium-201.

produced, due to the far lower myocardial oxygen demands associated with vasodilator stress compared to exercise. The possibility that the extraction fraction of radiotracers might be lower with vasodilator stress compared to exercise has also been suggested.

Withholding of caffeine

Methylxanthines, such as theophylline or caffeine, compete for the adenosine receptors, blocking adenosine binding and potentially eliminating the effects of dipyridamole or adenosine on coronary vasodilation. Since the half-life of caffeine is variable [70], with either dipyridamole or adenosine stress, it has been recommended that the patients be off caffeine-containing compounds for 24 hours prior to imaging. There is currently no effective means of identifying patients in whom the pharmacologic effects of adenosine or dipyridamole have been blocked by caffeine, since, in contrast to exercise, the heart rate or blood pressure response does not provide accurate information regarding response [71].

Antianginal medications prior to vasodilator stress

Traditionally, antianginal medications have not been withheld prior to stress testing with vasodilator agents to the extent they have been prior to exercise stress. However, data from several manuscripts suggest that the practice of withholding medications could improve the diagnostic yield. In a small clinical study, Sharir et al. demonstrated, however, that continued use of antianginal drugs (predominantly calcium-channel blockers and nitrates) prior to dipyridamole with low-level treadmill exercise thallium-201 MPS significantly reduced the extent and severity of perfusion defects, resulting in underestimated CAD [72]. Recently, β-blockers have also been shown to reduce the extent and severity of myocardial perfusion defects with dipyridamole technetium-99m sestamibi SPECT imaging [73]. In this study, patients underwent rest technetium-99m sestamibi MPS as well as three dipyridamole technetium-99m sestamibi MPS studies (after placebo, low-dose metoprolol (up to 10 mg), and high-dose metoprolol (up to 20 mg)). Sensitivity for detection of angiographic CAD was 85.7% with placebo versus 71.4% with low- and high-dose metoprolol. In comparison with placebo, the summed stress score, a marker of the extent and severity of the stress perfusion defects, was significantly lower ($p < 0.05$) with low- and high-dose metoprolol (12.0 ± 10.1 vs. 8.7 ± 9.0 and 9.3 ± 10.6, respectively). The summed difference score, a measure of the extent and severity of ischemia, also was significantly lower (8.4 ± 8.8 with placebo vs. 5.0 ± 6.7 ($p < 0.001$) and 5.4 ± 7.9 ($p < 0.01$) with low- and high-dose metoprolol, respectively).

Thus, in patients referred for vasodilator stress for diagnostic purposes, if the referring physician considers it safe to do so, we recommend withholding β-blockers and calcium blockers for 4–5 half-lives (e.g., 36–48 h) before testing [65], and long-acting nitrates on the day of the study. As with exercise, when the goal is to evaluate the effectiveness of medical therapy, stress testing is performed without taking the patient off medications.

Vasodilator stress protocols

Dipyridamole

Dipyridamole is usually infused at 0.142 mg/(kg min) for 4 minutes, although some investigators have recommended increasing the dose by 50% [74]. The maximal effect occurs approximately 3–4 minutes after termination of the infusion. Side effects are common and include nonspecific chest pain, shortness of breath, dizziness, and flushing. Death as a side effect is very rare, being noted in 1/10,000 in the largest study to date [75]. The side effects can usually be reversed by intravenous administration of aminophylline, usually 75–125 mg, although additional administration of nitroglycerin may occasionally be needed. Due to the potential side effect of severe bronchospasm, dipyridamole is contraindicated for patients with asthma.

Adenosine

Adenosine is infused intravenously, usually at a dose of 140 μg/(kg min) over 4–6 minutes, with administration of the radiopharmaceutical at 2 minutes with 4- or 5-minute infusions and at 3 minutes with the 6-minute infusion [76,77]. The dual-isotope adenosine stress protocol we currently employ is shown in Fig. 3.9. Minor and transient side effects occur more frequently with adenosine to those of dipyridamole. With adenosine, there is an increased incidence of advanced heart block. As the half-life of adenosine is very short (several seconds), side effects usually remit within 30–45 seconds of termination of the infusion. Aminophylline reversal is not required. Adenosine is considered contraindicated for patients with ≥1st-degree AV block, sick sinus syndrome, or for those

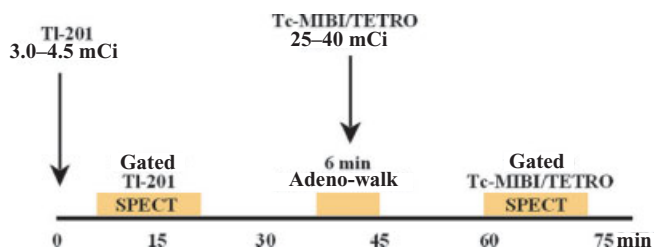

Figure 3.9 Combined low-level exercise/adenosine ("adeno-walk") dual-isotope SPECT acquisition protocol. Abbreviations: Adeno, adenosine; Tc-MIBI/TETRO, technetium-99m sestamibi or tetrofosmin; Tl-201, thallium-201.

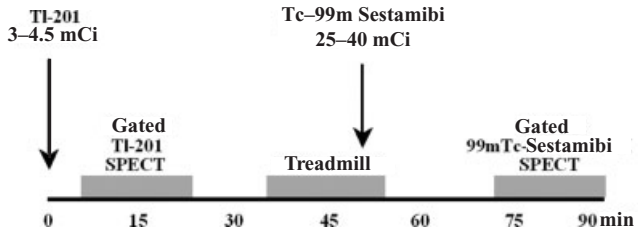

Figure 3.10 Separate acquisition rest thallium-201/exercise technetium-99m sestamibi dual-isotope MPS protocol.

with bronchospasm and in patients who are taking dipyridamole orally.

Vasodilator stress with low-level exercise

It has become increasingly common to combine vasodilator stress with low-level exercise (Fig. 3.10) [78]. This is generally accomplished by beginning exercise at the beginning of adenosine infusion or at the end of a dipyridamole infusion. The low-level exercise reduces splanchnic blood flow and thereby hepatic uptake of technetium-99m sestamibi or tetrofosmin, facilitating early postinfusion imaging with these tracers (as early as 15 minutes following injection) [79], compared to the 1-hour delay required when adjunctive exercise is not performed. Another key benefit is a marked reduction in the frequency as well as in the severity of side effects from the vasodilator stress agents, possibly due to the increased attention to the "task" of walking in these patients who usually cannot perform maximal exercise. There may be a slightly higher incidence of ischemia with combined exercise and pharmacologic stress, potentially adding to the diagnostic sensitivity of this study [80], through the mechanism of increasing regional wall motion abnormalities as discussed for exercise above. Being able to perform low-level exercise also provides additional prognostic information (Hach 2005 adenoscore). Given all of these advantages (and no perceived disadvantages), we perform the "adeno-walk" protocol with all adenosine infusions when possible, with the exception of patients with left bundle branch block or paced rhythm in whom it is preferable not to have the increased heart rate associated with exercise.

Some investigators have suggested that it would be desirable to have the patient exercising at his or her maximal capacity at the time of the injection of radioactivity – that time being determined by the peak effect of the vasodilator being used (in the middle of the adenosine infusion, 4 minutes following dipyridamole infusion). In addition to allowing quicker acquisition poststress, this approach has the advantages of inducing a greater degree of ischemia (potentially enhancing perfusion defect severity), decreasing noncardiac side effects due to the vasodilator, and providing some information about the patient's exercise tolerance. This maximal exercise/adenosine stress protocol is of potential interest but is not considered routine in most laboratories at the present time.

A2a agonists

There are three A2a agonists currently being evaluated for use as vasodilator stress agents. In general, these more specific agents are considered likely to result in a lower frequency of side effects and can be administered as a bolus rather than with an infusion. Although the agents potentially may be used even in patients with bronchospasm, this has not yet been studied.

Dobutamine stress

An alternative to vasodilator stress is inotropic stress, usually performed with dobutamine [81,82]. At present, dobutamine stress is usually utilized for patients with asthma or those with recent caffeine ingestion. Dobutamine stress is associated with a lower rate pressure product and a lower degree of hyperemia in the myocardial bed than with exercise (Fig. 3.8) [68,83]. Side effects are common, but are similar in frequency to what is observed with exercise and less frequent than with adenosine. The most common side effects are chest discomfort, palpitations, and shortness of breath. Hypotension or hypertension can also occur. Due to the strong catecholamine stimulation, premature ventricular complexes(PVCs) are common; however, serious arrhythmias or other side effects are rare [84]. The effects of dobutamine begin to wear off approximately 2 minutes after termination of the infusion, and seldom require reversal with intravenous administration of a rapid-acting β-blocker (e.g., metaprolol, esmolol).

Optimizing stress protocols

One of the fundamental advantages of MPS is its ability to obtain diagnostic studies in virtually all patients. To this end, appropriate patient preparation is necessary. We ask that all of our patients referred for either exercise or pharmacologic stress testing be off caffeine-containing compounds for 24 hours prior to testing. This gives us the flexibility to refrain from injecting the stress radiopharmaceutical when an inadequate response to exercise stress testing is observed, quickly substituting pharmacologic for exercise stress. In order to derive optimal diagnostic and prognostic information from a study, it is important that a maximal hyperemic state be achieved with MPS. For this reason, we have recommended that stress tests only be considered adequate if the heart rate achieved during exercise is concordant with a maximal exercise stimulus. For practical purposes, we have defined this level as 85% of the maximal predicted heart rate (220 – age). In order to maximize the opportunity to achieve greater than 85%

of the maximal predicted heart rate, we recommend that patients be taken off β-blockers for 48 hours (or at least 24 hours) prior to testing. This recommendation is accompanied by a recommendation from the referring physician not to exercise, between the time at which medications are stopped and that of the test. Patients should be fasting for 4 hours prior to testing. If patients fail to achieve greater than 85% of the maximal predicted heart rate, develop severe chest pain, or have greater than 2 mm of ST depression in the setting of a normal resting ECG, the stress radiopharmaceutical would not be injected and the study would be immediately converted to a vasodilator stress study. For patients scheduled for exercise SPECT, caffeine and caffeine-containing compounds should not be ingested for 24 hours prior to testing. Thus, if a patient fails to achieve 85% of the maximal predicted heart rate, the radioactive tracer should not be injected. Rather, pharmacologic stress with adenosine or dipyridamole should be immediately substituted, allowing for diagnostic test results.

In summary, we now recommend using the same set of instructions for all patients, regardless of whether they are scheduled for exercise or pharmacologic stress MPS. Thus all patients should be caffeine-free, allowing for immediate conversion from exercise to vasodilator stress, and all patients should be off antianginal medications if the referring physician feels it is safe to do so, giving the highest sensitivity for CAD detection in patients undergoing either exercise or pharmacologic stress MPS. Occasionally, referring physicians intentionally decide to test patients on their antianginal medications for purposes of risk stratification.

Left bundle branch block and right ventricular pacing

Patients with left bundle branch block may frequently demonstrate reversible defects in the septal wall in the absence of CAD [85]. The mechanism has been postulated to be a true septal ischemia that occurs in left bundle branch block in the presence of marked tachycardia. In a dog model comparing right ventricular pacing (mimicking left bundle branch block) to right atrial pacing, Hirzel et al. demonstrated with both microspheres and thallium-201 decreased septal uptake during tachycardia in right ventricular, but not in right atrial pacing. A recent clinical study has suggested that this perfusion defect indicates a true decrease in flow resulting from an increase in early diastolic compressive resistance, in turn caused by delayed ventricular relaxation [86]. In view of this pathophysiology, stress techniques that do not increase heart rate as markedly as exercise are preferred in left bundle branch block; i.e., adenosine or dipyridamole testing without walking is generally considered preferable in patients with left bundle branch block [87,88]. Matzer et al. demonstrated that the perfusion defect associated with left bundle branch block in the absence of left anterior descending CAD most commonly involves the interventricular septum with sparing of the apex of the left ventricular, a pattern which would be uncommon for left anterior descending CAD [89]. Recently, myocardial perfusion defects in the inferior and apical walls have also been reported in the absence of CAD in patients with prolonged right ventricular pacing [90]. Because of the relationship between the increase in heart rate and the presence of perfusion defects without CAD in left bundle branch block and paced ventricular rhythms, vasodilator stress is preferred over exercise in these patients (Class I indication in the recent guidelines) and the vasodilator stress protocols are performed without adjunctive low-level exercise [1].

Aortic stenosis

Exercise stress testing is generally not recommended in patients with significant aortic stenosis due to safety concerns. Although exercise testing is generally safe in asymptomatic patients [91,92], studies have shown low specificity with myocardial perfusion imaging for the diagnosis of CAD. Vasodilator stress has been reported to be effective in aortic stenosis patients. In a study of 35 patients with moderate to severe aortic stenosis, Samuels et al. demonstrated that adenosine stress MPS with a 6-minute infusion protocol was well tolerated [93]. In the 20 patients undergoing coronary angiography, the sensitivity for detection of CAD was 92% and the specificity was 71%. Although this small study did include some patients with severe aortic stenosis, in patients with critical aortic stenosis any form of stress testing (exercise, vasodilator, dobutamine) is considered contraindicated. CT coronary angiography may become increasingly used as an alternative to invasive angiography in the critical aortic stenosis patient.

Cedars-Sinai dual-isotope protocol

Our current routine clinical protocol is shown in Figs. 3.6, 3.9, and 3.10. For the separate acquisition study, a standard weight-adjusted dose of 3–4.5 mCi of thallium-201 is injected intravenously at rest. Rest thallium-201 SPECT is begun 5 minutes after injection. Immediately following thallium-201 SPECT, the patient is prepared for treadmill exercise. At near-maximal exercise, a weight-adjusted dose of 25–40 mCi of technetium-99m sestamibi is injected. (See Table 2.3 in Chapter 2 for a list of rest and stress weight-adjusted doses.) The patient then exercises for 1 minute at maximal workload, and for an additional 2 minutes at one stage lower. Technetium-99m sestamibi SPECT is begun 15 minutes after injection. Both the rest thallium-201 and stress technetium-99m sestamibi

acquisitions use a high-resolution collimator, 180° acquisition over 64 projections, and 25–45 seconds per projection. Female patients are imaged with their bra off and with the breasts in a natural-dependent position, for both rest and stress imaging. In thallium-201 SPECT imaging, two energy windows are used: a 30% symmetric window for the 68–80-keV photopeak, and a 20% window for the 167-keV photopeak. For technetium-99m sestamibi SPECT, a 15% window centered on the 140-keV peak is used (this window is narrower than that used with other technetium-99m sestamibi protocols, in order to reduce scatter from thallium-201). With the separate acquisition dual-isotope protocol, completion of the entire procedure is possible in less than 2 hours. Chapter 2 has a detailed discussion of the technical aspects of image acquisition. An example of a normal study is shown in Fig. 3.11. A study demonstrating extensive perfusion defects is shown in Fig. 3.12.

One advantage of a rest/stress protocol is that the rest perfusion can be evaluated prior to stress testing, just as the rest ECG is evaluated for acute changes prior to stress treadmill testing. Aboul-Enein et al. recently reported on 139 patients (rest group) at our institution who had no history of myocardial infarction or coronary artery bypass surgery and were referred for stress MPS but whose stress test was canceled due to unexpected resting perfusion defects (summed rest score $\geq$4) [94]. Of these, 60 patients (43.2%) were referred for angiography after MPS (6.0 ± 11.5 days). Angiographic referral rates and results were compared to those of a diagnostic population ($n = 3565$) who demonstrated stress-induced perfusion defects (summed stress score $\geq$4) (stress group) on rest/stress MPS. The frequency of referral for angiography was higher in the rest group (43.2% vs. 19.8%, $p < 0.0001$). Also, the rest group more frequently had significant CAD ($\geq$70% stenosis) (95% vs. 80%, $p = 0.008$) and critical CAD ($\geq$90% stenosis) (80% vs. 66%, $p = 0.038$). Thus the rest/stress sequence for MPS enables the identification of patients with unexpected rest perfusion defects, usually secondary to critical CAD, in whom unnecessary stress testing can be avoided. An example of a patient with

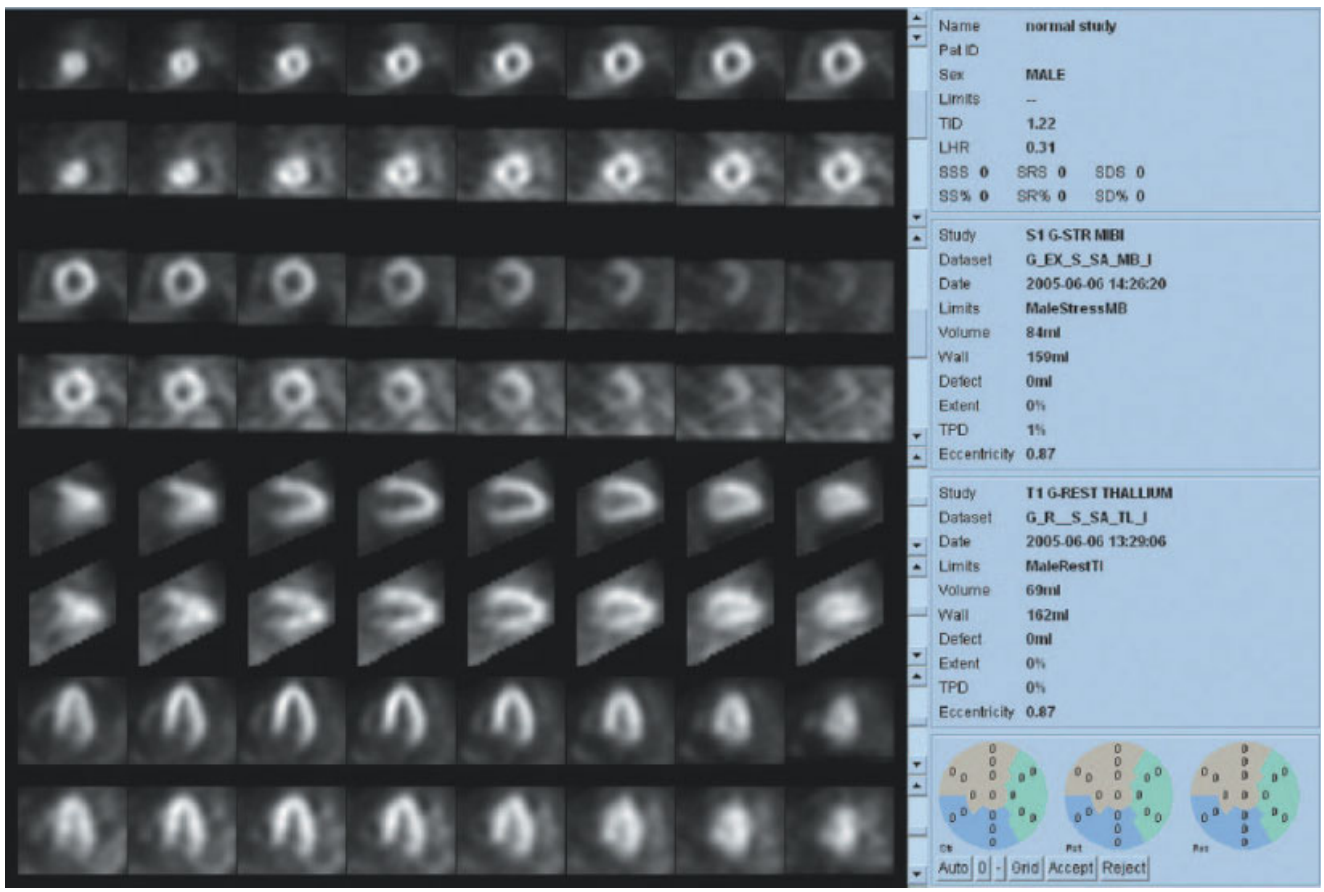

(a)

Figure 3.11 Normal exercise stress technetium-99m sestamibi and rest thallium-201 MPS images (a) and quantitative perfusion analysis (b) using the dual-isotope protocol.

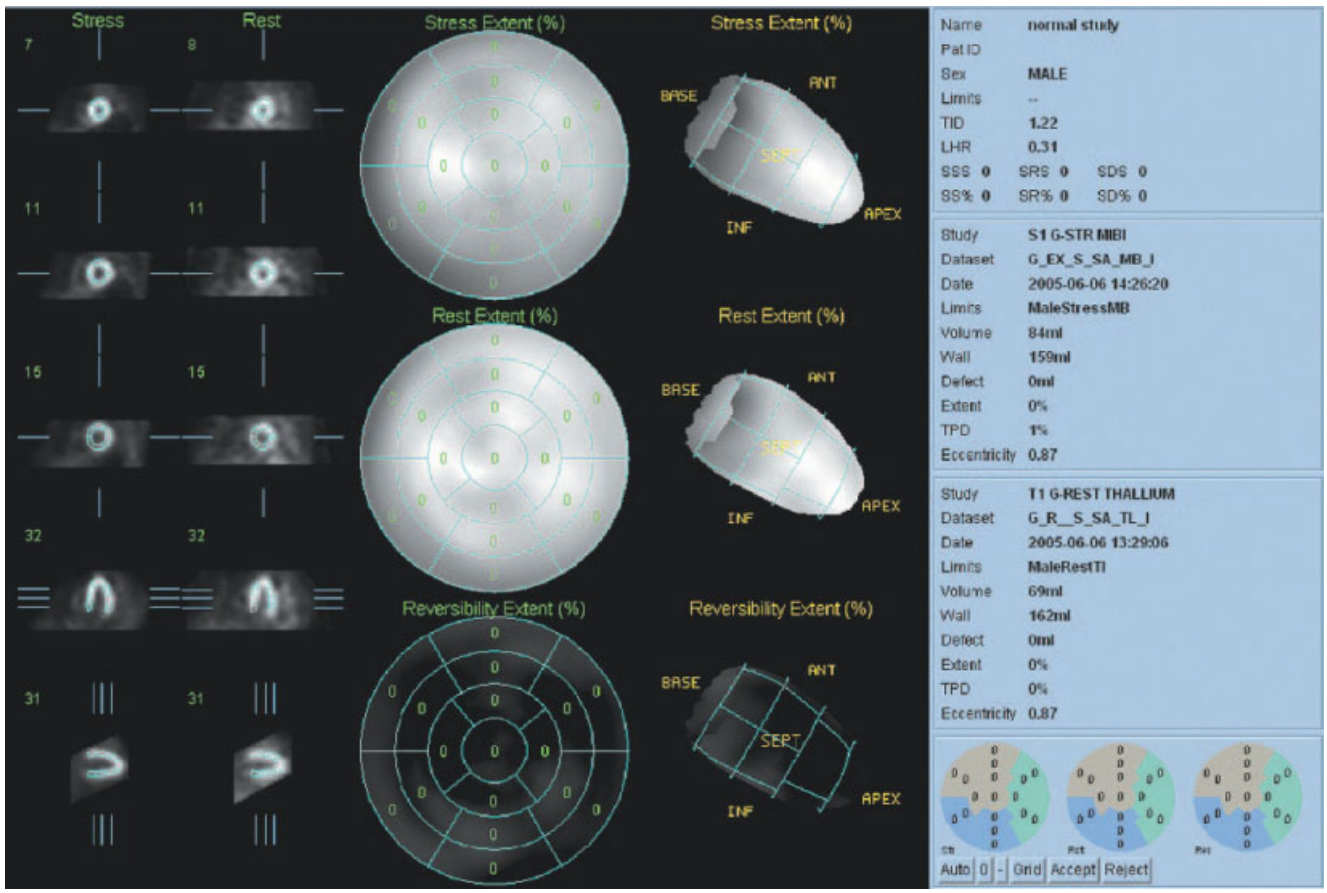

(b)

Figure 3.11 (*Continued*)

an unexpected resting perfusion defect leading to cancellation of the stress study is shown in Fig. 3.13.

Another advantage of the dual-isotope approach over standard rest/stress technetium-99m sestamibi approaches relates to the use of thallium-201 for the evaluation of defect reversibility in patients with resting thallium-201 defects [35,49]. This advantage derives from the redistribution of thallium-201 into areas of ischemic but viable myocardium. Patients with resting thallium-201 defects can be brought back for 24-hour imaging the next day [12], or a rest/redistribution study can be completed before the stress technetium-99m sestamibi injection (Fig. 3.4). At 24-hour, the contribution of technetium into the thallium-201 window would be minimal since only one-sixteenth of the injected technetium-99m sestamibi (half-life = 6 h) dose would remain due to physical decay, compared to a much higher proportion of thallium-201 (half-life = 73 h), and some of the technetium-99m would have washed out from the myocardium [21].

Incorporation of 24-hour rest/redistribution thallium-201 scintigraphy into the dual-isotope protocol provides the detection of an additional 8–15% of reversible segments, which would go undetected by rest scintigraphy alone [37]. Our protocol for late redistribution imaging is illustrated in Fig. 3.4A, and a patient with late reversibility identified by this approach and undetected by rest/stress imaging is shown in Fig. 3.5.

Prone imaging

One of the most difficult areas of interpretation of MPS is the differentiation of decreases in apparent myocardial tracer distribution that are artifactual (and due to attenuation) from those due to true hypoperfusion. Gated SPECT is frequently useful in making this distinction. The problem with relying on gated SPECT alone for this purpose, however, is that true myocardial perfusion defects due to subendocardial infarction, associated with a normal contraction pattern, could be falsely attributed to attenuation. We [95] and others [96,97] have previously shown that prone imaging decreases the frequency of attenuation artifacts in the inferior wall, and also decreases motion artifact.

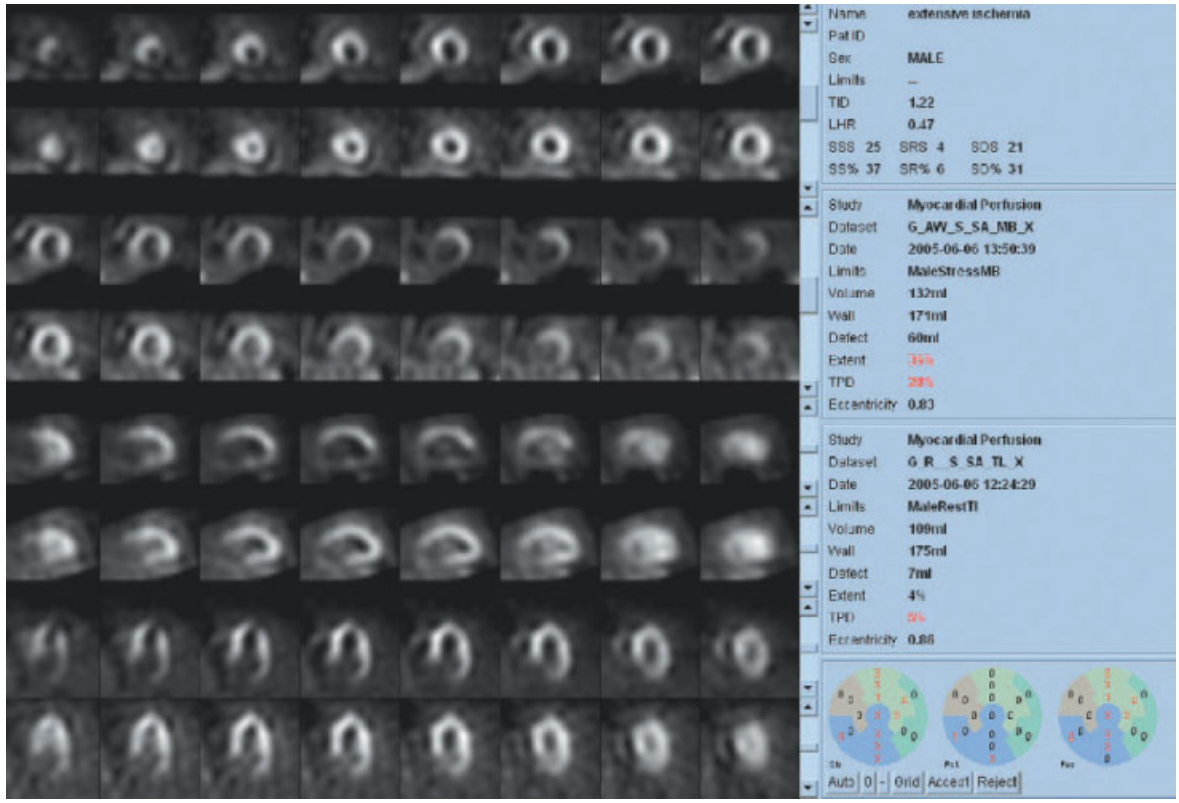

(a)

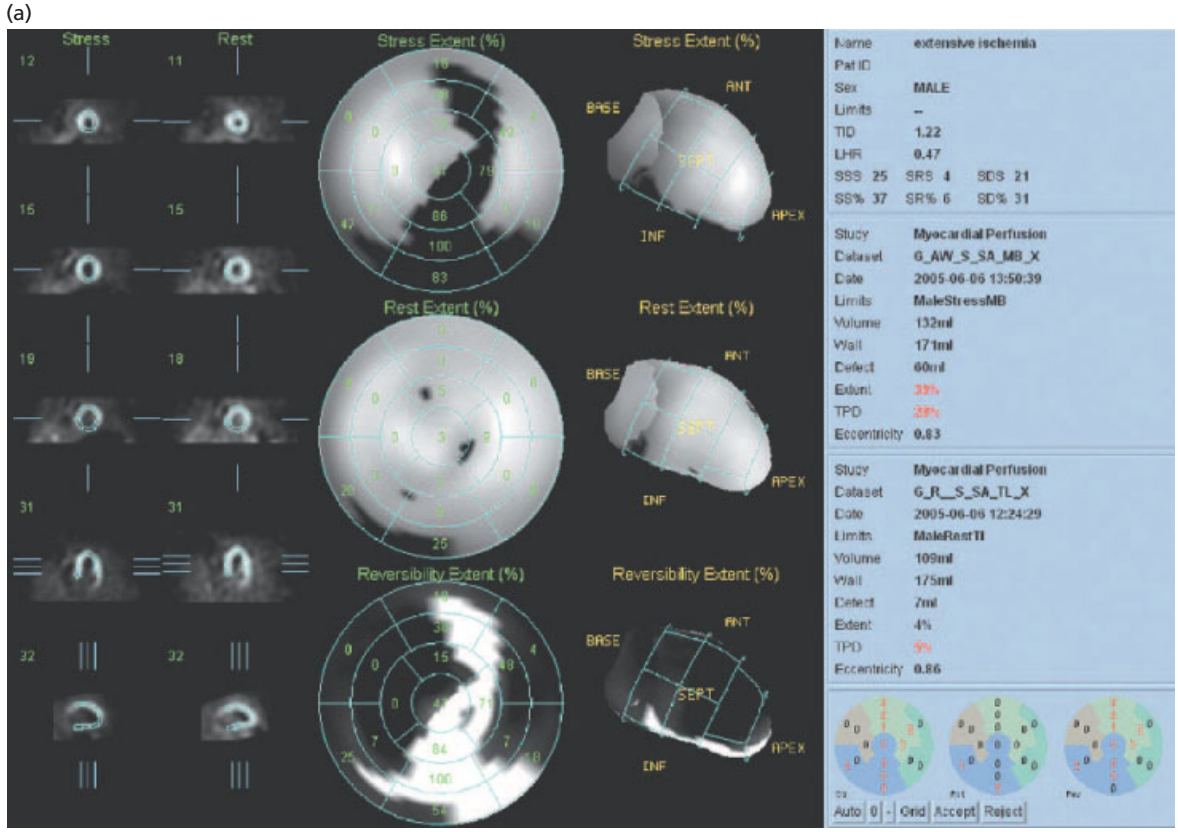

(b)

Figure 3.12 Adenosine technetium-99m sestamibi and rest thallium-201 MPS images (a) and quantitative perfusion analysis (b) in a patient with extensive perfusion defects involving the diagonal and right coronary artery territories. By visual scoring of perfusion, the summed stress score (SSS) was 25 (37% of myocardium), the summed rest score (SRS) was 4 (6% of myocardium), and the summed difference score (SDS) was 21 (31% of myocardium).

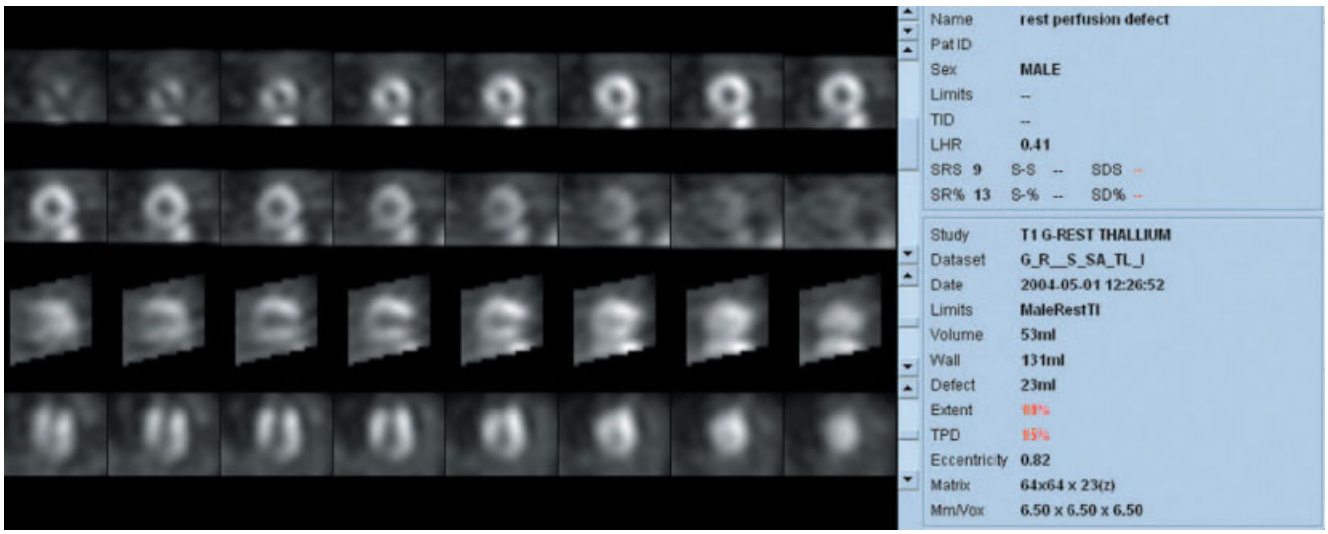

Figure 3.13 Rest thallium-201 MPS images are displayed for a patient presenting to the emergency department with chest pain. A 12-lead ECG was normal, as was the troponin level (<0.1). A stress ECG 2 years earlier was reportedly normal. Since the patient's chest pain had resolved, a stress myocardial perfusion study was ordered. On rest thallium-201 imaging the patient was found to have a large severe resting perfusion defect (18% of myocardium) in the left anterior descending coronary artery distribution. The resting perfusion defects were presumed to be acute and therefore stress testing was canceled and the patient admitted. His subsequent troponin level 12 hours later was elevated at 28 (normal, <0.4) and coronary angiography demonstrated an 80% stenosis in the mid left anterior descending coronary artery.

The prone study is performed with the detectors employed for an additional acquisition, with image acquisition from under the patient lying prone. Prone imaging alone, however, may be associated with artifactual anteroseptal defects due to the more pronounced sternal attenuation in this position. As a consequence, taking advantage of the lack of redistribution of technetium-99m sestamibi, we perform both supine and prone technetium-99m sestamibi imaging on our patients (Fig. 3.14), and have employed this as our standard clinical practice for approximately 10 years. In our laboratories, the nongated prone images are performed for 40% shorter time than are the gated supine images. Approximately 90% of our patients are able to have both supine and prone imaging. Hayes et al. have recently reported that patients with inferior wall defects on supine MPS but normal prone MPS have a low risk of subsequent cardiac events, similar to that of patients with normal supine-only studies [98]. A patient example illustrating the advantage of this approach is shown in Fig. 3.15. We have recently reported the development, validation, and application of a quantitative method for computer-based interpretation of combined supine and prone sestamibi SPECT images [99]. With this approach, supine and prone images are compared to their respective normal databases and only regions found concordantly abnormal by both positions are considered abnormal. The combined quantitation has demonstrated an increase in the normalcy rate without a loss of specificity. In daily practice, we have found that the addition of prone imaging greatly enhances observer confidence in overall scan interpretation (see Chapter 5).

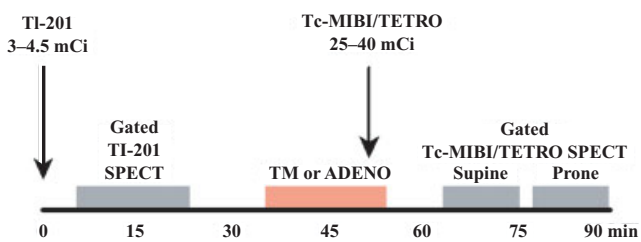

Figure 3.14 Combined supine and prone, separate acquisition dual-isotope SPECT protocol.

Attenuation correction

All the major scintillation camera manufacturers now provide hardware and software implementation of attenuation correction protocols, which have undergone various degrees of validation [100–105]. In general, these attenuation corrections are imperfect, reducing but not eliminating apparent perfusion defects due to soft tissue attenuation in normal patients. At times, true perfusion defects might be obscured or eliminated by application of these approaches. The artifactual elimination of perfusion defects is usually due to filtering or due to scatter from adjacent organs, which becomes more apparent after attenuation correction. Because of these limitations, it is prudent that attenuation-corrected tomographic data sets be visualized simultaneously with noncorrected data sets.

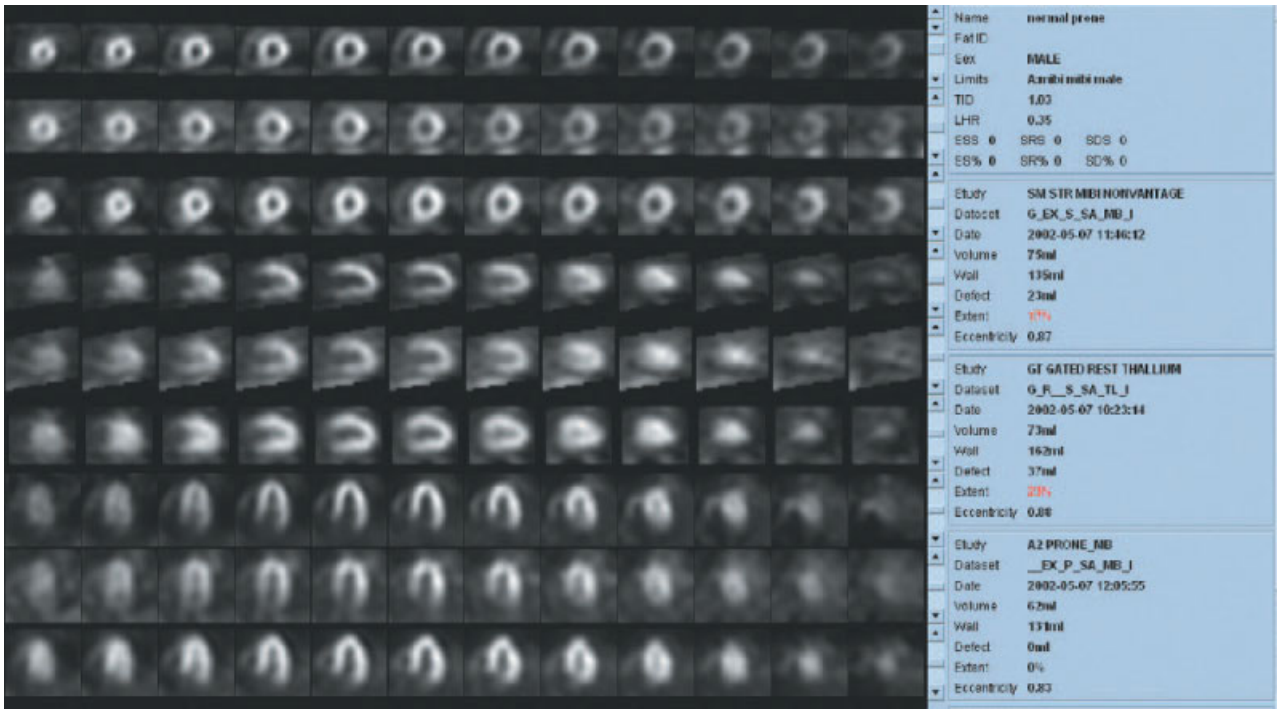

(a)

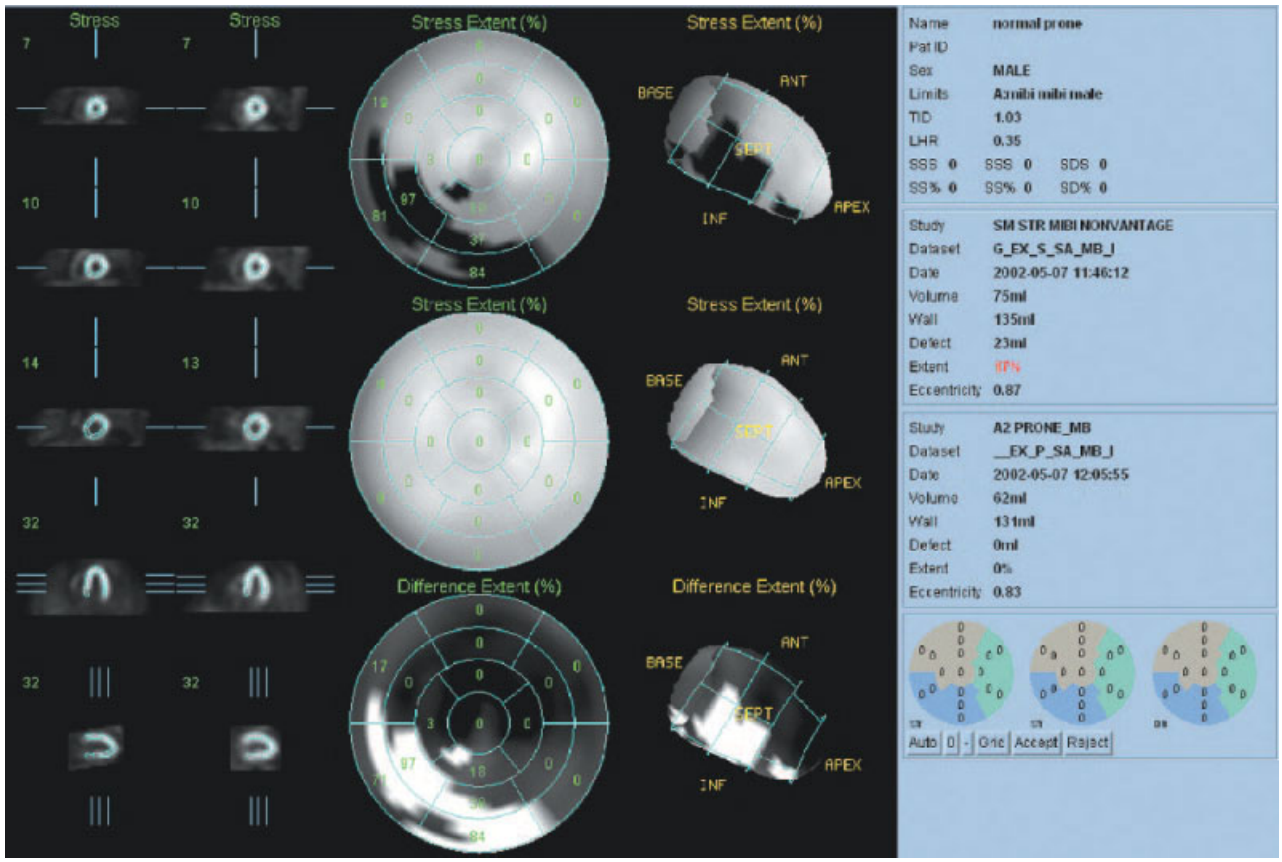

(b)

Figure 3.15 Supine (top) and prone (bottom) exercise technetium-99m sestamibi SPECT images (a), with rest thallium-201 images in the middle, in a patient who had a prior study demonstrating reversible inferior wall defects. He was referred to a cardiologist who referred the patient to Cedars-Sinai for a repeat study specifically with prone imaging. The supine images again demonstrate a large stress perfusion defect in the inferior wall (17% of myocardium), which is not seen on the prone images that are entirely normal. On the basis of the combined images, the MPS examination was interpreted as normal. The quantitative perfusion analysis of the supine and prone stress images is displayed in part (b).

The interpreter should be aware that because of the imperfection in present-day attenuation correction algorithms, a uniform distribution of radioactivity throughout the myocardium cannot be expected. Furthermore, the normal regional distribution of counts on a segment-by-segment basis may be different in attenuation-corrected images than in non-attenuation-corrected images. Thus, the normal regional distribution of counts in the attenuation-corrected images should be taken into account prior to segmental scoring.

Bateman et al. recently reported preliminary data on 494 rest/stress technetium-99m sestamibi MPS studies [106]. All studies were read twice: once with attenuation corrected images and once with non-attenuation-corrected images and ECG gating. Attenuation correction led to improved specificity (86% vs. 64%, $p < 0.001$) and no change in sensitivity, thus suggesting that attenuation correction could reduce the frequency of unnecessary angiograms.

Heller et al. also recently reported a study in which 10 experienced nuclear cardiologists independently interpreted 90 stress-only ECG-gated technetium-99m sestamibi images in a sequential fashion: MPS alone, MPS plus ECG-gated data, and attenuation-corrected MPS with ECG-gated data [107]. With stress MPS data alone, only 37% of studies were interpreted as definitely normal or abnormal, with a very high perceived need for rest imaging (77%). Attenuation-corrected data significantly increased the number of studies characterized as definitely normal or abnormal (84%, $p < 0.005$) and significantly reduced the perceived need for rest imaging (43%, $p < 0.005$). If confirmed, these findings may lead to improved laboratory efficiency and diagnostic accuracy. In the future, it is likely that attenuation correction will become routine, and that the principal method utilized for generating the attenuation maps will be CT with hybrid SPECT/CT systems.

References

1. Klocke FJ, Baird MG, Lorell BH, et al. ACC/AHA/ASNC guidelines for the clinical use of cardiac radionuclide imaging [American College of Cardiology Web Site].2003. Available at: http://www.acc.org/clinical/guidelines/radio/index.pdf, (last accessed date April 10, 2006).
2. Gibbons RJ, Abrams J, Chatterjee K, et al. ACC/AHA 2002 guideline update for the management of patients with chronic stable angina [American College of Cardiology Web Site]. 2002. Available at: http://www.acc.org/clinical/guidelines/stable/stable.pdf, (last accessed date April 10, 2006).
3. Eagle KA, Berger PB, Calkins H, et al. ACC/AHA guideline update for perioperative cardiovascular evaluation for noncardiac surgery [American College of Cardiology Web Site]. 2002. Available at: http://www.acc.org/clinical/guidelines/perio/update/pdf/perio_update.pdf, (last accessed date April 10, 2006).
4. Antman EM, Anbe DT, Armstrong PW, et al. ACC/AHA guidelines for the management of patients with ST-elevation myocardial infarction [American College of Cardiology Web Site]. 2004. Available at http://www.acc.org/clinical/guidelines/stemi/index.pdf, (last accessed date April 10, 2006).
5. Gould KL, Lipscomb K, Hamilton GW. Physiologic basis for assessing critical coronary stenosis. Instantaneous flow response and regional distribution during coronary hyperemia as measures of coronary flow reserve. American Journal of Cardiology 1974;33(1):87–94.
6. Nielsen AP, Morris KG, Murdock BS, Bruno FP, Cobb FR. Linear relationship between the distribution of thallium-201 and blood flow in ischemic and nonischemic myocardium during exercise. Circulation 1980;61:797–801.
7. L'Abbate A, Biagin A, Michelassic C, et al. Myocardial kinetics of thallium and potassium in man. Circulation 1979;60:776–785.
8. Strauss HW, Harrison BS, Pitt B. Thallium-201: noninvasive determination of the regional distribution of cardiac output. Journal of Nuclear Medicine 1977;18(12):1167–1170.
9. Bradley-Moore PR, Lebowitz E, Greene M, et al. Tl-201 for medical use: II. Biologic behavior. Journal of Nuclear Medicine 1975;16:156–160.
10. Angello DA, Wilson RA, Palac RT. Effect of eating on thallium-201 myocardial redistribution after myocardial ischemia. American Journal of Cardiology 1987;60(7):528–533.
11. Berman D, Maddahi J, Charuzi Y, et al. Rate of redistribution in Tl-201 exercise myocardial scintigraphy: inverse relationship to degree of coronary stenosis [abstract]. Circulation 1978;58(Suppl 2):II-63.
12. Gutman J, Berman DS, Freeman M, et al. Time to completed redistribution of thallium-201 in exercise myocardial scintigraphy: relationship to the degree of coronary artery stenosis. American Heart Journal 1983;106(5, Pt 1):989–995.
13. Li Q-S, Frank TL, Franceschi D, et al. Technetium-99m methoxyisobutyl isonitrile (RP30) for quantification of myocardial ischemia and reperfusion in dogs. Journal of Nuclear Medicine 1988;29:1539–1548.
14. Sinusas AJ, Bergin JD, Edwards NC, et al. Redistribution of ^{99m}Tc-sestamibi and ^{201}Tl in the presence of a severe coronary artery stenosis. Circulation 1994;89:2332–2341.
15. Krivokapich J, Smith GT, Huang SC, et al. 13N ammonia myocardial imaging at rest and with exercise in normal volunteers. Quantification of absolute myocardial perfusion with dynamic positron emission tomography. Circulation 1989;80(5):1328–1337.
16. Leppo JA, Meerdink DJ. Comparison of the myocardial uptake of a technetium-labeled isonitrile analogue and thallium. Circulation Research 1989;65(3):632–639.
17. Hurwitz GA, Blais M, Powe JE, Champagne CL. Stress/injection protocols for myocardial scintigraphy with 99mTc-sestamibi compared with 201Tl: implications of early post-stress kinetics. Nuclear Medicine Communications 1996;17(5):400–409.

18. Udelson JE. Choosing a thallium-201 or technetium 99m sestamibi imaging protocol. Journal of Nuclear Cardiology 1994;1(5, Pt 2):S99-S108.
19. Dahlberg ST, Leppo JA. Myocardial kinetics of radiolabeled perfusion agents: basis for perfusion imaging. Journal of Nuclear Cardiology 1994;1(2, Pt 1):189–197.
20. Jain D, Wackers FJ, Mattera J, McMahon M, Sinusas AJ, Zaret BL. Biokinetics of technetium-99m-tetrofosmin: myocardial perfusion imaging agent: implications for a one-day imaging protocol. Journal of Nuclear Medicine 1993;34(8):1254–1259.
21. Wackers FJ, Berman DS, Maddahi J, et al. Technetium-99m hexakis 2-methoxyisobutyl isonitrile: human biodistribution, dosimetry, safety, and preliminary comparison to thallium-201 for myocardial perfusion imaging. Journal of Nuclear Medicine 1989;30(3):301–311.
22. Chan SY, Brunken RC, Czernin J, et al. Comparison of maximal myocardial blood flow during adenosine infusion with that of intravenous dipyridamole in normal men. Journal of the American College of Cardiology 1992;20(4):979–985.
23. Soman P, Taillefer R, DePuey GE, Udelson J, Lahiri A. Improved detection of reversible ischemia by Tc-99 sestamibi compared to Tc-99m tetrofosmin SPECT imaging in mild to moderate CAD [abstract]. Journal of Nuclear Cardiology 1999;6:S35.
24. Soman P, Tailleker R, Udelson JE, DePuey GE, Lahiri A. Enhanced detection of reversible perfusion defects by Tc-99m sestamibi compared to Tc-99m tetrofosmin during vasodilater stress SPECT imaging in mild-to-moderate coronary artery disease. Journal of the American College of Cardiolog 2001;37:458–462.
25. Maublant JC, Marcaggi X, Lusson JR, et al. Comparison between thallium-201 and technetium-99m methoxyisobutyl isonitrile defect size in single-photon emission computed tomography at rest, exercise and redistribution in coronary artery disease. American Journal of Cardiology 1992;69(3):183–187.
26. Narahara KA, Villanueva-Meyer J, Thompson CJ, Brizendine M, Mena I. Comparison of thallium-201 and technetium-99m hexakis 2-methoxyisobutyl isonitrile single-photon emission computed tomography for estimating the extent of myocardial ischemia and infarction in coronary artery disease. American Journal of Cardiology 1990;66(20):1438–1444.
27. Meerdink DJ, Leppo JA. Experimental properties of technetium-99m agents: myocardial transport of perfusion imaging agents. American Journal of Cardiology 1990;66:9E–15E.
28. Leppo JA, Meerdink DJ. Comparative myocardial extraction of two technetium-labeled BATO derivatives (SQ30217,SQ30214) and thallium. Journal of Nuclear Medicine 1990;31:67–74.
29. Chua T, Kiat H, Germano G, et al. Technetium-99m teboroxime regional myocardial washout in subjects with and without coronary artery disease. American Journal of Cardiology 1993;72(9):728–734.
30. Chua T, Kiat H, Germano G, et al. Rapid back to back adenosine stress/rest technetium-99m teboroxime myocardial perfusion SPECT using a triple-detector camera. Journal of Nuclear Medicine 1993;34(9):1485–1493.
31. Kiat H, Berman DS, Maddahi J, et al. Late reversibility of tomographic myocardial thallium - 201 defects: an accurate marker of myocardical viability. Journal of the American College of cardiology 1988;12:1456–1463.
32. Dilsizian V, Rocco TP, Freedman NM, Leon MB, Bonow RO. Enhanced detection of ischemic but viable myocardium by the reinjection of thallium after stress-redistribution imaging [see comments]. New England Journal of Medicine 1990;323(3):141–146.
33. Dilsizian V, Smeltzer WR, Freedman NM, Dextras R, Bonow RO. Thallium reinjection after stress-redistribution imaging. Does 24-hour delayed imaging after reinjection enhance detection of viable myocardium? Circulation 1991;83(4):1247–1255.
34. Basu S, Senior R, Raval U, Lahiri A. Superiority of nitrate-enhanced 201Tl over conventional redistribution 201Tl imaging for prognostic evaluation after myocardial infarction and thrombolysis [see comments]. Circulation 1997;96(9):2932–2937.
35. Pohost GM, Zir LM, Moore RH, McKusick KA, Guiney TE, Beller GA. Differentiation of transiently ischemic from infarcted myocardium by serial imaging after a single dose of thallium-201. Circulation 1977;55(2):294–302.
36. Pagley PR, Beller GA, Watson DD, Gimple LW, Ragosta M. Improved outcome after coronary bypass surgery in patients with ischemic cardiomyopathy and residual myocardial viability. Circulation 1997;96(3):793–800.
37. Wagdy HM, Christian TF, Miller TD, Gibbons RJ. The value of 24-hour images after rest thallium injection. Nuclear Medicine Communications 2002;23(7):629–637.
38. Yang LD, Berman DS, Kiat H, et al. The frequency of late reversibility in SPECT thallium-201 stress-redistribution studies. Journal of the American College of Cardiology 1990;15(2):334–340.
39. Bateman TM. Nuclear cardiology in private practice. Journal of Nuclear Cardiology 1997;4(2, Pt 2):S184–S188.
40. Mahmarian JJ, Boyce TM, Goldberg RK, Cocanougher MK, Roberts R, Verani MS. Quantitative exercise thallium-201 single photon emission computed tomography for the enhanced diagnosis of ischemic heart disease [see comments]. Journal of the American College of Cardiology 1990;15(2):318–329.
41. Mahmarian J. State of the art for coronary artery disease detection: thallium-201. In Zaret BL, Beller G, edis. Nuclear Cardiology: State of the Art and Future Directions. 2nd edn. St. Louis, MO: Mosby; 1998:237–272.
42. Friedman J, Van Train K, Maddahi J, et al. "Upward creep" of the heart: a frequent source of false-positive reversible defects during thallium-201 stress-redistribution SPECT. Journal of Nuclear Medicine 1989;30(10):1718–1722.
43. Berman DS, Kiat H, Maddahi J. The new 99mTc myocardial perfusion imaging agents: 99mTc-sestamibi and 99mTc-teboroxime. Circulation 1991;84(3, Suppl):I7–I21.
44. Berman D, Kiat H, Germano G, et al. 99m Tc-sestamibi SPECT. In: DePuey EG, Berman DS, Garcia EV, eds. Cardiac SPECT Imaging. New York: Raven Press; 1995:121–146.

45. Van Train KF, Areeda J, Garcia EV, et al. Quantitative same-day rest-stress technetium-99m-sestamibi SPECT: definition and validation of stress normal limits and criteria for abnormality. Journal of Nuclear Medicine 1993;34(9):1494–1502.
46. Buell U, Dupont F, Uebis R, et al. 99Tcm-methoxy-isobutyl-isonitrile SPECT to evaluate a perfusion index from regional myocardial uptake after exercise and at rest. Results of a four hour protocol in patients with coronary heart disease and in controls. Nuclear Medicine Communications 1990;11(2):77–94.
47. Heo J, Kegel J, Iskandrian AS, Cave V, Iskandrian BB. Comparison of same-day protocols using technetium-99m-sestamibi myocardial imaging. Journal of Nuclear Medicine 1992;33(2):186–191.
48. Taillefer R, Gagnon A, Laflamme L, Gregoire J, Leveille J, Phaneuf DC. Same day injections of Tc-99m methoxy isobutyl isonitrile (hexamibi) for myocardial tomographic imaging: comparison between rest-stress and stress-rest injection sequences. European Journal of Nuclear Medicine 1989;15(3):113–117.
49. Marzullo P, Parodi O, Reisenhofer B, et al. Value of rest thallium-201/technetium-99m sestamibi scans and dobutamine echocardiography for detecting myocardial viability. American Journal of Cardiology 1993;71(2):166–172.
50. Berman DS, Kiat HS, Van Train KF, Germano G, Maddahi J, Friedman JD. Myocardial perfusion imaging with technetium-99m-sestamibi: comparative analysis of available imaging protocols. Journal of Nuclear Medicine 1994;35(4):681–688.
51. Sciagrà R, Bisi G, Santoro GM, et al. Comparison of baseline-nitrate technetium-99m sestamibi with rest-redistribution thallium-201 tomography in detecting viable hibernating myocardium and predicting postrevascularization recovery. Journal of the American College of Cardiology 1997;30(2):384–391.
52. He Z, Verani M. Evaluation of myocardial viability by myocardial perfusion imaging: Should nitrates be used? Journal of Nuclear Cardiology 1998;5:527–532.
53. Kiat H, Germano G, Friedman J, et al. Comparative feasibility of separate or simultaneous rest thallium-201/stress technetium-99m-sestamibi dual-isotope myocardial perfusion SPECT. Journal of Nuclear Medicine 1994;35(4):542–548.
54. de Jong HW, Beekman FJ, Viergever MA, van Rijk PP. Simultaneous (99m)Tc/(201)Tl dual-isotope SPET with Monte Carlo-based down-scatter correction. European Journal of Nuclear Medicine and Molecular Imaging 2002;29(8):1063–1071.
55. Weinmann P, Faraggi M, Moretti JL, Hannequin P. Clinical validation of simultaneous dual-isotope myocardial scintigraphy. European Journal of Nuclear Medicine and Molecular Imaging 2003;30(1):25–31.
56. Nakamura M, Takeda K, Ichihara T, et al. Feasibility of simultaneous stress 99m-Tc-sestamibi/rest 201-Tl dual isotope myocardial perfusion SPECT in the detection of coronary artery disease. Journal of Nuclear Medicine 1999;40:895–903.
57. Bateman T, Case J, Moutray K, et al. Clinical evaluation of a novel dual-simultaneous SPECT myocardial perfusion protocol: blinded comparison to dual-sequential images [abstract]. Journal of the American College of Cardiology 1999; 33(2, Suppl A):418A.
58. Berman DS, Kiat H, Friedman JD, et al. Separate acquisition rest thallium-201/stress technetium-99m sestamibi dual-isotope myocardial perfusion single-photon emission computed tomography: a clinical validation study. Journal of the American College of Cardiology 1993;22(5):1455–1464.
59. Friedman JD, Berman DS, Kiat H, et al. Rest and treadmill exercise first-pass radionuclide ventriculography: validation of left ventricular ejection fraction measurements. Journal of Nuclear Cardiology 1994;1(4):382–388.
60. Bateman TM, Berman DS, Heller GV, et al. American Society of Nuclear Cardiology position statement on electrocardiographic gating of myocardial perfusion SPECT scintigrams. Journal of Nuclear Cardiology 1999;6(4):470–471.
61. Germano G, Erel J, Kiat H, Kavanagh PB, Berman DS. Quantitative LVEF and qualitative regional function from gated thallium-201 perfusion SPECT. Journal of Nuclear Medicine 1997;38(5):749–754.
62. Lauer MS, Francis GS, Okin PM, Pashkow FJ, Snader CE, Marwick TH. Impaired chronotropic response to exercise stress testing as a predictor of mortality. JAMA 1999;281(6):524–529.
63. Azarbal B, Hayes SW, Lewin HC, Hachamovitch R, Cohen I, Berman DS. The incremental prognostic value of percentage of heart rate reserve achieved over myocardial perfusion single-photon emission computed tomography in the prediction of cardiac death and all-cause mortality: superiority over 85% of maximal age-predicted heart rate. Journal of the American College of Cardiology 2004;44(2):423–430.
64. Lauer MS. Chronotropic incompetence: ready for prime time. Journal of the American College of Cardiology 2004;44(2):431–432.
65. Gerson MC. Reduction in dipyridamole-induced single-photon emission computed tomography myocardial defect size by beta-blockers: time to re-examine the patient preparation protocol for pharmacologic stress testing. Journal of the American College of Cardiology 2003;42(8):1484–1486.
66. Verani MS. Adenosine thallium-201 myocardial perfusion scintigraphy. American Heart Journal 1991;122:269–278.
67. Takeishi Y, Chiba J, Abe S, Yamaki M, Tomoike H. Adenosine-induced heterogeneous perfusion accompanies myocardial ischemia in the presence of advanced coronary artery disease. American Heart Journal 1994;127(5):1262–1268.
68. Iskandrian AS, Verani MS, Heo J. Pharmacologic stress testing: mechanism of action, hemodynamic responses, and results in detection of coronary artery disease. Journal of Nuclear Cardiology 1994;1(1):94–111.
69. Iskandrian A. State of the art for pharmacologic stress imaging. In Zaret BL, Beller G, eds. Nuclear Cardiology: State of the Art and Future Directions. 2nd edn. St. Louis, MO: Mosby; 1998:312–330.
70. Smits P, Thien T, van't Laar A. Circulation effects of coffee in relation to the pharmacokinetics of caffeine. American Journal of Cardiology 1985;56:958–963.

71. Amanullah AM, Berman DS, Kiat H, Friedman JD. Usefulness of hemodynamic changes during adenosine infusion in predicting the diagnostic accuracy of adenosine technetium-99m sestamibi single-photon emission computed tomography (SPECT). American Journal of Cardiology 1997;79(10):1319–1322.
72. Sharir T, Rabinowitz B, Livschitz S, et al. Underestimation of extent and severity of coronary artery disease by dipyridamole stress thallium-201 single-photon emission computed tomographic myocardial perfusion imaging in patients taking antianginal drugs. Journal of the American College of Cardiology 1998;31(7):1540–1546.
73. Taillefer R, Ahlberg AW, Masood Y, et al. Acute beta-blockade reduces the extent and severity of myocardial perfusion defects with dipyridamole Tc-99m sestamibi SPECT imaging. Journal of the American College of Cardiology 2003;42(8):1475–1483.
74. Picano E, Marini C, Pirelli S, et al. Safety of intravenous high-dose dipyridamole echocardiography. American Journal of Cardiology 1992;70:252–258.
75. Lette J, Tatum JL, Fraser S, et al. Safety of dipyridamole testing in 73,806 patients: the Multicenter Dipyridamole Safety Study. Journal of Nuclear Cardiology 1995;2(1):3–17.
76. Verani MS, Mahmarian JJ. Myocardial perfusion scintigraphy during during maximal coronary artery vasodilation with adenosine. American Journal of Cardiology 1991;67:12D–17D.
77. Verani MS, Mahmarian JJ, Hixson JB, et al. Diagnosis of coronary artery disease by controlled coronary vasodilation with adenosine and thallium-201 scintigraphy in patients unable to exercise. Circulation 1990;82:80–87.
78. Pennell DJ, Mavrogeni SI, Forbat SM, Karwatowski SP, Underwood SR. Adenosine combined with dynamic exercise for myocardial perfusion imaging. Journal of the American College of Cardiology 1995;25(6):1300–1309.
79. Parikh A, Kiat H, Kang X, Cohen I, Friedman J, Berman D. Addition of low level treadmill exercise to adenosine stress Tc-99m sestamibi myocardial perfusion SPECT allows for early post-stress imaging [abstract]. Journal of Nuclear Medicine 1996;37(5):59P.
80. Hayes S, Dhar S, Cordero H, et al. First pass radionuclide angiography adds incremental value to adenosine low level treadmill exercise Tc-99m sestamibi SPECT for detecting multivessel coronary artery disease [abstract]. Journal of Nuclear Medicine 1998;39(5):102P.
81. Mason JR, Palac RT, Freeman ML, et al. Thallium scintigraphy during dobutamine infusion: nonexercise-dependent screening test for coronary disease. American Heart Journal 1984;107(3):481–485.
82. Pennell DJ, Underwood SR, Swanton RH, Walker JM, Ell PJ. Dobutamine thallium myocardial perfusion tomography. Journal of the American College of Cardiology 1991;18(6):1471–1479.
83. Cerqueira MD. Pharmacologic stress versus maximal-exercise stress for perfusion imaging: which, when, and why? Journal of Nuclear Cardiology 1996;3(6, Pt 2): S10–S14.
84. Elhendy A, Valkema R, van Domburg RT, et al. Safety of dobutamine-atropine stress myocardial perfusion scintigraphy. Journal of Nuclear Medicine 1998;39:1662-1666.
85. Hirzel HO, Senn M, Nuesch K, et al. Thallium-201 scintigraphy in complete left bundle branch block. American Journal of Cardiology 1984;53(6):764–769.
86. Skalidis EI, Kochiadakis GE, Koukouraki SI, Parthenakis FI, Karkavitsas NS, Vardas PE. Phasic coronary flow pattern and flow reserve in patients with left bundle branch block and normal coronary arteries. Journal of the American College of Cardiology 1999;33(5):1338–1346.
87. Rockett J, Wood W, Moinuddim M. Intravenous dipyridamole thallium-201 SPECT imaging in patients with left bundle branch block. Clinical Nuclear Medicine 1990;15:401–407.
88. O'Keefe J, Bateman T, Barnhart C. Adenosine thallium-201 is superior to exercise thallium-201 for detecting coronary artery disease in patients with left bundle branch block. Journal of the American College of Cardiology 1993;21:1332–1338.
89. Matzer L, Kiat H, Friedman JD, Van Train K, Maddahi J, Berman DS. A new approach to the assessment of tomographic thallium-201 scintigraphy in patients with left bundle branch block. Journal of the American College of Cardiology 1991;17(6):1309–1317.
90. Tse H, Lau C. Long-term effect of right ventricular pacing on myocardial perfusion and function. Journal of the American College of Cardiology 1997;29:744–749.
91. Atwood JE, Kawanishi S, Myers J, Froelicher VF. Exercise testing in patients with aortic stenosis. Chest 1988;93(5):1083–1087.
92. Clyne CA, Arrighi JA, Maron BJ, Dilsizian V, Bonow RO, Cannon RO, III. Systemic and left ventricular responses to exercise stress in asymptomatic patients with valvular aortic stenosis. American Journal of Cardiology 1991;68(15):1469–1476.
93. Samuels B, Kiat H, Friedman JD, Berman DS. Adenosine pharmacologic stress myocardial perfusion tomographic imaging in patients with significant aortic stenosis. Diagnostic efficacy and comparison of clinical, hemodynamic and electrocardiographic variables with 100 age-matched control subjects. Journal of the American College of Cardiology 1995;25(1):99–106.
94. Aboul-Enein FA, Hayes SW, Matsumoto N, Friedman JD, Germano G, Berman DS. Rest perfusion defects in patients with no history of myocardial infarction predict the presence of a critical coronary artery stenosis. Journal of Nuclear Cardiology 2003;10(6):656–662.
95. Kiat H, Van Train KF, Friedman JD, et al. Quantitative stress-redistribution thallium-201 SPECT using prone imaging: methodologic development and validation. Journal of Nuclear Medicine 1992;33(8):1509–1515.
96. Esquerré JP, Coca FJ, Martinez SJ, Guiraud RF. Prone decubitus: a solution to inferior wall attenuation in thallium-201 myocardial tomography. Journal of Nuclear Medicine 1989;30(3):398–401.
97. Segall GM, Davis MJ. Prone versus supine thallium myocardial SPECT: a method to decrease artifactual inferior

wall defects [see comments]. Journal of Nuclear Medicine 1989;30(4):548–555.
98. Hayes SW, De Lorenzo A, Hachamovitch R, et al. Prognostic implications of combined prone and supine acquisitions in patients with equivocal or abnormal supine myocardial perfusion SPECT. Journal of Nuclear Medicine 2003;44(10):1633–1640.
99. Nishina H, Slomka P, Abidov A, et al. Combined supine and prone quantitative myocardial perfusion SPECT: method development and clinical validation in patients with no known coronary artery disease. Journal of Nuclear Medicine 2006;47:51–58.
100. Ficaro EP, Fessler JA, Shreve PD, Kritzman JN, Rose PA, Corbett JR. Simultaneous transmission/emission myocardial perfusion tomography. Diagnostic accuracy of attenuation-corrected 99mTc-sestamibi single-photon emission computed tomography. Circulation 1996;93(3):463–473.
101. Cullom S, Hendel R, Liu L, Garcia E, White M, Berman D. Diagnostic accuracy and image quality of a scatter, attenuation and resolution compensation method for Tc-99m cardiac SPECT: preliminary results [abstract]. Journal of Nuclear Medicine 1996;37(5):81P.
102. Hendel RC, Berman DS, Cullom SJ, et al. Multicenter clinical trial to evaluate the efficacy of correction for photon attenuation and scatter in SPECT myocardial perfusion imaging. Circulation 1999;99:2742–2749.
103. Ficaro EA, Kritzman JN, Hawman PC, DeBruin SW, Corbett JR. Initial clinical validation of profile attenuation correction: comparison to the University of Michigan modified STEP method. Journal of Nuclear Medicine; 1999;40:90P.
104. Links J, Becker L, Rigo P, et al. Combined attenuation, depth-dependent blur, and motion corrections in cardiac SPECT: a multicenter trial. Journal of Nuclear Medicine; 1999: 89P.
105. Gallowitsch HJ, Sykora J, Mikosch P, et al. Attenuation-corrected thallium-201 single-photon emission tomography using a gadolinium-153 moving line source: clinical value and the impact of attenuation correction on the extent and severity of perfusion abnormalities. European Journal of Nuclear Medicine 1998;25(3):220–228.
106. Bateman TM, Heller GV, Johnson LL, et al. Does attenuation correction add value to non-attenuation corrected ECG-gated technetium-99m sestamibi SPECT? Journal of Nuclear Cardiology 2003;10(1):S91.
107. Heller GV, Bateman TM, Johnson LL, et al. Clinical value of attenuation correction in stress-only Tc-99m sestamibi SPECT imaging. Journal of Nuclear Cardiology 2004;11(3):273–281.

4 Quantification of myocardial perfusion

Piotr J. Slomka
Daniel S. Berman
Guido Germano

Introduction

Operator independent, quantitative assessment of regional myocardial perfusion is a principal competitive advantage of nuclear cardiology over other modalities [1,2]. This assessment is now nearly fully automated using a variety of approaches. The potential of such automated processing is reliable reader-independent and laboratory-independent results, which would improve accuracy of a single assessment and facilitate assessment of the interval change.

This chapter will review various computational techniques designed for quantification of parameters related to myocardial perfusion. It will also review the validations performed for these measurements, and will discuss the remaining limitations of quantification. We will also describe recent developments and improvements in the quantification of myocardial perfusion. Since clinically applied myocardial perfusion SPECT quantification techniques do not perform "absolute" quantification of counts, the term "quantification" in this chapter is used to describe "relative quantification" of perfusion.

Basic techniques

Overview of the quantification process

A block diagram representing typical computing steps needed for the extraction of the quantitative perfusion parameters from projection acquisition data is shown in Fig. 4.1. Ideally, all these steps are performed in a fully automated fashion and most current computer systems provide this facility; however, manual interaction may be required in some cases. For example, manual interaction may be required to assist the computer program in defining the region for left ventricle (LV) reconstruction and in selecting angles for reorientation. In this section, we will describe specific steps in this process. In a subsequent section, we will discuss other approaches in myocardial perfusion quantification in which some of the steps presented in the diagram are combined or eliminated.

Obviously, the quantification program depends on the quality of the raw projection data. The quantification may be inaccurate due to the inadequate number of counts, improper peaking, improper positioning of the rotating camera, or excessive motion of the patient (see Chapter 7). The performance of the quantification program also depends on preprocessing steps during image reconstruction or reorientation, whether automatic or manual. Manual steps in the processing introduce inter- and intraobserver variability to the results, and by definition prohibit fully automated analysis of the data [3]. Therefore efforts have been undertaken to automate the whole image processing chain starting from the reconstruction of the data and ultimately objectify the interpretation of myocardial perfusion images.

LV reconstruction

As noted above, LV reconstruction can be performed in a fully automatic fashion. Acquired projection images are reconstructed by filtered backprojection or by iterative reconstruction techniques into a series of transaxial planes [4]. Separate optimization of reconstruction parameters for stress and rest studies may be required because of the difference in count statistics [5]. In general, unless attenuation maps are available [5], no attenuation correction is performed. Often image reconstruction is limited in the Z-axis only to the LV cardiac region to exclude extracardiac activity. This cardiac region can be selected automatically [6], or it can be adjusted manually by selecting the appropriate transaxial slice range. Performance of subsequent image processing steps (LV segmentation and reorientation) may depend on the selection of these slice limits. During this step it is important to review the projection

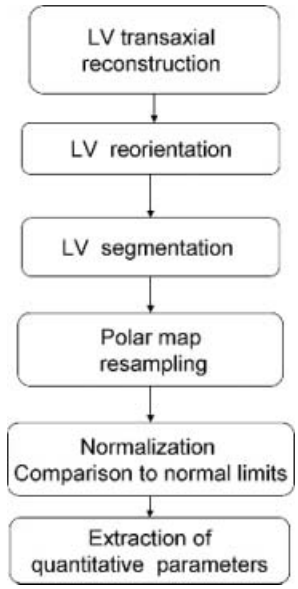

Figure 4.1 Overview of the quantification process.

data with respect to patient motion, and apply correction if needed [7]. Motion artifacts often affect the quantification of myocardial perfusion, since the relative count distribution in the myocardium is altered. Without motion correction, comparison to normal limits (generated from data without motion) may produce false-positive results [7,8].

Automatic LV reorientation

LV reorientation is not strictly required for the automatic extraction of the perfusion parameters from the reconstructed data, but it is convenient to represent LV images as short-axis data and reoriented images have become standard for data display. Most computer approaches use as input reoriented short-axis data. This reorientation can be performed automatically. Incorrect alignment of the myocardium during quantification procedures may introduce discrepancies in the perfusion quantification results [8].

In efforts to automate image alignment, geometric methods were developed for reorienting the skeleton representation of the LV [9–11]. In this early approach, no significant difference was demonstrated between manual and automatic alignment [10]. Another approach, using principal-axis transformation, was originally proposed by Faber et al. [12]. Mullick et al. proposed a method that uses three-dimensional (3D) polygonal representation of the ventricular surface to compute the orientation parameters [13]. Germano et al. developed an automatic technique based on fitting the ellipsoid to the segmented left ventricle and validated performance of the technique in 400 patients with a success rate of 98.5% [14]. Three-dimensional registration techniques accomplish this step intrinsically during alignment of transverse data with the templates [15–17].

LV segmentation

In imaging, segmentation refers to the separation of a region or a structure of interest from the remainder of an image. Automatic segmentation of the left ventricular myocardium – the structure of interest for assessment of myocardial perfusion – is typically performed using short-axis image slices. This segmentation is to some extent dependent on the "correctness" of the reorientation of the short-axis images. The boundaries that are used for myocardial perfusion assessment can be based on various computational techniques, many of which were initially applied and validated for measurement of the ejection fraction [18–22]. When applied to ungated "summed" images, these techniques are used to provide boundaries of the left ventricular myocardium. For example, the Quantitative Perfusion SPECT (QPS) program from Cedars-Sinai applies an identical LV segmentation algorithm for gated studies of left ventricular function and the ungated studies for myocardial perfusion [23]. It should be noted that the segmentation of gated and ungated data may be independent of each other; therefore, the detection of contours should be verified visually for both gated and ungated data. Errors in LV segmentation may lead to significantly erroneous results in myocardial perfusion quantification. In most cases, these will be false-positive results. Figure 4.2 presents an example of spurious quantification defect caused by incorrect definition of myocardial contours in the base.

Most commercially available software packages will allow manual override of the automatic segmentation. An example of the manual override page for the QPS program is shown in Fig. 4.3. If manual override has been exercised by the user, the quantitative results will be associated with operator variability even if derived in an otherwise fully automated manner. In the case of the QPS program, the manual override allows the user to define the mask and constrain the LV region to a specific geometrical shape. The contour detection, however, is always performed automatically. In practice, fully manual 3D contour definition is usually not attempted (or offered as an option) due to large number of slices and contours that would need to be adjusted and the errors associated with the multiple interactions.

Polar sampling

Most quantitative schemes (not 3D voxel methods) utilize some sort of polar sampling or circumferential sampling

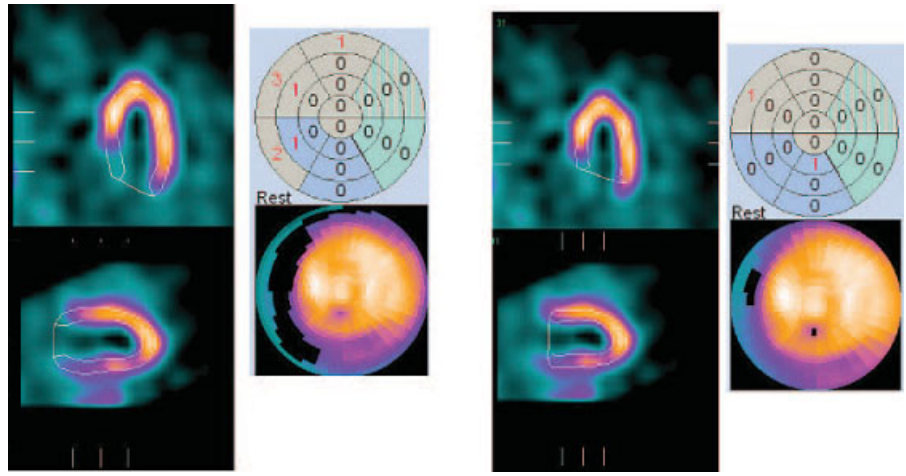

Figure 4.2 An example of improper contour definition on the quantification results. Note spurious defect in the septal wall and a summed stress score of 8. After correction of the contours the defect disappears and the summed stress score is 2.

in order to extract a limited number of perfusion samples from the myocardium [24,25]. In short-axis image orientation, these samples are performed using a base geometrical shape, for example, hybrid spherical-cylindrical [26], by the CEqual application or ellipsoidal model by QPS [23]. 3D/4DMSPECT from University of Michigan utilizes equidistant sampling of the myocardium based on the length of the myocardium from base to apex, with angular sampling adjusted for the smaller radii in the distal to apical regions [27].

As an example, the QPS program from Cedars-Sinai extracts raw myocardial counts from profiles normal to the

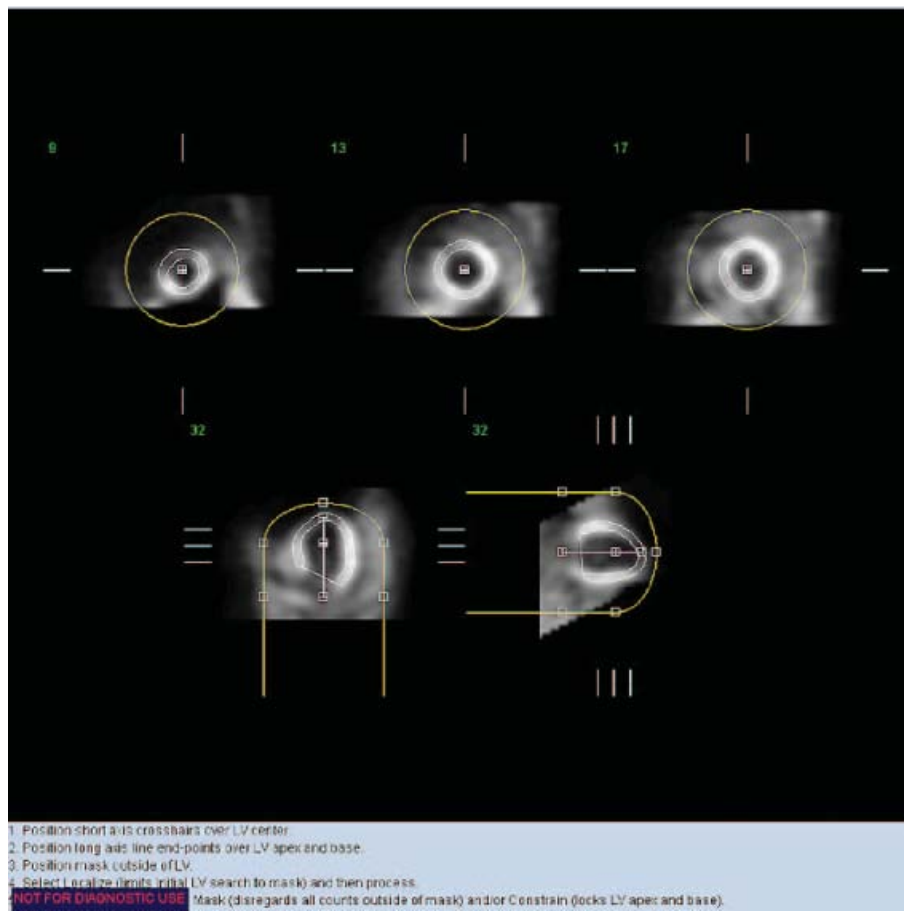

Figure 4.3 A manual adjustment of the LV mask and constrain in the QPS software. The user can interactively adjust a smooth 3D boundary around the LV. Contour detection will be limited to this 3D region. In addition, the position of the apex and base can be "locked" to a given location.

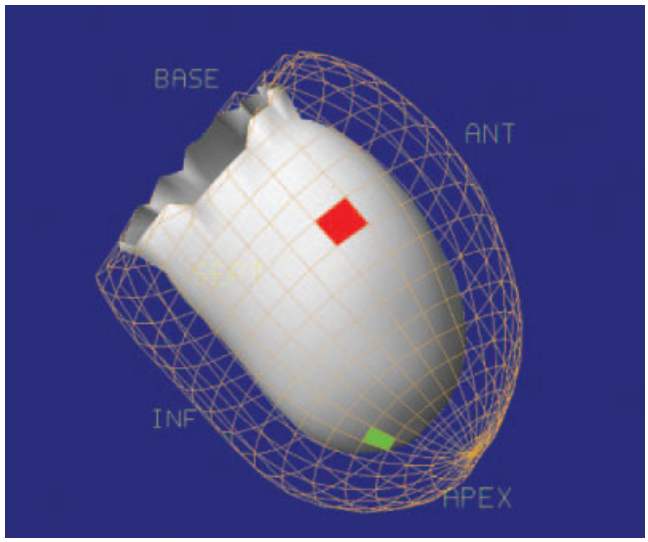

Figure 4.4 The polar perfusion samples have different corresponding areas, depending on the location in the myocardium. Mid-ventricular samples (red) are generally bigger than the apical samples (green). This effect needs to be accounted for during the computation of the defect size.

LV surfaces and average count densities between epi- and endocardial surfaces obtained for each profile individually [23]. The number of profiles and the angular samples is standardized for all patients and is 20 and 36, respectively, in the QPS program. Thus all the myocardial perfusion information is contained in a 20 × 36 matrix (720 samples). In Fig. 4.4, the epicardial surface of the LV is shown as a quadrilateral grid, where each quadrilateral corresponds to one perfusion sample. In QPS, each sample is obtained as the average of the counts between the epi- and endocardial contours for a given ray perpendicular to the LV surface. In other applications, maximum counts on the ray perpendicular to the LV surface are used [26], which is shown to correlate to the average counts in phantoms due to partial volume effects [28]. Note that due to such geometrical approach, a given myocardial sample may have different myocardial volume associated with it than another. For example, in Fig. 4.4, the apical samples (green) have smaller volumes than the mid-ventricular samples (red). Therefore the geometric volumes associated with each perfusion samples must be computed and used by the quantification program for calculation of quantitative parameters such as extent of the perfusion defect.

In order to simplify the display of perfusion information extracted in this manner a polar map display has been developed for graphical presentation to the user (Fig. 4.5) [29]. This kind of display is used extensively in clinical practice. Polar maps create a bull's eye plot based on the extracted samples mapped on the circle. Note that as with any polar map, these polar map plots of myocardial perfusion distort the relative sizes of various regions and are therefore used for qualitative analysis only, allowing the observer a quick review of perfusion information on one image. In order to present this information in a less distorted manner, 3D methods have been utilized [30]. An example of polar maps and corresponding 3D surface display with color-coded perfusion defect from the Cedars-Sinai QPS program is shown in Fig. 4.6.

Although polar or circumferential resampling is the most popular scheme, other approaches have been implemented utilizing 3D voxel analysis, which considers all voxels within the left ventricular myocardium without polar sampling [15,16] or sampling of vertical long-axis images [31]. In some other applications, average segmental perfusion counts have been computed directly in a small number of segments without using individual perfusion samples [21].

Comparison to normal limits

Most quantitative techniques for myocardial perfusion rely on the comparison to normal limits. In such methods a normal database of gender-matched patients is stored in the form of polar map samples. Gender-matched limits are required in non attenuation-corrected SPECT since the normal distribution of males and females is significantly different (Fig. 4.7). Subsequently, polar maps of a given abnormal patient are compared to the normal distribution and the differences visualized on the polar map display

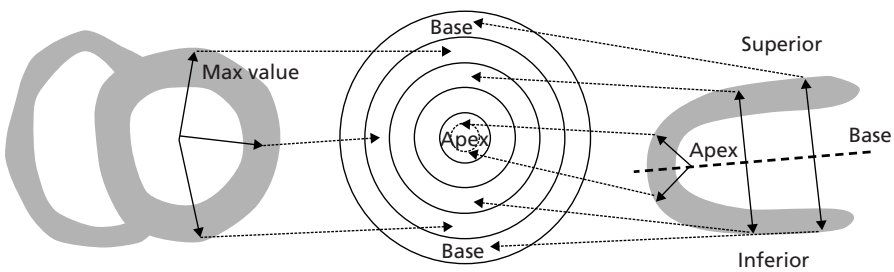

Figure 4.5 Polar map sampling of perfusion data.

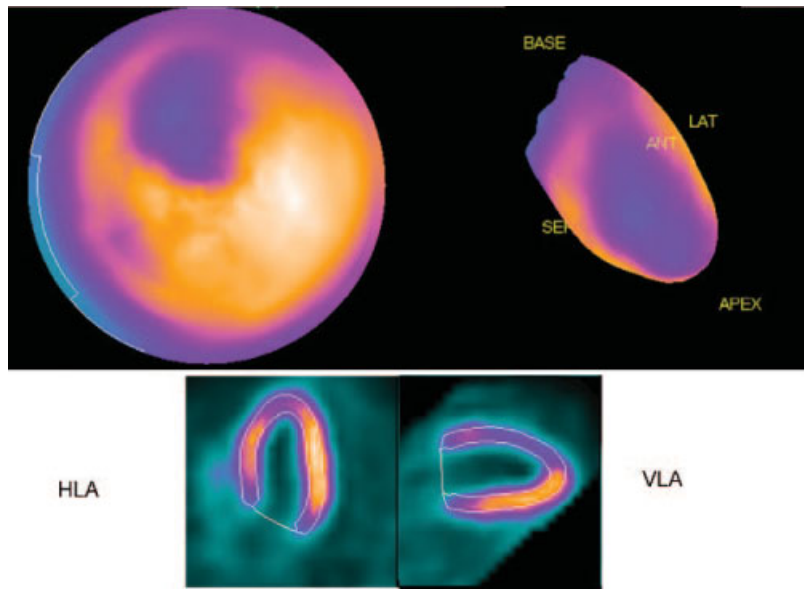

Figure 4.6 Polar map (top right) and 3D shape-preserving representation of the perfusion information. Note the apparent deformation of the defect on the polar map display to geometrical sampling. Corresponding horizontal long-axis (HLA) and vertical long-axis (VLA) slices with superimposed contours are shown in the bottom panel.

as color-coded images (colors corresponding to the number of standard deviations below the normal average) and blackout maps [24]. Several types of comparisons to normal ranges can be obtained [26].

Most existing software applications used in clinical practice, such as 4D-MSPECT from University of Michigan [32], Perfit from Nuclear Diagnostics/University of Western Ontario [33], Emory Toolbox from Emory University [19]), and QPS software from Cedars-Sinai [23], apply normal-limit methods to derive defect size. An example of the blackout map derived by comparison to gender-matched normal limits by the QPS quantification [34] is shown in Fig. 4.8.

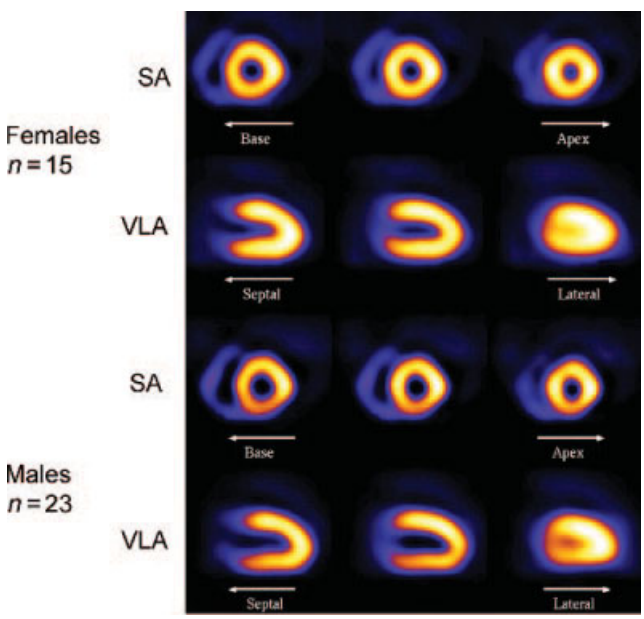

Figure 4.7 Short-axis and vertical long-axis image slices derived from composite 3D templates created from stress Tc-99m sestamibi SPECT normal studies of females ($n = 15$) (top) and males ($n = 23$) (bottom). Note the evident inferior wall artifact in the male template. Abbreviations: SA, short axis; VLA, vertical long axis. (Reproduced with permission from [16].)

In the normal-limit-based systems, the number of perfusion samples for each test-patient needs to be equalized to the standard number of samples in the normal database. In this way, the individual patient perfusion data have the same number of perfusion samples as each of the patients in the normal file. Thus a form of spatial normalization is typically performed resampling the raw patient polar maps results to standardized dimensions of polar samples [26].

Attenuation-corrected normal limits

Normal-limit quantification can be utilized for the data reconstructed with attenuation correction (AC) but require the use of separate attenuation-corrected normal limits. Normal limits still need to be applied, rather than thresholding technique, since images with AC do not have perfectly uniform distribution within the myocardium. For example, after AC a 10–15% decrease in activity in the apex has been observed relative to the uniform activity distribution in the distal and proximal regions of the myocardium of due to partial volume effects [35,36]. In addition, extracardiac activity can spill over into left ventricular region [37], creating an apparent nonuniformity of count distribution.

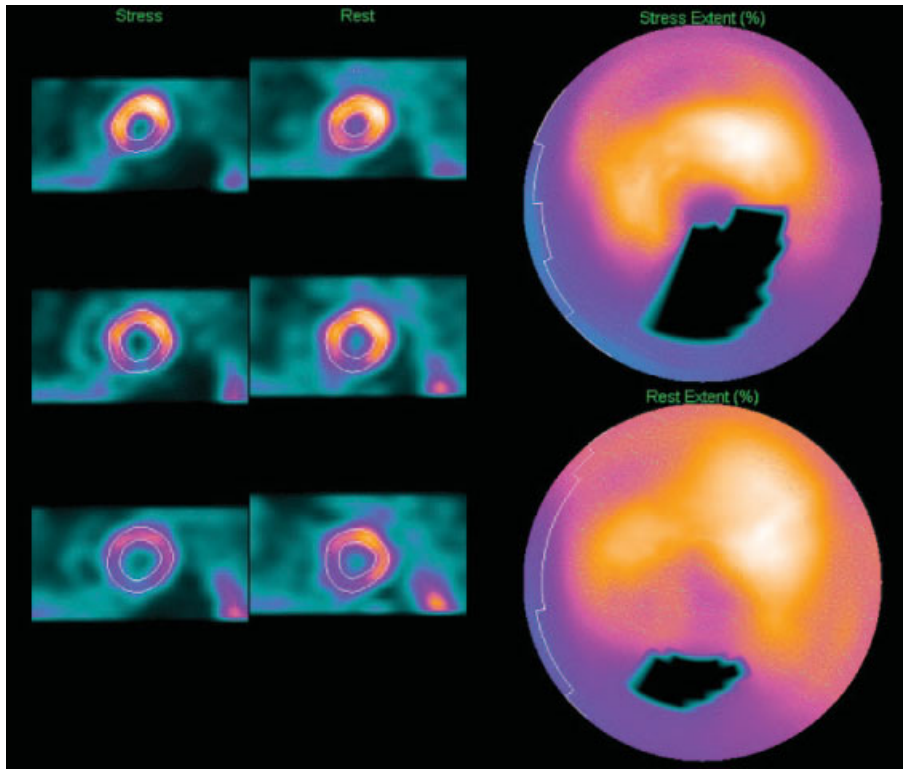

Figure 4.8 Short-axis stress and rest images and corresponding stress (top right) and rest (bottom right) blackout maps derived by the quantitative software obtained by masking the polar map pixels below normal limits.

If the AC algorithm is sufficiently robust, the normal limits can be simplified after AC by combining genders since the differences between males and females may no longer be statistically significant [35,38] (Fig. 4.9). In relatively small studies, improved diagnostic performance of automatic quantification with the aid of attenuation-corrected normal limits has been shown, and may be particularly useful in obese population and in patients with left main disease [38,39].

Combined prone and supine quantification

In order to improve specificity, we have routinely performed combined supine and prone imaging at Cedars-Sinai for over 10 years (see Chapter 6). Until recently, this practice reduced our reliance on quantification, since the quantitative method had been applied only to the supine images. In a recent study, a combined automatic image quantification using images acquired in prone and supine orientation was shown to improve the diagnostic performance (increased specificity) in a manner similar to what had been reported with attenuation-corrected studies [40] (Fig. 4.10). In fact, the combined prone/supine quantification was superior to the expert visual reader interpretation, despite the influence of the patient's clinical state on the visual reading as described in Chapter 6. We now routinely employ this approach in our image analysis and have found that the combined supine prone analysis ("prone plus") has resulted in increased reliance of our expert interpreters on the quantitative computer output. Of interest, we have preliminary data showing that the combined supine/prone assessment is also useful in eliminating artifact due to breast attenuation [41].

Count normalization

All of the techniques described in this chapter quantify relative decrease of perfusion in a portion of the LV as compared to the rest of the myocardium (which is assumed to be normal). Therefore when comparing a given patient's data to the normal limits, some form of count normalization (patient to normal limits) must be performed. Simple normalization schemes are typically not effective since normalization to total counts in the myocardium would over normalize studies with large defects and normalization to maximum counts may be skewed by occasional hot spots or heterogeneous distribution of normal counts in the myocardium (hot lateral wall).

Previously, uniform standard deviation thresholds were deemed not optimal due to the non-Gaussian distribution of normalized counts [25] and regional modifications of standard deviation thresholds (ranging from 1.75 to 3.75) were derived by receiver operator characteristics (ROC) analysis [42]. However, this compensation was required

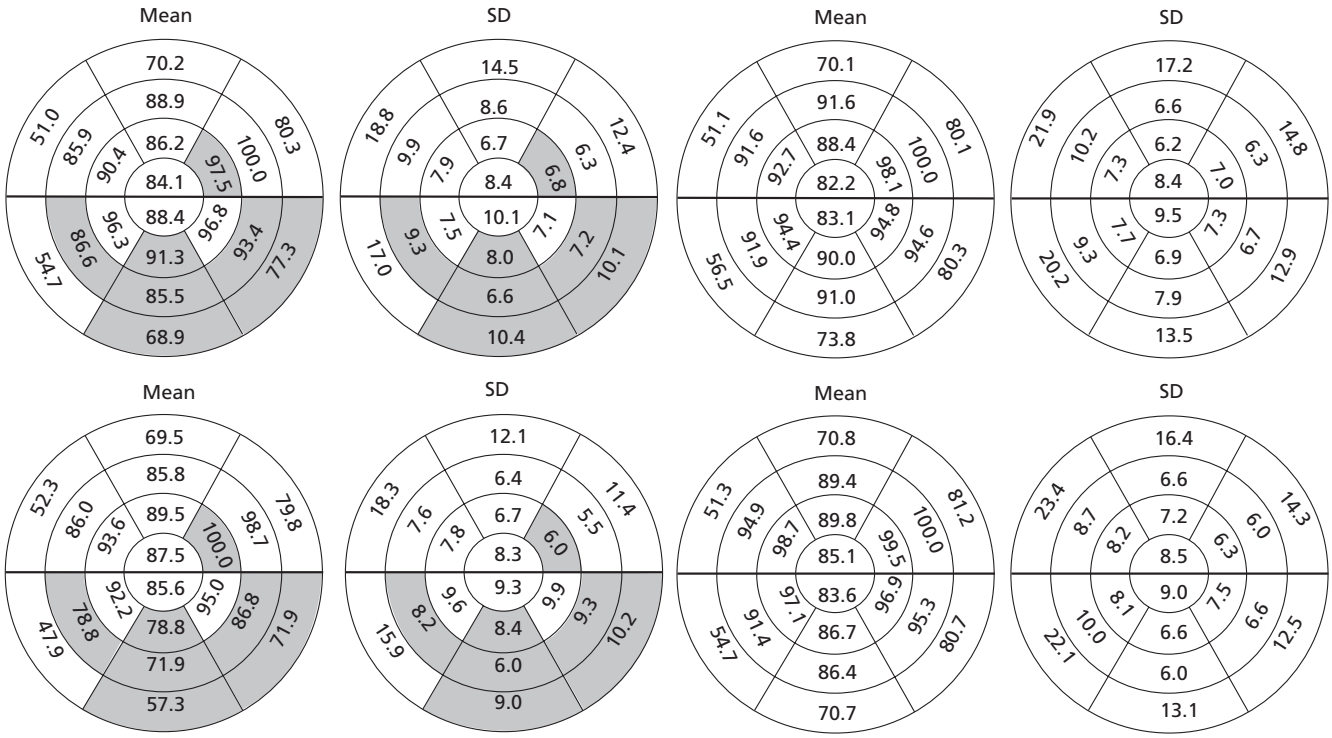

Figure 4.9 Segmental comparison of gender-matched uncorrected (left two columns) and gender-independent attenuation corrected (right two columns) normal myocardial perfusion distributions (mean and corresponding SD) (results for women are shown in the top row and those for men are shown in the bottom row). Segmental comparisons are expressed as percentage of maximum regional uptake. Segments highlighted in gray are statistically significantly different between genders ($p < 0.01$). (Reproduced with permission from [38].)

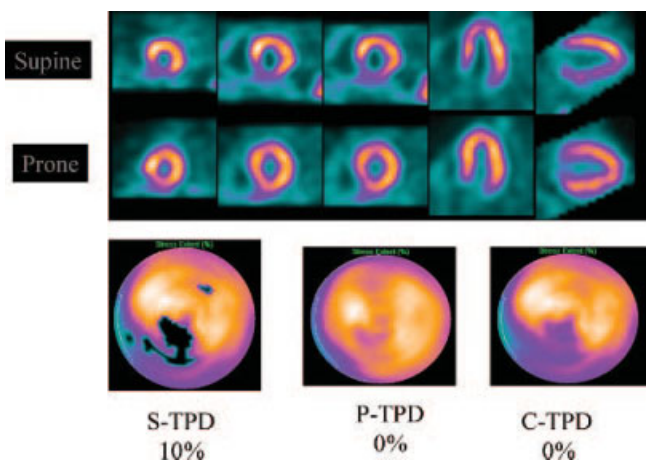

Figure 4.10 Example of supine and prone image quantification using appropriate supine and prone normal limits in a normal Tc-99m stress study of a 69-year-old male with atypical angina (confirmed by angiography). Supine quantification (S-TPD) shows defect of 10% due to significant AC. Prone quantification (P-TPD) shows no defect. Combined (C-TPD) prone–supine quantification shows no defect [40].

due to non-Gaussian count distribution caused by the normalization of intersubject profiles to the maximum [25] or a given percentile [43]. Recent techniques apply more complex normalization schemes which allow the use of uniform standard deviation threshold (typically 2.5 SD or equivalent 3.0 average deviations) and therefore would not require the per segment or per region optimization of the abnormality thresholds [34]. Williams et al. found significant differences in quantification results due to normalization effects [44]. The count normalization techniques have a significant effect on the final results and may preclude direct comparison of the results between various methods.

Quantitative perfusion parameters

Various quantitative parameters related to perfusion can be derived from myocardial perfusion scans. They are summarized in Table 4.1. In general, there are global parameters and regional parameters that allow automated localization of the defects. These parameters are most commonly obtained by the comparison to normal limits [23,24,26,34,42].

Table 4.1 Quantitative measures of myocardial perfusion.

Global	Regional	Description	Typical abnormal threshold
X		Percentage of the LV surface or volume where perfusion counts are below normal limit. Can also be expressed in absolute units (ml) [23,34,42].	3–5%
X		Average number of standard deviation below normal limits within the area of the defect [34,35,45]	2.5
X		Perfusion deficit in the myocardium obtained by integrating severity values in all polar map pixels belonging to the defect [34,45]	3–5%
X	X	Quantitative segmental scores in 17- or 20-segment model. When summed they provide global measure [23,34]	Score 4
	X	Percentage of the defect within a defined vascular territory. Vascular territories can be defined by empirical maps or geometrical models [23,34,35,42]	3–10%
X		A relative measure of change in counts between stress and rest or serial stress estimated by direct pixel-by-pixel comparison of serial or sequential images [46–48]	2–10%

We have recently described a perfusion deficit measure that combines defect extent and severity in one variable, and thus represents a measure of missing counts. This approach was adopted based on prior work from this laboratory documenting that both the extent and the severity of perfusion defects influence the prognostic power of myocardial perfusion imaging [49]. For example in the Cedars-Sinai QPS module, the variable total perfusion deficit (TPD) is defined in the following manner:

$$\mathrm{TPD} = 100\% \times \sum_{a=0}^{a<A} \sum_{p=0}^{p<P} \frac{score(a,\, p)}{4AP} \tag{4.1}$$

where a, p are the radial coordinates of the polar map, A, P are the maximum number of samples in each dimension, and $score(a,\, p)$ is the pixel score at the polar map location $(a,\, p)$. The theoretical maximum value for TPD is 100% for a case with no visible uptake (less than 70%) [34]. A similar concept has been used by other quantification packages. For example, Fig. 4.11 demonstrates the measure of hypoperfusion derived from circumferential profiles by Liu et al. [45] used in their Wackers-Liu quantification software, which is similar in concept to the total perfusion deficit.

Some techniques allow derivation of certain perfusion parameters without the use of normal limits. For example, in the Mayo Clinic approach, the determination of the defect size is performed using the threshold-based method [50,51]. This technique has been extensively validated for clinical trial endpoints [52,53]. The method assumes that the myocardium can be considered as a sum of cylinders. Five representative slices are chosen (basal,

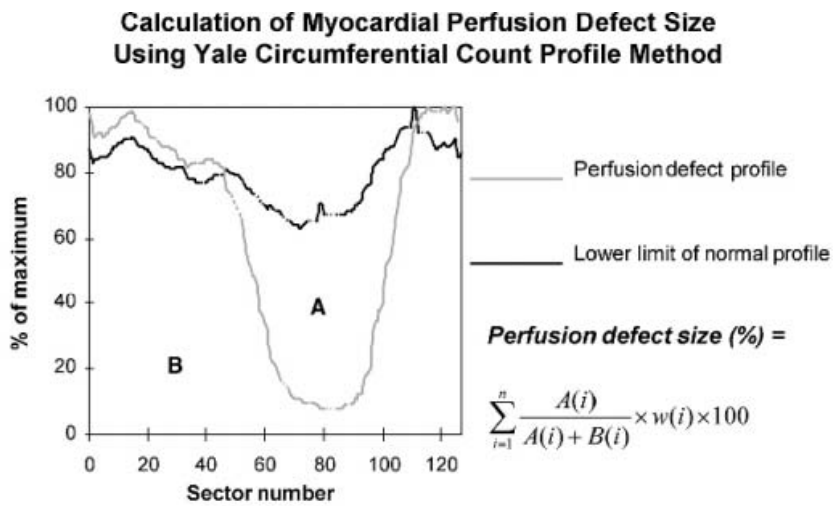

Figure 4.11 Principle of quantification of myocardial perfusion defect size from circumferential profiles applied by Liu et al. [45].

mid-ventricle, apical, and two more between base and mid-ventricle and between mid-ventricle and apex). For each slice, a circumferential count profile is generated and the fraction of counts that drop below 60% of the maximum counts in the profile is considered to represent the fraction of that slice that is infarcted. The percentage of infarcted myocardium is then calculated knowing the volume and the infarcted fraction of each slice. One problem with the threshold approach is that it does not take into account the regional variation in counts associated with non attenuation-corrected data. Recently, methods for direct stress–rest or serial change measures have been described that obtain regional perfusion parameters without the need for inter-patient normal databases [46]; however, this technique requires a reference baseline scan (see Recent Developments in Perfusion Quantification section in this chapter).

The abnormal threshold for each of the quantitative perfusion measures is specific to a particular definition and implementation. Typical reported ranges for several variables are shown in Table 4.1.

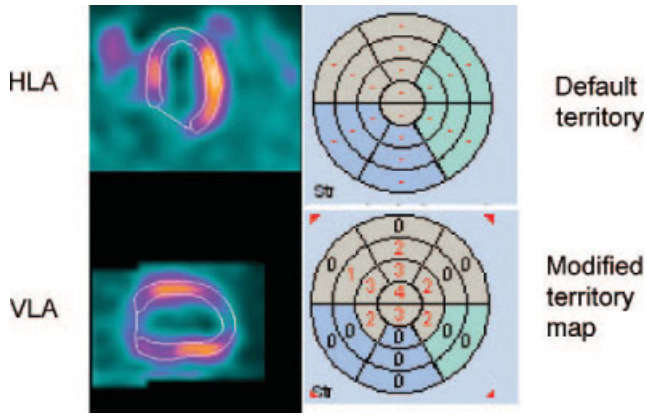

Figure 4.12 Example of dynamic territory maps in a case with 100% proximal LAD stenosis (confirmed by coronary angiography). Stress Tc-99m-sestamibi HLA and VLA images are shown on the left. Default segmental assignment to territories is shown in top-right panel (brown-LAD, green-LCX, blue-RCA). Dynamic assignment based on the segmental perfusion scores is shown at the bottom right. Note that two lateral segments changed the assignment from LCX to LAD; the dynamic assignment allowed correct identification of LAD single vessel disease.

Regional quantification and localization of defects

From a clinical perspective, it is frequently important to assign a perfusion defect to a given vascular territory. This task can be performed automatically by the quantification software. One approach is to utilize predefined vascular territory maps defined in polar map [42] or voxel coordinates [54]. Subsequently, the extent of the perfusion defect within a given territory can be computed and thresholds of the disease in a given territory can be established. Another approach is to use segmental definition and dynamically apply a set of rules which will assign a segment to a vascular territory based on the pattern of the perfusion scores [43], creating dynamic vascular maps. An example of such a dynamically created territory based on the 17-segment model is shown in Fig. 4.12.

Performance of the automatic assignment of the defect to the correct vascular territory is reduced in comparison to the overall detection of coronary artery disease (CAD) in most reported studies [34,35,43,55] due in part to variable vessel anatomy and imprecise territory maps. Ultimately, methods that would include patient-specific coronary anatomy maps could prove more accurate [56]. Such maps could become available routinely with emerging SPECT/CT or PET/CT systems, allowing for improved localization of the perfusion defects [57].

Segmental scoring models

Although accurate automatic quantification of perfusion is the preferred goal, it is often required for the observer to visually rate the perfusion deficit of the LV on a global or regional basis. As described in Chapter 7, a convenient segmental scoring system has been designed for this purpose [58], dividing the polar maps into arbitrary segmental definitions. Subsequently, users can score perfusion on a per-segment basis on a given scale (for example, 0 (normal) to 4 (absent uptake)). Such segmental scoring has been described with the number of segments ranging from 9 to 400. For purposes of standardizing the approach, the 17-segment model is now recommended [59]. Segmental scores can be summed to provide a global visual measure of the perfusion deficit combining extent and severity such as summed stress score (SSS) or summed rest score (SRS) [58].

Computer quantification can be utilized to provide the "first guess" of the visual scores for the user [60]. Such computer-derived scores can then be further adjusted by the user if required. The computer-generated scores can be obtained by comparison of perfusion samples to the low-likelihood normal limits and generating an average severity score per segment [32,34] on a given scale resembling user scoring. In some approaches, segmental scores have been derived automatically by training the system with a large number of user-defined scores and maximizing the agreement between the user- and computer-derived scores [23].

Computer-derived segmental scores are rounded off to integer values and use coarse segment boundaries, unlike continuous variables such as defect extent or perfusion deficit. Therefore they may be inaccurate for small defects that are located between two segments. However,

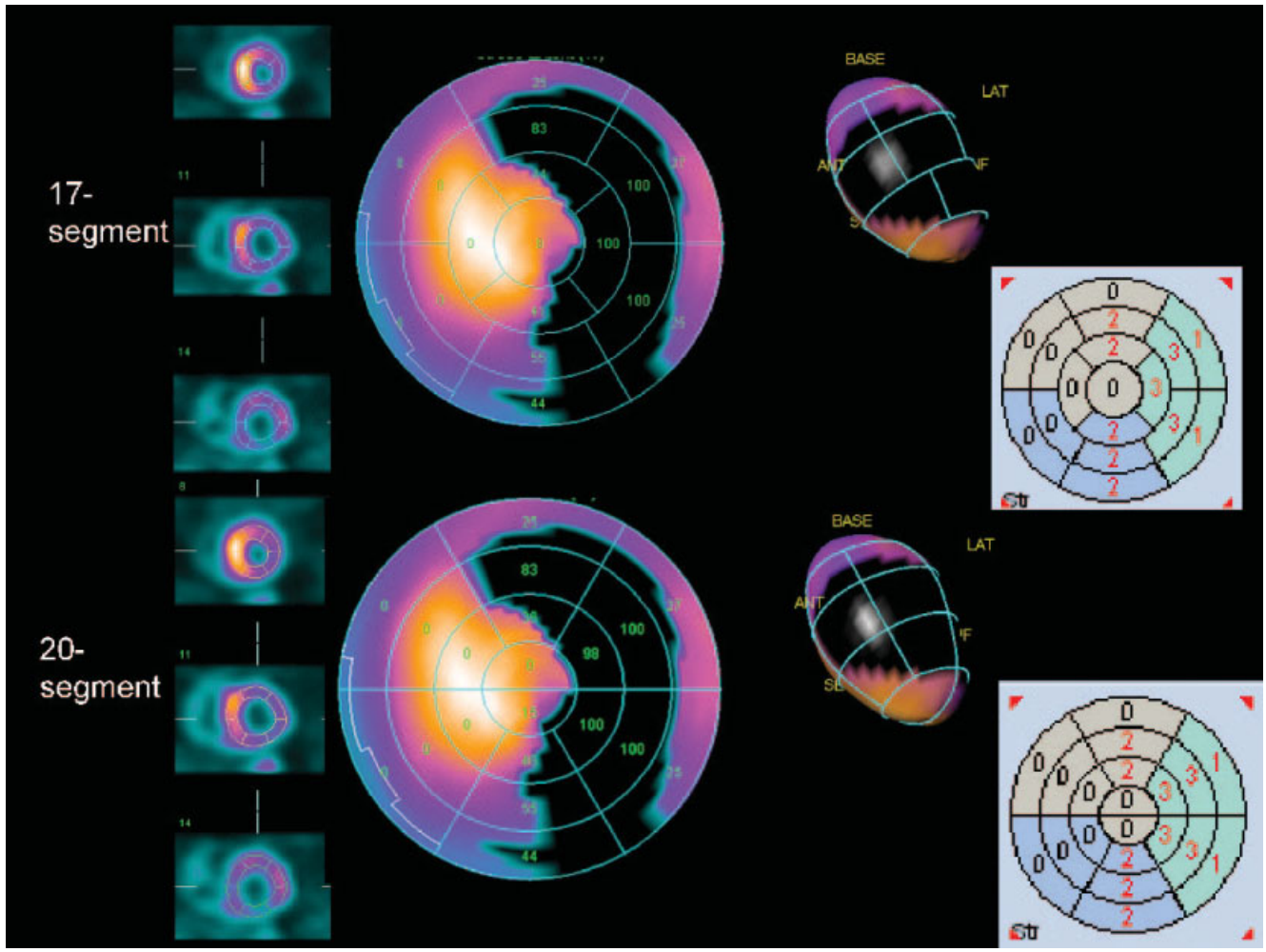

Figure 4.13 An example of a 17-segment and 20-segment quantification of stress Tc-99m-sestamibi scan in a 74-year-old male with triple vessel disease (confirmed by coronary angiography). Summed stress score for this patient was 23 with the 20-segment model and 20 with the 17-segment model. TPD is 27%. Seventeen-segment quantification results are presented in the top row and 20-segment results are presented in the bottom row. In each row, segment maps are superimposed on original slices, polar maps, 3D surfaces, and scores.

the advantage of scoring approach is that it provides the interpreter a manner for interacting with or correcting the quantitative, computer-derived data. For example, a quantitative polar map may show a perfusion defect in a region of obvious breast attenuation. The interpreter generally has difficulty in "correcting" the standard quantitative display. The computer-based segmental scoring approach provides a convenient manner by which the reader can adjust the automatically generated scores. Such computer-aided scoring is commonly used in clinical practice [61,62]. Figure 4.13 shows an example of perfusion defect scored automatically in 17- and 20-segment models. Segments can be displayed as a 2D grid or superimposed on image slices and/or on a 3D surface. Algorithms have been devised to convert visually or automatically defined scores between the 17- and 20-segment models [63].

Validation

Validation by coronary angiography

Validation of quantitative myocardial perfusion is challenging since there is no widely available equivalent "gold standard" to which the results can be compared. The most commonly used comparison made is to coronary angiography [34,43,54,55]. The angiographic test accurately defines vessel morphology in the assessment of CAD; it also forms a basis for treatment of CAD [64]. Although coronary angiography has been shown to be limited in demonstrating the effect of the lesion in the artery on the perfusion of the myocardial tissue [65], it remains the most commonly employed standard for validation of

Table 4.2 Sensitivity and specificity for detection of CAD (≥70% stenosis) by stress SPECT Tc-99m without AC, by automatic quantification methods.

Author	Sensitivity	Specificity	No. of patients
Van Train [55]	87%	36%	161
Sharir [43]	88%	88%	93
Ficaro [35]	72%	71%	60
Slomka [34]	93%	79%	256
Rubello [67]	93%	61%	120

myocardial perfusion SPECT assessments. The results of the test can be presented as an ROC curve for the detection of angiographic disease, expressing sensitivity/specificity for using a particular quantitative threshold.

One difficulty with angiographic validation is referral bias [66]. Regarding test specificity, since the results of nuclear testing are now used to determine whether patients go to coronary angiography, there is a paucity of normal patients with normal SPECT referred for the catherization. Since these patients typically present with clinical symptoms, often there can be underlying abnormality even without a significant stenosis. Consequently, specificity performance defined by this "gold standard" may be substantially lower than the actual clinical specificity. Therefore, our laboratory previously described the use of the "normalcy rate" as a proxy for specificity by using an additional population with low likelihood of the disease (based on age, sex, symptoms, and the results of stress ECG testing, but not based on the nuclear test results), but in whom angiography is not performed [55]. Furthermore, while angiography can be used as a "gold standard" only for the task of detection of coronary disease, it is generally not considered an accurate standard for perfusion defect sizing.

Some of the results of the automated quantitative analysis (no visual analysis) of stress Tc-99m sestamibi studies without AC validated by coronary angiography are presented in Table 4.2.

Validation by cardiac magnetic resonance imaging

While rest/stress assessment of myocardial perfusion by magnetic resonance imaging (MRI) is not yet considered a standard, delayed-enhancement MRI (DE-MRI) has been shown to be a highly accurate method for the noninvasive estimation of infarct size and location, in the setting of either acute [68,69] or chronic myocardial infarction [70,71]. DE-MRI is now widely accepted as the gold standard for the quantitative estimation of infarct size and thus could be used for validation of the perfusion defect size measurement by SPECT. In one recent study, quantitative normal-limit analysis (4D-MSPECT; University of Michigan, Ann Arbor) [32] was applied to compare defect sizes in patients with acute infarcts measured by 4-hour delayed ^{201}Tl with defect sizes obtained by DE-MRI [72]. Infarct sizes have also been measured by the QPS software on resting Tc-99m SPECT and compared to DE-MRI [73,74]. In a recent study, we validated the performance of simplified normal-limit quantification in QPS for the detection and sizing of infarcts by resting Tl-201 imaging using DE-MRI as a gold standard in 82 patients [75]. We found correlation (r) of size to be 0.85 and ROC area under curve for the detection to be 0.90. Figure 4.14 shows a comparison between a defect size on SPECT and DE-MRI. The threshold-based quantification technique was also found to correlate well with DE-MRI data [76]. Discrepancies between SPECT and DE-MRI are attributed to partial volume effects in case of nontransmural defects [77].

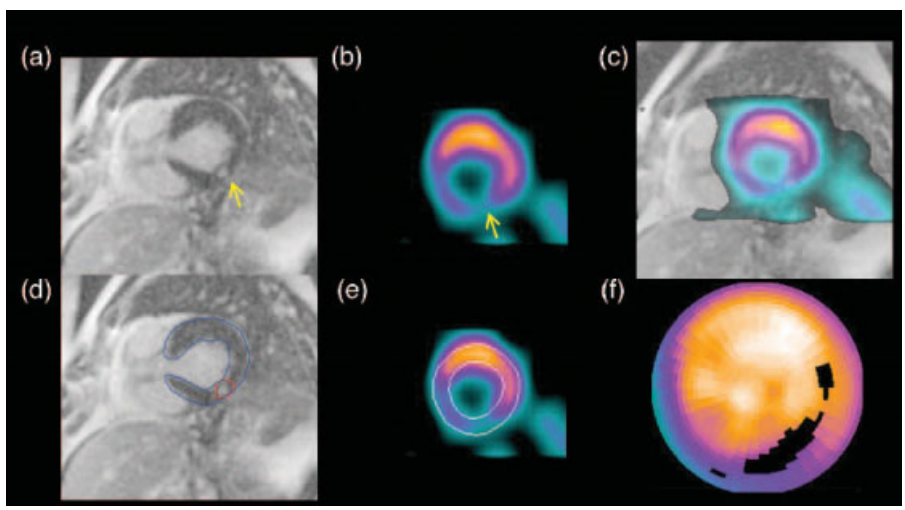

Figure 4.14 An example of delayed enhancement MRI with a small defect. Defect quantification results were 0.8% by MRI , 6% by EXT SPECT, and 5.7% by SPECT TPD . In the top row, we show MRI slice with the defect with marked infarct region (red) (a), corresponding slice from delayed Tl-201 rest SPECT (b), and fused MRI-SPECT image (c). In the bottom row, we show the vertical long axis of DE-MRI with the same defect (d), corresponding vertical long axis SPECT image (e), and results of polar map quantification (f). Arrows point to the defect location on panels (a), (b), (d), and (e). (Reproduced with permission from [75].)

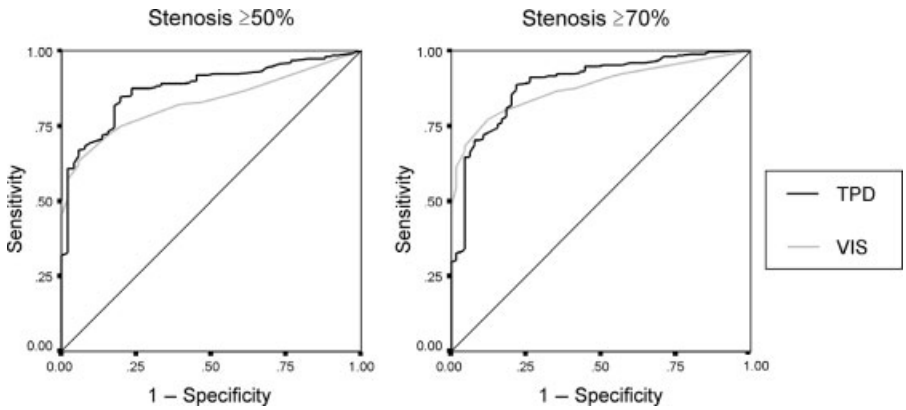

Figure 4.15 ROC curves for detection of CAD (≥50% and ≥70% stenosis cutoff) for total perfusion deficit (TPD) and visual scoring (VIS) for the overall test population ($n = 256$) [34]. The difference between TPD and VIS is statistically significant for a 50% stenosis cutoff. (Reproduced with permission from [34].)

The size of the hypoperfusion region can be obtained at stress and rest with MRI [78,79] and can be compared to SPECT [80,81]. However, since perfusion MRI is a first-pass technique and has limitations, including incomplete coverage of the ventricle, it is not yet the best validator for SPECT quantification. The agreement between SPECT quantification and MRI perfusion findings has been found to be only moderate [82].

Other validation approaches

Validation of myocardial perfusion SPECT quantification for defect sizing has also been performed in animal models [83,84] and in phantom studies [45,85]. These approaches, however, are of limited use in the evaluation of quantitative software tools as applied to patient studies, when images are compared with the database of normal scans to derive measures of perfusion defect extent and severity. In a unique study, validation of infarct size measurements by Tc-99m-sestamibi SPECT was performed histologically in 15 patients undergoing heart transplants [86], which is perhaps the ultimate validation method.

Other methods for validation can utilize the comparison to visual reading of segmental scores and the agreement of the quantification with the human experts [43]. However, it is possible that visual experts could actually underperform in comparison to a well-tuned algorithm. For example, our group has recently shown that the detection of coronary disease defined as greater than or equal to 50% stenosis was actually better by the quantitative software than by visual analysis [34] (Fig. 4.15). In an indirect approach, the relationship of automatic quantitative perfusion defect size and severity to functional parameters can be evaluated assuming that good correlation should be obtained [87]. Some studies suggest variability in the measurements obtained by different quantitative SPECT techniques [88–90], which is most likely due to different assumptions and different mathematical models used by these techniques. In the future, it is likely that such inter-software differences will be resolved by the use of the external gold standards for calibration.

Table 4.3 summarizes various approaches to the validation of myocardial perfusion quantification results with references, and lists the specific limitations of each approach.

Limitations

Instrumentation limitations

Due to inhomogeneous attenuation properties of the thorax, the effect of scatter and attenuation may cause artifacts in myocardial SPECT [92]. The presence of scatter reduces spatial resolution in the images, resulting in image blurring and spillover of extracardiac activity to the left ventricular region. Attenuation of photons causes a relative decrease of the observed activity in regions located deeper in the body. The amount of attenuation depends also on the character of the surrounding tissue. Scatter and attenuation contribution increases from the apex to the base of the heart. Thus, hypoperfused regions in basal areas can be more difficult to detect. Moreover, depth-dependent spatial resolution of projection images may cause reconstruction artifacts, especially with 180° and noncircular orbits [93]. Since photon absorption is greater for lower energies, the effect of scatter and attenuation is more severe with Tl-201 than with Tc-99m based agents. Attenuation artifacts in women are caused also by breast tissue, which reduces the activity in the anterior region [94].

Although several approaches proposed to reduce the degrading effects of attenuation and scatter are being implemented in clinical practice [95,96], there are remaining controversies [97–99] and significant variability in characteristics of various implementations [100]. There have been only few studies evaluating the effects and performance of fully automatic quantification algorithms with and without such correction methods [35].

Table 4.3 Summary of validation approaches for quantitative myocardial perfusion SPECT.

Gold standard	What can be validated	Description and references	Limitations
Coronary angiography	Detection of CAD	Compare the presence of significant stenosis (≥50% or ≥70%) to the quantitative results [34,43,46,54,55]	Referral bias. Paucity of suitable normal population Interobserver variability of coronary angiography. Severity of stenosis not related to defect size
DE-MRI	Detection and size of infarcts	Use presence and size of infarct on delayed enhancement MRI as a gold standard for resting perfusion data [75]	Delayed enhancement MRI only applicable to infarct size Quantitation of perfusion MRI is not yet widely established Limited sampling by MRI Manual definition of infarct size on MRI Applicable to rest scans only
Pathology	Detection and size of infarcts	Use pathological quantification of the extent and severity of scarred and normal myocardium as a reference [83,84,86]	Usually limited to animal models or transplant patients Not applicable to stress perfusion. Technically challenging
Physical Phantoms	Detection, size, and severity of defects	Place physical defects of varying size in phantom [27,45,52,85]	Not possible to validate normal-limit-based techniques No realistic anatomical variations, no cardiac motion
Other quantitative packages	Reproducibility	Compare results between different quantitative methods [88,89]	Different mathematical models and definitions of quantitative parameters, Lack of gold standard PET suffers from some of the same limitations as SPECT (e.g., relative rather than absolute measurements in routine clinical practice)
PET	Detection of CAD, extent of defects	Compare quantitative SPECT and PET parameters [91]	Comparison of relative perfusion SPECT to absolute blood flow measurements by PET not yet reported

Motion artifacts

SPECT acquisition requires that a patient remain still during the scan; motion results in artifacts on the reconstructed images, which can often lead to false-positive results. Image quantification algorithms are very sensitive to motion artifacts [8]. Analysis of raw projection images is recommended to reveal such errors [101,102]. Shorter acquisition times and specialized devices providing good arm support for patients reduce chances of patient motion during the procedure. It is possible to detect and compensate for the patient movement after the acquisition, by applying motion correction algorithms [7,103,104]. Respiratory motion can be another reason for motion artifacts, especially after exercise. SPECT acquisition, which can last up to 20 minutes, is performed over many cardiac cycles. Heart motion, another source of artifacts, can be reduced by utilizing the motion-frozen technique [105]. An example of erroneous image quantification due to patient motion artifacts is shown in Fig. 4.16.

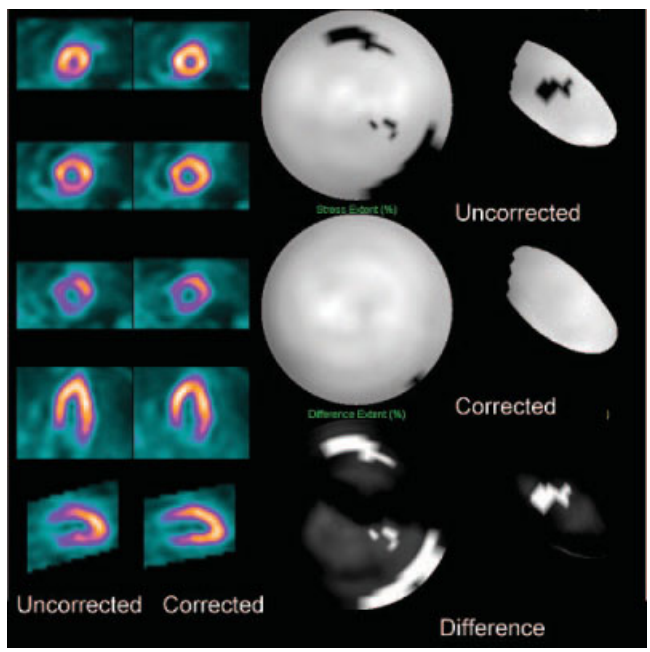

Figure 4.16 An example of false-positive quantification results due to patient motion. Uncorrected and corrected images, polar maps, and scores are shown. Polar map with the differences between study with and without motion is also shown, illustrating the effect of motion on the count distribution.

Physiological limitations

Even if the imaging of the radiotracer distribution in the heart was perfect, a false-positive or false-negative diagnosis and quantification results can occur due to various

physiological factors. Patients may not be stressed adequately and therefore the expected effect on myocardial perfusion may not occur. Superimposed radioactivity in the abdomen may degrade the image quality and elevate counts in the inferior region [36]. If such a spurious increase in uptake is observed on the rest study and compared to the normal stress study, it can imitate a relative decrease of uptake under stress. Alternatively, it can mask a defect on either a rest or stress study. Other reasons for abnormal studies are noncoronary diseases of the heart such as left bundle branch block [106], or myocardial hypertrophy [107]. An unusual contraction of the heart can also lead to the misinterpretation of defects on both rest and stress studies [108]. Balanced ischemia due to triple vessel disease can lead to entirely false-negative findings. More commonly in triple vessel disease, there is substantial underestimation of the size of the ischemic zone as zone supplied by the least stenoses artery or arteries may be the most normally perfused and might appear normal [1,109] (see Chapter 6).

Recent developments in perfusion quantification

Voxel-based quantification

An alternative approach to quantification of myocardial perfusion is voxel-based analysis of counts and registration of patient images to 3D templates created from studies of normal patients [15,16] (Fig. 4.17). A general-purpose algorithm is applied to perform automatic segmentation and realignment of the myocardial image to the template and subsequent voxel-based comparison to normal limits. Image voxels are marked directly on the image slices without using polar map sampling. Typical steps performed in the 3D quantification process are illustrated in Fig. 4.18. The results of 3D voxel quantification and corresponding standard polar map quantification are shown in Fig. 4.19. Potential advantages of the 3D approach are (1) direct visualization of defects on image slices, (2) no need for arbitrary geometrical models, and (3) integration of 3D alignment and quantification. This 3D voxel-based registration method was also recently applied in the direct quantification of ischemia [46].

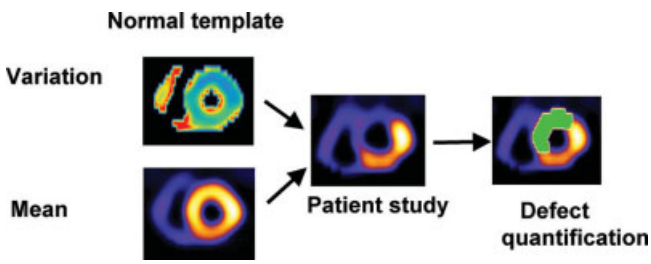

Figure 4.17 The principle of 3D voxel-based quantification. Registered and resized patient study is compared to 3D templates (3D mean and variation maps). Hypoperfused voxels below normal limits are marked directly on image slices.

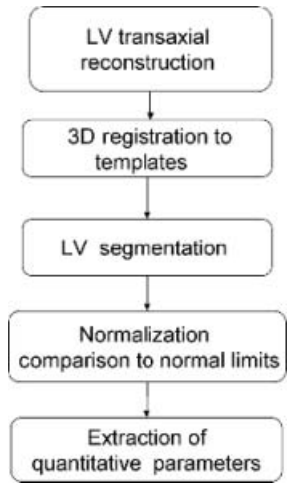

Figure 4.18 Overview of the steps in 3D voxel-based quantification.

Motion-frozen quantification

Myocardial perfusion SPECT images are blurred due to movement of cardiac walls. However, the gated SPECT technique permits the acquisition of separate 3D images corresponding to several portions of the cardiac cycle. If gated SPECT acquisition is performed, each view is divided into a number of images (usually 8 to 16) containing counts corresponding to particular segments of the average cycle based on the ECG signal. Although each gated

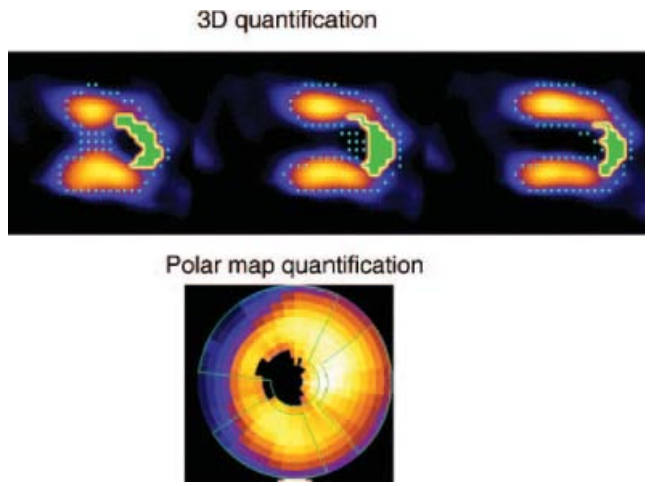

Figure 4.19 Example of the voxel-based and equivalent polar map disease quantification in a case with stress Tc-99m-sestamibi scan with LAD [33].

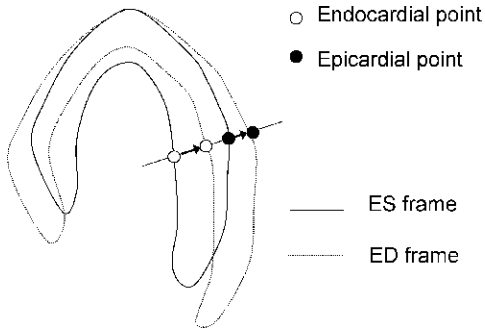

Figure 4.20 Diagram illustrating generation of source and target equivalent points, which can be used to warp gated image frames to one common position (for example, end-diastolic). Both endo- and epi-cardial surfaces are used to create two "displacement vectors" for each normal profile. (Reproduced with permission from [105].)

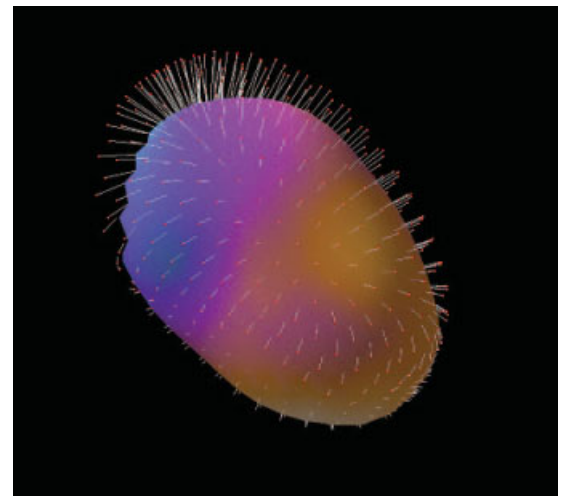

Figure 4.21 Illustration of the "displacement vectors" used in image warping, indicating the amount of cardiac motion between the end-diastolic and end-systolic frames. End-systolic epicardial surface is shown with perfusion data represented in color. "Displacement vectors" (white) show the local motion between the end-systolic and end-diastolic positions. The end-diastolic position of the epicardial surface is marked with red points. (Reproduced with permission from [105].)

segment contains fewer counts than conventional SPECT images, the blur due to heart motion is reduced. Most myocardial perfusion imaging protocols utilize gating during image acquisition as recommended by the American Society of Nuclear Cardiology [110]. It has been previously suggested that analysis of gated end-diastole (ED) frames only, can improve the detection of CAD in females [111]. However, ED images are not suitable for reliable computer quantification, since they contain counts from a limited portion of the cardiac cycle. Therefore, image quantification and analysis of perfusion has been most commonly performed on summed (added) image frames from all cardiac cycles, without consideration for cardiac motion.

Recently, a novel "motion-frozen" display and quantification technique for gated myocardial perfusion imaging has been proposed to address this issue [105]. The "motion-frozen" technique utilizes all gated frames for perfusion quantification, taking into account cardiac motion. This technique eliminates image blurring due to cardiac motion, with noticeable improvement in image quality. "Motion-freezing" of perfusion data is accomplished by detection and subsequent motion tracking of the LV endo- and epicardial borders, with an established LV myocardial contour extraction algorithm such as QGS [18]. Subsequently, 3D nonlinear image warping is applied to all phases of the gated data, deforming each image phase to match the position of the ED phase (Fig. 4.20). In Fig. 4.21, we show the extent of cardiac motion on a typical gated myocardial perfusion scan by displaying the end-systolic to end-diastolic displacement vectors. The warped images can be summed, forming "motion-frozen" perfusion images. Such "motion-frozen" perfusion images have the visual appearance similar to the ED frames but are less noisy since they contain counts from all or most cardiac cycles (Fig. 4.22).

Image quantification algorithms can use the motion information in polar map coordinates to derive cardiac motion-corrected polar maps. "Motion-frozen" quantification can be performed using polar maps that are created from individual polar map samples for each portion of the cardiac cycle, as defined by the gated 3D contours. Nonlinear image warping does not need to be performed for quantification in polar map coordinates. Such "motion-frozen" quantification technique has been demonstrated to improve the diagnostic performance in a selected group of patients [112]. The improvement in image quality is more likely to resolve borderline findings in patients with high ejection fractions, in which cardiac motion significantly reduces the image resolution. Furthermore, cardiac motion becomes the dominant degrading effect as the image resolution increases. Therefore, this technique may become of great importance in PET imaging or future high-resolution SPECT imaging.

Direct quantification of ischemia

Myocardial ischemia is detected by comparing stress perfusion images to images obtained at rest. Hypoperfusion defects that are larger at stress than at rest indicate the presence of ischemia. In typical quantification protocols, the stress and rest data are fitted separately to a geometrical polar map model. Subsequently, polar maps are created independently for stress and rest patient data and are compared to the respective stress and rest normal limits. Alternatively, separate reversibility limits can be established as applied to delayed Tl-201 imaging [113]. A

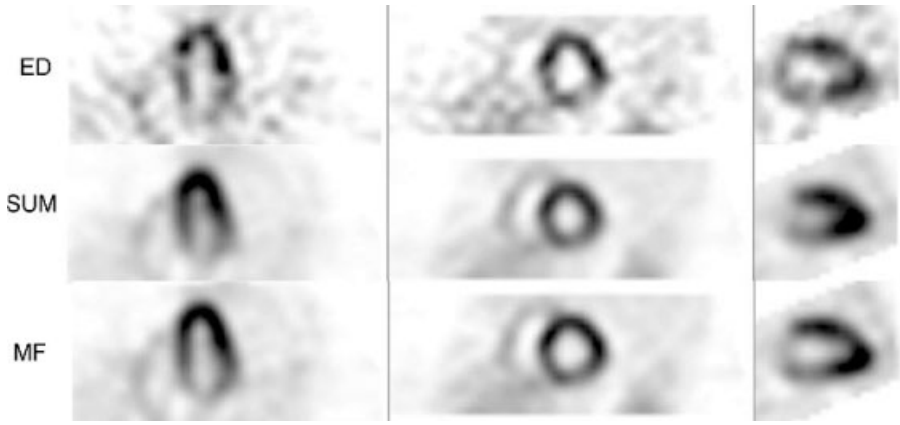

Figure 4.22 "Motion-frozen" perfusion images compared to the summed perfusion images in the case of double vessel disease confirmed by angiography (100% LAD occlusion and 80% LCX occlusion). Both standard quantification technique and visual analysis of summed data identified only the LAD lesion; the additional LCX lesion was identified only by the "motion-frozen" quantification. (Reproduced with permission from [105].)

semiquantitative visual segmental scoring system is also used to assess the extent and severity of ischemia by the summed difference score (SDS), derived as the difference between summed stress score (SSS) and summed rest score (SRS) [114].

One limitation of such indirect approach for the estimation of ischemia is that the orientation and position differences between stress and rest images can occur since no direct stress–rest alignment is performed. Such misalignment can confound the quantitative results. Furthermore, the normal limits are based on *inter*-patient comparisons; therefore these may not accurately reflect normal limits of *intra*-patient changes, such as those observed between rest and stress. Thus, a change might not be significant on stress when compared to the normal population stress scans using the standard database approach, but there still may be a detectable stress–rest count change for a given patient. Moreover, separate stress and rest count normalization factors are calculated for paired scans when these scans are compared to their normal limits, compounding quantification errors.

Recently, a new quantification method for direct measure of ischemia derived from paired rest–stress scans was introduced by our group [46]. This quantification is accomplished by 3D image coregistration of rest and stress images and voxel-by-voxel estimation of differences in 3D without utilizing normal limits for stress and rest. After image registration and normalization, the stress–rest count difference is derived from the voxels contained only within the 3D left ventricular volume. Only stress contours are used since rest scans have been spatially aligned to the stress scans in 3D. Image registration allows for the anisotropic adjustment in size to compensate for the possible Transient Ischemic Dilation (TID) effects [46]. Since the same contours are used for stress and rest quantification, the errors due to possible differences in the definition of the valve plane are eliminated. The voxel count differences are then divided by the total rest counts, resulting in a relative count change measure, given by the equation below:

$$\text{CHANGE} = 100\% \times \Big\{ \sum_{x,y,z} [R(x,y,z) \times \text{NF} - S(x,y,z)] / \times \sum_{x,y,z} R(x,y,z) \Big\}$$

where $R(x, y, z)$ and $S(x, y, z)$ are counts in rest and stress images at voxel position x, y, z, and NF is the global stress–rest count normalization factor. Changes between stress and rest images can be overlaid on raw stress slices and are rendered using a separate continuous color table and transparency function similar to the techniques used in image fusion, highlighting the rest–stress changes (Fig. 4.23). This technique allows direct localization of significant changes detected by the computer on image slices.

When such direct quantification technique was applied and tested for detection of CAD in patients without known infarcts, it performed equivalent to or better than the standard normal-limit-based technique. When compared for prediction of stenosis, the area under the ROC curve was significantly better for the new change measure than for standard measures such as SSS or defect extent obtained by existing quantitative approaches, which utilize normal databases [34]. These findings suggest that the quantification of ischemia could potentially be simplified for laboratories that do not have the capabilities and/or resources to derive their own normal databases, and are not able to use the standard sets of normal limits typically available with the quantification software due to their use of "unsupported" protocols or equipment.

Quantification of serial changes

Similar registration techniques can be applied to the analysis of serial changes. Analysis of serial changes by traditional techniques requires two separate comparisons to the normal database, which is not optimal due to

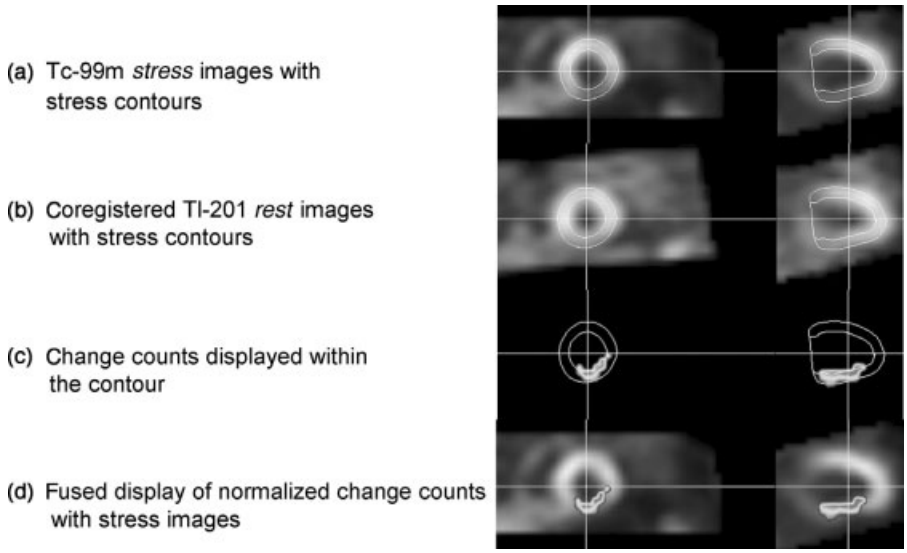

Figure 4.23 3D visualization of the ischemic stress–rest change of 4.5%. (Reproduced with permission from [46].)

possible contour mispositioning, multiple normalization procedures, and intersubject variability [115]. Sensitive methods for detection and estimation of changes in myocardial perfusion over time could improve confidence in using myocardial perfusion SPECT for these applications [47, 62, 116–118].

De Kemp et al. have devised a serial perfusion quantification method in which direct serial comparisons were applied [119]. They estimated the precision of SPECT perfusion and wall-thickening measurements from the gated residuals, after fitting the count data sector by sector to a modified sinusoid [48]. The resulting standard errors are used to create polar maps of the T-statistic, showing significant differences between serial scans (Fig. 4.24). When two scans are different, the distribution of T-statistics deviates from the theoretical t-distribution. Regional changes are localized after adjustment of the p value for test-retest repeatability and image smoothness.

Serial changes in paired stress scans have been also determined in a preliminary study by a technique based on 3D image registration [121]. It has been found that in patients with normal perfusion, the average positive or negative changes determined by the new approach were smaller than changes obtained by an existing quantitative scheme (changes in visual or quantitative SSS scores). At the same time, the new measure has detected a higher number of patients with improved perfusion in the revascularization group.

Another voxel-based technique for the quantification of serial changes was recently presented and uniquely validated in measuring reperfusion after the revascularization procedure using serial coronary angiography results as a gold standard [122]. Patient images were automatically registered to the 3D reference templates, which were used instead of 2D polar maps. Subsequently, the perfusion changes were considered only within the volume of the significant hypoperfusion detected in the first study. Using such approach, it has been established that the voxel-based technique was able to distinguish between patient groups with patent versus reoccluded coronary arteries when standard visual segmental scoring was not able to achieve that goal. The voxel-based quantification was also the only technique able to distinguish patients with patent

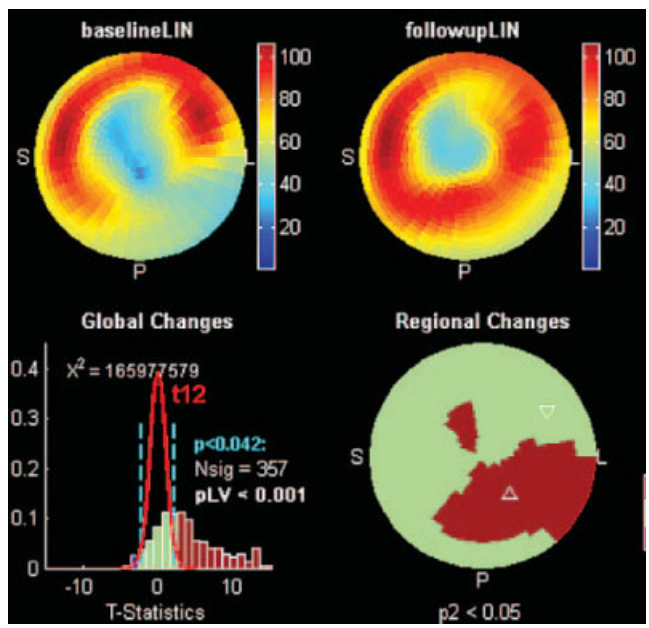

Figure 4.24 An example of serial quantification approach. Significant perfusion increases (red) are detected after coronary bypass surgery ($p < 0.05$). (Reproduced with permission from [120].)

arteries, when analysis was restricted to the volume of the initial ischemic defect.

These results suggest that the measurements of serial perfusion changes in SPECT using direct comparisons may be more sensitive than standard quantitative or visual approaches. These findings are significant because many of the previously published clinical trials evaluating myocardial perfusion changes after various therapies have used global measures such as visual SSS [58] or quantitative defect extents [123]. The improved new quantification techniques may be able to detect more subtle perfusion changes occurring over time.

Computer-aided interpretation of quantitative results

Expert systems for the final interpretation of the quantitative data have been proposed [124,125]. In such systems, polar map samples are typically used as input to a set of rules. The expert system can suggest which areas of the myocardium are hypoperfused and potentially help to avoid false-positive findings due to well-known artifacts. Performance of such system was shown to be comparable to human readers [126]. Others applied artificial neural network analysis to the bull's eye quantification [127–130] or segmental quantification results [131] and combined the perfusion data with clinical results [132]. In one study, the values of pixels on the polar map were used as input weights to the network. The results suggested that the neural network system scored better than an average radiology resident but slightly worse than an experienced radiologist [129]. Such techniques have the potential to further reduce the variability and subjectivity of the myocardial perfusion test, providing a consistently high level of diagnosis. However, the "black-box" character of the algorithms based on neural networks will remain problematic from the regulatory point of view.

References

1. Berman D, Hachamovitch R, Shaw L, Hayes S, Germano G. Nuclear cardiology. In Fuster V, ed. Hurst's the Heart. 11th edn. New York: McGraw-Hill Medical Publishing Division; 2004:563–597.
2. Wackers FJ. Science, art, and artifacts: how important is quantification for the practicing physician interpreting myocardial perfusion studies? Journal of Nuclear Cardiology 1994;1(5, Pt 2):S109–S117.
3. Garcia EV. Quantitative myocardial perfusion single-photon emission computed tomographic imaging: quo vadis? (Where do we go from here?) Journal of Nuclear Cardiology 1994;1(1):83–93.
4. Bai J, Hashimoto J, Suzuki T, et al. Comparison of image reconstruction algorithms in myocardial perfusion scintigraphy. Annals of Nuclear Medicine 2001;15(1):79–83.
5. Updated imaging guidelines for nuclear cardiology procedures, part 1. [Comment On: Journal of Nuclear Cardiology Jan–Feb 2001;8(1):4–9]. Journal of Nuclear Cardiology 2001;8(1):G5–G58.
6. Germano G, Kavanagh PB, Chen J, et al. Operator-less processing of myocardial perfusion SPECT studies. Journal of Nuclear Medicine 1995;36(11):2127–2132.
7. Matsumoto N, Berman DS, Kavanagh PB, et al. Quantitative assessment of motion artifacts and validation of a new motion-correction program for myocardial perfusion SPECT. Journal of Nuclear Medicine 2001;42(5):687–694.
8. DePuey EG, Garcia EV. Optimal specificity of thallium-201 SPECT through recognition of imaging artifacts [see comments]. Journal of Nuclear Medicine 1989;30(4):441–449.
9. He ZX, Maublant JC, Cauvin JC, Veyre A. Reorientation of the left ventricular long-axis on myocardial transaxial tomograms by a linear fitting method [published erratum appears in Journal of Nuclear Medicine Nov 1991;32(11):2070]. Journal of Nuclear Medicine 1991;32(9):1794–1800.
10. Cauvin JC, Boire JY, Maublant JC, Bonny JM, Zanca M, Veyre A. Automatic detection of the left ventricular myocardium long axis and center in thallium-201 single photon emission computed tomography. European Journal of Nuclear Medicine 1992;19(12):1032–1037.
11. deKemp RA, Nahmias C. Automated determination of the left ventricular long axis in cardiac positron tomography. Physiological Measurement 1996;17(2):95–108.
12. Faber TL, Stokely EM. Orientation of 3-D structures in medical images. IEEE Transactions on Pattern Analysis and Machine Intelligence 1988;10(5):626–633.
13. Mullick R, Ezquerra NF. Automatic determination of LV orientation from SPECT data. IEEE Transactions on Medical Imaging 1995;14(1):88–99.
14. Germano G, Kavanagh PB, Su HT, et al. Automatic reorientation of three-dimensional, transaxial myocardial perfusion SPECT images [see comments]. Journal of Nuclear Medicine 1995;36(6):1107–1114.
15. Declerck J, Feldmar J, Goris ML, Betting F. Automatic registration and alignment on a template of cardiac stress and rest reoriented SPECT images. IEEE Transactions on Medical Imaging 1997;16(6):727–737.
16. Slomka PJ, Hurwitz GA, Stephenson J, Cradduck T. Automated alignment and sizing of myocardial stress and rest scans to three-dimensional normal templates using an image registration algorithm [see comments]. Journal of Nuclear Medicine 1995;36(6):1115–1122.
17. Goris ML, Pace WM, Maclean M, Yee A, Kwan A. Three-dimensional quantitative analysis of scintigraphic tomographic images after elastic transformation to a template. Surgical Technology International 2000;IX:81–90.
18. Germano G, Kiat H, Kavanagh PB, et al. Automatic quantification of ejection fraction from gated myocardial perfusion SPECT. Journal of Nuclear Medicine 1995;36(11):2138–2147.
19. Faber TL, Cooke CD, Folks RD, et al. Left ventricular function and perfusion from gated SPECT perfusion images:

an integrated method. Journal of Nuclear Medicine 1999; 40(4):650–659.
20. Itti E, Rosso J, Hammami H, Benayoun S, Thirion JP, Meignan M. Myocardial tracking, a new method to calculate ejection fraction with gated SPECT: validation with Tl-201 versus planar angiography. Journal of Nuclear Medicine 2001;42(6):845–852.
21. Cachin F, Lipiecki J, Mestas D, et al. Preliminary evaluation of a fuzzy logic-based automatic quantitative analysis in myocardial SPECT. Journal of Nuclear Medicine 2003;44(10): 1625–1632.
22. Liu Y, Sinusas A, Khaimov D, Gebuza B, Wackers F. New hybrid count- and geometry-based method for quantification of left ventricular volumes and ejection fraction from ECG-gated SPECT: methodology and validation. Journal of Nuclear Cardiology 2005;12(1):55–65.
23. Germano G, Kavanagh PB, Waechter P, et al. A new algorithm for the quantitation of myocardial perfusion SPECT, I: technical principles and reproducibility. Journal of Nuclear Medicine 2000;41(4):712–719.
24. Garcia EV, Van Train K, Maddahi J, et al. Quantification of rotational thallium-201 myocardial tomography. Journal of Nuclear Medicine 1985;26(1):17–26.
25. Maddahi J, Van Train K, Prigent F, et al. Quantitative single photon emission computed thallium-201 tomography for detection and localization of coronary artery disease: optimization and prospective validation of a new technique [see comments]. Journal of the American College of Cardiology 1989;14(7):1689–1699.
26. Garcia EV, Cooke CD, Van Train KF, et al. Technical aspects of myocardial SPECT imaging with technetium-99m sestamibi. American Journal of Cardiology 1990;66(13): 23E–31E.
27. Kritzman J, Ficaro E, Liu Y, Wackers F, Corbett J. Evaluation of 3-D MSPECT for quantification of Tc-99m sestamibi defect size [abstract]. Journal of Nuclear Medicine 1999;40(5): 181P.
28. Galt JR, Garcia EV, Robbins WL. Effects of myocardial wall thickness on SPECT quantification. IEEE Transactions on Medical Imaging 1990;9(2):144–150.
29. Caldwell JH, Williams DL, Harp GD, Stratton JR, Ritchie JL. Quantitation of size of relative myocardial perfusion defect by single-photon emission computed tomography. Circulation 1984;70(6):1048–1056.
30. Cooke CD, Vansant JP, Krawczynska EG, Faber TL, Garcia EV. Clinical validation of three-dimensional color-modulated displays of myocardial perfusion [see comments]. Journal of Nuclear Cardiology 1997;4(2, Pt 1): 108–116.
31. Benoit T, Vivegnis D, Foulon J, Rigo P. Quantitative evaluation of myocardial single-photon emission tomographic imaging: application to the measurement of perfusion defect size and severity. European Journal of Nuclear Medicine 1996;23(12):1603–1612.
32. Ficaro E, Kritzman J, Corbett J. Development and clinical validation of normal Tc-99m sestamibi database: comparison of 3D-MSPECT to CEqual [abstract]. Journal of Nuclear Medicine 1999;40(5):125P.
33. Slomka PJ, Radau P, Hurwitz GA, Dey D. Automated three-dimensional quantification of myocardial perfusion and brain SPECT. Computerized Medical Imaging and Graphics 2001;25(2):153–164.
34. Slomka PJ, Nishina H, Berman DS, et al. Automated quantification of myocardial perfusion SPECT using simplified normal limits. Journal of Nuclear Cardiology 2005;12(1):66–77.
35. Ficaro EP, Fessler JA, Shreve PD, Kritzman JN, Rose PA, Corbett JR. Simultaneous transmission/emission myocardial perfusion tomography. Diagnostic accuracy of attenuation-corrected 99mTc-sestamibi single-photon emission computed tomography. Circulation 1996;93(3):463–473.
36. Links JM, Becker LC, Anstett F. Clinical significance of apical thinning after attenuation correction. Journal of Nuclear Cardiology 2004;11(1):26–31.
37. Hutton BF, Osiecki A. Correction of partial volume effects in myocardial SPECT. Journal of Nuclear Cardiology 1998;5(4):402–413.
38. Grossman GB, Garcia EV, Bateman TM, et al. Quantitative Tc-99m sestamibi attenuation-corrected SPECT: development and multicenter trial validation of myocardial perfusion stress gender-independent normal database in an obese population. Journal of Nuclear Cardiology 2004;11(3):263–272.
39. Duvernoy CS, Ficaro EP, Karabajakian MZ, Rose PA, Corbett JR. Improved detection of left main coronary artery disease with attenuation-corrected SPECT. Journal of Nuclear Cardiology 2000;7(6):639–648.
40. Nishina H, Slomka PJ, Abidov A, et al. Combined supine and prone quantitative myocardial perfusion SPECT: method development and clinical validation in patients with no known coronary artery disease. Journal of Nuclear Medicine, 2006;47(1):51–58.
41. Nishina H, Slomka PJ, Abidov A, et al. Combined supine-prone quantitive myocardial perfusion SPECT improves detection of coronary artery disease and normalcy rates on women [abstract]. Journal of Nuclear Medicine 2005;46(Suppl 2):8P.
42. Van Train KF, Areeda J, Garcia EV, et al. Quantitative same-day rest-stress technetium-99m-sestamibi SPECT: definition and validation of stress normal limits and criteria for abnormality. Journal of Nuclear Medicine 1993;34(9):1494–1502.
43. Sharir T, Germano G, Waechter PB, et al. A new algorithm for the quantitation of myocardial perfusion SPECT, II: validation and diagnostic yield. Journal of Nuclear Medicine 2000;41(4):720–727.
44. Williams KA, Schuster RA, Williams KA Jr, Schneider CM, Pokharna HK. Correct spatial normalization of myocardial perfusion SPECT improves detection of multivessel coronary artery disease. Journal of Nuclear Cardiology 2003;10(4):353–360.
45. Liu YH, Sinusas AJ, DeMan P, Zaret BL, Wackers FJ. Quantification of SPECT myocardial perfusion images: methodology and validation of the Yale-CQ method. Journal of Nuclear Cardiology 1999;6(2):190–204.
46. Slomka PJ, Nishina H, Berman DS, et al. Automatic quantification of myocardial perfusion stress-rest change: a

new measure of ischemia. Journal of Nuclear Medicine 2004;45(2):183–191.
47. Faber TL, Galt JR, Chen J, Tsui BMW, Garcia EV. Detecting changes in myocardial perfusion. In Lemke HU, Vannier MW, Inamura AG, Farman K, Reiber JH, eds. CARS 2002. Springer, New York, NY, 2002:879–883.
48. deKemp RA, Hart R, Klein R, et al. Serial changes in perfusion and wall-thickening with gated-stress SPECT and direct paired comparison (DPC) analysis [abstract]. Journal of Nuclear Medicine 2003;44:53P.
49. Ladenheim ML, Pollock BH, Rozanski A, et al. Extent and severity of myocardial hypoperfusion as predictors of prognosis in patients with suspected coronary artery disease. Journal of the American College of Cardiology 1986;7(3):464–471.
50. O'Connor MK, Hammell T, Gibbons RJ. In vitro validation of a simple tomographic technique for estimation of percentage myocardium at risk using methoxyisobutyl isonitrile technetium 99m (sestamibi). European Journal of Nuclear Medicine 1990;17(1–2):69–76.
51. Chareonthaitawee P, Christian TF, O'Connor MK, et al. Noninvasive prediction of residual blood flow within the risk area during acute myocardial infarction: a multicenter validation study of patients undergoing direct coronary angioplasty. American Heart Journal 1997;134(4):639–646.
52. O'Connor MK, Leong LK, Gibbons RJ. Assessment of infarct size and severity by quantitative myocardial SPECT: results from a multicenter study using a cardiac phantom. Journal of Nuclear Medicine 2000;41(8):1383–1390.
53. Gibbons RJ, Valeti US, Araoz PA, Jaffe AS. The quantification of infarct size. Journal of the American College of Cardiology 2004;44(8):1533–1542.
54. Slomka PJ, Hurwitz GA, St. Clement G, Stephenson J. Three-dimensional demarcation of perfusion zones corresponding to specific coronary arteries: application for automated interpretation of myocardial SPECT. Journal of Nuclear Medicine 1995;36(11):2120–2126.
55. Van Train KF, Garcia EV, Maddahi J, et al. Multicenter trial validation for quantitative analysis of same-day rest-stress technetium-99m-sestamibi myocardial tomograms. Journal of Nuclear Medicine 1994;35(4):609–618.
56. Faber TL, Santana CA, Garcia EV, et al. Three-dimensional fusion of coronary arteries with myocardial perfusion distributions: clinical validation. Journal of Nuclear Medicine 2004;45(5):745–753.
57. von Schulthess GK. Positron emission tomography versus positron emission tomography/computed tomography: from "unclear" to "new-clear" medicine. Molecular Imaging and Biology 2004;6(4):183–187.
58. Berman DS, Kiat H, Friedman JD, et al. Separate acquisition rest thallium-201/stress technetium-99m sestamibi dual-isotope myocardial perfusion single-photon emission computed tomography: a clinical validation study. Journal of the American College of Cardiology 1993;22(5):1455–1464.
59. Cerqueira MD, Weissman NJ, Dilsizian V, et al. Standardized myocardial segmentation and nomenclature for tomographic imaging of the heart: a statement for healthcare professionals from the Cardiac Imaging Committee of the Council on Clinical Cardiology of the American Heart Association. Journal of Nuclear Cardiology 2002;9(2):240–245.
60. Germano G, Kavanagh PB, Berman DS. An automatic approach to the analysis, quantitation and review of perfusion and function from myocardial perfusion SPECT images. International Journal of Cardiac Imaging 1997;13(4):337–346.
61. Berman DS, Kang X, Van Train KF, et al. Comparative prognostic value of automatic quantitative analysis versus semiquantitative visual analysis of exercise myocardial perfusion single-photon emission computed tomography. Journal of the American College of Cardiology 1998;32(7): 1987–1995.
62. Hendel RC, Henry TD, Rocha-Singh K, et al. Effect of intracoronary recombinant human vascular endothelial growth factor on myocardial perfusion: evidence for a dose-dependent effect. Circulation 2000;101(2):118–121.
63. Berman D, Abidov A, Kang X, et al. Prognostic validation of a 17-segment score derived from a 20-segment score for myocardial perfusion SPECT interpretation. Journal of Nuclear Cardiology 2004;11(4):414–423.
64. Johnson M. Principles and practice of coronary angiography. In DJ S, ed. Cardiac Imaging: A Companion to Braunwald's Heart Disease. Philadelphia: W.B. Saunders Co.; 1996:220–251.
65. White CW, Wright CB, Doty DB, et al. Does visual interpretation of the coronary arteriogram predict the physiologic importance of a coronary stenosis? New England Journal of Medicine 1984;310(13):819–824.
66. Rozanski A, Diamond GA, Berman D, Forrester JS, Morris D, Swan HJ. The declining specificity of exercise radionuclide ventriculography. New England Journal of Medicine 1983;309(9):518–522.
67. Rubello D, Zanco P, Candelpergher G, et al. Usefulness of 99mTc-MIBI stress myocardial SPECT bull's-eye quantification in coronary artery disease. Quaterly Journal of Nuclear Medicine 1995;39(2):111–115.
68. Ingkanisorn WP, Rhoads KL, Aletras AH, Kellman P, Arai AE. Gadolinium delayed enhancement cardiovascular magnetic resonance correlates with clinical measures of myocardial infarction. Journal of the American College of Cardiology 2004;43(12):2253–2259.
69. Fieno DS, Kim RJ, Chen E-L, Lomasney JW, Klocke FJ, Judd RM. Contrast-enhanced magnetic resonance imaging of myocardium at risk: distinction between reversible and irreversible injury throughout infarct healing. Journal of the American College of Cardiology 2000;36(6):1985–1991.
70. Wu E, Judd RM, Vargas JD, Klocke FJ, Bonow RO, Kim RJ. Visualisation of presence, location, and transmural extent of healed Q-wave and non-Q-wave myocardial infarction. Lancet 2001;357(9249):21–28.
71. Klein C, Nekolla SG, Bengel FM, et al. Assessment of myocardial viability with contrast-enhanced magnetic resonance imaging – comparison with positron emission tomography. Circulation 2002;105(2):162–167.
72. Lund GK, Stork A, Saeed M, et al. Acute myocardial infarction: evaluation with first-pass enhancement and delayed enhancement MR imaging compared with 201Tl SPECT imaging. Radiology 2004;232(1):49–57.

73. Mahrholdt H, Wagner A, Holly TA, et al. Reproducibility of chronic infarct size measurement by contrast-enhanced magnetic resonance imaging. Circulation 2002;106(18): 2322–2327.
74. Hedstrom E, Palmer J, Ugander M, Arheden H. Myocardial SPECT perfusion defect size compared to infarct size by delayed gadolinium-enhanced magnetic resonance imaging in patients with acute or chronic infarction. Clinical Physiology and Functional Imaging 2004;24(6):380–386.
75. Slomka PJ, Fieno D, Thomson L, et al. Automatic detection and size quantification of infarcts by myocardial perfusion SPECT: clinical validation by delayed-enhancement MRI. Journal of Nuclear Medicine 2005;46(5):728–735.
76. Ibrahim T, Nekolla SG, Hornke M, et al. Quantitative measurement of infarct size by contrast-enhanced magnetic resonance imaging early after acute myocardial infarction: comparison with single-photon emission tomography using Tc99m-sestamibi. Journal of the American College of Cardiology 2005;45(4):544–552.
77. Wagner A, Mahrholdt H, Holly TA, et al. Contrast-enhanced MRI and routine single photon emission computed tomography (SPECT) perfusion imaging for detection of subendocardial myocardial infarcts: an imaging study. Lancet 2003; 361(9355):374–379.
78. Vallee JP, Sostman HD, MacFall JR, et al. MRI quantitative myocardial perfusion with compartmental analysis: a rest and stress study. Magnetic Resonance in Medicine 1997;38(6):981–989.
79. Nagel E, Klein C, Paetsch I, et al. Magnetic resonance perfusion measurements for the noninvasive detection of coronary artery disease. Circulation 2003;108(4):432–437.
80. Ishida N, Sakuma H, Motoyasu M, et al. Noninfarcted myocardium: correlation between dynamic first-pass contrast-enhanced myocardial MR imaging and quantitative coronary angiography. Radiology 2003;229(1):209–216.
81. Panting JR, Gatehouse PD, Yang GZ, et al. Echo-planar magnetic resonance myocardial perfusion imaging: parametric map analysis and comparison with thallium SPECT. Journal of Magnetic Resonance Imaging 2001;13(2):192–200.
82. Keijer JT, van Rossum AC, Wilke N, et al. Magnetic resonance imaging of myocardial perfusion in single-vessel coronary artery disease: implications for transmural assessment of myocardial perfusion. Journal of Cardiovascular Magnetic Resonance 2000;2(3):189–200.
83. Prigent F, Maddahi J, Garcia EV, Resser K, Lew AS, Berman DS. Comparative methods for quantifying myocardial infarct size by thallium-201 SPECT. Journal of Nuclear Medicine 1987;28(3):325–333.
84. Sinusas AJ, Trautman KA, Bergin JD, et al. Quantification of area at risk during coronary occlusion and degree of myocardial salvage after reperfusion with technetium-99m methoxyisobutyl isonitrile. Circulation 1990;82(4):1424–1437.
85. Kirac S, Wackers FJ, Liu YH. Validation of the Yale circumferential quantification method using 201Tl and 99mTc: a phantom study. Journal of Nuclear Medicine 2000;41(8):1436–1441.
86. Medrano R, Lowry RW, Young JB, et al. Assessment of myocardial viability with 99mTc sestamibi in patients undergoing cardiac transplantation. A scintigraphic/pathological study. Circulation 1996;94(5):1010–1017.
87. Kang X, Berman DS, Van Train KF, et al. Clinical validation of automatic quantitative defect size in rest technetium-99m-sestamibi myocardial perfusion SPECT. Journal of Nuclear Medicine 1997;38(9):1441–1446.
88. De Sutter J, Van de Wiele C, D'Asseler Y, et al. Automatic quantification of defect size using normal templates: a comparative clinical study of three commercially available algorithms. European Journal of Nuclear Medicine 2000;27(12):1827–1834.
89. Svensson A, Akesson L, Edenbrandt L. Quantification of myocardial perfusion defects using three different software packages. European Journal of Nuclear Medicine and Molecular Imaging 2004;31(2):229–232.
90. Ceriani L, Verna E, Giovanella L, Bianchi L, Roncari G, Tarolo GL. Assessment of myocardial area at risk by technetium-99m sestamibi during coronary artery occlusion: comparison between three tomographic methods of quantification. European Journal of Nuclear Medicine 1996;23(1):31–39.
91. Stewart RE, Schwaiger M, Molina E, et al. Comparison of rubidium-82 positron emission tomography and thallium-201 SPECT imaging for detection of coronary artery disease. American Journal of Cardiology 1991;67(16):1303–1310.
92. Galt JR, Cullom J, Garcia EV. Attenuation and scatter compensation in myocardial perfusion SPECT. Seminars in Nuclear Medicine 1999;29(3):204–220.
93. Maniawski PJ, Morgan HT, Wackers FJ. Orbit-related variation in spatial resolution as a source of artifactual defects in thallium-201 SPECT [see comments]. Journal of Nuclear Medicine 1991;32(5):871–875.
94. Johnson LL. Sex specific issues relating to nuclear cardiology. Journal of Nuclear Cardiology 1995;2(4):339–348.
95. Hendel RC, Berman DS, Cullom SJ, et al. Multicenter clinical trial to evaluate the efficacy of correction for photon attenuation and scatter in SPECT myocardial perfusion imaging. Circulation 1999;99(21):2742–2749.
96. Bateman TM, Cullom SJ. Attenuation correction single-photon emission computed tomography myocardial perfusion imaging. Seminars in Nuclear Medicine 2005;35(1): 37–51.
97. Wackers FJ. Attenuation correction, or the emperor's new clothes? [editorial; comment]. Journal of Nuclear Medicine 1999;40(8):1310–1312.
98. Wackers FJT. Should SPET attenuation correction be more widely employed in routine clinical practice? Against. European Journal of Nuclear Medicine and Molecular Imaging 2002;29(3):412–415.
99. Ficaro EP. Should SPET attenuation correction be more widely employed in routine clinical practice? For. European Journal of Nuclear Medicine and Molecular Imaging 2002;29(3):409–412.
100. O'Connor MK, Kemp B, Anstett F, et al. A multicenter evaluation of commercial attenuation compensation techniques in cardiac SPECT using phantom models. Journal of Nuclear Cardiology 2002;9(4):361–376.

101. Friedman J, Berman DS, Van Train K, et al. Patient motion in thallium-201 myocardial SPECT imaging. An easily identified frequent source of artifactual defect. Clinical Nuclear Medicine 1988;13(5):321–324.
102. DePuey EGr. How to detect and avoid myocardial perfusion SPECT artifacts. Journal of Nuclear Medicine 1994;35(4):699–702.
103. Cooper JA, Neumann PH, McCandless BK. Detection of patient motion during tomographic myocardial perfusion imaging. Journal of Nuclear Medicine 1993;34(8):1341–1348.
104. Germano G, Chua T, Kavanagh PB, Kiat H, Berman DS. Detection and correction of patient motion in dynamic and static myocardial SPECT using a multi-detector camera. Journal of Nuclear Medicine 1993;34(8):1349–1355.
105. Slomka PJ, Nishina H, Berman DS, et al. "Motion-frozen" display and quantification of myocardial perfusion. Journal of Nuclear Medicine 2004;45(7):1128–1134.
106. Campeau RJ, Garcia OM, Colon R, Agusala M, Correa OA. False-positive Tc-99m sestamibi SPECT in a patient with left bundle branch block. Clinical Nuclear Medicine 1993;18(1): 40–42.
107. Bartram P, Toft J, Hanel B, et al. False-positive defects in technetium-99m sestamibi myocardial single-photon emission tomography in healthy athletes with left ventricular hypertrophy. European Journal of Nuclear Medicine 1998;25(9):1308–1312.
108. Eisner RL, Schmarkey LS, Martin SE, et al. Defects on SPECT "perfusion" images can occur due to abnormal segmental contraction. Journal of Nuclear Medicine 1994;35(4):638–643.
109. Martin W, Tweddel AC, Hutton I. Balanced triple-vessel disease: enhanced detection by estimated myocardial thallium uptake. Nuclear Medicine Communications 1992;13(3):149–153.
110. Klocke FJ, Baird MG, Lorell BH, et al. ACC/AHA/ASNC guidelines for the clinical use of cardiac radionuclide imaging. Executive summary – A report of the American College of Cardiology/American Heart Association Task Force on Practice Guidelines (ACC/AHA/ASNC Committee to revise the 1995 guidelines for the clinical use of cardiac radionuclide imaging). Journal of the American College of Cardiology 2003;42(7):1318–1333.
111. Taillefer R, DePuey EG, Udelson JE, Beller GA, Benjamin C, Gagnon A. Comparison between the end-diastolic images and the summed images of gated 99mTc-sestamibi SPECT perfusion study in detection of coronary artery disease in women. Journal of Nuclear Cardiology 1999;6(2):169–176.
112. Slomka PJ, Nishina H, Kavannagh P, Berman DS, Germano G. "Motion-frozen" myocardial perfusion gated SPECT [abstract]. Circulation 2003;108:SIV-456.
113. Klein JL, Garcia EV, DePuey EG, et al. Reversibility bull's-eye: a new polar bull's-eye map to quantify reversibility of stress-induced SPECT thallium-201 myocardial perfusion defects. Journal of Nuclear Medicine 1990;31(7):1240–1246.
114. Berman DS, Hachamovitch R, Kiat H, et al. Incremental value of prognostic testing in patients with known or suspected ischemic heart disease: a basis for optimal utilization of exercise technetium-99m sestamibi myocardial perfusion single-photon emission computed tomography. Journal of the American College of Cardiology 1995;26(3):639–647.
115. Slomka PJ, Berman DS, Germano G. Quantification of serial changes in myocardial perfusion. Journal of Nuclear Medicine 2004;45(12):1978–1980.
116. Berman DS, Kang XP, Schisterman EF, et al. Serial changes on quantitative myocardial perfusion SPECT in patients undergoing revascularization or conservative therapy. Journal of Nuclear Cardiology 2001;8(4):428–437.
117. Schwartz RG, Pearson TA, Kalaria VG, et al. Prospective serial evaluation of myocardial perfusion and lipids during the first six months of pravastatin therapy: coronary artery disease regression single photon emission computed tomography monitoring trial. Journal of the American College of Cardiology 2003;42(4):600–610.
118. Udelson JE, Dilsizian V, Laham RJ, et al. Therapeutic angiogenesis with recombinant fibroblast growth factor-2 improves stress and rest myocardial perfusion abnormalities in patients with severe symptomatic chronic coronary artery disease. Circulation 2000;102(14):1605–1610.
119. deKemp RA, Ruddy TD, Hewitt T, Dalipaj MM, Beanlands RS. Detection of serial changes in absolute myocardial perfusion with 82Rb PET. Journal of Nuclear Medicine 2000;41(8):1426–1435.
120. Hart R, Ruddy TD, Beanlands RS, deKemp RA. Statistical parametric imaging of heart function with ECG-gated perfusion scans. In SPIE Regional Meeting on Optoelectronics, Photonics, and Imaging, 2002;TD01:379–382.
121. Slomka P, Nishina H, Akincioglu C, et al. Method for detection of serial myocardial perfusion SPECT changes by 3D volume-based image registration. Journal of American College of Cardiology 2005;45(3)(suppl): 1112–1170, 285A.
122. Itti E, Klein G, Rosso J, et al. Assessment of myocardial reperfusion after myocardial infarction using automatic 3-dimensional quantification and template matching. Journal of Nuclear Medicine 2004;45(12):1981–1988.
123. Patel AD, Iskandrian AE. Role of single photon emission computed tomography imaging in the evaluation of therapy for angina pectoris. American Heart Journal 2003;145(6):952–961.
124. Haddad M, Adlassnig K-P, Porenta G. Feasibility analysis of a case-based reasoning system for automated detection of coronary heart disease from myocardial scintigrams. Artificial Intelligence in Medicine 1997;9(1):61–78.
125. Garcia EV, Herbst MD, Cooke CD, et al. Knowledge-based visualization of myocardial perfusion tomographic images. In Proceedings of the First Conference on Visualization in Biomedical Computing; 1990:157–161.
126. Garcia EV, Cooke CD, Folks RD, et al. Diagnostic performance of an expert system for the interpretation of myocardial perfusion SPECT studies. Journal of Nuclear Medicine 2001;42(8):1185–1191.
127. Lindahl D, Palmer J, Ohlsson M, Peterson C, Lundin A, Edenbrandt L. Automated interpretation of myocardial SPECT perfusion images using artificial neural networks. Journal of Nuclear Medicine 1997;38(12):1870–1875.
128. Hamilton D, Riley PJ, Miola UJ, Amro AA. A feed forward neural network for classification of bull's-eye myocardial

perfusion images. European Journal of Nuclear Medicine 1995;22(2):108–115.

129. Fujita H, Katafuchi T, Uehara T, Nishimura T. Application of artificial neural network to computer-aided diagnosis of coronary artery disease in myocardial SPECT bull's-eye images of Nuclear Medicine 1992;33(2):272–276.
130. Allison JS, Heo J, Iskandrian AE. Artificial neural network modeling of stress single-photon emission computed tomographic imaging for detecting extensive coronary artery disease. American Journal of Cardiology 2005;95(2):178–181.
131. Porenta G, Dorffner G, Kundrat S, Petta P, Duit-Schedlmayer J, Sochor H. Automated interpretation of planar thallium-201-dipyridamole stress-redistribution scintigrams using artificial neural networks [see comments]. Journal of Nuclear Medicine 1994;35(12):2041–2047.
132. Haraldsson H, Ohlsson M, Edenbrandt L. Value of exercise data for the interpretation of myocardial perfusion SPECT. Journal of Nuclear Cardiology 2002;9(2):169–173.

5 Quantification of ventricular function

Guido Germano
Daniel S. Berman

Introduction

Concomitant with the increased adoption of gated perfusion SPECT protocols (see Chapter 2), the past 10 years have witnessed a substantial increase in the development and use of algorithms for the quantitation of global and regional ventricular function, using gated SPECT. In fact, it is now estimated that essentially all gamma cameras used for cardiac SPECT are directly connected to a computer or workstation running gated SPECT software for function quantitation, at least in the United States. Table 5.1 presents a synopsis of published data on commercially available quantitative gated SPECT algorithms, including their principles of operation and the validation of parameters they quantitate [1–87]. The aim of this chapter is to describe the available algorithms for quantitation and the accuracy and reproducibility of the quantitative measurements.

Review of available algorithms

Several software approaches for the analysis of ventricular function from gated SPECT are currently commercially available. Although their operation is more thoroughly described in the references quoted in Table 5.1, it is useful to briefly summarize the main concepts behind each class of algorithms.

Cedars-Sinai's QGS™

The Cedars-Sinai Quantitative Gated SPECT (QGS™) software [1] operates in the three-dimensional space and utilizes the gated short-axis data sets after stacking them together to form a three-dimensional image volume. All aspects of this algorithm operate automatically, with the option for manual interaction. The software's first step involves the automatic segmentation of the left ventricular (LV) myocardium, based on initial heuristic thresholding, binarization, and clusterification of the three-dimensional image, followed by iterative cluster refinement using pixel erosion and pixel growing. The iterative process is terminated when a mask consistent with the expected size, shape, and location of the LV is obtained. Once the LV has been isolated, its center of mass is automatically determined and rays are drawn from it according to a spherical sampling model. The local maxima along all rays define a first estimate of the three-dimensional midmyocardial surface, which is then fitted to an ellipsoid. The best-fit ellipsoid can be used to estimate the LV's sphericity [88], and also defines a new sampling coordinate system, along which new rays are drawn and count profiles measured normally to the myocardium. These count profiles are fitted to asymmetric Gaussian curves. The Gaussian' maxima represent the final estimate of the midmyocardial surface, while the endocardial and epicardial surfaces are determined on the basis of the Gaussians standard deviations, and the valve plane is determined by fitting a plane to the most basal myocardial points (Fig. 5.1). The constraint of preservation of myocardial mass throughout the cardiac cycle is imposed and further refines the endocardial and epicardial surfaces. Surfaces can usually be accurately determined even in the apparent absence of perfusion (Fig. 5.2) because (1) Gaussian fitting operates on the segmented but nonthresholded image, and is thus able to "pick up" very low levels of perfusion that are visually hidden in the darkest portions of the gray or color scale used, and (2) the algorithm seeks to preserve the continuity of the three-dimensional myocardial surface gradients by extrapolating those points that are immediately adjacent to the nonperfused area. Endocardium, epicardium, and valve plane are calculated for each gating interval. LV cavity volumes are calculated by multiplying the individual voxel volume by the number of voxels contained in the three-dimensional space bound by the endocardium

Table 5.1 A review of published quantitative algorithms for gated perfusion SPECT.

	Institution					
	Cedars-Sinai	**Emory University**	**University of Michigan**	**Stanford University**	**Yale University**	**Various others**
Commercial name	QGS™, AutoQUANT™	EGS™, Cardiac Toolbox™	3D-MSPECT™, 4D-MSPECT™	MultiDim™	GSCQ™	N/A
Operation	Automatic	Automatic	Automatic	Semiautomatic	Automatic	Semiautomatic
Dimensionality	3-D	3-D	3-D	3-D	3-D	2-D
Method	Gaussian fit [1,2]	Partial volume [3,4]	Gradient [5,6]	Moment [7,8]	Maximal pixel, partial volume [9]	Partial volume [10–13], Threshold [14–16], Elastic surface [17], Image inversion [18]
Validation of LVEF	First pass [1,19–22], MUGA [22–36], 3-D MUGA [37,38], MRI [39–51], 2-D echo [30,52–60], 3-D echo [61], contrast ventricular [37,53,62,63], EBCT [64], thermodilution [65]	First pass [4], MUGA [31,34], MRI [4,43,47], 2-D echo [58] (58)	MUGA [31,34], 2-D echo [59], MRI [50,51,66,67], contrast ventricular [6,68]	First pass [69], MUGA [8,27,70], 2-D echo [70,71]	First pass [22], MUGA [9,22,72]	First pass [18], MUGA [14,16,17,34,73], MRI [74,75], 2-D echo [58], contrast ventricular [18,76,77]
Diastolic parameters	MUGA [32,33,35,38]					
volumes	MUGA [27,28,30,34,36], 3-D MUGA [37,78], MRI [39–51], 2-D echo [52,54–56,58,60,79], 3-D echo [61,80], contrast ventricular [37,62,78], thermodilution [65,81], excised hearts[82]	First pass [4], MUGA [34], MRI [4,43,47], 2-D echo [58]	MUGA [34], MRI [5,50,51,66], excised hearts [82]	First pass [69], MUGA [27], contrast ventricular [70]	Excised hearts [82]	MUGA [16,34], 2-D echo [58,83], contrast ventricular [77]
WM	Visual [2]	MUGA [84]	MRI [85]			2-D echo [86]
WT	Visual [2]	2-D echo [87]				

Abbreviations: EBCT, electron beam computed tomography; echo, echocardiography; LVEF, left ventricular ejection fraction; MRI, magnetic resonance imaging; MUGA, planar blood pool; WM, wall motion; WT, wall thickening

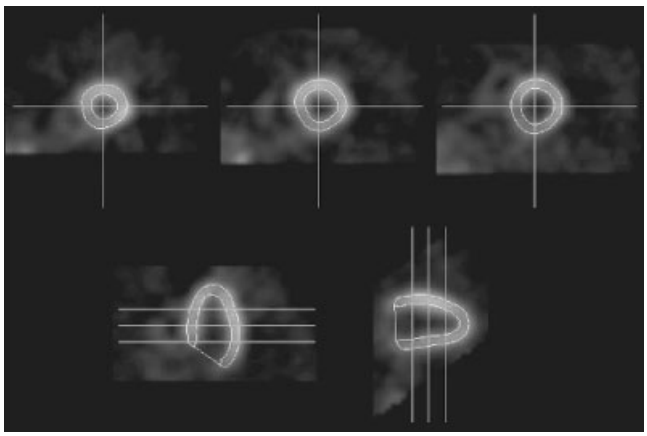

Figure 5.1 (top) Apical, mid, and basal short-axis slices and (bottom) horizontal (left) and vertical (right) long-axis slices with overlayed endocardial and epicardial contours for a normal patient, as determined by QGS. Crosshair lines indicate the short-axis and long-axis sections considered.

and the valve plane. The largest and the smallest LV cavity volumes correspond to end-diastole and end-systole, from which the ejection fraction is derived. All volumes can also be graphed in a "time–volume curve," from whose derivative it is possible to quantify various parameters of diastolic function [32]. The algorithm further measures regional motion as the excursion of the three-dimensional endocardial surface from end-diastole to end-systole, using a modification of the centerline method [89]. Segmental thickening is calculated using both geometric (distance between epicardium and endocardium) and count considerations (apparent count increase from end-diastole to end-systole, due to the partial volume effect) [2].

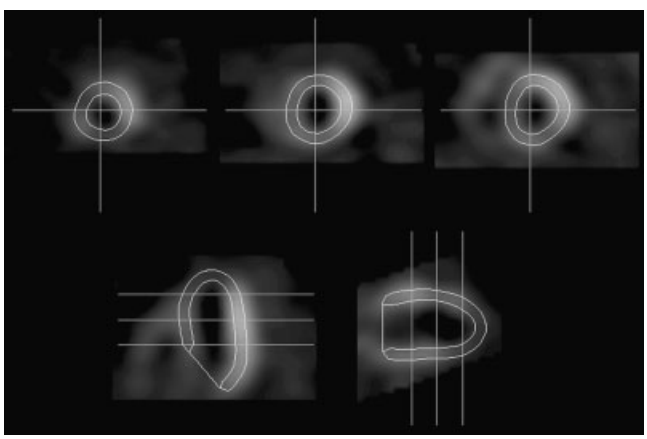

Figure 5.2 Short- and long-axis slices with QGS-overlayed contours in a patient with a severe and extensive perfusion defect in the left anterior descending coronary artery territory.

Emory University's EGS™

The Emory Gated SPECT (EGS™) software [4] operates on a volumetric set of short-axis slices. The LV is automatically isolated by iterative threshold adjustment of candidate objects near the middle of the volume. Quantitative parameters (center, radius, apex, and base) are automatically determined using iterative refinement that reduces the possibility of errors caused by extracardiac activity or large perfusion defects. Additional processing is performed to define an LV base consisting of two intersecting planes: a flat base plane in the lateral half of the LV and an angled base fit to the septal valve plane. The LV is then sampled using a hybrid coordinate system [90]. The center of the coordinate system is the LV long axis, and the search space is limited by the LV radius, apex, and base. In the basal and medial portion of the LV, samples are taken 9° apart by using cylindrical coordinates. The apical hemisphere is sampled using spherical coordinates, approximately every 12°. The sample at each angle is the detected maximal count value, assumed to occur at the center of the imaged myocardium, and this set of sampled points is used to create the LV model. Since the myocardium is usually thinner than the reconstructed "full width half maximum" (FWHM) – typically 1.2–1.5 cm – and the partial volume effect is a concern [91]; the endocardial and epicardial boundary points are estimated by subtracting and adding 5 mm to all radii in the end-diastolic frame. In other words, an assumption is made that the myocardium is approximately 10 mm thick at end-diastole [92–94]. Wall thickening throughout the cardiac cycle is computed using a Fourier analysis of the size–intensity relationship [3]. For each quantitative perfusion sample, a time–intensity curve is created, and its Fourier transform is computed to replace the discrete temporal samples by a continuous curve, thus promoting temporal resolution. The phase and amplitude of the first harmonic of the transform are used to calculate percent thickening (with respect to the end-diastolic frame) for all frames in the cardiac cycle. Since the myocardial thickness at end-diastole is presumed to be uniformly 10 mm, the percent thickening information can be used to approximate "absolute" myocardial thickness at each sampled point in the LV, at every gated frame. For each gating interval, endocardial and epicardial boundary points are determined by the same process of subtracting and adding one half of the myocardial thickness to the myocardial center. The surface points are connected into a contiguous triangle mesh defining the endocardial and epicardial surfaces. The volume enclosed by the endocardial surface points is the endocardial chamber volume. The difference between epicardial volume and endocardial volume is the myocardial volume; myocardial mass is obtained by multiplying the volume by a density of 1.05 g/ml. Finally, ejection

fraction is calculated from the end-diastolic and end-systolic volumes.

University of Michigan's 4D-MSPECT™

The University of Michigan's 4D-MSPECT™ software [68] provides an automated algorithm for estimating the LV endocardial and epicardial surfaces for myocardial perfusion tomographic images. The algorithm, operating on the three-dimensional time-varying image volume, utilizes gradient operators in conjunction with segmented images and a contiguity constraint to provide the initial surface estimate for the endocardial and epicardial surfaces. Using a cylindrical/spherical sampling system [85], weights are assigned on the basis of the measured intensity profiles within the initial surface boundaries. Using these weights and the estimated curvature of the heart, two-dimensional and one-dimensional weighted splines are utilized to fill in missing data (i.e., perfusion defects) while minimizing the inclusion of splanchnic activity. Using the intensity profiles bounded by these new surfaces, a Gaussian fit is used to find the peak activity and an estimate of the myocardial thickness. To compensate for the limited resolution of emission tomography, the myocardial thickness at end-diastole (corresponding to the maximal endocardial volume) is scaled to provide an average thickness of 10 mm. This scale factor, in conjunction with a myocardial mass constraint, is used to adjust the myocardial thickness throughout the cardiac cycle. Using these endocardial surface contours, the deviation of the image volume from the optimal LV center and long-axis orientation is computed. If the LV center position is in error (i.e., >0.1 pixels), the sampling coordinate system is adjusted and the surface algorithm is restarted. If the long axis of the LV is found to deviate more than 0.1° from the optimal orthogonal axis, the LV image volume is rotated, the sampling coordinate system is adjusted, and the surface algorithm is restarted. This iterative procedure is capped at five iterations, but usually converges with two to three iterations. The automatic realignment and centering algorithm has been found to significantly improve the reproducibility of global and regional quantitative measures of the LV perfusion and function [95]. From the final endocardial surfaces, the LV chamber volume curve through the cardiac cycle is defined. LV ejection fraction (LVEF) and volumes at end-diastole and end-systole are calculated and cardiac output is computed on the basis of the end-diastolic volume (EDV) and end-systolic volume (ESV) and heart rate. If the study was acquired with sufficient temporal resolution ($\geq$16 frames), diastolic function parameters, such as peak filling and peak emptying rates and the time position to these peak rates, are computed from harmonic analysis of the time–volume curve. Myocardial volume and mass are computed from the volume defined between the endocardial and epicardial surfaces. Regional wall motion is estimated from the change between the end-systolic and end-diastolic endocardial surface positions, using a three-dimensional modification of the centerline method [96]. The algorithm for estimating regional wall thickening utilizes the partial volume effect inherent to current emission tomographic imaging systems where the relative change in peak myocardial intensity from end-diastole to end-systole is related to the change in myocardial thickness.

Stanford University's MultiDim™

The Stanford University algorithm underlying the MultiDim™ software [7,8] is based on the three-dimensional analysis of count distribution moments in the short-axis image volume. The software starts by requiring manual placement of an ellipsoidal mask around the myocardium in the operator-determined end-diastolic frame, with the goal of eliminating extracardiac structures containing activity. This masking is followed by the thresholding of the pixels inside the ellipsoid to 35% of the maximal pixel count throughout the cardiac cycle. Then, short-axis images in each time interval are shifted upward or downward, so as to ensure that the image plane dividing the image volume in 90–10% count proportions is the same for all time intervals. The stacked short-axis images form a three-dimensional image volume, which is sampled (along equally spaced longitudinal and latitudinal angles) using rays originating at the center of the LV cavity. For each ray-associated count profile, the following three parameters are calculated: (1) the maximum in the profile; (2) the first moment of the count distribution along the ray, representative of the average location of the myocardial wall; and (3) the second moment of the count distribution along the ray (the standard deviation of the count distribution around the mean), representative of the myocardial wall thickness. All the samples corresponding to a specific parameter and time frame are collected in a bidimensional vector similar to the commonly used polar (Bulls eye) map. Then, the evolution in time of each given point (myocardial segment) is assessed in terms of the phase and amplitude of the first harmonic of the Fourier series describing the sequential values of a parameter at the point during the cardiac cycle. In particular, regional wall motion is derived from the phase and amplitude of the cyclic wave representing the temporal variation of the first moment of the count distribution, while wall thickening is derived from phase and amplitude of the cyclic wave representing the temporal variation of the product of the maximum perfusion and the second moment of the count distribution.

Yale University's GSCQ™

Yale University's GSCQ™ software [9] performs an initial smoothing of the gated SPECT images by pixel-by-pixel convolution in the temporal domain, using a digital filter with kernel values of (1, 2, 1). An estimate of the LV's "mid-wall" is determined from the ungated short and horizontal long-axis SPECT images using a maximal count search scheme and a hybrid cylindrical–spherical sampling model. Then, that estimate is refined by a median count search applied to images from all gated SPECT intervals. A myocardial thickness of 12 mm is assumed for the gated sector in which the median count is detected. Myocardial thickness for the remaining gated intervals in the corresponding sector is calculated as the median thickness (12 mm) weighted by the ratio of the sector count to the median count. The thickness calculation is performed on all sectors of all gated SPECT slices, with endocardial and epicardial edges determined by expanding the mid-wall edge inward and outward, respectively, based upon the total counts within the predefined endocardial and epicardial areas in each sector. LV cavity volumes are calculated as the individual voxel's volume multiplied by the total number of voxels enclosed in the endocardial edges, with the LVEF being derived from the EDV and ESV.

The GSCQ™ algorithm quantifies regional wall thickening by generating circumferential maximal count profiles consisting of 128 sectors (short-axis slices) or 64 sectors (horizontal long-axis slices) from each frame of gated SPECT slices, then measuring count changes in each sector (i) from the end-diastolic to the end-systolic interval as $[ES(i)-ED(i)]/ED(i) \times 100\%$ [97]. ED is defined as the first frame following the R-wave trigger, and ES is defined as the frame with maximal sectorial count density. Gated circumferential count profiles are first normalized to the maximal value of all 128 sectors (64 for the apical cap) during a cardiac cycle. The changes in regional function are subsequently normalized to the end-diastolic counts in each sector, to better appreciate wall thickening independent of regional myocardial radiotracer uptake. Ultimately, the normalized maximal thickening profile is displayed in conjunction with the lower limit of normal wall thickening (mean thickening in normal subjects – 2SD). The severity and extent of abnormal thickening is expressed as minimal wall thickening in a given anatomic zone (anterior, septal, inferior, lateral) and as percent of the circumferential profile.

Other approaches

Partial volume-based methods

The partial volume effect was initially described by Hoffman et al. with regard to positron emission tomography (PET) [98], and expresses the fact that, in nuclear medicine imaging, the average counts measured in a structure or an organ are proportional not only to the amount of activity contained in this structure but also to the size of the structure itself, this latter dependence being particularly strong for structures less than twice the FWHM resolution of the imaging system. The result of this phenomenon is that a "recovery coefficient curve" can be built that links the average counts contained in a region of interest (ROI) centered on various sections of the myocardium and the thickness of that section, as shown in Fig. 5.3. Quantitative algorithms based on the partial volume effect, like those by Smith et al. [11] and Mochizuchi et al. [12], assume a linear relationship between the increase in maximal counts in a myocardial segment from diastole to systole and the physical thickening of this segment in the same time interval. The LVEF can then be calculated by modeling the LV as an ellipsoid with constant myocardial volume, and measuring an average "index of myocardial thickening" [11]. A variation on the partial volume approach has been described by Buvat et al. [13]. This algorithm uses the segmental count increase from diastole to systole as a proxy for wall thickening and integrates it with a geometric estimate of the actual wall thickness at diastole and systole (hybrid method).

Threshold-based methods

One algorithm, proposed by DePuey and Nichols [14,15], utilizes a pair of operator-selected, gated vertical long-axis (VLA) and horizontal long-axis (HLA) midventricular images, and determines the midmyocardial and endocardial borders in these images at end-diastole and end-systole, by radial sampling originating from the LV cavity center and bound by empirically determined percent thresholds (a function of the minimum LV cavity counts and the maximum myocardial counts). For each short-axis slice that contains part of the VLA and HLA contours, a short cylinder is built that has an ellipsoidal section defined by the "height" of the VLA and the "width" of the HLA in that short-axis plane. End-diastolic and end-systolic LV cavity volumes are derived by summing all ellipsoid cylinders at end-diastole and end-systole, as commonly done in biplanar echocardiography [99]. A recent enhancement to this algorithm involves transforming the gated SPECT images to allow better visualization of myocardial thickening ("brightening-mapping") and motion ("motion mapping") in severely hypoperfused myocardial regions [14].

A different threshold-based algorithm described by Yang and Chen [100] defines the end-diastolic myocardial contours as the isocount curves corresponding to 60% of the maximal myocardial pixel counts, while the

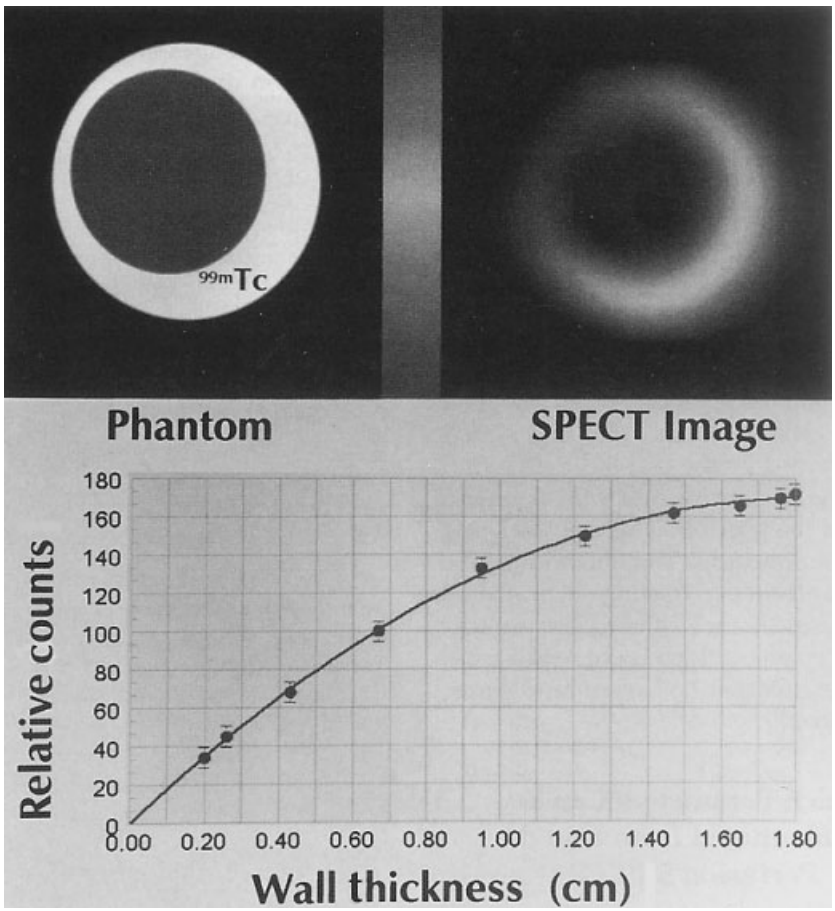

Figure 5.3 Partial volume effect: (top left) section of an asymmetrical phantom containing a uniform concentration of ^{99m}Tc, and (top right) transaxial SPECT image of the phantom obtained using a standard gamma camera: the thinner regions of the phantom appear to contain a lower concentration of activity. The relationship between "wall thickness" and corresponding maximum count value is shown in the graph, and has been previously referred to as the "recovery coefficient curve" [98]. (Reproduced with permission from [11].)

end-systolic contours are empirically and iteratively determined from the percent threshold that causes the LV mass at end-systole to be within 5% of that at end-diastole. The ejection fraction is then calculated from the LV cavity areas of three midventricular short-axis images, while regional thickening is estimated from their end-diastolic and end-systolic epicardium-endocardium distances. A refinement of this algorithm uses count gradients to help define the isocount levels for the end-diastolic and end-systolic contours [84].

In another algorithm, proposed by Nakata et al. [16], a spline curve with a threshold of 30% of peak activity is initially used in horizontal and vertical long-axis images to isolate the myocardium from extracardiac activity. Then, count profile curves are drawn across the myocardium, with the epicardium's location estimated to correspond to 50% of each profile's maximum count. The endocardial location is determined instead using a mathematical formula that depends on the size of the LV cavity, thus accounting for the possible marked asymmetry of the count profile in small ventricles and/or at end-systole. Myocardial wall thickening can be either derived from the end-diastolic and end-systolic epicardium-endocardium distances, or estimated from the partial volume-related regional count density increases from end-diastole to end-systole [101].

The elastic surface and image inversion methods

In the algorithm proposed by Stegger et al. [17], the midmyocardial surface of the LV is represented by an elastic surface over which the myocardial activity distribution exerts an attracting force proportional to the regional count uptake. The shape of the midmyocardial surface is modeled as the solution to a second-order partial differential equation, and various constraints and local "weights" are employed to minimize the influence of extracardiac activity. In a manner similar to that used in the QGS^{TM}algorithm, the elastic surface approach "patches up" areas of reduced or absent perfusion by promoting the continuity of count gradients calculated from adjacent areas of preserved perfusion. The endocardial and epicardial surfaces are postulated to be equidistant from the midmyocardium and are determined following the calculation of the regional myocardial thickness,

during which process the added constraint of constant myocardial volume throughout the cardiac cycle can be applied.

The image inversion method described by Williams and Taillon [18] exploits the fact that the contrast between the perfused myocardium and the LV cavity is preserved when one horizontal and one vertical long-axis images per gating interval are digitally inverted. In essence, with this technique, counts are produced within the LV chamber, and the change in these counts reflects the volumetric alterations occurring in the LV during systole. If a master ROI is manually placed around the LV chamber counts at end-diastole, ROIs can be automatically generated for each frame of the cardiac cycle, using a center of mass and the combination derivative-threshold border detection technique. The ejection fraction is then calculated for each long-axis data set as the end-diastolic counts minus the end-systolic counts, divided by the end-diastolic counts. This method of edge detection and ejection fraction determination is the same as that commonly employed for gated planar blood pool equilibrium analysis, except that no background correction is utilized.

Function parameters that can be quantified from gated perfusion SPECT

A wide variety of global and regional function variables can be measured from gated SPECT. Quantifiable global parameters of function from gated perfusion SPECT include LVEF, end-diastolic and end-systolic LV cavity volumes, mass, and transient ischemic dilation (TID) of the LV based on gated or ungated volumes. Diastolic function assessment was initially not thought to be possible with gated SPECT, but recent research shows it is feasible if a sufficient number of gating intervals are acquired [32,33,38,102–104]. Right ventricular (RV) quantitation is generally not performed with gated SPECT except in very special cases [105]. In the absence of RV hypertrophy, RV quantitation is difficult because the RV myocardium is thinner and on a per-gram basis has lower blood flow than the LV, hence taking up much less radioactivity than the LV. Because of these factors, the RV is frequently poorly visualized. In addition, the geometric shape of the RV is less straightforward to model than that of the LV. Consequently, when it is performed, the RV assessment is based on selected two-dimensional slices and cannot be applied to all imaged patients. Regional parameters of function quantitated from gated perfusion SPECT images include LV myocardial wall motion and thickening. This section will review the published validations of quantitative measurements of global and regional LV function parameters.

LVEF

Quantitative measurements of LVEF using gated perfusion SPECT are usually volume-based methods rather than count-based methods. In particular, the time–volume curve allows to identify the end-diastolic and end-systolic LV cavity volumes (Fig. 5.4), from which the ejection fraction is calculated as

$$\%\text{LVEF} = (\text{EDV} - \text{ESV})/\text{EDV} \times 100$$

Virtually all published validation studies of gated perfusion SPECT LVEF measurements by commercially available algorithms are presented in Table 5.2, along with details about the studies [1,4,6,8,9,19–50,52–71]. It is apparent that the agreement between gated SPECT and gold standard measurements of LVEF is generally very good to excellent. Indeed, it has been pointed out that the two-dimensional gold standards may be intrinsically less accurate than gated SPECT algorithms operating in the three-dimensional space, because of geometric assumptions required by the former [1].

Arrhythmias and gating errors

At the outset, it should be noted that premature ventricular contractions (PVCs) have a much greater effect on function measurements with gated SPECT than premature atrial contractions (PACs), due to the known effects of the PVCs on contractility – in both the PVC and the post-PVC beat – that are not associated with the PACs. As the ultimate example of this phenomenon, the EF measurements in patients with atrial fibrillation are generally considered to be relatively accurate except in circumstances where it is marked beat length variability.

The effect of cardiac arrhythmias on LVEF quantification must be discussed in the context of the particular cardiac beat length acceptance strategy employed. If counts from rejected beats can be accumulated in an "extra frame" with a particular camera/computer system, a narrow acceptance window is preferred (as seen in Chapter 2). This approach allows accurate binning of only the data acquired in a regular rhythm for the assessment of ventricular function, and then summation of counts from all of the beats for the assessment of myocardial perfusion. While with this approach arrhythmias would still be expected to compromise the overall count statistics of the gated images, this compromise would affect all frames equally. The extent of the problem can be easily gauged from the relative number of counts in the extra frame, as well as the appearance of the number of counts in the gated images. Overall, little published data exists on the effect of arrhythmias on quantitative LVEF measurements in conjunction with narrow acceptance windows.

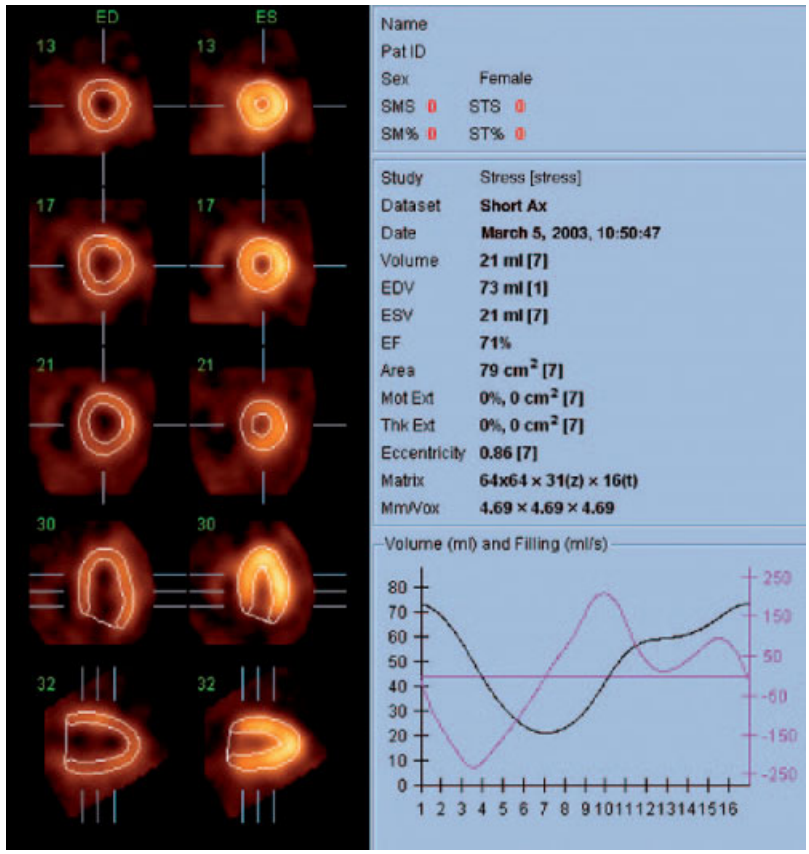

Figure 5.4 The volumes bound by the endocardium and the valve plane at end-diastole (left column) and end-systole (middle column) are the highest and lowest point on the black time–volume curve (in this patient, frames 1 and 7, respectively), from which the LVEF is calculated. The red curve is the derivative of the time–volume curve, from which parameters of diastolic function can be quantified.

When a wide acceptance window is used during acquisition because the extra frame is not available, on the other hand, greater problems and risks exist. For starters, count losses may occur even when a 100% acceptance window is used, if a substantial proportion of the heartbeats occurs at less than 50% or at more than 150% of their expected duration. In these cases, the gating software may also wait one or more additional beats before resuming triggering and binning after a rejected event. Such count loss can not only affect function measurements but also result in artifactual perfusion defects [106]. A practical rule of thumb has been proposed, on the basis of which gated SPECT acquisitions would be reported only if at least 80% of a patient's cardiac beats follow a regular rhythm [107]. It should also be recognized that a patient with a regular rhythm at the inception of the study may develop an arrhythmia during the acquisition.

In a patient with arrhythmia, it is important to understand to what extent quantitative measurement of LVEF, volumes, and regional function are affected by such arrhythmias so that a postacquisition decision can be made as to whether the gated component of the study should be reported. A comprehensive analysis of the influence of arrhythmias on quantitative gated SPECT assessment by the QGS™ and EGS™ algorithms has been performed by Nichols et al., through computer simulation of "consistently variable" heart rate, transient tachycardia, and atrial fibrillation in conjunction with a 100% acceptance window [108,109]. By paired $t-$test analysis these investigators found that substantial changes could be demonstrated in LVEF, EDV, and ESV, which could lead to misclassification of individual patients with respect to abnormality. In general, regional myocardial thickening assessment was deemed to be compromised more by the presence of arrhythmias than global function measurements were [109]. A more recent report by Kasai et al. [110] points out that both arrhythmias and various gating errors are capable of causing severe deformations of the time–volume curve from which EDV, ESV, and LVEF are calculated, naturally resulting in quantitative errors (Fig. 5.5). Finally, it has been reported that simulated T wave triggering in a portion of the cardiac beats in a gated SPECT acquisition causes a decrease in the quantitatively measured LVEF; the decrease is linearly proportional to the percentage of erroneous triggers, and has a summative effect with decreases related to simulated patient motion [111].

The above considerations stress the importance of routinely reviewing the time–volume curve for the purpose of quality-controlling the quantitative results. This topic will be examined in detail in Chapters 6 and 7. Suffice it to

Table 5.2 Validations of quantitative measurements of LVEF from gated perfusion SPECT.

Method	Gold standard	No. of patients	Spearman's *r* (LVEF)	Isotope	References
QGS™	First pass	65	0.91	^{99m}Tc sestamibi	[1]
QGS™	First pass	44	0.92	I-123 BMIPP	[19]
QGS™	First pass	63	0.85	^{99m}Tc sestamibi	[20]
QGS™	First pass	63	0.84	^{201}Tl	[20]
QGS™	First pass	365	0.74	^{99m}Tc sestamibi, ^{99m}Tc tetrofosmin	[21]
QGS™	First pass	117	0.74	^{99m}Tc sestamibi	[22]
QGS™	MUGA	50	0.92	^{99m}Tc sestamibi	[23]
QGS™	MUGA	36	0.87–0.92	^{201}Tl	[24]
QGS™	MUGA	40	0.93	^{99m}Tc tetrofosmin	[25]
QGS™	MUGA	40	0.93	^{201}Tl	[26]
QGS™	MUGA	21	0.7	^{201}Tl	[27]
QGS™	MUGA	21	0.87	^{99m}Tc tetrofosmin	[28]
QGS™	MUGA	55	0.94	^{201}Tl	[29]
QGS™	MUGA	62	0.94	^{99m}Tc sestamibi, ^{99m}Tc tetrofosmin	[30]
QGS™	MUGA	25	0.89	^{99m}Tc sestamibi	[31]
QGS™	MUGA	24	0.95	^{99m}Tc tetrofosmin	[32]
QGS™	MUGA	48	0.91–0.94	^{99m}Tc tetrofosmin	[33]
QGS™	MUGA	24	0.85	^{99m}Tc sestamibi	[22] (22)
QGS™	MUGA	30	0.82	^{99m}Tc sestamibi	[34]
QGS™	MUGA	52	0.90	^{99m}Tc sestamibi	[35]
QGS™	MUGA	36	0.93	^{99m}Tc tetrofosmin	[36]
QGS™	MUGA	36	0.91	I-123 BMIPP	[36]
QGS™	3-D MUGA	10	0.97	^{99m}Tc tetrofosmin	[37]
QGS™	3-D MUGA	25	0.93	^{99m}Tc sestamibi	[38]
QGS™	MRI	17	0.93	^{99m}Tc tetrofosmin	[39]
QGS™	MRI	15	0.88	^{99m}Tc tetrofosmin	[40]
QGS™	MRI	25	0.93	^{99m}Tc tetrofosmin	[41]
QGS™	MRI	20	0.94	^{99m}Tc sestamibi	[42]
QGS™	MRI	20	0.92	^{201}Tl	[42]
QGS™	MRI	31	0.85	^{99m}Tc sestamibi	[43]
QGS™	MRI	16	0.89	^{99m}Tc sestamibi	[44]
QGS™	MRI	22	0.90	^{99m}Tc tetrofosmin	[45]
QGS™	MRI	21	0.85	^{99m}Tc tetrofosmin	[46]
QGS™	MRI	30	0.72	^{99m}Tc sestamibi	[47]
QGS™	MRI	15	0.89–0.90	unknown	[48]
QGS™	MRI	50	0.82	^{99m}Tc tetrofosmin	[49]
QGS™	MRI	54	0.90	^{99m}Tc sestamibi	[50]
QGS™	2-D echo	35	0.79	^{99m}Tcsestamibi	[52]
QGS™	2-D echo	57	0.85	^{99m}Tc tetrofosmin	[53]
QGS™	2-D echo	52	0.82	^{201}Tl	[54]
QGS™	2-D echo	50	0.90	^{99m}Tc sestamibi	[55]
QGS™	2-D echo	180	0.72–0.79	^{99m}Tc sestamibi, ^{201}Tl	[56]
QGS™	2-D echo	72	0.76–0.86	^{201}Tl	[57]
QGS™	2-D echo	33	0.75	^{99m}Tc sestamibi	[58]
QGS™	2-D echo	30	0.77–0.86	^{99m}Tc tetrofosmin	[59]
QGS™	2-D echo	32	0.83	^{99m}Tc tetrofosmin	[60]
QGS™	3-D echo	18	0.80	^{201}Tl	[61]
QGS™	Contrast ventriculography	12	0.85	^{99m}Tc tetrofosmin	[53]
QGS™	Contrast ventriculography	10	0.97	^{99m}Tc tetrofosmin	[37]
QGS™	Contrast ventriculography	229	0.78	^{99m}Tc tetrofosmin	[62]
QGS™	Contrast ventriculography	74	0.92	^{99m}Tc tetrofosmin	[63]
QGS™	Contrast ventriculography	56	0.78–0.89	^{99m}Tc sestamibi	[63]
QGS™	EBCT	10	0.94	^{99m}Tc sestamibi	[64]
QGS™	Thermodilution	21	0.84	^{99m}Tc sestamibi	[65]

(*continued*)

Table 5.2 (*Continued*)

Method	Gold standard	No. of patients	Spearman's *r* (LVEF)	Isotope	References
EGS™	First pass	79	0.82	^{99m}Tc sestamibi	[4]
EGS™	MUGA	25	0.88	^{99m}Tc sestamibi	[31]
EGS™	MUGA	30	0.78	^{99m}Tc sestamibi	[34]
EGS™	MRI	10	0.88	^{99m}Tc sestamibi	[4]
EGS™	MRI	31	0.81	^{99m}Tc sestamibi	[43]
EGS™	MRI	30	0.70	^{99m}Tc sestamibi	[47]
EGS™	2-D echo	33	0.72	^{99m}Tc sestamibi	[58]
4D-MSPECT™	MUGA	25	0.82	^{99m}Tc sestamibi	[31]
4D-MSPECT™	MUGA	30	0.69	^{99m}Tc sestamibi	[34]
4D-MSPECT™	2-D echo	30	0.84–0.86	^{99m}Tc tetrofosmin	[59]
4D-MSPECT™	MRI	26	0.97	^{99m}Tc sestamibi	[66]
4D-MSPECT™	MRI	22	0.93	unknown	[67]
4D-MSPECT™	MRI	54	0.89	^{99m}Tc sestamibi	[50]
4D-MSPECT™	Contrast ventriculography	90	0.81	^{99m}Tc sestamibi	[68]
4D-MSPECT™	Contrast ventriculography	97	0.87	unspecified	[6]
MultiDim™	First pass	20	0.86	^{99m}Tc sestamibi	[69]
MultiDim™	MUGA	50	0.93	^{99m}Tc tetrofosmin	[8]
MultiDim™	MUGA	40	0.94	^{99m}Tc tetrofosmin	[25]
MultiDim™	MUGA	19	0.7	^{201}Tl	[27]
MultiDim™	MUGA	32	0.75–0.88	^{201}Tl	[70]
MultiDim™	2-D echo	49	0.73	^{99m}Tc sestamibi	[71]
GSCQ™	First pass	117	0.78	^{99m}Tc sestamibi	[22]
GSCQ™	MUGA	24	0.88	^{99m}Tc sestamibi	[22]
GSCQ™	MUGA	30	0.90	^{99m}Tc sestamibi	[9]
Total		3652	0.86		

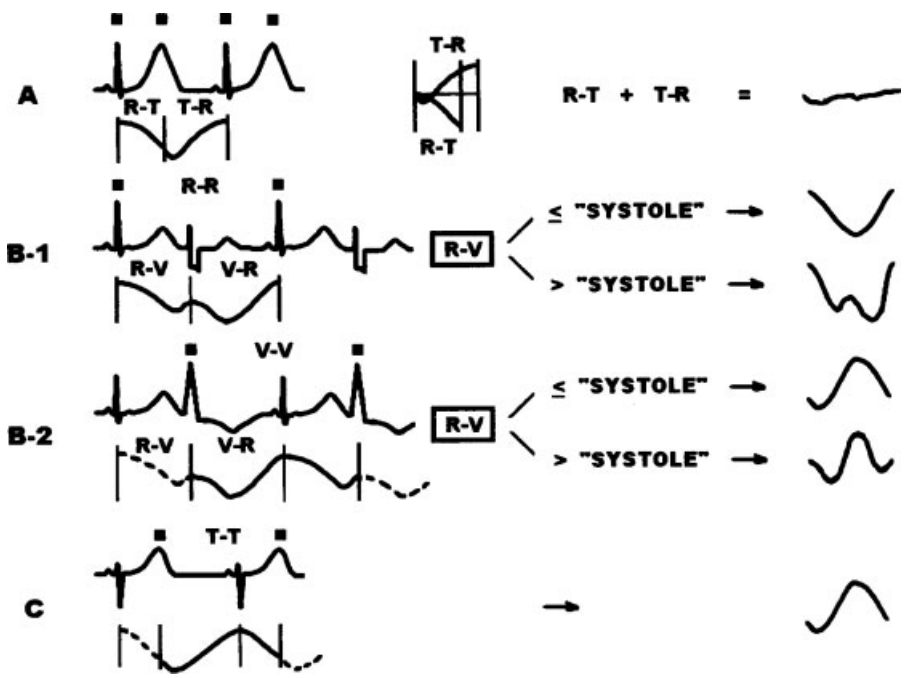

Figure 5.5 Potential errors in electrocardiographic (ECG) gating. If the ECG gate senses the R–R interval incorrectly, an erroneous time–volume curve will be produced. (a) Both T and R waves trigger the ECG gate. (b) The original R waves are sensed for B-1 and the ventricular premature beats are sensed for B-2. Two entire cardiac cycles are involved in the sensed R–R interval for B-1 and B-2. (c) The T waves are sensed instead of R waves. R–T, T–R, R–R, R–V, V–R, and V–V each represent an interval, respectively. Abbreviation: V, ventricular premature beat; square, trigger for gating. (Reproduced with permission from [110].)

say that if the time–volume curve is obviously deformed, or if the frequency of PVCs is more than 20%, great caution should be exercised regarding whether to report cardiac function assessments.

Number of gating intervals

While most gated SPECT measurements of LVEF in the literature have been derived from images acquired using 8-frame gating, 16-frame gating is becoming increasingly popular (see Chapters 2 and 3). Sixteen-frame gating requires additional data storage and processing time and could result in images with unacceptably low counts. However, it can also provide more accurate estimates of LVEF, since there is more precise end-systolic imaging. We recommend 16-frame gating in centers using multidetector cameras. At least 16-frame acquisition is considered essential for diastolic function assessment. The relationship between 8-frame and 16-frame measurements of gated SPECT LVEF has been quantitatively investigated for Cedars-Sinai's QGS™algorithm [1,29,32,33,48,112–115] and for Yale's GSCQ™algorithm [72]. As expected, 8-frame gating was found to underestimate LVEF by 2–4.5 (QGS™) to 6 (WLCQ™) percentage points, due to the undersampling of the time–volume curve (Figs. 5.6 and 5.7). However, the degree of underestimation is remarkably uniform over a wide range of ejection fractions, with no apparent trend demonstrated by Bland–Altman analysis (Fig. 5.8). In other words, 8-frame gating has been shown to lead to an average LVEF underestimation of 3.7–4 LVEF percentage points in comparison with 16-frame gating. It is, therefore, possible to derive a proxy for "16-frame LVEF" by adding 4% points to the LVEFs measured by QGS™ from 8-frame gated data. Obviously,

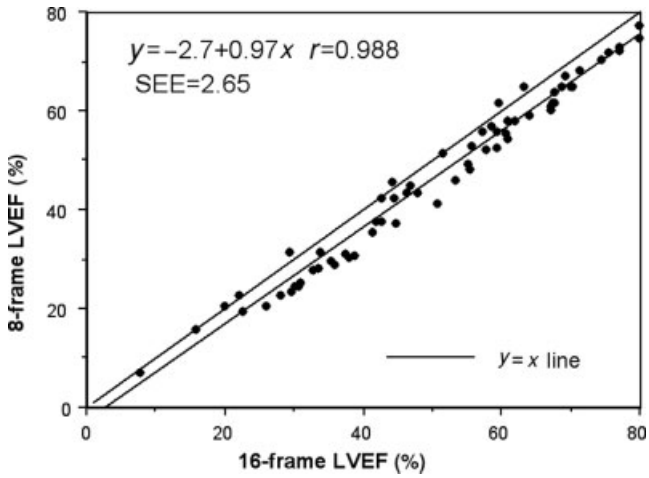

Figure 5.7 LVEFs measured by QGS, on 65 patients, using 16-frame and 8-frame gated ^{99m}Tc-sestamibi SPECT, showing that the latter underestimates LVEF [1]. The correlation between the two measurements is excellent and the standard error of the estimate (SEE) low, making their relationship quite predictable.

although generally true, this relationship will not apply to all the patients. While 8-frame gated SPECT imaging does not allow for meaningful measurement of diastolic function [116], it has been suggested that 12-frame imaging may be adequate [102] and that 16-frame imaging is quite effective [103]. Thirty-two-frame imaging is also feasible and results in an excellent agreement with a MUGA standard [32,33,35,38,104] (Table 5.3).

Count statistics and choice of radioisotopes

Quantitative measurements of LVEF, EDV, and ESV have been reported to be quite independent of count statistics,

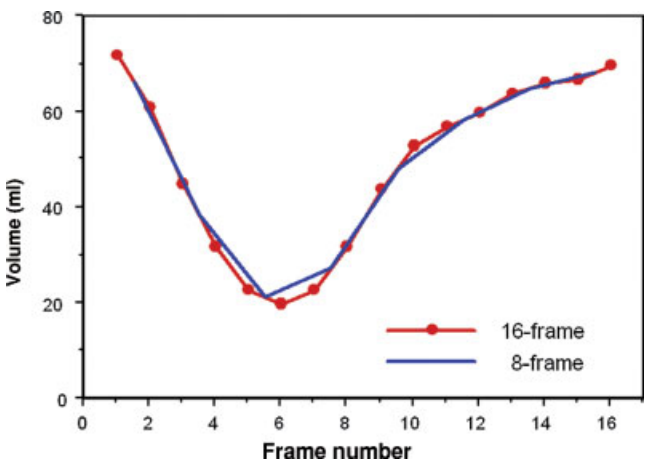

Figure 5.6 Eight-frame gating "smooths" the time–volume curve compared to 16-frame gating, yielding slightly lower EDVs, higher ESVs, and lower LVEF, principally due to imprecise definition of true end-systole.

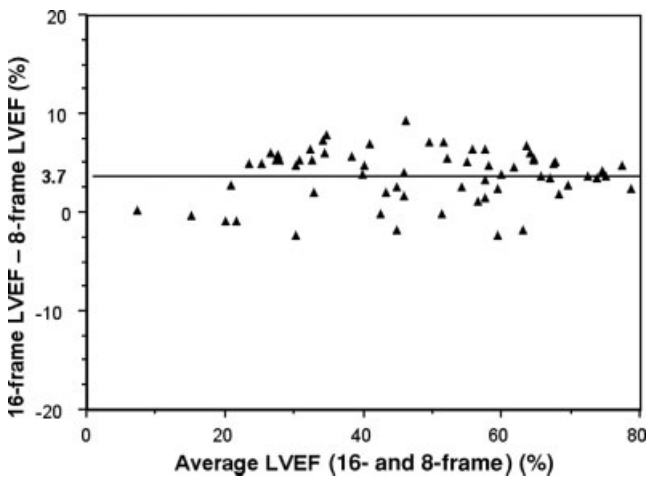

Figure 5.8 Bland–Altman analysis of the data in Fig. 5.7 shows essentially no trend in the underestimation of LVEF across LVEF ranges by 8-frame gating, with the average decrease being 3.7 LVEF percentage points [1].

Table 5.3 Validations of quantitative measurements of diastolic function from gated perfusion SPECT.

Method	Gold standard	No. of patients	Parameter	Spearman's *r*	Isotope	References
QGS™	MUGA	24	PER	0.87	^{99m}Tc tetrofosmin	[32]
QGS™	MUGA	24	TPER	0.84	^{99m}Tc tetrofosmin	[32]
QGS™	MUGA	24	1/3 FF	0.87	^{99m}Tc tetrofosmin	[32]
QGS™	MUGA	24	PFR	0.92	^{99m}Tc tetrofosmin	[32]
QGS™	MUGA	24	TPFR	0.89	^{99m}Tc tetrofosmin	[32]
QGS™	MUGA	48	PFR	0.51–0.75	^{99m}Tc tetrofosmin	[33]
QGS™	MUGA	25	PER	0.90	^{99m}Tc sestamibi	[38]
QGS™	MUGA	25	PFR	0.68	^{99m}Tc sestamibi	[38]
QGS™	MUGA	25	1/3 FF	0.83	^{99m}Tc sestamibi	[38]
QGS™	MUGA	52	PER	0.88	^{99m}Tc sestamibi	[35]
QGS™	MUGA	52	PFR	0.80	^{99m}Tc sestamibi	[35]
QGS™	MUGA	52	1/3 FF	0.82	^{99m}Tc sestamibi	[35]
Total		149		0.83		

Abbreviations: 1/3 FF, 1/3 filling fraction; PER, peak ejection rate; PFR, peak filling rate; TPER, time to peak ejection rate; TPFR, time to peak filling rate

and accurate even when calculated from low-count (high-noise) images acquired using the "fast" gated SPECT technique [117–120], as well as simulated noisy acquisitions [121]. While this finding would be expected to also apply to gated SPECT images acquired following low-dose and high-dose radionuclide injections [122], it has been reported that small differences may exist [114], and further investigation of this issue is warranted. In the authors' opinion, it is likely that differences between quantitative results in high-count and low-count images will be at least in part related to the quantitative algorithms' difficulties in identifying the location of the valve plane with the latter images.

Quantitative measurements may also depend on the type of radionuclide used. As it was originally suggested with respect to nongated dual isotope SPECT imaging (rest ^{201}Tl/poststress ^{99m}Tc sestamibi), resolution differences should be minimized by employing the same low-energy-high-resolution collimator for the ^{201}Tl and ^{99m}Tc acquisitions [123]. This approach is also advocated for gated SPECT imaging. Nevertheless, it is to be expected that ^{201}Tl images will be more "blurred" than ^{99m}Tc sestamibi or ^{99m}Tc tetrofosmin images, due both to the increased amount of Compton scatter associated with ^{201}Tl and the use of a smoother pre-reconstruction filter. This would translate into a mild overestimation of ^{201}Tl LVEF and moderate underestimation of ^{201}Tl EDV and ESV compared to ^{99m}Tc-based LVEF, EDV, and ESV, respectively, as reported for the QGS™ algorithm [42,124–126] and shown in Fig. 5.9 with respect to LVEF. Given the many published validations of quantitative gated ^{201}Tl SPECT measurements against various gold standards [24,26,27,29,42,43,54,57,61,70,125,127,128], it is unlikely that major quantitative discrepancies exist between ^{201}Tl- and ^{99m}Tc-based gated SPECT, as long as the studies are properly acquired and processed. This was also demonstrated in direct comparisons between separate [124,125] and simultaneous dual isotope gated SPECT acquisitions [20, 129].

Finally, it is reasonable to expect that the use of ^{201}Tl will exacerbate the overestimation of LVEF in small ventricles; the use of zoomed acquisition and/or reconstruction strategies may be able to counter that phenomenon, as will be discussed later in this chapter. While there are lower count rates associated with clinical doses of thallium-201 than with the ^{99m}Tc agents, we still use and recommend the use of 16-frame gating when multidetector cameras are employed.

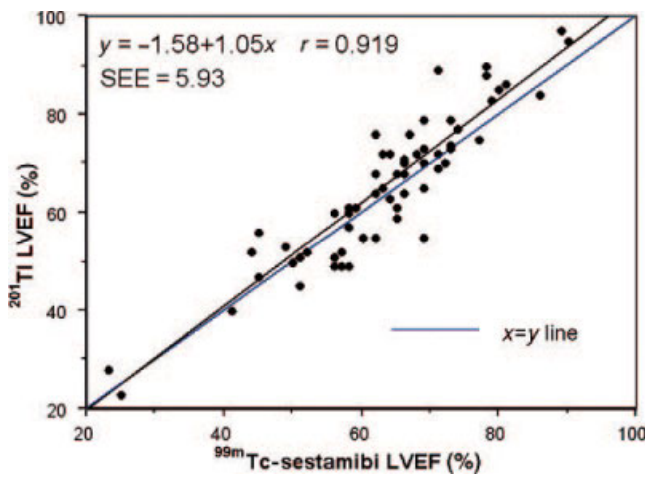

Figure 5.9 Relationship between the LVEF measured by QGS in a nonischemic 64-patient population studied with gated ^{99m}Tc sestamibi and ^{201}Tl SPECT [124].

Collimators, filter cutoffs, and reconstruction techniques

The known dependency of gated SPECT image resolution on the type of collimator used should not be of excessive concern, as long as a high-resolution parallel hole collimator is used for all patients. However, the effect of specialized collimators (fan beam, cone beam, etc.) on the quantitative measurements of LVEF has not been investigated in great detail, and the results are not clear. Some studies comparing the QGS™ algorithm in the same patient population using both a parallel hole and a "cardio focal" collimator have reported almost identical results [119,130] as well as substantially different results [131].

To the extent that pre- or post-reconstruction filtering changes the resolution of the gated SPECT images, it can also affect the quantitative LVEF measured, most likely in a manner dependent on the particular algorithm used. Figure 5.10 shows the quantitative LVEF, measured by QGS™, as a function of the critical or cutoff frequency of the Butterworth pre-reconstruction filter, for a normal patient and an abnormal patient undergoing gated ^{99m}Tc-sestamibi SPECT imaging. The algorithm was found to be relatively insensitive to the level of filtering of the projection images, as long as the cutoff is greater than about 0.15 on the 0–0.5 scale, as also confirmed by other investigators [132–134]. An even lesser degree of variability is expected to be associated with the use of different filters having the same cutoff [132,135]. Of course, image resolution is not exclusively determined by filtering, being also a function of radio pharmaceutical choice and LV size – dependency on the latter will be discussed in detail later in the chapter.

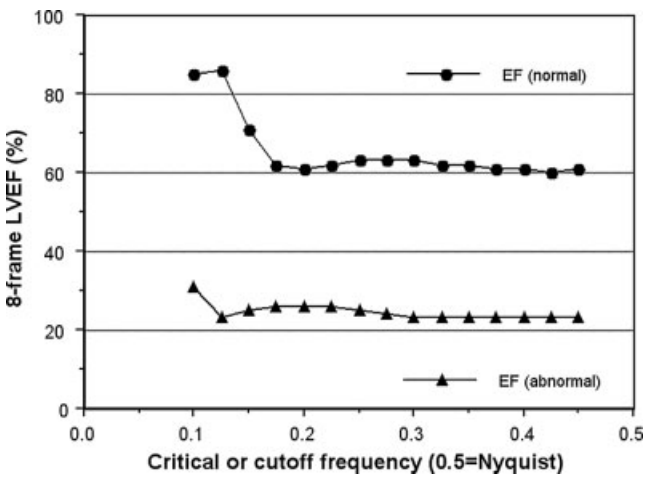

Figure 5.10 LVEF measured by QGS in a normal (top) and an abnormal patient (bottom) undergoing gated ^{99m}Tc-sestamibi SPECT, as a function of the pre-reconstruction filter cutoff. Values ≤ 0.15 (on a 0–0.5 scale) or ≤ 0.30 (on a 0–1 scale) can lead to overestimation of the LVEF, due to "LV cavity obliteration."

Finally, it has been reported that filtered back projection and iterative reconstruction result in statistically equivalent measurements of LVEF, EDV, ESV, and regional wall motion [136–140], particularly if the number of iterations has been optimized [141]. Iterative reconstruction may help reduce artifacts in the inferoseptal myocardium [142], with consequent improvement in the success rate of the quantitative algorithm as well as its quantitative accuracy, and has been found to yield marginally better correlation with a planar blood pool standard than filtered back projection did [143].

Influence of perfusion defects on function measurements

The dependency of gated SPECT LVEF, EDV, and ESV measurements on the presence and size of perfusion defects is, to some extent, a function of the specific quantitative algorithm used [144]. However, it is remarkable that a large number of published reports have shown the absence of major discrepancies between true LVEF and measured LVEF in patients with large perfusion defects and/or low LVEFs [6,9,20,25,29,30,39,45,48,57,59,63,68,71, 74,75,77,115, 120,145–153]. With algorithms not operating on thresholded images, a possible reason for these findings is that low levels of perfusion often exist that are detected by the algorithm but are not visible because of the particular gray or color scale used. This phenomenon can be verified by saturating the scale, that is, allocating all colors or gray levels to the low-count portion of the image (Fig. 5.11). Nevertheless, most quantitative gated SPECT algorithms will be unable to track edges in large aneurysms, because quantitation generally proceeds from an approach based on the assumption of a regular or "smooth" LV shape. While this approach is quite helpful in ensuring that the areas of extracardiac uptake be not erroneously considered as myocardium, it may frequently cause the aneurysm to be "cut off" (excluded), with consequent underestimation of the ESV and overestimation of the LVEF.

Small LVs and myocardial hypertrophy

The accuracy of quantitative LVEF measurements depends on the actual size of the LV as well as on its reconstructed size. It has been shown that the relatively low resolution of nuclear cardiology images can lead to the apparent shrinkage or even obliteration of the LV cavity in patients with small ventricles, particularly at end-systole, the end result being an overestimation of the LVEF [134,155–159]. It should be clear that this is not so much a limitation of the various quantitative gated SPECT algorithms, but one of nuclear cardiology itself (a human operator would be just as likely to have difficulty

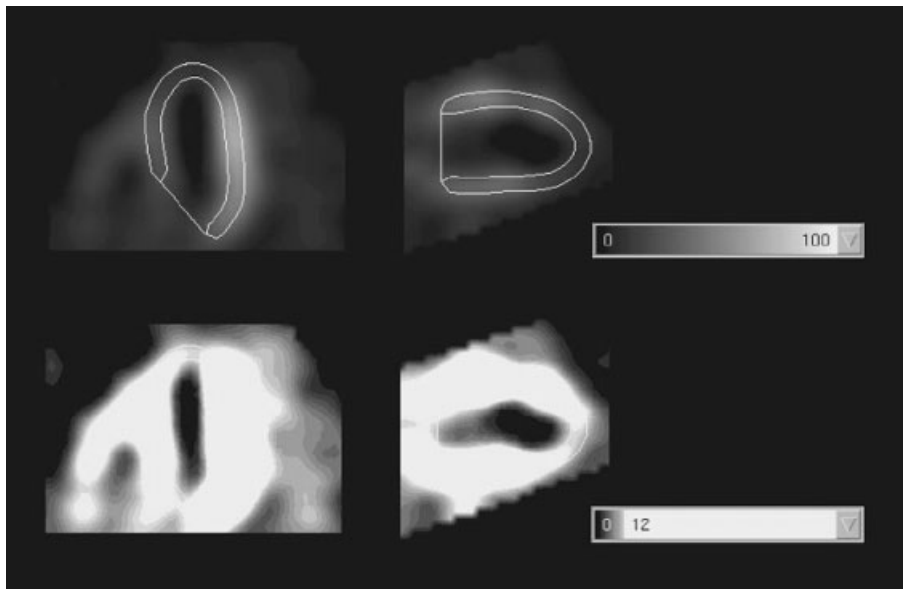

Figure 5.11 "Saturating" the gray or color scale by allocating all its values to the low-count portion of the image (bottom row) allows to verify the general accuracy of contours derived by the quantitative algorithm in areas of apparent "absent" perfusion (top row). (Reproduced with permission from [154].)

identifying the ESV in Fig. 5.12). It is reasonable to presume that if the LV is magnified, preferably in acquisition (by employing a larger acquisition zoom) or, less ideally, in reconstruction (by employing zoomed centered or zoomed off-axis reconstruction, as shown in Fig. 2.19), the amount of LVEF overestimation would decrease [156,160–165]. This is equivalent to using a larger image matrix size (100^2 or 128^2 pixels instead of the conventional 64^2), since each pixel would then correspond to a smaller portion of the myocardium [134]. A refinement of imaging technique, therefore, might include a brief planar acquisition followed by the choice of zoom (or matrix size) most appropriate for a given patient, based on the observed heart size [166]. Alternatively, it has been proposed that numerical modeling and compensation of blurring be used in patients with small hearts [167,168]. We do not favor customization of gated SPECT acquisition and/or processing parameters based on individual patients' characteristics, and prefer to report LVEFs as being "in the normal range" or "higher than 75%" whenever overestimation of quantitative LVEF occurs due to small LV size.

The thickness of the myocardium is also an issue, since nuclear cardiology techniques do not have sufficient resolution to measure it with extreme accuracy [2]. Most quantitative gated SPECT algorithms are either calibrated for the range of thicknesses most typically encountered in clinical practice [1], or assume a fixed myocardial thickness [4,72]; consequently, the endocardial and epicardial contours will be incorrectly positioned in patients with LV hypertrophy, and quantitative gated SPECT LVEFs are likely to be underestimated [169,170].

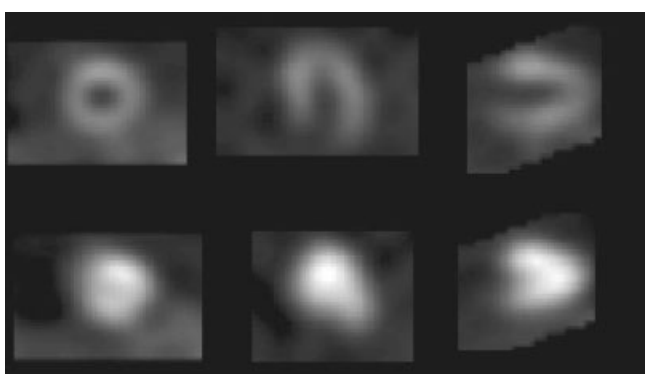

Figure 5.12 End-diastolic (top) and end-systolic (bottom) midventricular short (left) and horizontal (middle) and vertical (right) long-axis images for a gated ^{99m}Tc-sestamibi SPECT patient with a small LV.

Motion

While it has long been known that patient or organ motion during nongated myocardial perfusion SPECT acquisitions may cause artifactual perfusion defects [171–173], and the relationship between various types and degrees of motion and quantitative perfusion assessment has been characterized for single- and dual-detector camera systems [174], less data exists on the effect of motion on quantitative LVEF assessment in gated SPECT imaging. A recent report by Matsumoto et al., on the basis of the simulation of nine different patterns of motion during dual-detector acquisitions in clinical patients, suggests that LVEF measurements by QGS^{TM} are relatively independent of motion in larger hearts (EDV $>$ 60 ml) whereas progressive overestimation of LVEF occurs in smaller hearts (EDV $<$50 ml). Patient motion was generally found to cause

underestimation of EDV and ESV, mostly related to apparent shrinkage of the LV cavity, with artifactual myocardial wall motion abnormalities reported in larger hearts [175]. Furthermore, it has been suggested that gated myocardial perfusion SPECT may be more sensitive to patient motion than planar [111] and gated blood pool SPECT [176], with simulated motion of as little as 6.7 mm resulting in decrease of quantitatively measured gated SPECT LVEF [111].

Attenuation, scatter, and resolution compensation

Attenuation correction of gated SPECT images does not appear to greatly affect quantitative measurements of LVEF, as demonstrated by the fact that differences less than 5% between LVEFs from attenuation-corrected and standard gated SPECT were reported for two different quantitative algorithms [177], and small, not clinically significant, differences in LVEFs and volumes were found with a third algorithm [178].

LVEFs were found to be quite comparable in a large population of patients undergoing back-to-back supine and prone gated SPECT acquisitions, despite the different attenuation characteristics of the two settings [179,180], and similarly good agreement was found for gated SPECT acquisitions performed with the patient in the supine and upright positions [181]. A more recent report confirms the statistical equivalence for quantitative LVEFs and ESVs derived from consecutive supine and prone rest gated SPECT acquisitions – however, differences were found for the EDVs, stroke volumes (SVs), and heart rates. The authors of this report suggest that the effects seen were mostly physiological as opposed to technical or algorithm-related.

The use of resolution recovery approaches has been reported to have little effect on LVEF [138]. Quantitative differences in LVEF, EDV, and ESV found in images before and after correction for attenuation, scatter, and variable resolution are likely to be related to changes in the apparent LV cavity size caused by the correction algorithm itself, and, in the authors' opinion, their possible artifactual nature ought to be carefully considered.

Normal limits

It is generally accepted in cardiology that the cutoff between a normal LVEF and an abnormal LVEF is 50% [182,183], and some may be tempted to consider that number as an absolute threshold. However, we have seen that quantitative measurements of LVEF from gated SPECT images depend on a number of factors – as an example, a patient's LVEF could be measured as 48 or 52%, depending on whether an 8-frame or 16-frame acquisition protocol was employed. It is therefore essential to think of limits of normality for gated SPECT measurements of global cardiac function in the context of the specific imaging approach used. Normal limits for LVEF and LV volumes have been reported mostly for 8-frame gating [9,184–190], and appear to be gender-specific [126,188–196] and possibly age-specific [194], but independent of the type of camera used [189]. Conflicting reports exist on normal limits' dependence on the specific radioisotope used [126,189]. Table 5.4 presents some published data relative to QGS™ and 8-frame gating: with respect to that setting, it may be prudent to consider LVEFs greater than 50% as definitely normal and LVEFs lower than 40% as definitely abnormal, with clinical judgment and integration of additional data needed in the 40–50% range (see also Chapters 6 and 8). It is extremely important to realize that normal limits for parameters of global cardiac function will likely be different for different quantification algorithms [9,50,188,193,197–199], despite the generally good cross-algorithm reproducibility.

Table 5.4 Normal limits for quantitative measurements of global LV function from 8-frame gated perfusion SPECT images, using the QGS™ algorithm.

References	Gender	LVEF (%)	EDV (ml)	ESV (ml)	EDV (ml/m^2)	ESV (ml/m^2)
[187]	M + F	45	120	70		
[189]	F	50	91	40		
	M	43	119	5		
[190]	F	50	100	42	56	25
	M	45	142	65	70	32

Gated PET

Of note, it has recently been suggested that algorithms developed for gated SPECT quantitation may be directly applicable to gated PET quantitation, despite differences in isotope energy and image resolution: radioisotopes of interest in this regard would be 18-FDG [153,210–225], 13-N [226–228], 15-O [229], and 82-Rb [230–234]. Even though most validations have proved satisfactory (see also Chapter 12), it is likely that improvements can be achieved by modifying the gated SPECT algorithms in such a way as to take advantage of the superior resolution of the gated PET images (G. Germano, personal communication, 2005).

Volumes

It should be appreciated that one can usually more accurately measure ratios of the LV cavity volumes, such as

the LVEF or the TID ratio [235], than the volumes themselves – for example, errors in the determination of end-diastolic and end-systolic volumes would be expected to occur in the same general direction, and therefore would at least partially cancel out when the ratio of the volumes is calculated for LVEF calculation purposes [1]. Consequently, validation of quantitative LVEF measurements does not necessarily imply validation of the end-diastolic and end-systolic volume measurements from which the LVEF is derived. Errors in the absolute measurement of LV cavity volumes can be attributed, in part, to the same factors that affect the measurement of LVEF. Specifically, (a) in comparison with 16-frame gating, the use of 8-frame gating will artificially increase ESVs and have little effect on EDVs, as shown in Fig. 5.6, and (b) both EDV and ESV will be underestimated when quantitative analysis is performed on unzoomed images of small ventricles, especially with lower resolution radioisotopes. In addition, absolute volume measurements can be adversely affected by incorrect listing of the pixel size in the image header. Pixel size is usually automatically calculated by modern cameras, on the basis of knowledge of field of view and zoom information. However, older cameras or "hybrid" systems (where one manufacturer's camera is interfaced to another manufacturer's computer) may not be set up to transfer pixel size information from the gantry, and may assume a "standard" value (i.e., 1 cm) as default. Whenever in doubt, the accuracy of the pixel size stored in the image header should be checked by imaging a test pattern (e.g., 2-point sources separated by a known distance), and counting the number of pixels between the points' centroids in the reconstructed image.

Above considerations notwithstanding, a large body of published evidence suggests that quantitative measurements of absolute LV cavity volumes from gated perfusion SPECT images agree well with established standards, as summarized in Table 5.5 [4,27,28,30,34,36,37,39–50,52,54–56,58,60–62,65,66,69,70,78–81].

As it is reasonable to expect given the frequent association of ventricular enlargement and compromised cardiac function, there is an inverse relationship between quantitative measurements of LVEF and LV cavity volumes [204,236]. With respect to the QGS^{TM}algorithm, Figs. 5.13, 5.14, and 5.15 show the relationships between quantitative LVEF and end-diastolic, end-systolic, and summed gated (ungated) LV cavity volumes measured in 926 patients who underwent 8-frame gated ^{99m}Tc-sestamibi SPECT. The best fit to the data is provided in all cases by a negative exponential model, although linear regression also yields very good correlation. Interestingly, displaying the same data in a table format (Tables 5.6, 5.7, and 5.8) demonstrate that, no matter whether the end-diastolic, end-systolic, or ungated LV cavity volume is considered, thresholds exist which allow to identify the study to be considered likely to be associated with a normal (>50%) or abnormal (≤40%) LVEF based on the volume measurement alone, with relatively high accuracy. The relationship between the summed gated LV cavity volume and the EDV and ESV measured by QGS^{TM}was investigated in the same 926-patient population described above. As Fig. 5.16 shows, LV cavity volumes from ungated or summed gated images are more similar to ESVs than to EDVs. This finding suggests that the effect on perceived myocardial counts of the apparent increase caused by myocardial thickening at systole (partial volume effect [98]) is stronger than that of the relatively longer duration of the diastolic phase of the cardiac cycle.

Regional myocardial wall motion and thickening

Regional function assessment plays an important role in the clinical application of gated myocardial perfusion SPECT. Often the presence of a regional function abnormality with a normal LVEF provides the necessary evidence by which to consider an overall SPECT study or a vascular territory abnormal. There is no agreement as to whether the focus should be on quantifying myocardial wall motion or thickening: the former has traditionally been evaluated by nuclear cardiologists in conjunction with blood pool studies (and is found by many as being easier to categorize visually – see Chapter 6), while the latter is uniquely suited to take advantage of the partial volume effect and its effect on gated perfusion SPECT images. Many think that the two measurements are essentially equivalent, because in order to thicken the myocardium must necessarily move (and vice versa). While this is generally true, there are exceptions. For instance, small infarcted portions of the myocardium can be "tethered" by surrounding healthy cardiac muscle, thus appearing as having normal motion but absent thickening. On the other hand, it is well known that typically postcardiac surgery patients appear to exhibit septal dyskinesia (paradoxical septal motion) in the presence of normal septal thickening, with possible concomitant overestimation of motion in the lateral myocardial wall [237–241]. While the above phenomena suggest that thickening is potentially a more accurate parameter of myocardial function than motion, the authors believe that it is important to evaluate both regional motion and thickening, whether the assessment is done visually or quantitatively.

Technical considerations

Quantitation and validation of regional myocardial function measurements from gated perfusion SPECT are more challenging, compared to global function.

With respect to thickening, it has been pointed out earlier in this chapter that nuclear cardiology images do not have

Table 5.5 Validations of quantitative measurements of volumes from gated perfusion SPECT.

Method	Gold standard	# Patients	Spearman's *r* (EDV)	Spearman's *r* (ESV)	Isotope	References
QGS™	MUGA	21	0.7	0.7	^{201}Tl	[27]
QGS™	MUGA	21	0.73	0.83	^{99m}Tc tetrofosmin	[28]
QGS™	MUGA	62	0.88	0.95	^{99m}Tc sestamibi, ^{99m}Tc tetrofosmin	[30]
QGS™	MUGA	30	0.88	–	^{99m}Tc sestamibi	[34]
QGS™	MUGA	36	0.85	0.82	^{99m}Tc tetrofosmin	[36]
QGS™	MUGA	36	0.85	0.75	I-123 BMIPP	[36]
QGS™	3-D MUGA	10	0.95	0.97	^{99m}Tc tetrofosmin	[37]
QGS™	3-D MUGA	16	0.98	0.93	^{99m}Tc sestamibi	[78]
QGS™	MRI	17	0.81	0.90	^{99m}Tc tetrofosmin	[39]
QGS™	MRI	15	0.95	0.94	^{99m}Tc tetrofosmin	[40]
QGS™	MRI	25	0.81	0.92	^{99m}Tc tetrofosmin	[41]
QGS™	MRI	20	0.92	0.97	^{99m}Tc sestamibi	[42]
QGS™	MRI	20	0.85	0.94	^{201}Tl	[42]
QGS™	MRI	31	0.91	0.92	^{99m}Tc sestamibi	[43]
QGS™	MRI	16	0.89	0.93	^{99m}Tc sestamibi	[44]
QGS™	MRI	22	0.84	0.87	^{99m}Tc tetrofosmin	[45]
QGS™	MRI	21	0.94	0.95	^{99m}Tc tetrofosmin	[46]
QGS™	MRI	30	0.91	0.92	^{99m}Tc sestamibi	[47]
QGS™	MRI	15	0.94	0.96–0.97	^{99m}Tc sestamibi	[48]
QGS™	MRI	50	0.90	–	^{99m}Tc tetrofosmin	[49]
QGS™	MRI	54	0.92	0.96	^{99m}Tc sestamibi	[50]
QGS™	2-D echo	35	0.88	0.91	^{99m}Tc sestamibi	[52]
QGS™	2-D echo	52	0.70	0.71	^{201}Tl	[54]
QGS™	2-D echo	180	0.87–0.89	0.86–0.90	^{99m}Tc sestamibi, ^{201}Tl	[56]
QGS™	2-D echo	50	0.87	0.90	^{99m}Tc sestamibi	[55]
QGS™	2-D echo	33	0.90	0.94	^{99m}Tc sestamibi	[58]
QGS™	2-D echo	49	0.86	0.86	^{99m}Tc tetrofosmin	[79]
QGS™	2-D echo	32	0.94	0.96	^{99m}Tc tetrofosmin	[60]
QGS™	3-D echo	18	0.94	0.97	^{201}Tl	[61]
QGS™	3-D echo	8	0.99	0.99	^{99m}Tc sestamibi	[80]
QGS™	Contrast ventriculography	10	0.93	0.97	^{99m}Tc tetrofosmin	[37]
QGS™	Contrast ventriculography	229	0.67	0.79	^{99m}Tc tetrofosmin	[62]
QGS™	Contrast ventriculography	16	0.92	–	^{99m}Tc sestamibi	[78]
QGS™	Thermodilution	21	0.86	0.94	^{99m}Tc sestamibi	[65]
QGS™	Thermodilution	24	0.89	0.94	^{99m}Tc sestamibi	[81]
EGS™	First pass	79	0.85	0.91	^{99m}Tc sestamibi	[4]
EGS™	MUGA	30	0.89	–	^{99m}Tc sestamibi	[34]
EGS™	MRI	10	0.97	0.99	^{99m}Tc sestamibi	[4]
EGS™	MRI	31	0.90	0.91	^{99m}Tc sestamibi	[43]
EGS™	MRI	30	0.90	0.92	^{99m}Tc sestamibi	[47]
EGS™	2-D echo	33	0.90	0.94	^{99m}Tc sestamibi	[58]
4D-MSPECT™	MUGA	30	0.85	–	^{99m}Tc sestamibi	[34]
4D-MSPECT™	MRI	26	0.95	0.98	^{99m}Tc sestamibi	[66]
4D-MSPECT™	MRI	54	0.89	0.96	^{99m}Tc sestamibi	[50]
MultiDim™	First pass	20	0.93	0.92	^{99m}Tc sestamibi	[69]
MultiDim™	MUGA	19	0.7	0.7	^{201}Tl	[27]
MultiDim™	Contrast ventricular	32	0.87–0.93	0.90–0.94	^{201}Tl	[70]
Total		1719	0.88	0.91		

sufficient resolution for myocardial thickness to be accurately measurable [2] – consequently, thickening cannot be accurately derived solely on the basis of the change in measured myocardial thickness from diastole to systole. Most quantification approaches rely, to some degree, on the partial volume effect, which relates the increase in apparent myocardial count density from diastole to systole to the underlying increase in myocardial thickness. The curve

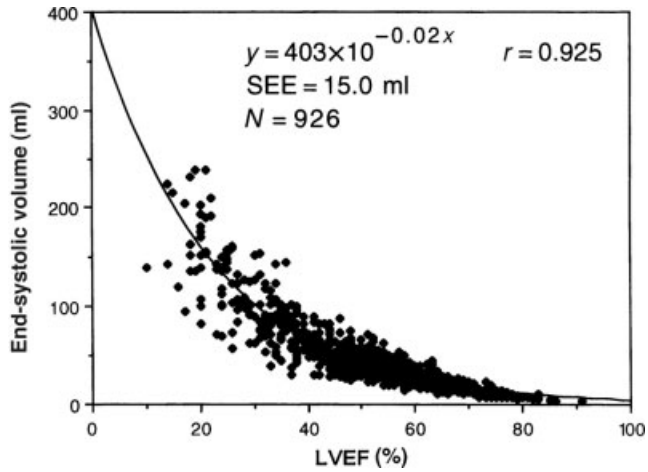

Figure 5.13 Relationship between ejection fractions and ESVs. (Modified and reproduced with permission from [204].)

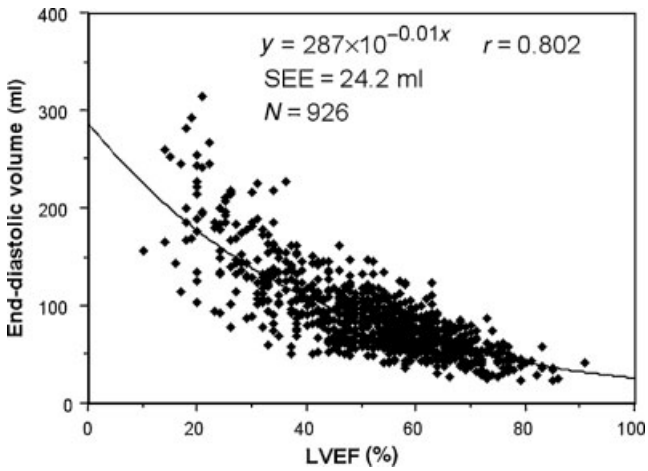

Figure 5.14 Relationship between ejection fractions and EDVs. (Modified and reproduced with permission from [204].)

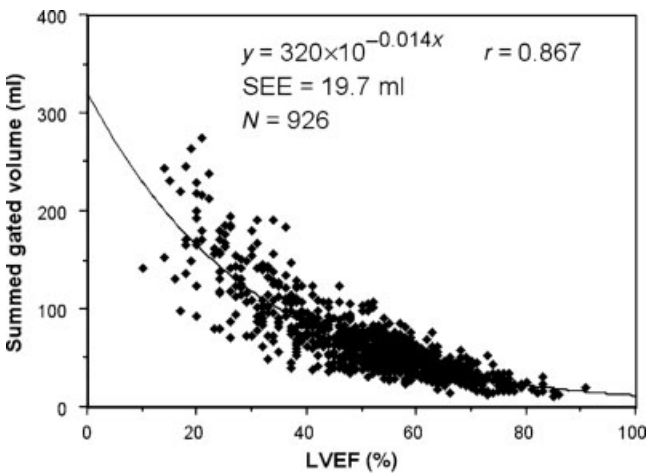

Figure 5.15 Relationship between ejection fractions and summed gated volumes. (Modified and reproduced with permission from [204].)

Table 5.6 Relationship between end-diastolic volume and left ventricular ejection fraction (LVEF) calculated from the same gated SPECT study*.

	End-diastolic volumes		
LVEF	**>155 ml**	**50–155 ml**	**<50 ml**
≤ 40%	61	128	0
40–50%	2	191	1
>50%	0	437	106

*Patients in Tables 5.6–5.8 are the same as in [204]. These data, however, were not reported.

that describes this relationship is assumed to be linear for the range of myocardial thicknesses most commonly encountered in clinical practice (Figure 5.3) [11], but of course that is only an approximation.

Other technical challenges associated with the measurement of regional function from gated perfusion SPECT are related to the rotation and translation of the heart, as well as to the choice of an appropriate reference system. The very nature of cardiac motion causes areas of the myocardium to move between image slices from diastole to systole, thus requiring accurate evaluation of regional function to be performed in the three-dimensional space and with a number of samples that are constant across gating intervals [1,2]. Even three-dimensional quantitative algorithms, however, do not account for the rotation of the heart during systole [242]. Methods for the quantification and correction of myocardial rotation have been

Table 5.7 Relationship between end-systolic volume and left ventricular ejection fraction (LVEF) calculated from the same gated SPECT study.

	End-systolic volumes		
LVEF	**>90 ml**	**25–90 ml**	**<25 ml**
≤ 40%	93	111	0
40–50%	0	197	1
>50%	0	282	242

Table 5.8 Relationship between "ungated" (summed) volume and left ventricular ejection fraction (LVEF) calculated from the same gated SPECT study.

	Ungated (summed) volumes		
LVEF	**>125 ml**	**38–125 ml**	**<38 ml**
≤ 40%	86	127	0
40–50%	0	188	2
> 50%	0	331	192

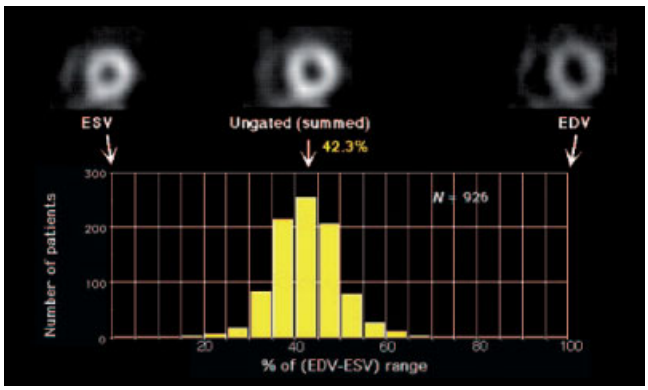

Figure 5.16 Histogram of the ungated (summed) LV cavity volume within the (ESV to EDV) range, as determined by QGS in 926 patients [204].

proposed for nonnuclear modalities [243] and more recently for gated SPECT [244,245], but these solutions are not widely implemented and are likely to be problematic, mainly because of the insufficient resolution of the gated SPECT image set. Incidentally, it has been demonstrated that correction for myocardial rotation has very little effect in the assessment of the basal two-thirds of the LV [99,246], and its clinical relevance in assessing the distal one third of the LV is uncertain [99]. The authors believe that the adoption of the three-dimensional, coordinateless "centerline" approach utilized by our and other algorithms to quantify myocardial motion [2,85,89] avoids the inaccuracies deriving from the use of a fixed or floating reference system [99], albeit without specifically addressing cardiac rotation and translation.

Validation of absolute measurements of regional function

One would ideally want to validate the absolute quantitative measurements of regional wall motion and thickening, generated by a three-dimensional algorithm applied to gated perfusion SPECT images, against a three-dimensional gold standard. Quantitative gated MRI is the natural candidate for that purpose, given its high spatial and temporal resolution, but several concerns exist with respect to its three-dimensional nature. With current protocols, and unlike gated SPECT, the various MRI slices that compose a three-dimensional volume are not acquired simultaneously, but during a series of breathholds. Even if a "navigator" technique is used, this approach is associated with some degree of misalignment within the image volume. Also, the reliance on short-axis images characteristic of MRI protocols makes it difficult to precisely identify the location of the valve planes, which is sometimes not even covered by the MRI acquisition, especially in patients with larger hearts. Despite these drawbacks, MRI is accepted as the gold standard for function assessments at the present time. It is surprising that only a few validations of gated SPECT measurements by MRI exist.

Importantly, even if a larger number of published reports existed comparing absolute quantitative measurements of regional wall motion and thickening by gated SPECT and other reference techniques in the same patient populations, validation would be difficult. Some method for precise registration of images from different techniques would be needed.

It has been reported by several investigators using different algorithms that regional function quantitatively assessed from gated SPECT images of normal patients is markedly nonuniform [247–253], as shown in Figs. 5.17 and 5.18. On the other hand, the nonnuclear literature comprises both findings of substantial regional heterogeneity of thickening [254–259] and findings of reasonable thickening uniformity [260,261], as discussed by Corbett et al. [262]. The nonuniformity of quantitative gated SPECT regional function is probably due to a combination

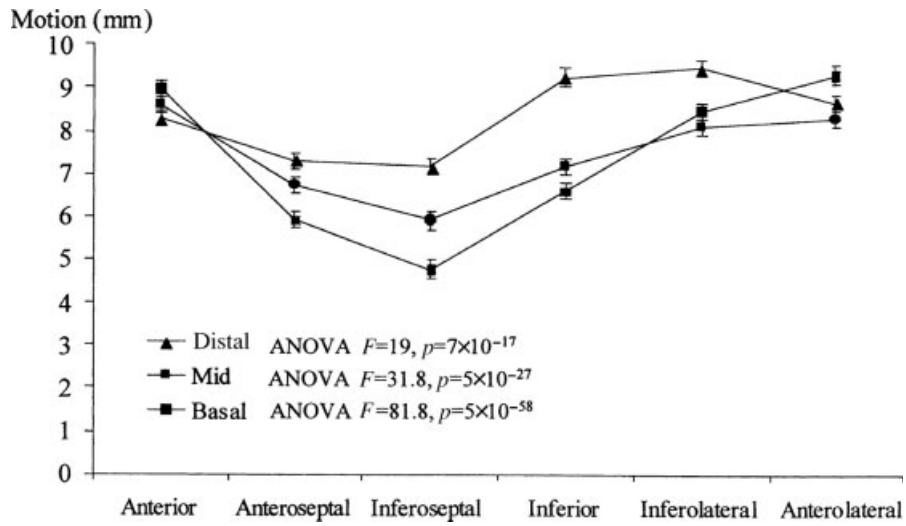

Figure 5.17 Circumferential variations in normal LV myocardium's segmental motion at distal, mid, and basal ventricular levels. (Reproduced with permission from [252].)

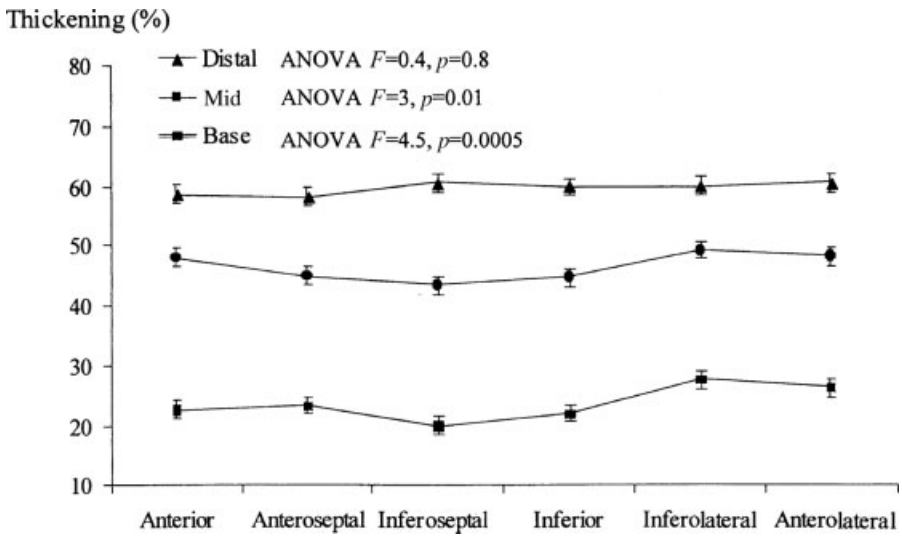

Figure 5.18 Circumferential variations in normal left ventricular (LV) myocardium's segmental thickening at distal, mid, and basal ventricular levels. (Reproduced with permission from [252].)

of physiology (the septal wall of the LV moves less than the lateral wall, since it is attached to the RV) and partial volume effects specific to nuclear cardiology (the apex of the LV, being thinner than other areas, appears to move and thicken more because it lies in a steeper region of the count density recovery curve [98]). At any rate, normal gated SPECT regional LV function displayed using the traditional two-dimensional polar map (Bulls eye) format will result in a darker area at the septum for the motion map, and a brighter area at the apex for the thickening map (see Figs. 5.19 and 5.20), making it virtually impossible to visually assess function normalcy from polar maps.

In addition to the heterogeneity of regional function in a given patient, the clinical significance of absolute regional function quantification is hampered by the rather large variations in "normal" regional function across patients; as summarized by Katz et al. for echocardiography, *normal segmental cavity shrinkage has been reported to vary from 0 (i.e., akynesis) to 100% and segmental wall thickening to vary from 0 to 150%* [99], and magnetic resonance imaging (MRI) studies have also reported a normal thickening range of 18–100% [257]. Nonetheless, as with SPECT perfusion quantification, quantitative thresholds defining gated SPECT LV wall motion and thickening abnormality can

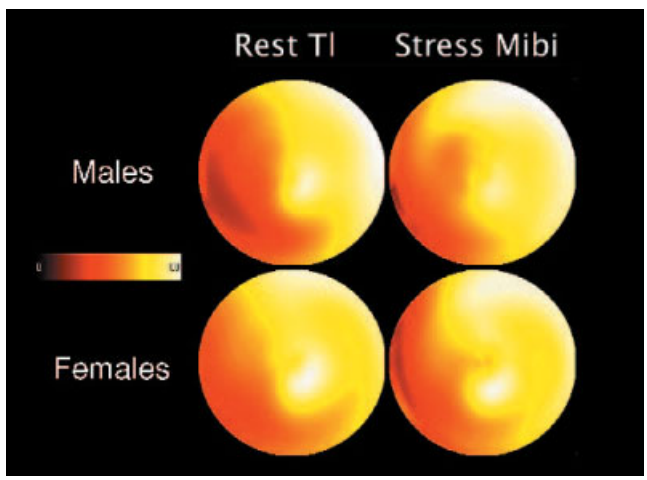

Figure 5.19 Polar maps showing average myocardial wall motion in 30 normal men and 30 normal women imaged using Cedars' rest ^{201}Tl/stress ^{99m}Tc-sestamibi separate dual isotope protocol. Note that "normal" motion is usually less at the septum compared to the lateral wall, a finding independent of patient gender and radioisotope used. (Modified and reproduced with permission from [263].)

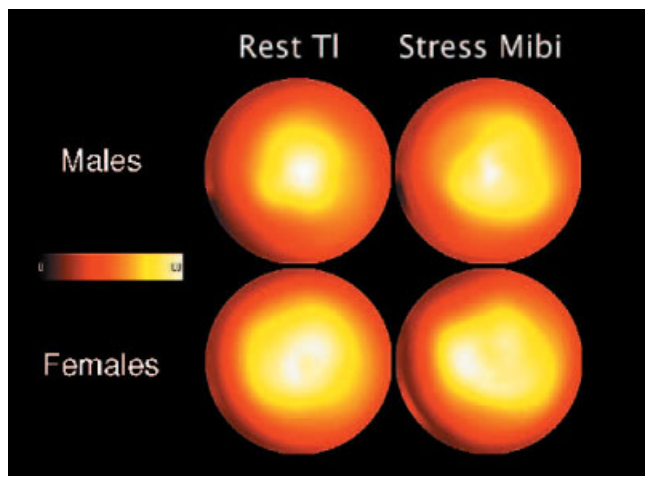

Figure 5.20 Polar maps showing average myocardial wall thickening in 30 normal males and 30 normal females imaged using Cedars' rest ^{201}Tl/stress ^{99m}Tc-sestamibi separate dual isotope protocol. Note that "normal" thickening is usually higher at the apex than at the base, a finding independent of patient gender and radioisotope used. (Modified and reproduced with permission from [263].)

be derived on the basis of the mean and standard deviation of these parameters in a normal patient population [264–267]. With respect to specific implementations, investigators using the EGS^{TM}algorithm have found a gender dependency of thickening, although its effect was muted when small LV patients were purged from the analysis [268]. The QGS^{TM}algorithm uses one set of normal limits for wall motion and one for wall thickening [252], on the basis of the authors' experience that normal patterns of regional function are reasonably independent of patient gender and choice of radioisotope (Figs. 5.19 and 5.20).

Semiquantitative assessment

As a practical alternative to the absolute quantification of regional LV function parameters from gated SPECT images, semiquantitative classifications that are based on segmental visual assessment have been proposed. A popular model divides the LV myocardium into 20 or 17 segments, and assigns to each of them a score varying from 0 to 5 for motion, and from 0 to 3 for thickening, as discussed in detail in Chapter 6. Underlying this class of approaches is the assumption that visual assessment of regional function from gated perfusion SPECT and other reference imaging modalities will correlate well, despite the possible modality-dependent differences described in the previous section. This assumption has been verified by several investigators with respect to regional myocardial wall motion and thickening, as shown in Table 5.9 [41,42,44,269,270].

Categorical scoring of segmental myocardial wall motion and thickening can also be accomplished automatically, by defining ranges for the absolute measurements obtained by a quantitative gated SPECT algorithm. A simplified approach assigning scores of 0, 1–2, 3, 4, and 5 to quantitative motion of more than 5, 3–5, 1–3, 0–1, and less than 0 mm in any myocardial segment (regardless of location) resulted in exact agreement 72.6% and kappa = 0.433 between expert visual scores and QGS^{TM}-generated scores, in a population of 79 clinical patients with a wide range of LVEFs [2]. In the same patients, assigning scores of 0, 1–2, 3, and 4 to quantitative thickening of more than 30%, 15–30%, 5–15%, and less than 5% in any myocardial segment (again, regardless of location) resulted in exact agreement 74.7% and kappa = 0.408. When the regional heterogeneity of normal function was taken into account by making the QGS^{TM}quantitative ranges segment-specific, exact agreement improved to 80% for motion (kappa = 0.71) and 86% for thickening (kappa = 0.68) [252]. In this latter approach, scoring thresholds were automatically determined by an iterative process aimed at maximizing the agreement between computer-generated and expert scores. Results obtained for the 4D-MSPECT^{TM} algorithm [271] confirm the above findings. While it has been pointed out that visual scores represent a suboptimal gold standard by which to validate gated SPECT measurements of quantitative wall motion and thickening [262], it has been shown that quantitative measurements are extremely reproducible [202], being directly related to the high degree of automation of the algorithm that generated them, and can potentially be very useful in serial imaging for the assessment of medical therapy or surgical intervention [241]. The reproducibility of quantitative gated SPECT measurements will be examined in more detail in the next section.

As discussed in Chapter 6 with respect to perfusion scores, segmental wall motion and thickening scores can also be summed to produce a "summed motion score" and a "summed thickening score." Whether these semiquantitative measures of global LV function contain incremental diagnostic and prognostic value over the LVEF is currently unclear.

As previously mentioned, displays of quantitative regional myocardial wall motion and thickening can be implemented using the traditional two-dimensional polar map (Bull's eye) format, as demonstrated in Fig. 5.21, or overlayed onto the three-dimensional epicardial or endocardial surface, as commonly done for gated blood pool

Table 5.9 Validations of quantitative measurements of regional myocardial wall motion and thickening from gated perfusion SPECT.

Parameter	Gold standard	No. of patients	No. of segments	Classification	Exact agreement	Kappa	References
Motion	MRI	25	13	5-point	92%	0.82	[41]
Motion	MRI	20	9	4-point	82–84%	0.70–0.73	[42]
Motion	MRI	28	9	6-point	78%	0.66	[269]
Motion	2-D echo	43	16	6-point	91%	0.68	[270]
Thickening	MRI	20	9	4-point	84–87%	0.71–0.76	[42]
Thickening	MRI	16	13	4-point	76%	0.62	[44]
Thickening	MRI	28	9	5-point	78%	0.62	[269]
Thickening	2-D echo	43	16	4-point	90%	0.62	[270]
TOTAL		223			84%	0.69	

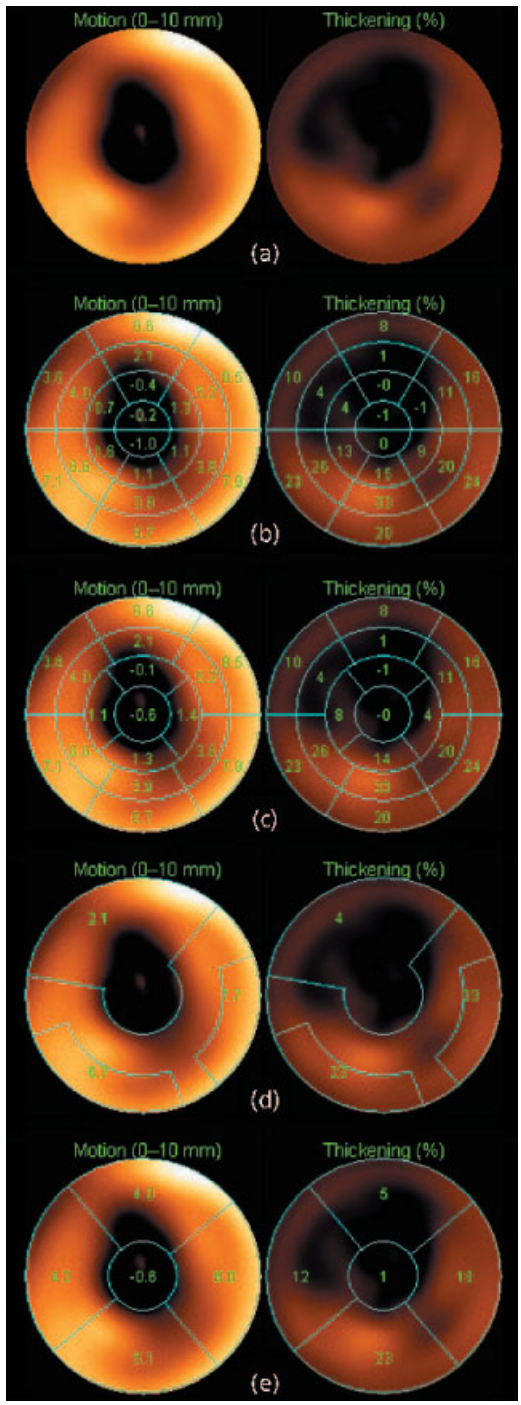

Figure 5.21 Polar or "Bulls eye" maps displaying (a) regional myocardial wall motion and thickening patterns, and their average quantitative values for (b) the 20-segment model, (c) the 17-segment model, (d) the three-coronary territories model, and (e) a wall-based model.

SPECT (Fig. 5.22). It has been reported that global myocardial contractility can be calculated using the time–volume curve from gated perfusion SPECT, and expressed via a normalized elastance curve [272].

Reproducibility of global and regional quantitative function measurements

Reproducibility vs. repeatability

In the authors' opinion, there is inconsistency in the usage of the term *reproducibility*. For the purposes of our discussion, we shall distinguish between reproducibility and repeatability as follows.

Repeatability assessment involves applying a quantitative gated SPECT algorithm to two separately acquired image sets belonging to the same patient (images ideally acquired without changes in the acquisition protocol or patient condition), and measuring the difference between the quantitative results. Low repeatability can be due to either (a) changes in the acquisition setup (the patient moved, the radiopharmaceutical uptake pattern changed, gating abnormalities occurred); (b) changes in the reconstruction and reorientation parameters used to generate the tomographic images input to the algorithm; (c) changes in the way the quantitative algorithm operated, or was applied to the data; and/or (d) true physiological variation in the patient's state at imaging. In other words, repeatability is a measure of the combined "stability" of the quantitative algorithm, the gated SPECT acquisition protocol itself, and the patient. Image registration strategies [273] can be applied prior to the use of a quantitative algorithm in order to improve its repeatability [274], as explained in detail in Chapter 4.

We consider *reproducibility* of measurements of global and regional function from gated SPECT images to refer to applying a quantitative algorithm twice to the same image set, and therefore to be proportional to the degree to which the algorithm is automated. Measurements from automatic, "push-button" algorithms that operate in a deterministic manner are, by definition, perfectly reproducible [1] – published reports suggesting otherwise reflect the incorporation, in the reproducibility calculations, of either (a) operator-performed reconstruction and reorientation or (b) manual override of algorithm-generated contours in some of the patients. Semiautomatic algorithms that systematically require some sort of operator intervention (slice selection, manual isolation of the LV, manual identification of the LV cavity center, etc.) can be evaluated in terms of their *interobserver reproducibility* (agreement between measurements by two different individuals using the same algorithm on the same patient) and *intraobserver reproducibility* (agreement between measurements by the same individual using the same algorithm on the same patient). As a general rule, one would expect intraobserver reproducibility to be at least as high as interobserver reproducibility, and reproducibility to be at least as high as repeatability. Of note, an algorithm can be perfectly

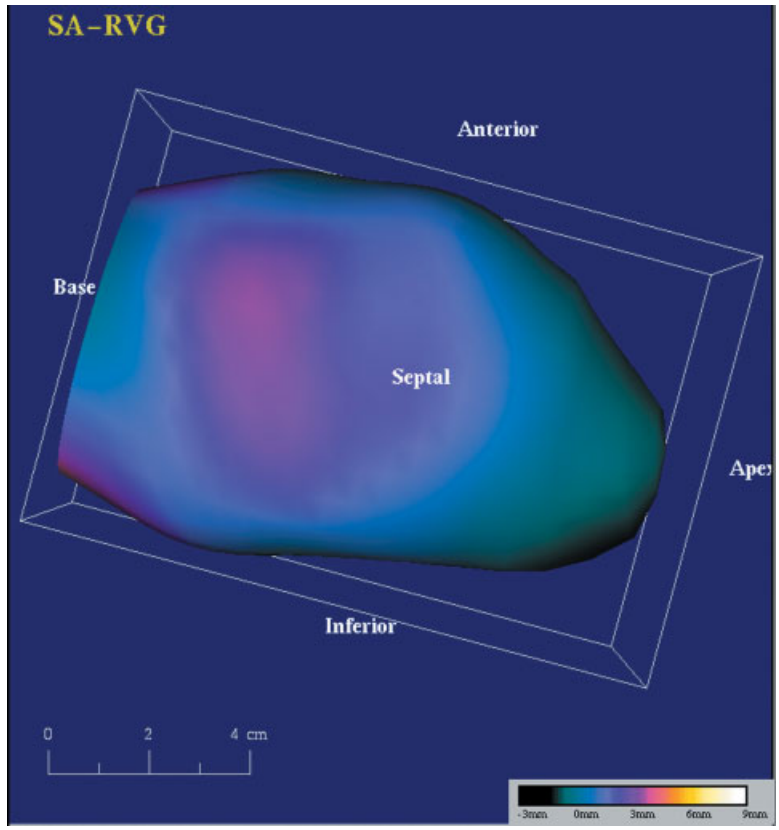

Figure 5.22 Three-dimensional representation of the endocardial surface with superimposed color-coded quantitative wall motion, for a patient with low LVEF and marked hypokinesis in the LAD coronary artery territory (courtesy of Edward J. Ficaro, PhD).

reproducible in general but require (in a small percentage of the studies processed) adjustments to compensate for inaccuracies in the identification or outlining of the myocardium: it is customary to address this situation by reporting the *success rate* of the algorithm, or the percentage of cases in which no modifications were required [1]. Modifications can be effected using various degrees of human interaction, from simply "masking out" portions of the image set and reapplying the automatic algorithm (Fig. 5.23) to constraining the location of the apex and basal plane, or manually drawing or altering myocardial contours, and will typically result in intra- and interobserver reproducibilities that are very high but less than 100%.

The published results concerning the reproducibility and repeatability of measurements of quantitative function parameters from gated perfusion SPECT for commercially available algorithms (Table 5.10) demonstrate very good to excellent agreement between independent measurements [1,2,8,19,28,30–32,34,36,48,56,69,119,124,125,128,153,179,200–209]. Even semiautomatic algorithms that require minor operator intervention (slice selection, manual isolation of the LV, manual identification of the LV cavity center, etc.) generally enjoy equal or greater reproducibility than conventional nuclear or nonnuclear techniques used for LV function assessment [275]. As quantitative gated perfusion SPECT becomes an increasingly important tool in the sequential evaluation of patients with progressing disease or undergoing medical or surgical therapy [241,276–285], it is obvious that the reproducibility and repeatability of a particular algorithm must be known to correctly identify significant changes in a patient [274].

Stunning

An admittedly extreme, worst-case example of nonrepeatability is the finding of differences in quantitative gated SPECT measurements of LVEF (or regional wall motion) at rest compared to poststress. While no one would consider this to be a fair test of repeatability, historically many validations of poststress gated SPECT quantitation have used as reference a planar study acquired at rest, implicitly assuming that LV function 1-hour after exercise is equal to resting function. Indeed, that is often not the case, and "nonrepeatabilities" found in this context have important clinical meaning.

Johnson et al. first reported in 1997 that of 61 patients with reversible ischemia imaged using a 2-day, treadmill stress and rest gated ^{99m}Tc-sestamibi SPECT protocol, 22

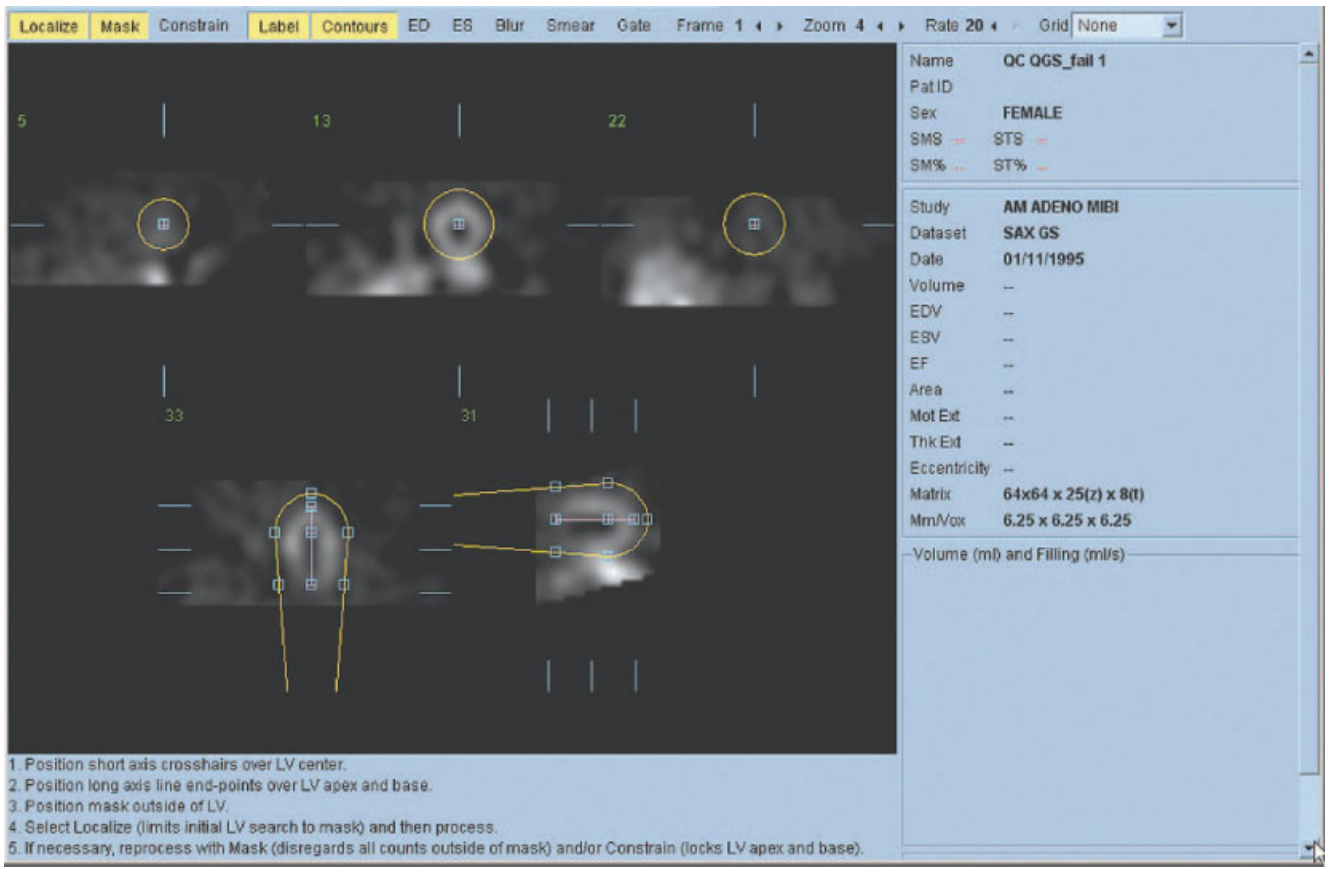

Figure 5.23 "Manual" processing option in QGS™. If the automatic algorithm did not produce satisfactory endocardial/epicardial contours (most commonly due to high extracardiac activity), a mask can be used to redefine the portion of the image volume on which the algorithm is to operate.

(36%) had significantly lower poststress LVEF than the rest LVEF [201]. The threshold of ±5.2% (2SD) for statistically significant differences had been determined from a separate group of 15 patients undergoing serial rest gated SPECT on consecutive days. The authors attributed the reduction in LVEF in those 22 patients to postischemic myocardial stunning persisting 30 minutes poststress, noting that all 20 patients in yet another group without reversible ischemia demonstrated excellent agreement between the poststress and rest quantitative LVEF measurements.

The association between reversible ischemia and a decrease in the poststress LVEF has been successively reported by a large number of investigators for exercise stress [286–296] and even for pharmacological stress [286,297–304]. It has been suggested that subendocardial ischemia rather than stunning might be the main causing factor for the apparent LVEF decrease, because quantitative algorithms might fail to adequately trace the endocardium in regions with the greatest ischemia and thus underestimate LVEF [305]; however, studies designed around sequential poststress gated SPECT acquisitions using ^{99m}Tc-based (nonredistributing) radiopharmaceuticals have shown that systolic dysfunction tends to resolve over time in spite of persisting stress perfusion defects, implying that true stunning is at least a partial cause of the observed phenomenon [303,306–308]. Interestingly, poststress decreases in LVEF have been reported even in the patients with normal perfusion [298,309] and are associated with significant CAD [310] and adverse prognosis.

In addition to poststress decreases in global LV function, regional wall motion abnormalities present poststress have been described [300,311–313], and may be easier to detect than abnormalities in global poststress function [295,300,311,314,315]. Poststress diastolic dysfunction has also been found associated with systolic dysfunction in patients with angina [316].

While myocardial stunning is a well-recognized phenomenon in conjunction with both treadmill stress [317,318] and adenosine vasodilator stress [319–321], there

Table 5.10 Reproducibility and repeatability of quantitative gated SPECT measurements.

Method	Type of analysis	Parameter	Agreement	No. of patients	References
QGS™	Reproducibility	LVEF	$r = 1$, SEE = 0%	65	[1]
QGS™	Reproducibility	EDV	$r = 1$, SEE = 0 ml	65	[1]
QGS™	Reproducibility	ESV	$r = 1$, SEE = 0 ml	65	[1]
QGS™	Reproducibility	WM	% Agreement = 100%	79	[2]
QGS™	Reproducibility	WT	% Agreement = 100%	79	[2]
QGS™	Reproducibility (intraobserver)*	LVEF	$r = 0.99$, SEE = 2.4%	21	[28]
QGS™	Reproducibility (intraobserver)*	EDV	$r = 0.99$, SEE = 3.2 ml	21	[28]
QGS™	Reproducibility (intraobserver)*	ESV	$r = 0.99$, SEE = 3.2 ml	21	[28]
QGS™	Reproducibility (intraobserver)*	LVEF	$r = 0.99$	25	[31]
QGS™	Reproducibility (intraobserver)*	LVEF	$r = 0.99$	30	[34]
QGS™	Reproducibility (interobserver)*	LVEF	$r = 0.99$, SEE = 2.2%	25	[31]
QGS™	Reproducibility (interobserver)*	EDV	$r = 0.99$, SEE = 3.3 ml	25	[31]
QGS™	Reproducibility (interobserver)*	ESV	$r = 0.99$, SEE = 2.7 ml	25	[31]
QGS™	Reproducibility (interobserver)*	LVEF	$r = 1$	25	[31]
QGS™	Reproducibility (interobserver)*	LVEF	$r = 0.99$, SEE = 1.8%	20	[30]
QGS™	Reproducibility (interobserver)*	EDV	$r = 1$, SEE = 5.2 ml	20	[30]
QGS™	Reproducibility (interobserver)*	ESV	$r = 1$, SEE = 5.0 ml	20	[30]
QGS™	Reproducibility (interobserver)*	LVEF/EDV/ESV	$r = 0.99$ (^{201}Tl)	30	[200]
QGS™	Reproducibility (interobserver)*	"	$r = 0.99$–1.00 (^{99m}Tc)	26	[200]
QGS™	Reproducibility (interobserver)*	LVEF	$r = 1.00$	30	[34]
QGS™	Reproducibility (interobserver)*	LVEF	$r = 0.99$	36	[36]
QGS™	Reproducibility (interobserver)*	EDV	$r = 0.97$	36	[36]
QGS™	Reproducibility (interobserver)*	ESV	$r = 0.98$	36	[36]
QGS™	Repeatability	LVEF	$r = 0.98$, SD = 2.6%	15	[201]
QGS™	Repeatability	LVEF	$r = 0.92$, SD = 5.5%	26	[128]
QGS™	Repeatability	EDV	$r = 0.98$, SD = 12 ml	26	[128]
QGS™	Repeatability	ESV	$r = 0.98$, SD = 9.5 ml	26	[128]
QGS™	Repeatability	LVEF	$r = 0.98$, SD = 3%	25	[128]
QGS™	Repeatability	EDV	$r = 0.98$, SD = 8 ml	25	[128]
QGS™	Repeatability	ESV	$r = 0.99$, SD = 5 ml	25	[128]
QGS™	Repeatability	WM	$r = 0.95$, kappa = 0.81	31	[202]
QGS™	Repeatability	WT	$r = 0.88$, kappa = 0.71	31	[202]
QGS™	Repeatability (8-frame vs. 16-frame)	LVEF	$r = 0.99$, SEE = 2.65%	65	[1]
QGS™	Repeatability (8-frame vs. 16-frame)	LVEF	$r = 0.99$	15	[48]
QGS™	Repeatability (8- frame vs. 32-frame)	EDV	$r = 0.99$	24	[32]
QGS™	Repeatability (8- frame vs. 32-frame)	ESV	$r = 0.99$	24	[32]
QGS™	Repeatability (16- frame vs. 32-frame)	EDV	$r = 1.00$	24	[32]
QGS™	Repeatability (16- frame vs. 32-frame)	ESV	$r = 1.00$	24	[32]
QGS™	Repeatability (180° vs. 360°)	LVEF	$r = 0.98$, SEE = 3.4%	30	[203]
QGS™	Repeatability (180° vs. 360°)	EDV + ESV	$r = 0.99$, SEE = 5.6 ml	30	[203]
QGS™	Repeatability (prone/supine)	LVEF	$r = 0.93$, SD = 3.2%	180	[179]
QGS™	Repeatability (prone/supine)	EDV	$r = 0.97$, SD = 6.2 ml	180	[179]
QGS™	Repeatability (prone/supine)	ESV	$r = 0.98$, SD = 4.8 ml	180	[179]
QGS™	Repeatability (gated/non-gated)	V	$r = 0.99$, SEE = 5.1 ml	926	[204]
QGS™	Repeatability (standard/fast)	LVEF	$r = 0.97$, SD = 3.4%	20	[119]
QGS™	Repeatability (standard/fast)	EDV	$r = 0.99$, SD = 7.1 ml	20	[119]
QGS™	Repeatability (standard/fast)	ESV	$r = 0.99$, SD = 6.3 ml	20	[119]
QGS™	Repeatability (standard/fast)	LVEF	$r = 0.98$, SEE = 3.4%	25	[205]
QGS™	Repeatability (standard/fast)	EDV	$r = 0.98$	25	[205]
QGS™	Repeatability (different cameras)	LVEF	$r = 0.88$	79	[206]
QGS™	Repeatability (follow-up)	LVEF	$r = 0.87$	1880	[207]
QGS™	Repeatability (^{201}Tl/^{99m}Tc)	LVEF	$r = 0.92$, SEE = 6.3%	121	[124]
QGS™	Repeatability (^{201}Tl/^{99m}Tc)	LVEF	$r = 0.87$, SD = 6%	40	[125]
QGS™	Repeatability (^{201}Tl/^{99m}Tc)	EDV	$r = 0.96$, SD = 15.5 ml	40	[125]

(*continued*)

Table 5.10 (*Continued*)

Method	Type of analysis	Parameter	Agreement	No. of patients	References
QGS™	Repeatability (^{201}Tl/^{99m}Tc)	ESV	$r = 0.97$, SD = 11.5 ml	40	[125]
QGS™	Repeatability (18FDG/^{99m}Tc)	LVEF	$r = 0.85$–0.94	101	[153]
QGS™	Repeatability (123I/^{99m}Tc)	LVEF	$r = 0.95$, SEE = 5%	44	[19]
QGS™	Repeatability (123I/^{99m}Tc)	LVEF	$r = 0.94$	36	[36]
QGS™	Repeatability (123I/^{99m}Tc)	EDV	$r = 0.93$	36	[36]
QGS™	Repeatability (123I/^{99m}Tc)	ESV	$r = 0.95$	36	[36]
QGS™	Repeatability (123I/^{201}Tl)	LVEF	$r = 0.84$	20	[208]
QGS™	Repeatability (rest/poststress, ^{99m}Tc)	LVEF	$r = 0.90$, SEE = 6.1%	31	[56]
QGS™	Repeatability (rest/poststress, ^{99m}Tc)	EDV	$r = 0.97$, SEE = 13.0 ml	31	[56]
QGS™	Repeatability (rest/poststress, ^{99m}Tc)	ESV	$r = 0.98$, SEE = 9.6 ml	31	[56]
QGS™	Repeatability (sequential poststress, ^{99m}Tc)	LVEF	$r = 0.98$, 2SD = 5.5%	26	[200]
QGS™	Repeatability (sequential poststress, ^{99m}Tc)	EDV	$r = 0.99$, 2SD = 14.1 ml	26	[200]
QGS™	Repeatability (sequential poststress, ^{99m}Tc)	ESV	$r = 1.00$, 2SD = 9.4 ml	26	[200]
QGS™	Repeatability (rest/poststress, ^{201}Tl)	LVEF	$r = 0.89$, SEE = 6.8%	29	[56]
QGS™	Repeatability (rest/poststress, ^{201}Tl)	EDV	$r = 0.97$, SEE = 9.7 ml	29	[56]
QGS™	Repeatability (rest/poststress, ^{201}Tl)	ESV	$r = 0.98$, SEE = 8.3 ml	29	[56]
QGS™	Repeatability (sequential rest, ^{201}Tl)	LVEF	$r = 0.92$, SD = 6%	20	[125]
QGS™	Repeatability (sequential rest, ^{201}Tl)	EDV	$r = 0.95$, SD = 14.5 ml	20	[125]
QGS™	Repeatability (sequential rest, ^{201}Tl)	ESV	$r = 0.97$, SD = 9.5 ml	20	[125]
QGS™	Repeatability (sequential rest, ^{201}Tl)	LVEF	$r = 0.93$, 2SD = 10.3%	30	[200]
QGS™	Repeatability (sequential rest, ^{201}Tl)	EDV	$r = 0.98$, 2SD = 24.1 ml	30	[200]
QGS™	Repeatability (sequential rest, ^{201}Tl)	ESV	$r = 0.99$, 2SD = 18.6 ml	30	[200]
QGS™	Repeatability (sequential rest, ^{201}Tl)	LVEF	$r = 0.94$	55	[209]
QGS™	Repeatability (sequential rest, ^{201}Tl)	EDV	$r = 0.99$	55	[209]
QGS™	Repeatability (sequential rest, ^{201}Tl)	ESV	$r = 0.99$	55	[209]
EGS™	Reproducibility (intraobserver)*	LVEF	$r = 0.98$	25	[31]
EGS™	Reproducibility (interobserver)*	LVEF	$r = 0.98$	25	[31]
EGS™	Reproducibility (intraobserver)*	LVEF	$r = 0.98$	30	[34]
EGS™	Reproducibility (interobserver)*	LVEF	$r = 0.98$	30	[34]
4D-MSPECT™	Reproducibility (intraobserver)*	LVEF	$r = 0.96$	25	[31]
4D-MSPECT™	Reproducibility (interobserver)*	LVEF	$r = 0.96$	25	[31]
4D-MSPECT™	Reproducibility (intraobserver)*	LVEF	$r = 0.98$	30	[34]
4D-MSPECT™	Reproducibility (interobserver)*	LVEF	$r = 0.98$	30	[34]
4D-MSPECT™	Repeatability (different cameras)	LVEF	$r = 0.89$	79	[206]
MultiDim™	Reproducibility (intraobserver)	LVEF	$r = 0.97$, SD = 4.5%	50	[8]
MultiDim™	Reproducibility (interobserver)	LVEF	$r = 0.88$, SD = 4.7%	50	[8]
MultiDim™	Reproducibility	LVEF	$r = 0.97$, SEE = 3.7%	49	[69]

Abbreviations: r, Spearman's correlation coefficient; SEE, standard error of the estimate; SD = standard deviation of the paired absolute difference between measurements; V, ungated (summed) volume; WM, wall motion; WT, wall thickening

*Includes reproducibility of reconstruction/reorientation process and/or manual override of algorithmic results in some of the patients.

is less agreement on its duration. With respect to quantitative gated SPECT imaging, published reports range from less than 30 minutes [307] to 1 hour or more with exercise stress [288,322] or pharmacologic stress [297,300]. The frequency with which poststress decreases in LV function are encountered in a clinical laboratory will likely depend, to a large extent, on the type of patients imaged, with published data ranging from 5 to 10% [56,57,323,324] to as many as 44% of patients [298]. In general, the finding is considered to be due to severe ischemia occurring during stress, and is usually associated with a critical (>90%) coronary stenosis (see Chapter 6).

Cross-algorithm reproducibility

Cross-algorithm reproducibility is defined as the agreement between quantitative measurements performed by two different algorithms on the same patient. If the two algorithms are completely automatic, cross-algorithm reproducibility less than 100% will reflect only the different manner in which the algorithms operate; if not,

Table 5.11 Cross-algorithm reproducibility for commercially available quantitative gated SPECT software.

Method	No. of patients	Parameter	Agreement	References
QGS™vs. EGS™	33	EDV, ESV	$r > 0.94$	[83]
QGS™vs. EGS™	97	LVEF	$r = 0.72$	[325]
QGS™vs. EGS™	246	LVEF	$r = 0.90$	[326]
QGS™vs. EGS™	246	EDV	$r = 0.91$	[326]
QGS™vs. EGS™	246	ESV	$r = 0.95$	[326]
QGS™vs. EGS™	246	LVEF	$r = 0.90$	[327]
QGS™vs. EGS™	246	EDV	$r = 0.91$	[327]
QGS™vs. EGS™	246	ESV	$r = 0.94$	[327]
QGS™vs. EGS™	1006	LVEF	$r = 0.93$	[328]
QGS™vs. EGS™	1006	EDV	$r = 0.93$	[328]
QGS™vs. EGS™	1006	ESV	$r = 0.80$	[328]
QGS™vs. EGS™	50	LVEF	$r = 0.87$	[197]
QGS™vs. EGS™	50	EDV	$r = 0.89$	[197]
QGS™vs. EGS™	50	ESV	$r = 0.92$	[197]
QGS™vs. EGS™	122	LVEF	$r = 0.89$, SEE = 6.4%	[198]
QGS™vs. EGS™	30	LVEF	$r = 0.95$	[34]
QGS™vs. EGS™	30	EDV	$r = 0.98$	[34]
QGS™vs. EGS™	30	LVEF	$r = 0.95$, SEE = 3.9%	[47]
QGS™vs. 4D-MSPECT™	30	LVEF	$r = 0.91$	[34]
QGS™vs. 4D-MSPECT™	30	EDV	$r = 0.98$	[34]
QGS™vs. 4D-MSPECT™	129	LVEF	$r = 0.94$	[329]
QGS™vs. 4D-MSPECT™	129	EDV	$r = 0.97$	[329]
QGS™vs. 4D-MSPECT™	129	ESV	$r = 0.98$	[329]
QGS™vs. 4D-MSPECT™	54	LVEF	$r = 0.92$	[50]
QGS™vs. 4D-MSPECT™	54	EDV	$r = 0.96$	[50]
QGS™vs. 4D-MSPECT™	54	ESV	$r = 0.96$	[50]
QGS™vs. MultiDim™	40	LVEF	$r = 0.93$, SEE = 6.8%	[25]
QGS™vs. MultiDim™	40	EDV	$r = 0.97$, SEE = 20 ml	[25]
QGS™vs. MultiDim™	40	ESV	$r = 0.98$, SEE = 20 ml	[25]
QGS™vs. MultiDim™	43	LVEF	$r = 0.86$	[144]
QGS™vs. MultiDim™	43	EDV	$r = 0.96$	[144]
QGS™vs. MultiDim™	43	ESV	$r = 0.97$	[144]
QGS™vs. MultiDim™	122	LVEF	$r = 0.42$, SEE = 10.9%	[198]
QGS™vs. GSCQ™	110	LVEF	$r = 0.87$	[330]
QGS™vs. GSCQ™	110	EDV	$r = 0.90$	[330]
QGS™vs. GSCQ™	110	ESV	$r = 0.90$	[330]
QGS™vs. GSCQ™	158	LVEF	$r = 0.89$	[22]
QGS™vs. GSCQ™	122	LVEF	$r = 0.82$, SEE = 10.2%	[198]
EGS™vs. 4D-MSPECT™	30	LVEF	$r = 0.94$	[34]
EGS™vs. 4D-MSPECT™	30	EDV	$r = 0.96$	[34]
EGS™vs. MultiDim™	122	LVEF	$r = 0.38$, SEE = 10.6%	[198]
EGS™vs. GSCQ™	122	LVEF	$r = 0.71$, SEE = 9.3%	[198]
MultiDim™vs. GSCQ™	122	LVEF	$r = 0.19$, SEE = 12.4%	[198]

intra- and interobserver variabilities will also detract from the agreement.

Most studies analyzing cross-algorithm reproducibility have shown strong linear correlation between measurements of the same parameters by different algorithms, as demonstrated by the high Spearman *r* values in Table 5.11 [22,25,34,47,50,83,144,197,198,325–330]. However, it has also been demonstrated that systematic differences and biases between the algorithms' measurements do exist, as reflected in the fact that the slope of the correlation lines is in many cases substantially different from 1. In practical terms, this necessitates the use of algorithm-specific diagnostic and prognostic thresholds and prevents the direct merging of differently analyzed data in the context of multicenter trials [50,58,122,134,326,328,329, 331].

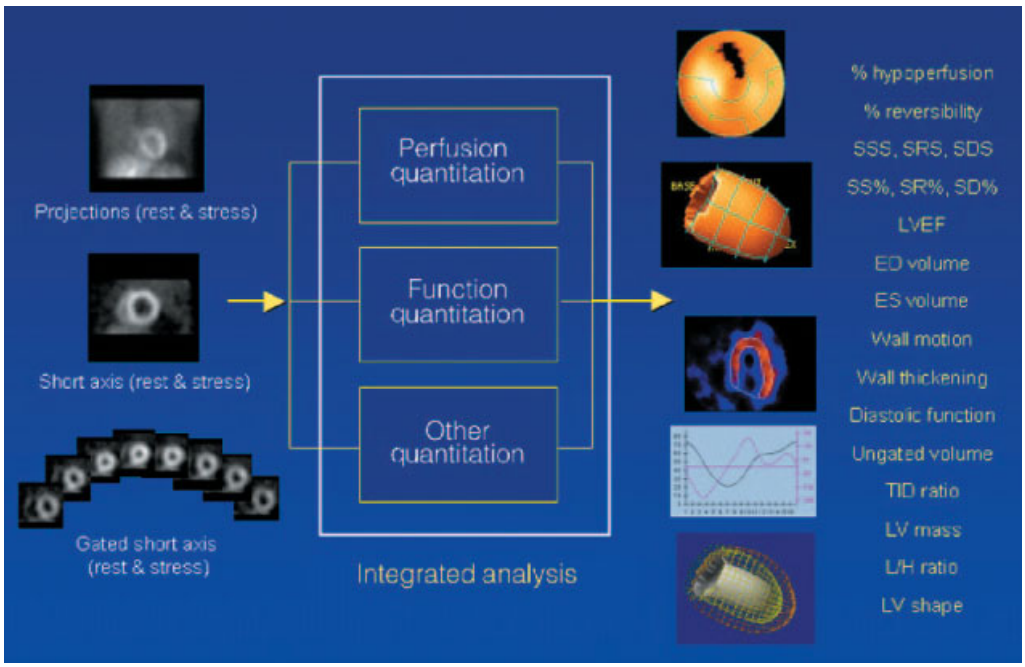

Figure 5.24 Quantitative parameters derivable from a rest/stress gated perfusion SPECT protocol.

Reporting of quantitative perfusion and data

Quantitative gated perfusion SPECT imaging greatly increases the number of important parameters that can be objectively and reproducibly measured using nuclear cardiology. As described in Chapter 3, at Cedars-Sinai our patients undergo a "separate dual-isotope" protocol [123], using 16-frame gated SPECT at rest (3–4.5 mCi of ^{201}Tl) and 15–60 minutes after stress (25–40 mCi of ^{99m}Tc sestamibi). The projection data and short-axis gated and ungated data are routinely, simultaneously, and automatically analyzed as shown in Fig. 5.24, and the following quantitative parameters extracted: (a) percent hypoperfused myocardium and percent ischemic myocardium [266,332]; (b) summed stress, summed rest, and summed difference scores, both model-specific [333,334] and model-independent (normalized to the worst possible score in a particular model) [335]; (c) rest and poststress LVEF [1]; (d) percent dysfunctional myocardium and regional myocardial wall motion and thickening scores [2,252], with model-specific and model-independent (normalized) summed wall motion (SWM) and wall thickening (SWT) scores; (e) rest and stress LV cavity volumes, both gated and ungated [204]; (f) TID ratio based on the ungated LV cavity volumes [235,303]; (g) rest and stress lung/heart ratios (LHRs) [336]; (h) LV mass [337,338]; and (i) LV sphericity [88].

Quantitative information related to perfusion can be presented as shown in Fig. 5.25, with (a) side-by-side display of representative short- and long-axis images for the rest and stress portion of the study; (b) 17-segment (or 20-segment if desired), territory-based or myocardial wall-based demarcation lines overlayed onto the images themselves, the two-dimensional polar maps and the three-dimensional perfusion maps (the latter two expressing in parametric format raw values, extent, or severity); and (c) a graphical and numeric assessment of defect extent and reversibility, including summed severity scores and TID. Quantitative information related to function can be presented, in similar fashion, as shown in Fig. 5.26, where (a) the side-by-side short- and long-axis images now represent the end-diastolic and end-systolic gating frames; (b) two-dimensional polar maps for regional perfusion, myocardial wall motion, and wall thickening are displayed together with three-dimensional "surface maps"; and (c) the time–volume curve accompanies numeric determinations of EDV, ESV, SV, and LVEF. To achieve meaningful correlation of the regional quantitative perfusion and function measurements, it is essential that the segments to which such measurements refer be intrinsically aligned. To this end, current generation quantitative algorithms follow an "integrated" software approach focusing on a common coordinate system and sampling scheme for the assessment of the perfusion and function components of a gated SPECT acquisition [4,339]. Some brief observations regarding quantitation of parameters other than perfusion and function are presented below.

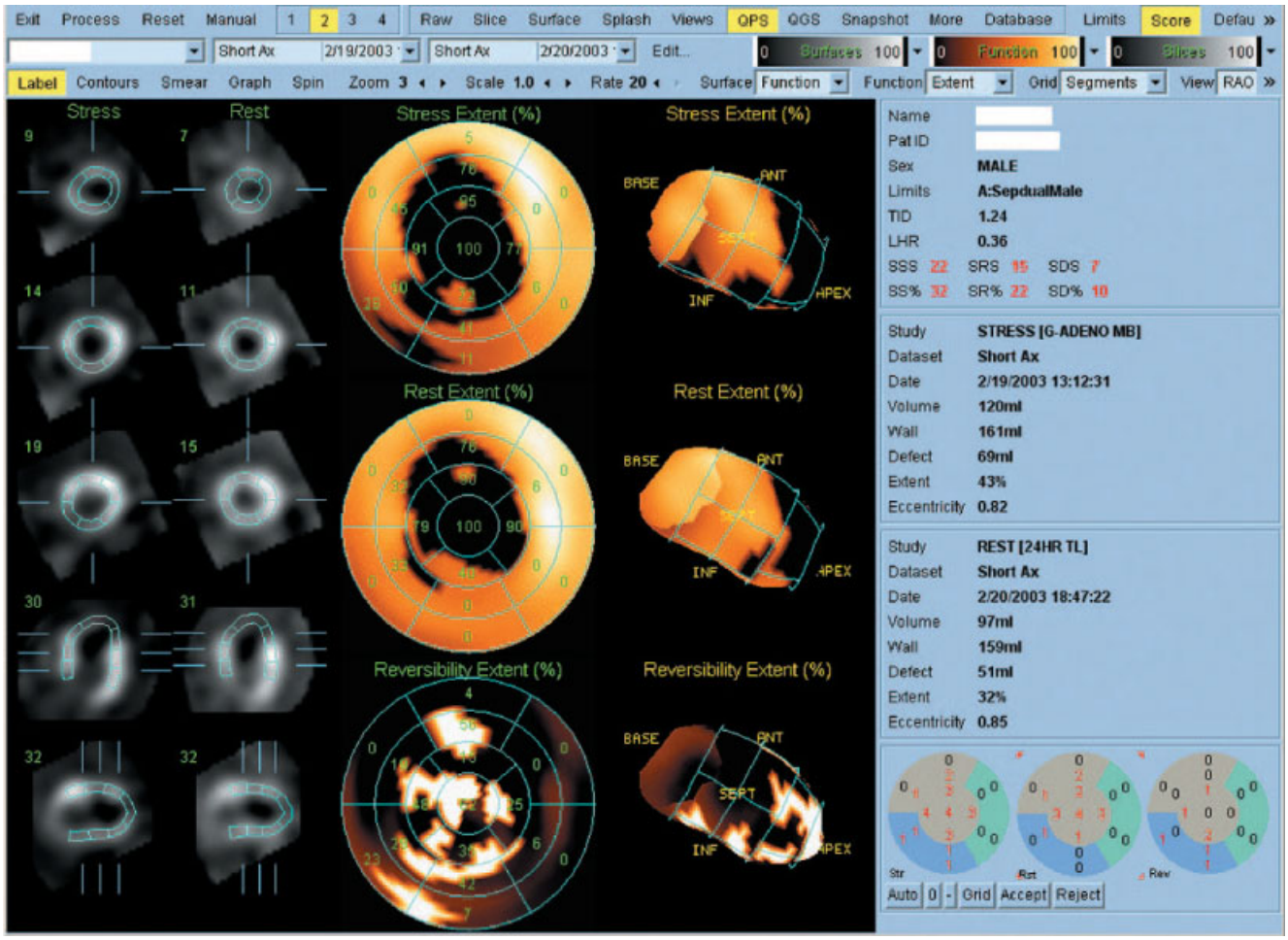

Figure 5.25 Cedars-Sinai's Quantitative Perfusion SPECT (QPS™): display of quantitative perfusion information for a patient with ischemia in the mid left anterior descending territory.

Lung/heart ratio

While the LHR was initially measured from anterior planar images, this ratio can also be assessed from the raw data acquired during SPECT. Several projection images from a SPECT acquisition can be summed to improve count statistics for the purposes of LHR calculation [339]. The LV is isolated in this composite image by manually or automatically generating an ROI that encompasses it, and a similar ROI is placed on the adjacent lung. The LHR is then computed as the simple ratio of the maximal or average pixel count in the LV and lung ROIs. In patients with coronary artery disease (CAD), it has long been reported that the LHR is a moderately sensitive and specific marker of severe and extensive CAD when used in conjunction with ^{201}Tl, with its threshold for abnormality being approximately 0.5 [340]. It has also been shown to be of prognostic significance, adding to the assessment of perfusion defects. Later experience with ^{99m}Tc sestamibi suggests that the LHR has a similar role at somewhat lower values (0.44) with ^{99m}Tc-based radioisotopes, provided that imaging is performed closely following injection [336].

TID ratio

The TID ratio is simply the ratio of the ungated LV cavity volume poststress and at rest. As previously discussed, the TID ratio measured by SPECT may reflect true stress-induced stunning of the LV, extensive subendocardial ischemia, or a combination of the two mechanisms. Nevertheless, this parameter has been demonstrated to be a moderately sensitive and highly specific marker of severe and extensive CAD [235], with higher specificity than the LHR. Of note, multiple investigators have reported that TID ratio and LHR are not correlated (i.e., it is quite unlikely to find them both to be abnormal in any given

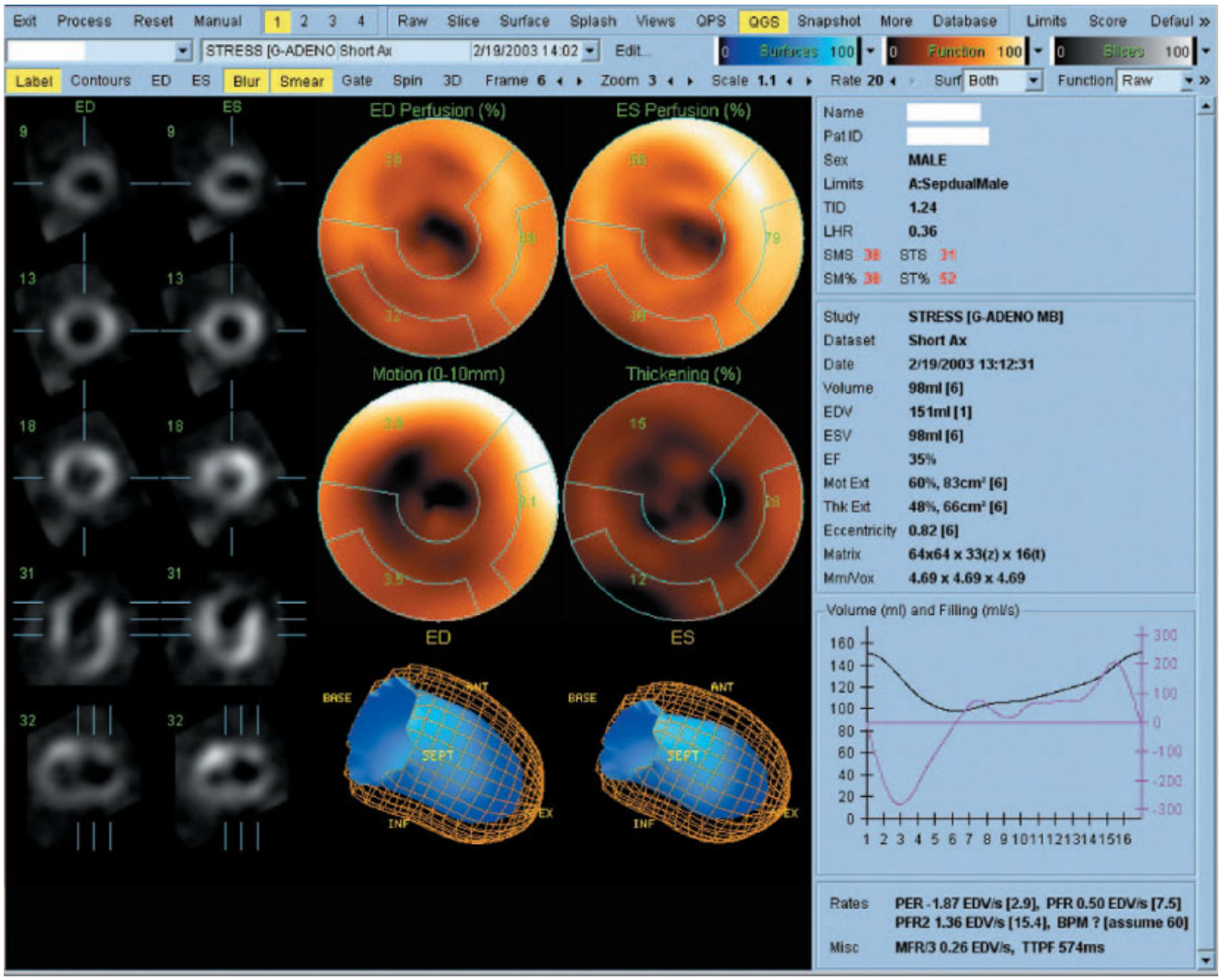

Figure 5.26 Cedars-Sinai's QGS: display of quantitative function information for the same patient as in Fig. 5.25.

patient [341,342]), which makes them ideal complementary measurements.

The threshold for TID ratio abnormality depends on the choice of rest and poststress radioisotopes, method of stress, and possibly patient gender [343,344], but appears to be relatively independent of the particular quantitative algorithm used; published values range from 1.14 for a same-day postexercise/rest ^{99m}Tc-sestamibi protocol [344] to 1.22–1.23 for a rest ^{201}Tl/postexercise ^{99m}Tc-sestamibi protocol [235,344], with pharmacologic stress producing somewhat higher thresholds, as high as 1.36 with adenosine stress and dual isotope myocardial perfusion SPECT [345,346]. It is also possible to derive the TID ratio from end-diastolic or end-systolic LV cavity volumes [347], although the implications and potential advantages of this approach have not been studied in depth.

Myocardial mass

This parameter is also conceptually easy to measure, being derived as the volume bound by the epicardial surface, endocardial surface, and valve plane multiplied by the myocardial density. One could think of the myocardial volume as the area of the midmyocardial surface (between the epicardial and endocardial surfaces) multiplied by the myocardial thickness. As previously discussed, since it is difficult to accurately measure the latter due to the relatively low resolution of SPECT images [2], myocardial mass is not assessed with as high accuracy by SPECT as are volumes and ejection fraction [337,348–351], although both reproducibility and stress/rest repeatability of LV mass measurements by SPECT can be expected to be very high [348,349,352]. Of note, some investigators have reported very good agreement of reference and

SPECT LV mass measurements on the basis of the assumption of uniform thickness for the myocardial wall [4,66,353], which should translate into the possibility of using the SPECT midmyocardial LV surface area as a good proxy for the LV volume.

LV shape

The LV can be reasonably approximated by a prolate ellipsoid [1], and consequently it is easy to estimate its shape using the major and minor axes of the ellipsoid that best fits it. The closer the axes in size, the closer the ellipsoid becomes to a sphere, a case consistent with LV remodeling associated with congestive heart failure or other pathologies. A potentially more accurate algorithm for shape assessment has also been proposed that is based on the regional search for the maximal distance between endocardial surface points [88].

References

1. Germano G, Kiat H, Kavanagh PB, et al. Automatic quantification of ejection fraction from gated myocardial perfusion SPECT. Journal of Nuclear Medicine 1995;36(11):2138–2147.
2. Germano G, Erel J, Lewin H, Kavanagh PB, Berman DS. Automatic quantitation of regional myocardial wall motion and thickening from gated technetium-99m sestamibi myocardial perfusion single-photon emission computed tomography. Journal of the American College of Cardiology 1997;30(5):1360–1367.
3. Cooke CD, Garcia EV, Cullom SJ, Faber TL, Pettigrew RI. Determining the accuracy of calculating systolic wall thickening using a fast Fourier transform approximation: a simulation study based on canine and patient data. Journal of Nuclear Medicine 1994;35(7):1185–1192.
4. Faber TL, Cooke CD, Folks RD, et al. Left ventricular function and perfusion from gated SPECT perfusion images: an integrated method. Journal of Nuclear Medicine 1999;40(4):650–659.
5. Faber TL, Stokely EM, Peshock RM, Corbett JR. A model-based four-dimensional left ventricular surface detector. IEEE Transactions on Medical Imaging 1991;10(3):321–329.
6. Chugh A, Ficaro EP, Moscucci M, Kritzman JN, Corbett JR. Quantification of left ventricular function by gated perfusion tomography: testing of a new fully automatic algorithm [abstract]. Journal of the American College of Cardiology 2001;37(2):394A.
7. Goris ML, Thompson C, Malone LJ, Franken PR. Modelling the integration of myocardial regional perfusion and function. Nuclear Medicine Communications 1994;15(1):9–20.
8. Everaert H, Franken PR, Flamen P, Goris M, Momen A, Bossuyt A. Left ventricular ejection fraction from gated SPET myocardial perfusion studies: a method based on the radial distribution of count rate density across the myocardial wall. European Journal of Nuclear Medicine 1996;23(12):1628–1633.
9. Liu Y, Sinusas A, Khaimov D, Gebuza B, Wackers F. New hybrid count- and geometry-based method for quantification of left ventricular volumes and ejection fraction from ECG-gated SPECT: methodology and validation. Journal of Nuclear Cardiology 2005;12(1):55–65.
10. Marcassa C, Marzullo P, Parodi O, Sambuceti G, L'Abbate A. A new method for noninvasive quantitation of segmental myocardial wall thickening using technetium-99m 2-methoxy-isobutyl-isonitrile scintigraphy – results in normal subjects. Journal of Nuclear Medicine 1990;31(2):173–177.
11. Smith WH, Kastner RJ, Calnon DA, Segalla D, Beller GA, Watson DD. Quantitative gated single photon emission computed tomography imaging: a counts-based method for display and measurement of regional and global ventricular systolic function. Journal of Nuclear Cardiology 1997;4(6):451–463.
12. Mochizuki T, Murase K, Fujiwara Y, Tanada S, Hamamoto K, Tauxe WN. Assessment of systolic thickening with thallium-201 ECG-gated single-photon emission computed tomography: a parameter for local left ventricular function. Journal of Nuclear Medicine 1991;32(8):1496–1500.
13. Buvat I, Bartlett ML, Kitsiou AN, Dilsizian V, Bacharach SL. A "hybrid" method for measuring myocardial wall thickening from gated PET/SPECT images. Journal of Nuclear Medicine 1997;38(2):324–329.
14. Nichols K, DePuey EG, Rozanski A. Automation of gated tomographic left ventricular ejection fraction. Journal of Nuclear Cardiology 1996;3(6, Pt 1):475–482.
15. DePuey EG, Nichols K, Dobrinsky C. Left ventricular ejection fraction assessed from gated technetium-99m-sestamibi SPECT. Journal of Nuclear Medicine 1993;34(11):1871–1876.
16. Nakata T, Katagiri Y, Odawara Y, et al. Two- and three-dimensional assessments of myocardial perfusion and function by using technetium-99m sestamibi gated SPECT with a combination of count- and image-based techniques. Journal of Nuclear Cardiology 2000;7(6):623–632.
17. Stegger L, Biedenstein S, Schäfers KP, Schober O, Schäfers MA. Elastic surface contour detection for the measurement of ejection fraction in myocardial perfusion SPET. European Journal of Nuclear Medicine 2001;28(1):48–55.
18. Williams KA, Taillon LA. Left ventricular function in patients with coronary artery disease assessed by gated tomographic myocardial perfusion images. Comparison with assessment by contrast ventriculography and first-pass radionuclide angiography. Journal of the American College of Cardiology 1996;27(1):173–181.
19. Inubushi M, Tadamura E, Kudoh T, et al. Simultaneous assessment of myocardial free fatty acid utilization and left ventricular function using 123I-BMIPP-gated SPECT. Journal of Nuclear Medicine 1999;40(11):1840–1847.
20. He ZX, Cwajg E, Preslar JS, Mahmarian JJ, Verani MS. Accuracy of left ventricular ejection fraction determined by gated myocardial perfusion SPECT with Tl-201 and Tc-99m sestamibi: comparison with first-pass radionuclide angiography. Journal of Nuclear Cardiology 1999;6(4):412–417.

21. Vallejo E, Dione DP, Sinusas AJ, Wackers FJ. Assessment of left ventricular ejection fraction with quantitative gated SPECT: accuracy and correlation with first-pass radionuclide angiography. Journal of Nuclear Cardiology 2000;7(5):461–470.
22. Lam PT, Wackers FJT, Liu YH. Validation of a new method for quantification of left ventricular function from ECG-gated SPECT [abstract]. Journal of Nuclear Medicine 2001;42(5):93P–94P.
23. Moriel M, Germano G, Kiat H, et al. Automatic measurement of left ventricular ejection fraction by gated SPECT Tc-99m sestamibi: a comparison with radionuclide ventriculography [abstract]. Circulation 1993;88(4):I–486.
24. Bateman T, Case J, Saunders M, et al. Gated SPECT LVEF measurements using a dual-detector camera and a weight-adjusted dosage of thallium-201 [abstract]. Journal of the American College of Cardiology 1997;29(2, Suppl A): 263A.
25. Everaert H, Bossuyt A, Franken PR. Left ventricular ejection fraction and volumes from gated single photon emission tomographic myocardial perfusion images: comparison between two algorithms working in three-dimensional space. Journal of Nuclear Cardiology 1997;4(6):472–476.
26. Carpentier P, Benticha H, Gautier P, Sulman C. Thallium 201 gated SPECT for simultaneous assessment of myocardial perfusion, left ventricular ejection fraction and qualitative regional function [abstract]. Journal of Nuclear Cardiology 1999;6(1, Pt 2):S39.
27. Daou D, Helal B, Colin P, et al. Are LV ejection fraction (EF), end diastolic (EDV) and end systolic volumes (ESV) measured with rest Tl-201 gated SPECT accurate [abstract]? Journal of Nuclear Cardiology 1999;6(1, Pt 2):S31.
28. Yoshioka J, Hasegawa S, Yamaguchi H, et al. Left ventricular volumes and ejection fraction calculated from quantitative electrocardiographic-gated ^{99m}Tc-tetrofosmin myocardial SPECT. Journal of Nuclear Medicine 1999;40(10): 1693–1698.
29. Manrique A, Koning R, Cribier A, Véra P. Effect of temporal sampling on evaluation of left ventricular ejection fraction by means of thallium-201 gated SPET: comparison of 16- and 8-interval gating, with reference to equilibrium radionuclide angiography. European Journal of Nuclear Medicine 2000;27(6):694–699.
30. Chua T, Yin LC, Thiang TH, Choo TB, Ping DZ, Leng LY. Accuracy of the automated assessment of left ventricular function with gated perfusion SPECT in the presence of perfusion defects and left ventricular dysfunction: correlation with equilibrium radionuclide ventriculography and echocardiography. Journal of Nuclear Cardiology 2000;7(4):301–311.
31. Higuchi T, Nakajima K, Taki J, Yoneyama T, Tonami N. Accuracy and reproducibility of four softwares for the left-ventricular function with ECG-gated myocardial perfusion SPECT [abstract]. Journal of Nuclear Cardiology 2001;8(1):S64.
32. Kikkawa M, Nakamura T, Sakamoto K, et al. Assessment of left ventricular diastolic function from quantitative electrocardiographic-gated ^{99m}Tc-tetrofosmin myocardial SPET (ERRATA in vol 28, pg 1579, 2001). European Journal of Nuclear Medicine 2001;28(5):593–601.
33. Kumita S, Cho K, Nakajo H, et al. Assessment of left ventricular diastolic function with electrocardiography-gated myocardial perfusion SPECT: comparison with multigated equilibrium radionuclide angiography. Journal of Nuclear Cardiology 2001;8(5):568–574.
34. Nakajima K, Higuchi T, Taki J, Kawano M, Tonami N. Accuracy of ventricular volume and ejection fraction measured by gated myocardial SPECT: comparison of 4 software programs. Journal of Nuclear Medicine 2001;42(10):1571–1578.
35. Higuchi T, Nakajima K, Taki J, Kinuya S, Bunko H, Tonami N. Assessment of left ventricular systolic and diastolic function based on the edge detection method with myocardial ECG-gated SPET. European Journal of Nuclear Medicine 2001;28(10):1512–1516.
36. Nanasato M, Ando A, Isobe S, et al. Evaluation of left ventricular function using electrocardiographically gated myocardial SPECT with I-123- labeled fatty acid analog. Journal of Nuclear Medicine 2001;42(12):1747–1756.
37. Paul A, Hasegawa S, Yoshioka J, et al. Left ventricular volume and ejection fraction from quantitative gated SPECT: comparison with gated pool SPECT and contrast ventriculography [abstract]. Journal of Nuclear Medicine 1999;40(5):178P.
38. Higuchi T, Nakajima K, Taki J, Yoneyama T, Tonami N. The accuracy of left-ventricular time volume curve derived from ECG-gated myocardial perfusion SPECT [abstract]. Journal of Nuclear Cardiology 2001;8(1):S18.
39. He Z, Vick G, Vaduganathan P, Verani M. Comparison of left ventricular volumes and ejection fraction measured by gated SPECT and by cine magnetic resonance imaging [abstract]. Journal of the American College of Cardiology 1998;31(2, Suppl A):44A.
40. Atsma D, Kayser H, Croon C, et al. Good correlation between left ventricular ejection fraction, endsystolic and enddiastolic volume measured by gated SPECT as compared to magnetic resonance imaging [abstract]. Journal of the American College of Cardiology 1999;33(2, Suppl A): 436A.
41. Vaduganathan P, He ZX, Vick GW, III, Mahmarian JJ, Verani MS. Evaluation of left ventricular wall motion, volumes, and ejection fraction by gated myocardial tomography with technetium 99m-labeled tetrofosmin: a comparison with cine magnetic resonance imaging. Journal of Nuclear Cardiology 1999;6(1, Pt 1):3–10.
42. Tadamura E, Kudoh T, Motooka M, et al. Assessment of regional and global left ventricular function by reinjection T1-201 and rest Tc-99m sestamibi ECG-gated SPECT: comparison with three-dimensional magnetic resonance imaging. Journal of the American College of Cardiology 1999;33(4):991–997.
43. Vansant J, Pettigrew R, Faber T, et al. Comparison and accuracy of two gated-SPECT techniques for assessing left ventricular function defined by cardiac MRI [abstract]. Journal of Nuclear Medicine 1999;40(5):166P.

44. Tadamura E, Kudoh T, Motooka M, et al. Use of technetium-99m sestamibi ECG-gated single-photon emission tomography for the evaluation of left ventricular function following coronary artery bypass graft: comparison with three-dimensional magnetic resonance imaging. European Journal of Nuclear Medicine 1999;26(7):705–712.
45. Bax JJ, Lamb H, Dibbets P, et al. Comparison of gated single-photon emission computed tomography with magnetic resonance imaging for evaluation of left ventricular function in ischemic cardiomyopathy. American Journal of Cardiology 2000;86(12):1299–1305.
46. Bavelaar-Croon CD, Kayser HW, van der Wall EE, et al. Left ventricular function: correlation of quantitative gated SPECT and MR imaging over a wide range of values. Radiology 2000;217(2):572–575.
47. Faber TL, Vansant JP, Pettigrew RI, et al. Evaluation of left ventricular endocardial volumes and ejection fractions computed from gated perfusion SPECT with magnetic resonance imaging: comparison of two methods. Journal of Nuclear Cardiology 2001;8(6):645–651.
48. Roelants V, Gerber B, Vanoverschelde J. Comparison between 16- and 8-interval gating for the evaluation of LV function with G-SPECT in patients with history of myocardial infarction and severe ischemic cardiomyopathy: a comparison to MRI [abstract]. Journal of Nuclear Cardiology 2003;10(1):S6.
49. Thorley PJ, Plein S, Bloomer TN, Ridgway JP, Sivananthan UM. Comparison of Tc-99m tetrofosmin gated SPECT measurements of left ventricular volumes and ejection fraction with MRI over a wide range of values. Nuclear Medicine Communications 2003;24(7):763–769.
50. Lipke CSA, Kuhl HP, Nowak B, et al. Validation of 4D-MSPECT and QGS for quantification of left ventricular volumes and ejection fraction from gated Tc-99m-MIBI SPET: comparison with cardiac magnetic resonance imaging. European Journal of Nuclear Medicine and Molecular Imaging 2004;31(4):482–490.
51. Schaefer W, Lipke C, Kuehl H, Koch K, Nowak B, Buell U. Validation of 4D-MSPECT and QGS for quantification of left ventricular volumes and ejection fraction from gated Tc-99m MIBI SPECT: comparison with cardiac magnetic resonance imaging [abstract]. Journal of Nuclear Medicine 2004;45(5):177P.
52. Zanger D, Bhatnagar A, Hausner E, et al. Automated calculation of ejection fraction from gated Tc-99m sestamibi images – comparison to quantitative echocardiography [abstract]. Journal of Nuclear Cardiology 1997;4(1, Pt 2):S78.
53. Di Leo C, Bestetti A, Tagliabue L, et al. ^{99m}Tc-tetrofosmin gated-SPECT LVEF: correlation with echocardiography and contrastographic ventriculography [abstract]. Journal of Nuclear Cardiology 1997;4(1, Pt 2):S56.
54. Bateman T, Magalski A, Barnhart C, O'Keefe J, Jones P. Global left ventricular function assessment using gated SPECT-201: comparison with echocardiography [abstract]. Journal of the American College of Cardiology 1998;31 (2, Suppl A):441A.
55. Mathew D, Zabrodina Y, Mannting F. Volumetric and functional analysis of left ventricle by gated SPECT: a comparison with echocardiographic measurements [abstract]. Journal of the American College of Cardiology 1998;31(2, Suppl A): 44A.
56. Cwajg E, Cwajg J, He ZX, et al. Gated myocardial perfusion tomography for the assessment of left ventricular function and volumes: comparison with echocardiography. Journal of Nuclear Medicine 1999;40(11):1857–1865.
57. Bacher-Stier C, Müller S, Pachinger O, et al. Thallium-201 gated single-photon emission tomography for the assessment of left ventricular ejection fraction and regional wall motion abnormalities in comparison with two-dimensional echocardiography. European Journal of Nuclear Medicine 1999;26(12):1533–1540.
58. Nichols K, Lefkowitz D, Faber T, et al. Echocardiographic validation of gated SPECT ventricular function measurements. Journal of Nuclear Medicine 2000;41(8):1308–1314.
59. Gayed IW, Cid E, Boccalandro F. Correlation of left ventricular ejection fraction using Gated SPECT automated programs with echocardiography. Journal of Nuclear Medicine 2001;42(5):177P–178P.
60. Vourvouri EC, Poldermans D, Bax JJ, et al. Evaluation of left ventricular function and volumes in patients with ischaemic cardiomyopathy: gated single-photon emission computed tomography versus two-dimensional echocardiography. European Journal of Nuclear Medicine 2001;28(11):1610–1615.
61. Akinboboye O, El-Khoury Coffin L, Sciacca R, Bergmann S, Blood D, King D. Accuracy of gated SPECT thallium left ventricular volumes and ejection fractions: comparison with three-dimensional echocardiography [abstract]. Journal of the American College of Cardiology 1998;31(2, Suppl A):85A.
62. Abe M, Kazatani Y, Fukuda H, Tatsuno H, Habara H, Shinbata H. Left ventricular volumes, ejection fraction, and regional wall motion calculated with gated technetium-99m tetrofosmin SPECT in reperfused acute myocardial infarction at super-acute phase: comparison with left ventriculography. Journal of Nuclear Cardiology 2000;7(6):569–574.
63. Atsma DE, Bavelaar-Croon CDL, Germano G, et al. Good correlation between gated single photon emission computed myocardial tomography and contrast ventriculography in the assessment of global and regional left ventricular function. International Journal of Cardiac Imaging 2000;16(6):447–453.
64. Toba M, Ishida Y, Fukuchi K, Fukushima K, Takamiya M. Application of ECG-gated Tc-99m sestamibi cardiac imaging to patients with arrhythmogenic right ventricular dysplasia (ARVD) [abstract]. Journal of Nuclear Cardiology 1999; 6(1, Pt 2):S41.
65. Germano G, VanDecker W, Mintz R, et al. Validation of left ventricular volumes automatically measured with gated myocardial perfusion SPECT [abstract]. Journal of the American College of Cardiology 1998;31(2, Suppl A):43A.
66. Cahill J, Chen M, Corbett J, Quaife R. Validation of three-dimensional analysis method for calculation of the LV mass and ejection fraction using Tc-99m Sestamibi gated-SPECT

perfusion imaging: comparison between 4D-MSPECT and magnetic resonance imaging [abstract]. Journal of Nuclear Medicine 2003;44(5):197P.
67. Cahill J, Chen M, Ficaro E, Corbett J, Quaife R. Validation of 4D-MSPECT analysis method for Tc-99m gated blood pool tomography: comparison of LV ejection fractions and volumes to magnetic resonance imaging [abstract]. Journal of Nuclear Cardiology 2003;10(4):S20.
68. Ficaro E, Quaife R, Kritzman J, Corbett J. Accuracy and reproducibility of 3D-MSPECT for estimating left ventricular ejection fraction in patients with severe perfusion abnormalities [abstract]. Circulation 1999;100(18):I–26.
69. Schwartz R, Thompson C, Mixon L, Eckdahl J, Burns G. Gated SPECT analysis with 3-D wall parametrization method: accurate and reproducible evaluation of left ventricular volumes and ejection fraction [abstract]. Circulation 1995;92(8):I–449.
70. Vera P, Manrique A, Pontvianne V, Hitzel A, Koning R, Cribier A. Thallium-gated SPECT in patients with major myocardial infarction: effect of filtering and zooming in comparison with equilibrium radionuclide imaging and left ventriculography. Journal of Nuclear Medicine 1999;40(4):513–521.
71. Schwartz R, Eckdahl J, Thompson C. 3-D wall parametrization method for quantitative LVEF of gated SPECT sestamibi with LV dysfunction and severe perfusion defects [abstract]. Journal of Nuclear Cardiology 1995;2(2):S114.
72. Navare SM, Wackers FJT, Liu YH. Comparison of 16-frame and 8-frame gated SPET imaging for determination of left ventricular volumes and ejection fraction. European Journal of Nuclear Medicine and Molecular Imaging 2003;30(10):1330–1337.
73. Calnon DA, Kastner RJ, Smith WH, Segalla D, Beller GA, Watson DD. Validation of a new counts-based gated single photon emission computed tomography method for quantifying left ventricular systolic function: comparison with equilibrium radionuclide angiography. Journal of Nuclear Cardiology 1997;4(6):464–471.
74. Stollfuss JC, Haas F, Matsunari I, et al. Regional myocardial wall thickening and global ejection fraction in patients with low angiographic left ventricular ejection fraction assessed by visual and quantitative resting ECG-gated ^{99m}Tc-tetrofosmin single-photon emission tomography and magnetic resonance imaging. European Journal of Nuclear Medicine 1998;25(5):522–530.
75. Stollfuss JC, Haas F, Matsunari I, et al. ^{99m}Tc-tetrofosmin SPECT for prediction of functional recovery defined by MRI in patients with severe left ventricular dysfunction: additional value of gated SPECT. Journal of Nuclear Medicine 1999;40(11):1824–1831.
76. Adiseshan P, Corbett J. Quantification of left ventricular function from gated tomographic perfusion imaging: development and testing of a new algorithm [abstract]. Circulation 1994;90(4):I–365.
77. Nichols K, Tamis J, DePuey EG, Mieres J, Malhotra S, Rozanski A. Relationship of gated SPECT ventricular function parameters to angiographic measurements. Journal of Nuclear Cardiology 1998;5(3):295–303.
78. Nakajima K, Higuchi T, Taki J, et al. Quantitative gated SPECT with myocardial perfusion and blood-pool studies to determine ventricular volumes and stroke volume ratio in congenital heart diseases [abstract]. Journal of Nuclear Cardiology 2003;10(1):S11.
79. Zuber E, Rosfors S. Effect of reversible hypoperfusion on left ventricular volumes measured with gated SPECT at rest and after adenosine infusion. Journal of Nuclear Cardiology 2000;7(6):655–660.
80. Cittanti C, Mele D, Colamussi P, et al. Determination of left ventricular volume and ejection fraction by g-SPECT myocardial perfusion scintigraphy. A comparison with quantitative 3-D echocardiography [abstract]. Journal of Nuclear Cardiology 1999;6(1, Pt 2):S34.
81. Iskandrian AE, Germano G, VanDecker W, et al. Validation of left ventricular volume measurements by gated SPECT ^{99m}Tc-labeled sestamibi imaging. Journal of Nuclear Cardiology 1998;5(6):574–578.
82. Hwang WS, Fernando GP, Natale D, et al. Comparison and validation of 3 gated SPECT programs for volume determination using ventricular casts of excised canine hearts [abstract]. Journal of Nuclear Medicine 2001;42(5):46P–47P.
83. Nichols K, Lefkovitz D, Faber T, et al. Ventricular volumes compared among three gated SPECT methods and echocardiography [abstract]. Journal of the American College of Cardiology 1999;33(2, Suppl A):409A.
84. Yang KT, Chen HD. Evaluation of global and regional left ventricular function using technetium-99m sestamibi ECG-gated single-photon emission tomography. European Journal of Nuclear Medicine 1998;25(5):515–521.
85. Faber TL, Akers MS, Peshock RM, Corbett JR. Three-dimensional motion and perfusion quantification in gated single-photon emission computed tomograms. Journal of Nuclear Medicine 1991;32(12):2311–2317.
86. Nichols K, DePuey EG, Krasnow N, Lefkowitz D, Rozanski A. Reliability of enhanced gated SPECT in assessing wall motion of severely hypoperfused myocardium: echocardiographic validation. Journal of Nuclear Cardiology 1998;5(4):387–394.
87. Fukuchi K, Uehara T, Morozumi T, et al. Quantification of systolic count increase in technetium-99m-MIBI gated myocardial SPECT. Journal of Nuclear Medicine 1997;38(7):1067–1073.
88. Abidov A, Slomka P, Hayes S, et al. Left ventricular shape index assessed by gated myocardial perfusion SPECT: a new scintigraphic marker of congestive heart failure [abstract]. Journal of Nuclear Medicine 2004;45(5):176P.
89. Sheehan FH, Dodge HT, Mathey D, Brown BG, Bolson EL, Mitten S. Application of the centerline method: analysis of change in regional left ventricular wall motion in serial studies. In: Computers in Cardiology. Ninth Meeting of Computers in Cardiology; 1983; Seattle, WA: IEEE Computer Society Press; 1983:97–100.
90. Garcia EV, Cooke CD, Van Train KF, et al. Technical aspects of myocardial SPECT imaging with technetium-99m sestamibi. American Journal of Cardiology 1990;66(13):23E–31E.

91. Galt JR, Garcia EV, Robbins WL. Effects of myocardial wall thickness on SPECT quantification. IEEE Transactions on Medical Imaging 1990;9(2):144–150.
92. Pflugfelder PW, Sechtem UP, White RD, Higgins CB. Quantification of regional myocardial function by rapid cine MR imaging. American Journal of Roentgenology 1988;150(3):523–529.
93. Kaul S, Wismer GL, Brady TJ, et al. Measurement of normal left heart dimensions using optimally oriented MR images. American Journal of Roentgenology 1986;146(1):75–79.
94. Byrd BJ, Schiller NB, Botvinick EH, Higgins CB. Normal cardiac dimensions by magnetic-resonance imaging. American Journal of Cardiology 1985;55(11):1440–1442.
95. Ficaro E, Lee B, Kritzman J, Corbett J. Automatic realignment and centering of gated perfusion SPECT: effect on quantitative reproducibility [abstract]. Journal of Nuclear Medicine 2003;44(5):198P.
96. Sheehan FH, Stewart DK, Dodge HT, Mitten S, Bolson EL, Brown BG. Variability in the measurement of regional left ventricular wall motion from contrast angiograms. Circulation 1983;68(3):550–559.
97. Shen MY, Liu YH, Sinusas AJ, et al. Quantification of regional myocardial wall thickening on electrocardiogram-gated SPECT imaging. Journal of Nuclear Cardiology 1999;6(6):583–595.
98. Hoffman EJ, Huang SC, Phelps ME. Quantitation in positron emission computed tomography: 1. Effect of object size. Journal of Computer Assisted Tomography 1979;3(3):299–308.
99. Katz A, Force T, Folland E, Aebischer N, Sharma S, Parisi A. Echocardiographic assessment of ventricular systolic function. In: Marcus ML, Braunwald E, eds. Marcus Cardiac Imaging : A Companion to Braunwald's Heart Disease. 2nd edn. Philadelphia: Saunders; 1996:297–324.
100. Yang KT, Chen HD. A semi-automated method for edge detection in the evaluation of left ventricular function using ECG-gated single-photon emission tomography. European Journal of Nuclear Medicine 1994;21(11):1206–1211.
101. Kasai T, DePuey EG, Ali Shah A. Decreased septal wall thickening in patients with left bundle branch block. Journal of Nuclear Cardiology 2004;11(1):32–37.
102. Higuchi T, Taki J, Yoneyama T, Kawano M, Tonami N. Diastolic and systolic parameters obtained by myocardial ECG-gated perfusion study [abstract]. Journal of Nuclear Medicine 2000;41(5):160P.
103. Nakajima K, Taki J, Kawano M, et al. Diastolic dysfunction in patients with systemic sclerosis detected by gated myocardial perfusion SPECT: an early sign of cardiac involvement. Journal of Nuclear Medicine 2001;42(2):183–188.
104. Sakamoto K, Nakamura T, Zen K, et al. Identification of exercise-induced left ventricular systolic and diastolic dysfunction using gated SPECT in patients with coronary artery disease. Journal of Nuclear Cardiology 2004;11(2):152–158.
105. Alexanderson E, Espinola N, Meavel A, Victoria D. Assessment of ventricular perfusion and function with nuclear scan and echocardiography in patients with corrected transposition of great arteries [abstract]. Journal of Nuclear Cardiology 2003;10(1):S66.
106. Germano G, Nichols K, Cullom S, Faber T, Cooke C. Gated perfusion SPECT: technical considerations. In: DePuey EG, Garcia EV, Berman DS, eds. Cardiac SPECT imaging Ed. Vol. II. 2nd edn. Philadelphia: Lippincott, Williams & Wilkins; 2001:103–115.
107. Cullom SJ, Case JA, Bateman TM. Electrocardiographically gated myocardial perfusion SPECT: technical principles and quality control considerations. Journal of Nuclear Cardiology 1998;5(4):418–425.
108. Nichols K, Dorbala S, DePuey EG, Yao SS, Sharma A, Rozanski A. Influence of arrhythmias on gated SPECT myocardial perfusion and function quantification. Journal of Nuclear Medicine 1999;40(6):924–934.
109. Nichols K, Yao SS, Kamran M, Faber TL, Cooke CD, DePuey EG. Clinical impact of arrhythmias on gated SPECT cardiac myocardial perfusion and function assessment. Journal of Nuclear Cardiology 2001;8(1):19–30.
110. Kasai T, DePuey EG, Shah AA, Merla VC. Impact of gating errors with electrocardiography gated myocardial perfusion SPECT. Journal of Nuclear Cardiology 2003;10(6):709–711.
111. Djaballah W, Muller M, Bertrand A, et al. Gated SPECT assessment of left ventricular function is sensitive to small patient motions and to low rates of triggering errors: a comparison with equilibrium radionuclide angiography. Journal of Nuclear Cardiology 2005;12(1):78–85.
112. Imai K, Azuma Y, Nakajima S, Yamazaki S, Iwano K, Hayafune N, et al. Frames a cardiac cycle in quantitative gated SPECT (QGS) for clinical use: 8 versus 16 [abstract]. Journal of Nuclear Cardiology 1999;6(1, Pt 2):S17.
113. Cohade C, Taillefer R, Gagnon A, Benjamin C, Lajeunesse S. Comparison of different radionuclide methods, including gated SPECT (GS), for determination of left ventricle ejection fraction (LVEF) [abstract]. Journal of Nuclear Medicine 2000;41(5):6P.
114. Cohade C, Taillefer R, Gagnon A, Lejeunesse S, Benjamin C. Effect of the number of frames per cardiac cycle and the amount of injected dose of radionuclide on the determination of left ventricular ejection fraction (LVEF) with gated SPECT myocardial perfusion imaging (GS) [abstract]. Journal of Nuclear Medicine 2000;41(5):154P.
115. Manrique A, Vera P, Hitzel A, Koning R, Cribier A. 16-interval gating improves thallium-201 gated SPECT LVEF measurement in patients with large myocardial infarction [abstract]. Journal of the American College of Cardiology 1999;33(2, Suppl A):436A–437A.
116. Damrongpipatkij Y, Mohammed F, Brown E, Alhaddad I, Heller E. Quantitative cardiac SPECT: measuring diastolic function [abstract]. Journal of Nuclear Medicine 2000;41(5):154P.
117. Mazzanti M, Germano G, Kiat H, Friedman J, Berman DS. Fast technetium 99m-labeled sestamibi gated single-photon emission computed tomography for evaluation of myocardial function. Journal of Nuclear Cardiology 1996;3(2):143–149.

118. Everaert H, Vanhove C, Defrise M, Franken P. Ultra-fast (3 minutes) gated myocardial perfusion SPET studies using a 3-head gamma camera and cardiofocal collimators [abstract]. Journal of Nuclear Medicine 1997;38(5):28P.
119. Everaert H, Vanhove C, Franken PR. Gated SPET myocardial perfusion acquisition within 5 minutes using focussing collimators and a three-head gamma camera. European Journal of Nuclear Medicine 1998;25(6):587–593.
120. Everaert H, Vanhove C, Franken PR. Low-dose dobutamine gated single-photon emission tomography: comparison with stress echocardiography. European Journal of Nuclear Medicine 2000;27(4):413–418.
121. Vanhove C, Muylle K, Franken P. Minimal count level required for quantification of left ventricular function with gated myocardial perfusion tomography [abstract]. European Journal of Nuclear Medicine 2002;29(Suppl 1): S218.
122. Franken PR, Everaert H, Momen A, Vanhove C. Comparison of three automatic software to measure left ventricular cavity volume and ejection fraction from perfusion gated tomograms [abstract]. European Journal of Nuclear Medicine 1999;26(9):1076.
123. Berman DS, Kiat H, Friedman JD, et al. Separate acquisition rest thallium-201/stress technetium-99m sestamibi dual-isotope myocardial perfusion single-photon emission computed tomography: a clinical validation study. Journal of the American College of Cardiology 1993;22(5):1455–1464.
124. Germano G, Erel J, Kiat H, Kavanagh PB, Berman DS. Quantitative LVEF and qualitative regional function from gated thallium-201 perfusion SPECT. Journal of Nuclear Medicine 1997;38(5):749–754.
125. Lee DS, Ahn JY, Kim SK, et al. Limited performance of quantitative assessment of myocardial function by thallium-201 gated myocardial single-photon emission tomography. European Journal of Nuclear Medicine 2000;27(2):185–191.
126. Hyun I, Kim D, Seo J, et al. Normal parameters of left ventricular volume and ejection fraction measured by gated myocardial perfusion SPECT: comparison of Tc99m MIBI and TI-201 [abstract]. European Journal of Nuclear Medicine 2002;29(Suppl 1):S205.
127. He Z, Mahmarian J, Preslar J, Verani M. Correlations of left ventricular ejection fractions determined by gated SPECT with thallium and sestamibi and by first-pass radionuclide angiography [abstract]. Journal of Nuclear Medicine 1997;38(5):27P.
128. Hyun I, Kwan J, Park K, Lee W. Reproducibility of gated perfusion SPECT for the assessment of myocardial function: comparison with ^{201}Tl and ^{99m}Tc MIBI [abstract]. Journal of Nuclear Medicine 2000;41(5):125P.
129. Case A, Bateman T, Cullom S, Moutray K, O'Keefe J, McGhie A. Validation of Tl-201 LVEF measurements using simultaneous acquired Tc-99m-sestamibi/Tl-201 ECG-gated SPECT perfusion scintigraphy [abstract]. Journal of Nuclear Medicine 1999;40(5):159P.
130. Everaert H, Vanhove C, Hamill JJ, Franken PR. Cardiofocal collimators for gated single-photon emission tomographic myocardial perfusion imaging. European Journal of Nuclear Medicine 1998;25(1):3–7.
131. Groch M, Takamiya Y, Groch P, Erwin W. Quantitative gated myocardial SPECT: effect of collimation on left ventricular ejection fraction [abstract]. Journal of Nuclear Cardiology 1999;6(1, Pt 2):S85.
132. Bjering K, Larsen W, Seierstad T, Bach-Gansmo T, Skretting A, Bogsrud T. Effects of changing cutoff frequency and powerfactor in the Butterworth filter for quantitative gated myocardial SPECT using Cedar-Sinai's QGS [abstract]. European Journal of Nuclear Medicine 2003;30(Suppl 2):S263–S264.
133. Khalil M, El-Motairi T, Shehab F, Omar A, Mohammed A, Elgazzar A. The effect of filter cut-off on the reproducibility of QGS and ECTb in LV functional estimation: comparison with gated blood pool [abstract]. Journal of Nuclear Medicine 2004;45(5):225P.
134. Hambye AS, Vervaet A, Dobbeleir A. Variability of left ventricular ejection fraction and volumes with quantitative gated SPECT: influence of algorithm, pixel size and reconstruction parameters in small and normal-sized hearts. European Journal of Nuclear Medicine and Molecular Imaging 2004;31(12):1606–1613.
135. Wright GA, McDade M, Martin W, Hutton I. Quantitative gated SPECT: the effect of filtering on left ventricular ejection fraction measurements [abstract]. Journal of Nuclear Medicine 2001;42(5):94P.
136. Daou D, Pointurier I, Coaguila C, et al. Does iterative reconstruction as compared to filtered backprojection increase the accuracy of Tl-201 gated SPECT for the measurement of LVEF [abstract]? Journal of Nuclear Medicine 2001;42(5):174P.
137. Daou D, Pointurier I, Coaguila C, et al. Iterative reconstruction and filtered backprojection of 201-Tl gated SPECT provide similar accuracy for the measurement of LVEF [abstract]. European Journal of Nuclear Medicine 2001;28(8):PS609.
138. Daou D, Pointurier I, Coaguila C, et al. Performance of OSEM and depth-dependent resolution recovery algorithms for the evaluation of global left ventricular function in Tl-201 gated myocardial perfusion SPECT. Journal of Nuclear Medicine 2003;44(2):155–162.
139. Gayed I, Mar M, Broemeling L, et al. Comparison between iterative versus filtered back projection processing of myocardial perfusion studies [abstract]. Journal of Nuclear Medicine 2004;45(5):226P.
140. Mar M, Broemeling L, Erwin W, Campbell R, Miller S, Gayed I. Effect of iterative reconstruction on left ventricular ejection fraction and volume [abstract]. Journal of Nuclear Medicine 2004;45(5):121P.
141. Dobbeleir A, Deryk S, Van Hove C, Franken P. Influence of number of Osem iterations on gated SPECT ejection fraction calculation [abstract]. European Journal of Nuclear Medicine 2003;30(Suppl 2):S260.
142. Germano G, Chua T, Kiat H, Areeda JS, Berman DS. A quantitative phantom analysis of artifacts due to hepatic activity in technetium-99m myocardial perfusion SPECT studies. Journal of Nuclear Medicine 1994;35(2):356–359.

143. Cittanti C, Leonelli ES, Colamussi P, et al. Back-projection vs iterative ^{99m}Tc-Sestamibi gated-SPECT reconstruction in the evaluation of left ventricular ejection fraction and volumes: a comparison with contrast left ventriculography [abstract]. European Journal of Nuclear Medicine 2001;28(8): OS159.
144. Véra P, Koning R, Cribier A, Manrique A. Comparison of two three-dimensional gated SPECT methods with thallium in patients with large myocardial infarction. Journal of Nuclear Cardiology 2000;7(4):312–319.
145. Al-Khori F, McNelis P, Van Decker W. Reliability of gated SPECT in assessing left ventricular ejection fraction in ventricles with scarred myocardium [abstract]. Journal of Nuclear Cardiology 1999;6(1, Pt 2):S26.
146. Giubbini R, Terzi A, Rossini P, Milan E. Gated myocardial perfusion single photon emission tomography (GSPECT) in the evaluation of left ventricular ejection fraction in CAD patients with previous myocardial infarction [abstract]. Journal of Nuclear Cardiology 1999;6(1, Pt 2):S58.
147. Bax J, Lamb H, Dibbets P, et al. Comparison between LV volumes and LVEF assessed by MRI and gated SPECT in patients with severe ischemic LV dysfunction [abstract]. Journal of Nuclear Medicine 1999;40(5):45P.
148. Dibbets P, Bax JJ, Lamb H, et al. Direct comparison of LVEF and LV volumes assessed by gated SPECT and MRI in patients with chronic coronary artery disease and severely reduced LV function [abstract]. European Journal of Nuclear Medicine 1999;26(9):962.
149. Itti E, Damien P, Rosso J, Meignan M, Benayoun S, Thirion J. Assessment of ejection fraction by 201-Thallium gated tomography in extended myocardial infarction: repeatability in a rest-redistribution study and accuracy versus planar angiography [abstract]. Journal of the American College of Cardiology 2000;35(2, Suppl A):481A.
150. Itti E, Rosso J, Damien P, Auffret M, Thirion JP, Meignan M. Assessment of ejection fraction with Tl-201 gated SPECT in myocardial infarction: precision in a rest-redistribution study and accuracy versus planar angiography. Journal of Nuclear Cardiology 2001;8(1):31–39.
151. Boccalandro F, Gayed I, Cid E. Effect of myocardial perfusion defects on the accuracy of left ventricular ejection fraction using gated SPECT [abstract]. Circulation 2001;104(17): II–584.
152. Chen K, Tan RS, Keng F, et al. Accuracy of gated perfusion single-photon emission tomography for left ventricular ejection fraction assessment in the presence of large perfusion defects: correlation with cardiac magnetic resonance [abstract]. Journal of the American College of Cardiology 2002;39(5):394A.
153. Shen R, Liu X, Shi R, et al. Evaluation of LVEF by F-18-FDG gated SPECT using dual isotope simultaneous acquisition: comparison between patients with perfusion-metabolism mismatch and match [abstract]. Journal of Nuclear Medicine 2003;44(5):59P.
154. Germano G, Berman DS. On the accuracy and reproducibility of quantitative gated myocardial perfusion SPECT [editorial; comment]. Journal of Nuclear Medicine 1999;40(5): 810–813.
155. Case J, Cullom S, Bateman T, Barnhart C, Saunders M. Overestimation of LVEF by gated MIBI myocardial perfusion SPECT in patients with small hearts [abstract]. Journal of the American College of Cardiology 1998;31(2, Suppl A,): 43A.
156. Nakajima K, Taki J, Higuchi T, et al. Gated SPET quantification of small hearts: mathematical simulation and clinical application. European Journal of Nuclear Medicine 2000;27(9):1372–1379.
157. Ford PV, Chatziioannou SN, Moore WH, Dhekne RD. Overestimation of the LVEF by quantitative gated SPECT in simulated left ventricles. Journal of Nuclear Medicine 2001;42(3):454–459.
158. Kelles A, Martin P, Tran-ngoc E, et al. Influence of ventricle size on the results of left ventricular ejection fraction found by quantitative gated SPECT [abstract]. European Journal of Nuclear Medicine 2001;28(8):OS244.
159. El-Maghraby T, El-Rahman N. Clinical relevance of left ventricular volumes and function assessed by gated SPECT in paediatric patients. International Journal of Cardiac Imaging 2004;20(2):127–134.
160. Schwartz R, Mixon L, Germano G, Chaudhary I, Armstrong K, Mackin M. Gated SPECT reconstruction with zoom and depth dependent filter improves accuracy of volume and LVEF in small hearts [abstract]. Journal of Nuclear Cardiology 1999;6(1, Pt 2):S17.
161. Ezuddin S, Sfakianakis G, Pay L, Sanchez P. Comparative study to determine the effect of different zoom factors on the calculation of LVEF from gated myocardial perfusion SPECT with Tl-201 and Tc-99m-sestamibi in patients with small hearts [abstract]. Journal of Nuclear Medicine 1999;40(5):169P.
162. Nakajima K, Taki J, Higuchi T, Kawano M, Tonami N. Factors affecting volume measurement of small heart by gated SPECT [abstract]. Journal of Nuclear Medicine 2000;41(5):99P.
163. Manrique A, Gardin I, Brasse D, Sanson A, Vera P. Effect of reconstruction parameters on LV volume measurements from Tl-201 SPECT: a phantom study [abstract]. Journal of Nuclear Cardiology 2001;8(1):S71.
164. Imai K, Tajima O, Sakamoto H, et al. A newly developed maneuver, Field Change Conversion (FCC), has enabled more accurate evaluation of the left ventricular volume on quantitative gated SPECT (QGS) analysis [abstract]. Journal of Nuclear Cardiology 2003;10(1):S18.
165. Maruno H, Mori K, Saitoh K, Okazaki A. Dynamic cardiac beating phantom in imitation of small left ventricle and evaluation of improved accuracy of SPECT LVEF, EDV, ESV by decreasing pixel size for small ventricle [abstract]. Journal of Nuclear Medicine 2003;44(5):194P.
166. Nakajima K, Taki J, Taniguchi M, et al. Gated myocardial SPECT in pediatric patients: is it reliable? [abstract] Journal of Nuclear Medicine 1999;40(5):204P.
167. Case J, Bateman T, Cullom S, O'Keefe J, Moutray K, Saunders M. Improved accuracy of SPECT LVEF using numerical modeling of ventricular image blurring for patients with small hearts [abstract]. Journal of the American College of Cardiology 1999;33(2, Suppl A):436A.

168. Faber T, Cooke C, Folks R, Santana C, Garcia E. Correction of artifactually high EF from gated perfusion SPECT in small ventricles [abstract]. Journal of Nuclear Cardiology 2000;7(4):S20.
169. Santos M, Lewin H, Hayes S, Friedman J, Berman D, Germano G. A potential cause for underestimation of LVEF by QGS [abstract]. Journal of Nuclear Cardiology 2001;8(4):S130.
170. Kasai T, DePuey E, Shah A, Suma V. Threshold methods for myocardial edge detection with gated SPECT lead to underestimation of LVEF in patients with left ventricular hypertrophy [abstract]. Journal of Nuclear Cardiology 2003;10(4):S8.
171. Friedman J, Berman DS, Van Train K, et al. Patient motion in thallium-201 myocardial SPECT imaging. An easily identified frequent source of artifactual defect. Clinical Nuclear Medicine 1988;13(5):321–324.
172. Eisner RL. Sensitivity of SPECT thallium-201 myocardial perfusion imaging to patient motion [editorial; comment]. Journal of Nuclear Medicine 1992;33(8):1571–1573.
173. Cooper JA, Neumann PH, McCandless BK. Effect of patient motion on tomographic myocardial perfusion imaging [see comments]. Journal of Nuclear Medicine 1992;33(8):1566–1571.
174. Matsumoto N, Berman DS, Kavanagh PB, et al. Quantitative assessment of motion artifacts and validation of a new motion-correction program for myocardial perfusion SPECT. Journal of Nuclear Medicine 2001;42(5):687–694.
175. Matsumoto N, Berman DS, Kavanagh PB, et al. Effect of patient motion on quantitative left ventricular volume and regional wall motion in ECG-gated myocardial perfusion SPECT [abstract]. Journal of Nuclear Medicine 2001;42(5): 175P.
176. Daou D, Coaguila C, Benada A, et al. Impact of patient movement on the robustness of gated myocardial perfusion SPECT (GSPECT) and radionuclide angiography SPECT (RNA SPECT) for the measurement of left ventricular ejection fraction (LVEF) [abstract]. Journal of Nuclear Medicine 2004;45(5):232P.
177. Ficaro E, Kritzman J, Hamilton T, Mitchell T, Corbett J. Effect of attenuaton corrected myocardial perfusion SPECT on left ventricular ejection fraction estimates [abstract]. Journal of Nuclear Medicine 2000;41(5):166P–167P.
178. Tsakin V, Liu Y, Wackers F. Differential effects of acquisition orbits and attenuation correction on assessments of left ventricular volumes and ejection fraction gated using SPECT/CT imaging in normal volunteers [abstract]. Journal of Nuclear Medicine 2004;45(5):398P–399P.
179. Berman D, Germano G, Lewin H, et al. Comparison of post-stress ejection fraction and relative left ventricular volumes by automatic analysis of gated myocardial perfusion single-photon emission computed tomography acquired in the supine and prone positions. Journal of Nuclear Cardiology 1998;5(1):40–47.
180. Schaefer W, Lipke C, Kaiser H, Nowak B, Kuehl H, Buell U. Effects of supine and prone acquisition in gated Tc-99m MIBI SPECT on left ventricular volumes, stroke volume, ejection fraction and heart rate [abstract]. Journal of Nuclear Medicine 2004;45(5):121P.
181. Kubo N, Mabuchi M, Katoh C, et al. Validation of left ventricular function using gated SPECT with a scintillation crystal and semiconductor detectors camera system: a study of dynamic myocardial phantom [abstract]. Journal of Nuclear Medicine 2002;43(5):199P–200P.
182. Kennedy JW, Baxley WA, Figley MM, Dodge HT, Blackmon JR. Quantitative angiocardiography. I. The normal left ventricle in man. Circulation 1966;34(2):272–278.
183. Sheehan F. Applications of contrast ventriculography. In: Marcus ML, Braunwald E, eds. Marcus Cardiac Imaging: A Companion to Braunwald's Heart Disease. 2nd edn. Philadelphia: Saunders, 1996:187–199.
184. Kang X, Berman D, Germano G, et al. Normal parameters of left ventricle volume and ejection fraction measured by gated myocardial perfusion SPECT [abstract]. Journal of the American College of Cardiology 1999;33(2, Suppl A): 409A.
185. Case J, Bateman T, Moutray K, Cullom S. Establishing normal limits for LVEF from ECG-gated resting Tl-201 myocardial perfusion SPECT imaging [abstract]. Journal of Nuclear Cardiology 1999;6(1, Pt 2):S116.
186. Fujino S, Masuyama K, Kanayama S, et al. Early and delayed technetium-99m labeled sestamibi myocardial ECG-gated SPECT by QGS program in normal volunteers [abstract]. Journal of Nuclear Medicine 1999;40(5):180P.
187. Sharir T, Germano G, Kavanagh PB, et al. Incremental prognostic value of post-stress left ventricular ejection fraction and volume by gated myocardial perfusion single photon emission computed tomography. Circulation 1999;100(10):1035–1042.
188. Rozanski A, Nichols K, Yao SS, Malholtra S, Cohen R, DePuey EG. Development and application of normal limits for left ventricular ejection fraction and volume measurements from ^{99m}Tc-sestamibi myocardial perfusion gates SPECT. Journal of Nuclear Medicine 2000;41(9):1445–1450.
189. Ababneh AA, Sciacca RR, Kim B, Bergmann SR. Normal limits for left ventricular ejection fraction and volumes estimated with gated myocardial perfusion imaging in patients with normal exercise test results: influence of tracer, gender, and acquisition camera. Journal of Nuclear Cardiology 2000;7(6):661–668.
190. Sharir T, Germano G, Kang XP, Cohen I, Friedman JD, Berman DS. Prognostic value of post-stress left ventricular volume and ejection fraction by gated myocardial perfusion single photon emission computed tomography in women: gender related differences in normal limits and outcome [abstract]. Circulation 2002;106(19):II–523.
191. De Bondt P, De Sutter J, De Winter F, Van de Wiele C, Dierckx R. Normal values of left ventricular ejection fraction (LVEF) and left ventricular volumes (LVV) measured by gated myocardial SPECT in women and men at rest and after bicycle or dipiridamole (DIP) stress testing [abstract]. Journal of Nuclear Medicine 2000;41(5):159P.
192. Ababneh A, Sciacca R, Bergmann S. Normal limits for left ventricular ejection fraction, end-diastolic, and end-systolic volume as estimated with gated perfusion imaging [abstract]. Circulation 2000;102(18):II–724.

193. Sharir T, Germano G, Friedman J, et al. Prognostic value of gated myocardial perfusion single photon emission computed tomography in women versus men [abstract]. Circulation 2000;102(18):II–544.
194. De Bondt P, Van de Wiele C, De Sutter J, De Winter F, De Backer G, Dierckx RA. Age- and gender-specific differences in left ventricular cardiac function and volumes determined by gated SPET. European Journal of Nuclear Medicine 2001;28(5):620–624.
195. Kim J, Kim N. Normal LVEF measurements are significantly higher in females assessed by ^{99m}Tc-MIBI and tetrofosmin quantitative gated myocardial perfusion SPECT: age and gender matched statistical analysis [abstract]. Journal of Nuclear Medicine 2003;44(5): 106P.
196. Ficaro F, Kritzman J, Stephens G, Corbett J. Gender specific differences in normal ranges of cardiac functional parameters from gated SPECT [abstract]. Journal of Nuclear Medicine 2003;44(5):205P–206P.
197. Santana CA, Garcia EV, Folks R, Krawczynska EG, Cooke CD, Faber TL. Comparison of normal values of left ventricular function between two programs: QGS and emory cardiac toolbox (ECTB) [abstract]. Journal of Nuclear Medicine 2001;42(5):166P.
198. Krasnow J, Trask I, Dahlberg S, Margulis G, Leppo J. Automatic determination of left ventricular function (LVEF) by gated SPECT; comparison of four quantitative software programs [abstract]. Journal of Nuclear Cardiology 2001;8(4):S138.
199. Kang D, Kim M, Kim Y. Functional data of gated myocardial perfusion SPECT by QGS and 4D-MSPECT program cannot exchanged each other (sic) [abstract]. Journal of Nuclear Medicine 2004;45(5):225P.
200. Hyun IY, Kwan J, Park KS, Lee WH. Reproducibility of Tl-201 and Tc-99m sestamibi gated myocardial perfusion SPECT measurement of myocardial function. Journal of Nuclear Cardiology 2001;8(2):182–187.
201. Johnson LL, Verdesca SA, Aude WY, et al. Postischemic stunning can affect left ventricular ejection fraction and regional wall motion on post-stress gated sestamibi tomograms [see comments]. Journal of the American College of Cardiology 1997;30(7):1641–1648.
202. Paeng JC, Lee DS, Cheon GJ, Lee MM, Chung JK, Lee MC. Reproducibility of an automatic quantitation of regional myocardial wall motion and systolic thickening on gated Tc-99m- sestamibi myocardial SPECT. Journal of Nuclear Medicine 2001;42(5):695–700.
203. Vanhove C, Franken PR, Defrise M, Bossuyt A. Comparison of 180 degrees and 360 degrees data acquisition for determination of left ventricular function from gated myocardial perfusion tomography and gated blood pool tomography. European Journal of Nuclear Medicine and Molecular Imaging 2003;30(11):1498–1504.
204. Germano G, Kavanagh PB, Kavanagh JT, Wishner SH, Berman DS, Kavanagh GJ. Repeatability of automatic left ventricular cavity volume measurements from myocardial perfusion SPECT. Journal of Nuclear Cardiology 1998;5(5):477–483.
205. Kumita S, Kumazaki T, Cho K, et al. Rapid data acquisition protocol in ECG-gated myocardial perfusion SPECT with Tc-99m-tetrofosmin. Annals of Nuclear Medicine 1998;12(2):71–75.
206. Kritzman J, Ficaro E, Corbett J. Reproducibility of 3-D MSPECT for quantitative gated SPECT sestamibi perfusion analysis [abstract]. Journal of Nuclear Medicine 2000;41(5):166P.
207. Lewin H, Berman D, Hayes S, Friedman J, Germano G. Clinical reproducibility of post-stress gated myocardial perfusion SPECT imaging [abstract]. Journal of Nuclear Medicine 2000;41(5):160P.
208. Agostini D, Filmont J, Darlas Y, Dronne F, Bouvard G. LVEF and LV volumes determinations with gated 123I-MIBG SPECT in dystrophic myotony [abstract]. Journal of Nuclear Medicine 2000;41(5):49P.
209. Rubio A, Garcia-Burillo A, Gonzalez-Gonzalez J, et al. Interstudy repeatability of gated-spect quantitative parameters [abstract]. European Journal of Nuclear Medicine 2002;29(Suppl 1):S208.
210. Willemsen A, Siebelink H, Blanksma P, Paans A. Left ventricle ejection fraction determination with gated 18FDG-PET [abstract]. Journal of Nuclear Medicine 1999;40(5):166P.
211. Willemsen AT, Siebelink HJ, Blanksma PK, Paans AM. Automated ejection fraction determination from gated myocardial FDG-PET data. Journal of Nuclear Cardiology 1999;6(6):577–582.
212. Inubushi M, Ishida Y, Fukuchi K, Fukushima K, Sasako K. Myocardial viability assessment using 18F FDG gated PET [abstract]. Journal of Nuclear Medicine 2000;41(5):157P.
213. Santana C, Soler M, Cooke C, et al. Determination of left ventricular ejection fraction (LVEF) from ECG-gated FDG PET studies: validation with contrast ventriculography [abstract]. Journal of Nuclear Medicine 2000;41(5):163P.
214. deKemp R, Van Kriekinge S, Germano G, Aung M, Ruddy T, Beanlands R. LV ejection fraction with gated FDG studies on a partial-ring PET scanner [abstract]. Journal of Nuclear Medicine 2000;41(5):88P.
215. Shen R, Shi R, Liu X, et al. Evaluation of left-ventricular ejection fraction by Tc-99m-MIBI/F-18-FDG gated myocardial tomography with dual isotope simultaneous acquisition [abstract]. Journal of Nuclear Cardiology 2001;8(1):S18.
216. Kanayama S, Matsunari I, Yoneyama T, Matsudaira M, Hisada K, Takekoshi N. ECG gated FDG and Tc-perfusion SPECT in normals: comparison with cine MRI [abstract]. Journal of Nuclear Cardiology 2001;8(1):S75.
217. Block S, Schaefer W, Nowak B, et al. Comparison of left ventricular ejection fraction calculated by EGG-gated PET and contrast left ventriculography [abstract]. Journal of Nuclear Medicine 2001;42(5):169P.
218. Matsunari I, Kanayama S, Yoneyama T, et al. Comparison between gated Tc-99m-MIBI and 18F-FDG SPECT for the measurement of left ventricular function [abstract]. Journal of Nuclear Medicine 2002;43(5):191P.
219. Schaefer WM, Lipke CSA, Nowak B, et al. Validation of an evaluation routine for left ventricular volumes, ejection fraction and wall motion from gated cardiac FDG PET: a comparison with cardiac magnetic resonance imaging.

European Journal of Nuclear Medicine and Molecular Imaging 2003;30(4):545–553.
220. Takahashi N, Inoue T, Yamakawa Y, Umemura S. Clinical usefulness of ECG gated 18 F-FDG PET for estimating myocardial viability and function [abstract]. Journal of Nuclear Medicine 2003;44(5):7P.
221. Nowak B, Sinha AM, Schaefer WM, et al. Cardiac resynchronization therapy homogenizes myocardial glucose metabolism and perfusion in dilated cardiomyopathy and left bundle branch block. Journal of the American College of Cardiology 2003;41(9):1523–1528.
222. Saab G, deKemp RA, Ukkonen H, Ruddy TD, Germano G, Beanlands RSB. Gated fluorine 18 fluorodeoxyglucose positron emission tomography: determination of global and regional left ventricular function and myocardial tissue characterization. Journal of Nuclear Cardiology 2003;10(3):297–303.
223. Muylle K, Franken P, Van Hove C, Everaert H, Bossuyt A. Left ventricular function measured by QGS algorithm from 18FDG gated PET heart studies [abstract]. European Journal of Nuclear Medicine 2003;30(Suppl 2):S261.
224. Schaefer WM, Lipke CSA, Nowak B, et al. Validation of QGS and 4D-MSPECT for quantification of left ventricular volumes and ejection fraction from gated F-18-FDG PET: comparison with cardiac MRI. Journal of Nuclear Medicine 2004;45(1):74–79.
225. Slart R, Bax JJ, de Jong RM, et al. Comparison of gated PET with MRI for evaluation of left ventricular function in patients with coronary artery disease. Journal of Nuclear Medicine 2004;45(2):176–182.
226. Kanayama S, Matsunari I, Hirayama A, Kitayama M, Matsui S, Takekoshi N. Automatic quantitation of left ventricular volumes, and ejection fraction by ECG-gated N-13-ammonia PET in patients with coronary artery disease [abstract]. Journal of Nuclear Medicine 2002;43(5):187P.
227. Kanajama S, Matsunari I, Hirayama A, et al. Global and regional left ventricular function assessed by ECG gated N-13 ammonia PET in patients with coronary artery disease [abstract]. Journal of Nuclear Cardiology 2003;10(1):S79.
228. Matsunari I, Kanayama S, Yoneyama T, et al. ECG-gated N-13 Ammonia PET to assess global and regional left ventricular function in patients with myocardial infarction: comparison with MRI [abstract]. Journal of Nuclear Medicine 2003;44(5):85P.
229. Rajappan K, Livieratos L, Camici PG, Pennell DJ. Measurement of ventricular volumes and function: A comparison of gated PET and cardiovascular magnetic resonance. Journal of Nuclear Medicine 2002;43(6):806–810.
230. Santana C, Folks R, Cooke C, Faber T, Garcia E. Rubidium-82 myocardial perfusion PET: development and validation of combined normal limits [abstract]. Journal of Nuclear Cardiology 2001;8(4):S134.
231. Cullom SJ, Meyer AF, Case JA, McGhie IA, Bateman TM. Preliminary evaluation of LSO-based PET for ECG-gating of rest/stress Rb-82 perfusion studies [abstract]. Journal of Nuclear Medicine 2002;43(5):197P.
232. Case J, Cullom S, Bateman T, Saunders M, Moutray K. Reproducibility of left ventricular function measurements using ECG gated Rb-82 cardiac PET imaging [abstract]. Journal of Nuclear Cardiology 2003;10(1):S80.
233. Case J, Bateman T, Moser K, Cullom S, Herstenstein G. Comparison of LVEF measurements from ECG-gated Rb-82 myocardial perfusion PET and Tc-99m sestamibi myocardial perfusion SPECT [abstract]. Journal of Nuclear Cardiology 2003;10(4):S13.
234. Almeida O, Machac J, Travis J, et al. Measurement of left ventricular ejection fraction with gated cardiac Rubidium-82 positron emission Tomography [abstract]. Journal of Nuclear Medicine 2004;45(5):224P.
235. Mazzanti M, Germano G, Kiat H, et al. Identification of severe and extensive coronary artery disease by automatic measurement of transient ischemic dilation of the left ventricle in dual-isotope myocardial perfusion SPECT. Journal of the American College of Cardiology 1996;27(7):1612–2160.
236. Yao S, Chandra P, Cohen R, Nichols K, DePuey E, Rozanski A. Factors influencing resting left ventricular ejection fraction measurements by technetium-99m sestamibi myocardial perfusion gated SPECT [abstract]. Journal of Nuclear Medicine 1998;39(5):45P.
237. De Nardo D, Caretta Q, Mercanti C, et al. Effects of uncomplicated coronary artery bypass graft surgery on global and regional left ventricular function at rest. Study by equilibrium radionuclide angiocardiography. Cardiology 1989;76(4):285–292.
238. Canclini S, Rossini P, Terzi A, et al. Gated SPECT (GSPECT) evaluation of septal wall motion after cardiac surgery [abstract]. Journal of Nuclear Medicine 2000;41(5):125P.
239. Imran MB, Morita K, Adachi I, et al. Comparison between segmental wall motion and wall thickening in patients with coronary artery disease using quantitative gated SPECT software. International Journal of Cardiac Imaging 2000;16(4):283–291.
240. Younis G, Fares M, Shea R, Udelson J. Septal asynchrony by gated SPECT imaging: correlation with perfusion, function, and clinical data [abstract]. Journal of Nuclear Cardiology 2001;8(4):S135.
241. Taki J, Higuchi T, Nakajima K, et al. Electrocardiographic gated Tc-99m-MIBI SPECT for functional assessment of patients after coronary artery bypass surgery: comparison of wall thickening and wall motion analysis. Journal of Nuclear Medicine 2002;43(5):589–595.
242. Nichols K, Cooke C, Faber T, Garcia E, Kamran M, DePuey E. Detection of cardiac torque from gated myocardial perfusion tomograms [abstract]. Journal of Nuclear Medicine 2000;41(5):45P.
243. Perman WH, Creswell LL, Wyers SG, Moulton MJ, Pasque MK. Hybrid DANTE and phase-contrast imaging technique for measurement of three-dimensional myocardial wall motion. Journal of Magnetic Resonance Imaging 1995;5(1):101–106.
244. Nichols K, Kamran M, Cooke D, et al. Cardiac torque quantified from myocardial perfusion gated SPECT [abstract]. Circulation 2000;102(18):II-724–725.
245. Nichols K, Kamran M, Cooke CD, et al. Feasibility of detecting cardiac torsion in myocardial perfusion gated

SPECT data. Journal of Nuclear Cardiology 2002;9(5):500–507.
246. Mirro MJ, Rogers EW, Weyman AE, Feigenbaum H. Angular displacement of the papillary muscles during the cardiac cycle. Circulation 1979;60(2):327–333.
247. Cooke C, Garcia E, Folks R, Ziffer J. Myocardial thickening and phase analysis from Tc-99m sestamibi multiple gated SPECT: development of normal limits [abstract]. Journal of Nuclear Medicine 1992;33(5):926–927.
248. Shirakawa S, Hattori N, Tamaki N, et al. Assessment of left ventricular wall thickening with gated ^{99m}Tc-MIBI SPECT–value of normal file. Kaku Igaku 1995;32(7):643–650.
249. Itoh Y, Adachi I, Kohya T, et al. Heterogeneity in myocardial perfusion, wall motion and wall thickening with Tc-99m-sestamibi quantitative gated SPECT in normal subjects [abstract]. Journal of Nuclear Medicine 1999;40(5):165P.
250. Adachi I, Morita K, Imran MB, et al. Heterogeneity of myocardial wall motion and thickening in the left ventricle evaluated with quantitative gated SPECT. Journal of Nuclear Cardiology 2000;7(4):296–300.
251. Chua T, Lee CY, Keng F, Ding ZP, Lim YL. Automated quantitation of regional function by gated perfusion tomography: determination of a normal range and correlation with echocardiography for detection of abnormal wall motion [abstract]. Journal of the American College of Cardiology 2001;37(2):393A–394A.
252. Sharir T, Berman DS, Waechter PB, et al. Quantitative analysis of regional motion and thickening by gated myocardial perfusion SPECT: normal heterogeneity and criteria for abnormality. Journal of Nuclear Medicine 2001;42(11):1630–1638.
253. Grossman G, Folks R, Faber T, Halkar R, Cooke C, Garcia E. Normal limits of systolic wall thickening in gated myocardial perfusion studies [abstract]. Journal of Nuclear Medicine 2003;44(5):86P.
254. Haendchen RV, Wyatt HL, Maurer G, et al. Quantitation of regional cardiac function by two-dimensional echocardiography. I. Patterns of contraction in the normal left ventricle. Circulation 1983;67(6):1234–1245.
255. Pandian NG, Skorton DJ, Collins SM, Falsetti HL, Burke ER, Kerber RE. Heterogeneity of left ventricular segmental wall thickening and excursion in 2-dimensional echocardiograms of normal human subjects. American Journal of Cardiology 1983;51(10):1667–1673.
256. Fisher MR, von Schulthess GK, Higgins CB. Multiphasic cardiac magnetic resonance imaging: normal regional left ventricular wall thickening. American Journal of Roentgenology 1985;145(1):27–30.
257. Sechtem U, Sommerhoff BA, Markiewicz W, White RD, Cheitlin MD, Higgins CB. Regional left ventricular wall thickening by magnetic resonance imaging: evaluation in normal persons and patients with global and regional dysfunction. American Journal of Cardiology 1987;59(1):145–151.
258. Moore CC, Lugo-Olivieri CH, McVeigh ER, Zerhouni EA. Three-dimensional systolic strain patterns in the normal human left ventricle: characterization with tagged MR imaging. Radiology 2000;214(2):453–466.
259. Kramer U, Miller S, Helber U, et al. Variability in the MR tomographic determination of myocardial function and perfusion parameters in healthy subjects. Rofo-Fortschritte Auf Dem Gebiet Der Rontgenstrahlen Und Der Bildgebenden Verfahren 2000;172(7):609–614.
260. Young AA, Axel L. 3-Dimensional motion and deformation of the heart wall – estimation with spatial modulation of magnetization – a model-based approach. Radiology 1992;185(1):241–247.
261. Beyar R, Weiss JL, Shapiro EP, Graves WL, Rogers WJ, Weisfeldt ML. Small apex-to-base heterogeneity in radius-to-thickness ratio by 3-dimensional magnetic-resonance-imaging. American Journal of Physiology 1993;264(1):H133–H140.
262. Corbett JR, Ficaro EP. Gated SPECT and the visual gold standard: gold standard or not? Invited commentary. Journal of Nuclear Medicine 2001;42(11):1639–1642.
263. Germano G, Berman D. Regional and global ventricular function and volumes from single-photon emission computed tomography perfusion imaging. In: Zaret BL, Beller GA, eds. Clinical Nuclear Cardiology. Mosby: Elsevier; 2005:189–211.
264. Van Train KF, Areeda J, Garcia EV, et al. Quantitative same-day rest-stress technetium-99m-sestamibi SPECT: definition and validation of stress normal limits and criteria for abnormality. Journal of Nuclear Medicine 1993;34(9):1494–1502.
265. Ficaro E, Kritzman J, Corbett J. Development and clinical validation of normal Tc-99m sestamibi database: comparison of 3D-MSPECT to CEqual [abstract]. Journal of Nuclear Medicine 1999;40(5):125P.
266. Germano G, Kavanagh PB, Waechter P, et al. A new algorithm for the quantitation of myocardial perfusion SPECT. I: technical principles and reproducibility. Journal of Nuclear Medicine 2000;41(4):712–719.
267. Kirac S, Wackers FJ, Liu YH. Validation of the Yale circumferential quantification method using ^{201}Tl and ^{99m}Tc: a phantom study. Journal of Nuclear Medicine 2000;41(8):1436–1441.
268. Grossman G, Folks R, Faber T, et al. Gender differences in normal limits of systolic wall thickening in SPECT myocardial perfusion studies [abstract]. Journal of Nuclear Cardiology 2003;10(4):S13.
269. Gunning MG, Anagnostopoulos C, Davies G, Forbat SM, Ell PJ, Underwood SR. Gated technetium-99m-tetrofosmin SPECT and cine MRI to assess left ventricular contraction. Journal of Nuclear Medicine 1997;38(3):438–442.
270. Chua T, Kiat H, Germano G, et al. Gated technetium-99m sestamibi for simultaneous assessment of stress myocardial perfusion, postexercise regional ventricular function and myocardial viability. Correlation with echocardiography and rest thallium-201 scintigraphy. Journal of the American College of Cardiology 1994;23(5):1107–1114.
271. Ficaro EP, Kritzman JN, Corbett JR. Automatic segmental scoring of myocardial wall thickening and motion: validation of a new semi-quantitative algorithm [abstract]. Journal of Nuclear Medicine 2001;42(5):171P.
272. Lee DS, Kim KM, Kim SK, et al. Development of a method for measuring myocardial contractility with gated myocardial

SPECT and arterial tonometry. Journal of Nuclear Cardiology 1999;6(6):657–663.
273. Slomka PJ, Nishina H, Berman DS, et al. Automatic quantification of myocardial perfusion stress-rest change: a new measure of ischemia. Journal of Nuclear Medicine 2004;45(2):183–191.
274. De Winter O, De Bondt P, Van De Wiele C, De Backer G, Dierckx RA, De Sutter J. Day-to-day variability of global left ventricular functional and perfusional measurements by quantitative gated SPECT using Tc-99m tetrofosmin in patients with heart failure due to coronary artery disease. Journal of Nuclear Cardiology 2004;11(1):47–52.
275. Hoffmann R, Lethen H, Marwick T, et al. Analysis of interinstitutional observer agreement in interpretation of dobutamine stress echocardiograms. Journal of the American College of Cardiology 1996;27(2):330–336.
276. Cheon G, Lee D, Kim S, et al. Evaluation of improvement of myocardial perfusion and function after "off-pump" coronary artery bypass graft surgery by gated myocardial SPECT [abstract]. Journal of Nuclear Medicine 1999;40(5): 163P.
277. Giubbini R, Rossini PL, Fallanca F, et al. Sestamibi gated spect for monitoring the effects of revascularization in patients with previous myocardial infarction [abstract]. European Journal of Nuclear Medicine 1999;26(9):1060.
278. Higuchi T, Taki J, Nakajima K, et al. Assessment of global and septal function after uncomplicated coronary artery bypass surgery by gated myocardial SPECT [abstract]. European Journal of Nuclear Medicine 1999;26(9):961.
279. Nakajima T, Imai K, Azuma Y, et al. Follow-up of regional left ventricular function in patients with acute myocardial infarction by quantitative gated SPECT (QGS) [abstract]. Journal of Nuclear Cardiology 1999;6(1, Pt 2):S60.
280. Tanaka R, Nakamura T. Serial evaluation of myocardial blood flow and cardiac function using Tc-99m tetrofosmin gated SPECT before and after reperfusion therapy in patients with acute myocardial infarction [abstract]. Journal of Nuclear Medicine 2001;42(5):166P–167P.
281. Nakajima T, Nagaoka Y, Handa S, Suzuki Y. Assessment of the reverse remodeling effect of beta-blocker in chronic heart failure by LV volumes obtained from the quantitative gated SPECT using ^{99m}Tc-tetrofosmin [abstract]. Journal of Nuclear Cardiology 2001;8(1):S24.
282. De Sutter JH, De Winter O, Tavernier R, De Bondt P, Van de Wiele C, Dierckx RA. Adverse left ventricular remodeling assessed by tetrofosmin gated SPET in patients with life-threatening ventricular arrhythmias late after myocardial infarction [abstract]. Journal of Nuclear Medicine 2001;42(5):1P.
283. Kasama S, Toyama T, Kumakura H, et al. Myocardial contractile reserve determined by dobutamine stress Tc-99m tetrofosmin quantitative gated SPECT predicts late spontaneous improvement in cardiac function in patients with recent-onset dilated cardiomyopathy. Journal of Nuclear Cardiology 2003;10(6):607–614.
284. Ban K, Nakajima T, Nagaoka M, Suzuki Y, Tanabe T, Handa S. Assessment of the long-term effects of beta-blocker in chronic heart failure by LV volumes and functions obtained from QGS using ^{99m}Tc tetrofosmin SPECT [abstract]. Journal of Nuclear Cardiology 2003;10(1):S67.
285. Sciagra R, Giaccardi M, Porciani MC, et al. Myocardial perfusion imaging using gated SPECT in heart failure patients undergoing cardiac resynchronization therapy. Journal of Nuclear Medicine 2004;45(2):164–168.
286. Bateman T, Case J, Moutray K, Cullom S, O'Keefe J. Is there clinical value in measuring LVEF both post-stress and at rest during ECG-gated myocardial perfusion SPECT scintigraphy? [abstract] Journal of the American College of Cardiology 1999;33(2, Suppl A):482A–483A.
287. Hashimoto J, Kubo A, Iwasaki R, et al. Gated single-photon emission tomography imaging protocol to evaluate myocardial stunning after exercise. European Journal of Nuclear Medicine 1999;26(12):1541–1546.
288. Imai K, Nakajima T, Azuma Y, et al. Presence of stunning after stress test, evaluated by myocardial perfusion imaging with quantitative gated SPECT (QGS) [abstract]. Journal of Nuclear Cardiology 1999;6(1, Pt 2):S38.
289. Camilletti J, Campisi R, Glezer L, Mele A. Abnormal response of post-stress left-ventricular ejection fraction in patients with inducible ischaemia [abstract]. Journal of Nuclear Cardiology 2001;8(1):S39.
290. Cho I, Chun K, Won K, et al. Comparison of left ventricular function at post-stress with left ventricular function at rest in patients with an acute myocardial infarction: evaluation with gated SPECT [abstract]. Journal of Nuclear Cardiology 2001;8(1):S106.
291. Furuyama H, Iwado Y, Yoshinaga K, et al. Transient LV dysfunction in ischemic myocardium due to post-exercise stunning not subendocardial hypoperfusion. Comparative study with exercise and pharmacological stress gated myocardial SPECT [abstract]. Journal of Nuclear Medicine 2001;42(5):179P.
292. Itti E, Levy M, Pouillart F, Perez T, Rosso J, Meignan M. Evolution of Tl-201 gated SPECT ejection fraction from rest to stress in patients with myocardial infarction [abstract]. Journal of Nuclear Medicine 2001;42(5):178P.
293. Heiba SI, Santiago J, Mirzaitehrane M, Jana S, Dede F, Abdel-Dayem HM. Transient postischemic stunning evaluation by stress gated Tl- 201SPECT myocardial imaging: effect on systolic left ventricular function. Journal of Nuclear Cardiology 2002;9(5):482–490.
294. Hickman M, Jeetley P, Sabharwal N, et al. Extent of reversible myocardial perfusion abnormality determines the degree of post ischaemic stunning [abstract]. Journal of Nuclear Cardiology 2003;10(1):S39.
295. Mazzanti M, Cianci G, Carini G, et al. Post exercise regional and global myocardial stunning after gated SPECT in asymptomatic subjects with increased absolute cardiovascular risk (NIDOT Project) [abstract]. Journal of Nuclear Cardiology 2003;10(1):S12.
296. Verberne HJ, Dijkgraaf MGW, Somsen GA, van Eck-Smit BLF. Stress-related variations in left ventricular function as assessed with gated myocardial perfusion SPECT. Journal of Nuclear Cardiology 2003;10(5):456–463.
297. Arai Y, Mizuno S, Ohsato K, et al. Dypiridamole induced stunning continues for at least one hour in patients with

coronary artery disease: evaluation with quantitative gated SPECT [abstract]. Journal of Nuclear Cardiology 1999; 6(1,Pt 2):S47.
298. Garcia-Burillo A, Canela T, Cordero JA, Richart JA, Palleres C, Roca I. Measurement of left ventricular ejection fraction (EF) by means of exercise and rest GATED-SPET ^{99m}Tc-tetrofosmin [abstract]. European Journal of Nuclear Medicine 1999;26(9):1066.
299. Roelants V, Rombaut E, Marchandise B, et al. New insight for the post-dobutamine left ventricular function evaluated by gated sestamibi perfusion SPECT [abstract]. Journal of Nuclear Medicine 1999;40(5):169P.
300. Lee DS, Yeo JS, Chung JK, Lee MM, Lee MC. Transient prolonged stunning induced by dipyridamole and shown on 1- and 24-hour poststress ^{99m}Tc-MIBI gated SPECT. Journal of Nuclear Medicine 2000;41(1):27–35.
301. Chun KA, Cho IH, Won KJ, et al. Pharmacologic stress-induced stunning: evaluation with quantitative gated SPECT [abstract]. Journal of Nuclear Medicine 2001;42(5): 95P.
302. Beretta M, Rener A, Vidal I, et al. Demonstration of myocardial stunning after dipyridamole stress test with gated perfusion SPECT [abstract]. Journal of Nuclear Cardiology 2001;8(1):S77.
303. Abidov A, Berman DS. Transient ischemic dilation associated with poststress myocardial stunning of the left ventricle in vasodilator stress myocardial perfusion SPECT: true marker of severe ischemia? Journal of Nuclear Cardiology 2005;12(3):258–260.
304. Hung GU, Lee KW, Chen CP, Lin WY, Yang KT. Relationship of transient ischemic dilation in dipyridamole myocardial perfusion imaging and stress-induced changes of functional parameters evaluated by Tl-201 gated SPECT. Journal of Nuclear Cardiology 2005;12(3):268–275.
305. Bonow RO. Gated myocardial perfusion imaging for measuring left ventricular function [editorial; comment]. Journal of the American College of Cardiology 1997;30(7):1649–1650.
306. Alexanderson E, Lorenzo A, Unzek S, Rubinstein J, Bialostozky D. Influence of myocardial ischemia over ventricular function evaluated with GATED SPECT [abstract]. Journal of Nuclear Medicine 2001;42(5):170P.
307. Toba M, Kumita S, Cho K, et al. Temporal changes of cardiac function after exercise stress assessed by gated myocardial perfusion SPECT [abstract]. Journal of Nuclear Cardiology 2003;10(1):S19.
308. Toba M, Kumita S, Cho K, Ibuki C, Kumazaki T, Takano T. Usefulness of gated myocardial perfusion SPECT imaging soon after exercise to identify postexercise stunning in patients with single-vessel coronary artery disease. Journal of Nuclear Cardiology 2004;11(6):697–703.
309. Bestetti A, Alessi A, Triulzi A, di Leo C, Tagliabue L, tarolo G. The stunning phenomenon assessed by gated SPECT in CAD patients with fixed perfusion defects [abstract]. Journal of Nuclear Cardiology 2001;8(1):S105.
310. Abidov A, Hayes S, Friedman J, et al. Ischemic stunning and transient ischemic dilation are important diagnostic markers of significant CAD in patients with normal myocardial perfusion SPECT [abstract]. Journal of Nuclear Medicine 2003;44(5):3P.
311. Sharir T, Bacher-Stier C, Dhar S, et al. Identification of severe and extensive coronary artery disease by post-exercise regional wall station abnormalities in Tc-99m sestamibi gated single-photon emission computed tomography. American Journal of Cardiology 2000;86(11):1171–1175.
312. Emmett L, Iwanochko RM, Freeman MR, Barolet A, Lee DS, Husain M. Reversible regional wall motion abnormalities on exercise technetium-99m-gated cardiac single photon emission computed tomography predict high-grade angiographic stenoses. Journal of the American College of Cardiology 2002;39(6):991–998.
313. Petix N, Sestini S, Marcucci G, et al. Can the reversible regional wall motion abnormalities on stress gated Tc-99m sestamibi SPECT predict a future cardiac event? Journal of Nuclear Cardiology 2005;12(1):20–31.
314. Paul AK, Hasegawa S, Yoshioka J, et al. Characteristics of regional myocardial stunning after exercise in gated myocardial SPECT. Journal of Nuclear Cardiology 2002;9(4):388–394.
315. Sharir T. Role of regional myocardial dysfunction by gated myocardial perfusion SPECT in the prognostic evaluation of patients with coronary artery disease [editorial]. Journal of Nuclear Cardiology 2005;12(1):5–8.
316. Kawasaki T, Sakatani T, Mani H, Kamitani T, Kawasaki S, Sugihara H. Systolic and diastolic stunning 30 min after exercise in patients with angina pectoris: evaluation with gated Tc-99m-tetrofosmin SPECT [abstract]. European Journal of Nuclear Medicine 2001;28(8):PS361.
317. Homans DC, Sublett E, Dai XZ, Bache RJ. Persistence of regional left ventricular dysfunction after exercise-induced myocardial ischemia. Journal of Clinical Investigation 1986;77(1):66–73.
318. Ambrosio G, Betocchi S, Pace L, et al. Prolonged impairment of regional contractile function after resolution of exercise-induced angina – evidence of myocardial stunning in patients with coronary artery disease. Circulation 1996;94(10): 2455–2464.
319. Kloner RA, Jennings RB. Consequences of brief ischemia: stunning, preconditioning, and their clinical implications. Circulation 2001;104(25, Pt 2):3158–3167.
320. Kloner RA, Jennings RB. Consequences of brief ischemia: stunning, preconditioning, and their clinical implications. Circulation 2001;104(24, Pt 1):2981–2989.
321. Druz RS, Akinboboye OA, Grimson R, Nichols KJ, Reichek N. Postischemic stunning after adenosine vasodilator stress. Journal of Nuclear Cardiology 2004;11(5):534–541.
322. Haidar M, Daou D, Gharzeddine L, Sarda L, Lebtahi R, Le Guludec D. Impact of time to imaging on the detection of left ventricular dysfunction with stress ^{201}TI gated SPECT [abstract]. European Journal of Nuclear Medicine 2002;29(Suppl 1):S130.
323. Taillefer R, Cohade C, Gagnon A, Lajeunesse S, Benjamin C. Is the left ventricle post-stress stunning a frequent finding on gated SPECT (GS) myocardial perfusion imaging? [abstract] Journal of Nuclear Medicine 2000;41(5):6P.

324. De Winter O, De Sutter JH, Van de Wiele C, De Bondt P, De Winter F, Dierckx RA. How frequent is a decrease of left ventricular ejection fraction post bicycle stress measured by gated SPET: results from a European single-centre prospective database [abstract]. Journal of Nuclear Medicine 2001;42(5):176P–177P.
325. Sias T, Calnon D, Beller G, Watson D. Comparison of two algorithms for calculation of left ventricular ejection fraction using gated single photon emission tomography (SPECT) myocardial perfusion images [abstract]. Journal of the American College of Cardiology 1999;33(2, Suppl A):436A.
326. Nichols K, Folks R, Cooke D, Faber T, Garcia E. Comparisons between "ECTb" and "QGS" software to compute left ventricular function from myocardial perfusion gated SPECT data [abstract]. Journal of Nuclear Cardiology 2000;7(4):S20.
327. Nichols K, Santana CA, Folks R, et al. Comparison between ECTb and QGS for assessment of left ventricular function from gated myocardial perfusion SPECT. Journal of Nuclear Cardiology 2002;9(3):285–293.
328. Lewis T, Grewal K, Calnon D. Discrepancies in estimating left-ventricular volumes and ejection fraction by two commercially available gated SPECT algorithms: comparison to echocardiography [abstract]. Journal of Nuclear Cardiology 2001;8(1):S18.
329. Dede F, Narin Y. Can different software programs give the same functional measurements in ECG gated SPECT: comparison of two software programs [abstract]. European Journal of Nuclear Medicine 2002;29(Suppl 1):S209.
330. Liu Y, Harrell C, Tsatkin V, et al. Evaluation of a new quantification method for gated SPECT imaging: comparison with the quantitative gated SPECT (QGS) method in patients [abstract]. Journal of Nuclear Cardiology 2001;8(1):S65.
331. Boussaha MR, Storto G, Antonescu C, Delaloye AB. Ejection fraction evaluation by gated myocardial perfusion SPECT: comparison between gated SPECT quantification (GSQ) and emory cardiac tool box (ECTB) [abstract]. European Journal of Nuclear Medicine 2001;28(8):OS240.
332. Sharir T, Germano G, Waechter PB, et al. A new algorithm for the quantitation of myocardial perfusion SPECT. II: validation and diagnostic yield. Journal of Nuclear Medicine 2000;41(4):720–727.
333. Hachamovitch R, Berman DS, Kiat H, et al. Exercise myocardial perfusion SPECT in patients without known coronary artery disease: incremental prognostic value and use in risk stratification. Circulation 1996;93(5):905–914.
334. Hachamovitch R, Berman DS, Kiat H, et al. Effective risk stratification using exercise myocardial perfusion SPECT in women: gender-related differences in prognostic nuclear testing. Journal of the American College of Cardiology 1996;28(1):34–44.
335. Berman D, Abidov A, Kang X, et al. Prognostic validation of a 17-segment score derived from a 20-segment score for myocardial perfusion SPECT interpretation. Journal of Nuclear Cardiology 2004;11(4):414–423.
336. Bacher-Stier C, Sharir T, Kavanagh PB, et al. Postexercise lung uptake of ^{99m}Tc-sestamibi determined by a new automatic technique: validation and application in detection of severe and extensive coronary artery disease and reduced left ventricular function. Journal of Nuclear Medicine 2000;41(7):1190–1197.
337. Akimboboye O, Germano G, Idris O, et al. Estimation of left ventricular mass by gated SPECT: comparison with 3D echocardiography [abstract]. Journal of Nuclear Cardiology 1999;6(1, Pt 2):S38.
338. Mochizuki T, Murase K, Tanaka H, Kondoh T, Hamamoto K, Tauxe WN. Assessment of left ventricular volume using ECG-gated SPECT with technetium-99m-MIBI and technetium-99m-tetrofosmin. Journal of Nuclear Medicine 1997;38(1):53–57.
339. Germano G, Kavanagh PB, Berman DS. An automatic approach to the analysis, quantitation and review of perfusion and function from myocardial perfusion SPECT images. International Journal of Cardiac Imaging 1997;13(4):337–346.
340. Homma S, Kaul S, Boucher CA. Correlates of lung/heart ratio of thallium-201 in coronary artery disease. Journal of Nuclear Medicine 1987;28(10):1531–1535.
341. Hansen CL, Sangrigoli R, Nkadi E, Kramer M. Comparison of pulmonary uptake with transient cavity dilation after exercise thallium-201 perfusion imaging. Journal of the American College of Cardiology 1999;33(5):1323–1327.
342. Daou D, Coaguila C, Delahaye N, Houzet F, Lebtahi R, Le Guludec D. Discordance between exercise SPECT lung TI-201 uptake and left ventricular transient ischemic dilation in patients with CAD. Journal of Nuclear Cardiology 2004;11(1):53–61.
343. Madison S, Dalipaj M, Ruddy T. Effects of gender and stress on transient ischemic dilation ratios in normals [abstract]. Journal of Nuclear Cardiology 2003;10(1):S85.
344. Kritzman JN, Ficaro EP, Corbett JR. Post-stress LV dilation: The effect of imaging protocol, gender and attenuation correction [abstract]. Journal of Nuclear Medicine 2001;42(5):50P.
345. Abidov A, Bax JJ, Hayes SW, et al. Transient ischemic dilation ratio of the left ventricle is a significant predictor of future cardiac events in patients with otherwise normal myocardial perfusion SPECT. Journal of the American College of Cardiology 2003;42(10):1818–1825.
346. Berman D, Hachamovitch R, Shaw L, Hayes S, Germano G. Nuclear cardiology. In: Fuster V, ed. Hurst's the Heart. 11th edn. New York: McGraw-Hill Medical Publication Division; 2004:563–597.
347. Bestetti A, Di Leo C, Alessi A, Tegliabue L, Tarolo GL. Transient left ventricular dilation during myocardial perfusion gated-SPECT in hypertensive patients [abstract]. European Journal of Nuclear Medicine 2001;28(8):OS239.
348. Manchikalapudi P, Biederman R, Doyle M, et al. Validation of left ventricular mass by SPECT sestamibi imaging [abstract]. Journal of Nuclear Cardiology 2000;7(4):S18.
349. Maruyama K, Hasegawa S, Mu X, et al. Assessment of left ventricular mass index by quantitative gated myocardial SPECT: comparison with echocardiography [abstract]. Journal of Nuclear Medicine 2000;41(5):153P.
350. Ahn BC, Lee J, Lee SW, Kwak DH, Chae SC, Lee KB. Left ventricular mass measured with quantitative gated myocardial perfusion SPECT: comparison with echocardiography [abstract]. Journal of Nuclear Medicine 2001;42(5):94P.

351. Lee J, Ahn B, Kim S, Song H, Bom H, Lee K. Measurement of left ventricular mass with gated myocardial SPECT in women without perfusion defects: comparison with echocardiography [abstract]. Journal of Nuclear Medicine 2002;43(5):177P.
352. Ahn B, Lee J, Lee S, Lee K, Bom K. Myocardial mass and functional parameters of left-ventricle (LV) measured with gated SPECT: comparison between stress and rest imaging in patients with no perfusion defect [abstract]. Journal of Nuclear Cardiology 2001;8(1):S12.
353. Faber T, Folks R, Cooke C, Vansant J, Pettigrew R, Garcia E. Left ventricular mass from ungated perfusion images: comparison with MRI [abstract]. Journal of Nuclear Medicine 1997;38(5):20P.

6 Interpretation and reporting of gated myocardial perfusion SPECT

Daniel S. Berman
Guido Germano

Introduction

A systematic approach to the interpretation of gated SPECT is essential to the optimal utilization of this modality. Since the assessments of perfusion and function are intimately related, this chapter will address the interpretation and reporting of the combination of perfusion and function in gated myocardial perfusion SPECT (MPS). The reader is directed to three key references in this regard: the Imaging Guidelines for Nuclear Cardiology Procedures Part 2 from the American Society of Nuclear Cardiology (ASNC) [1], the American Heart Association (AHA) Scientific Statement on Standardized Myocardial Segmentation and Nomenclature for Tomographic Imaging of the Heart [2], and the ASNC Consensus Statement: Reporting of Radionuclide Myocardial Perfusion Imaging Studies [3]. As with MPS in general, careful attention to all aspects of camera–computer system quality control is essential to ensure the adequacy of gated MPS studies. These quality control measures include verification of camera peaking, detector(s) uniformity, alignment, center of rotation, and closeness to the patient. With regard to the injected radiopharmaceuticals, care must be taken to document that the radiopharmaceutical tagging was appropriate, an adequate dose was injected, and no infiltration of radioactivity occurred. Although the routine technical aspects of quality control are often delegated to a technologist, the physician interpreting the studies must be aware of the quality control procedures in effect in the laboratory, so as to ensure the adequacy of those procedures.

Initial patient information

Due to the subjective nature of a scan interpretation, it is generally recommended that all scans first be interpreted without the knowledge of the patient's clinical state. It is important, however, to know the patient's height, weight, gender, and if female, bra size, in order to be able to best recognize possible soft tissue artifacts (see also Chapter 7). If the study is an exercise study, the exercise heart rate achieved (expressed both in beats per minute and as percent of the maximal predicted rate) and the exercise duration should be known. These factors are of particular help in avoiding overstatement of clinical interpretations based on normal results; for example, if the patient's achieved heart rate is less than 80% of the maximal predicted rate, a "normal" study must be interpreted as nondiagnostic with respect to the presence of coronary artery disease (CAD) or risk stratification [4]. In this regard, it should be noted that the most important heart rate is that achieved at the time of injection. Care should be taken to appropriately identify patients whose peak heart rate was adequate but in whom the radiopharmaceutical was injected at a premature point during exercise; for example, if a patient achieves 100% of maximal predicated heart rate (MPHR), but the tracer was injected at 70% of MPHR, a normal MPS study would be considered "nondiagnostic" for purposes of diagnosis or risk stratification of CAD.

Inspection of the raw projection data

The most important step in quality control of SPECT is the review of the raw data, consisting of the projection images prior to filtering and reconstruction. The most useful method for such a review is the endless loop "cinematic" display of the rotating projection images. Although the study has been acquired as a gated SPECT study, the summed or "ungated" projection images are displayed for this purpose (see Chapter 2).

General observations

The raw projection images should be inspected to ensure they were acquired over the appropriate acquisition arc (generally RAO 45° to LPO 45°) and to be certain that the

heart was completely within the field of view throughout the acquisition. Truncation, referring to having a part of the heart outside of the field of view, often results in artifactual perfusion defects. The raw images also provide useful information regarding count statistics. Studies in which the raw projection data reveal a subjectively poor count rate must be interpreted with caution, since inadequate count statistics can be a source of artifactual defects. In addition to overall assessment of count statistics, the reader should be considering the apparent count density in the individual projection images. Major variation in the count density of the images manifests itself as "flashing" of the cine display and is often related to gating error (see Chapter 2). When severe dropout or absence of counts is noted in one or more images resulting in marked "flashing," the acquisition should be repeated, if possible. If repeat imaging is not possible, interpretation should be made with great caution, since gating artifacts frequently result in underestimation of regional and global function and can even be a source of artifactual perfusion defects.

Patient motion

Inspection of the rotating projection images in a cine display provides a convenient and accurate method for detecting patient motion or "upward creep" of the heart [5]. Careful attention should be paid to patient motion in the vertical (craniocaudal) and lateral (horizontal) direction, since either can be associated with an artifactual defect that may go undetected by simple inspection of the tomographic slices. We employ a three-point score for motion, with 0 = no motion, 1 = slight motion, and 2 = moderate to severe motion [6]. In general, a score of 1 is insufficient to cause an artifactual defect, while a score of 2 is frequently associated with an artifactual defect [6]. Immediately after the image acquisition, the technologist should assess the raw data for motion and if moderate to severe motion is noted, the acquisition should be repeated. When slight (score of 1) motion is observed, the images might first be reconstructed. If a perfusion defect is present, consideration should be given to repeating the image acquisition. When acquisition is repeated, it is often preferable to perform it in the prone position, since this position is associated with less patient motion than the supine position [7] (see Chapter 3). Figure 6.1a illustrates an apparent perfusion defect in typical SPECT images reconstructed from projection images, corresponding to moderate (two-pixel, score = 2) motion on visual inspection. Figure 6.1b represents the reconstructed SPECT images from this same patient's study when the acquisition was repeated in the prone position. No motion was associated with the second acquisition, and the reconstructed images demonstrate no perfusion defect. If a validated motion correction algorithm is available, it could be applied to projection data sets in which motion is observed [8]. It should be noted, however, that motion correction does not work adequately with severe motion and frequently fails in lateral motion [8]. If motion correction is applied, both the uncorrected and the motion-corrected tomograms should be presented to the reading physician for interpretation. Importantly, the routine application of motion correction algorithms and presentation to the reader of only motion-corrected images is not recommended, since in unusual circumstances the application of the motion correction process could produce an artifactual defect.

Dual-detector 90° cameras

It is worthy of note that while most efficient from the standpoint of acquisition time [9], the dual-detector 90° configuration accentuates the problems associated with patient motion. In a 64-projection acquisition with a dual-detector 90° camera, 32 projections would be obtained by each detector. With most types of motion, the greatest difference between projections is noted between the first and last (1 and 32 for the first detector). Since the first projection of the first detector (projection 1) and the first of the second detector (projection 33) are acquired at the same time and with the patient in exactly the same position, if the patient moved at any time during the acquisition, the motion is usually most evident between projections 32 and 33. Unfortunately, this greatest discrepancy between data sets occurs in a portion of the acquisition which is highly sensitive to motion – at approximately a 45° LAO view of the heart, a view generally associated with relatively high myocardial count rates. Because of this problem, cameras with dual detectors oriented at 90° are more subject to motion artifacts than cameras with single detector or triple detectors, and require a higher degree of vigilance for motion (and perhaps a lower threshold for repeating the acquisition) than the other types of cameras. The accentuation of patient motion between frames 32 and 33 was responsible for the artifactual defect in the patient study presented in Fig. 6.1a.

Attenuation

As explained in detail in Chapter 7, inspection of the rotating projection images provides an opportunity for detecting sources of attenuation artifacts. In female patients, for example, the degree of breast attenuation can be estimated with reasonable accuracy by an experienced observer looking at the projection data. Special attention should be paid when comparing differing data sets (e.g., stress/rest, stress/redistribution, supine/prone) side by side in order

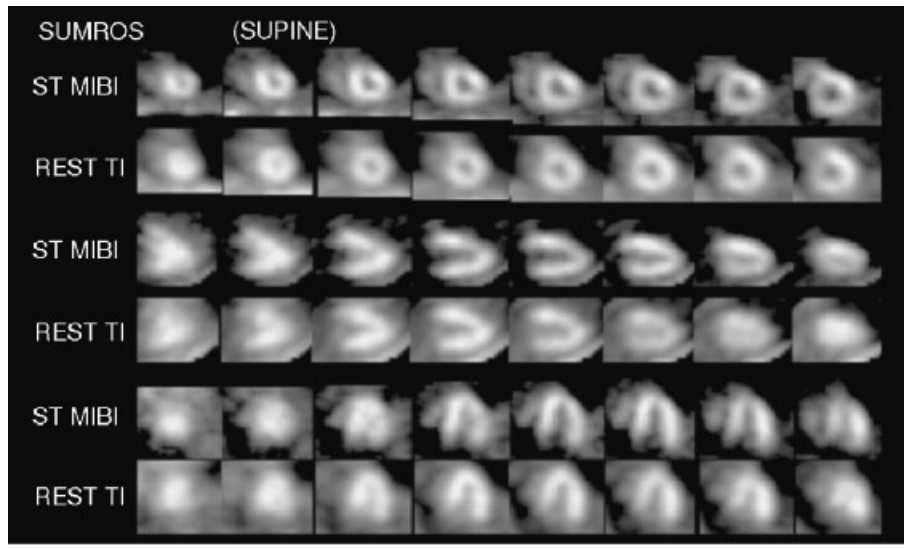

(a)

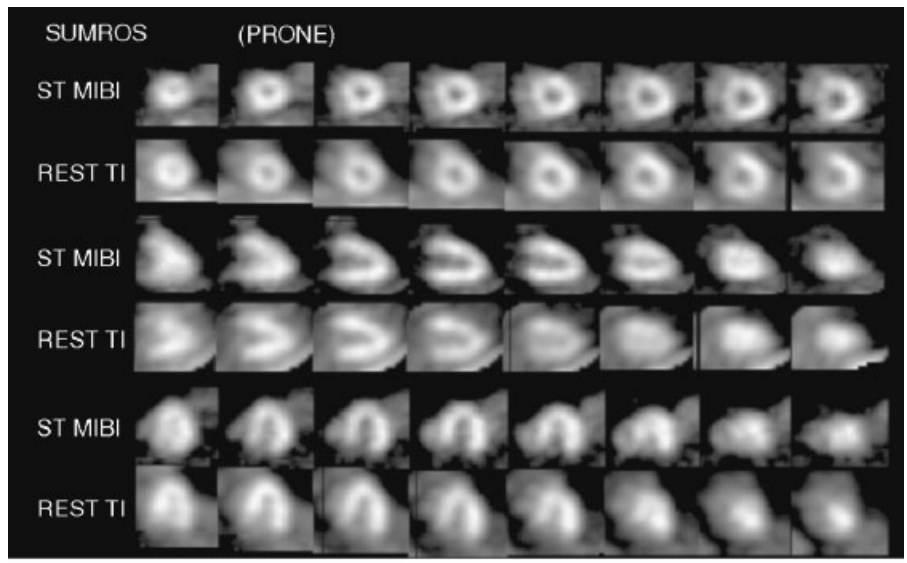

(b)

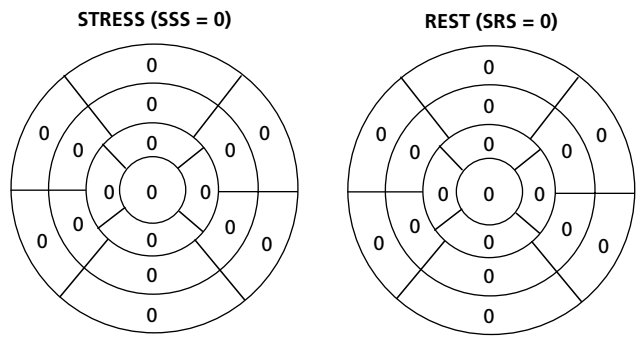

(c)

Figure 6.1 (a) Exercise Tc-99m sestamibi/rest thallium-201 MPS images in a 69-year-old female with multiple risk factors for CAD and an abnormal stress ECG, but no chest discomfort. An apparent perfusion defect is noted in the anterior and inferolateral left ventricular walls, suggestive of disease in the diagonal branch of the LAD coronary artery and the left circumflex coronary artery. Inspection of raw projection images, however, revealed evidence of marked patient motion (see part (b)). (b) Exercise Tc-99m sestamibi/rest thallium-201 MPS images obtained in the prone position at stress, in the same patient whose supine images were illustrated in part (a). In the prone position there was no evidence of motion on the raw projection images, and the study was deemed to be normal. The overall report of this study, based on the combined images, was that the scan was normal. The false suggestion of disease in the diagonal branch of the LAD and left circumflex was avoided by the use of prone imaging. (c) Polar map display of the five-point semiquantititave score assignment at stress (left) and rest (right) of the patient shown in parts (a) and (b). The score of zero in all segments defines a completely normal study. For the remainder of the chapter, these semiquantitative polar maps will be illustrated *only* when an abnormality is present.

to determine whether the position of the attenuating structure changed between acquisitions. Although artifactual attenuation perfusion defects are usually nonreversible on inspection of the tomographic slices, breast or other attenuation artifacts may appear to be reversible if the attenuating breast or other body part (e.g., arm) was in a different location on the two acquisitions. Other sources of attenuation artifacts observed with the help of the rotating image display include subdiaphragmatic structures and general body fat. Many of the attenuation artifacts can be appreciated by repeating the acquisition in the prone position [7] (Fig. 6.1b), since the location of the attenuating structure frequently shifts. Prone acquisition is particularly useful to minimize diaphragmatic attenuation, but also can be of help with general soft tissue attenuation and breast attenuation [35]. An example of supine/prone imaging's ability to clarify breast attenuation is also shown in Fig. 6.2.

Extra cardiac uptake

The raw projection data should also be examined for evidence of extra cardiac radioactivity uptake, perhaps the most important example of this occurring with occult

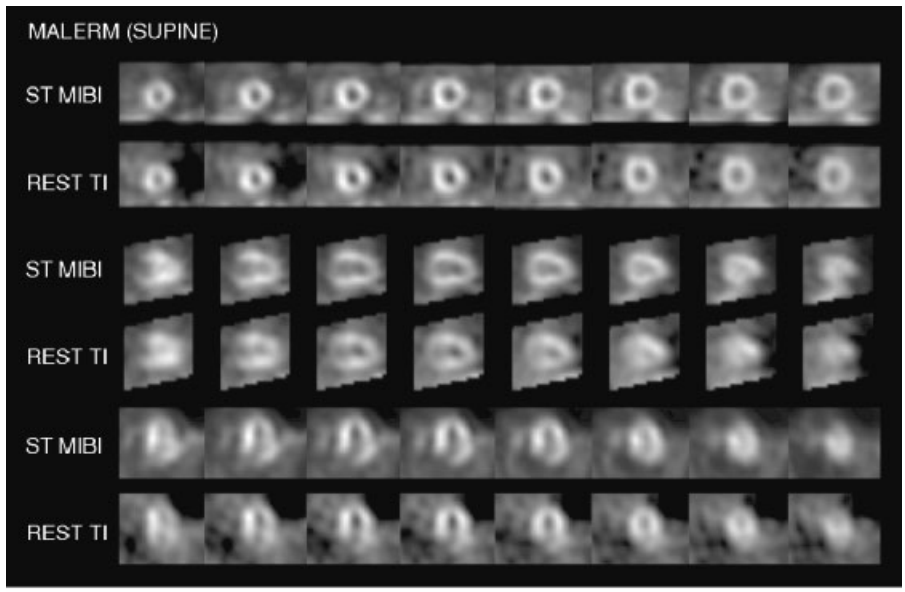

(a)

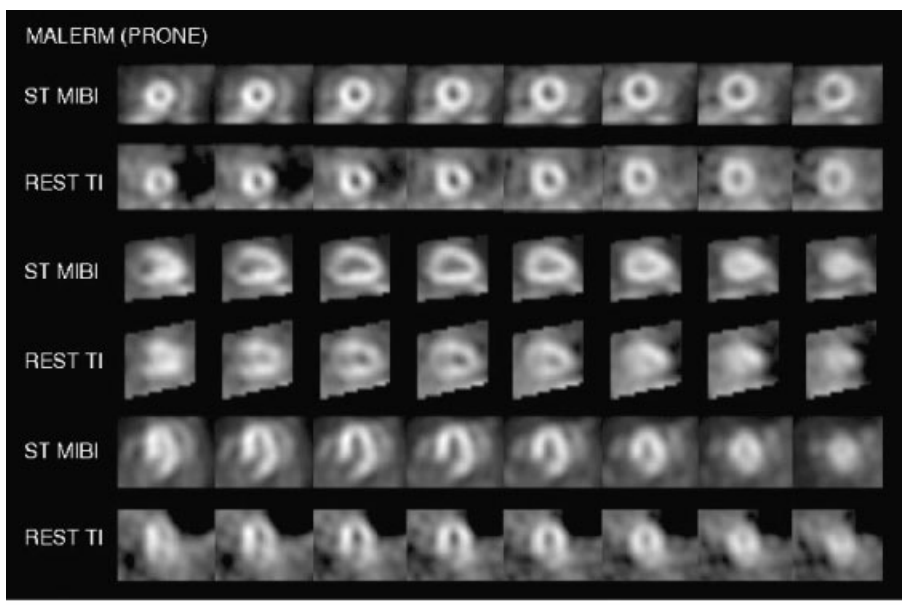

(b)

Figure 6.2 (a) Adenosine stress Tc-99m sestamibi/rest thallium-201 MPS images in an asymptomatic 69-year-old female with ischemic stress ECG. A small perfusion defect is noted in the anterior left ventricular walls on supine stress image. (b) Images obtained in the prone position after stress in the same patient whose supine stress images were illustrated in part (a). No defect was found. Based on the combined images, the scan result was normal. Instead of being consistent with disease in the diagonal branch of the LAD, the study was interpreted as normal and simply manifesting breast attenuation.

cancer. Given the reduced reliance on standard chest x-rays as routine procedures, it is not uncommon for the first evidence of cancer in the thorax to come from an incidental observation at the time of myocardial perfusion scintigraphy. Indeed, Tc-99m sestamibi and Tl-201 have been utilized for cancer detection as well as for myocardial perfusion imaging [10,11]. An example of a patient with previously undiagnosed cancer detected by the rotating projection images of a MPS study is shown in Fig. 6.3. Lung cancer, lymphoma, and breast cancer are the most common kinds of cancers detected through this approach. Often thyroid tissue, the liver, gall bladder, spleen, and kidneys are in the field of view, and should be inspected for possible abnormality.

Lung uptake

The degree of lung uptake of myocardial perfusion tracers should be noted from visual inspection of the raw projection images. Additionally, the lung/heart ratio can be quantified automatically or manually. Quantification is performed by placing two regions of interest over the most normal cardiac zone and a representative pulmonary region of an anterior or LAO 45° projection image, and determining the lung/heart ratio from the mean pixel counts in selected regions. Quantitative lung/heart ratios for Tl-201 have been reported to have an upper limit of normal of 0.54 [12–14], while for Tc-99m sestamibi, we have reported the upper limit of normal to be 0.44 [15]. Given the similar biodistributions of tetrofosmin and sestamibi, it is

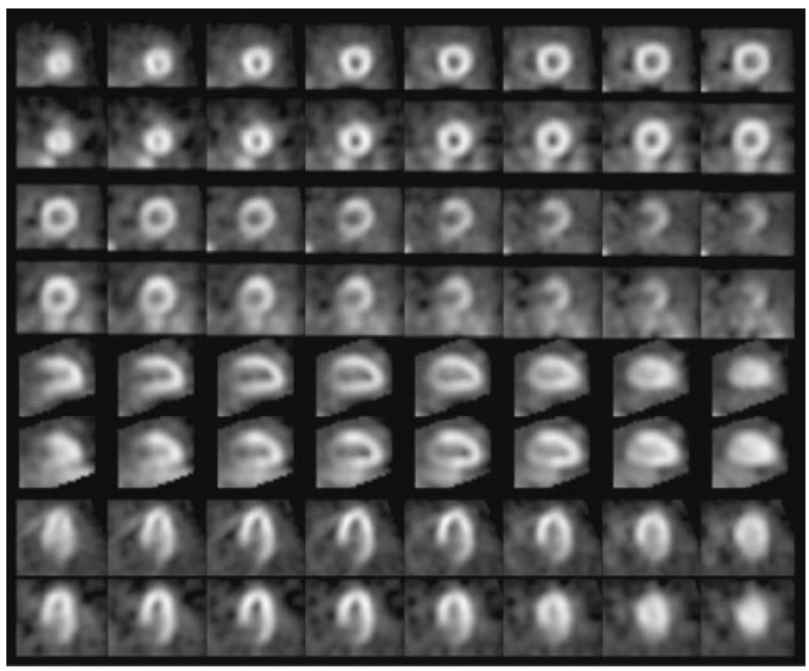

(a)

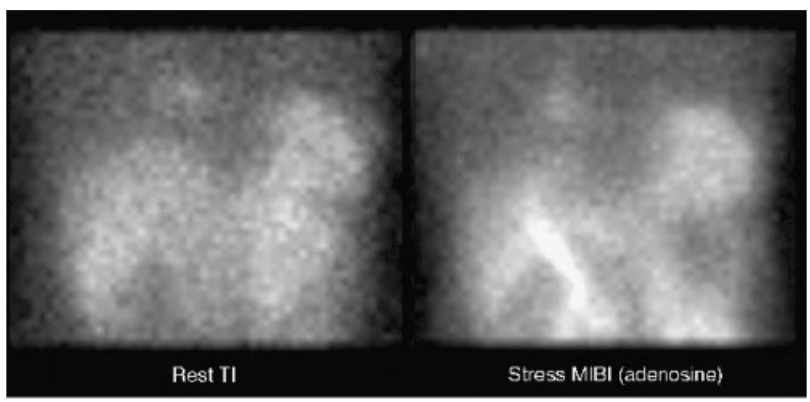

(b)

Figure 6.3 Adenosine stress Tc-99m sestamibi/rest thallium-201 MPS images in an 82-year-old female patient with breast cancer. The myocardial images are normal (a). Selected anterior view projection images from the rest thallium-201 (left) and stress sestamibi (right) study illustrated in part (b). The presence of focal increased uptake in the right breast is observed. Patient underwent mastectomy after diagnosis.

likely that the 0.44 ratio would also apply to tetrofosmin [16]. From a visual analysis standpoint, a four-point scale is recommended, with 0 = no lung uptake, 1 = mild (and probably insignificant) lung uptake, 2 = moderate lung uptake (clearly evident but not equal to that of the heart), and 3 = severe lung uptake (equal to or greater than cardiac uptake). In general, there is a strong linear correlation relationship between the degree of lung uptake and the pulmonary capillary wedge pressure at the time of injection [17,18]. Thus, increase in lung on rest scans uptake implies increased resting wedge pressure, and increased uptake on poststress scans suggests increased wedge pressure during stress. Diffuse inflammation of the lungs can cause increased lung uptake of the myocardial perfusion tracers without increase in wedge pressure, as might be seen in conditions such as sarcoidosis, pulmonary fibrosis, or even chronic smoking.

Hepatic/gastrointestinal uptake

The scan reader should be aware of the importance of the degree of tracer uptake in the liver and the gastrointestinal tract adjacent to the heart. If excessive, consideration should be given to repeating image acquisition after a delay of 1 hour (if Tc-99m sestamibi or tetrofosmin is used), or after having the patient drink a large amount of water to distend the stomach and displace the liver and bowel. As explained in Chapter 7, increased radioactivity in structures adjacent to the heart can be a source of artifacts on the reconstructed tomograms. In particular, either artifactual decrease in severity of true perfusion defects may occur (due to scatter from the adjacent "hot" source) or an artifactual myocardial perfusion defect may be created by the mathematics of the reconstruction process (cancellation of counts in regions immediately adjacent to "hot" objects) [19].

Assessment of myocardial perfusion from SPECT images

Display

Committees of the American Heart Association, American College of Cardiology, and Society of Nuclear Medicine have agreed to a uniform approach to SPECT image display, based on the reorientation of images (slices) relative to the axis of orientation of the heart in the chest [20]. The reoriented slices are termed the short-axis, vertical long-axis, and horizontal long-axis images. We recommend that the display used for analysis, whether on computer screen or transparency film, include all of these images. It is also recommended that images from different acquisitions (e.g. stress/rest, rest/redistribution, stress/redistribution) be appropriately aligned and displayed simultaneously in interleaved fashion. As for image normalization, there are two widely used approaches. Each series (short-axis, vertical long-axis, and horizontal long-axis images) can be normalized to the pixel with the highest count in the entire series (series normalization). This approach provides the most intuitively accurate assessment of the presence, extent, and severity of perfusion defects, although it presents the drawbacks of lack of ideal display for each individual slice, sensitivity to focal hot spots, and insensitivity to basal perfusion defects. Alternatively, each tomographic slice can be normalized to the brightest pixel within that slice ("frame normalization"). This approach provides ideal display of each individual slice, is less sensitive to the problem of basal attenuation, and is the approach that has been utilized for the last 15 years at Cedars-Sinai Medical Center. Comparison of frame normalization and series normalization for a normal stress/rest study is illustrated in Figs. 6.4 and 6.5.

Quality control

The short-and long-axis images should first be inspected for overall adequacy of counts, appropriateness of the axis chosen for reorientation, and slice selection. If the wrong axis of reorientation is chosen or slices are misaligned, artifactual defects (frequently reversible) can result. It is also important to note at this time whether all the slices are visualized. Although important, this step of the quality control is clearly secondary to the essential step of raw data review described above. We recommend including a comment regarding the overall quality of a study in the report. (e.g. 5 = excellent; 4 = good; 3 = fair; 2 = poor; 1 = uninterpretable)

Segmentation, nomenclature, and scoring

Segmentation

A writing group of AHA, with representation from the American College of Cardiology, ASNC, the American Society of Echocardiography, the Society for Cardiac Angiography and Intervention, and the North American Society of Cardiac Imaging – the principal North American societies dealing with cardiac imaging, has recommended the use of a standardized approach to segmentation and nomenclature for all tomographic cardiac imaging modalities [2]. Division of the heart into 17 segments for assessment of the left ventricular myocardium and the left ventricular cavity was recommended [2]. The 17-segment system was chosen over the 20-segment system, since it most closely represented the proportions of the left ventricle observed on autopsy examination. The

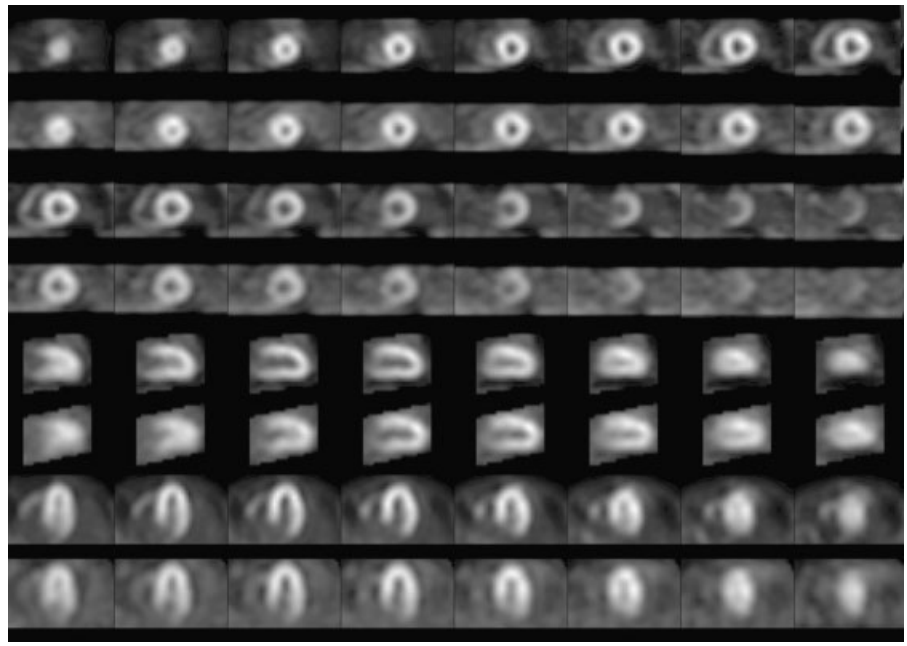

Figure 6.4 Example of normal dual-isotope MPS using frame normalization in a 50-year-old male with atypical chest pain.

20-segment system divides the basal, mid, and apical short-axis slices into 6 segments each and assigned 2 segments to the apex. As such, it overweighted the smaller apical short axis and the apex. By reducing the number of segments in the apical short axis to 4 and considering the apex as a single segment, these segments comprise 30% of the left ventricle compared to 40% with the 20-segment system, more closely corresponding to autopsy data in which these segments comprised 21% of the left ventricle [21]. We now routinely use the 17-segment approach in our interpretation and reporting.

Nomenclature

The AHA writing group also recommended that each of the 17 segments have a distinct name (as well as a number),

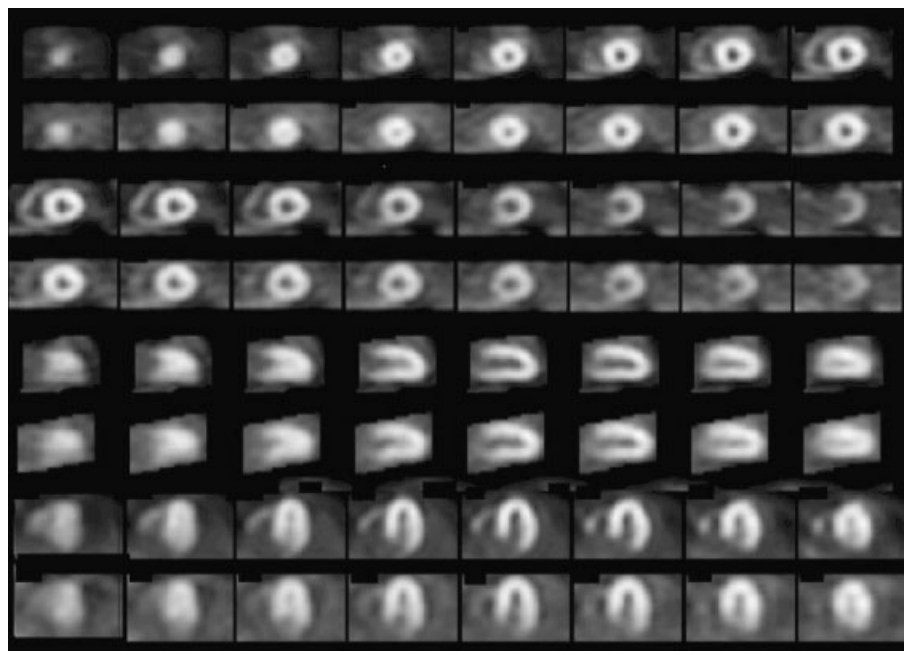

Figure 6.5 Normal dual-isotope MPS study demonstrating the use of the series normalization display. The patient is the same as is illustrated in Fig. 6.4. Note the differences in the appearance of the more basal short-axis slices, as well as the apical short-axis slices, with the series normalization approach.

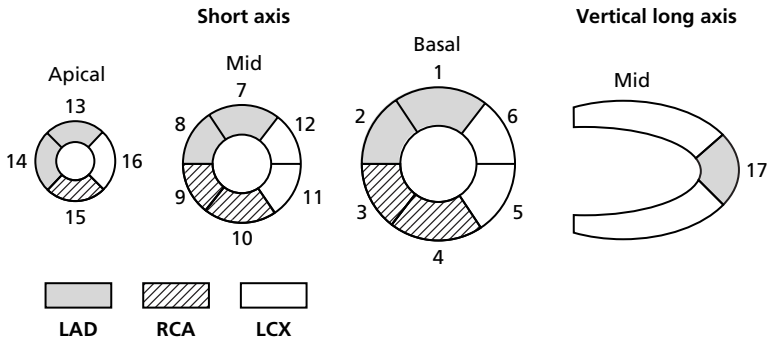

Figure 6.6 Assignment of the 17 myocardial segments to the territories of the left anterior descending (LAD), right coronary artery (RCA), and the left circumflex coronary artery (LCX). (Adapted with permission from [2].)

as indicated in Fig. 6.6. The short axis contains 16 segments in three representative slices termed basal, mid, and apical. The vertical long axis contains the 17th segment – the apex. The nomenclature is simple and based on anatomic orientation. The short-axis slices are divided into anterior, inferior, lateral (the term posterior has been discarded), and septal segments. These four terms without modifiers are used for the apical short-axis slice. The mid and basal short-axis slices are divided into 6 segments, and the respective septal and lateral walls are divided into anteroseptal and inferoseptal and anterolateral and inferolateral segments (Fig. 6.6).

Segmental scoring

Each segment is scored using a five-point system (Table 6.1). The score of 0 is used for normal and 4 for visually absent uptake. Severe reduction of uptake is scored as 3. The score of 2 is used for a moderate defect, but one in which the reader is quite confident that the defect is real. The score of 1 implies a mild or "equivocal" reduction in uptake. The principal function of this score is to express that there is a possibility that the region could be abnormal, but it also could represent a normal variant due to attenuation or artifactual cause. The score of 1 should be used sparingly as a mean of conveying a degree of uncertainty in segmental interpretation.

Of note, it is essential that the observer take into account the normal regional variation of count distribution typical of myocardial perfusion scintigraphy before assigning a perfusion score. For example, the basal interventricular septum (membranous septum) has reduced blood flow and (because of its depth) is subject to greater attenuation than other portions of the myocardium. This "normal septal dropout," frequently observed as an apparent defect on the basal septal slices, should be assigned a score of 0 rather than a score suggesting the presence of abnormality. Similarly, if an apparent defect is considered to represent an attenuation artifact, it would be appropriate to score the involved segments with "0" or "1," depending on the confidence with which the finding can be attributed to attenuation rather than to a true decrease in perfusion.

Since perfusion defects imply a severe reduction in myocardial perfusion, it is not surprising that scores of 3 or 4 usually signify the presence of a critical (≥90%) coronary stenosis. We previously observed that approximately 90% of the time, these severe perfusion defects were associated with critical stenoses [23,24]. We routinely include a statement that a 90% or greater coronary stenosis is likely when reporting severe perfusion defects. Importantly, however, for the more common perfusion defect with a score of 2, no comment is made regarding the severity of the associated coronary stenosis, since multiple factors may reduce the apparent severity of a perfusion defect even in the presence of a critical stenosis (e.g., low heart rate at the time of tracer injection, balanced reduction in flow throughout the myocardium, well functioning collateral vessels).

Table 6.1 Segmental scoring: each segment is scored using a five-point system.

0 = normal
1 = slight (equivocal) reduction of uptake
2 = moderate reduction of uptake (usually implies a significant abnormality)
3 = severe reduction of uptake
4 = absence of radioactive uptake [1,22]

Summed scores

The segmental scoring systems lend themselves to the derivation of summed scores, initially described in our laboratery which can be considered global indices of perfusion [25]. The summed stress score (SSS) is defined as the sum of the stress scores for all of the segments. The summed rest score (SRS) is defined as the sum of the rest scores or redistribution scores, and the summed difference score (SDS), measuring the degree of reversibility, is defined as the difference between the SSS and the SRS. These summed scores are to perfusion what the ejection fraction

index is to ventricular function – single parameters reflecting overall perfusion defects. Specifically, the SSS is the perfusion analog of the peak exercise ejection fraction, the SRS is the perfusion analog of the resting ejection fraction, and the SDS is the perfusion analog of the change in ejection fraction with stress.

While in general these scores are simple summations of the scores given to the 17 segments, there are situations in which this is not the case. For example, we "ignore" the score of 1 for purposes of generating the summed scores, if the region showed this mild 1 finding on both rest and stress images. Therefore, multiple segments with stress/rest scores of 1,1 would be considered 0,0 for purposes of deriving summed scores. Similarly, if the rest score is higher than the rest score when sestamibi or tetrofosmin is used for stress, this difference is ignored in summed scoring – i.e., a score of 2, 3 would be converted to a 2, 2 for summed scoring, so that it does not detract from the SDS.

Based on our previous prognostic work, with the 20-segment model [26,27], summed stress scores of less than 4 are considered normal or nearly normal, summed stress scores of 4–8 are considered mildly abnormal, summed stress scores of 9–13 moderately abnormal, and summed stress scores of greater than 13 severely abnormal. An example of a patient with a mildly abnormal scan (SSS of 6) is illustrated in Figs. 6.7a–6.7c. When a 17-segment system is applied, the absolute cutoffs for defining these degrees of abnormality need to be slightly altered. This need would be even more apparent if the number of segments were even more disparate, e.g., 14 segments as used by the Mayo Clinic for years and the 12 segments employed at Duke University. Since large databases from multiple centers have been developed based on segmental scoring with multiple different systems, it has become apparent that a system which can express the degree of abnormality in a consistent manner with varying numbers of segments would be preferable to simple summed scores (see % myocardium abnormal, below).

% myocardium abnormal

In order to express the extent and severity of MPS perfusion defects in a more intuitive manner, and in order to employ a system that could be applied with a segmental scoring system using any number of segments, we have recently proposed that the extent of myocardial perfusion abnormality is more effectively expressed as a percent of the myocardium abnormal rather than as a simple summed score [28]. The % myocardium abnormal is derived from the summed stress, summed rest, and summed difference scores by normalizing them to the maximal score for a particular scoring model – i.e., by dividing by the maximum score and multiplying by 100. For example, in a 0–4 score/20-segment system, the maximum score would be 80, and in a 0–4 score/17-segment system, the maximum score is 68. Figure 6.8 illustrates the manner in which this assessment is effective with 17- or 20-segment scoring systems in prediction of cardiac mortality in a population of 16,020 patients from the Cedars-Sinai nuclear cardiology database, who were followed up for a mean of 2.1 years. The cardiac mortality rate is seen to rise steadily as a function of the % myocardium abnormal at stress with either segmental approach, and there were no significant differences between the 17- and 20-segment systems when analyzed in this normalized manner [29].

We now routinely report the % myocardium with stress, rest, and reversible defects, both in our daily clinical practice and in publications. Consistent with our previous terminology for defects by SSS and the 20-segment system (noted above), we consider $< 5\%$ to be normal (corresponding to a score of < 4 with either the 20- or 17-segment system). Defects between 5 and 9% are termed mild, those between 10 and 14% moderate, and $\geq$ greater than or equal to 15% are called severe.

Ascribing abnormalities to coronary vascular territories

As illustrated in Fig. 6.6, the 17 myocardial segments can be ascribed to individual coronary territories [2,24,30] and the distribution of SPECT abnormalities provides information regarding the location of coronary artery stenoses. Representative examples of SPECT defect locations associated with various individual coronary artery stenoses are shown in Figs. 6.9a and 6.9b and the corresponding polar maps of these examples are shown in Fig. 6.10. The coronary assignment is variously assigned border between specific vessels territories, depending on the pattern of perfusion defect abnormality in the adjacent segments. This pertains most commonly to the inferoseptal and inferolateral walls, but also applies to the anterolateral wall. Regarding the septum, if an inferoseptal or anteroseptal segment, but not both, were present (excluding the basal inferoseptal segment, which is generally a right coronary artery territory), the septal abnormalities would be assigned to the left anterior descending (LAD) or right coronary artery, depending on which of these vessels had a perfusion defect. Similarly, if an inferolateral or anterolateral defect, but not both, were present in patients with adjacent defects in either the anterior or inferior wall, the lateral wall defect would be assigned to the vessel attributed to the neighboring defect and not considered to be indicative of multi-vessel disease. These are general associations, which may vary in an individual patient based on variations in coronary anatomy.

For purposes of reporting (see section on Likelihood of angiographically significant CAD below), ascribing a

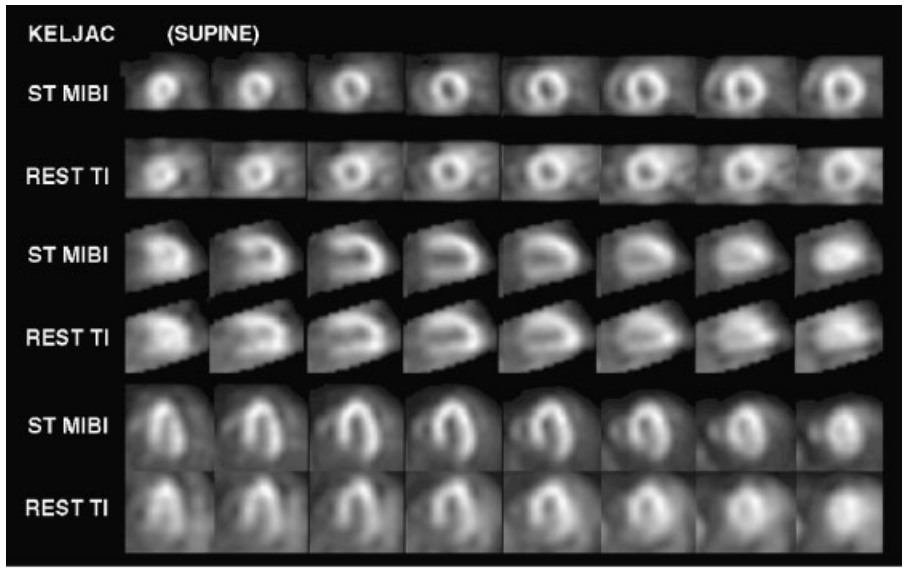

(a)

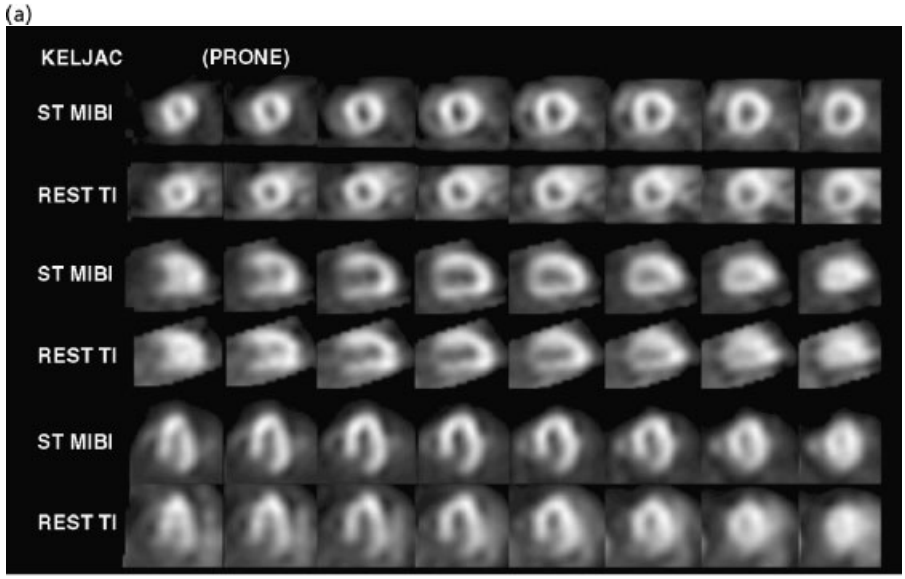

(b)

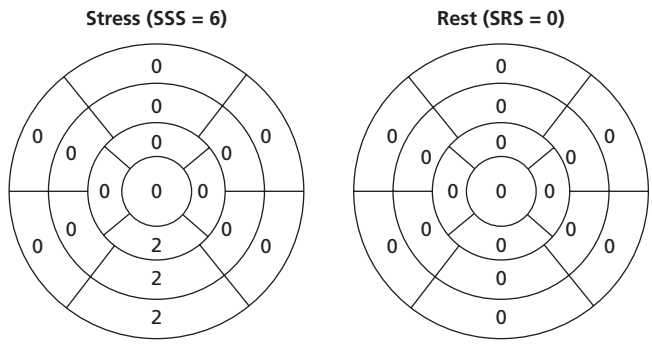

(c)

Figure 6.7 Exercise/rest dual-isotope MPS images of a 67-year-old male with typical angina. Supine sestamibi images are illustrated in part (a), and prone sestamibi images in part (b). In both figures, the rest thallium-201 images are the same and were obtained in the supine position. A small reversible defect is noted in the inferior wall. The SSS, derived from the prone images, is 6 (8.8% myocardium), constituting a mild abnormality, while the SRS is 0 (c). Subsequent coronary angiography was performed, and revealed an 80% stenosis of the posterior-descending branch of the right coronary artery. The patient was successfully treated with medical therapy. This case illustrates the persistence of an inferior wall defect in the prone position, allowing the study to be confidently interpreted as definitely abnormal and not mistaken as showing only diaphragmatic artifact (for comparison, see Fig. 1.2).

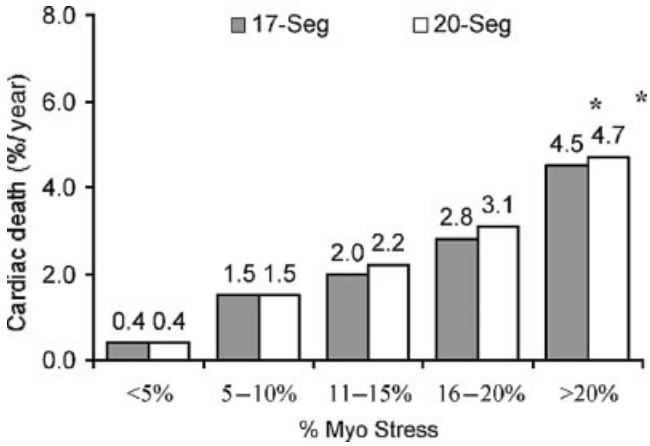

Figure 6.8 Annual rate of cardiac death as a function of % stress defect by 17- vs. 20-segment scoring system. Note the similarity of death rates using the 17- and 20-segment systems when expressed as % myocardium. $^{*}p < 0.001$ across the groups. Abbreviation: % Myo stress: % myocardium abnormal at stress. (Adapted with permission from [29].)

segmental perfusion defect to a specific coronary artery is influenced by the pattern of abnormality observed in other segments, and, of course, by the specifics of a patient's coronary anatomy, if known. For example, in Figs. 6.9 and 6.10, the patient with diagonal branch abnormality shows a lateral wall abnormality in the apical short-axis slice, but only anterior wall abnormalities in the mid and basal short-axis slices. Rather than consider the apical lateral wall abnormality as representing involvement of the left circumflex, this isolated lateral wall finding, contiguous with a more extensive abnormality in the diagonal territory, is attributed to the diagonal vessel disease. In determining the overall interpretation (from definitely normal to definitely abnormal), the degree to which an apparent perfusion defect corresponds to a known coronary vascular territory is taken into account. Perfusion defects that fail to correspond to a standard vascular territory are more likely to be artifacts than those corresponding to typical vascular distributions.

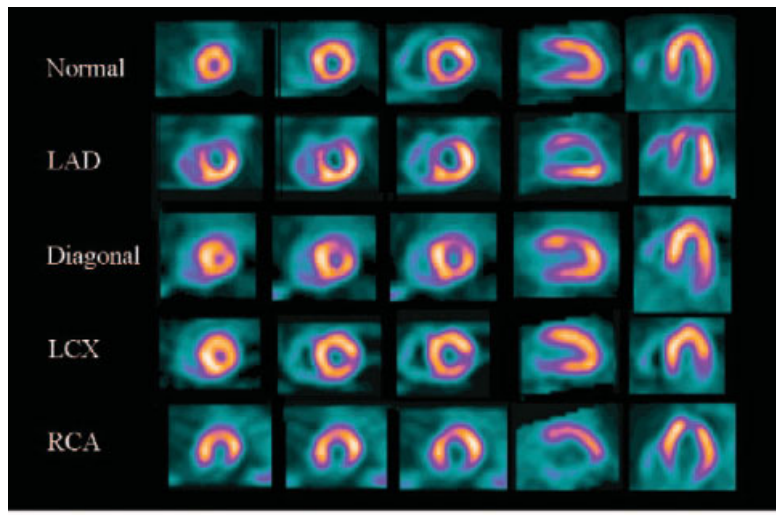

(a)

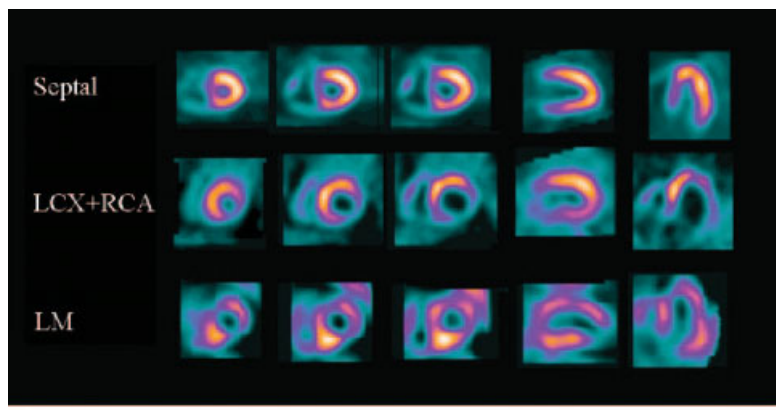

(b)

Figure 6.9 (a) Examples of typical stress perfusion patterns corresponding to normal (top) and various single territory abnormalities. Coronary angiographic findings in these patients were as follows: LAD coronary artery proximal 95% stenosis; diagonal (occluded proximal first diagonal artery); left circumflex (LCX) coronary artery: occluded first marginal artery branch; right coronary artery (RCA): mid 95% stenosis. All patients had no evidence of myocardial infarction and normal MPS at rest. From left to right, the images represent distal short axis, mid short axis, basal short axis, mid vertical long axis, and mid horizontal long axis. These patients showed the typical distributions of perfusion defects associated with the specific coronary arteries involved (adapted with permission from [31]). (b) Stress MPS images demonstrating more complex patterns associated with known coronary lesions in patients with normal resting perfusion images and no history of prior myocardial infarction. Septal: trapped septal perforator coronary artery (ischemia in the territory of the first septal coronary artery in a patient with critical LAD coronary artery stenoses proximal and distal to the septal perforator take off and patent right posterior descending coronary artery, vein grafts to the left circumflex marginal coronary artery and patent LAD internal mammary graft); LCX plus RCA: occlusion of proximal left circumflex and proximal right coronary arteries; LM: subtotal left main coronary artery stenosis. (Adapted with permission from [31].)

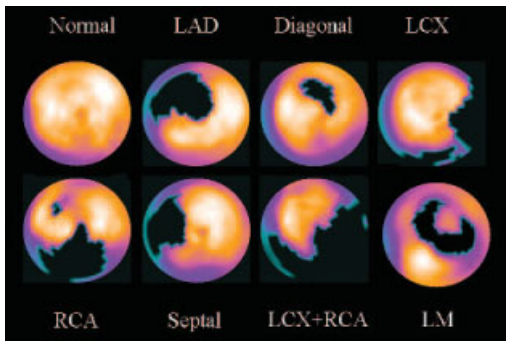

Figure 6.10 Quantitative polar maps (QPS) of the studies illustrated in Fig. 6.9. The abnormally perfused zones are shown by the areas in black. (Adapted with permission from [31].)

Attenuation corrected images

Recently, several camera manufacturers have provided commercially available implementation of attenuation correction protocols [32,33]. In general, these attenuation corrections are imperfect, usually reducing but not eliminating apparent perfusion defects due to soft tissue attenuation in normal patients. In addition, at times, true perfusion defects might be obscured or eliminated by application of these approaches. The artifactual elimination of perfusion defects is usually due to filtering or due to scatter from adjacent organs, which becomes more apparent after attenuation correction. The latter is frequently observed when there is a moderate or greater amount of radioactivity in the liver or bowel, in which case an inferior wall defect might be missed with application of attenuation correction. Because of these limitations, it is currently recommended that attenuation-corrected tomographic data sets be visualized simultaneously with noncorrected data sets. The interpreter should be aware that because of the imperfection in present-day attenuation correction algorithms, a uniform distribution of radioactivity throughout the myocardium cannot be expected. Furthermore, the normal regional distribution of counts on a segment-by-segment basis may be different in attenuation-corrected images than in non-attenuation-corrected images. Thus, the normal regional distribution of counts in the attenuation-corrected images should be taken into account prior to segmental scoring. Preliminary data have suggested that robust attenuation correction may be possible when SPECT/CT systems are employed, due to the vastly improved quality of the attenuation map provided by recent generation CT scanners. An example of a patient in whom attenuation correction allowed a study with an attenuation artifact to be called normal is shown in Fig. 6.11.

Semiquantitative scoring of multiple images

Not uncommonly, the interpreter has more than one data set available for scoring (attenuation corrected/nonattenuation corrected, supine/prone). In these cases, all data sets should be taken into account prior to assigning the segmental scores or categorizing the overall study from normal to abnormal. In combined supine and prone imaging, for example, a segment is generally scored according to the most normal uptake shown. If a defect is seen in the inferior wall in supine imaging but not in prone imaging, for example, the inferior wall segments are scored as "0." Conversely, if the anteroseptal wall is normal in supine imaging but demonstrates a defect in prone

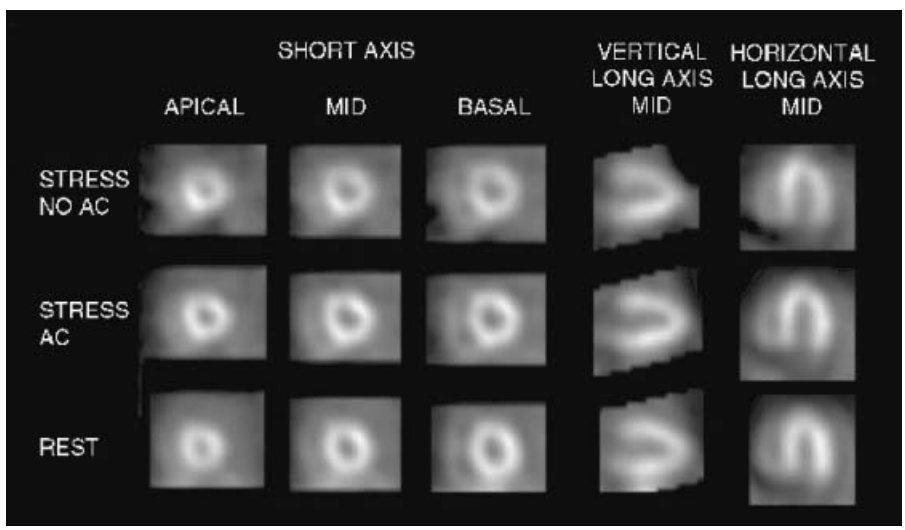

Figure 6.11 Example of attenuation correction (AC) of stress MPS in a 46-year-old obese female with body mass index 37 and a low likelihood of CAD. Apparent anterior and lateral perfusion defects are shown in stress without attenuation-corrected image, which are not seen in the attenuation-corrected image.

imaging (a common artifact with prone acquisition), segments in that region would also be scored as "0."

Quantitative analysis

It is recommended that semiquantitative visual analysis and quantitative analysis be assessed simultaneously. As described in Chapters 4 and 5, a variety of quantitative approaches have been developed, most of which compute myocardial counts in the various myocardial segments and display these counts using a two-dimensional or three-dimensional polar map. Most commonly, abnormalities are then defined by comparison of a patient's polar map to the polar maps derived from gender-matched normal patients. Due to the objective nature of the analyses, quantitative assessments are more reproducible than visual assessments and are particularly useful in assessing interval change when patients are evaluated serially, particularly when extensive abnormalities are observed. Examples of this application of serial quantitative analyses are illustrated in Figs. 6.12 and 6.13. Recent advances offer promise of greatly increasing the clinical utility of quantitative analysis. Examples of these improvements are the assessment of change following precise image registration [34], which may be of particular use in assessing ischemia. Most recently, we have found that an automatic method to incorporate both supine and prone imaging in the quantitative analysis has become of great value in our laboratories in which combined supine/prone imaging is routine [35]. A similar recent development incorporating attenuation-corrected images and non-attenuation-corrected images into a single quantitation is also highly useful.

Visual analysis remains the final step in clinical interpretation of MPS. Currently, our method of reading has evolved into an automatic quantitative computer analysis with visual overread. Prior to modifying the computer scores, the interpreter should look at the perfusion images with "contours on" and "contours off." This is an essential quality control step to ensure that the computer-selected myocardial regions have been correctly selected. If necessary, manual resetting of the limits of the computer search is performed at this time, and the study is reprocessed for quantitative assessment. Of note, the "contours on" and "contours off" steps should be repeated separately for the perfusion and function portions of the study.

After this initial quality control step, the computer-derived 17-segment scores are modified by the expert interpreter based on visual interpretation. Visual modification is essential in accounting for a variety of artifactual patterns that can be recognized by visual inspection (e.g., breast attenuation, motion artifact, noncoronary patterns) and not yet by computer analysis. The most frequent alteration changes segmental scores to 0 or 1 in areas considered visually to represent attenuation artifact, and changes "borderline" computer segmental scores of 1 (mild/equivocal) to 2 (moderate, definite) or 0 (normal). Since the incorporation of combined supine/prone normal limits [35], the proportion of cases and segments in which the scores are altered by visual analysis in our laboratories has been markedly reduced.

Assessment of myocardial viability

Questions of myocardial viability arise when there is abnormally contracting myocardium without clear evidence of myocardial infarction. In such myocardial segments, viability is implied with the myocardial perfusion tracers if the degree of uptake at rest, redistribution, or following nitrate-augmented rest injection is normal or nearly normal. If a region has severely reduced or absent uptake of radioactivity in these settings, it is considered to be nonviable. Areas with moderate reduction of counts in these conditions (score 2 at redistribution or nitrate-augmented rest) are usually partially viable, and patients in this group have a variable response in terms of postoperative improvement. Although some have suggested that a single cutoff point (chosen as a percentage of maximal counts in the myocardium) is predictive of viability in a region in question [36,37], we recommend the use of the number of standard deviations below normal, since the latter takes into account the rather marked normal reduction in counts that occurs in the inferior wall and non-attenuation-corrected MPS images. Of note, a growing body of evidence suggests that fluorine-18-deoxyglucose positron emission tomography (F-18 FDG PET) not uncommonly demonstrates viability in regions considered nonviable by even optimally performed SPECT. When decisions regarding proceeding with myocardial revascularization are being made on the basis of the SPECT findings, we now frequently recommend FDG PET or late enhancement imaging with cardiac MRI in further assessment of patients with SPECT evidence of extensive scarring and no or only minimal viable myocardium.

Figure 6.14 shows an example of a patient with a large nonreversible defect on stress sestamibi and 24-hour rest thallium SPECT in whom clear evidence of viability was shown by rest F-18 FDG PET.

"Nonperfusion" abnormalities

In addition to perfusion defects, several nonperfusion abnormalities should be observed and, when present, described. They include size of the left ventricle, transient ischemic dilation (TID) of the left ventricle [38–41], right

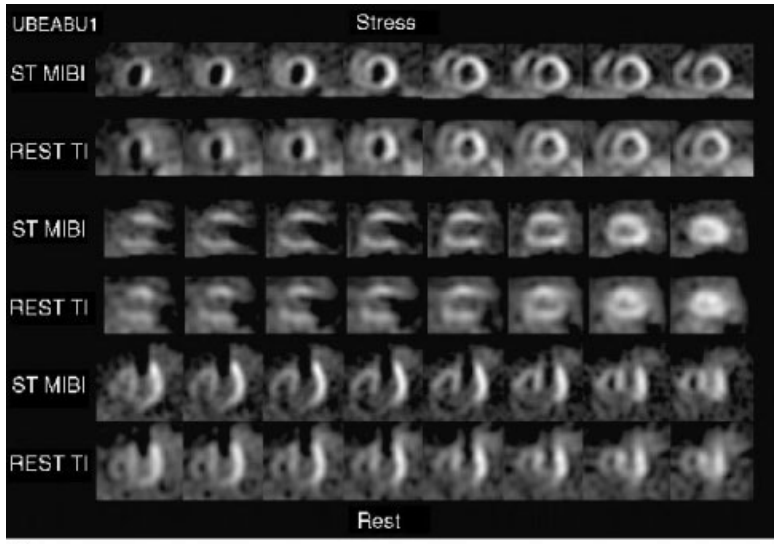

(a)

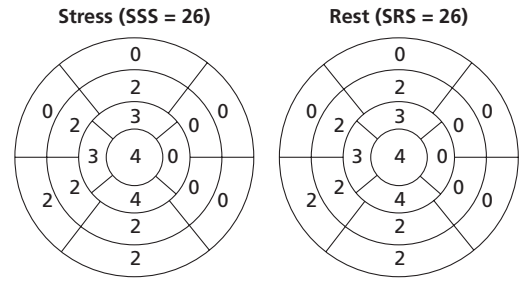

(c)

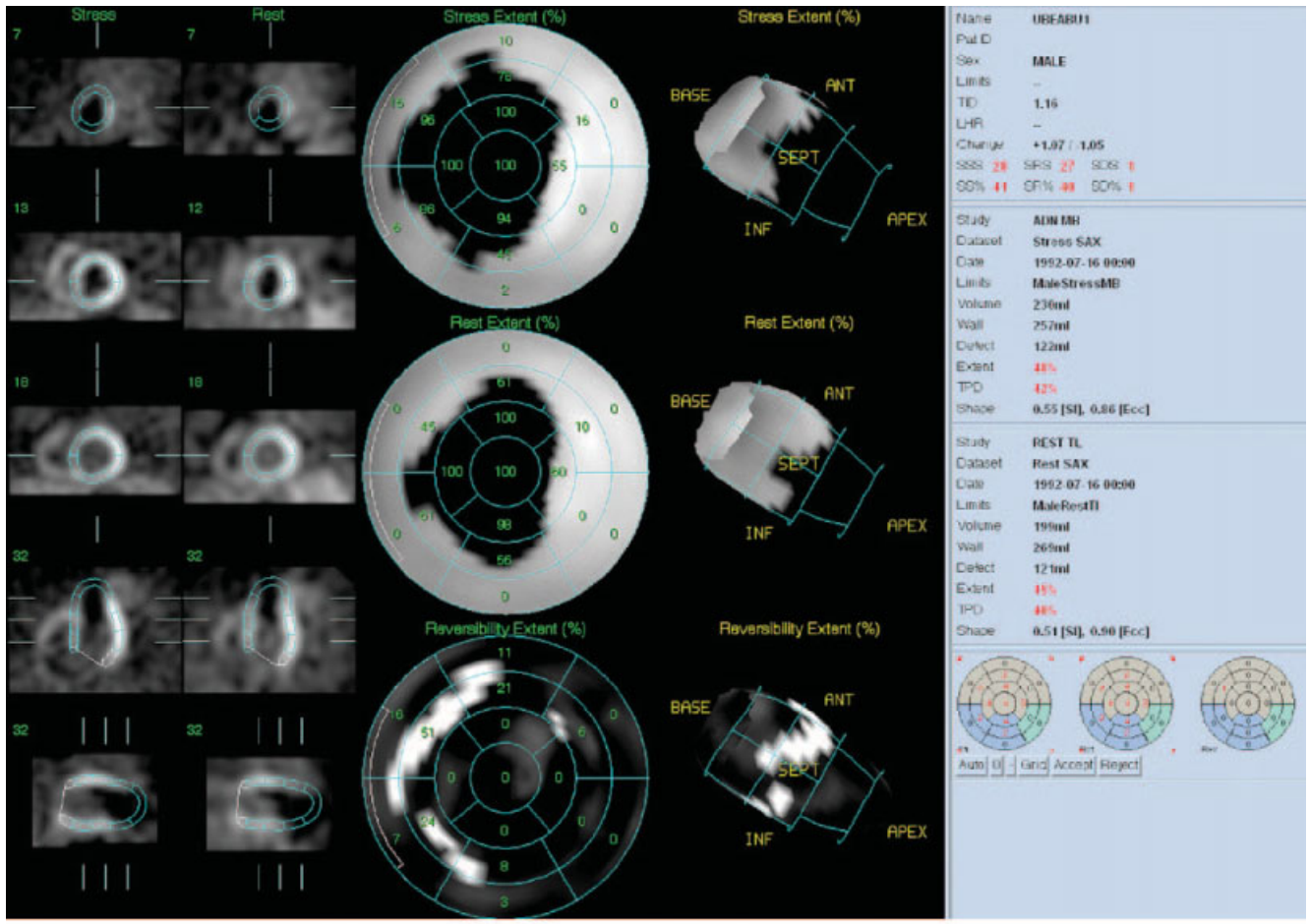

(b)

Figure 6.12 Adenosine stress sestamibi/rest thallium-201 MPS images (a) in a 76-year-old diabetic male with prior myocardial infarction. The type and distribution of the scintigraphic abnormalities are consistent with a large prior myocardial infarction in the anterior wall, septum, inferior wall, and apex. An extensive nonreversible defect by quantitative perfusion SPECT (QPS) is noted throughout the LAD coronary artery territory (b).

ventricle myocardial uptake pattern, and right ventricular size. As noted before, a note should also be made of abnormalities of lung uptake or other abnormal extracardiac activity.

TID is considered present when the left ventricular cavity appears to be significantly larger in the poststress images than in the resting images. The degree of enlargement needed depends on the imaging protocol used. For example, with dual-isotope protocols, the greater Compton scatter associated with Tl-201 causes the myocardial walls to appear intrinsically thicker (and the cavity smaller) in Tl-201 rest images compared to poststress Tc-99m sestamibi images [39]. Therefore, a greater degree of transient enlargement must be evident for a dual-isotope study to be considered to demonstrate transient ischemic dilation. The ventricular size can easily be measured by slight modifications of the quantitative gated SPECT algorithms described in Chapter 4. We have found that the upper limit of normal for transient ischemic dilation with *exercise* dual-isotope imaging is 1.22 (Table 6.2). Patients who have transient ischemic dilation of the left ventricle (transient ischemic dilation >1.22) are likely to have severe and extensive CAD (>90% stenosis of the proximal LAD coronary artery, or of multiple vessels) [39]. With *adenosine* stress, for unknown reasons, the upper limit of normal for transient ischemic dilation is higher – being 1.36 with dual-isotope SPECT [40]. For single-isotope studies, the upper normal is likely to be lower, and would be lowest when 2-day protocols are employed, since the images would have similar myocardial counts and would be generated using identical filters. Upper normal in this setting is likely to be approximately 1.1 [42]. Since different filters are used with low dose rest/high dose stress 1-day protocols, the upper normal. It should be noted that the term "transient ischemic dilation" is imprecise. What is referred to as transient ischemic dilation may at times be caused by an apparent cavity dilation secondary to diffuse subendocardial ischemia (obscuring the endocardial border). This phenomenon is likely to explain why "transient ischemic dilation" may be seen for several hours following stress, when true cavity dilation is probably no longer present. The pattern of transient ischemic dilation of the left ventricle has similar clinical implications whether it is observed on exercise or pharmacologic stress studies [40,42]. Examples of patients illustrating transient ischemic dilation of the left ventricle are shown in Figs. 6.7, 6.15, and 6.16.

Overall assessment of myocardial perfusion

An overall interpretation of the myocardial perfusion scan is recommended, prior to incorporation of the clinical information. To minimize the use of an equivocal category, we advocate using a five-point scoring system (normal, probably normal, equivocal, probably abnormal, abnormal) predominantly based on the segmental score but also on other considerations including the degree to which the scan abnormality conforms to a known vascular coronary territory, the presence of transient ischemic dilation or lung uptake, and the heart rate achieved (on exercise studies). This overall interpretation is subjective, but guidance is provided by the criteria for abnormality listed in Table 6.3.

Table 6.2 Suggested thresholds for TID.

	Exercise	Pharmacologic Stress
Dual isotope rest T1-201/stress Tc-99 m	1.22	1.36
Same day low dose/high dose Tc-99 m	1.15	1.20
2 day Tc-99 m or stress/redistribution T1-201	1.1	1.15

Assessment of ventricular function from gated SPECT images

As with the assessment of myocardial perfusion, a systematic approach to the assessment of ventricular function from the gated SPECT portion of the study is recommended, which is based on a combination of review of automatic quantitative measurements (as described in Chapter 5) and visual assessment. Careful attention to regional function assessment is particularly helpful in identifying patients with extensive CAD, since in multivessel disease with balanced reduction in flow, perfusion defects may underestimate this extent. It is also helpful in deciding whether borderline perfusion defects are due to soft tissue attenuation or due to true perfusion abnormalities.

Quality control

As with myocardial perfusion, assessment of adequacy of the technical quality of the data is, of course, an integral part of the interpretation of gated SPECT. Inspection of the rotating "summed" raw projection images is frequently a source of information regarding inadequacy of the data. As previously noted, observation of "flashing" usually indicates that a gating error has occurred, resulting in the acquisition of a widely different number

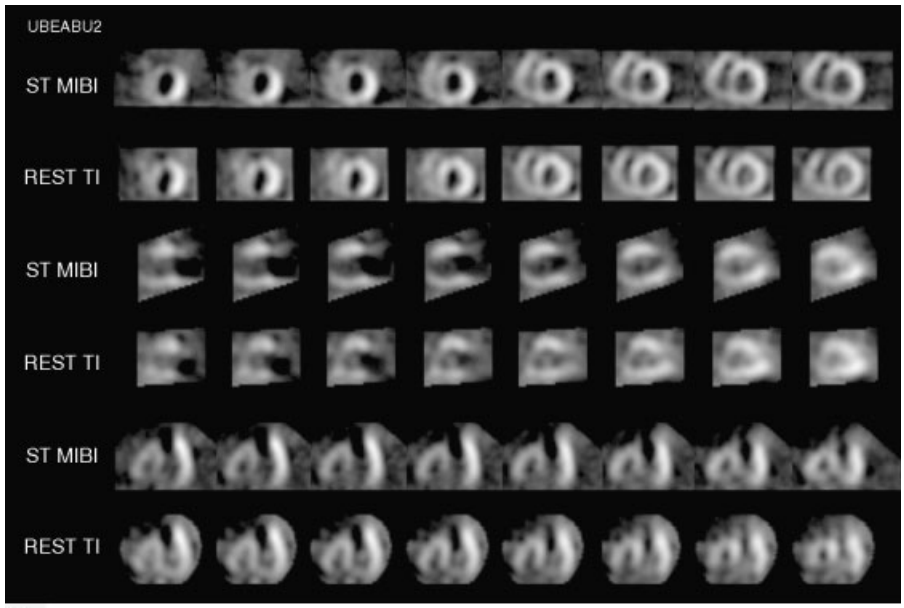

(a)

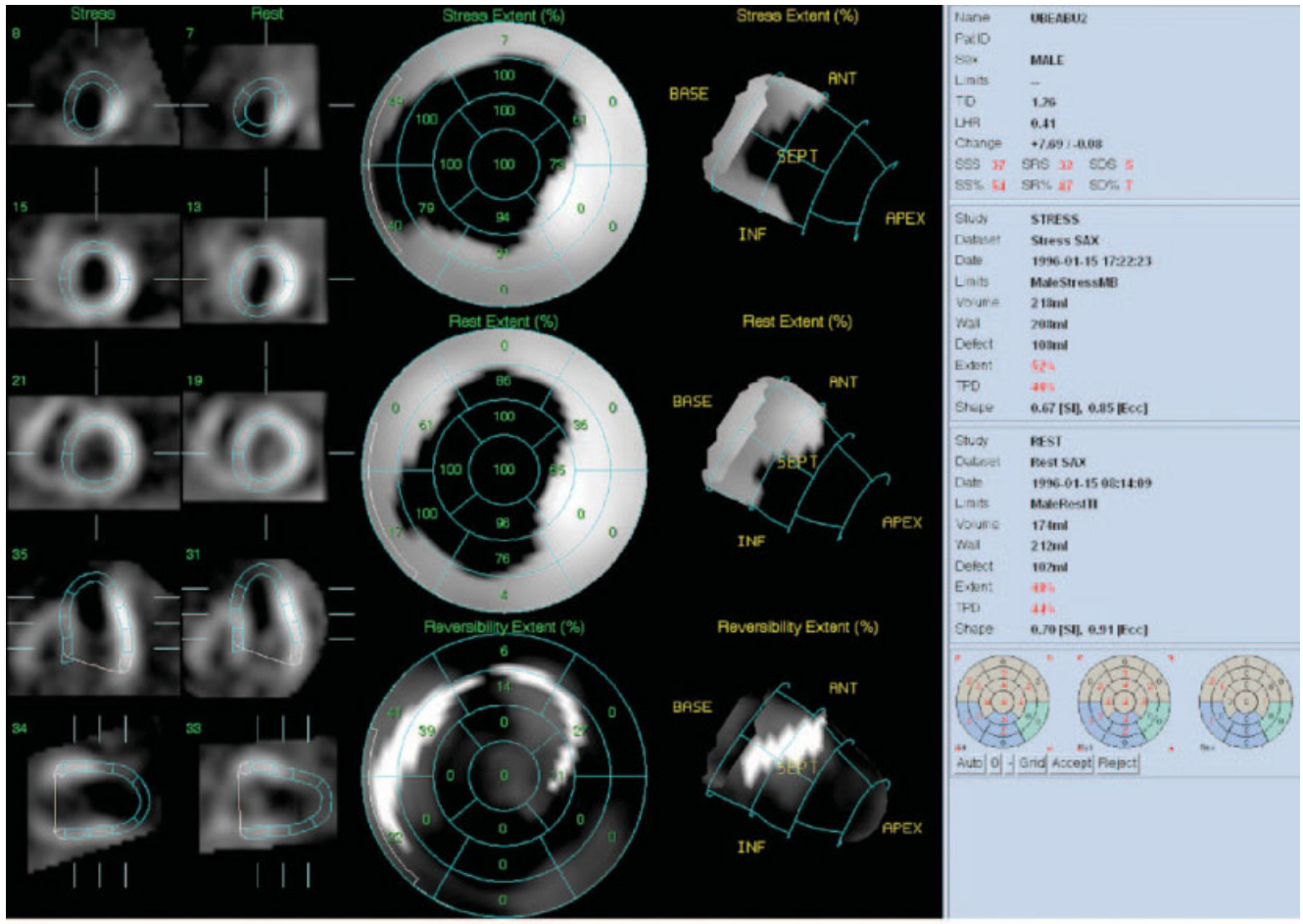

(b)

Figure 6.13 Adenosine stress sestamibi/rest thallium-201 MPS performed 3.5 years later in the same patient as in Fig. 6.12. The extensive nonreversible defect revealed a little change in myocardial perfusion images (a) and quantitative perfusion SPECT (b). By visual analysis, a great deal of time is required to determine the absence of change, while by quantitative analysis the absence of significant change is quickly apparent.

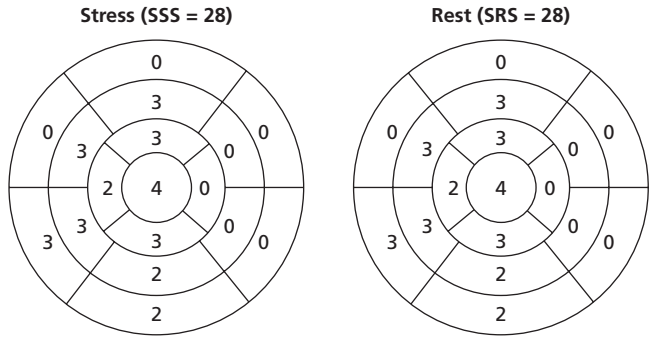

Figure 6.13 (*Continued*)

of cardiac cycles at different angles along the acquisition arc. As with multiple gated equilibrium blood pool studies, quality control would be enhanced through evaluation of a heart-rate histogram providing objective documentation of the adequacy of gating, as explained in detail in Chapter 2; however, most manufacturers do not supply this heart-rate histogram for gated SPECT at the present time.

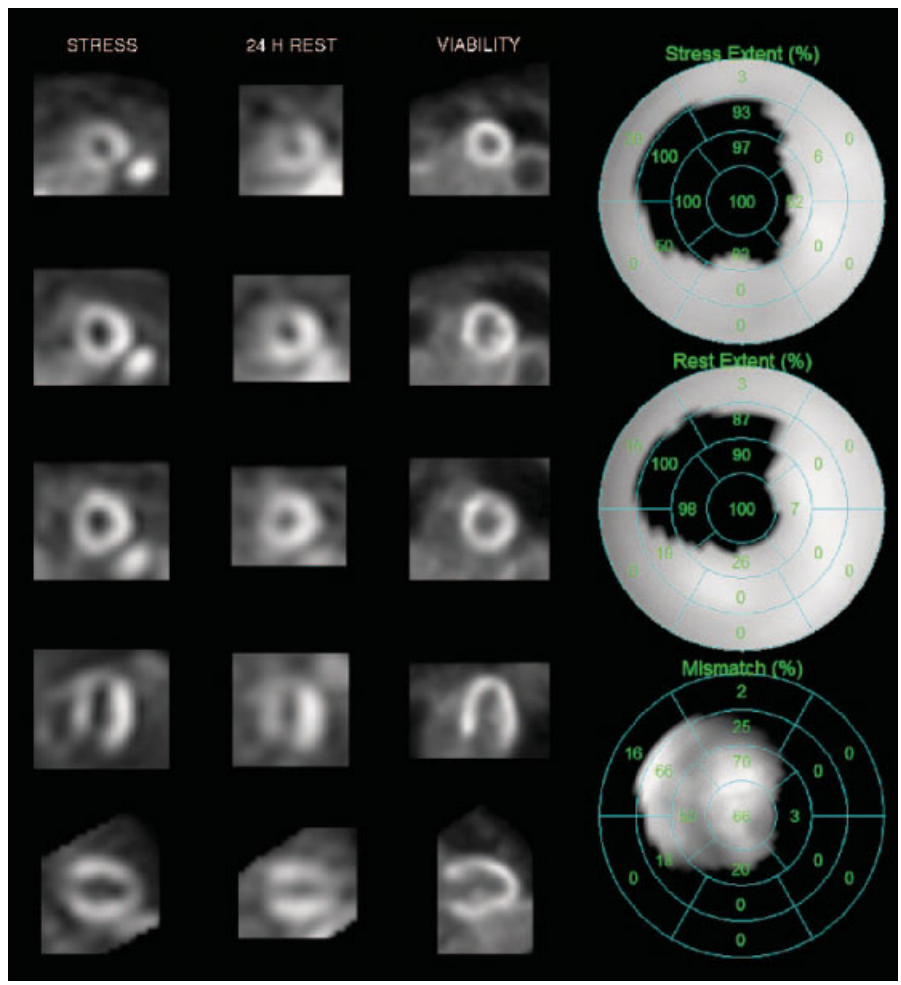

Figure 6.14 Exercise stress sestamibi (left), and 24-hour redistribution (after rest injection) thallium-201 (middle) MPS and glucose loaded F-18 FDG PET (right) from Cedars-Sinai Medical Center in a 73-year-old female with prior myocardial infarction and recent atypical angina. A large nonreversible defect was apparent by SPECT. FDG PET revealed only a small defect in the anterior wall, with almost the entire myocardium being viable. The polar maps show abnormal zones on stress (top) and redistribution thallium (middle) MPS and the area of mismatch (bottom) by quantitative PET analysis. Based on the PET documentation of viability, the patient underwent PCI with a stent to the LAD.

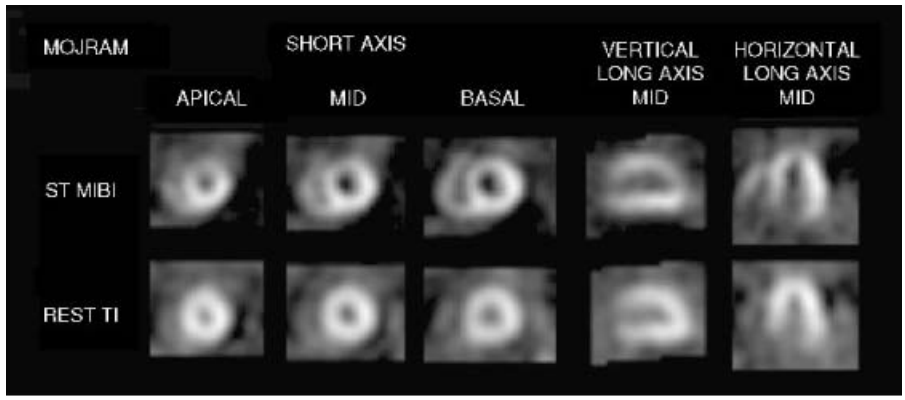

(a)

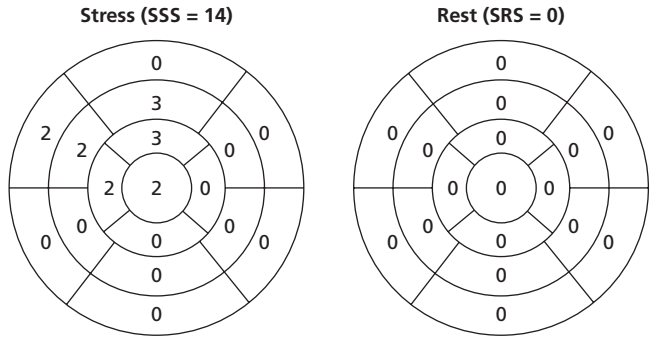

(b)

Figure 6.15 Exercise sestamibi/rest thallium-201 MPS in a 43-year-old diabetic male with typical angina. A severe reversible defect is seen throughout the LAD coronary artery territory (a). (b). There is also transient ischemic dilation of the left ventricle. The distribution of the findings and their severity allowed the report to state: "The distribution of scintigraphic abnormalities and their type indicate the presence of at least a critical (greater than 90%) stenosis of the proximal LAD coronary artery." Subsequent coronary angiography revealed a proximal to mid 95% stenosis in LAD coronary artery and no other vessel disease.

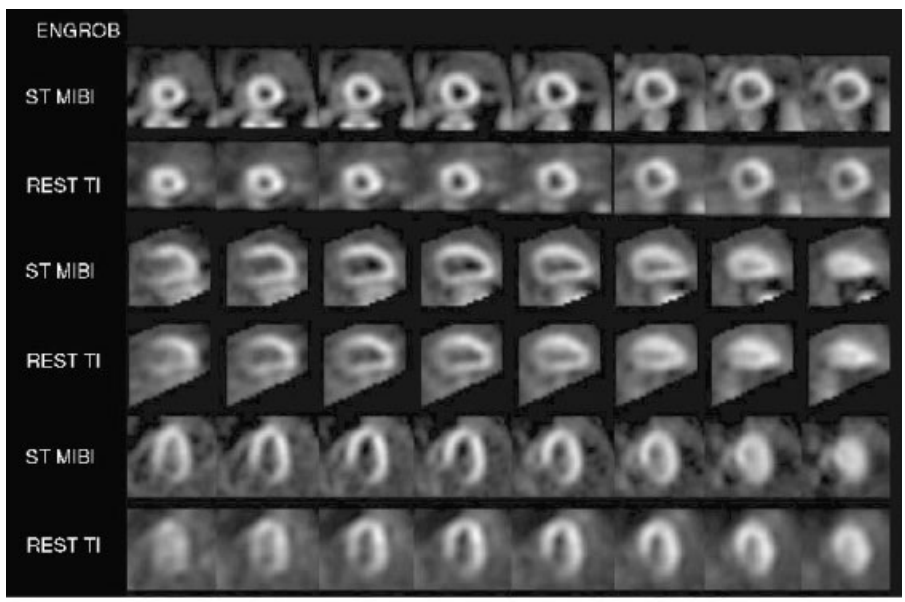

(a)

Figure 6.16 Adenosine stress sestamibi/rest thallium-201 MPS images in an asymptomatic 77-year-old male. The myocardial perfusion images are normal. Resting and post-adenosine ejection fraction are 38 and 32%, and there was adenosine-induced wall motion abnormality in the anterior wall. The transient ischemic dilation ratio is elevated at 1.44. Coronary angiography revealed a >90% stenosis in the proximal segment of the LAD coronary artery.

Table 6.3 Visual criteria for abnormality (exercise or phamacologic testing)*.

Normal	All segments = 0
Probable normal	Few segments = 1
Equivocal	Multiple reversible = 1 1 segment = 2
Probably abnormal	2 segments = 2
Definitely abnormal	≥3 segments = 2 ≥1 segments ≥3

Note: Weighing toward abnormal if defects are reversible, conform to a standard coronary territory, are associated with transient ischemic dilation or lung uptake.
*Overall interpretation of myocardial perfusion SPECT.

Time–volume curve

Overall inadequacy of the gating process can frequently be detected by inspection of the time–volume curve. This curve is derived from quantitative gated SPECT algorithms [9], and provides an assessment of the left ventricular cavity site at various phases of the cardiac cycle. Figure 6.17 illustrates an example of quantitative gated SPECT results, including the time–volume curve. Note that the frame with the largest volume is the first frame, corresponding to end-diastole, and that the overall curve has a characteristic U shape. An example of faulty gating resulting in an incorrect time–volume curve is illustrated in Fig. 6.18. When the time–activity curve is clearly inappropriately timed, the gated SPECT data are generally considered nondiagnostic. The rotating summed projection images should also be evaluated for count statistics; at times, the count density in the overall summed images may be adequate for the interpretation of perfusion SPECT data, but is inadequate for the assessment of wall motion and wall thickening from the individual gated frames.

Display

Because each image is now displayed over 8 or preferably 16 frames of the cardiac cycle, we have found that

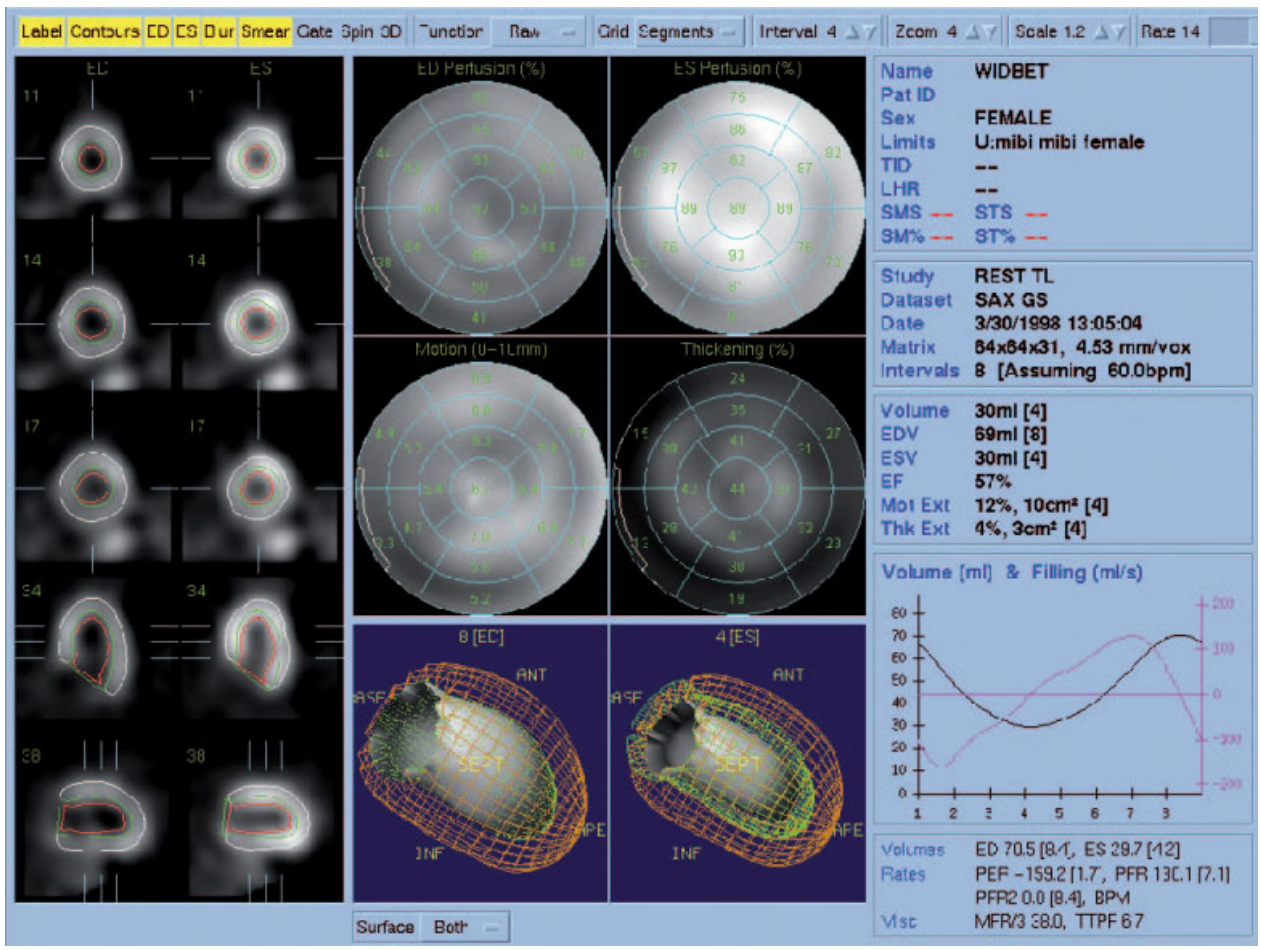

Figure 6.17 Quantitative adenosine stress gated SPECT (QGS) analysis of an 83-year-old female following stenting of the proximal LAD coronary artery. Left ventricular ejection fraction is 57%, with normal left ventricular wall motion and volumes.

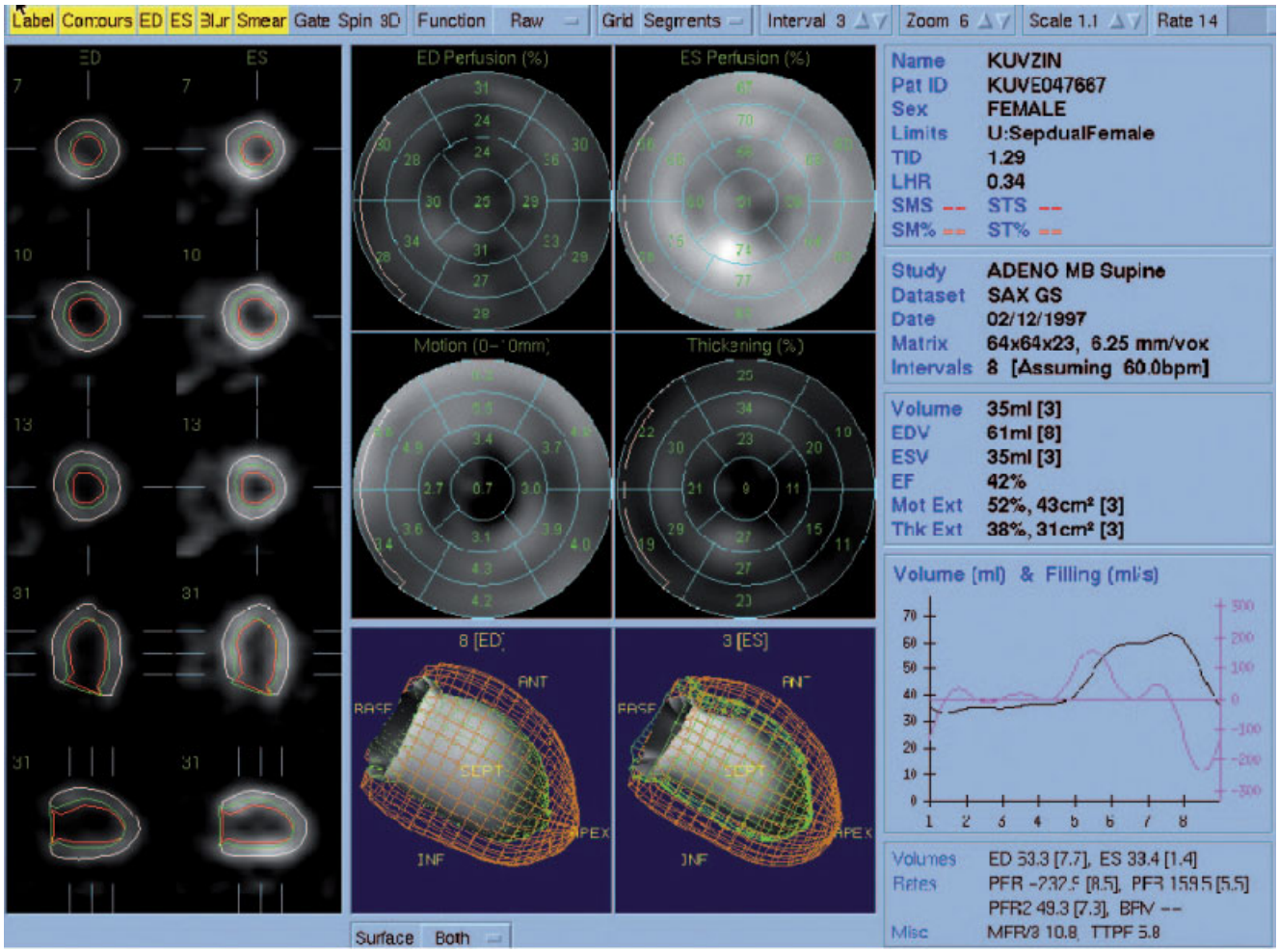

Figure 6.18 Quantitative gated SPECT (QGS) analysis of a patient with a gating artifact. The gating artifact is evident by the nonphysiologic shape of the volume curve (lower right). In the presence of this type of gating artifact, the study should be repeated. If repeating is not possible, the ventricular function parts of the gated SPECT study should not be reported.

displaying all myocardial slices simultaneously results in too much information to interpret easily. We therefore recommend a five-slice display in which three representative short-axis slices (apical, mid-ventricular, and basal) as well as one vertical long-axis and one horizontal long-axis mid-ventricular tomogram are displayed. The appropriate slices are automatically selected by computer software [9], and the five-slice display is viewed in a "cine" format, alternating between the "*contours on*" and the "*contours off*" mode. This alternation is one of the most important quality control measure to verify that the endocardial and epicardial surfaces determined by the algorithm were appropriate for computation of left ventricular ejection fraction and left ventricular volumes, and also provides necessary quality control information if the derived three-dimensional representation of contours are to be used in the assessment of regional function.

17-segment wall motion analysis

We recommend that the same 17 segments utilized for perfusion assessment be used for the visual assessment of regional ventricular function. A diagrammatic representation of the five slices chosen for analysis and the six-point motion scoring system (0 = normal, 1 = mild (equivocal) hypokinesis, 2 = moderate hypokinesis, 3 = severe hypokinesis, 4 = akinesis, 5 = dyskinesis) is illustrated in Fig. 6.19. As noted, the assignment of the segmental regional wall motion scores is based on what is "normal" for a given region. This approach assumes that the observer is familiar with the range of motion that is normal for a given segment, just as he or she would be expected to be familiar with the range of "normal" perfusion in a given segment. Wall motion analysis is performed by visualizing the endocardial edge of the left ventricle, a process

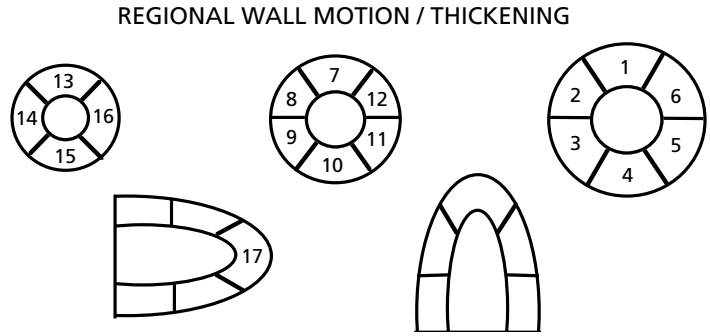

Figure 6.19 Illustration of the method for semiquantitative visual assessment of gated MPS. *Scores are based on the "normal" motion or thickening for a region.

that is also aided by the alternation between "contours on" and "contours off." As a general rule, most experts suggest the use of a gray scale for the interpretation of regional wall motion. Once the contours have been verified as being correct, many readers utilize a three-dimensional representation of the function data ("views" in the QGS application), which provides three-dimensional contours in three different interactive perspectives.

17-segment wall thickening analysis

Visual assessment of wall thickening takes advantage of the direct relationship between the increase in the apparent brightness of a wall during the cardiac cycle (partial volume effect) [59] and the actual increase in its thickness. For purposes of wall thickening evaluation, many investigators recommend the use of a 10-step or other multiple-color scales as opposed to a gray or other monochromatic scale. The degree of all thickening is similarly scored with a 4-point system (0 = normal to 3 = absent thickening). In general, for a given short-axis slice, there is greater uniformity of "absolute" thickening than there is of wall motion, due to the greater effect of translational motion of the heart's long axis during systole on perceived regional wall motion than on thickening. With a 10-point color scale, there is usually at least a 2-color change from diastole to systole in normal zones. Figure 6.19 also illustrates our approach to visual assessment of segmental wall motion and wall thickening. In general, in the mid and distal short-axis slices, as well as in the apical slices, the mean normal thickening is approximately 40%. Given some variability, thickening of 20–30% would be considered mild (equivocal) reduction in thickening, thickening of 10–20% moderate to severe reduction in thickening, and less than 10% absent thickening. Thus, in these regions, no change in color on the 10-point color scale would be scored as 3 (absent thickening), a change of 1 color scale unit would be scored as 2 (moderate to severe definite reduction in thickening), and a color change of 2 grades would be considered mild (equivocal) reduction in thickening. Anything showing over 2 grades of thickening would be considered normal. In the basal short-axis slices, the mean degree of thickening observed is only 20%. In these regions, scores of 1 are generally not used. A score of 2 would be used for a single color scale change, suggesting the presence of hypokinesis, and no change in color scale would be scored as 3. These color differences appear to be applicable whether or not a perfusion defect is noted to be present; i.e., the changes scored are based on the starting point for a given segment, as illustrated by the color during diastole.

Discordance between wall motion and wall thickening

In general, regional wall motion and wall thickening abnormalities accompany each other. Due to this marked agreement, we have found it most convenient to score function in combined fashion for the 17 segments, only making note of whether wall motion and wall thickening are found to be discordant. The most common cause of discordance between wall motion and wall thickening is found in patients who have undergone bypass surgery; in these cases, "abnormal" wall motion with preserved thickening of the interventricular septum is an expected normal variant. Similar discordance between wall motion and wall thickening can also occur in left bundle branch block, where preserved thickening with abnormal motion

of the interventricular septum is also a common variant. At the edges of a large infarct, normal thickening with minimal or absent motion may be observed in the periinfarction zone, with reduced motion being due to the adjacent infarct. The presence of thickening is considered to be indicative of viable myocardium; conversely, "normal" wall motion of an abnormally perfused segment that does not thicken could be associated with passive inward motion of a nonviable myocardial region (tethering) due to hypercontractility of adjacent noninfarcted segments.

Combined rest/poststress regional function analysis

When available, the rest and poststress gated images should be compared to identify the development of new wall motion abnormality. Wall motion abnormalities that occur on poststress images but are not seen on resting images imply the presence of ventricular stunning, and are highly specific for the presence of CAD [44,45]. If resting gated SPECT studies are not available, a note should still be made of discrete regional wall motion or wall thickening abnormalities, since these can often be indicators of the presence of a severe coronary stenosis (≥90% diameter narrowing). This finding might be missed by perfusion defect assessment alone, particularly in patients with a greater degree of ischemia in a region other than that demonstrating the wall motion abnormality [45]. It is important to routinely report the patient's state at the time of gated SPECT acquisition, i.e., rest, 30-minute poststress, 1-hour poststress, etc. Of interest in protocol design, the earlier this acquisition is performed after stress, the more likely that the poststress wall motion abnormality will be observed.

Quantitative wall motion/wall thickening assessment

Ideally, quantitative methods for comparing the degree of wall motion and wall thickening of each segment of the left ventricle to the lower limit of normal would be available, and would augment the visual analysis of ventricular function from gated SPECT data. Algorithms for the automatic quantitative measurement of absolute endocardial motion and relative myocardial thickening between end-diastole and end-systole have been developed and validated [46,47].

Left ventricular volume

It has recently been demonstrated that quantitative assessments of absolute left ventricular cavity volumes correlate well with a variety of "gold standards" (see Table 5.3). We have also found the absolute measurement of left ventricular volume to be perfectly reproducible (repeated assessment in a given data set) [48] and highly repeatable (repeated data acquisition) [49,50] (see Table 5.5). If a validated method for measuring left ventricular volumes is available on a particular camera–computer system, it is recommended that this measurement be reported as a standard component of gated SPECT analysis. Volume measurements are helpful in prognostication [51], as well as in guiding the use of angiotensin-converting enzyme inhibitors [52]. Absolute left ventricular volumes tend to be underestimated in patients with very small hearts, as discussed in Chapter 5.

Overall interpretation of ventricular function

An overall interpretation of the ventricular function component of the gated SPECT examination is recommended, as it is for assessment of myocardial perfusion, and can be accomplished using the same scale with five gradations (from definitely normal to definitely abnormal). This overall interpretation is subjective, but guidance is provided by the criteria for abnormality listed in Table 6.3. In general, a study would be considered as showing abnormal function if a severe wall motion abnormality is present. If only a moderate wall motion abnormality is present, the determination as to whether the ventricular function portion of the study should be considered abnormal depends on the ejection fraction.

Modification of the interpretation of perfusion and function based on clinical information

The observer has now analyzed the perfusion and function portions of the gated perfusion SPECT examination without knowledge of the patient's clinical state. The final report, however, should be based on all clinically relevant data, including symptoms, risk factors, the results of exercise testing, the results of pharmacologic stress testing, and, when available, other information such as the results of coronary angiography. By convention, endorsed by the ASNC guidelines (1), this modification of the interpretation based on clinical information should not change the initial assessment by more than one category of abnormality, using the five-point scale for abnormality (Fig. 6.20). For example, if the initial interpretation was equivocal, the study could be considered probably normal in a patient with a low prescan likelihood of CAD; conversely, the equivocal study could be reported as probably abnormal in a high prescan likelihood setting (e.g., typical angina pectoris with multiple risk factors and an abnormal treadmill test). This modification has the effect of improving the overall concordance of information sent to clinicians (a

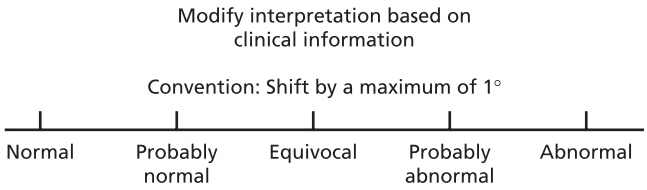

Figure 6.20 Interpretation of gated MPS showing convention for modification by a maximum of 1° based on clinical information.

type of "smoothing" function). It is of critical importance to exercise restraint, so that the maximal shift is one category in the five-point scale. Shifting by a greater extent would be confusing, in that it would no longer provide data representative of the scintigraphic study. If there is a clear discordance between clinical and scintigraphic data, this should be directly expressed in the "Comments" portion of the report, rather than being buried in the interpretation of the nuclear study per se.

Integration of information: reporting of gated MPS

Table 6.4 lists the items of information that an ideal nuclear cardiology report would contain, in addition to the scintigraphic information. The final report should represent a synthesis of nuclear and nonnuclear information. An example report is shown in Figs. 6.21a–c.

Likelihood of angiographically significant CAD

By convention, CAD is based on the presence of an hemodynamically significant coronary atherosclerotic plaque, as determined by coronary angiography or more recently by intravascular ultrasound or fractional flow reserve measurements. Coronary atherosclerosis is the term used for coronary plaques that do not demonstrate this degree of functional significance. Clinicians have learned to guide their management of patients in part by their assessment of this likelihood. When incorporating this likelihood into the final report, the interpreter assesses the prescan likelihood of CAD based on age, sex, symptoms, risk factors, and the results of the nonnuclear components of the stress testing. The postscan likelihood is then reported by incorporating the nuclear test results.

Table 6.4 Overall interpretation of function on gated MPS.

Criteria for global abnormality (16-frame gating)*			
Normal	≥50		All segments = 0
Probable normal	45–49	or	Few segments = 1
Equivocal	45–49	or	Multiple reversible = 1 1 segment = 2
Probably abnormal	41–45	or	2 segments = 2
Definitely abnormal	<40	or	≥1 segments ≥3

*Overall interpretation of ventricular function on gated myocardial perfusion SPECT.

Likelihood of a cardiac event

Since one of the principal applications of gated MPS is risk assessment, it is recommended that the interpreter consider incorporation of risk assessment in the final report. This complex subject is also covered in Chapter 8. For decades it has been recognized that the ejection fraction is a strong—if not the strongest—predictor of cardiac mortality. What the rest/stress myocardial perfusion studies add uniquely to this assessment is the extent and severity of ischemia. Recent data from Cedars-Sinai Medical Center have shown that the extent of ischemia is related to the likelihood of benefit from revascularization, adding a new dimension to risk assessment. After risk adjustment, Hachamovitch et al. [28] have reported that when no ischemia is present, patients in general have a lower mortality rate with medical management and when ≥greater than or equal to 10% ischemia is present, revascularization is associated with a lower mortality rate with revascularization than with medical therapy. Further analysis has demonstrated that this relationship holds up in patients with reduced ejection fraction. Thus, while patients with a very low ejection fraction have a high mortality rate, those who benefit from revascularization in terms of lowering this mortality rate appear to be identified by having extensive myocardial ischemia. Given these considerations, we now frequently incorporate a statement regarding the likelihood of survival benefit from revascularization in our reports. Examples of a study with extensive ischemia and a study with infarction but with no ischemia are illustrated in Figs. 6.21d and 6.22.

In patients undergoing exercise stress, the interpreter or the clinician is often comfortable in combining clinical and nuclear test results in assessing risk. For example, it is well known that factors such as brief exercise duration, abnormal % heart rate reserve achieved, exercise hypotension, and exercise-induced angina are high-risk markers. In contrast, in patients undergoing vasodilator stress, the clinician frequently finds it more difficult to make an overall assessment of risk, since exercise duration does not apply, symptoms during the stress are nonspecific, and less is known about heart rate and blood pressure responses. We have recently observed that abnormal heart rate and blood pressure responses during adenosine stress are of prognostic importance [53]. However, the clinician is still faced with a complex task in attempting to incorporate all findings in the risk assessment of patients undergoing adenosine perfusion SPECT.

CEDARS-SINAI

Rest/Stress Myocardial Perfusion

Patient Name: **Aaj, Ram**	Referring Physician:
Date of Study: **2006-02-22**	Doe John
ID Number: 999999 **Outpatient**	Phone (098) 765-4321
Age: 50 Sex: **M**	Fax (123) 456-7890

Background:

- Symptom: typical chest pain
- Risk factors: hypertension, diabetes, hypercholesterolemia
- Medications: HMG CoA reductase inhibitor
- Height: 65 in. Weight: 190 lbs. Body Mass Index (BMI): 31.6

Exercise Stress ECG Results:

- Exercise duration = 04:55 minutes; Rest HR 92; Peak HR 147 (86% of maximum-predicted)
- Blood Pressure: Rest: 164/100; Stress: 164/100
- Symptom during test: discomfort occured at 1 minute into exercise
- Reason for termination of exercise: generalized fatigue
- Resting ECG: incomplete right bundle branch block and possible left ventricular hypertrophy
- Stress ECG: -0.8mm downsloping ST depression in lead V5 and -1.5mm downsloping ST depression in lead AVF

Nuclear Results:

- Dual isotope gated SPECT [stress sestamibi (Prone and Supine) / rest thallium]
- Technical quality: good
- **Myocardial Perfusion:** overall defects as follows:

Vessel	Reversible
LAD	large (anteroseptal/anterior/septal/apical)

Total perfusion defect 21% myocardium (21% reversible, 0% fixed)
LV enlargement: no; Visual TID: yes; TID Ratio 1.39

- **Myocardial Function:**
  LVEF: Rest: 57%; Stress: 52%
  EDV: Rest: 83ml; Stress: 121ml
  Resting gated SPECT revealed an ejection fraction of 57% with end-diastolic volume of 83 ml. Left ventricular wall motion demonstrated moderate hypokinesis in the anterior wall.

Conclusion:				
	Perfusion	Abnormal (Reversible)	**Clinical Response**	Ischemic
	Function	Normal rest, worse after stress	**ECG Response**	Ischemic (S-T elevation)

These test results indicate a high (>90%) likelihood for the presence of angiographically significant coronary artery disease. The type and distribution of the scintigraphic abnormalities are most consistent with the following: in the LAD territory, a large amount of severe ischemia in the septal, anterior and apical walls. The severity of the anterior perfusion defect suggests that the LAD stenosis is critical (>90%). There is also transient ischemic dilation (TID) of the left ventricle which is a marker of severe and extensive coronary artery disease.

Thank you for referring this patient to us.

Sincerely yours,

Daniel S. Berman, M.D., FACC

Date printed: 2006-05-02 19:47

Figure 6.21 (a)–(c) Example standardized report from Cedars-Sinai Medical Center of patient RM whose images are in Fig. 6.15. Catheterization revealed a 95% LAD stenosis after the takeoff of the first diagonal.

CEDARS-SINAI

SPECT: Myocardial Perfusion

Patient Name: **Aaj, Ram**	Referring Physician:
Date of Study: **2006-02-22**	Doe John
ID Number: 999999 **Outpatient**	Phone (098) 765-4321
Age: 50 Sex: **M**	Fax (123) 456-7890

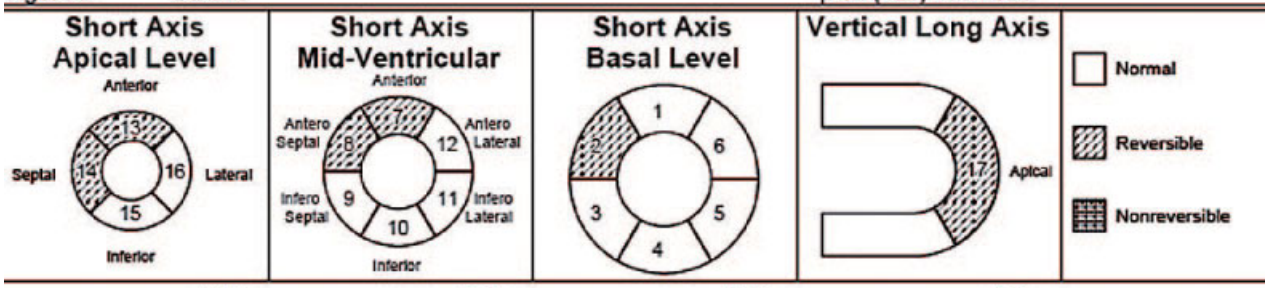

	S	R		S	R		S	R		S	R
13. Anterior	3	0	7. Anterior	3	0	1. Anterior	0	0			
			8. AnteroSeptal	2	0	2. AnteroSeptal	2	0			
14. Septal	2	0	9. InferoSeptal	0	0	3. InferoSeptal	0	0	17. Apical	2	0
15. Inferior	0	0	10. Inferior	0	0	4. Inferior	0	0			
			11. InferoLateral	0	0	5. InferoLateral	0	0			
16. Lateral	0	0	12. AnteroLateral	0	0	6. AnteroLateral	0	0			

0 =Normal
1 =Mildly reduced Equivocal
2 =Moderately Reduced
3 =Severely Reduced
4 =Absent Uptake

S = Stress R = Rest

Date of study	Results	%Total defects	%Reversible	%Fixed	Stress
2006-02-22	Abnormal	21%	21%	0%	Exercise

Exercise separate aquisition dual isotope gated myocardial perfusion SPECT using Tc-99m sestamibi (30.0 mCi) at stress and thallium-201 (3.5 mCi) at rest was performed using the rest/stress sequence. Sestamibi SPECT was performed in the supine and prone positions.

Findings: overall defects as follows:

Vessel	Reversible
LAD	large (anteroseptal/anterior/septal/apical)

Myocardial perfusion test result: definitely abnormal with reversible defect.

Daniel S. Berman, M.D., FACC

%Myocardium		%Reversible		%Fixed		Vessel Descriptions
Normal/Equivocal	0-4%	Normal	0-2%	Normal/Equivocal	0-4%	RCA (Right Coronary Artery)
Mild	5-9%	Mild	3-5%	Mild	5-9%	LAD (Left Anterior Descending)
Moderate	10-14%	Moderate	6-9%	Moderate	10-14%	LCX (Left Circumflex)
Severe	>14%	Severe	>10%	Severe	>14%	DIAG (Diagonal)

Date printed: 2006-05-02 19:47

Figure 6.21 (b)

CEDARS-SINAI

SPECT: Ventricular Function

Patient Name: Aaj, Ram
Date of Study: 2006-02-22
ID Number: 999999 Outpatient
Age: 50 Sex: M

Referring Physician:
Doe John
Phone (098) 765-4321
Fax (123) 456-7890

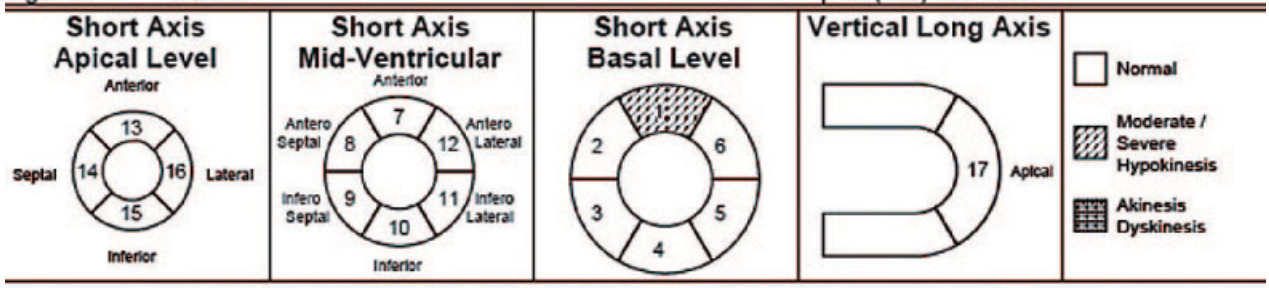

	S	R		S	R		S	R		S	R	
13. Anterior	0	0	7. Anterior	0	0	1. Anterior	2	2				0 =Normal
			8. AnteroSeptal	0	0	2. AnteroSeptal	0	0				1 =Mild Hypokinesis 2 =Moderate Hypokinesis
14. Septal	0	0	9. InferoSeptal	0	0	3. InferoSeptal	0	0	17. Apical	0	0	3 =Severe Hypokinesis
15. Inferior	0	0	10. Inferior	0	0	4. Inferior	0	0				4 =Akinesis 5 =Dyskinesis
			11. InferoLateral	0	0	5. InferoLateral	0	0				S = Stress R = Rest
16. Lateral	0	0	12. AnteroLateral	0	0	6. AnteroLateral	0	0				

LV Ejection Fraction
Rest: 57% Post Stress: 52%

End-diastolic volume
Rest: 83 ml Post Stress: 121 ml

TID Ratio 1.39

Resting gated SPECT revealed an ejection fraction of 57% with end-diastolic volume of 83 ml. Left ventricular wall motion demonstrated moderate hypokinesis in the anterior wall.

Wall motion results: definitely abnormal; normal rest, worse after stress

Daniel S. Berman, M.D., FACC

Date printed: 2006-05-02 19:47

Figure 6.21 (c)

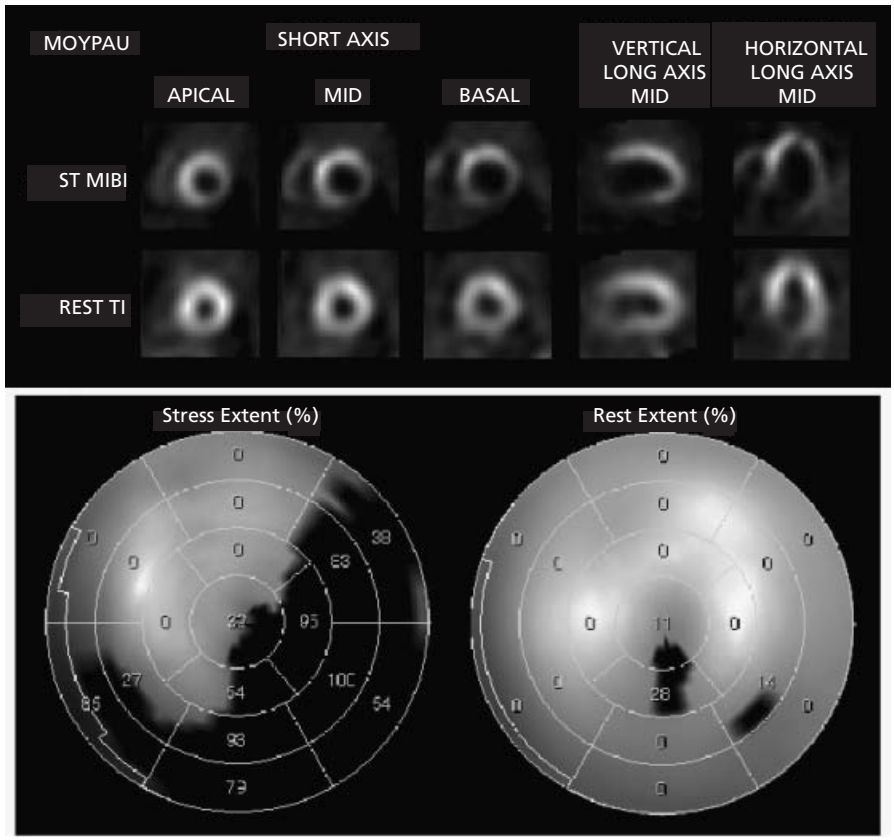

Figure 6.21 (d) Example of extensive reversible defect and low ejection fraction. Exercise MPS of an asymptomatic 54-year-old male with no history of CAD. Stress MPS shows a large reversible defect in the inferior, lateral, and basal inferoseptal walls. Postexericse gated MPS revealed 33% left ventricular ejection fraction with end-diastolic volume of 162 ml. The transient ischemic dilation ratio is elevated at 1.52. Coronary angiography revealed both occlusions of the left circumflex and the right coronary arteries. After bypass surgery, the SPECT study became normal as did the rest and poststress ejection fractions (images not shown).

In 2005, Hachamovitch et al. [54] described an adenosine score that takes into account the patients age, % myocardium ischemic, % myocardium "fixed," dyspnea as a presenting symptom (worse prognosis), the rest and peak heart rate during adenosine stress, the rest ECG, and whether the patient was able to perform low-level treadmill exercise along with the adenosine infusion. With this score, we now incorporate the likelihood of cardiac death with early revascularization or medical therapy as part of our routine reports. We are currently developing a similar score for exercise testing. The degree to which this form of risk reporting will be incorporated into final reports remains to be seen.

Components of the final report

Technical details

The final report should contain the patient's age, identification number, age, gender, height, weight, and the type

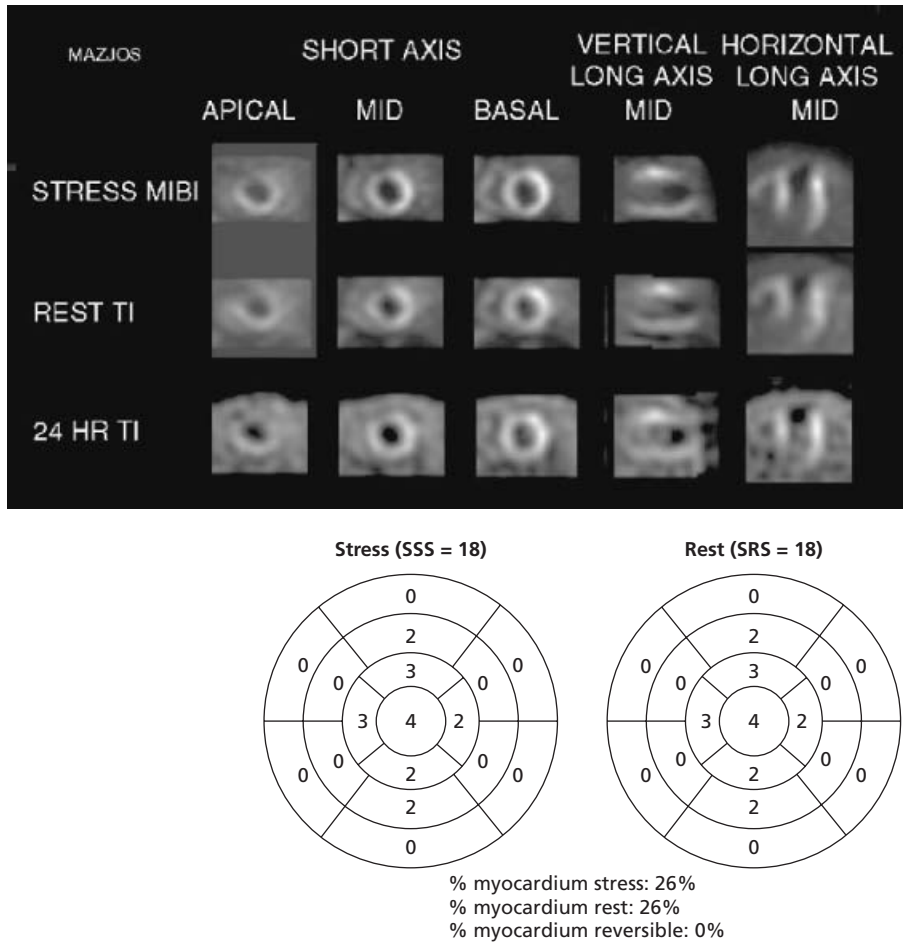

Figure 6.22 Example of extensive nonreversible defect and low ejection fraction. Exercise MPS of an 85-year-old male with history of myocardial infarction and symptom of shortness of breath. Stress MPS shows a large defect in the anterior and apical walls. Twenty-four-hour resting Tl-201 image shows no redistribution. Resting gated MPS revealed 29% left ventricular ejection fraction with end-diastolic volume of 184 ml. Poststress gated MPS showed a 28% ejection fraction with end-diastolic volume of 219 ml. There was no evidence of stress-induced ischemia in this patient (the % reversible was 0). Of note, at the present time, if the assessment of viability is critical to patient management, we would recommend either F-18 FDG or late enhancement MRI to further evaluate the likelihood of viable myocardium in the region with the fixed perfusion defect.

of study performed, and the reason for testing. With the exception of coronary angiography and other imaging test results, the information listed on Table 6.5 should be included in the descriptive portion of the report. The report should also contain the result of the assessments of myocardial perfusion and myocardial function, ideally employing both the semiquantitative multisegment analysis described above and quantitative analysis. As noted above, when describing the ventricular function portion of the study, the patient's state at the time of imaging should be reported (e.g., poststress, rest). As noted above, it is also recommended that a statement regarding the technical quality of the examination be made, so that studies of only marginal quality will be given appropriate weight by the referring physician. Also as noted above, if the level of stress achieved on an exercise study was suboptimal, a qualifying statement regarding the diagnostic or prognostic implications of the absence of ischemia should be provided.

Table 6.5 Interpretation of gated MPS showing convention for modification based on clinical information.

Clinical information and other test results that should be incorporated into the final report
• Risk factors
• Demographic information
• Reason for test
• Presenting symptoms
• Non-nuclear stress test results
Duration
Rest and peak heart rate
Rest and peak blood pressure
Symptoms
ST response
• Coronary angiography
• Other imaging tests

Table 6.6 Likelihood of angiographically significant CAD (≥50%).

<5–14%	Low
15–29%	Low intermediate
30–69%	Intermediate
70–85%	High intermediate
85–94%	High
95–98%	Very high
≥99%	Virtually diagnostic

Nuclear and nonnuclear information in the final report

We recommend that several summary statements be included as components of the final report, including the following:

1 In patients who are not known to have CAD, the postscan likelihood of angiographically significant CAD should be expressed. This likelihood can be calculated by using commercially available programs such as Cadenza [55], or look-up tables [56,57]. Table 6.6 lists the adjectives that we associate with the various postscan likelihoods of angiographically significant CAD.
2 In patients with known disease (post-angiography, post-myocardial infarction, post-coronary artery bypass grafting (CABG), post-percutaneous coronary intervention (PCI)) who are undergoing exercise studies, the postscan likelihood is referred to as the "likelihood of exercised-induced ischemia." In patients with known disease who are undergoing vasodilator stress, a more precise term the "likelihood of jeopardized myocardium" may be used. This distinction between "exercised-induced ischemia" and "jeopardized myocardium" is preferred since a large majority of patients demonstrating reversible defects (evidence of jeopardized myocardium) with vasodilator stress (dypridamole/adenosine) develop a perfusion imbalance during stress but do not actually develop "ischemia" [58]. From a practical standpoint, however, the attribution of the reversible perfusion defects seen with vasodilator stress to "ischemia" may be more clearly understood by the clinician than "jeopardized myocardium."
3 The extent, severity, and location of reversible defects should be reported and related to the likely coronary anatomy. As noted above, we now recommend that these variables be reported as % myocardium, by normalizing the patients summed perfusion scores to the maximum scores possible.
4 The extent and location of fixed defects (which might be referred to as "apparent scarring" or "prior myocardial infarction") should be described. In general, the terms "myocardial infarction" or "scarring" should be avoided unless late redistribution imaging is performed, since, as noted above, nonreversible defects may still be seen in areas with hibernating, viable myocardium.
5 The final summation should answer the specific question being asked by the referring physician. For example, if a patient postangioplasty is being referred for the evaluation of possible restenosis, the likelihood of restenosis should be directly addressed. If a patient is being referred with chest discomfort from the emergency department, the likelihood of an acute ischemic syndrome should be expressed.
6 Using the combined clinical information and scintigraphic scores, consideration should be given to incorporation of a statement regarding the patient's risk of subsequent cardiac event into the final report. Based on recent reports [28,54] the mortality risk with medical vs. revascularization therapy is also frequently included in our current reports.
7 If myocardial viability is being questioned, specific statements regarding the viability of abnormally contracting segments should be included.

"Automatic" report generation

Several commercially available packages are available to help automate the reporting process. With these systems the various components of the report can be automatically incorporated into the report after they have been input at various times during testing. For example, the demographic data, the historical information (e.g., history of prior CAD events or procedures, symptoms, risks factors), and the clinical observations at rest and stress (e.g., heart rates, blood pressures, clinical responses, exercise duration, ST segment changes) can all be entered into the system at the time of stress testing, and then sent electronically to the computer with which the final interpretation is being performed. Furthermore, such systems can provide a template for the interpreter by presenting the perfusion and function scores, left ventricular ejection fraction, and volume measurements assessed by computer algorithms as the starting place for the interpreter's subjective final interpretation. One of the principal advantages of this approach is that the detail of the elements of the report is all checked by the algorithm for internal consistency, so that errors in reporting are minimized. Additionally, the approach allows the interpreter to generate and fax the final report immediately at the time of final interpretation. We have routinely utilized this approach to report generation in our laboratory for approximately 7 years. A study with extensive ischemia, and a study with infarction but with no ischemia are illustrated in Figs. 6.21 and 6.22.

How to integrate information of perfusion and function from gated SPECT

As noted above, usually data relative to perfusion and function are similar. The classic examples of discordance that occur in the interventricular septum in patients who have undergone bypass surgery or in patients with left bundle branch block are expected, but should still be reported.

Unexpected discordance of data should be accompanied by a specific description of the discordance at the end of the final report. In our experience, the most common occurrences of discordance are in patients with cardiomyopathy. For example, if a patient has a very reduced left ventricular ejection fraction, a large left ventricle and no perfusion defect (the MPS study is normal, but its gated SPECT component is abnormal), we categorize this type of study as "abnormal, with left ventricular enlargement, but no perfusion defects." We would then add a statement such as "the findings of severe left ventricular enlargement and severe depression of left ventricular ejection fraction with no associated perfusion defect are most consistent with a dilated nonischemic cardiomyopathic process." In our laboratory, many patients with a report such as this will not undergo subsequent cardiac catherization. Further noninvasive confirmation of the absence of ischemic heart disease is, however, often recommended in our reports by suggesting coronary calcium testing, CT coronary angiography, or delayed enhancement cardiac magnetic resonance imaging. A somewhat less common but important additional source of discordance between perfusion and function data occurs in patients with ventricular remodeling following myocardial infarction. These patients will typically have large nonreversible perfusion defects with no reversible perfusion defects, but marked left ventricular enlargement and reduction of left ventricular ejection fraction and regional ventricular function out of proportion to the size of the perfusion defect. In those circumstances, a statement such as this is included in the final summation: "The left ventricular enlargement and marked left abnormality of ventricular function are out of proportion to the size of the perfusion defect. These findings are most compatible with ventricular remodeling." Depending on the clinical situation, we may add, "less likely, but still possible, is the possibility that the patient has an ischemic cardiomyopathic process with balanced reduction in flow." To make the latter statement, we would usually like to have further evidence of exercise-induced ischemia or jeopardized myocardium, such as marked chest discomfort, ST segment depression or unexpected akinesis/dyskinesis in zones with normal resting motion or normal resting perfusion. We often include in our reporting of these patients a recommendation that FDG PET or cardiac magnetic resonance be considered for further noninvasive confirmation of the absence of extensive jeopardized myocardium.

In dilated nonischemic cardiomyopathic processes and in ventricular remodeling, the portions of the left ventricle demonstrating normal perfusion but abnormal function are usually hypokinetic. When frank akinesis or dyskinesis is noted in zones that appear to have normal perfusion, the final report is weighed toward the possibility of an ischemic cardiomyopathy with balanced reduction in flow, since stress-induced stunning would be more likely to be associated with akinesis or dyskinesis than with ventricular remodeling or nonischemic cardiomyopathic processes.

The overall interpretation of gated MPS remains an art. Following the systematic approach recommended in this chapter allows this art to be refined and makes the results more reproducible from observer to observer and from center to center.

Acknowledgments

The authors gratefully acknowledge the excellent assistance of Xingping Kang, MD, in the preparation of this chapter and James Gerlach, CNMT, for technical assistance in preparation of the figures.

References

1. Imaging guidelines for nuclear cardiology procedures, part 2. American Society of Nuclear Cardiology. Journal of Nuclear Cardiology 1999;6(2):G47–G84.
2. Cerqueira MD, Weissman NJ, Dilsizian V, et al. Standardized myocardial segmentation and nomenclature for tomographic imaging of the heart: a statement for healthcare professionals from the Cardiac Imaging Committee of the Council on Clinical Cardiology of the American Heart Association. Circulation 2002;105(4):539–542.
3. Hendel RC, Wackers FJ, Berman DS, et al. American Society of Nuclear Cardiology consensus statement: reporting of radionuclide myocardial perfusion imaging studies. Journal of Nuclear Cardiology 2003;10(6):705–708.
4. Hachamovitch R, Hayes S, Friedman JD, et al. Determinants of risk and its temporal variation in patients with normal stress myocardial perfusion scans: what is the warranty period of a normal scan? Journal of the American College of Cardiology 2003;41(8):1329–1340.
5. Friedman J, Van Train K, Maddahi J, et al. "Upward creep" of the heart: a frequent source of false-positive reversible defects during thallium-201 stress-redistribution SPECT. Journal of Nuclear Medicine 1989;30(10):1718–1722.
6. Prigent FM, Hyun M, Berman DS, Rozanski A. Effect of motion on thallium-201 SPECT studies: a simulation and clinical study. Journal of Nuclear Medicine 1993;34(11):1845–1850.

7. Kiat H, Van Train KF, Friedman JD, et al. Quantitative stress-redistribution thallium-201 SPECT using prone imaging: methodologic development and validation. Journal of Nuclear Medicine 1992;33(8):1509–1515.
8. Matsumoto N, Berman DS, Kavanagh PB, et al. Quantitative assessment of motion artifacts and validation of a new motion-correction program for myocardial perfusion SPECT. Journal of Nuclear Medicine 2001;42(5):687–694.
9. Germano G, Kiat H, Kavanagh PB, et al. Automatic quantification of ejection fraction from gated myocardial perfusion SPECT. Journal of Nuclear Medicine 1995;36(11):2138–2147.
10. Piwnica-Worms D, Holman BL. Noncardiac applications of hexakis(alkylisonitrile) technetium-99m complexes [comment]. Journal of Nuclear Medicine 1990;31(7):1166–1167.
11. Waxman AD. The role of (99m)Tc methoxyisobutylisonitrile in imaging breast cancer. Seminars in Nuclear Medicine 1997;27(1):40–54.
12. Aksut SV, Mallavarapu C, Russell J, Heo J, Iskandrian AS. Implications of increased lung thallium uptake during exercise single photon emission computed tomography imaging. American Heart Journal 1995;130(2):367–373.
13. Jain D, Thompson B, Wackers FJ, Zaret BL. Relevance of increased lung thallium uptake on stress imaging in patients with unstable angina and non-Q wave myocardial infarction: results of the Thrombolysis in Myocardial Infarction (TIMI)-IIIB Study. Journal of the American College of Cardiology 1997;30(2):421–429.
14. Vaccarino RA, Johnson LL, Antunes ML, et al. Thallium-201 lung uptake and peak treadmill exercise first-pass ejection fraction. American Heart Journal 1995;129(2):320–329.
15. Bacher-Stier C, Sharir T, Kavanagh PB, et al. Postexercise lung uptake of 99mTc-sestamibi determined by a new automatic technique: validation and application in detection of severe and extensive coronary artery disease and reduced left ventricular function. Journal of Nuclear Medicine 2000;41(7):1190–1197.
16. Tsou SS, Sun SS, Kao A, Lin CC, Lee CC. Exercise and rest technetium-99m-tetrofosmin lung uptake: correlation with left ventricular ejection fraction in patients with coronary artery disease. Japanese Heart Journal 2002;43(5):515–522.
17. Liu P, Kiess M, Okada RD, et al. Increased thallium lung uptake after exercise in isolated left anterior descending coronary artery disease. American Journal of Cardiology 1985;55(13, Pt 1):1469–1473.
18. Martinez EE, Horowitz SF, Castello HJ, et al. Lung and myocardial thallium-201 kinetics in resting patients with congestive heart failure: correlation with pulmonary capillary wedge pressure. American Heart Journal 1992;123(2):427–432.
19. Germano G, Chua T, Kiat H, Areeda JS, Berman DS. A quantitative phantom analysis of artifacts due to hepatic activity in technetium-99m myocardial perfusion SPECT studies. Journal of Nuclear Medicine 1994;35(2):356–359.
20. The Cardiovascular Imaging Committee, American College of Cardiology; The Committee on Advanced Cardiac Imaging and Technology, Council on Clinical Cardiology, American Heart Association; and Board of Directors, Cardiovascular Council, Society of Nuclear Medicine. Standardization of cardiac tomographic imaging. Journal of the American College of Cardiology 1992;20(1):255–256.
21. Edwards WD, Tajik AJ, Seward JB. Standardized nomenclature and anatomic basis for regional tomographic analysis of the heart. Mayo Clinical Proceedings 1981;56(8):479–497.
22. Berman DS, Kiat H, Van Train K, Garcia E, Friedman J, Maddahi J. Technetium 99m sestamibi in the assessment of chronic coronary artery disease [see comments]. Seminars in Nuclear Medicine 1991;21(3):190–212.
23. Reisman S, Berman D, Maddahi J, Swan HJ. The severe stress thallium defect: an indicator of critical coronary stenosis. American Heart Journal 1985;110(1, Pt 1):128–134.
24. Matzer L, Kiat H, Van Train K, et al. Quantitative severity of stress thallium-201 myocardial perfusion single-photon emission computed tomography defects in one-vessel coronary artery disease. American Journal of Cardiology 1993;72(3):273–279.
25. Berman DS, Hachamovitch R, Kiat H, et al. Incremental value of prognostic testing in patients with known or suspected ischemic heart disease: a basis for optimal utilization of exercise technetium-99m sestamibi myocardial perfusion single-photon emission computed tomography. Journal of the American College of Cardiology 1995;26(3):639–647.
26. Hachamovitch R, Berman DS, Kiat H, et al. Exercise myocardial perfusion SPECT in patients without known coronary artery disease: incremental prognostic value and use in risk stratification. Circulation 1996;93(5):905–914.
27. Hachamovitch R, Berman DS, Shaw LJ, et al. Incremental prognostic value of myocardial perfusion single photon emission computed tomography for the prediction of cardiac death: differential stratification for risk of cardiac death and myocardial infarction. Circulation 1998;97(6):535–543.
28. Hachamovitch R, Hayes SW, Friedman JD, Cohen I, Berman DS. Comparison of the short-term survival benefit associated with revascularization compared with medical therapy in patients with no prior coronary artery disease undergoing stress myocardial perfusion single photon emission computed tomography. Circulation 2003;107(23):2900–2907.
29. Berman DS, Abidov A, Kang X, et al. Prognostic validation of a 17-segment score derived from a 20-segment score for myocardial perfusion SPECT interpretation. Journal of Nuclear Cardiology 2004;11:414–423.
30. Berman DS, Kiat H, Friedman JD, et al. Separate acquisition rest thallium-201/stress technetium-99m sestamibi dual-isotope myocardial perfusion single-photon emission computed tomography: a clinical validation study. Journal of the American College of Cardiology 1993;22(5):1455–1464.
31. Berman DS, Hachamovitch R, Shaw LJ, Hayes SW, Germano G. Nuclear cardiology. In Fuster V AR, O'Rourke RA, Roberts

R, King SB, Wellens HJJ, eds. Hurst's The Heart. 11th edn. New York: McGraw-Hill; 2004:563–597.
32. Ficaro EP, Fessler JA, Shreve PD, Kritzman JN, Rose PA, Corbett JR. Simultaneous transmission/emission myocardial perfusion tomography. Diagnostic accuracy of attenuation-corrected 99mTc-sestamibi single-photon emission computed tomography. Circulation 1996;93(3):463–473.
33. Cullom S, Hendel R, Liu L, Garcia E, White M, Berman D. Diagnostic accuracy and image quality of a scatter, attenuation and resolution compensation method for Tc-99m cardiac SPECT: preliminary results [abstract]. Journal of Nuclear Medicine 1996;37(5):81P.
34. Slomka PJ, Berman DS, Germano G. Quantification of serial changes in myocardial perfusion. Journal of Nuclear Medicine 2004;45(12):1978–1980.
35. Nishina H, Slomka PJ, Abidov A, et al. Combined supine and prone quantitative myocardial perfusion SPECT: method development and clinical validation in patients with no known coronary artery disease. Journal of Nuclear Medicine 2006;47(1):51–58.
36. Bonow R. Assessment of myocardial viability with thallium-201. In Beller G, ed. Nuclear Cardiology: State of the Art and Future Directions. 2nd edn. St. Louis, MO: Mosby; 1998:503–512.
37. Udelson JE, Coleman PS, Metherall J, et al. Predicting recovery of severe regional ventricular dysfunction. Comparison of resting scintigraphy with 201Tl and 99mTc-sestamibi. Circulation 1994;89(6):2552–2561.
38. Weiss AT, Berman DS, Lew AS, et al. Transient ischemic dilation of the left ventricle on stress thallium-201 scintigraphy: a marker of severe and extensive coronary artery disease. Journal of the American College of Cardiology. 1987;9:752–759.
39. Mazzanti M, Germano G, Kiat H, et al. Identification of severe and extensive coronary artery disease by automatic measurement of transient ischemic dilation of the left ventricle in dual-isotope myocardial perfusion SPECT. Journal of the American College of Cardiology 1996;27(7):1612–1620.
40. Abidov A, Bax JJ, Hayes SW, et al. Integration of automatically measured transient ischemic dilation ratio into interpretation of adenosine stress myocardial perfusion SPECT for detection of severe and extensive CAD. Journal of Nuclear Medicine 2004;45:1999–2007.
41. Abidov A, Bax JJ, Hayes SW, et al. Transient ischemic dilation ratio of the left ventricle is a significant predictor of future cardiac events in patients with otherwise normal myocardial perfusion SPECT. Journal of the American College of Cardiology 2003;42:1818–1825.
42. Berman DS, Yang LD, Slomka P, et al. Comparison of quantitative total perfusion deficit on same day rest Tl-201 and rest Tc-99m sestamibi myocaridal perfsuion SPECT [abstract]. Journal of Nuclear Medicine 2005;46:277P.
43. Chouraqui P, Rodrigues EA, Berman DS, Maddahi J. Significance of dipyridamole-induced transient dilation of the left ventricle during thallium-201 scintigraphy in suspected coronary artery disease. American Journal of Cardiology 1990;66(7):689–694.
44. Johnson LL, Verdesca SA, Aude WY, et al. Postischemic stunning can affect left ventricular ejection fraction and regional wall motion on post-stress gated sestamibi tomograms [see comments]. Journal of the American College of Cardiology 1997;30(7):1641–1648.
45. Sharir T, Bacher-Stier C, Dhar S, et al. Identification of severe and extensive coronary artery disease by postexercise regional wall motion abnormalities in Tc-99m sestamibi gated single-photon emission computed tomography. American Journal of Cardiology 2000;86(11):1171–1175.
46. Germano G, Erel J, Lewin H, Kavanagh PB, Berman DS. Automatic quantitation of regional myocardial wall motion and thickening from gated technetium-99m sestamibi myocardial perfusion single-photon emission computed tomography. Journal of the American College of Cardiology 1997;30(5):1360–1367.
47. Shen MY, Liu YH, Sinusas AJ, et al. Quantification of regional myocardial wall thickening on electrocardiogram-gated SPECT imaging. Journal of Nuclear Cardiology 1999;6(6):583–595.
48. Germano G, Berman DS. On the accuracy and reproducibility of quantitative gated myocardial perfusion SPECT [editorial; comment]. Journal of Nuclear Medicine 1999;40(5):810–813.
49. Berman DS, Kang X, Van Train KF, et al. Comparative prognostic value of automatic quantitative analysis versus semiquantitative visual analysis of exercise myocardial perfusion single-photon emission computed tomography. Journal of the American College of Cardiology 1998;32(7):1987–1995.
50. Germano G, Kavanagh PB, Kavanagh JT, Wishner SH, Berman DS, Kavanagh GJ. Repeatability of automatic left ventricular cavity volume measurements from myocardial perfusion SPECT. Journal of Nuclear Cardiology 1998;5(5):477–483.
51. White HD, Norris RM, Brown MA, Brandt PW, Whitlock RM, Wild CJ. Left ventricular end-systolic volume as the major determinant of survival after recovery from myocardial infarction. Circulation 1987;76(1):44–51.
52. Pfeffer MA, Braunwald E, Moye LA, et al., for The SAVE Investigators. Effect of captopril on mortality and morbidity in patients with left ventricular dysfunction after myocardial infarction. Results of the survival and ventricular enlargement trial. [see comments]. New England Journal of Medicine 1992;327(10):669–677.
53. Abidov A, Hachamovitch, R, Hayes, SW, et al. Prognostic impact of hemodynamic response to adenosine in patients older than age 55 years undergoing vasodilator stress myocardial perfusion study. Circulation 2003;107:2894–2899.
54. Hachamovitch R, Hayes SW, Friedman JD, Cohen I, Berman DS. A prognostic score for prediction of cardiac mortality risk after adenosine stress myocardial perfusion scintigraphy. Journal of the American College of Cardiology 2005;45(5):722–729.
55. Diamond GA, Staniloff HM, Forrester JS, Pollock BH, Swan HJ. Computer-assisted diagnosis in the noninvasive evaluation of patients with suspected coronary artery disease.

Journal of the American College of Cardiology 1983;1(2, Pt 1): 444–455.
56. Staniloff HM, Forrester JS, Berman DS, Swan HJ. Prediction of death, myocardial infarction, and worsening chest pain using thallium scintigraphy and exercise electrocardiography. Journal of Nuclear Medicine 1986;27(12):1842–1848.
57. Pryor DB, Shaw L, Harrell FE Jr, et al. Estimating the likelihood of severe coronary artery disease. American Journal of Medicine 1991;90(5):553–562.
58. Iskandrian AS, Verani MS, Heo J. Pharmacologic stress testing: mechanism of action, hemodynamic responses, and results in detection of coronary artery disease. Journal of Nuclear Cardiology 1994;1(1):94–111.
59. Smith WH, Kastner RJ, Calnon DA, Segalla D, Beller GA, Watson DD. Quantitative gated single photon emission computed tomography imaging: a counts-based method for display and measurement of regional and global ventricular systolic function. Journal of Nuclear Cardiology 1997;4:451–463.

7 Artifacts caused by and clarified by gated myocardial perfusion SPECT

E. Gordon DePuey

Introduction

One of the most important aspects of gated SPECT interpretation is the appropriate recognition of artifacts. This chapter deals with various SPECT artifacts and the way in which the interpretation of regional function can help identify the artifacts as well as the way in which ECG gating can actually contribute to artifacts. The reader is also referred to Chapter 6 for further consideration of these issues.

Soft tissue attenuation artifacts

Soft tissue attenuation artifacts are a common cause of false-positive myocardial perfusion SPECT [1]. Soft tissue attenuators such as the breast, the left hemidiaphragm, and lateral chest wall fat may mimic true perfusion defects. These artifacts usually appear as fixed defects and could be mistaken for myocardial scarring. However, if there is a shift in the position of the soft tissue attenuator from rest to stress, artifactual perfusion defects may show "reverse distribution" mimicking subendocardial infarction with a patent vessel [2–4], or reversible defects mimicking myocardial ischemia [2]. Gated perfusion SPECT has been demonstrated to be very helpful to differentiate soft tissue attenuation versus scar as a cause of fixed perfusion defects [1–3,5–7]. Whereas myocardial scarring usually demonstrates regional left ventricular dysfunction and decreased wall thickening, defects secondary to soft tissue attenuation would show normal motion and thickening. The principal exception to this would be a true moderate nonreversible defect in a region with partial thickness infarction, in which case the wall motion might be normal (see Chapter 6). Of note, however, in the setting of apparently reversible defects due to shifting soft tissue attenuation, gating is less helpful since normal regional function might be seen in ischemic regions as well as in regions with artifacts. Guidelines to incorporate gated SPECT to differentiate specific attenuation artifacts from scar are discussed below.

Breast attenuation

Breast attenuation is a common source of artifactual defects on SPECT. To detect this source, the planar projection images displayed in endless-loop cinematic format should be inspected carefully. These should be displayed in a linear gray scale (or a similar linear color scale) in order to accentuate the soft tissues. The position of the left breast should be ascertained. Usually a curvilinear "shadow" can be observed corresponding to the inferior and inferoposterior margins of the left breast. The breast shadow may lie over the anterior/anterolateral portion of the heart, or when pendulous, may be positioned posterolaterally, or even predominantly over the inferior wall of the heart. By determining the position of the breast soft tissue attenuation, the observer can anticipate the location of the corresponding myocardial perfusion SPECT attenuation artifact. Similarly, the thickness or density of the breast can be approximated by the degree of photopenia associated with the breast "shadow." For example, a small breast that is difficult to localize in the cine planar projection images is unlikely to create a significant attenuation artifact. In contrast, a large, dense breast that "eclipses" the heart in the cine planar projection images may create a severe, discrete attenuation artifact.

In the reconstructed tomographic slices the breast attenuation artifact will appear as a fixed defect, assuming that the breast has not shifted in position from the rest to stress images. If a single-day low-dose/high-dose Tc-99m agent protocol is employed, the attenuation artifact may appear more severe in the low count density resting images [8]. The location of the fixed or "reverse distribution" defect should correspond approximately to the location of the overlying breast "shadow" previously observed in the cine planar projection images.

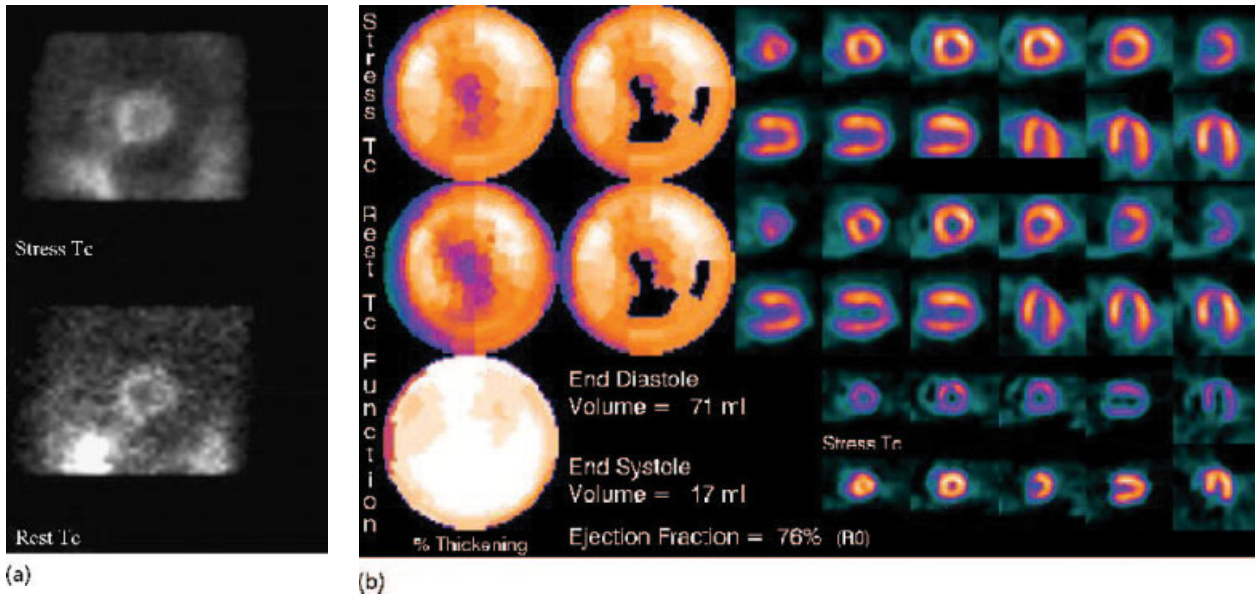

Figure 7.1 (a) Stress (top) and rest (bottom) planar projection images demonstrate a large, "circular," photopenic "shadow" overlying the entire heart in the left anterior oblique view. This breast "shadow" appears to "eclipse" the entire heart. (b) Stress and rest tomographic images demonstrate a moderately extensive, moderately severe, fixed decrease in tracer concentration in the apex and distal portion of the left ventricle. Quantitative perfusion polar plots wherein patient data are compared to female gender-matched normal files (Emory Toolbox® software) identify an "abnormal" decrease in tracer concentration in the apex and distal anterior wall. Gated post-stress tomograms demonstrate normal left ventricular wall motion and wall thickening, including that of the apex. Quantitative analysis of left ventricular wall thickening in polar plot format confirms the presence of normal left ventricular wall thickening. The combination of perfusion and functional findings favor breast attenuation rather than scar as the cause of the fixed apical perfusion defect.

Gated tomographic images will demonstrate normal regional wall motion and wall thickening in the distribution of the fixed defect if it is due to breast attenuation artifact. Inspection of regional wall motion in gated tomographic slices is particularly advantageous in determining if there is normal regional left ventricular function precisely in the distribution of the fixed perfusion defect. In three-dimensional gated displays it is usually more difficult to correlate regional function with the precise perfusion defect. Regional wall motion is best evaluated using a black and white display with some degree of thresholding (approximately 8–10% background subtraction) to enhance the endocardial border in order to evaluate regional wall motion. Wall thickening is usually better evaluated using a color scale because changes in intensity, proportional to wall thickening, may be evaluated with greater sensitivity in color than in black and white. Quantitative polar map displays of wall thickening may also be useful in differentiating normal versus abnormal wall thickening. Whereas determining changes in intensity from end-diastole to end-systole of a perfusion defect as compared to that of "normal" myocardium may be difficult by visual inspection alone, the quantitative displays can provide the percent change in count density of each pixel from end-diastole to end-systole and thereby help to objectify the analysis of wall thickening. However, each individual observer should choose the display with which he or she is best able to appreciate these parameters of wall motion and wall thickening. A case example of a patient with an anterior wall breast attenuation artifact is shown in Fig. 7.1.

Diaphragmatic attenuation

Diaphragmatic attenuation is also a common source of artifactual perfusion defects, particularly in men. As with identifying breast attenuation, a stepwise, systematic approach in image interpretation, incorporating gated SPECT images is advantageous in differentiating diaphragmatic attenuation artifact from scar as a cause of fixed inferior perfusion defects [9]. The planar projection images should be inspected in endless-loop cinematic format using a linear gray scale to ascertain the position of the left hemidiaphragm. Usually a photopenic "shadow" (albeit often indistinct) can be detected corresponding to air or fluid in the fundus of the stomach or under the left hemidiaphragm itself. If the shadow lies entirely below the inferior wall of the left ventricle in the planar projection images, diaphragmatic attenuation artifact is very unlikely. However, if the "shadow" overlies the inferior wall, particularly in the left lateral projection images, diaphragmatic attenuation artifact is more likely.

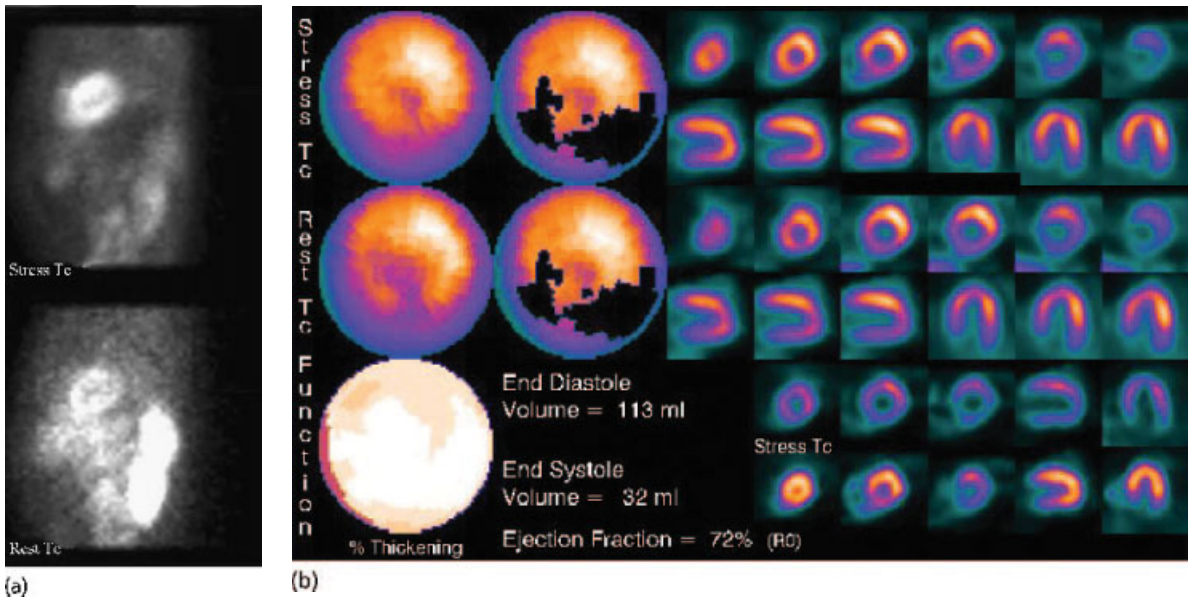

Figure 7.2 (a) In the planar projection images the location of the left hemidiaphragm can be identified as a curvilinear photopenic shadow. In this case example of a male patient the left hemidiaphragm is relatively high, and so diaphragmatic attenuation of the inferior wall of the left ventricle may be anticipated. (b) Stress and rest tomographic images demonstrate an extensive, moderately severe fixed defect in the inferior wall of the left ventricle. Quantitative perfusion polar plots wherein patient data are compared to male gender-matched normal files (Emory Toolbox® software). Gated tomograms demonstrate normal left ventricular wall motion and wall thickening. Quantitative analysis of wall thickening displayed in polar plot format similarly demonstrates normal inferior wall thickening, favoring inferior attenuation artifact rather than scar.

Tomographic images demonstrate a fixed inferior perfusion defect either with myocardial scarring or with diaphragmatic attenuation artifact. As noted above for breast attenuation, if a single-day rest/stress Tc-99m labeled imaging protocol is used, diaphragmatic attenuation artifacts may appear somewhat more marked in the low count density resting tomograms. In vertical long-axis tomograms, with diaphragmatic attenuation the inferior wall often appears to "taper" from apex to base, whereas with myocardial scarring the inferior perfusion defect often appears more discrete with an abrupt decrease in count density.

Gated perfusion tomograms will demonstrate normal wall motion and wall thickening if the fixed inferior defect is secondary to diaphragmatic attenuation. In contrast, inferior myocardial scarring usually exhibits decreased wall motion and wall thickening. Suggestions offered for evaluating wall motion and wall thickening in patients with suspected breast attenuation (see above) are equally helpful in evaluating the inferior myocardial wall. A case example of a patient with a diaphragmatic attenuation artifact is shown in Fig. 7.2 and a patient with a true inferior wall defect due to myocardial scarring is shown in Fig. 7.3.

Lateral chest wall attenuation

In obese individuals, lateral chest wall fat not only attenuates photons emanating from the myocardium but also increases the distance between the heart and the scintillation detector. Thereby, in such individuals, lateral chest wall fat may result in lateral wall attenuation artifacts that may mimic true perfusion defects. As for other soft tissue attenuators, inspection of the planar projection images in endless-loop cinematic format is of considerable value. A photopenic defect overlying the posterolateral wall of the left ventricle may be observed corresponding to a large, dense fat fold. Alternately, the attenuation effect may be diffuse, whereby the heart seems to "disappear" in the left lateral and left posterior oblique planar projections.

Either the discrete or diffuse attenuation effects of lateral chest wall soft tissue may create lateral wall myocardial attenuation artifacts that may simulate true perfusion defects in the circumflex coronary artery territory. Although these abnormalities may not be readily apparent by visual inspection of the perfusion tomograms, because the lateral wall may be less intense than the septum, abnormalities are accentuated when patient data are compared to gender-matched normal files (in which the lateral wall is "anticipated" to be more intense than the septum).

Gated tomograms will demonstrate normal wall motion and thickening of the lateral wall if the fixed defect is due to attenuation artifact, whereas abnormal wall motion and wall thickening may be observed in the presence of lateral myocardial scarring. A case example of a patient demonstrating lateral chest wall attenuation artifact is shown in Fig. 7.4.

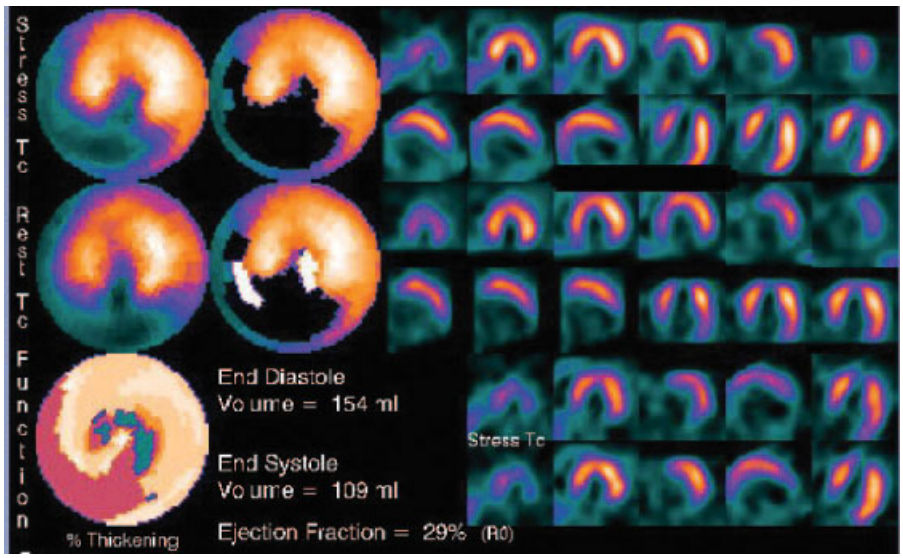

Figure 7.3 Stress and rest tomographic images demonstrate an extensive fixed defect in the inferior wall of the left ventricle. Gated tomograms demonstrate absent wall thickening. Count density is decreased to such a degree that in this color display inferior wall thickening cannot be adequately assessed. Quantitative analysis of wall thickening displayed in polar plot format demonstrates markedly decreased to absent inferior wall thickening, favoring inferior myocardial scarring rather than attenuation artifact as a cause of the fixed inferior defect.

In the case of lateral wall defects, gated imaging may be more difficult to interpret than in the case of anterior or inferior defects (as described above). During systole there is rotational and anterior translational motion of the heart. This motion tends to counterbalance the posterior, inward motion of the septum and accentuates the anterior motion of the posterolateral wall [10]. Therefore, even in the presence of myocardial scarring, there may appear to be preserved motion of the posterolateral wall. For this reason, it is important to evaluate not only wall motion but also wall thickening. Whereas a posterolateral scar may demonstrate relatively normal wall motion, abnormal wall thickening will be manifest as a failure to increase count density during systole. A case example of true posterolateral scan with preserved wall motion but abnormal wall thickening is shown in Fig. 7.5.

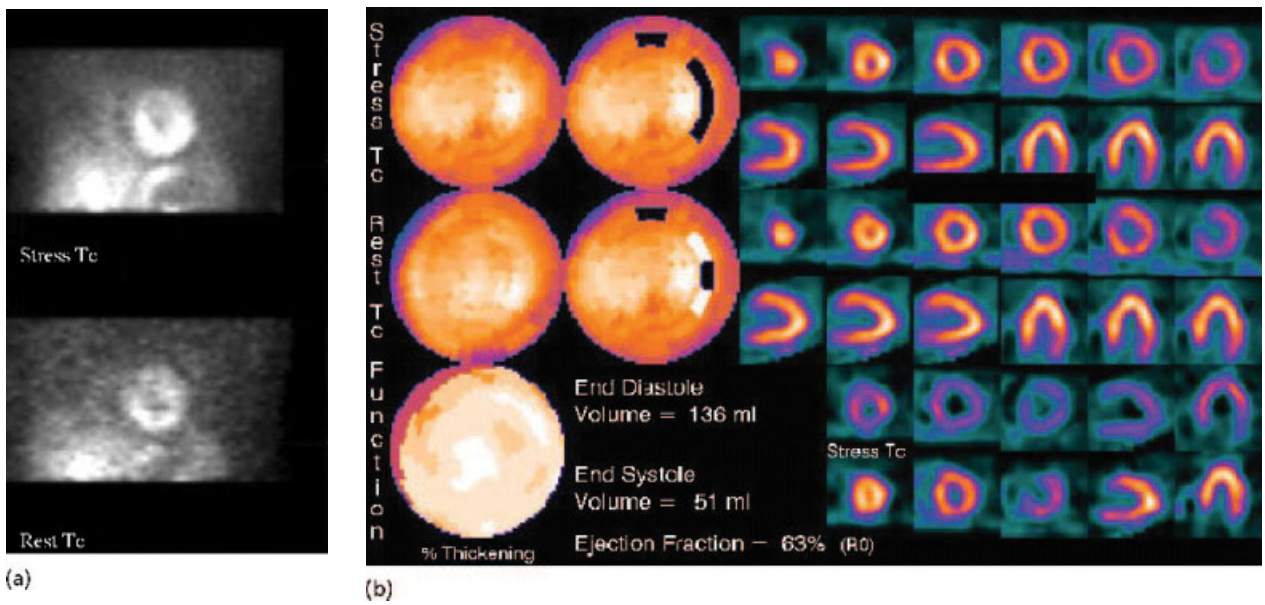

Figure 7.4 (a) In planar projection images it is apparent that this female patient is very obese, with a considerable distance between the lateral border of the left ventricle and the left lateral chest wall. (b) Stress and rest tomographic images demonstrate a moderate decrease in tracer concentration in the basal half of the posterolateral wall of the left ventricle. As compared to the septum, the lateral wall is less intense. This is an abnormal scan finding, since the lateral wall should normally be more intense than the septum. Gated tomograms demonstrate normal wall motion and wall thickening of the entire left ventricle, including that of the posterolateral wall. Quantitative analysis of wall thickening displayed in polar plot format similarly demonstrates normal posterolateral wall thickening, favoring lateral wall soft tissue attenuation artifact rather than scar as a cause of the fixed posterolateral defect.

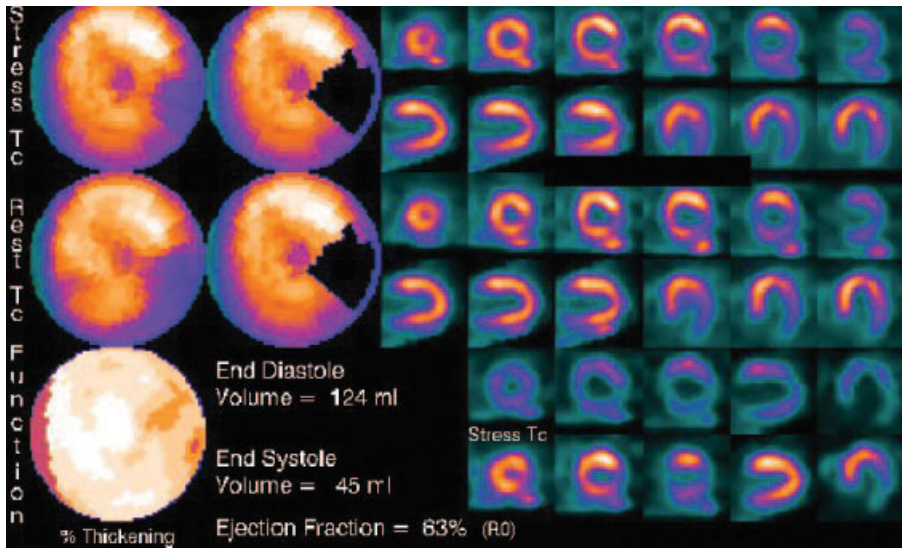

Figure 7.5 Stress and rest tomographic images demonstrate a marked fixed defect involving the basal half of the posterolateral wall of the left ventricle. Gated tomographic images demonstrate markedly decreased wall thickening of the fixed defect. However, posterolateral wall motion is relatively well preserved, most likely accounted for by the anterior translational motion of the heart during systole. Quantitative analysis of wall thickening displayed in polar plot format demonstrates markedly decreased posterolateral wall thickening, consistent with myocardial scarring rather than attenuation artifact as a cause of the fixed posterolateral defect.

Left arm attenuation

Although it is much preferred to image patients with both arms, or at least the left arm, raised above the head, in some patients, particularly those who are early postoperative or in those with arthritis, elevation of the left arm is sometimes not possible. Under such circumstances gated SPECT may be performed with the left arm by the patient's side [11]. The arm should be positioned as posteriorly as possible to minimize attenuation of the myocardium in the 180° SPECT imaging arc. Nevertheless, even with these precautions, lateral wall attenuation artifacts are frequently encountered when patients are imaged with the left arm down. These attenuation artifacts may be particularly severe because not only soft tissue but also bone attenuates photons emanating from the myocardium.

In the planar projection images viewed in a endless-loop cinematic format the position of the arm should be ascertained, particularly the position of the humerus in relation to the lateral/posterolateral wall of the left ventricle. It is particularly important to determine that the position of the arm is identical in the stress and rest images. Otherwise, variable attenuation in the stress and rest tomograms may be present, mimicking a reversible, i.e. ischemic, perfusion defect.

Unlike patients with lateral chest wall fat attenuation, because of the severity of attenuation caused by the humerus, localized attenuation encountered in patients imaged with the left arm down may be particularly marked. Therefore, in tomographic images left arm attenuation artifacts may appear relatively severe and discrete.

Gated tomographic images will exhibit normal wall motion and wall thickening in the case of left arm attenuation artifacts, whereas wall thickening and usually wall motion abnormalities will be expected in patients with posterolateral myocardial scars. As for patients with lateral chest wall fat attenuation artifacts, the observer should evaluate both wall motion and wall thickening since physiological anterior cardiac translational motion during systole may minimize wall motion abnormalities in patients with posterolateral scars.

Normal anatomic variants mimicking perfusion defects

Apical thinning

Variants in myocardial anatomy may mimic fixed perfusion defects. A fixed apical defect may be present due to "physiological apical thinning." The etiology of this scan finding is not precisely known, but it is postulated that a localized decrease in count density at the left ventricular apex may be secondary to actual anatomic thinning of the apex as compared to the remainder of the left ventricular myocardium. Alternately, the apex may appear thinner because spatial resolution of the apex is greatest since it is closest to the scintillation detector. Moreover, in most patients the apex is not attenuated by soft tissue. Of note, such apical defects may be accentuated with attenuation correction, presumably by "eliminating" soft tissue attenuation. Being closer to the collimator, the resolution of the apex is further enhanced, thereby making it appear even thinner [12]. Finally, SPECT artifacts due to center of rotation error, camera head misalignment, and patient motion are usually more marked at the left ventricular apex [2].

Because the apical defects described above are usually small and discrete, inspection of planar projection

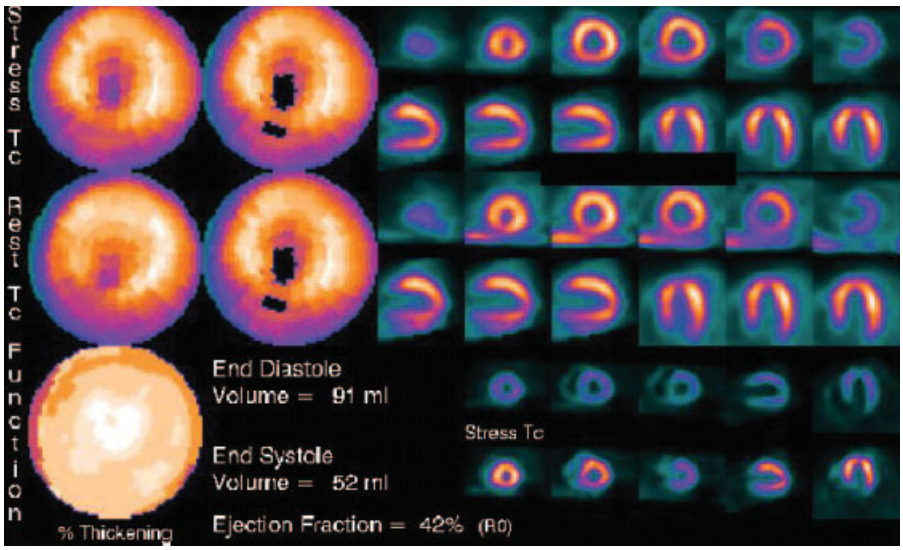

Figure 7.6 Stress and rest tomographic images demonstrate a small, moderately severe "cleft-like" defect at the apex of the left ventricle. Gated tomographic images clearly demonstrate normal wall motion and wall thickening of the apex. Quantitative analysis of wall thickening displayed in polar plot format similarly demonstrates normal myocardial wall thickening, including that of the apex, favoring "normal physiological apical thinning" rather than localized scarring as a cause of the fixed apical defect.

images is seldom of value in identifying such abnormalities. However, inspection of the planar projection images in endless-loop cinematic format is critical in identifying patient motion as a cause of such defects.

In horizontal long-axis and vertical long-axis tomograms "apical thinning" usually appears as a discrete, linear defect at the very apex of the left ventricle. True perfusion abnormalities due to coronary artery disease are usually larger, extending to the anterior or inferior walls.

Gated perfusion tomograms will exhibit normal wall motion and thickening in patients with "physiological apical thinning" or in those in whom the apical defects are due to patient motion or center of rotation error. Discrete apical myocardial scarring frequently produces a localized wall motion abnormality. A case example of physiological apical thinning is shown in Fig. 7.6.

The "11 o'clock" defect

Frequently discrete, linear defects extending through the myocardium are noted at approximately 11 o'clock and 7 o'clock in the short-axis tomograms. The precise cause of these defects is not known. However, because they are almost invariably located adjacent to the insertion points of the right ventricular myocardium as it joins the septum, they are most likely either anatomic variants or related to attenuation by the right ventricle myocardium and/or blood pool. An experienced observer generally has no difficulty in identifying these defects as artifacts/variants. However, gated perfusion SPECT may be of additional value in differentiating such artifacts from actual localized anteroseptal and inferoseptal myocardial scars. Regional wall motion and wall thickening will be entirely normal at the site of these septal artifacts/variants.

Artifacts associated with SPECT image normalization

When regions of the myocardium are increased in intensity due to image normalization to 100% of maximal myocardial count density, such areas will appear normal and other, remote areas may exhibit relatively decreased count density. These remote areas of relatively decreased count density may mimic true perfusion abnormalities. This phenomenon is called by some a "hot spot" artifact. If the erroneous normalization is equivalent at both stress and rest, defects will appear fixed, mimicking myocardial scar. However, if the source of increased myocardial count density is inconsistent from stress to rest, the normalization effect will be variable, and defects may appear reversible, or there may appear to be "reverse distribution." In the case of fixed defects, gated perfusion SPECT may be of considerable value in differentiating scar from normalization artifact.

Left ventricular hypertrophy

In patients with left ventricular hypertrophy there may be a diffuse increase in count density throughout the myocardium. Alternately, there may be a localized increase in count density, most often in the septum, papillary muscle, or apex [13]. Increased septal count density may be present in patients with idiopathic hypertrophic subaortic stenosis (IHSS), but may also be noted in patients with concentric myocardial hypertrophy because the septum

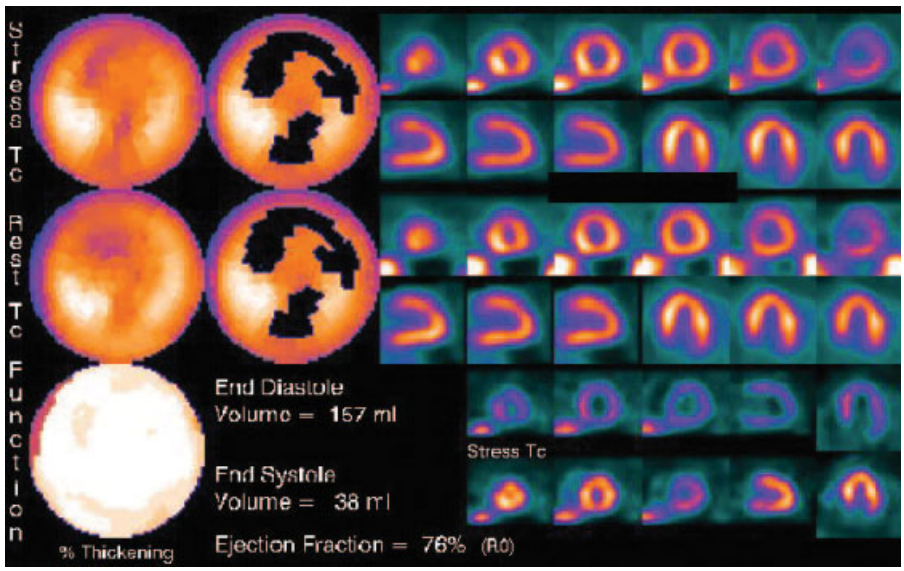

Figure 7.7 Stress and rest tomographic images in this woman with long-standing hypertension demonstrate a relative increase in tracer concentration and the septum and consequently a relative decrease in tracer concentration throughout the remainder of the left ventricular myocardium. Quantitative polar maps, comparing patient data to gender-matched normal limits, accentuate the relative decrease in tracer concentration in regions of myocardium apart from the septum. Gated tomographic images demonstrate normal left ventricular wall motion and wall thickening, including the areas of relatively decreased tracer concentration. Quantitative analysis of myocardial wall thickening displayed in polar plot format similarly demonstrates normal global left ventricular wall thickening. Scarring of the entire left ventricular myocardium, sparing only the septum, would be highly unlikely in the presence of such normal ventricular function. Therefore, combined perfusion and function findings favor increased septal count density secondary to left ventricular hypertrophy rather than myocardial scarring sparing only the septum as a cause of the fixed defects demonstrated by quantitative analysis.

hypertrophies to a slightly greater degree than the remainder of the left ventricle. Papillary muscle hypertrophy occurs commonly in patients with concentric myocardial hypertrophy, producing a localized "hot spot" in the lateral wall of the left ventricle. Localized apical hypertrophy, a variant of hypertrophic cardiomyopathy, frequently produces a localized increase in tracer concentration in the apex. Because of the process of SPECT image normalization, regions of myocardium remote from the septum, papillary muscle, or apex may exhibit relatively decreased count density.

Standard visual inspection of tomographic slices in these patients is often problematic because of this image normalization process. Often it is necessary for the interpreting physician to manually increase count density so that the localized septal, papillary muscle, or apex appears "hot," with remote areas of myocardium appearing "normal." However, interpreting physicians must be cautioned regarding the subjectivity of such manual image manipulation.

Gated perfusion imaging may be quite useful in differentiating an extensive area of myocardial scarring from a localized area of relatively increased tracer concentration. If the regions of decreased count density move and thicken normally, it is unlikely that they represent extensive myocardial scarring. Figure 7.7 illustrates a patient with increased septal count density due to left ventricular hypertrophy, and Fig. 7.8 shows a patient with relatively decreased inferior count density due to anterior papillary muscle hypertrophy.

Compton scatter

Compton scattered radiation from subdiaphragmatic structures such as the liver, stomach, or bowel may artifactually increase the count density of the inferior wall of the left ventricle. As described above for regions of relative myocardial hypertrophy, due to the process of image normalization, the artifactually increased count density of the inferior wall may appear "normal" (100% of maximal activity) and remote areas with relatively decreased activity may be misinterpreted as true perfusion defects. If the scatter artifact is identical in rest and stress tomograms, gating may be helpful in differentiating artifact from scar as a cause of the localized decreased in count density in areas remote from the inferior wall. However, in most instances the degree of scatter from subdiaphragmatic activity is variable from stress to rest, and therefore the process of image normalization creates variable artifacts in remote walls, mimicking ischemia rather than scar. For

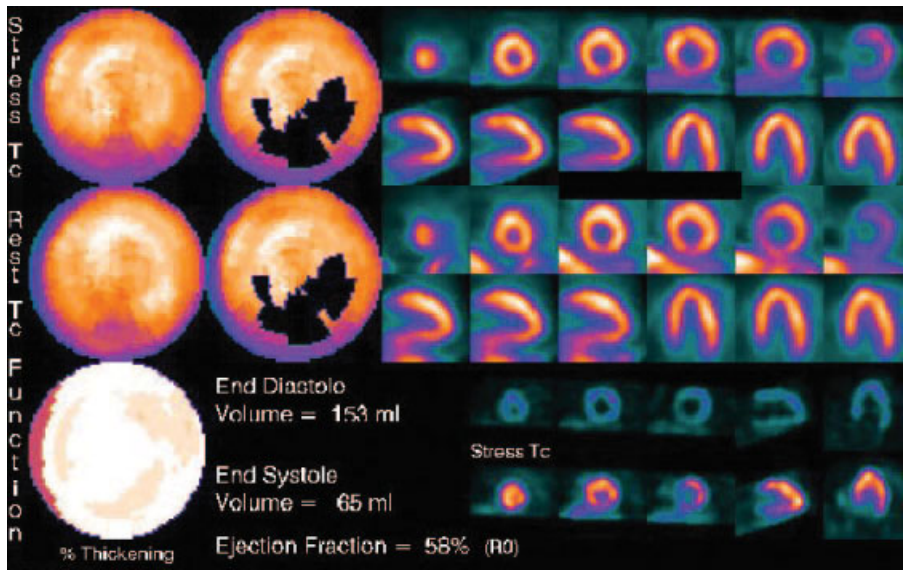

Figure 7.8 Stress and rest tomographic images in this man with long-standing hypertension demonstrate a relative increase in tracer concentration localized into the anterior wall of the left ventricle and the region of the anterior papillary muscle and consequently a relative decrease in tracer concentration throughout the remainder of the left ventricular myocardium, particularly the inferior wall. Quantitative polar maps, comparing patient data to gender-matched normal limits, accentuate the relative decrease in tracer concentration in regions of myocardium apart from the "hot" anterior papillary muscle. Gated tomographic images demonstrate normal left ventricular wall motion and wall thickening, including areas of relatively decreased tracer concentration. Quantitative analysis of myocardial wall thickening displayed in polar plot format similarly demonstrates normal global left ventricular wall thickening. These findings favor a localized anterior "hot spot" to which myocardial counts are normalized rather than scarring of the inferior wall.

this reason, gating is usually of relatively limited value in differentiating scatter artifacts from true perfusion defects.

Limitations of gated perfusion SPECT in differentiating artifacts from true perfusion defects

Myocardial ischemia

Gated perfusion imaging is of very limited value in differentiating stress-induced ischemia from a perfusion artifact that is present in the stress SPECT image only but not present at rest. Because the gated acquisition is performed poststress, usually 20–30 minutes postexercise or 30–45 minutes postpharmacologic stress, the post-stress gated images generally reflect *resting* left ventricular function. Only in the presence of post-stress myocardial stunning will a functional abnormality occur in the presence of a reversible perfusion defect [14] (see Chapters 5 and 6). The great majority of stress-induced perfusion abnormalities will demonstrate normal left ventricular function at the time of delayed SPECT image acquisition. Artifacts present in stress tomograms but not at rest will similarly demonstrate normal left ventricular function in post-stress gated images. Therefore, observation of ventricular function on gated perfusion SPECT is usually not helpful in differentiating stress-induced ischemia from artifacts present only in stress images.

Hibernating myocardium

In the presence of resting myocardial hypoperfusion, there is a down-regulation of left ventricular function, a mechanism useful to decrease myocardial oxygen demand in the face of diminished oxygen supply. Such a decrease in resting regional ventricular function has been termed "hibernating myocardium." While areas of hibernation are typically supplied by critical coronary stenoses, there is usually a perceptible worsening of myocardial perfusion on stress images in patients with hibernation. In many instances, however, the resting perfusion will be severely enough reduced so that additional stress-induced ischemia is not apparent. Therefore, gated perfusion SPECT may demonstrate a localized, fixed perfusion defect with an associated regional wall motion abnormality. The appearance of such an abnormality is identical to that of a myocardial scar with an associated regional wall motion abnormality. Therefore, gated perfusion SPECT is of limited value in differentiating viable, hibernating myocardium from myocardial scar [15,16] unless additional

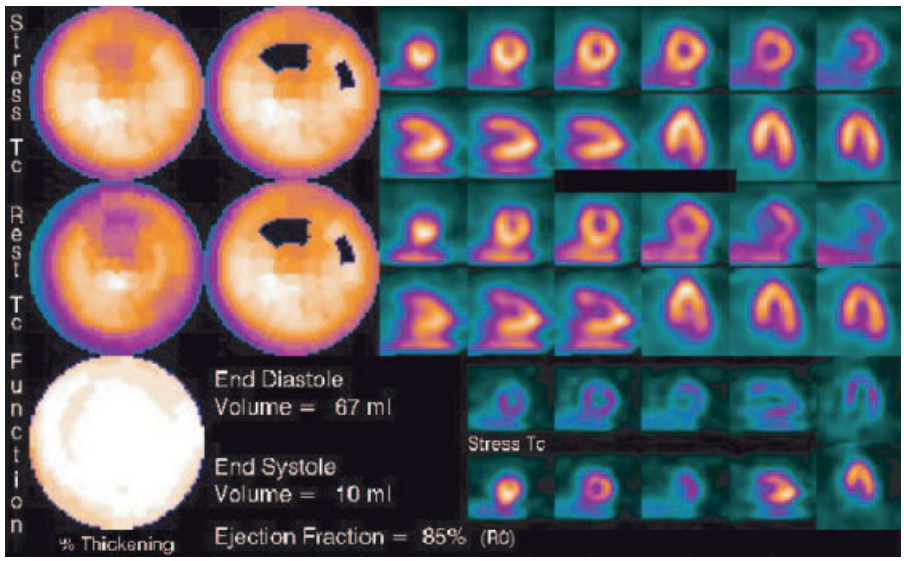

Figure 7.9 Stress tomographic images demonstrate a mild decrease in tracer concentration in the anterior wall of the left ventricle. In resting tomographic images the anterior defect is considerably more marked and extensive, findings consistent with "reverse distribution." These findings are corroborated in quantitative polar plots. Gated tomographic images demonstrate normal left ventricular wall motion and wall thickening, including that of the anterior wall. Quantitative analysis of myocardial wall thickening displayed in polar plot format similarly demonstrates normal global left ventricular wall thickening. This constellation of "reverse distribution" with normal regional wall motion and thickening may be observed either in a patient with soft tissue attenuation artifacts undergoing a single-day rest/stress Tc-99m protocol or in a patient with a nontransmural myocardial infarct with a patent proximal coronary artery. In this case example the severity and discrete nature of the anterior defect would favor the latter. The patient in this case example is a female who presented to the emergency department with an acute myocardial infarction and was sent immediately for percutaneous coronary angioplasty (PTCA) of the left anterior descending coronary artery. Post-PTCA coronary angiography demonstrated a patent left anterior descending, and cardiac enzymes suggested only a small degree of myocardial damage associated with the acute infarct.

gated SPECT imaging is performed after nitroglycerin or during low-dose dobutamine stress [17,18].

Nontransmural myocardial infarction

Nontransmural myocardial infarcts, i.e. subendocardial infarcts, with no additional stress-induced ischemia may produce fixed myocardial perfusion defects or defects demonstrating a "reverse distribution" [4]. However, regional left ventricular function may be preserved in the distribution of the infarct. Therefore, gated perfusion SPECT may demonstrate a fixed perfusion abnormality with normal left ventricular wall motion and, often, normal left ventricular wall thickening. This pattern is identical to that of a soft tissue attenuation artifact (see above). Therefore, a significant limitation of gated perfusion SPECT is the inability to differentiate nontransmural scarring with preserved regional function from soft tissue attenuation artifact. A potential advantage of attenuation correction is the ability to provide this differentiation. However, it should be cautioned that attenuation correction does not always completely compensate for soft tissue attenuation, and the differentiation of subendocardial scar from artifact may be suboptimal. Figure 7.9 illustrates a case example of subendocardial infarct with normal regional wall motion and wall thickening.

Nonischemic, dilated cardiomyopathy

In some patients with symptoms prompting gated SPECT imaging as an initial test, gated SPECT may provide the first diagnosis of a nonischemic dilated cardiomyopathy. Scans in such patients are typically characterized by biventricular dilation with global, biventricular dysfunction and the absence of perfusion defects or only minimal defects. However, when defects are seen in these patients that may be due to soft tissue attenuation, gated imaging is of limited value in differentiating myocardial scarring versus attenuation artifact because there is characteristically a marked, generalized decrease in regional wall motion and wall thickening. In patients with dilated cardiomyopathy, differentiation of diaphragmatic attenuation and inferior scarring is particularly problematic. In such patients diaphragmatic attenuation may be accentuated because the dilated heart lies low in the thorax. Moreover, blood within the dilated left ventricular cavity attenuates the inferior and inferoposterior walls, which lie most distant from the scintillation detector. Therefore, in such patients either

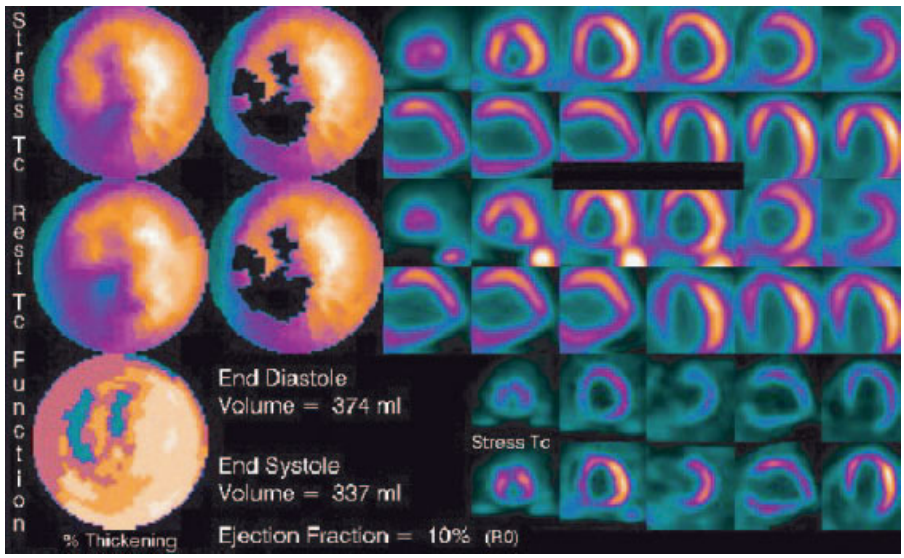

Figure 7.10 Stress and rest tomographic images in this male patient with a known cardiomyopathy demonstrate a markedly dilated, "globular" left ventricle. There is an extensive, moderate decrease in tracer concentration throughout the inferior wall. Quantitative perfusion polar plots identify the inferior defect as a moderately extensive, moderately severe abnormality. Gated tomographic images demonstrate marked, diffuse left ventricular hypokinesis. Left ventricular ejection fraction is 10%. There is a marked, diffuse decrease in myocardial wall thickening during systole. Quantitative analysis of myocardial wall thickening displayed in polar plot format similarly demonstrates a marked, diffuse decrease in wall thickening. Because of the diffuse left ventricular dysfunction, in this patient it is not possible to incorporate functional data to differentiate diaphragmatic attenuation versus inferior myocardial scarring as a cause of the fixed inferior perfusion defect. The etiology of this patient's cardiomyopathy was unknown. However, he had no prior history or electrocardiographic evidence of myocardial infarction. Therefore, based upon clinical information, the cause of the fixed inferior defect was most likely attributable to diaphragmatic attenuation.

prone imaging or attenuation correction is preferable to gated perfusion imaging to differentiate attenuation artifact from inferior scar [19]. A case example of dilated nonischemic cardiomyopathy with diaphragmatic attenuation artifact is illustrated in Fig. 7.10.

Artifacts Variable in Location and/or Severity in Stress Versus Rest SPECT Images

As mentioned previously, gated perfusion SPECT is of greatest value in differentiating fixed perfusion defects from localized myocardial scar. If the location and/or severity of an artifact differs in stress and rest images, the resultant apparent perfusion defect will likewise vary in location and severity, thus mimicking myocardial ischemia and/or "reverse distribution." Therefore, gated perfusion SPECT is of limited value in differentiating myocardial ischemia from artifact. Among the many examples of causes such variable artifacts are the following:

- Patient motion
- Flood field nonuniformity (The patient is usually positioned at different locations under the detector during stress and rest SPECT acquisitions.)
- Shifting breast position (The position of the left breast may shift under tight-fitting clothing, binders, with the bra on versus off, or with different degrees of elevation of the left arm.)
- Compton scattered radiation (The location and intensity of subdiaphragmatic tracer location usually varies from rest to stress, creating variable scatter artifacts.)

Instances in which interpretation of gated perfusion SPECT is problematic

Low count density

If gated perfusion SPECT images are count poor, they may be suboptimal to evaluate regional wall motion and wall thickening. While additional spatial and/or temporal smoothing may help define the endocardial borders and to determine temporal changes in count density proportional to wall thickening, there is no substitute for adequate count density, and caution should be exercised in interpreting regional function on count-poor images. A case example of low count density gated perfusion tomograms without and with additional spatial and temporal smoothing is shown in Fig. 7.11.

Inappropriate filtering

As described in Chapter 5, correct processing of gated perfusion tomograms is essential for their appropriate clinical

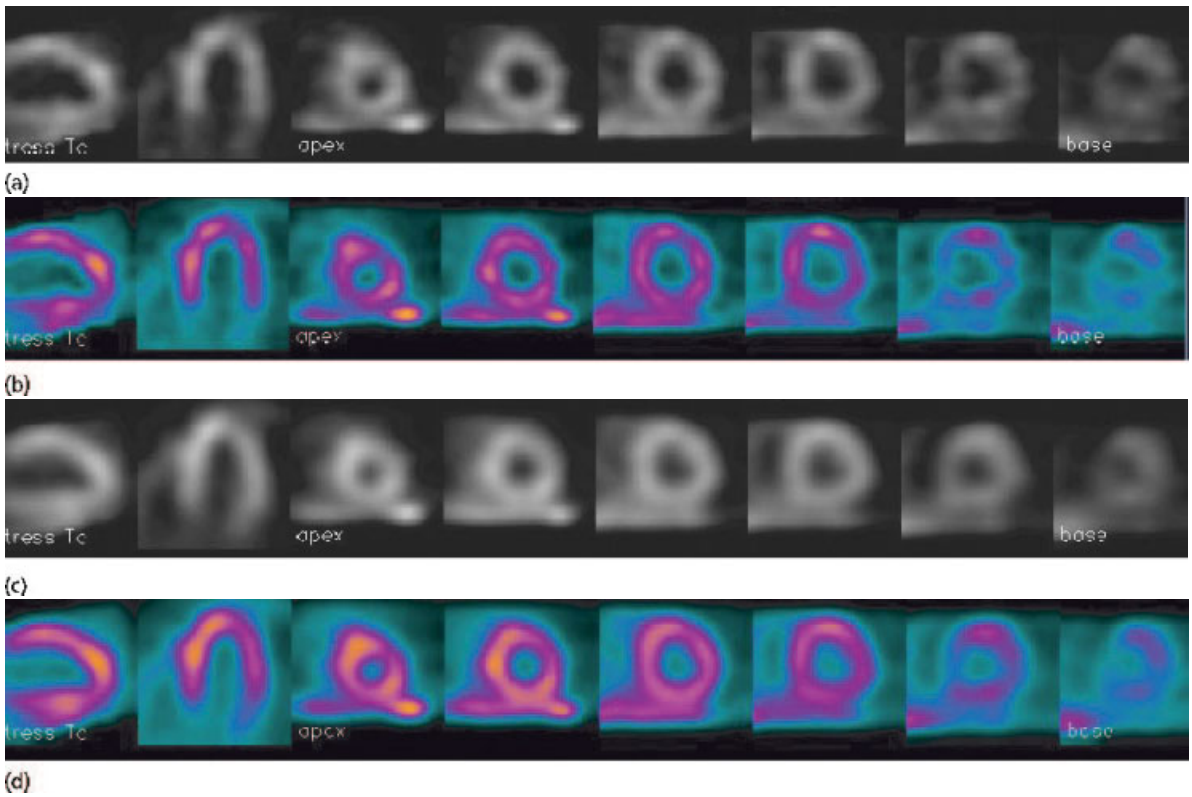

Figure 7.11 In this obese patient, gated post-stress tomograms were of low count density. (a) End-diastolic post-stress gated tomograms displayed in black and white, filtered according to the standard processing protocol (low count density resting filter applied to each of the eight frames of the post-stress gated tomograms). (b) End-diastolic post-stress gated tomograms displayed in color, filtered according to the standard processing protocol (low count density resting filter applied to each of the eight frames of the post-stress gated tomograms). (c) End-diastolic post-stress gated tomograms displayed in black and white, with additional spatial and temporal smoothing. (d) End-diastolic post-stress gated tomograms displayed in color, with additional spatial and temporal smoothing.

application. Similarly, to apply gated tomograms to help differentiate artifact versus myocardial scar, if gated images are count poor and if endocardial borders are not well defined, the assessment of wall motion and wall thickening may be suboptimal. Therefore, the interpreting physician cannot optimally apply gated perfusion SPECT to differentiate scar from artifact. A common error in processing gated SPECT tomograms is to use the same filter for the individual 8- or 16-frame-per-cardiac cycle images that is used for the summed tomograms. If the higher critical frequency filter used for the summed tomograms is applied to the lower count density gated tomograms, the latter will be "noisy" with suboptimal information.

Errors and artifacts caused by ECG gating

Incorrect gating

For appropriate gating of myocardial perfusion SPECT, the R-wave of each cardiac cycle must be identified. Electrocardiographic leads should be positioned to maximize R-wave amplitude. In patients with low R-wave voltage (anteroseptal myocardial infarction, for example) or in those with increased T-wave voltage (hyperkalemia, for example), the T-wave may trigger the gate instead of, or in addition to, the R-wave. Similar inappropriate triggering can occur in patients with paced rhythms, with gating on the pacing spike rather than the R wave. These gating errors often result in marked degradation of the gated SPECT tomograms. Less commonly tall, peaked P-waves will result in gating errors [20]. An example of erroneous gating on the R-wave and T-wave is shown in Fig. 7.12.

To prevent T-wave gating, the technologist should verify that the heart rate sensed by the ECG trigger corresponds to the patient's actual heart rate. Likewise, if possible, the position of the ECG trigger should be verified on the acquisition computer console or an ECG rhythm strip.

Arrhythmias

As discussed in Chapter 5, in order to maintain the integrity of the calculated left ventricular volume curve, it

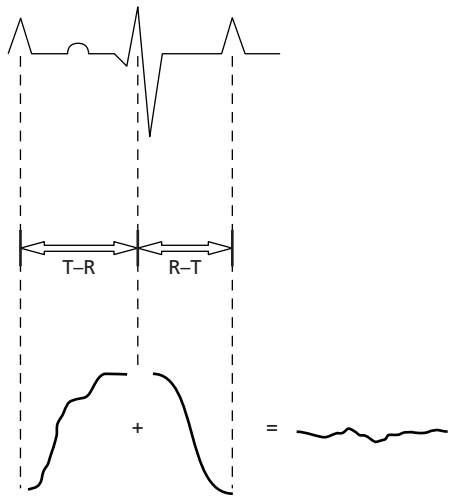

Figure 7.12 Low-voltage R-waves and tall T-waves may result in erroneous electrocardiographic gating. In this example both the R-wave and the T-wave are sensed by the electrocardiographic gate. As a result, one cardiac "cycle," the R–T interval, consists of only left ventricular systolic emptying, whereas the next "cycle," the T–R interval, consists of only left ventricular diastole. When these two consecutive "cycles" are summed, counts from each are averaged, resulting in an apparent marked decrease in left ventricular function.

is recommended that gated perfusion SPECT scans be acquired using some degree of arrhythmia rejection. Most commonly a "100%" window is selected, allowing cardiac cycle lengths up to 50% greater than and 50% shorter than the mean R–R interval to be accepted. Selection of a narrower window will improve the integrity of the left ventricular volume curve and theoretically result in a more accurate left ventricular ejection fraction. However, more cardiac cycles will be rejected, and the resulting count density of the summed perfusion tomograms will decrease. In contrast, increasing the arrhythmia acceptance window will result in fewer rejected beats. Count density of the summed perfusion tomograms will increase, but the integrity of the resulting left ventricular volume curve will suffer because cardiac cycles of greatly varying lengths will be averaged.

Also as discussed in Chapter 5, it has been demonstrated that due to the averaging of cardiac cycles of varying lengths, error may be introduced into quantification of regional myocardial wall thickening due to the disruption of the usual linear relationship between myocardial wall thickness and observed counts, associated with partial volume effects [21–24]. Nichols et al. reported that when arrhythmic rejection of irregular cardiac cycles (atrial fibrillation) occurred, in 28% of cases there was an artifactual increase in apparent wall thickening and in 40% of cases wall thickening artifactually decreased [23]. However, because individual gated frames are normalized to themselves throughout the heart cycle, functional values, including diastolic and systolic volume, are less affected by arrhythmias. These authors demonstrated that using either QGS® or Emory Toolbox® software such computer-simulated arrhythmias resulted in errors in ejection

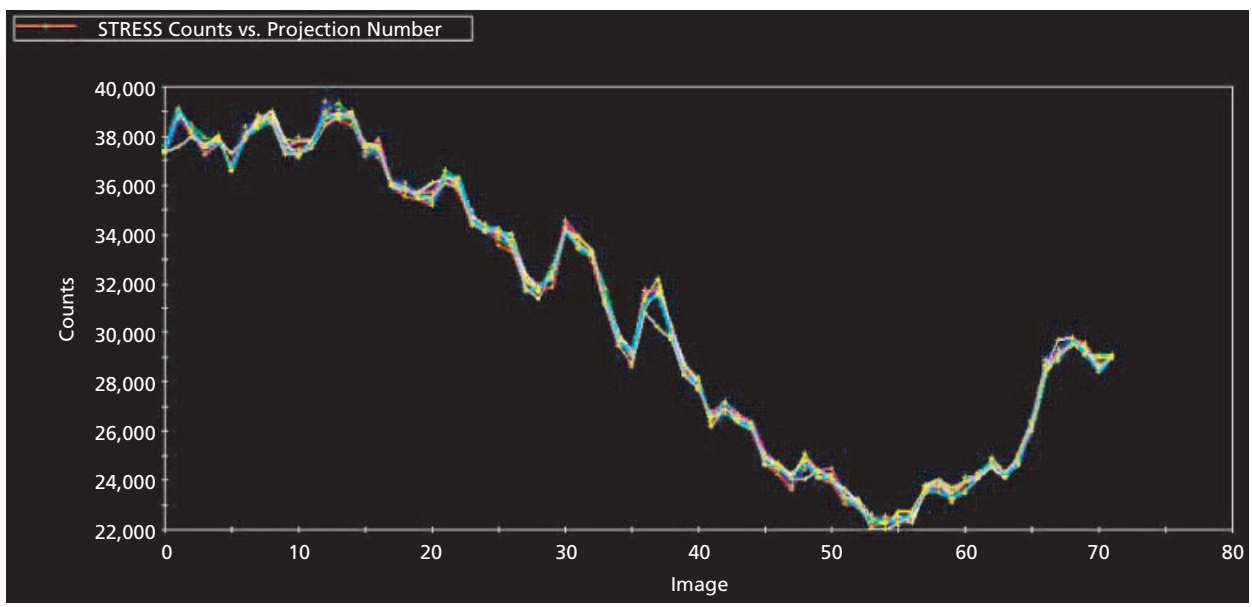

(a)

Figure 7.13 Quantitative analysis of planar projection cardiac count density in a patient with (a) no arrhythmia (GE Medical Systems®), (b) varying cardiac cycle length and "dropout" of data only in the eighth cardiac gating bin, (c) arrhythmia throughout the gated SPECT acquisition and resulting "dropout" of data in various cardiac gating bins, and (d) atrial fibrillation. Progressive "dropout" of data is observed in the diastolic gated frames.

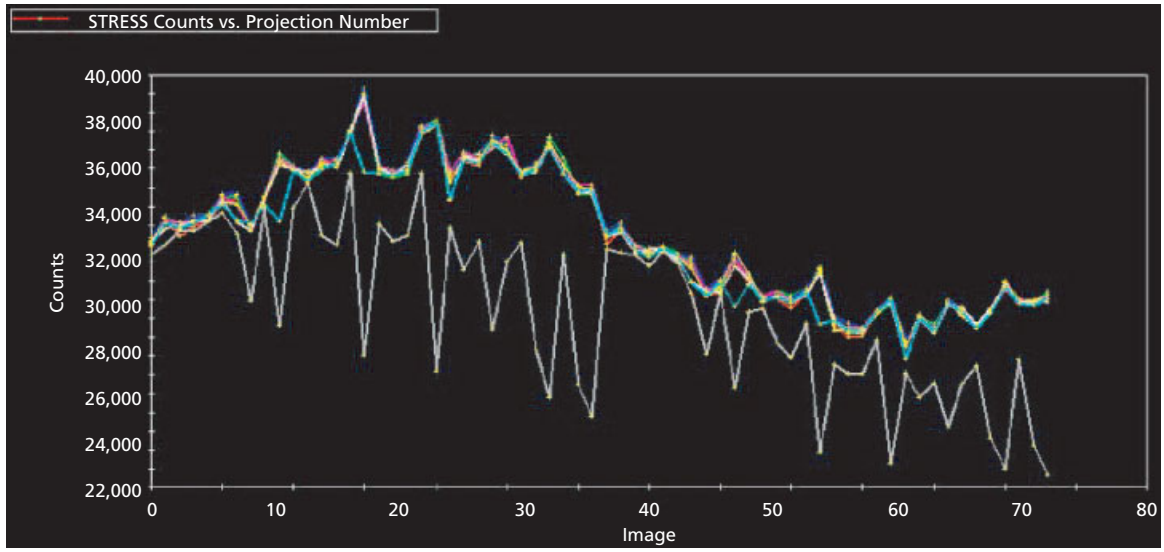

(b)

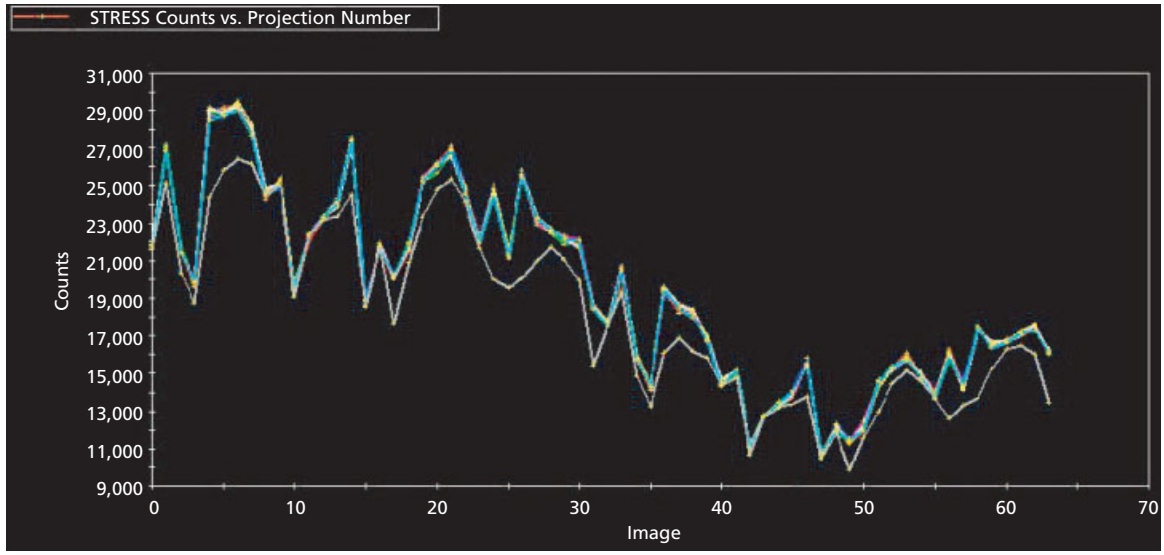

(c)

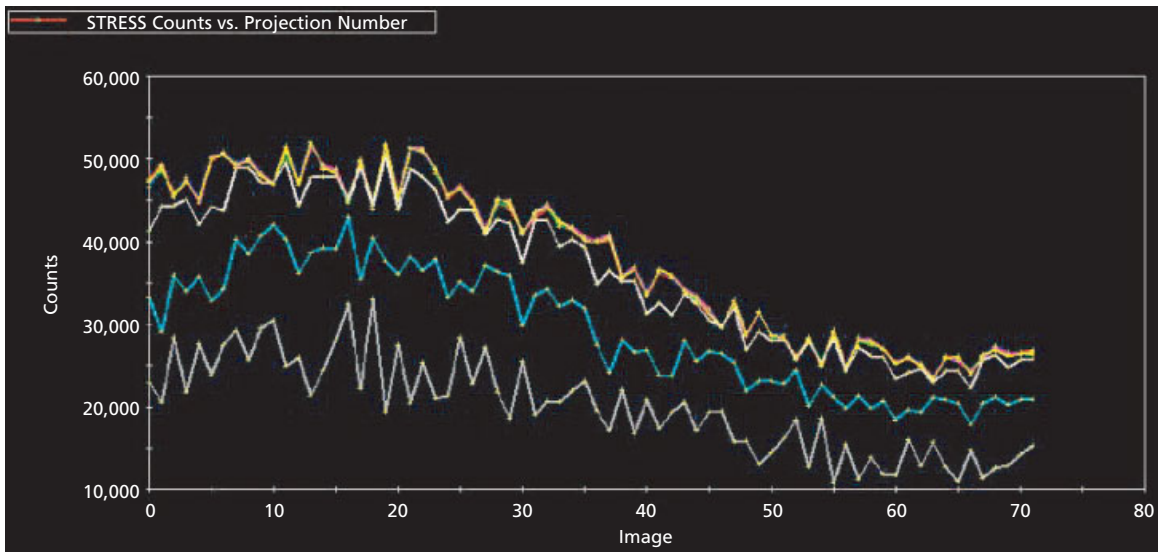

(d)

Figure 7.13 (*Continued*)

fraction, end-diastolic volume, and end-systolic volume of less than 5% [23].

With arrhythmia ("bad-beat") rejection, the overall count density of the summed tomographic images decreases. In low count density images there is greater statistical variation among pixels and thus a greater probability that artifactual regional perfusion abnormalities will be identified by either visual image inspection or quantitative analysis. Using computer-simulated arrhythmias (atrial fibrillation), Nichols et al. reported that by subjective visual analysis perfusion defects appeared to increase in severity in 33% of cases and decrease in severity in 12% of cases [23]. However, it was uncommon (fewer than 4% of cases) that such changes had an impact on visual scan interpretation. Nonetheless, the quality of tomograms, polar plots, and three-dimensional representation of myocardial perfusion degrades with decreasing image count density due to rejected arrhythmic cardiac cycles.

Software vendors have now introduced displays of cardiac image count density in individual planar projection images. Inspection of these quality control images is of value in determining the degree of arrhythmia and its effect on tomographic image count density (Fig. 7.13).

References

1. DePuey EG, Garcia EV. Optimal specificity of thallium-201 SPECT through recognition of imaging artifacts [see comments]. Journal of Nuclear Medicine 1989;30(4):441–449.
2. DePuey E. Artifacts in SPECT myocardial perfusion imaging. In DePuey EG, Berman DS, Garcia EV, eds. Cardiac SPECT Imaging. New York: Raven Press; 1995:169–200.
3. DePuey EGr. How to detect and avoid myocardial perfusion SPECT artifacts. Journal of Nuclear Medicine 1994;35(4):699–702.
4. Maddahi J, Berman DS. Reverse redistribution of thallium-201. Journal of Nuclear Medicine 1995;36(6):1019–1021.
5. DePuey EG, Rozanski A. Using gated technetium-99m-sestamibi SPECT to characterize fixed myocardial defects as infarct or artifact. Journal of Nuclear Medicine 1995;36(6): 952–955.
6. Fleischmann S, Koepfli P, Namdar M, Wyss CA, Jenni R, Kaufmann PA. Gated (99m) Tc-tetrofosmin SPECT for discriminating infarct from artifact in fixed myocardial perfusion defects. 2004;45(5):754–759.
7. Taillefer R, DePuey EG, Udelson JE, Beller GA, Latour Y, Reeves F. Comparative diagnostic accuracy of Tl-201 and Tc-99m sestamibi SPECT imaging (perfusion and ECG-gated SPECT) in detecting coronary artery disease in women. Journal of the American College of Cardiology 1997;29(1): 69–77.
8. Araujo W, DePuey EG, Kamran M, Undavia M, Friedman M. Artifactual reverse distribution pattern in myocardial perfusion SPECT with technetium-99m sestamibi. Journal of Nuclear Cardiology 2000;7(6):633–638.
9. DePuey E. A stepwise approach to myocardial perfusion SPECT interpretation. In Gerson M, ed. Cardiac Nuclear Medicine. 3rd edn. New York: McGraw-Hill; 1997:81–142.
10. Nichols K, Kamran M, Cooke CD, et al. Feasibility of detecting cardiac torsion in myocardial perfusion gated SPECT data. Journal of Nuclear Cardiology 2002;9(5):500–507.
11. Toma DM, White MP, Mann A, et al. Influence of arm positioning on rest/stress technetium-99m labeled sestamibi tomographic myocardial perfusion imaging. Journal of Nuclear Cardiology 1999;6(2):163–168.
12. DePuey E, Shahzad K. Attenuation correction versus gating to characterize Tc-99m sestamibi fixed defects as attenuation artifact or scar [abstract]. Journal of the American College of Cardiology 1998;31(2, Suppl A):175A.
13. DePuey EG, Guertler-Krawczynska E, Perkins JV, Robbins WL, Whelchel JD, Clements SD. Alterations in myocardial thallium-201 distribution in patients with chronic systemic hypertension undergoing single-photon emission computed tomography. American Journal of Cardiology 1988;62(4):234–238.
14. Johnson LL, Verdesca SA, Aude WY, et al. Postischemic stunning can affect left ventricular ejection fraction and regional wall motion on post-stress gated sestamibi tomograms [see comments]. Journal of the American College of Cardiology 1997;30(7):1641–1648.
15. DePuey E, Rozanski A, Ganti V, et al. The independence of regional asynergy and myocardial perfusion defect reversibility [abstract]. Journal of Nuclear Medicine 1993;34(5): 24P.
16. DePuey G, Ghesani M, Schwartz M, Friedman M, Nichols K. Comparative sensitivities of wall thickening, thallium uptake, and F-18 SPECT in detecting myocardial viability [abstract]. Journal of Nuclear Cardiology 1997;4(Suppl 1): S26.
17. Everaert H, Vanhove C, Franken PR. Assessment of perfusion, function, and myocardial metabolism after infarction with a combination of low-dose dobutamine tetrofosmin gated SPECT perfusion scintigraphy and BMIPP SPECT imaging. Journal of Nuclear Cardiology 2000;7(1): 29–36.
18. Leoncini M, Marcucci G, Sciagrà R, et al. Nitrate-enhanced gated technetium 99m sestamibi SPECT for evaluating regional wall motion at baseline and during low-dose dobutamine infusion in patients with chronic coronary artery disease and left ventricular dysfunction: comparison with two-dimensional echocardiography. Journal of Nuclear Cardiology 2000;7(5):426–431.
19. Hendel RC, Corbett JR, Cullom SJ, DePuey EG, Garcia EV, Bateman TM. The value and practice of attenuation correction for myocardial perfusion SPECT imaging: a joint position statement from the American Society of Nuclear Cardiology and the Society of Nuclear Medicine. Journal of Nuclear Medicine 2002;43(2):273–280.
20. DePuey E. Artifacts clarified by and caused by gated myocardial perfusion SPECT. In Germano G, Berman D, eds. Clinical

Gated Cardiac SPECT. Armonk, NY: Futura Publishing Company; 1999:183–237.
21. Galt JR, Garcia EV, Robbins WL. Effects of myocardial wall thickness on SPECT quantification. IEEE Transactions on Medical Imaging 1990;9(2):144–150.
22. Nichols K, Dorbala S, DePuey EG, Yao SS, Sharma A, Rozanski A. Influence of arrhythmias on gated SPECT myocardial perfusion and function quantification. Journal of Nuclear Medicine 1999;40(6):924–934.
23. Nichols K, Yao SS, Kamran M, Faber TL, Cooke CD, DePuey EG. Clinical impact of arrhythmias on gated SPECT cardiac myocardial perfusion and function assessment. Journal of Nuclear Cardiology 2001;8(1):19–30.
24. Yao S, Chandra P, Cohen R, Nichols K, DePuey E, Rozanski A. Factors influencing resting left ventricular ejection fraction measurements by technetium-99m sestamibi myocardial perfusion gated SPECT [abstract]. Journal of Nuclear Medicine 1998;39(5):45P.

8 Clinical value of combined perfusion and function imaging in the diagnosis, prognosis, and management of patients with suspected or known coronary artery disease

Rory Hachamovitch

Introduction

The introduction of widely available, validated software permitting reproducible measurements of gated SPECT ejection fraction and wall motion to be routinely performed as a part of clinical testing has generated considerable excitement and interest upon its release. Since the first edition of this text, gated SPECT functional measures have become a ubiquitous component of stress myocardial perfusion scintigraphy (MPS) studies and increasing evidence supports the use of gated MPS with respect to both diagnostic and prognostic endpoints. However, like many new additions to cardiologists' diagnostic armamentarium, the economic realities of today's medical marketplace dictate that all diagnostic modalities undergo rigorous evaluation particularly with respect to their clinical- and cost-effectiveness [1,2]. These data are necessary not only for gaining clinical acceptance for this modality among practicing physicians, but also for justifying reimbursement for this modality among payers.

Health care reform has forced a rethinking of the medical applications of testing modalities, their role, and the appropriate populations in which they should be applied. The evaluation of coronary artery disease (CAD), a widespread condition associated with significant morbidity and mortality that exist at epidemic levels in Western society, utilizes a number of testing modalities. Justification and ultimate validation of gated SPECT as one of these modalities will depend upon its ability to provide relevant clinical data over and above that available from the patient's clinical profile, cardiac history, and conventional stress SPECT imaging. Moreover, these data must be readily convertible to information that can be applied in patient care settings. This implies not only that a statistically significant gain in information need be measured, but that this information can be shown to enhance presently available patient care algorithms. Finally, and most importantly, it is the ultimate goal of stress imaging modalities to provide referring physicians with information that would permit them to identify which patients will accrue a survival benefit from various therapeutic options (e.g., medical therapy versus revascularization). Ideally, in the future, this will take the form of estimates of risk based on clinical, historical stress test, and imaging data that can be provided by a software package.

The goal of this chapter is to introduce the reader to the potential limitations of studies in this field, and to review the basic concept underlying the prognostic and diagnostic literature of this field, with a special emphasis on gated SPECT techniques. It is not the goal of this chapter to definitively review this area of the prognostic and diagnostic literature.

Epidemiological and statistical considerations in the measurement of test performance

Before evaluating the available literature appraising the performance characteristics of stress myocardial perfusion imaging using gated SPECT, an understanding of the pitfalls and limitations of the existing approaches is necessary. Unlike the case of therapeutic modalities, in which the success of treatment is readily measured by a reduction in morbidity or mortality, the efficacy of noninvasive testing is more difficult to determine. With the incorporation of stress imaging results in key decision-making steps, new and powerful referral biases have been introduced. These have amplified with the increased use of stress imaging. In order to make sense of counterintuitive, and even contradictory, results in the published literature, it is important to be aware of these biases, their causes, and whether they can be overcome.

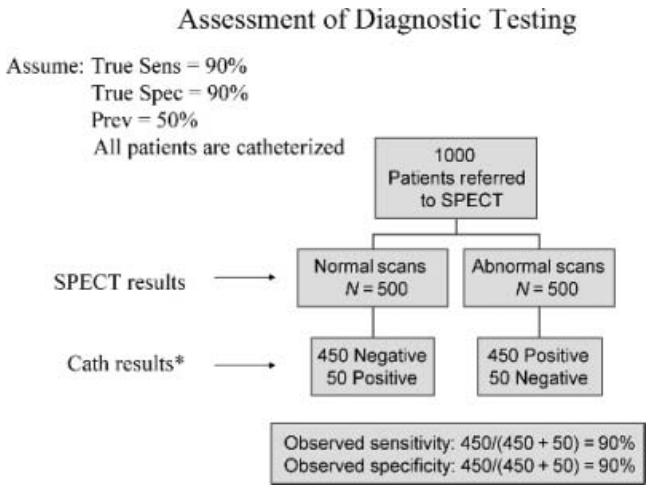

Figure 8.1 Assessment of diagnostic testing: outline of observed sensitivity (Sens) and specificity (Spec) determinations for a population with prevalence (Prev) of CAD of 50%, true sensitivity of 90%, and true specificity of 90%.

Referral bias

The fundamental flaw underlying an anatomy-based approach to defining the efficacy of noninvasive testing is the bias introduced by the necessity of referral to catheterization. As has been previously shown [1–5], the amount of ischemia present on the SPECT study is the best predictor of referral to catheterization. This results in a far greater number of patients with "positive" scans (either true or false positive) being referred to catheterization, compared to the number of patients with "negative" scans (true or false negative). Thus, the *measured* sensitivity of the nuclear testing (true positives divided by true positives plus false negatives) will be falsely raised by a small amount (since few false negatives are referred to catheterization). Similarly, the *measured* specificity of nuclear testing (true negatives divided by true negatives plus false positives) will be falsely lowered, since false positives will be referred to catheterization more frequently than true negatives. This phenomenon of test referral bias was first described by Rozanski and colleagues [6], using exercise wall motion studies.

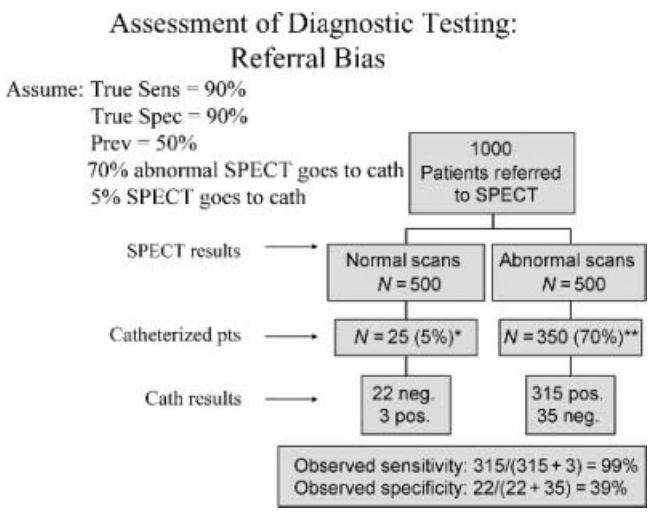

Figure 8.2 Assessment of diagnostic testing: outline of sensitivity and specificity determinations for a population with prevalence of CAD of 50%, true sensitivity of 90%, true specificity of 90%, and catheterization rates of 5% in normal scans and 70% in abnormal scans. Based on literature catheterization rates, *<5% following normal SPECT results [1,2,5,7] and **25–80% following abnormal SPECT results [2,5,7].

The extent by which test specificity will be lowered is dependent upon the referral rates to catheterization as a function of the SPECT results. A number of studies have shown that the referral rate to catheterization is very low (<5%) in the setting of a normal scan, and increases significantly as a function of scan abnormality – the presence of a markedly abnormal scan is associated with catheterization referral rates exceeding 60% [2–5,7–9]. A paradox is thus created in that, as nuclear testing evolves to greater levels of refinement and accuracy, and physicians base their decisions for subsequent treatment (and referral to a gold standard) upon the results of the SPECT study, the *specificity of nuclear testing will decline in proportion to its incorporation into clinical practice*. Furthermore, as appropriateness of care increases (catheterization in proportion to risk, expressed by scan abnormality), the performance characteristics of the test will decline. An example of this phenomenon is shown in Figs. 8.1 through 8.3. If a test is assumed to have positive and negative predictive values of 90%, and the population tested has a prevalence of CAD of 50%, sensitivity and specificity values of 90% will emerge if all patients are catheterized. However, if not all patients are referred to catheterization, and catheterization rates of 5 and 70% are assumed for normal and abnormal scans, respectively, sensitivity will increase to 99% and specificity will decrease to 39% (Fig. 8.2). Finally, if all abnormal SPECT are catheterized, but no normal SPECT are catheterized, the sensitivity will increase to 100% and specificity will decrease to 0% (Fig. 8.3). Hence, the *observed* sensitivity and specificity are inherently susceptible to the rates of post-SPECT catheterization in the cohort tested. Please note that the *actual* performance of the test is unchanged, but the population considered in the measurement of test performance has been altered. Unless the study design mandates catheterization in *all* patients (including patients with normal tests), the sensitivity and specificity values found may misrepresent the true predictive value of the test result.

Posttest referral bias in prognostic studies

The impact of posttest referral bias on the observed *prognostic* characteristics of stress SPECT is being increasingly

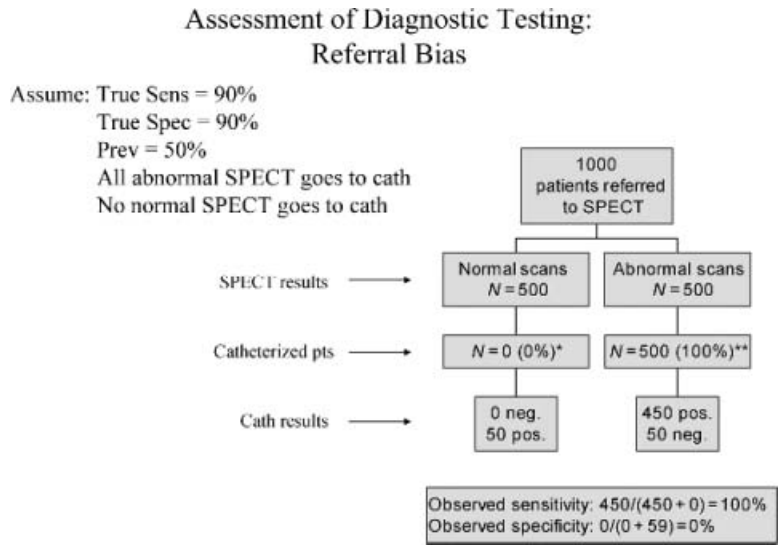

Figure 8.3 Assessment of diagnostic testing: outline of sensitivity and specificity determinations for a population with prevalence of CAD of 50%, true sensitivity of 90%, true specificity of 90%, and catheterization rates of 0% in normal scans and 100% in abnormal scans.

appreciated [10,11]. With respect to stress SPECT, posttest referral bias is usually thought of in the context of diagnostic testing, as outlined above. It has long been recognized that because of preferential referral of abnormal stress SPECT to catheterization and subsequent revascularization, and the relatively low referral rates after normal stress SPECT, a significant referral bias occurs. As we have described, this tends to lower specificity and slightly raise sensitivity, again due to the low referral rate of normal stress SPECT to catheterization. This phenomenon also impacts the observed prognostic value of stress SPECT. Since referral to revascularization after stress SPECT occurs in proportion to the extent and severity of ischemia present, and this revascularization alters the natural history of CAD, these patients have almost always been removed from prognostic analyses. Since increased use of, and trust in, stress SPECT results in increased revascularization rates, the impact of removing these high-risk patients reduces the number of patients found to have events after stress SPECT. Figure 8.4 shows event rates (observed and predicted, the latter based on a logistic regression model) in a subgroup of patients with moderate to severely abnormal stress SPECT (>10% of the total % myocardium abnormal) from a study of 1270 patients with pre-ETT (electrocardiographic exercise testing) likelihood greater than 0.85 and no prior myocardial infarction or revascularization who were followed up for 2.2 ± 1.2 years [9]. On the left side of the figure is shown the revealing high event rates for the medically treated patients in this study. On the right side is the event rates for the patients treated with early revascularization. The observed event rate is quite low (4.4%), due to the revascularization procedure and its impact on survival. Using a logistic regression model derived in the medically treated patients, the revascularized patients' event rates were estimated based on the assumption that *they would not have undergone revascularization*. This result is shown (10.9%) and is not dissimilar from the medically treated group on the left. Hence, the difference between the 14.6% and the 4.4% event rates (observed rates) reflects a treatment effect and a posttest referral bias. Had revascularization not been performed in 46% of these patients with marked abnormalities, the total number of events that occurred in the medically treated patients would have been greater, and the predictive value of stress SPECT improved. Of note, the vast majority of the MPS prognostic studies published to date are limited by this referral bias, both with respect to underestimation of event rates as well as in that

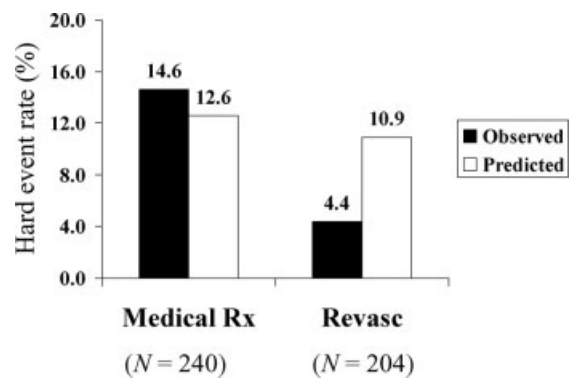

Figure 8.4 Impact of posttest referral bias on the observed *prognostic* characteristics of stress MPS. The figure (with permission from [9]) shows event rates (observed and predicted, the latter based on a logistic regression model) in a subgroup of patients with moderate to severely abnormal MPS (>10% of the total % myocardium abnormal) from a study of 1270 patients with pre-ETT likelihood greater than 0.85 and no prior myocardial infarction or revascularization who were followed up for 2.2 ± 1.2 years.

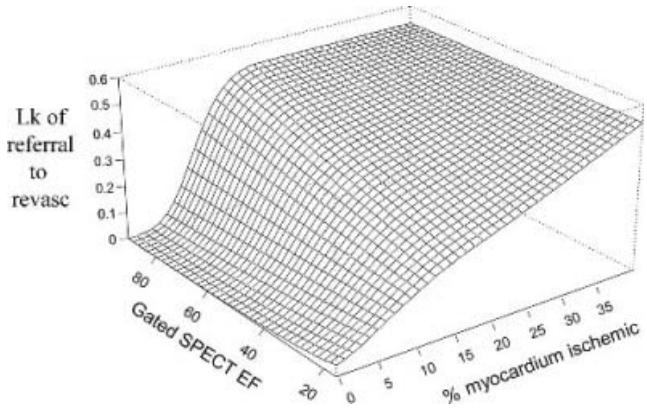

Figure 8.5 Multivariable, risk-adjusted relationship between gated ejection fraction and % myocardium ischemic with respect to prediction of likelihood of referral to revascularization based on a logistic regression model. Increase in likelihood $p < 0.0001$. Abbreviations: EF, ejection fraction; Lk, likelihood.

only patients treated medically after MPS are considered and analyzed.

A variety of other biases with respect to post-MPS referral to catheterization and revascularization are probably present as well. On the one hand, referral biases with respect to age, sex, and type of stress are probably not present [3,4,12]. On the other hand, a recent study showed that although physicians' poststress SPECT referral to catheterization and revascularization is strongly influenced by the extent and severity of inducible ischemia in patients without prior CAD presenting to stress SPECT, left ventricular ejection fraction (LVEF) does not influence this referral pattern [8] (Fig. 8.5). While this may be an appropriate referral pattern if inducible ischemia but not ejection fraction predicts patient benefit from revascularization, the impact of this referral pattern must be considered. Considering this in the context of the prognostic referral bias described above, this referral pattern would result in underestimation of risk as a function of inducible ischemia (since patients are being revascularized and their natural history altered in proportion to the amount of ischemia present) but a relatively stable and accurate estimation of risk relative to their LVEF (since ejection fraction is not impacting the referral to revascularization, their natural history relative to their ejection fraction is not altered).

Endpoints

An important question one must ask when either reading a study or planning a study is what is the endpoint in which we are interested? In general, the endpoints of noninvasive testing can be categorized as either anatomy-based (e.g., indicative of the presence of significant coronary artery stenoses) or outcomes-based (e.g., predictive of outcomes of interest, such as cardiac death, myocardial infarction).

The endpoints considered in this type of analysis usually include cardiac death and myocardial infarction. Other potential outcomes include clinical worsening late after testing (referral to revascularization is used as a surrogate for this outcome), hospitalization for cardiac causes, anginal status, or emergency room visits for chest pain [13]. By focusing on outcomes rather than anatomy, one can study the factors predictive of adverse events that patients experience, rather than anatomic patterns of disease that may (or may not) be associated with adverse events.

When applied to a population of patients with no history of CAD, the endpoint of interest is often the presence of anatomically significant CAD. The defining standard for the presence of this disease varies between studies. To date, most studies evaluating noninvasive testing toward an anatomic endpoint consider either 50 or 70% stenosis in one or more coronary arteries as the minimum lesion threshold for the presence of CAD. An alternative anatomic endpoint is the presence of CAD (defined at the time of catheterization) of a category shown to benefit from revascularization. This is the case for patients with three-vessel CAD, left main disease, and two-vessel disease with proximal left anterior descending artery involvement. Since patients with these anatomic patterns of CAD are more likely to undergo intervention, adjusting the criteria for abnormality will cause fewer patients with milder CAD (not in need of revascularization) to be identified as "positive."

The outcome of interest may vary considerably depending upon the question being asked in the study. Moreover, the variable that is most predictive may vary depending on the outcome of interest. In studying stress perfusion SPECT, for example, nonreversible defects may be the most important marker if cardiac death is used as an endpoint. Alternatively, ischemia by perfusion imaging may become a more important factor than nonreversible defects for outcomes related to unstable syndromes and progression of CAD (e.g., myocardial infarction, readmission with chest pain, late revascularization). For further discussion of statistical techniques, please refer to the Appendix.

Diagnostic testing

Nuclear testing for the diagnostic evaluation of CAD

Despite the limitations described above, stress myocardial perfusion imaging has been shown by numerous authors to have an outstanding accuracy for the detection of CAD (for reviews of this topic see [14–16]). Briefly, a number of authors have shown sensitivities for detection of CAD (≥70% stenosis) exceeding 80%, or even exceeding 90%

if Tc-99m sestamibi was used. As stated earlier, multiple studies in literature are difficult to compare or evaluate, due to the presence of both referral bias and variation in patient characteristics. To date, few studies have performed risk-adjusted analyses to better assess the accuracy of the nuclear modality. Furthermore, the specificity of SPECT has varied enormously, as explained earlier, due to the increase in referral bias over time. Although early studies using thallium-201 reported specificities exceeding 90% [16], the declining specificity of nuclear testing led to the development of the "normalcy rate" concept [17] in the attempt to correct for referral bias [18]. Normalcy is used as a surrogate for test specificity, and is expressed by the rate of normal studies in patients with a low likelihood of CAD. Indeed, the normalcy rate of stress SPECT has exceeded 80–90% in the hands of some investigators, particularly with Tc-99m sestamibi [14].

These values vary as a function of the number of diseased vessels present. The sensitivity of stress SPECT to detect disease (abnormal scan, irrespective of the number or size of defects present) has been reported as 79, 88, and 92% (thallium-201 planar), and 83, 93, and 95% (stress thallium-201 SPECT) for single-, double-, and triple-vessel CAD, respectively [16]. Although only 7% of patients with left main/three-vessel CAD have normal stress SPECT studies, only 69% have multivessel perfusion abnormalities by SPECT imaging [16]. This number can be enhanced by the use of adjunct markers, such as lung uptake, transient ischemic dilation of the left ventricle poststress, and, with thallium-201 imaging, thallium-201 washout rates [14,16]. While this increase in sensitivity could be real, the temporal relationships of these technical improvements raise the possibility that the increase between these approaches is due to the increasing reliance on test results in determining who undergoes coronary angiography.

What can gated SPECT add to the identification of CAD?

Given the relatively high accuracy rates associated with SPECT imaging, is there further information that can be gained by the use of gating as an adjunct? Taillefer and colleagues reported the results of a study comparing the accuracy of Tl-201 and Tc-99m sestamibi in a cohort of 115 women (85 with suspected CAD, 30 normal volunteers) [19]. Although no significant differences between the radiopharmaceuticals were found with respect to test sensitivity, test specificity was greater using Tc-99m sestamibi than Tl-201, predominantly due to a difference in those patients undergoing exercise stress. As shown in Fig. 8.6, imaging with Tc-99m sestamibi SPECT (both with and without gating) resulted in significantly greater specificity than with Tl-201 SPECT. The findings were far more

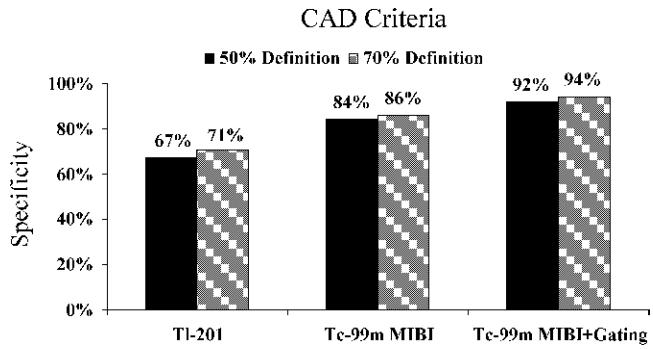

Figure 8.6 Specificities for detection of CAD using Tl-201 SPECT, Tc-99m sestamibi SPECT, and Tc-99m sestamibi SPECT with gating, and a 50% definition (black bars) or 70% definition (crosshatched bars) of CAD [19].

significant with gated Tc-99m SPECT studies than with ungated studies. Although the absolute differences between gated and ungated Tc-99m studies were striking, the study was underpowered to detect a statistically significant difference.

These findings supported previous work by DePuey and Rozanski [20], suggesting that the ability to observe myocardial contraction, in segments with fixed perfusion defects, would permit the nuclear reader to discern attenuation artifacts from true perfusion abnormalities. Choi et al. confirmed this finding and extended it to include gated SPECT studies performed using Tc-99m tetrofosmin [21]. In this study of 105 patients who underwent stress Tc-99m tetrofosmin gated SPECT, the probability of correctly identifying true disease was significantly increased with the addition of gated SPECT images.

The ability to discern between fixed defects associated with normal contraction and those accompanied by regional wall motion abnormalities suggests that the use of gated SPECT images may serve as an inexpensive alternative to attenuation correction software. DePuey and colleagues [22] reported that, with currently available technology, gated Tc-99m SPECT was superior to attenuation correction in differentiating scar from artifactual fixed defects. In a series of 110 patients, 53 (48%) of whom had fixed defects (75 total defects), attenuation correction failed to eliminate 26 of 51 fixed defects associated with normal wall motion. Furthermore, attenuation correction overcorrected counts in 11 of 24 defects that manifested normal wall motion. The overall reported sensitivity for identifying true defects as scar was 54% for attenuation correction and 92% for gated SPECT, while specificity was 49 and 98% for attenuation correction and gated SPECT, respectively.

The use of gating may thus result in an improvement in reader confidence in the interpretation rendered. Although this phenomenon is difficult to verify and quantitate, it is reasonable to expect that it would result in a

reduction in the number of "equivocal" scans reported. This hypothesis was examined by Smanio and colleagues [23]. In 285 consecutive patients (143 women, 142 men) who underwent stress SPECT imaging with Tc-99m sestamibi, all studies were initially interpreted and scored without viewing the gated SPECT images. Subsequently, the studies were rescored, allowing the readers to view the gated images. As a result, the number of "borderline" studies (borderline normal or borderline abnormal) was dramatically reduced from 89 to 29 (from 31 to 10% of the total). Furthermore, the addition of the gated images resulted in a significant increase in the number of patients with a $\leq$10% or less likelihood of CAD who were interpreted as normal (from 74 to 93%, $p < 0.0001$). A similar trend that did not reach statistical significance was found, in the sense that patients with documented CAD were reclassified as abnormal. Thus, physician confidence in scan interpretation does appear to increase following the addition of gated information, as documented by a reduction in equivocation regarding the results of perfusion studies.

The results of the studies discussed above are further enhanced by a study reported by Holly et al. [24]. This report was based on perfusion studies performed in 22 patients with low likelihood of CAD and 33 patients with known CAD, all of which were interpreted on two separate blind readings, once using gated SPECT and once using attenuation correction. In the patients with low likelihood of CAD, there was no difference in the overall scan interpretation or in the normalcy rate obtained using either attenuation correction or gated SPECT. In the patients with known CAD, there was a borderline significant ($p = 0.06$) trend in favor of a higher sensitivity for gated SPECT (83%) over attenuation correction (64%), and a significantly greater categorization toward an abnormal category with the use of gated SPECT compared to attenuation correction. Thus, as in the studies discussed above, a greater level of confidence was attained by the use of gated SPECT as an adjunct to conventional SPECT perfusion imaging.

Although a number of advantages are associated with the conversion from Tl-201 to Tc-99m-based agents (among which is the fact that the latter are better suited for gated SPECT), a potential detriment is that T1-201 lung uptake and myocardial washout rates have been demonstrated to be able to detect the presence of multivessel CAD. The potentials of the technetium-99m perfusion agents to assess lung uptake have not been fully explored. The use of gated SPECT, on the other hand, may help detect the presence of severe and/or extensive CAD by identifying poststress wall motion abnormalities in the presence of normal resting perfusion, or a lowering of ejection fraction poststress compared to rest.

In 1997, Johnson and colleagues [25] investigated whether ejection fraction values measured from poststress gated SPECT were similar to those obtained at rest as part of a 2-day gated sestamibi protocol. Of the 81 patients examined, 36% of those with reversible perfusion abnormalities had a poststress gated SPECT LVEF lower by 5% or more, compared to that obtained from rest Tc-99m sestamibi gated SPECT. This reduction in ejection fraction was also accompanied by significant elevation of both end-systolic and end-diastolic volumes, not present in those patients who did not demonstrate a stress-induced reduction in tracer uptake. In addition, a sevenfold greater reduction in chordal shortening was present in the patients with ischemia, compared to the remaining cohort. In all, this work suggests the possibility that stress-induced stunning may be a factor in stress SPECT imaging, and can be assessed using gated SPECT. Such a finding would naturally suggest the presence of severe underlying CAD.

Bateman and colleagues [26] extended these findings in their recent report on 763 patients who underwent stress-redistribution Tl-201 gated SPECT. They found that although few patients had a greater than 10% reduction in gated SPECT ejection fraction poststress relative to rest (3.5% of the initial cohort), these patients more frequently had lung uptake of Tl-201 (33% vs. 14%, $p < 0.05$), transient ischemic dilation of the left ventricle (89% vs. 24%, $p < 0.05$), and severe and extensive perfusion abnormalities (78% vs. 33%, $p < 0.05$). Most importantly, these patients also had a far greater frequency of multivessel CAD at the time of catheterization (37% vs. 8%). Further investigations are needed to determine the anatomic substrate responsible for the phenomenon of lowered ejection fraction poststress, as well as whether it represents persisting ischemia or true stress-induced stunning.

A well-recognized drawback of the use of SPECT techniques is the underestimation of the extent and severity of inducible ischemia due to balanced reduction, and hence, an underestimation of CAD extent and frequent misdiagnosis of patients with multivessel CAD. The role of gated SPECT in this situation was examined by Lima and colleagues from the University of Virginia [27]. To investigate whether the combined approach of perfusion and function with gated SPECT would enhance identification of these patients, a cohort of 143 patients with angiographic three-vessel CAD was identified and compared to a control group of 112 patients without three-vessel CAD. Stress SPECT was interpreted in a stepwise fashion – initially considering only perfusion data, and then interpreted using both perfusion and function data. In the cohort of patients with three-vessel CAD, significantly more abnormal segments per patient (6.2 ± 4.7 vs. 4.1 ± 2.8, $p < 0.001$) and more defects in multiple vascular territories (60% vs. 46%, $p < 0.05$) were identified by the combination of perfusion and function data compared to perfusion data alone. This was not found to be the case in the control group. Multivariable modeling revealed that patient age and the

number of vascular territories abnormal by either perfusion or function analysis are the most powerful predictors of three-vessel CAD and that functional data yielded incremental information over and above that yielded by pre-MPS and perfusion data for predicting the presence of three-vessel CAD. These results suggest that the use of gated data in conjuncture with stress perfusion can enhance the identification of multivessel CAD by stress SPECT.

Prognostic testing

Outcomes or risk-based assessment of testing

Although the various types of stress testing with or without imaging have long been considered in the context of anatomic endpoints – sensitivity, specificity, and accuracy for detection of significant epicardial stenoses – currently, they are more often considered in the context of a risk-based approach to patient management. This approach has become the accepted framework for considering both patient testing and management in the current era. Several basic principles underlie this approach and permit understanding of its application.

Our expanding understanding of the biochemical and structural basis of the pathophysiology of atherosclerosis has revealed that CAD is a dynamic process. Further, there is increasing evidence that the majority of cardiovascular events occur independent of fixed epicardial coronary stenoses as conventionally measured [28,29]. In contrast, there is evidence that abnormalities of coronary flow reserve are predictive of CAD events. It has long been recognized that a wide variation in flow reserve exists for any epicardial lesion, particularly in the setting of mild to moderate stenoses [30–33]. While flow reserve per se is not yet measured by SPECT, recent data suggest that assessment of regional myocardial perfusion defects using SPECT as the modality is more accurate and more cost-effective for identification of risk of cardiac event than identification of the presence and extent of anatomic CAD [34].

Whether assessing a patient or a modality, from a clinical perspective predicting patient survival or well being goes hand in hand with many preventive approaches to patient care [35]. By identifying the patient at risk, the so-called vulnerable patient, we can efficiently allocate more aggressive, expensive therapies targeting patients who will maximally derive a benefit from a given treatment. Hence, by focusing on outcomes rather than anatomy, one can evaluate gated SPECT with respect to factors predictive of adverse events that patients experience, rather than anatomic patterns of disease that may (or may not) be associated with adverse events.

Prognostic value of nuclear testing

A wealth of clinical research has shown that the extent and severity of stress perfusion defects are the predominant predictors of most post-MPS outcomes (for a review of this subject see [11,36,37]). This has been found to be the case irrespective of radiopharmaceutical, stress, and imaging protocol, as well as patient age, sex, history of previous CAD, or history of previous myocardial infarction [2,11,36,38,39]. Importantly, prognosis is independently predicted in these patients by both perfusion defect severity (a correlate of stenosis magnitude) and extent (a correlate of the amount of myocardium supplied by vessels with significant disease) [40]. It is important to note that metrics of perfusion incorporating extent and severity measures are more powerful predictors than those assessing defect extent or severity alone. This concept has been refined over time with respect to prediction of various endpoints, the differential prognostic implications of scar as opposed to reversible defects, and the relationship between defect extent and severity and risk. In addition to the assessment of regional myocardial perfusion, other indices from gated SPECT have been found to yield significant prognostic information. Lung uptake of thallium on stress images has been found to be a powerful predictor of outcome by Cox proportional hazards analysis, providing more information than perfusion variables [41]. Similarly, enlarged cardiac size and transient ischemic dilation have been found to be markers of higher risk [42–45]. With the advent of gated SPECT, several indices need to be considered as well, including left ventricular volumes, ejection fraction, and measures of potential stunning. The latter can be identified as the presence of poststress wall motion abnormality in the absence of rest defect if only stress SPECT is gated, or new poststress wall motion abnormality or decrease in ejection fraction if both rest and poststress images are gated. Finally, clinical information derived from the nonimaging stress portion of the examination should not be ignored, as it contains important predictors of adverse outcomes that add incremental value over conventional perfusion markers, as will be discussed later in this chapter.

Incremental prognostic value: conceptual basis

The determination of incremental prognostic value has become central to the evaluation of noninvasive testing [46,47]. The basic concept underlying incremental prognostic value is that a stress modality can add information over that provided by all information known about the patient prior to testing. Analytically, we assume that quantitative estimates of patient risk of adverse outcomes can be derived, and thus compared, usually by means of multivariable modeling. Since a finite number of factors

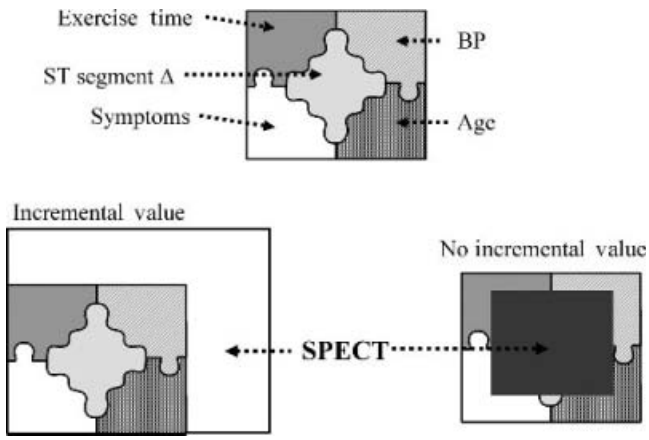

Figure 8.7 Schematic example of the concept of incremental value. The area of the puzzle shown at the top of the figure represents the amount of information known after ETT. A portion of this information is derived from patient age, and a portion from patient symptoms, yet more from ST segment change, exercise time, and blood pressure. The addition of SPECT information may result in an increase in the total amount of information known (lower left), with the white larger rectangle representing SPECT information. On the other hand, the addition of SPECT information may result in the additional information being redundant (nonincremental), despite being a greater source of information than any other source of information (e.g., any other piece of the puzzle), as shown on the lower right by the gray rectangle.

influence clinical patient risk, it is possible that a clinical domain or type of information may be conveyed by multiple variables (see Fig. 8.7 for example). One example of this potential information overlap is represented by the variables "history of previous myocardial infarction," "myocardial infarction by electrocardiographic criteria," "left ventricular ejection fraction," "left ventricular volume," and "resting left ventricular wall motion abnormalities." Although each of these variables is prognostically meaningful, there is considerable overlap between them from the perspective of information.

Significant correlation and overlap of information exists between these four variables. Similar (but less obvious) redundancy of information may also occur for other sources of risk estimation (clinical history, cardiac risk factors, results of exercise treadmill testing, results of stress perfusion testing, left ventricular function data). The measurement of incremental prognostic value addresses the question of whether the information provided by a particular test is unique, relative to the information already known based upon other tests or clinical sources.

In an era of cost containment in health care, this approach to the evaluation of testing becomes vital. The traditional questions of "Does nuclear testing predict risk?" or "Does nuclear testing risk stratify patients?" are reformulated as "Are the results of nuclear testing predictive of patient outcome, after known clinical information is considered (e.g., clinical risk factors and history, results of ETT)?" and "Does the application of the nuclear test result effectively risk stratify the cohort in question, after initial stratification by factors already known about the patient?" These issues are addressed by measuring:

1. the incremental *statistical* prognostic value of nuclear testing, that is, the prognostic information provided by the results of nuclear testing after previously known information (e.g., clinical data, exercise ECG) is considered.
2. the incremental *clinical* prognostic value of nuclear testing. In other words, after patients are risk stratified by clinical and/or exercise information, can nuclear testing further stratify patients into low- and high-risk groups such that the low-risk group will need no further testing and the high-risk cohort will require more aggressive treatment?
3. the incremental *economic* prognostic value of nuclear testing; that is, does the use of myocardial perfusion imaging result in greater cost–benefit or cost–utility when used as part of an overall patient strategy? This approach leads to the development of patient strategies that minimize the expense of testing, by referring to testing only those patients not at low or very high risk based on previous information. This cost-based perspective will be addressed in detail in Chapter 10.

These analyses are based upon an approach different from what was often used in the past. First, patient information must now be considered in a hierarchical fashion, beginning with clinical patient characteristics (very inexpensive) followed by exercise treadmill testing (ETT) (inexpensive), and only then considering data from nuclear testing (moderately expensive) and cardiac catheterization (more expensive). Second, the endpoints of the new approach are prognostic (e.g., occurrence of cardiac death and nonfatal myocardial infarction) rather than diagnostic (presence of significant coronary artery obstructions). Finally, this approach is pragmatic. Ready application to clinical scenarios and conversion of nuclear data to clinically relevant information become the focus of the analysis.

Incremental prognostic value of nuclear testing

The first published manuscript demonstrating the incremental prognostic value of nuclear testing was by Ladenheim and colleagues in 1987 [48]. In that study, the incremental prognostic value of perfusion data over clinical, historical, and ETT information was shown using a comparison of receiver operating characteristic (ROC) curves generated from logistic regression models [48]. Incremental value was clearly demonstrated in patients with abnormal resting ECGs, as well as in two-patient subgroups with normal rest ECGs – those with intermediate pretest

likelihood of CAD and ST depression on stress ECG and those with high pretest likelihood of CAD and discordant results.

Subsequently, these findings were extended to SPECT imaging. Using a Cox proportional hazards model after adjusting for clinical history and exercise results, the addition of stress perfusion SPECT information resulted in a dramatic and statistically significant increase in global χ^2 for the prediction of hard events, in a cohort of 2200 patients with no previously known catheterization, myocardial infarction, or revascularization (χ^2 increased from 31 to 169, $p < 0.001$) [2]. This demonstration of statistical incremental value by Hachamovitch and colleagues supported the use of a prognostic endpoint, even in a patient population in whom SPECT is usually thought of as a diagnostic test. This analytic approach has since been extended to a variety of other patient subsets. The same authors also assessed the incremental prognostic value of exercise myocardial SPECT in men versus women [39], finding that SPECT added incremental prognostic value in both sexes. Interestingly, the overall prognostic value of SPECT, and the efficiency of stratification provided by it, was greater in women than in men. Numerous other cohorts have been assessed in this manner (for overview, refer to [11,37]).

An alternative approach to this statistical approach to incremental value is one based on risk stratification. In this approach, a cohort is initially stratified, much as it would as a part of an initial clinical evaluation into low, intermediate, and high clinical risk groups (these strata are defined on the basis of pre-SPECT data). This was first shown by Berman and colleagues [1] (Fig. 8.8), who found that enhanced risk stratification was achieved by the addition of stress SPECT results in both patients with normal and abnormal resting ECGs. These findings have been extended to women [39], the elderly [38], patients without known prior CAD [2] (Fig. 8.9), and patients undergoing adenosine stress [49]. In all these studies, even after stratifying patients into low-, intermediate-, and high-risk groups based upon their prescan risk grouping, normal scans resulted in low risk in all subgroups, and the rate of hard events increased significantly with worsening scan results, a demonstration of clinical incremental value.

Risk stratification

Of the approaches described above, clearly that of enhanced risk stratification is clinically the most intuitive. Indeed, demonstration of clinically relevant risk stratification is the most useful approach for clinicians and has become the preferred manner in which to show the utility of stress imaging. In light of this, it is important to more rigorously evaluate and define what is meant by risk stratification, as well as what is clinically acceptable risk stratification.

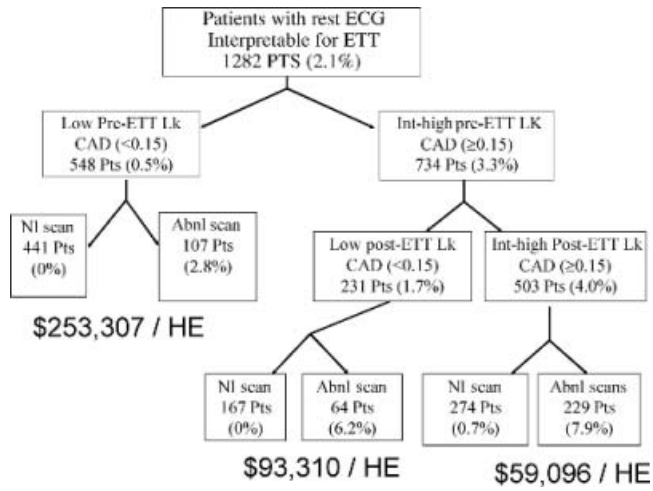

Figure 8.8 Outcomes, clinical-effectiveness, and cost-effectiveness after stress MPS (with permission modified from [1]) in a subset of 1282 patients who presented to MPS with rest ECG interpretable for ETT. These patients had a 2.1% hard event rate (cardiac death or nonfatal myocardial infarction) over a (20 ± 5)-month follow-up. As described in Figs. 8.1 and 8.2, the first stratification is based on clinical information, separating this cohort into low and intermediate-to-high risk groups (hard event rates: low pre-ETT likelihood – 0.5% versus intermediate-to-high likelihood – 3.3%). The latter group can be further stratified by ETT into low versus intermediate-to-high post-ETT likelihood of CAD (1.7% vs. 4.0% hard event rate, respectively). At this juncture, the results of MPS are applied to the three groups created: (1) low pre-ETT likelihood of CAD, (2) low post-ETT likelihood of CAD, and (3) intermediate-to-high post-ETT likelihood of CAD. In all three groups, normal MPS is associated, with low risk (0, 0, and 7.9% hard event rates, respectively). Significant risk stratification is also achieved in all three groups with the hard event rates greater in the setting of a normal versus abnormal MPS result. The cost-effectiveness ratios, expressed as cost per hard event detected, are in large yellow numbers at bottom. Despite significant risk stratification in all three groups, MPS only reached a reasonable level of cost-effectiveness in patients with intermediate-to-high post-ETT likelihood of CAD.

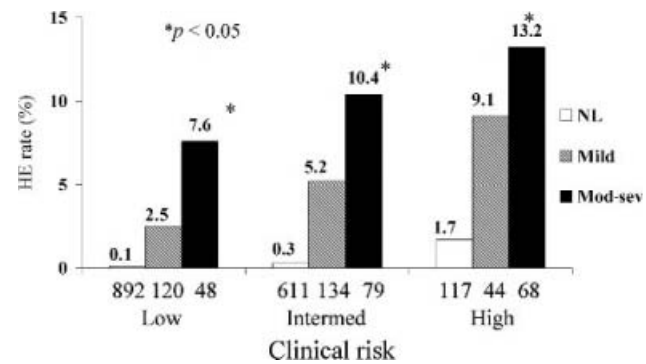

Figure 8.9 Frequency of hard events (over a follow-up of mean of 566 ± 142 days, 97% complete) in patients at low, intermediate, and high clinical risk as a function of the stress SPECT result (normal, mild, and moderately to severely abnormal) in a cohort of 2200 patients with no prior CAD referred to stress SPECT. Significant risk stratification is achieved in all clinical risk groups as a function of the scan result ($p < 0.05$). (From [2].)

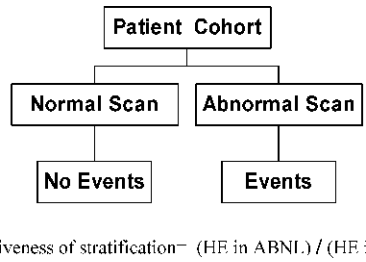

Figure 8.10 Scheme of the effectiveness of stratification. Abbreviation: HE, hard events.

Optimization of risk stratification

Based upon the prognostic studies performed to date, a number of requirements for optimal risk stratification by a noninvasive modality can be described.

1 A "negative" study should be associated with a very low event rate. The criteria generally referred to are a hard event rate (cardiac death or nonfatal myocardial infarction rate of <1% per year).
2 The event rate associated with an abnormal study should be greater than that associated with a normal study, and the relative risk and its associated confidence interval for an abnormal study relative to a normal study should exceed 1.0.

This relative risk defines the effectiveness of the stratification. The threshold for optimal risk stratification is specific to the particular endpoint of interest (e.g., cardiac death versus nonfatal myocardial infarction), and the effectiveness of stratification varies with the endpoint, as well. This finding significantly affects the application of nuclear testing as part of a testing strategy (Fig. 8.10).

With this in mind, it is important to consider that of the aggregate total number of events that occur in the overall cohort examined during the follow-up period, a significant proportion (>80–90%) should occur in the patient subset with abnormal scans. If more than 10–20% of all the events occur in the normal scan group, then it is feasible that either the event rate for normal scans in this group is too high (e.g., for testing to be efficient in this cohort, an event rate after normal studies far less than 1% is needed) or the overall population tested is at sufficiently low risk that noninvasive testing is inherently inefficient.

Normal scans

In the context of the above definitions, the pivotal role of normal scans must be appreciated. Clinically effective risk stratification is achieved because of the large number of patients identified as low risk by normal scans. Further, the cost-effectiveness of MPS risk stratification is attained by reclassifying large numbers of patients at low risk, hence not needing further testing. To date, extensive data exist defining the characteristics of normal scans.

Risk in general terms

In general, the event rate associated with a normal perfusion scan has been shown by numerous investigators to be less than 1% per year of follow-up. The most recent ACC/AHA/ASNC guidelines for the clinical use of cardiac radionuclide imaging [50] report that in 16 nonoverlapping studies, more than 27,000 patients with normal SPECT were followed for a mean of 26.8 months and were found to have a hard event rate of 0.6% per year. This rate has been found to be independent of radiopharmaceutical used (thallium-201 or Tc-99m) or type of stress (exercise or pharmacologic) [11,47,51]. This uniformly low event rate is also unaffected by pre- or post-ETT likelihood of CAD, presenting symptoms or patient sex, and is therefore crucial in applying nuclear testing to risk stratification. Based on the above data, any patient with a normal perfusion scan is at low risk; thus, in a prognosis-based approach to testing, these patients would appropriately not be referred to further invasive testing (i.e., catheterization). Similarly, an ASNC position paper on normal SPECT [52] states that both risk and subsequent resource utilization is very low after normal MPS, and that this finding is clinically appropriate in light of the risk associated with these studies.

Predictors of risk and its temporal component

While, in general, the overwhelming majority of patients with normal MPS are low risk and not in need of further evaluation for CAD, it is important to point out that the precise level of risk after normal MPS varies widely and, in many situations, exceeds the traditionally accepted less than 1% threshold. Studies in patients undergoing pharmacologic stress, a population at higher risk and more comorbidities than patients undergoing exercise, have reported hard event rates of 1.3–2.7% per year [3,53–56], suggesting that underlying clinical risk and prior CAD may influence event rates after a normal MPS. Although this concept is clinically sound, a significant number of patients with normal MPS and follow-up would be needed to demonstrate this point.

With this in mind, a recent study followed up 7300 patients with normal exercise or adenosine stress MPS for a mean period of 1.8 years, finding a cumulative event rate of 1.1% or 0.6% per year [57]. Analyses performed by the authors in this large cohort revealed several novel findings. First, despite the low overall rate of adverse events, consistent with previous studies, unadjusted rates of hard events (cardiac death or nonfatal myocardial infarction) were greater in certain patient subgroups. For example,

while patients without prior CAD had an event rate of 0.4% per year, those with known prior CAD had an event rate of 1.4%. Considering type of stress in combination with history of CAD revealed that in patients with prior CAD, hard event rates exceeded 1% per year irrespective of type of stress. However, even in the absence of prior CAD, although risk was very low in patients undergoing exercise stress (0.2% per year), risk was considerably greater in patients referred for adenosine stress (1.1% per year). An interrelationship was also found between the presence of diabetes mellitus and patient sex. Both men and women without diabetes mellitus were at very low risk after a normal study (0.3 and 0.5% per year, respectively), but this risk increased considerably in the setting of diabetes mellitus (1.0 and 1.8% per year, respectively). Survival modeling in this cohort revealed that several factors, including age, type of stress performed (exercise versus pharmacologic), patient sex, diabetes mellitus, and a history of prior CAD, were predictive of a higher risk of adverse events after a normal MPS. Not only were some patients at greater risk than others after a normal MPS, but a temporally dynamic component to this risk was present as well, such that patients with prior CAD had increasing risk with time after the normal MPS (e.g., they were at greater risk in their second year of follow-up compared to their first year) (Fig. 8.11a). These findings suggest the presence of a "warranty period" after a normal MPS such that the low risk associated with this scan result is temporally limited, thus potentially identifying a time point at which retesting after a normal study may be indicated for prognostic reasons. Finally, with respect to exercise stress, it appeared that risk was greater than 1% per year in patients who were unable to achieve greater than 80% predicted maximum heart rate (Fig. 8.11b). The important lesson is that while most patients are at low risk after a normal MPS, patients with normal MPS are a heterogeneous group and observed risk will vary according to their clinical and historical characteristics.

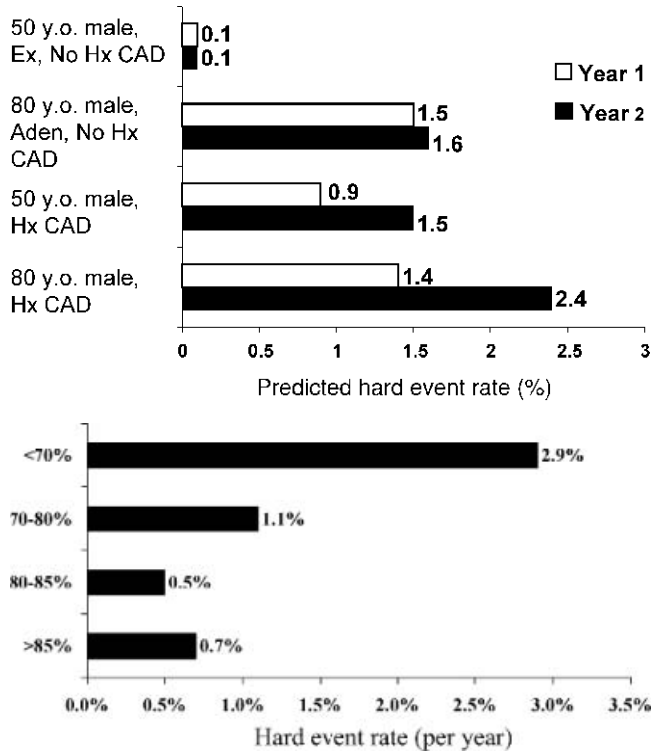

Figure 8.11 (a) Examples of predicted event rates in the first and second years after the index SPECT study [57]. The top pair of bars represents first and second year event rates in a 50-year-old male with no known CAD undergoing exercise stress. In comparison, an 80-year-old male with no known CAD undergoing adenosine stress would have significantly greater first and second year event rates. Of note, although the risk increases, the rates in the first and second years are not different. On the other hand, the counterparts of these two patients with CAD, as shown in the bottom two pairs of bars, would have significantly greater risk, the rate in the second year would exceed that in the first year and the change in risk between years one and two would increase as a function of age in the setting of known CAD. (b) Observed hard event rates per year in patients with normal exercise stress SPECT ($n = 5333$) as a function of predicted maximum heart rate achieved (<70%, 70–80%, 80–85%, or >85% of predicted maximum heart rate). (Based on [57].)

Elhendy and colleagues [58] also attempted to address the issue of the warranty period of a normal scan. On examining a cohort of 218 patients who had normal bicycle exercise stress Tc-99m sestamibi SPECT and were followed up for 7.4 ± 1.8 years, 10 myocardial infarction and 1 cardiac death occurred, with the annual mortality rate of 0.6% in the first five years and 1.8% between the sixth and eighth years. The annual hard cardiac event rate was 0.7% in the first five years and 1.5% between the sixth and eighth years. Although this study was underpowered to define the "warranty period" of a normal scan, they clearly brought to attention several of the more important issues involved.

In addition to the findings above, it is increasingly appreciated that in the setting of a normal pharmacologic stress SPECT study, the ECG response is also prognostically important, despite the presence of a normal SPECT. For example, the group from Yale University identified 228 patients who developed ischemic ECG changes during adenosine stress despite normal MPS [59] and were followed for over a 29-month period. These patients had more frequent adverse outcomes compared to age- and sex-matched controls who had normal adenosine stress MPS without the development of ischemic ECG changes. Studying a similar cohort, Klodas and colleagues from the Mayo Clinic reported that albeit an uncommon finding, the presence of an ischemic ECG response in the setting of a normal vasodilator stress SPECT was associated with increased risk of adverse events and multivessel CAD [60].

Challenging patients after normal stress MPS: are all normal MPS created equal?

Although most patients with normal MPS are low risk and can be managed conservatively, many challenging situations arise in this patient group during the course of daily clinical activities. As most readers are aware, it is possible for patients with significant epicardial CAD, particularly those with multivessel CAD, to have normal or near-normal MPS due to "normalization" of images. Because of this, there is a need to carefully examine MPS studies for ancillary markers suggestive of high risk. As noted above, these include transient ischemic dilation (either change in left ventricular shape or an increase in left ventricular size on stress versus rest), lung uptake of tracer, or evidence of left ventricular stunning poststress. In addition, the presence of an ischemic ECG response to stress, particularly in the setting of pharmacologic stress, or high-risk stress findings (ventricular ectopy or high degree block, abnormal hemodynamic response to exercise, severe, limiting symptoms, etc.) may raise suspicions of severe and/or extensive underlying CAD despite normal stress perfusion.

In a different category is the finding of significant left ventricular dysfunction (and possible enlargement) in the setting of normal perfusion. Although this may represent balanced reduction of stress flow, it may often represent nonischemic cardiomyopathy; nonetheless, the finding of transient ischemic dilation of the left ventricle in patients with otherwise completely normal perfusion scans has been shown to be associated with significantly higher risk than normal scans without this finding [45]. The clinical challenge in these settings is to determine whether the patient has a normal MPS or either significant epicardial CAD or nonischemic cardiomyopathy is present. This is an important differentiation since the former is at low risk and needs no further evaluation, while the latter may require further evaluation. In the past the only means to make a determination would be to refer the patient to catheterization and define the coronary anatomy. Currently, there are alternative noninvasive approaches that are particularly useful in patients who either prefer not to have invasive procedures or the procedure would present undue risk (e.g., abnormal renal function, poor access, peripheral vascular disease). The approaches that can be taken in these patients include the use of cardiac MRI with late contrast enhancement (see Chapter 13). The finding of late enhancement – the uptake of contrast on late imaging – is consistent with the presence of myocardial scar, suggesting CAD rather than nonischemic cardiomyopathy. Rest/stress cardiac MRI perfusion assessment can also be employed as this approach is able to define diffuse subendocardial ischemia. The absence of coronary calcium by CT would imply the presence of a nonischemic cardiomypathy. CT coronary angiography may also be useful in these patients, but further data are needed to substantiate this approach. Finally, the use of positron emission tomography (PET) in these patients with quantification of coronary flow reserve may also aid the evaluation of these patients. The limitation of PET in these circumstances is that many non-CAD processes – including cardiomyopathies – may also present with abnormal flow reserve. Combined PET/CT or SPECT/CT approaches may also prove useful in these patients, but data are currently lacking in this regard.

Decision making in patients with normal MPS

On the whole, patients with normal MPS can be managed conservatively. It must be noted that in a number of circumstances, particularly in the setting of left ventricular dysfunction and possible ischemic cardiomyopathy, the presence of ancillary finds suggestive of possible CAD or abnormal findings on the stress portion of the test, additional testing may be indicated to resolve discordance. Finally, there are many who believe that atherosclerosis testing may have a role in patients with normal MPS. If knowledge of whether atherosclerosis is present or not would influence subsequent management or direct the level of aggressiveness of preventive measures, atherosclerosis testing would have a role in these patients. At the current time, as described previously, there is, unfortunately, a lack of data to direct this approach.

Prognostic characteristics of abnormal scans

Event risk with abnormal scans. The prognostic characteristics of abnormal scans have been well described by an extensive literature. As illustrated conceptually in Fig. 8.12

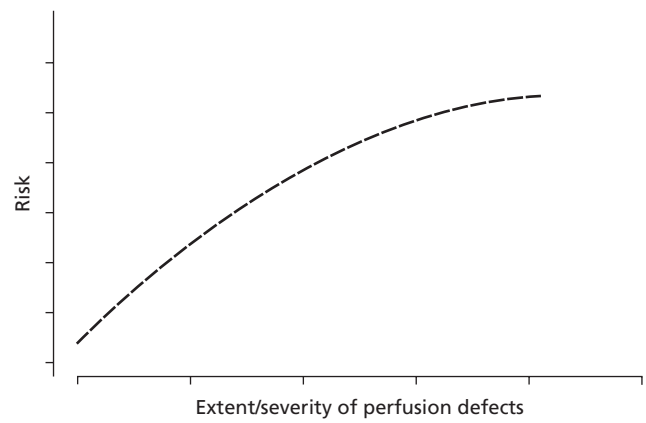

Figure 8.12 Relationship between extent and severity of stress perfusion defects on MPS and subsequent patient risk of adverse events on follow-up (from [61]). The generalized relationship shown in this figure is hypothetical, but representative of virtually all published studies. The shape of this curve stays fairly constant – risk increases with both extent and severity on stress MPS – but the overall curve can be shifted up or down by a number of factors that will be discussed later in this chapter.

[61], a close relationship exists between increasing extent and severity of scan abnormality and increasing patient risk of hard events or cardiac mortality [2,34,44,48,54,62–71]. The shape of this relationship holds true irrespective of the type of stress performed, the patient cohort examined (with respect to clinical characteristics or history of CAD), the type of isotope used, etc. Similarly, the risk of both cardiac death and nonfatal myocardial infarction increase as a function of scan abnormality. The flattened slope of this relationship (increase in mortality with increasing extent/severity of perfusion defect) is primarily related to the referral of the most ischemic patients to revascularization, resulting in their being censored from the prognostic publications. This referral bias was discussed above and will be discussed subsequently in more detail as well.

Table 8.1 Results of a meta-analysis of clinical trials comparing percutaneous revascularization to medical therapy.

Endpoint	Risk ratio (95% CI)	Strategy favored
Angina	0.70 (0.50–0.98)	percutaneous transluminal coronary angioplasty (PTCA)
Myocardial infarction (fatal and nonfatal)	1.42 (0.90–2.25)	Neither (trend to medical reaction)
Death	1.32 (0.65–2.70)	Neither
Need for PTCA	1.29 (0.71–3.36)	Neither
Need for coronary artery bypass surgery (CABG)	1.59 (1.09–2.32)	Medical reaction

Mildly abnormal perfusion scans

The concept of risk stratification was advanced a step further by the demonstration that stress SPECT may be able to differentiate those patients at risk of cardiac death versus those at risk of myocardial infarction.

As shown in Fig. 8.13, patients with moderately and severely abnormal scans were found to be at intermediate risk for both cardiac death and myocardial infarction [64]. However, patients with mildly abnormal perfusion studies (defined as <10% myocardium abnormal) with either exercise or vasodilator stress were at intermediate risk for myocardial infarction but at low risk for subsequent mortality (2.7 vs. 0.8 percent risk per year). Hence, patients with mildly abnormal scans were considered as having "flow-limiting" CAD, but unlikely to die from this disease over the next 2–3 years. A shown in Table 8.1, a recent meta-analysis of randomized clinical trials comparing medical therapy to medical therapy plus revascularization in patients defined angiographically to have mild CAD found that there were no differences between these approaches with respect to the endpoints of cardiac death, myocardial infarction, or need for downstream percutaneous coronary intervention (PCI). Medical therapy without revascularization was superior with respect to the need for downstream CABG. Of importance, however, is the fact that revascularization in these patients was a superior strategy with respect to relief of symptoms, as is widely known clinically. Extrapolating these results to noninvasive testing, it would appear that in general, patients with limited amounts of inducible ischemia, i.e., mildly abnormal SPECT, are unlikely to benefit from revascularization unless refractory symptoms are present. Thus, these patients may, despite their high likelihood of epicardial CAD, be candidates for medical therapy initially, and may be considered for revascularization only if they are refractory to medical therapy with respect to quality of life, functional status, anginal symptoms, or activity of daily living.

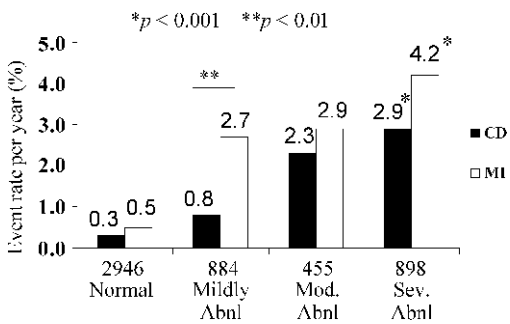

Figure 8.13 Annualized frequencies of cardiac death (red bars) and nonfatal myocardial infarction (white bars) in the setting of normal and mildly, moderately, and severely abnormal MPS (from [64]). This study followed 5183 patients both with and without prior CAD who underwent exercise or adenosine stress MPS. The frequencies of both cardiac death and nonfatal myocardial infarction increase significantly with increasing extent and severity of MPS abnormality. Importantly, the risk of cardiac death in the setting of a mildly abnormal scan (5–10% of the total % myocardium abnormal) is low (0.8% per year), while the risk of nonfatal myocardial infarction in this scan category is intermediate (2.7% per year). Given that myocardial infarction can be prevented by aggressive medical therapy, but not by revascularization, and that revascularization can only lower the risk of cardiac death (which is already low in this scan category), this study suggests the possibility that these patients should be treated with medical therapy rather than referral to catheterization unless issues pertaining to quality of life, functional status, or symptoms cannot be resolved.

While these findings still generally hold, several subgroups of patients with mildly abnormal perfusion scans and nonlimiting symptoms who have ancillary findings or comorbidities suggesting that SPECT might be underestimating risk have recently been described in whom coronary angiography would be appropriate to determine the need for revascularization as discussed below.

Moderately to severely abnormal perfusion scans

As risk of adverse events increases with the extent and severity of SPECT abnormalities, patients in these

categories of scan results are at greatest risk. Although both reversible and fixed stress perfusion defects are predictors of prognosis, those at highest risk of cardiac events are patients with extensive stress abnormalities. Multiple studies have described the highest event rates to be present in patients with moderate to severely abnormal with moderate to severely abnormal perfusion defects. These results extend to Tl-201 [48,69], Tc-99m sestamibi [54,68], and, more recently, Tc-99m tetrofosmin [72], as well as dual-isotope approaches [1,2,34,64,65,70].

Incremental value of non-SPECT data over SPECT information

More recently, an appreciation has been gained for factors that modulate the level of risk associated with any specific level of extent and severity found on MPS. In the section above on the prognostic implications of normal MPS, we discussed the variation in risk after a normal MPS with varying clinical and historical patient characteristics. Another important lesson learned from this finding is that pre-MPS data yield incremental value over MPS data for prediction of patient risk. This phenomenon was present in previous studies, but unappreciated. It was first pointed out by Berman and colleagues in a study evaluating the relationship between patient sex, diabetes mellitus, and risk after MPS [62]. As shown in Fig. 8.14, for any stress MPS defect size, patient risk varies as a function of whether the patient had diabetes mellitus, and what type of diabetes mellitus is present. This same relationship was previously shown, but not appreciated, in the study previously mentioned from Cedars-Sinai in 2200 patients without prior CAD who underwent stress MPS and had follow-up [2].

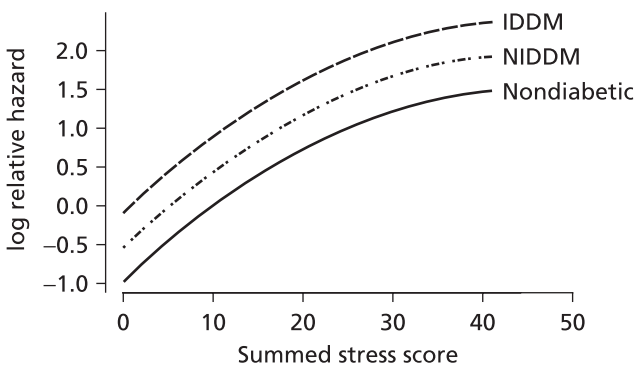

Figure 8.14 Predicted risk based on Cox proportional hazards model regression in a study of 6173 patients (2656 women and 2677 men) followed-up over 27.0 ± 8.8 months for cardiac death. Relationship between summed stress score (based on five point, 20-segment scoring) and log (natural) relative hazard from Cox proportional hazards modeling in patients with insulin-dependent diabetes mellitus, patients with non-insulin-dependent diabetes mellitus, and nondiabetic patients. Differences between curves are significant ($p < 0.0001$). (From [62].)

As seen in Fig. 8.9, if we focus on outcomes in the patients with mild scan abnormality, we find that the rate of hard events doubles at each increasing level of clinical risk, going from low to intermediate to high pre-MPS likelihood of CAD. Hence, not only does scan data provide incremental prognostic information over prescan information, but prescan data also yield incremental prognostic information over MPS results [2,3,57,62]. Thus, while patients with mildly abnormal MPS results generally are at low risk of cardiac death, this is not the case in the presence of significant comorbidities (e.g., advanced age [73], prior CAD [64], diabetes mellitus [62], atrial fibrillation [74], pharmacologic stress [64]). This phenomenon holds true not only for mildly abnormal SPECT results, but for normal SPECT, as discussed above, as well [57].

Nonperfusion/function markers of risk

Although a number of perfusion SPECT-derived variables are often mentioned as being clinically relevant and prognostically predictive, only the extent or the extent and severity of stress perfusion defects are reported in most manuscripts dealing with SPECT and prognosis. While in some studies these other variables were not analyzed, in many this has been due to the considerable overlap that exists between the various individual variables. Often mentioned variables include

1. total extent and severity of stress SPECT defects
2. total extent and severity of fixed SPECT defects
3. total extent and severity of reversible SPECT defects
4. total number of defects present (extent measure only)
5. presence of multivessel perfusion abnormalities
6. transient ischemic dilation of the left ventricle
7. lung uptake of the tracer
8. stress-induced stunning
9. LVEF
10. left ventricular volumes

First, as will be discussed below in greater detail, clinical, historical, and demographic data (such as age, cardiac risk factors, history of prior CAD) must be considered and weighed as markers of risk. In addition, the results of stress ETT must be taken into account. This includes not only exercise-induced symptoms and ST segment changes, but also multiple other factors such as pre-ETT likelihood of CAD, change in systolic and diastolic blood pressure with stress, work capacity (particularly in female patients), heart rate response, ectopy (stress or recovery), and heart rate recovery.

A number of investigators have put forward scores or algorithms of various levels of complexity to determine the post-ETT likelihood of CAD or risk of adverse events. These include complex scores such as CADENZA, or simpler scores, such as the Duke Treadmill Score [75,76] and other, more recently derived indices [77–79]. All of these

have subsequently been revalidated in external cohorts after the initial derivation and validation. The most important concept underlying these post-ETT estimates is the need to weigh multiple factors other than symptoms and ST segment change in summarizing the ETT result. Indeed, the ETT result should not be considered as either "positive" or "negative," but as reflecting either a low, intermediate, or high post-ETT likelihood of CAD or risk of adverse events.

In addition to the above factors, separate, unique factors must be considered for patients undergoing vasodilator stress. Although vasodilator stress is widely used as an adjunct to stress imaging, its results are not as intuitive to clinicians as are those of exercise treadmill testing. Although clinicians are accustomed and trained to understand and apply exercise tolerance, stress-induced symptoms, and both hemodynamic and chronotropic competence, the same cannot be said regarding vasodilator stress results. Symptoms experienced by patients during vasodilator stress are not predictors of coronary disease or of evidence of ischemia, and ST segment changes during vasodilator stress have lower sensitivity than during exercise. While some reduction of blood pressure and increase in heart rate are usually observed during vasodilator stress, the clinical significance and prognostic importance of different patterns of hemodynamic responses during vasodilator stress have not been well described. Recently, Abidov and colleagues [80] investigated 3444 patients who underwent adenosine stress SPECT with no additional exercise as an adjunct and were followed up for 2 years. Cox proportional hazards analysis revealed that after adjusting for all other significant factors, the failure to increase heart rate with vasodilator stress and a higher resting heart rate were both associated with increasing cardiac mortality.

The patient with high pre-ETT likelihood of CAD

Traditionally, the patient with high pre-ETT likelihood of CAD has been considered a candidate for direct referral to catheterization without noninvasive testing. The rationale for this approach has been that on Bayesian grounds even a normal MPS would not reduce the patient's likelihood of CAD to a sufficiently low level that further testing would not be necessary. Consequently, these patients have traditionally been considered candidates for catheterization rather than MPS.

However, this situation highlights the difference between anatomic and prognostic strategies for testing. A recent study addressed the role of stress MPS for risk stratification in 1021 patients with high pre-ETT or high post-ETT likelihood of CAD and no prior CAD [9]. As shown in Fig. 8.15, significant risk stratification is achieved and, importantly, the risk of cardiac death after a normal, or even mildly abnormal, scan is low. Hence, in this cohort, only 240 patients, or 21% of patients, would need

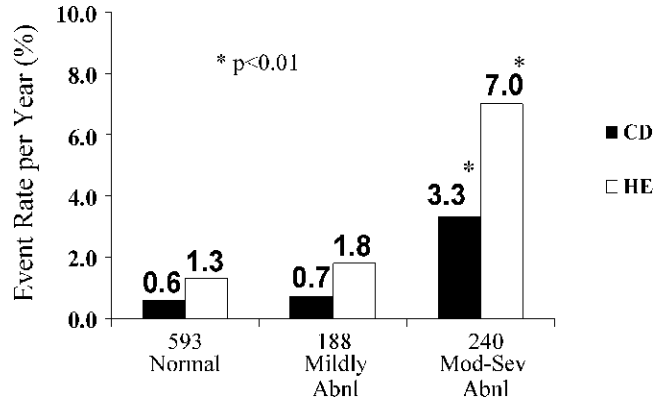

Figure 8.15 Frequency of cardiac death (red bars) and nonfatal myocardial infarction (white bars) in patients with high pre-ETT likelihood of CAD referred to MPS (from [9]). Patients were followed up for 2.2 ± 1.2 years after MPS. Frequency of outcomes are shown in normal, mildly abnormal, and moderately to severely abnormal MPS results. With respect to both outcomes, annualized rates of both cardiac death and nonfatal myocardial infarction increase across MPS categories. However, patients with both normal and mildly abnormal MPS are at low risk of cardiac death. Hence, of 1021 patients represented, only 240 would require catheterization on prognostic grounds.

further evaluation for CAD on the basis of risk. Given this excellent yield for testing (79% of patients reclassified as low risk of cardiac death), this study revealed that in patients with high pre-ETT likelihood of CAD, MPS was a cost-saving strategy compared to the use of ETT (followed by MPS) or direct referral to catheterization (as usually recommended). Hence, although from the perspective of a traditional Bayesian approach to noninvasive testing catheterization would appear to be a superior strategy, a risk-based strategy yields a different approach. This finding is an important lesson in that these two strategies do not always yield equivalent results, and that it is important to examine outcomes data before committing to a clinical strategy. With this mind, in patients with high pre-ETT likelihood CAD, stress MPS appears to be an acceptable, and potentially cost-saving, alternative to direct referral to catheterization.

Challenges to the use of pharmacologic stress

It must be noted that we have also gained insight with respect to the potential impact of the manner in which stress was performed on the prognostic implications of the scan result. It is generally accepted that exercise stress MPS is performed with the patient off antiischemic medications [50] whenever possible. Since these medications may limit or prevent the occurrence of ischemia during the exercise test, the sensitivity of the exercise perfusion study for the diagnosis of CAD is lower in patients taking such agents. Hence, the protocol at many laboratories

has been that patients on antiischemic medications do not undergo exercise stress but instead undergo vasodilator stress. Although, as discussed above, exercise stress yields parameters that can be used to assess the adequacy of stress (exercise duration, peak heart rate, predicted maximum heart rate achieved, etc.), no such parameters exist for vasodilator stress. Unfortunately, accumulating data suggest that contrary to initial beliefs, the use of vasodilator stress in patients who have taken antiischemic medications underestimated the presence of disease and the extent and severity of inducible ischemia. Sharir and colleagues [81] reported on 26 patients who underwent dipyridamole stress SPECT twice, the first without and the second with antiischemic medications. Compared to the perfusion defects seen on the studies performed on medications, those performed in the absence of the effects of antiischemic medications revealed significantly larger and more severe reversible defects. Quantitative software analysis indicated larger perfusion defects on stress images in the left anterior descending coronary artery ($25 \pm 21\%$ vs. $17 \pm 15\%$, $p = 0.003$), left circumflex coronary artery ($56 \pm 35\%$ vs. $48 \pm 36\%$, $p = 0.03$), and right coronary artery ($36 \pm 27\%$ vs. $25 \pm 24\%$, $p = 0.008$) territories. Of concern, the sensitivity for detection of CAD in any individual territory was significantly reduced (sensitivities for these three territories: 93% vs. 64%, 79% vs. 50%, and 100% vs. 70%, respectively; $p < 0.004$ for the first two comparisons). The overall individual vessel sensitivity of MPS off versus on medications was 92% vs. 62% ($p = 0.000003$). These results strongly suggest the need to discontinue antiischemic medications use prior to vasodilator stress MPS when the study is being performed for purposes of risk stratification or diagnosis. The mechanism by which this probably occurs is the preferential vasodilation of abnormal coronary arteries by the antiischemic medication, thus defeating the steal phenomenon on which vasodilator stress is based. Both previous and subsequent studies have supported these conclusions [82–84].

The mechanism of vasodilator stress described above can also be undermined by the use of caffeine-containing substances prior to SPECT. This would act to reduce or eliminate the ability to detect inducible ischemia. Numerous studies have reported that hemodynamic responses to vasodilators are not useful in identifying patients in whom the pharmacologic effects of adenosine or dipyridamole have been blocked by caffeine and a failure of heart rate or blood pressure to change with vasodilator stress does not imply lack of myocardial perfusion response [85,86]. Although most laboratories request that patients do not consume caffeine-containing substances prior to testing, stress laboratories are dependent on individual patients reporting the use of caffeine. This is unfortunate when studies reporting the accuracy of patient reporting are considered. Of patients denying caffeine use in the 12 hours prior to SPECT, 40% were serum caffeine positive while 74% of patients denying caffeine use in the prior 24 hours were serum caffeine positive [87,88]. These studies indicate a need for vigilance on the part of laboratory staff when performing vasodilator stress studies.

Considerations in patients with an abnormal scan

A simplistic approach to decision making after MPS would be to manage all patients with normal MPS conservatively and to consider catheterization in all patients after abnormal MPS. Unfortunately, extremes of resource utilization currently exist such that in some centers, this approach is actually practiced. Equally unfortunate is the remarkably low rate of resource utilization in the setting of certain centralized health care systems. Increasingly, advances in our knowledge of outcomes have increased the sophistication of the approach to identifying which patients are candidates for catheterization after abnormal MPS. Two distinct classes of criteria for catheterization after MPS exist. First, patients with refractory symptoms suggestive of CAD, irrespective of MPS results, are candidates for catheterization to define the underlying disease process to direct attempts at symptom relief. As noted above, angiographic data from randomized clinical trials, even in the setting of mild CAD, suggest an invasive approach is superior to medical management for relief of symptoms. Second, if the issue regarding a patient is survival free of cardiac death, the data from prospective randomized clinical trials clearly demonstrate that a relative survival benefit is to be gained through revascularization if extensive CAD is present. It is important to note that the absolute survival benefit is a function of several factors related to underlying patient risk, such as LVEF and various indices of clinical risk. As we will discuss subsequently, it is probably possible in most patients to identify who will benefit from revascularization as a function of MPS results.

Added value of gated SPECT

Given the relatively short time that gated SPECT has seen widespread use, it is not surprising that there are limited reports with respect to its added value or role in risk stratification. In the first published report from the Cedars-Sinai group including poststress gated SPECT, LVEF provided incremental information over perfusion defect extent and severity for the prediction of cardiac death [67] (Fig. 8.16). Surprisingly, this study showed that after consideration of LVEF, SPECT perfusion data no longer was predictive of adverse outcomes. This was recently identified as due to a referral bias in which patients with greatest extent and severity of ischemia were preferentially sent for early revascularization, the highest risk patients revascularized and thus censored from assessment of the prognostic value

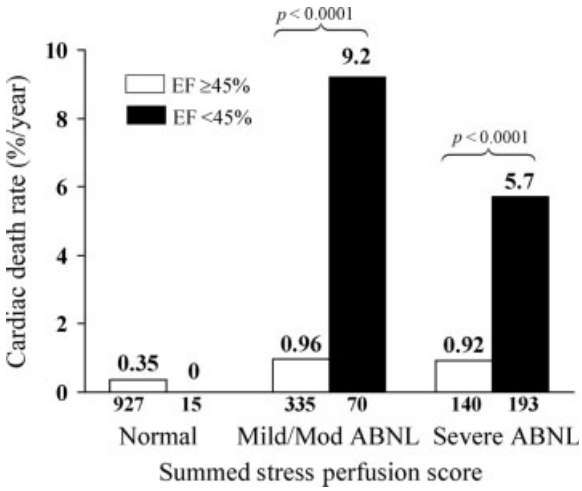

Figure 8.16 Frequency of cardiac death per year in patients as a function of scan result (normal, mild to moderately abnormal, and severely abnormal) and poststress ejection fraction by quantitative gated SPECT greater than or equal to 45% (left) and less than 45% (right). Significant differences ($p < 0.0001$) are present between lower and higher poststress ejection fraction in both abnormal scan groups. Numbers under the bars represent *N*. (From [89].)

of the test. Conversely, LVEF did not influence this referral process; hence, the risk associated with LVEF was not impacted by revascularization selection [8].

Data from this group also showed a role for left ventricular volumes from the gated information in risk stratification of patients. Indeed, left ventricular end-systolic volume provided added information over poststress LVEF for prediction of cardiac death [90]. Further, this group later reported that perfusion variables are stronger predictors of nonfatal myocardial infarction, while after risk-adjustment poststress ejection fraction was not predictive of nonfatal myocardial infarction [89].

A recent report by Thomas and colleagues [44] from a community-based nuclear cardiology laboratory followed 1612 consecutive patients undergoing stress SPECT over a follow-up period of 24 ± 7 months (0.2% lost to follow-up). Overall, patients with normal versus abnormal SPECT had hard event rates of 0.4%, compared with 2.3%, respectively ($p < 0.0001$). Further, these authors found that poststress ejection fraction added incremental value over pre-SPECT and perfusion data. Even after adjusting for these variables, each 1% change in LVEF was associated with a 3% increase in risk of adverse events. Unlike the Cedars-Sinai studies, perfusion data also added incrementally over ejection fraction data. In both patients with ejection fraction less than 40% and those with ejection fraction greater than or equal to ≥40%, the results of stress perfusion risk stratified patient risk (Fig. 8.17). A subsequent report by Travin and colleagues reported a series of 3207 patients who underwent stress SPECT and were followed-up for adverse events [68]. The authors found that both abnormal wall motion and abnormal ejection fraction were associated with increased risk; an abnormal gated SPECT wall motion score was associated with an annual event rate of 6.1% compared with 1.6% for a normal score, and an abnormal versus a normal LVEF was associated with an event rate of 7.4% versus 1.8%, respectively (both comparisons $p < 0.001$). Similar to previous studies, myocardial infarction was predicted by the number of territories with a perfusion defect but not by ejection fraction. On the other hand, as reported by Thomas et al., cardiac death was predicted by the number of territories with a perfusion defect and an abnormal ejection fraction. Finally, also as reported before, the results of gated SPECT added incremental value over both normal and abnormal SPECT perfusion.

Bias, treatment selection, and a reassessment of post-MPS strategy

To date, algorithms formulated to assist with the management of patients after stress SPECT have focused on the extent and severity of stress abnormalities as the basis for decision making. More recently, LVEF has been considered as a second parameter to assist in this as well. The data to support these approaches, and those preceded

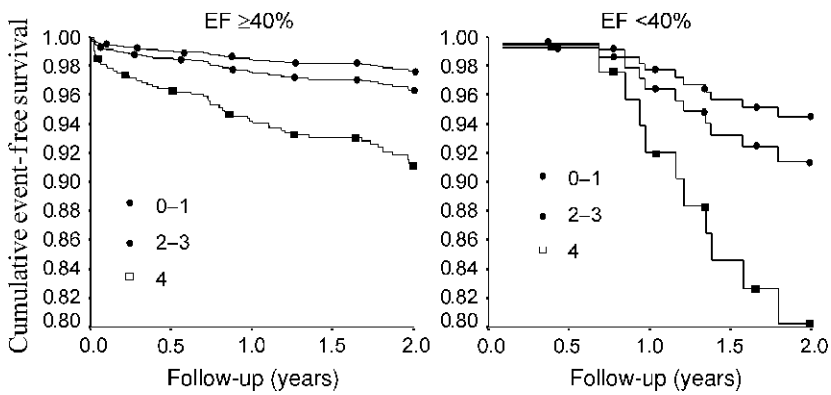

Figure 8.17 Cumulative event-free survival in patients as a function of reversibility score (0–1, 2–3, 4) as a function of poststress ejection fraction by quantitative gated SPECT greater than or equal to 40% (left) and less than 40% (right). Significant risk stratification is achieved by perfusion results in both ejection fraction categories. (From [44].)

it, were based on studies that censored, or removed, patients who were treated with revascularization early (60–90 days) after MPS. The rationale behind this was that since the decision to refer a patient to revascularization early after MPS was based on the MPS result, this "self-fulfilling prophecy" resulted in a reduction in event rates and the predictive value of MPS results. Recently, it has been found that this pattern of early revascularization has sufficient impact on post-MPS survival, and that even with censoring these early revascularizations [9], a significant underestimation of patient risk with markedly abnormal MPS occurs, contributing to a plateau effect of the defect size–risk relationship (Fig. 8.12) [61]. Consequently, the vast majority of the MPS prognostic studies published to date are limited by this referral bias, both with respect to underestimation of event rates as well as in that only patients treated medically after MPS are considered and analyzed.

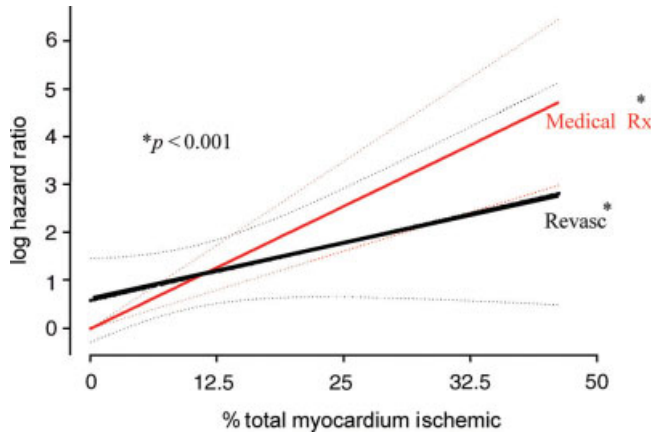

Figure 8.18 The primary results from a study of 10,627 patients with no prior myocardial infarction or revascularization that compared survival with revascularization versus medical therapy (from [3]). The two lines (with 95% confidence intervals) shown represent patients treated with revascularization (yellow line) and with medical therapy (red line). These lines define the relationship between the % myocardium ischemic and patient risk (as defined by the log of the hazard ratio). Importantly, these two lines cross (indicating a statistical interaction) such that patients with little or no ischemia (left side of graph) had lower risk with medical therapy compared with revascularization, while with increasing ischemia extent and severity a progressive survival benefit was accrued with revascularization relative to medical therapy. Importantly, in the range of ischemia values associated with a survival benefit with revascularization, the absolute benefit of revascularization (number for lives saved per 100 patients treated, years of life gained with revascularization) increased as a function of underlying clinical risk, as well as in women compared to men, diabetics compared to nondiabetics, adenosine stress compared to exercise stress, and the elderly compared to younger patients.

Impact of treatment selection on patient survival

The biases described above have recently been overcome by the application of advanced statistical techniques to analyze the relationship between MPS results, post-MPS survival, and post-MPS treatment given in a cohort of patients treated with either revascularization or medical therapy after MPS. This study of 10,627 patients without prior CAD undergoing exercise or adenosine stress MPS made several significant findings [3]. First, as previously described, both % myocardium fixed (fixed defects) and % myocardium ischemic (ischemic defects) were predictive of cardiac death, the latter more so than the former. However, only ischemia predicted which patients would fare better with revascularization or medical therapy. Patients with little or no ischemia had superior outcomes with medical therapy, while with increasing ischemia extent and severity revascularization had progressively superior survival benefit over medical therapy (Fig. 8.18). Further, the magnitude of improvement of survival (absolute benefit) varied as a function of underlying clinical risk, as described above with randomized clinical trials of revascularization versus medical therapy. Patients who were older, diabetic, women, or undergoing adenosine stress had greater survival benefit with revascularization at any level of ischemia.

Risk versus benefit driven strategies

Based on these results, a different approach to post-MPS patient management might be proposed as shown in Fig. 8.19. Rather than basing decision making on LVEF or extent and severity of stress defects, as previous algorithms have done, inducible ischemia by SPECT could be the basis of this decision making. Further, rather than basing decision making on risk – who is at greater risk, who is at low risk, we can base algorithms on identification of which patients may benefit from revascularization, and which probably will not. Hence, it could be possible to limit referral to catheterization to those patients who may accrue a survival benefit. Of course, the limitations of failure of the standard, normalized "relative" perfusion defect assessment of SPECT to detect diffuse ischemia must be recognized as a potential source of misclassifying high-risk patients as low risk.

Patients without inducible ischemia

These patients, not candidates for catheterization in this algorithm, consist of two distinct groups, those with normal MPS, discussed above, and those with abnormal MPS but no jeopardized myocardium. Several points must be made regarding the latter group. First, viability imaging becomes crucial in these patients because if any viable myocardium is detected, they may be reclassified into the next category of patients. While substantial viability is needed to improve outcomes with revascularization, some

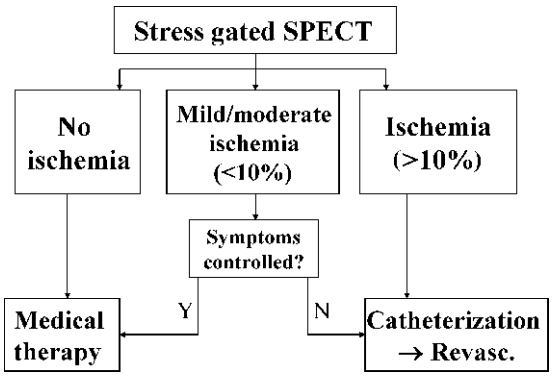

Figure 8.19 Flow diagram representing possible post-MPS management. Based on the above comments regarding the survival benefits of medical therapy versus revascularization, post-MPS decision making is based on the presence and amount of inducible ischemia. Patients without inducible ischemia are not listed as candidates for catheterization and/or revascularization. If the MPS is without ischemia because it is normal, then the reason for this is clear, and only risk factor modification can be recommended. On the other hand, if the MPS is abnormal without significant inducible ischemia, there is unlikely to be any survival benefit to be accrued with revascularization. If left ventricular function is significantly compromised, evaluation for transplantation in these patients may be indicated. A number of potential exceptions and challenges may arise in these patients, and these are discussed in the text.

viability techniques (e.g., SPECT, low-dose dobutamine echo) might underestimate viability. Second, while preventive measures are recommended in all patients in all algorithms, arguably in these patients "preventive measures" (and medical therapy) include not only those aimed at atherosclerosis prevention, but also those aimed at prevention of left ventricular remodeling and deterioration of left ventricular function. Finally, if neither inducible ischemia nor hibernation is present, and left ventricular dysfunction is found, consideration should be given for recommendation for transplant evaluation, when appropriate.

Patients with greater than 10% myocardium ischemic
These patients are similar to those with "mildly" abnormal scans described above. Although their MPS study is abnormal, unless refractory symptoms compromise of quality of life or limitations in functional status are present, it is unclear what benefit could be accrued by referral of this patient to revascularization. On the other hand, referral to catheterization should be considered in a number of instances in these patients. A potential pitfall of this approach is the patient with a severe (>90%) stenosis of the mid-first diagonal artery and a moderate lesions in the posterior descending artery and the proximal left circumflex vessel (70%). Due to balanced reduction, this patient may have a stress MPS showing only severe defects of the mid and distal anterior wall, or the distal anterior and anterolateral walls, with less than 10% of their myocardium ischemic. Hence, any suggestion that the limited amount of ischemia shown is due to balanced reduction should prompt further attention to this patient. Accordingly, in the presence of stress-induced stunning, transient ischemic dilation, lung uptake, ischemia on the nonnuclear stress portion of the examination, or any finding suggestive of underestimation of ischemia by perfusion imaging, catheterization may be indicated. Further, in diagnostic patients, if the study revealed no or minimal fixed defect (as opposed to a small amount of inducible ischemia with extensive scar), the finding by atherosclerosis testing of severe abnormalities in vascular distributions other than that where the perfusion defect is located may be an indication for catheterization. The potential dilemmas of this approach point to a potentially important advantage of SPECT/CT or PET/CT, that is, the potential to acquire a calcium score or CT angiography on all stress perfusion studies.

Patients with greater than 10% myocardium ischemic
These patients are relatively more clear-cut compared to those above. Recent data described above indicate that these patients will accrue a survival benefit from revascularization. It is important to note that "myocardium ischemic" incorporates both inducible ischemia and hibernating myocardium; hence, it is important to perform viability studies to identify those patients with borderline amounts of inducible ischemia who may qualify for this category. By performing viability imaging, patients who at first appear to have little or no jeopardized myocardium may turn out to have sufficient myocardium at risk to justify catheterization.

Incremental prognostic value of gated SPECT: what can gated SPECT add to perfusion findings?

Above we described the impact of including both patients treated medically along with those treated with early revascularization on the results of survival analyses. Importantly, this approach allowed, for the first time, a means by which to identify on the basis of noninvasive testing which patients are likely to accrue a survival benefit with one therapeutic approach compared to another [3]. However, this study did not include data regarding left ventricular function or LVEF; hence, the interrelationship of inducible ischemia and left ventricular function has not been defined. These data have, however, been reported in preliminary form [91]. In this report, the authors examined the hypothesis that while ejection fraction predicts the risk of cardiac death, only measures of ischemia will identify which patients will accrue a survival benefit from revascularization compared to medical therapy

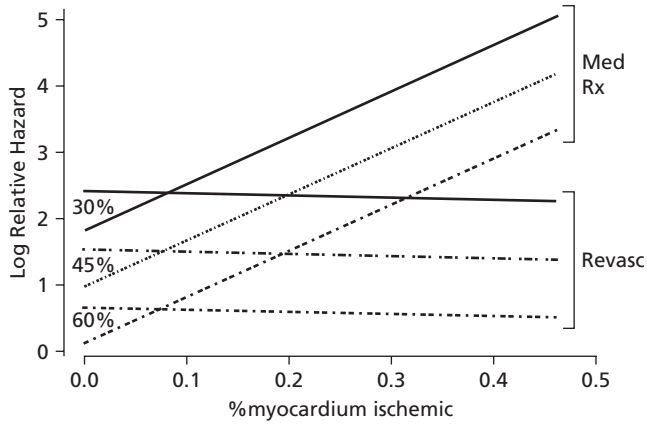

Figure 8.20 Predicted relationship based on Cox proportional hazards modeling between log hazard ratio versus % myocardium ischemic in patients treated medically ("Med Rx") versus early revascularization (Revasc) after stress SPECT. Three pairs of lines are shown for poststress LVEFs of 30, 45, and 60%. Within each pair, patient risk is unchanged across values of % myocardium ischemic with early revascularization, and increases significantly in patients treated medically. With decreasing ejection fraction, risk in both early revascularization and medically treated patients increases for any level of % myocardium ischemic. This increase in risk demonstrates the incremental value of LVEF over other factors. Similarly, the increase in risk with increasing % myocardium ischemic in the setting of medical therapy demonstrates the incremental value of SPECT measures of inducible ischemia. Finally, the differential risk with medical therapy versus revascularization identified by % myocardium ischemic demonstrates its ability to identify treatment benefit. Model $p < 0.00001$.

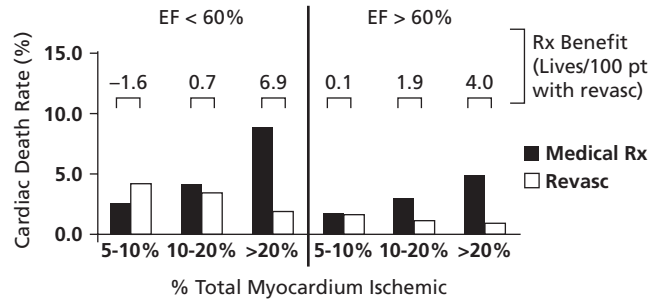

Figure 8.21 Predicted cardiac death rates based on final Cox proportional hazards model for patients with ejection fraction less than 60% versus greater than 60%. Results further stratified by % myocardium ischemic: 5–10%, 10–20%, and 20% or more. Within each category of inducible ischemia, predicted cardiac death rates are shown separately for medical therapy after stress SPECT (black bars) versus early revascularization (white bars). In both low and high ejection fraction subgroups, the risk associated with revascularization is significantly lower in the setting of marked ischemia. The number of lives saved per 100 patients treated (difference between predicted survival with early revascularization versus medical therapy) is shown over the bars. The number of lives saved per 100 patients treated is significant in patients with 20% myocardium ischemic, and is greater with low than high ejection fraction. Model $p < 0.0001$.

after stress SPECT. In this study, 5366 consecutive patients without prior revascularization were followed up for 2.8 ± 1.2 years, during which 146 cardiac deaths occurred (2.7%, 1.0% per year). After adjusting for pre-SPECT data, and a propensity score to adjust for nonrandomized treatment assignment, the authors found several interesting findings. First, as has been previously shown [67], LVEF was the most powerful predictor of cardiac death. Also, as shown before [44,68], stress perfusion results added incremental value over ejection fraction for prediction of cardiac death (Fig. 8.20). Most importantly, only the % myocardium ischemic was able to identify which patients would accrue a survival benefit with revascularization over medical therapy. Importantly, with respect to a relative benefit (which patients will have an improved survival with revascularization over medical therapy), only inducible ischemia was a predictor. On the other hand, LVEF played a crucial role in identifying the absolute benefit (number of lives saved per 100 treated, number of years of life gained with treatment) for a given patient (Figs. 8.20 and 8.21). This finding is similar to the meta-anlysis of randomized clinical trials data discussed above comparing medical therapy with revascularization [92]. Prediction of absolute benefit after stress SPECT is also a function of clinical risk factors, as previously described [3], such as patient age, sex, diabetes mellitus, and type of stress performed.

Predicting patient risk in individual patients

Given the recent findings described above, it is important to ask whether we can successfully predict risk in an individual patient after MPS. The ASNC Imaging Guidelines stated in 1999 that "some large laboratories have enough internal follow-up data to be able to statistically predict outcomes (death and nonfatal myocardial infarction) on the basis of perfusion image scores. If such data are available, incorporation of the likelihood of an adverse event in the report is highly desirable" [93]. However, this challenge is more daunting than initially appreciated when the above data are taken into account. First, it appears that in light of the referral bias to catheterization, and the obfuscation of event rates by post-MPS therapy selection, if this prediction of outcomes is to be attempted, risk estimation needs to consider post-MPS therapy as part of the equation. Second, in the context of the previous paragraph, for reasonably accurate estimates of risk to be put forward, a number of variables other than MPS results would be needed to be taken into account, as they add incremental value over the MPS results.

This year the first such score for MPS results was published [73]. This score was based on 5873 consecutive patients who underwent adenosine stress MPS and were followed up for a mean of 2.2 ± 1.1 years. Follow-up was

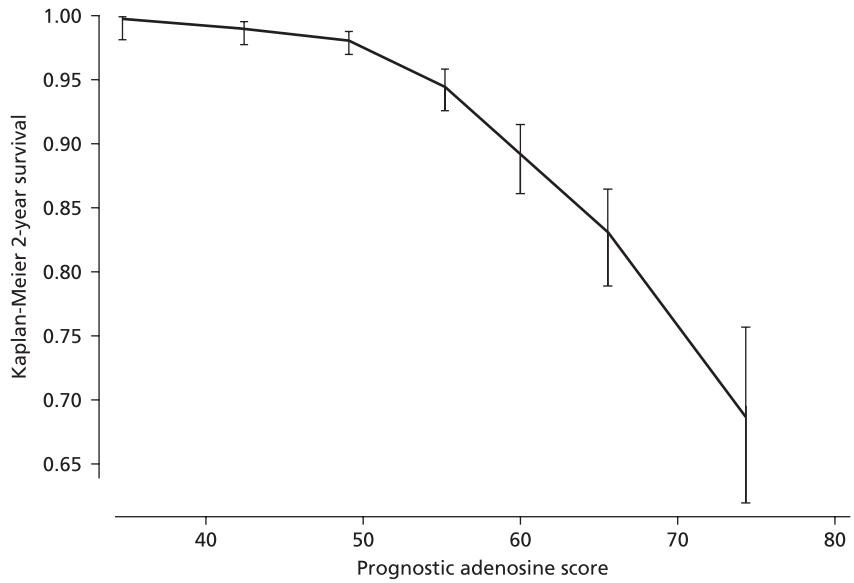

Figure 8.22 Kaplan–Meier 2-year survival as a function of prognostic score in the overall population. Bars represent 95% confidence intervals. $p < 0.0001$ (log-rank) across prognostic score. These bars are centered at the mean prognostic score values of seven subgroups (mean value and *n*): (1) 34.4, 387; (2) 42.3, 710; (3) 49.1, 1528; (4) 55.3, 909; (5) 60.2, 601; (6) 65.9, 458; (7) 74.9, 163. By calculating the adenosine prognostic score for patients, the result can be noted on the *X*-axis of this graph, a line drawn vertically to the survival curve, and a second line drawn horizontally to the *Y*-axis to determine the patients 2-year likelihood of survival free of cardiac death. Separate scores can be determined for medical therapy and treatment with revascularization for a patient, and the difference between the two constituting patient benefit.

94% complete and 387 cardiac deaths occurred during the follow-up period (6.6% mortality rate). This score was derived and internally validated using a split set validation with a Cox proportional hazards model. Several scores were reported, but the primary score is:

[age (decades) × 5.19] + [% myocardium ischemic (per 10%) × 4.66] + [% myocardium fixed (per 10%) × 4.81] + [diabetes mellitus × 3.88] + [if patient treated with early revascularization, 4.51] + [if dyspnea was a presenting symptom, 5.47] + [resting heart rate (per 10 beats) × 2.88] − [peak heart rate (per 10 beats) × 1.42] + [ECG score× 1.95] [if patient treated with early revascularization, % myocardium ischemic (per 10%) × 4.47] [73].

The ECG score consisted of 0.628 (if any block was present on ECG) + 0.724 (if left ventricular hypertrophy with repolarization abnormalities were present) + 0.832 (if premature ventricular beat(s) were present) + 0.331 (if nonspecific ST-T wave changes were present). Two separate scores can be calculated with this formula: one if the patients are treated medically and the other if they are treated with revascularization. Hence, this score not only estimates patient risk, but, in addition, identifies patient benefit with one therapy in comparison to another (Fig. 8.22).

Identification of risk versus identification of benefit

The potential to identify patient benefit introduces a new paradigm for stress imaging. A patient with extensive perfusion defects that are reversible is clearly at high risk, but also potentially has a significant benefit from revascularization. On the other hand, a patient with extensive defect but little ischemia is also at high risk of adverse outcomes, but will accrue little or no benefit from revascularization. This concept can be extended to a variety of situations. In any of them, rather than identifying a set of characteristics on MPS associated with high risk, and assuming that all these patients will have improved outcomes if treated invasively, we can now narrow our focus to those individuals who may benefit from this approach. This approach greatly improves the clinical-effectiveness and cost-effectiveness of MPS by increasing the number of patients classified as not potentially benefiting from revascularization without compromising patient outcomes.

Appendix

Statistical considerations in the determination of incremental value

In order to determine incremental value, the model should be derived in a *stepwise* fashion (clinical variables are entered first, then exercise variables, and finally nuclear variables). The statistical term for this approach is to *force* the initial clinical and exercise data *into* the multivariable model prior to the addition of the nuclear data. By forcing in the prenuclear information, the risk information not already contained in the prenuclear data can be successively assessed. The amount of information present in each step of this analysis (each successive model generated) is expressed by a test statistic such as χ^2, or, alternatively, by an ROC area. Unfortunately, the result of the analysis expressed as a test statistic is unintuitive, and its significance is unclear – e.g., what is the value of a unit of χ^2? Furthermore, this method is usually limited to the evaluation of

large patient populations, since a substantial number of outcome events are required for a meaningful analysis to be performed, and this is not always the case in patient subgroups [46,47,51,94].

Incremental clinical value

Although various multivariable analytic approaches can determine incremental prognostic value, the application of the analytic test results to patient stratification cannot be readily effected. The use of Kaplan–Meier survival curves permits determination of incremental prognostic value in a clinically more realistic manner. Generally, Kaplan–Meier curves are used to measure differences in survival rates between two patient cohorts. The patients are separated into lower and higher clinical risk groups (on the basis of clinical or clinical plus exercise test variables such as likelihood of CAD, exercise tolerance, ECG characteristics, etc.), and the survival rates over time of these two groups are compared. Each of these groups can potentially be further stratified by the results of nuclear testing. A significant difference in the survival rates between patients with normal and abnormal nuclear scans, either in the low or high clinical risk groups, demonstrates that even after clinical stratification, further information (in the form of further stratification) was added by nuclear testing. The advantages of this approach include the ability to test a clinically applicable or relevant threshold for clinical or exercise variables in a strategic manner, as well as the ability to analyze survival in a manner analogous to a clinical strategy. In addition, there are no clear-cut requirements for the number of outcome events, thus easing the performance of subgroup analysis.

Statistical evaluation of noninvasive testing

Several methods have been used to evaluate the performance of noninvasive testing. These include several multivariable analyses (e.g., multiple linear regression, multiple logistic regression, Cox proportional hazards models) and Kaplan–Meier survival analysis. Multivariable analysis is a statistical method that relates a number of predictor variables to an outcome of interest (e.g., cardiac events). Using this approach, it is possible to assess the effect of each individual predictor variable (e.g., perfusion abnormalities) after accounting for the effect of several other predictive factors (e.g., sex, age, risk factors, anginal symptoms). Differing approaches are used depending upon the outcome of interest. Multiple linear regression is used when the endpoint is a continuous variable (a number that has ordered, multiple possible values, such as blood pressure or cholesterol value). In the case of a variable that can assume one of two values (yes or no, CAD or no CAD), a binary logistic regression is used. If the outcome can be classified in one of several categories or levels, other types of logistic models can be applied (ordinal logistic, polytomous logistic) [95–98]. The use of logistic regression, either binary for the prediction of the presence of CAD or ordinal for prediction of grades of CAD (e.g., none, <90% single vessel, two vessel, three vessel/left main), permits assessment of test accuracy after adjusting for the variation in underlying patient characteristics. When survival data are modeled, a Cox proportional hazards analysis is usually performed. A Cox model incorporates information about both the occurrence of the outcomes (cardiac death, myocardial infarction) and the time between beginning of follow-up and occurrence of the event (time to event) [99]. Thus, it is not only relevant for this analysis that a patient had an event of interest, the amount of time to the event is also considered (e.g., a patient death occurring 1 week after the index timepoint is weighted more than if it occurred 1 year after the index timepoint) [95,97,100].

The results of these analyses can be compared using ROC) curve analysis [101–103]. The ROC curve represents the relation between a test's true positive rate (sensitivity) and false positive rate (1-specificity) as the threshold for abnormality is changed. The power of a model can be expressed as the area underneath its ROC curve, a measure that reflects the discriminatory power of the test in question independent of factors such as diagnostic threshold, baseline event rate in the study sample, or selection bias [48]. ROC curves have a potential area ranging from 0 to 1; an area of 0.5 corresponds to no discriminatory power, while an area of 1 defines perfect discrimination. ROC curve analysis can be applied to multivariable modeling by plotting each model's true positive and true negative rates at all possible thresholds of event probability. A comparison of models using ROC curves evaluates the diagnostic discrimination of the models, independently of a threshold of abnormality.

Risk-adjusted survival rates

An important approach to the analysis and subsequent understanding of outcomes data involves the use of multivariable methods to evaluate a modality with respect to its incremental prognostic value, or ability to risk stratify after adjusting for other clinical or historical factors (or the results of other tests, such as ETT or perfusion SPECT). Risk-adjusted survival curves can be developed that stratify patients by normal (≥50%) versus abnormal (<50%) gated SPECT ejection fractions. These curves, representing the rates of hard events over time, can be adjusted for the type of stress performed (exercise or adenosine),

the results of perfusion SPECT assessment, any history of prior revascularization or myocardial infarction, and the underlying clinical risk of the patients. Preliminary analysis has shown that gated SPECT ejection fraction yields incremental prognostic value over perfusion SPECT and all other clinical information known about the patient. Furthermore, it appears to do so in a clinically relevant manner (risk stratification), since it identifies a low-risk patient subgroup not in need of further testing.

References

1. Berman DS, Hachamovitch R, Kiat H, et al. Incremental value of prognostic testing in patients with known or suspected ischemic heart disease: a basis for optimal utilization of exercise technetium-99m sestamibi myocardial perfusion single-photon emission computed tomography [erratum appears in Journal of the American College of Cardiology Mar 1, 1996;27(3):756]. Journal of the American College of Cardiology 1995;26(3):639–647.
2. Hachamovitch R, Berman DS, Kiat H, et al. Exercise myocardial perfusion SPECT in patients without known coronary artery disease: incremental prognostic value and use in risk stratification. Circulation 1996;93(5):905–914.
3. Hachamovitch R, Hayes SW, Friedman JD, Cohen I, Berman DS. Comparison of the short-term survival benefit associated with revascularization compared with medical therapy in patients with no prior coronary artery disease undergoing stress myocardial perfusion single photon emission computed tomography. Circulation 2003;107(23):2900–2907.
4. Hachamovitch R, Berman DS, Kiat H, et al. Gender-related differences in clinical management after exercise nuclear testing. Journal of the American College of Cardiology 1995;26(6):1457–1464.
5. Bateman TM, O'Keefe JH Jr, Dong VM, et al. Coronary angiographic rates after stress single-photon emission computed tomographic scintigraphy. Journal of Nuclear Cardiology 1995;2:217–223.
6. Rozanski A, Diamond GA, Berman D, Forrester JS, Morris D, Swan HJ. The declining specificity of exercise radionuclide ventriculography. New England Journal of Medicine 1983;309(9):518–522.
7. Nallamothu N, Pancholy SB, Lee KR, Heo J, Iskandrian AS. Impact on exercise single-photon emission computed tomographic thallium imaging on patient management and outcome. Journal of Nuclear Cardiology 1995;2(4):334–338.
8. Hachamovitch R, Hayes SW, Friedman JD, et al. Is there a referral bias against revascularization of patients with reduced LV ejection fraction? influence of ejection fraction and inducible ischemia on post-SPECT management of patients without history of CAD. Journal of the American College of Cardiology 2003;42(7):1286–1294.
9. Hachamovitch R, Hayes S, Friedman J, Cohen I, Berman D. Stress myocardial perfusion SPECT is clinically effective and cost-effective in risk-stratification of patients with a high likelihood of CAD but no known CAD. Journal of the American College of Cardiology 2004;43:200–208.
10. Hachamovitch R, Shaw L, Berman DS. Methodological considerations in the assessment of noninvasive testing using outcomes research: pitfalls and limitations. Progress in Cardiovascular Diseases 2000;43(3):215–230.
11. Berman DS, Hachamovitch R, Shaw LJ, Germano G, Hayes S. Nuclear cardiology. In Fuster V, Alexander RW, King S, O'Rourke RA, Wellens HJJ, eds. Hurst's The Heart. New York, NY: McGraw-Hill; 2004:525–565.
12. Amanullah AM, Berman DS, Erel J, et al. Incremental prognostic value of adenosine myocardial perfusion single-photon emission computed tomography in women with suspected coronary artery disease. American Journal of Cardiology 1998;82(6):725–730.
13. Shaw LJ, Hachamovitch R, Eisenstein EL, Kesler KL, Heller GV, Miller DD. A primer of biostatistic and economic methods for diagnostic and prognostic modeling in nuclear cardiology: Part I. Journal of Nuclear Cardiology 1996;3(6, Pt 1):538–545.
14. Berman D, Kiat H, Germano G, et al. 99mTc-sestamibi SPECT. In DePuey EG, Berman DS, Garcia EV, eds. Cardiac SPECT Imaging. New York: Raven Press; 1995:121–146.
15. Iskandrian AE, Heo J, Nallamothu N. Detection of coronary artery disease in women with use of stress single-photon emission computed tomography myocardial perfusion imaging. Journal of Nuclear Cardiology 1997;4(4):329–335.
16. Maddahi J, Rodrigues E, Kiat H, Van Train K, Berman D. Detection and evaluation of coronary artery disease by thallium-201 myocardial perfusion scintigraphy. In DePuey EG, Berman DS, Garcia EV, eds. Cardiac SPECT Imaging. New York: Raven Press; 1995:103–120.
17. Rozanski A, Diamond GA, Forrester JS, Berman DS, Morris D, Swan HJ. Alternative referent standards for cardiac normality. Implications for diagnostic testing. Annals of Internal Medicine 1984;101(2):164–171.
18. Berman DS, Garcia, EV, Maddahi, J. Thallium-201 myocardial scintigraphy in the detection and evaluation of coronary artery disease. In Berman D, Mason, DT, eds. Clinical Nuclear Cardiology. 1st edn. New York: Grune and Stratton; 1981:49–106.
19. Taillefer R, DePuey EG, Udelson JE, Beller GA, Latour Y, Reeves F. Comparative diagnostic accuracy of Tl-201 and Tc-99m sestamibi SPECT imaging (perfusion and ECG-gated SPECT) in detecting coronary artery disease in women. Journal of the American College of Cardiology 1997;29(1):69–77.
20. DePuey EG, Rozanski A. Using gated technetium-99m-sestamibi SPECT to characterize fixed myocardial defects as infarct or artifact. Journal of Nuclear Medicine 1995;36(6):952–955.
21. Choi JY, Lee KH, Kim SJ, et al. Gating provides improved accuracy for differentiating artifacts from true lesions in equivocal fixed defects on technetium 99m tetrofosmin perfusion SPECT. Journal of Nuclear Cardiology 1998;5(4):395–401.
22. DePuey E, Shahzad K. Attenuation correction versus gating to characterize Tc-99m sestamibi fixed defects as attenuation artifact or scar [abstract]. Journal of the American College of Cardiology 1998;31(2, Suppl. A):175A.

23. Smanio PE, Watson DD, Segalla DL, Vinson EL, Smith WH, Beller GA. Value of gating of technetium-99m sestamibi single-photon emission computed tomographic imaging. Journal of the American College of Cardiology 1997;30(7):1687–1692.
24. Holly T, Parker M, Leonard S, Toth B, Hendel R. Comparative diagnostic accuracy of gated SPECT and attenuation correction in myocardial perfusion imaging [abstract]. Circulation 1997;96(8, Suppl. 1):I-442.
25. Johnson LL, Verdesca SA, Aude WY, et al. Postischemic stunning can affect left ventricular ejection fraction and regional wall motion on post-stress gated sestamibi tomograms. Journal of the American College of Cardiology 1997;30(7):1641–1648.
26. Bateman T, Case J, Cullom S, Barnhart C, O'Keefe J. Myocardial stunning detected by exercise gated SPECT Tl-201: a new scintigraphic marker of severe extensive CAD [abstract]. Journal of the American College of Cardiology 1998;31(2, Suppl. A):519A.
27. Lima RS, Watson DD, Goode AR, et al. Incremental value of combined perfusion and function over perfusion alone by gated SPECT myocardial perfusion imaging for detection of severe three-vessel coronary artery disease. Journal of the American College of Cardiology 2003;42(1):64–70.
28. Naghavi M, Libby P, Falk E, et al. From vulnerable plaque to vulnerable patient: a call for new definitions and risk assessment strategies: Part II. Circulation 2003;108(15):1772–1778.
29. Naghavi M, Libby P, Falk E, et al. From vulnerable plaque to vulnerable patient: a call for new definitions and risk assessment strategies: Part I. Circulation 2003;108(14):1664–1672.
30. Miller DD, Donohue TJ, Younis LT, et al. Correlation of pharmacological 99mTc-sestamibi myocardial perfusion imaging with poststenotic coronary flow reserve in patients with angiographically intermediate coronary artery stenoses. Circulation 1994;89:2150–2160.
31. Daimon M, Watanabe H, Yamagishi H, et al. Physiologic assessment of coronary artery stenosis by coronary flow reserve measurements with transthoracic Doppler echocardiography: comparison with exercise thallium-201 single piston emission computed tomography. Journal of the American College of Cardiology 2001;37(5):1310–1315.
32. Joye JD, Schulman DS, Lasorda D, Farah T, Donohue BC, Reichek N. Intracoronary Doppler guide wire versus stress single-photon emission computed tomographic thallium-201 imaging in assessment of intermediate coronary stenoses. Journal of the American College of Cardiology 1994;24(4):940–947.
33. Miller DD, Donohue TJ, Wolford TL, Kern MJ, Bergmann SR. Assessment of blood flow distal to coronary artery stenoses. Correlations between myocardial positron emission tomography and poststenotic intracoronary Doppler flow reserve. Circulation 1996;94(10):2447–2454.
34. Hachamovitch R, Berman DS, Kiat H, Cohen I, Friedman JD, Shaw LJ. Value of stress myocardial perfusion single photon emission computed tomography in patients with normal resting electrocardiograms: an evaluation of incremental prognostic value and cost-effectiveness. Circulation 2002;105(7):823–829.
35. Califf RM, Armstrong PW, Carver JR, D'Agostino RB, Strauss WE. 27th Bethesda Conference: matching the intensity of risk factor management with the hazard for coronary disease events. Task Force 5. Stratification of patients into high, medium and low risk subgroups for purposes of risk factor management. Journal of the American College of Cardiology 1996;27(5):1007–1019.
36. Brown KA. Prognostic value of thallium-201 myocardial perfusion imaging. A diagnostic tool comes of age. Circulation 1991;83(2):363–381.
37. Zaret BL, Beller GA. Clinical Nuclear Cardiology: State of the Art And Future Directions. 3rd edn. New York: Mosby-Year Book; 2004.
38. Shaw LJ, Miller DD, Romeis JC, et al. Prognostic value of noninvasive risk stratification in younger and older patients referred for evaluation of suspected coronary artery disease. Journal of the American Geriatrics Society 1996;44(10):1190–1197.
39. Hachamovitch R, Berman DS, Kiat H, et al. Effective risk stratification using exercise myocardial perfusion SPECT in women: gender-related differences in prognostic nuclear testing. Journal of the American College of Cardiology 1996;28(1):34–44.
40. Ladenheim ML, Pollock BH, Rozanski A, et al. Extent and severity of myocardial hypoperfusion as predictors of prognosis in patients with suspected coronary artery disease. Journal of the American College of Cardiology 1986;7(3):464–471.
41. Gill JB, Ruddy TD, Newell JB, Finkelstein DM, Strauss HW, Boucher CA. Prognostic importance of thallium uptake by the lungs during exercise in coronary artery disease. New England Journal of Medicine 1987;317(24):1486–1489.
42. McClellan JR, Travin MI, Herman SD, et al. Prognostic importance of scintigraphic left ventricular cavity dilation during intravenous dipyridamole technetium-99m sestamibi myocardial tomographic imaging in predicting coronary events. American Journal of Cardiology 1997;79(5): 600–605.
43. Veilleux M, Lette J, Mansur A, et al. Prognostic implications of transient left ventricular cavitary dilation during exercise and dipyridamole-thallium imaging. Canadian Journal of Cardiology 1994;10(2):259–262.
44. Thomas GS, Miyamoto MI, Morello AP, et al. Technetium99m based myocardial perfusion imaging predicts clinical outcome in the community outpatient setting: the nuclear utility in the community ("nuc") study. Journal of the American College of Cardiology 2004;43(2):213–223.
45. Abidov A, Bax JJ, Hayes SW, et al. Transient ischemic dilation of the left ventricle is a significant predictor of future cardiac events in patients with otherwise normal myocardial perfusion SPECT. Journal of the American College of Cardiology 2003;42(10):1818–1825.
46. Hachamovitch R, Berman DS, Morise AP, Diamond GA. Statistical, epidemiological and fiscal issues in the evaluation of patients with coronary artery disease. Quaterly Journal of Nuclear Medicine 1996;40(1):35–46.
47. Hachamovitch R, Shaw L, Berman D. Prognostic assessment in chronic coronary artery disease. American College of Cardiology Highlights 1997;Summer:4–8.

48. Ladenheim ML, Kotler TS, Pollock BH, Berman DS, Diamond GA. Incremental prognostic power of clinical history, exercise electrocardiography and myocardial perfusion scintigraphy in suspected coronary artery disease. American Journal of Cardiology 1987;59(4):270–277.
49. Hachamovitch R, Berman DS, Kiat H, et al. Incremental prognostic value of adenosine stress myocardial perfusion single-photon emission computed tomography and impact on subsequent management in patients with or suspected of having myocardial ischemia. American Journal of Cardiology 1997;80(4):426–433.
50. Klocke FJ, Baird MG, Lorell BH, et al. ACC/AHA/ASNC guidelines for the clinical use of cardiac radionuclide imaging–executive summary: a report of the American College of Cardiology/American Heart Association Task Force on practice guidelines (ACC/AHA/ASNC Committee to revise the 1995 guidelines for the clinical use of radionuclide imaging). Journal of the American College of Cardiology 2003;42(7):1318–1333.
51. Berman DS, Hachamovitch R. Risk assessment in patients with stable coronary artery disease: incremental value of nuclear imaging. Journal of Nuclear Cardiology 1996;3(6, Pt 2):S41–S49.
52. Bateman TM. Clinical relevance of a normal myocardial perfusion scintigraphic study. American Society of Nuclear Cardiology. Journal of Nuclear Cardiology 1997;4(2, Pt 1): 172–173.
53. Stratmann HG, Tamesis BR, Younis LT, Wittry MD, Miller DD. Prognostic value of dipyridamole technetium-99m sestamibi myocardial tomography in patients with stable chest pain who are unable to exercise. American Journal of Cardiology 1994;73(9):647–652.
54. Heller GV, Herman SD, Travin MI, Baron JI, Santosocampo C, McClellan JR. Independent Prognostic value of intravenous dipyridamole with Tc-99m sestamibi tomographic imaging in predicting cardiac events and cardiac-related hospital admissions. Journal of American College of Cardiology 1995;26(5):1202–1208.
55. Parisi AF, Hartigan PM, Folland ED. Evaluation of exercise thallium scintigraphy versus exercise electrocardiography in predicting survival outcomes and morbid cardiac events in patients with single- and double-vessel disease. Findings from the Angioplasty Compared to Medicine (ACME) Study. Journal of the American College of Cardiology 1997;30(5):1256–1263.
56. Calnon DA, McGrath PD, Doss AL, Harrell FE Jr, Watson DD, Beller GA. Prognostic value of dobutamine stress technetium-99m-sestamibi single-photon emission computed tomography myocardial perfusion imaging: stratification of a high-risk population. [comment]. Journal of the American College of Cardiology 2001;38(5):1511–1517.
57. Hachamovitch R, Hayes S, Friedman JD, et al. Determinants of risk and its temporal variation in patients with normal stress myocardial perfusion scans: what is the warranty period of a normal scan? Journal of the Ameriacn College of Cardiology 2003;41(8):1329–1340.
58. Elhendy A, Schinkel AF, van Domburg RT, Bax JJ, Poldermans D. Comparison of late outcome in patients with versus without angina pectoris having reversible perfusion abnormalities during dobutamine stress technetium-99m sestamibi single-photon emission computed tomography. American Journal of Cardiology 2003;91(3):264–268.
59. Abbott BG, Afshar M, Berger AK, Wackers FJ. Prognostic significance of ischemic electrocardiographic changes during adenosine infusion in patients with normal myocardial perfusion imaging [comment]. Journal of Nuclear Cardiology 2003;10(1):9–16.
60. Klodas E, Miller TD, Christian TF, Hodge DO, Gibbons RJ. Prognostic significance of ischemic electrocardiographic changes during vasodilator stress testing in patients with normal SPECT images [comment]. Journal of Nuclear Cardiology 2003;10(1):4–8.
61. Hachamovitch R, Berman DB. The use of nuclear cardiology in clinical decision making. Seminars in Nuclear Medicine 2004;35(1):62–72.
62. Berman DS, Kang X, Hayes SW, et al. Adenosine myocardial perfusion single-photon emission computed tomography in women compared with men. Impact of diabetes mellitus on incremental prognostic value and effect on patient management. Journal of the American College of Cardiology 2003;41(7):1125–1133.
63. Giri S, Shaw LJ, Murthy DR, et al. Impact of diabetes on the risk stratification using stress single-photon emission computed tomography myocardial perfusion imaging in patients with symptoms suggestive of coronary artery disease. Circulation 2002;105(1):32–40.
64. Hachamovitch R, Berman DS, Shaw LJ, et al. Incremental prognostic value of myocardial perfusion single photon emission computed tomography for the prediction of cardiac death: differential stratification for risk of cardiac death and myocardial infarction. Circulation 1998;97(6):535–543.
65. Kang X, Berman DS, Lewin HC, et al. Incremental prognostic value of myocardial perfusion single photon emission computed tomography in patients with diabetes mellitus. American Heart Journal 1999;138(6, Pt 1):1025–1032.
66. Sharir T, Germano G, Kang XP, Cohen I, Friedman JD, Berman DS. Prognostic value of post-stress left ventricular volume and ejection fraction by gated myocardial perfusion single photon emission computed tomography in women: gender related differences in normal limits and outcome [abstract]. Circulation 2002;106:II-523.
67. Sharir T, Germano G, Kang X, et al. Prediction of myocardial infarction versus cardiac death by gated myocardial perfusion SPECT: risk stratification by the amount of stress-induced ischemia and the poststress ejection fraction. Journal of Nuclear Medicine 2001;42(6):831–837.
68. Travin MI, Heller GV, Johnson LL, et al. The prognostic value of ECG-gated SPECT imaging in patients undergoing stress Tc-99m sestamibi myocardial perfusion imaging. Journal of Nuclear Cardiology 2004;11(3):253–262.
69. Vanzetto G, Ormezzano O, Fagret D, Comet M, Denis B, Machecourt J. Long-term additive prognostic value of thallium-201 myocardial perfusion imaging over clinical and exercise stress test in low to intermediate risk patients: study in 1137 patients with 6-year follow-up. Circulation 1999;100(14):1521–1527.

70. Zellweger MJ, Lewin HC, Lai S, et al. When to stress patients after coronary artery bypass surgery? Risk stratification in patients early and late post-CABG using stress myocardial perfusion SPECT: implications of appropriate clinical strategies. Journal of the American College of Cardiology 2001;37(1):144–152.
71. Marwick TH, Shaw LJ, Lauer MS, et al. The noninvasive prediction of cardiac mortality in men and women with known or suspected coronary artery disease. Economics of Noninvasive Diagnosis (END) Study Group. American Journal of Medicine 1999;106(2):172–178.
72. Shaw LJ, Hendel RC, Borges-Neto S, et al. Prognsotic value of normal exercise and adenosine (99m)Tc-tetrofosmin SPECT imaging: results from the multicenter registry of 4,728 patients. Journal of Nuclear Medicine 2003;44(2):134–139.
73. Hachamovitch R, Hayes SW, Friedman JD, Cohen I, Berman DS. A prognostic score for prediction of cardiac mortality risk after adenosine stress myocardial perfusion scintigraphy. Journal of the American College of Cardiology 2005;45:722–729.
74. Abidov A, Hachamovitch R, Rozanski A, et al. Prognostic implications of myocardial perfusion SPECT in patients with chronic atrial fibrillation. Journal of the American College of Cardiology 2004;44(5):1062–1070.
75. Mark DB, Hlatky MA, Harrell FE Jr, Lee KL, Califf RM, Pryor DB. Exercise treadmill score for predicting prognosis in coronary artery disease. Annals of Internal Medicine 1987;106(6):793–800.
76. Mark DB, Shaw L, Harrell FE, et al. Prognostic value of a treadmill exercise score in outpatients with suspected coronary artery disease. New England Journal of Medicine 1991;325(12):849–853.
77. Morrow K, Morris CK, Froelicher VF, et al. Prediction of cardiovascular death in men undergoing noninvasive evaluation for coronary artery disease. Annals of Internal Medicine 1993;118(9):689–695.
78. Morris CK, Morrow K, Froelicher VF, et al. Prediction of cardiovascular death by means of clinical and exercise test variables in patients selected for cardiac catheterization. American Heart Journal 1993;125(6):1717–1726.
79. Ho KT, Miller TD, Hodge DO, Bailey KR, Gibbons RJ. Use of a simple clinical score to predict prognosis of patients with normal or mildly abnormal resting electrocardiographic findings undergoing evaluation for coronary artery disease. Mayo Clinical Proceedings 2002;77(6):515–521.
80. Abidov A, Hachamovitch R, Hayes SW, et al. Prognostic impact of hemodynamic response to adenosine in patients older than age 55 years undergoing vasodilator stress myocardial perfusion study. Circulation 2003;107(23):2894–2899.
81. Sharir T, Rabinowitz B, Livschitz S, et al. Underestimation of extent and severity of coronary artery disease by dipyridamole stress thallium-201 single-photon emission computed tomographic myocardial perfusion imaging in patients taking antianginal drugs. Journal of the American College of Cardiology 1998;31(7):1540–1546.
82. Taillefer R, Ahlberg AW, Masood Y, et al. Acute beta-blockade reduces the extent and severity of myocardial perfusion defects with dipyridamole Tc-99m sestamibi SPECT imaging. Journal of the American College of Cardiology 2003;42(8):1475–1483.
83. Mahmarian JJ, Fenimore NL, Marks GF, et al. Transdermal nitroglycerin patch therapy reduces the extent of exercise-induced myocardial ischemia: results of a double-blind, placebo-controlled trial using quantitative thallium-201 tomography. Journal of the American College of Cardiology 1994;24:25–32.
84. Lewin HC, Hachamovitch R, Harris AG, et al. Sustained reduction of exercise perfusion defect extent and severity with isosorbide mononitrate (Imdur) as demonstrated by means of technetium 99m sestamibi. Journal of Nuclear Cardiology 2000;7(4):342–353.
85. Smits PCF, Aengevaeren WR, Wackers FJ, Thien T. False-negative dipyridamole-thallium-201 myocardial imaging after caffeine infusion. Journal of Nuclear Cardiology 1991;32(8):1538–1541.
86. Stanek EJMG, Charland SL. Xanthine interference with dipyridamole-thallium-201 myocardial imaging. Annals of Pharmacotherapy 1995;29(4):425–427.
87. Jacobson AFCM, Raisys V, Shattuc S. Serum caffeine levels after 24 hours of caffeine abstention: observations on clinical patients undergoing myocardial perfusion imaging with dipyridamole or adenosine. European Journal of Nuclear Medicine 1994;21:23–26.
88. Majd-Ardekani J, Clowes P, Menash-Bonsu V, Nunan TO. Time for abstention from caffeine before an adenosine myocardial perfusion scan. Nuclear Medicine Communications 2000;21(4):361–364.
89. Sharir T, Germano G, Lewin H, et al. Prognostic value of myocardial perfusion and function by gated SPECT in the prediction of non-fatal myocardial infarction and cardiac death [abstract]. In American Heart Association 72d Scientific Sessions 1999; Atlanta; 1999.
90. Sharir T, Germano G, Kavanagh PB, et al. Incremental prognostic value of post-stress left ventricular ejection fraction and volume by gated myocardial perfusion single photon emission computed tomography. Circulation 1999;100(10):1035–1042.
91. Hachamovitch R HS, Cohen I, Germano G, Berman DS. Inducible ischemia is superior to EF for identification of short-term survival benefit with revascularization vs. medical therapy [abstract]. Circulation 2002;106: II-523.
92. Yusuf S, Zucker D, Peduzzi P, et al. Effect of coronary artery bypass graft surgery on survival: overview of 10-year results from randomised trials by the Coronary Artery Bypass Graft Surgery Trialists Collaboration [see comments] [published erratum appears in Lancet Nov. 19, 1994;344(8934):1446]. Lancet 1994;344(8922):563–570.
93. American Society of Nuclear Cardiology. Imaging guidelines for nuclear cardiology procedures, Part 2. Journal of Nuclear Cardiology 1999;6(2):G47–G84.

94. Berman D, Hachamovitch R, Lewin H, Friedman J, Shaw L, Germano G. Risk stratification in coronary artery disease: implications for stabilization and prevention. American Journal of Cardiology 1997;79(12B):10–16.
95. Harrell FJ. Regression Modeling Strategies. New York: Springer-Verlag; 2001.
96. Harrell FE, Margolis PA, Gove S, et al. Development of a clinical prediction model for an ordinal outcome: The World Health Organization Multicentre Study of clinical signs and etiological agents of pneumonia, sepsis and meningitis in young infants. Statistics in Medicine 1998;17(8):909–944.
97. Harrell FE Jr, Lee KL, Mark DB. Multivariable prognostic models: issues in developing models, evaluating assumptions and adequacy, and measuring and reducing errors. Statistics in Medicine 1996;15(4):361–387.
98. Harrell FE Jr, Lee KL, Pollock BG. Regression models in clinical studies: determining relationships between predictors and response. Journal of the National Cancer Institute 1988;80(15):1198–1202.
99. Cox D. Regression models and life tables (with discussion). Journal of the Royal Statistical. Series B, Methodological 1972;34:187–220.
100. Harrell FE Jr, Lee KL, Califf RM, Pryor DB, Rosati RA. Regression modelling strategies for improved prognostic prediction. Statistics in Medicine 1984;3(2):143–152.
101. Hanley JA, McNeil BJ. The meaning and use of the area under a receiver operating characteristic (ROC) curve. Radiology 1982;143(1):29–36.
102. Hanley JA. Receiver operating characteristic (ROC) methodology: the state of the art. Critical Reviews in Diagnostic Imaging 1989;29(3):307–335.
103. McNeil BJ, Hanley JA. Statistical approaches to the analysis of receiver operating characteristic (ROC) curves. Medical Decision Making 1984;4(2):137–150.

9 Assessment of myocardial perfusion and left ventricular function in acute coronary syndromes: implications for gated myocardial perfusion SPECT

Fahim H. Jafary
James E. Udelson

Introduction

For over 20 years, radionuclide myocardial perfusion imaging has played an important role in diagnosis as well as risk stratification for patients suffering from acute ischemic coronary syndromes. Early studies using planar thallium imaging documented the superior ability of this technique to assess both the presence and location of myocardial infarction (MI) and more accurately predict the site of coronary disease involvement in unstable syndromes than ECG findings alone. More recently, the use of Tc-99m-based agents such as sestamibi in the early hours of an infarct has provided important information on area at risk in the setting of the coronary occlusion, while a follow-up study done several days later provides information on final infarct size as well as myocardial salvage, when both sets of images are compared. Stress perfusion imaging in the early aftermath of acute coronary syndromes as well as acute myocardial infarction (AMI) carries powerful prognostic information for risk-stratifying stable patients. Over the last few years, perfusion imaging has also been increasingly used among patients with chest pain syndromes in emergency department (ED) who do not have clear-cut ECG changes. Several published studies now consistently demonstrate extremely high negative predictive value for ruling out acute ischemia, as well as powerful risk stratification information for those with positive tests. Thus, the use of SPECT perfusion imaging techniques is widely utilized in the setting of acute ischemic coronary syndromes.

An entirely separate body of literature exists regarding the importance of left ventricular function in all of these clinical settings, that is, among patients with unstable angina, those with MI, and those in the ED setting. Assessment of regional and global left ventricular function in those settings has most often been performed using echocardiography as a separate test from the radionuclide myocardial perfusion imaging information.

Recent advances in hardware and software technology have allowed the combined assessment of stress and rest myocardial perfusion with resting (or poststress) measures of regional and global left ventricular function using gated SPECT imaging. The time and cost involved to provide the functional information beyond the perfusion information is quite modest and significantly lower than a separate examination using echocardiography, radionuclide ventriculography, or other methods such as magnetic resonance imaging (MRI). As documented in Chapter 5, gated SPECT determination of left ventricular ejection fraction as well as left ventricular volumes has been extensively validated against contrast ventriculography, two-dimensional (2D) echocardiography, radionuclide angiography, and MRI as gold standards using a variety of software packages and radioisotopes [1].

There is a growing body of literature that examines the combined assessment of perfusion and function in the same patients using gated SPECT imaging in the aftermath of acute ischemic syndromes or in the ED setting. Given the clear importance of left ventricular function in these clinical scenarios, however, it is likely that the addition of functional information to the perfusion data will provide a significant increment in information content in terms of risk stratification for future outcomes, as well as potentially providing important information for initial patient medical management. Also, given the relatively low cost of providing this information using gated SPECT technology, the necessary increment to obtain cost-effectiveness is modest.

Based on the growing availability of gated SPECT myocardial perfusion imaging, this report will attempt to assess the potential incremental value of adding functional information to the perfusion information in acute coronary syndromes. By carefully reviewing the individual prognostic value of perfusion imaging and left ventricular function and then examining studies that have combined functional and perfusion assessment, we hope to

gain insight into the added value of combining both pieces of information into one test.

Assessment of myocardial perfusion and left ventricular function following acute ST-elevation MI

Recent data indicate that there are approximately 1.5 million patients who develop an AMI annually in the United States. Among all patients suffering an acute infarction, approximately one-third are fated to die, with half of those deaths occurring within an hour of the onset of symptoms. Among survivors of the initial symptomatology, there has been a steady and favorable decline in mortality over the past three decades [2–4], likely related to improvements in aggressive early detection and treatment. Historically, these improvements have included the use of cardiac care units for intensive monitoring and early response to arrhythmias, and in the more recent era thrombolytic therapy and primary angioplasty, as well as other pharmacologic interventions to limit infarct size and progressive left ventricular dysfunction following infarction.

Among the survivors of the early hospital course of AMI, the underlying risk profile for subsequent mortality and recurrent infarction is quite variable. This risk profile ranges from the patient with a small infarction, single-vessel disease, and preserved left ventricular function who is at very minor risk for death or recurrent events over the subsequent year to the patient with a large index infarction, left ventricular dysfunction, and remaining viable myocardium jeopardized by severe obstructive coronary disease remote from the infarct-related artery, whose prognosis is quite grim.

Clinical variables and syndromes during the hospitalization for AMI identify a patient subgroup at very high risk in whom there is general agreement that early catheterization and intervention is indicated. These include patients with postinfarct recurrent ischemic pain, persistent hemodynamic instability including heart failure and cardiogenic shock, evidence of a mechanical complication such as mitral regurgitation or ventricular septal defect, and recurrent significant arrhythmias remote from the immediate acute infarct period [5].

The majority of patients surviving the initial acute infarction period will, however, have a relatively stable and uncomplicated course. In these patients, current guidelines generally recommend noninvasive risk stratification prior to hospital discharge. There are several reasons why profiling an individual patient's risk prior to discharge may be preferable to later postdischarge testing. A substantial proportion of morbidity and mortality in the year after MI occurs in the early weeks. Delaying stress testing for 3–6 weeks may result in missing this important cohort of patients [6]. Moreover, exercise testing with or without an imaging modality prior to discharge will allow the clinician to formulate an exercise prescription for the patient in preparation for post-MI cardiac rehabilitation.

Certain demographic and clinical variables can be identified which stratify stable post-MI patients into relatively higher or relatively lower risk groups following MI, such as age greater than 70 [7], diabetes [8], female gender [9], and patients with prior anterior infarcts [10,11]. However, the power of the stratification based on these variables is not generally thought to be sufficient to drive clinical decisions regarding catheterization. Few studies have carefully addressed the incremental value of stress testing with or without an imaging modality over and above all clinical and demographic variables in the post-MI setting.

Risk stratification following ST-elevation MI

A large body of literature documents three major determinants of natural history risk following an index acute infarction. These factors include residual resting left ventricular function, the extent of ischemic jeopardized myocardium, and the susceptibility to ventricular arrhythmias. Residual left ventricular function following an MI is related to final infarct size, which in turn is related to the potential myocardium at risk during the initial coronary occlusion. The residual extent of ischemic jeopardized myocardium following infarction is a consequence of the extent and severity of coronary artery disease (CAD) both within and remote from the infarct-zone-related artery. Susceptibility to malignant ventricular arrhythmias is a consequence of numerous factors, with important contributions from the degree of left ventricular dysfunction and the presence of inducible ischemia.

Thus, measures of left ventricular function and the extent of inducible ischemia would be expected to provide important prognostic information in the aftermath of AMI. Such data have the potential to guide management decisions regarding catheterization and subsequent intervention. Common practice in the United States often involves catheterization following MI in a majority of patients. Current guidelines, however, suggest that there is an important and potentially large subgroup of patients who are stable following an MI and who will not benefit in terms of natural history from catheterization and intervention, as they are already at relatively low risk for natural history events such as recurrent MI or cardiac related death. To the extent that noninvasive imaging of myocardial perfusion, inducible ischemia, and left ventricular function following an MI can provide powerful risk stratification information (and of particular importance provide information identifying a low-risk cohort), it follows that such testing will be extremely useful and potentially cost-effective by identifying the cohort of patients most likely

to benefit from further invasive management. There are numerous studies in the literature documenting the importance of detecting ischemia within or remote from the infarct zone. A separate body of literature has clearly and consistently documented the importance of left ventricular function in determining late outcome. Recent studies have analyzed the combined data on perfusion and function, and those few studies have involved separate noninvasive tests for these variables. Gated SPECT imaging, on the basis of its comprehensive ability to provide all of this important information, has the potential to be the single most important test in the stable patient following an MI.

Assessment of myocardial perfusion and inducible ischemia after AMI

One of the earliest and largest studies to examine the value of perfusion imaging data on the presence and extent of inducible ischemia in stable patients following MI was published by Gibson and colleagues in 1983 [12]. In this report, 140 consecutive patients with AMI and a stable in-hospital course underwent submaximal treadmill exercise testing in conjunction with planar thallium-201 imaging and coronary angiography prior to discharge. All predischarge assessments of electrocardiographic ischemia, scintigraphic ischemia, and the angiographic extent of CAD had statistically significant risk stratification value. However, the thallium-201 scintigraphic data contained the most robust information on stratifying risk, in that a low-risk thallium-201 image (defined as one thallium defect, no reversible defects, or no lung uptake) was associated with an extremely low-risk natural history outcome, with 6% of patients suffering cardiac events during 3-year follow-up (Fig. 9.1). In contrast, patients with a "low-risk" exercise test (defined as no ST depression or exercise-induced angina) had a 25% incidence of cardiac events on follow-up, while patients with a "low-risk" coronary angiogram (defined as zero- or one-vessel disease) had a 22% incidence of subsequent events. This important study not only defined the significant role played by scintigraphic perfusion imaging in detecting the presence of ischemia in post-MI testing, but also illustrated important points regarding the assessment of risk stratification testing variables in any situation. *Statistically significant* risk stratification may be obtained by a host of demographic, clinical, and testing variables when the prevalence of events is compared in a "low-risk" group and a "high-risk" group as defined by a specific variable. However, statistical difference in outcomes between the two groups does not necessarily translate into *clinically relevant* risk stratification information. In order for any variable or test result to be useful for clinical decision making, a "low-risk" test must be associated with a very low risk outcome such that conservative therapy can comfortably follow.

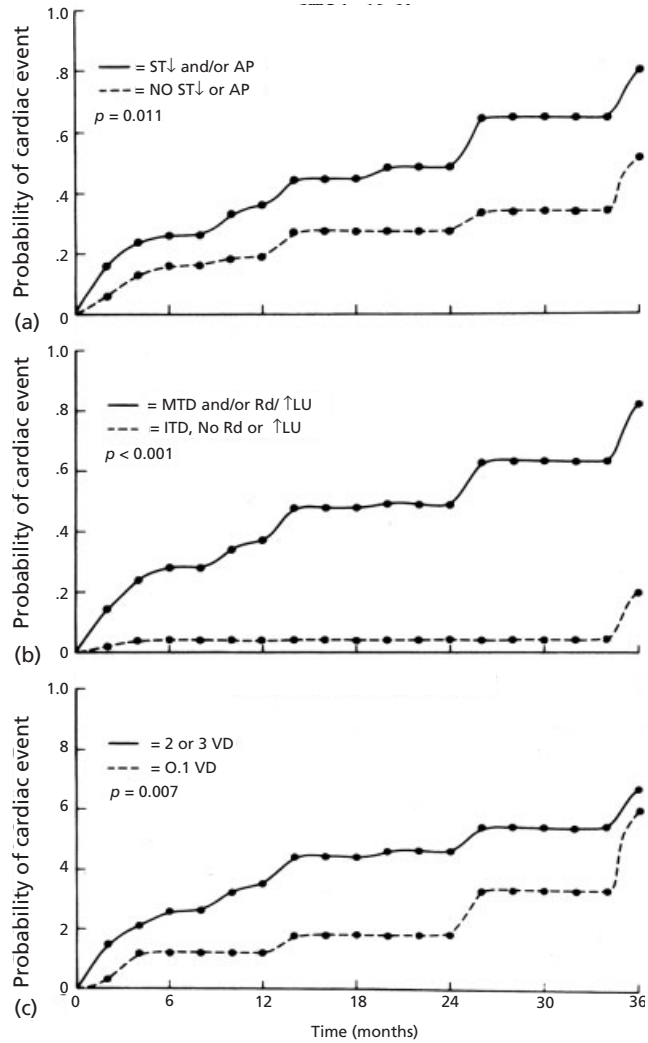

Figure 9.1 Probability of cardiac events in relation to different parameters acquired prior to hospital discharge: submaximal exercise test data (a), thallium-201 scintigraphy (b), and coronary angiography (c). Solid lines represent patients with high-risk characteristics (ST depression or angina, multiple thallium-201defects, reversible defects or lung uptake by scintigraphy, two- or three-vessel disease by angiography); dashed lines represent the defined low-risk test characteristics. Note the wide separation of the event curves between high- and low-risk patients as detected by thallium-201 scintigraphy, suggesting more powerful risk stratification. The perfusion data also identified a very low risk outcome group more clearly than the treadmill or angiographic data. Abbreviations: AP, angina pectoris; ↑Lu, increased lung uptake of thallium; MTD, thallium defects involving multiple vascular regions; Rd, redistribution; SMXT, submaximal treadmill exercise testing; ST↓, ST depression; 1TD, thallium defect in one vascular region; VD, vessel disease. (Reprinted with permission from [12].)

In the years following the report by Gibson et al. [12], many studies emerged which consistently identified the presence of inducible ischemia in the aftermath of AMI as a powerful predictor of subsequent outcome events [12–30]. These results are summarized in Table 9.1.

Table 9.1 Predictive value of stress myocardial perfusion imaging following MI.

Study	*N*	Time since MI	Thrombolytic therapy	Follow-up	Protocol	Imaging	Events death (and/or MI)		Predictors of cardiac events	
							N	%	Reversible defects	Other
Gibson et al. [12]	140	Predischarge	–	15 mo	Submax	Planar Tl-201	50	35.4	+	Lung uptake
Hung et al. [13]	117	3 wk	–	11.6 mo	Submax Naughton	Planar Tl-201	8	6.8	+	Change in EF by exercise RVG
Leppo et al. [14]	51	Predischarge	–	19 mo	Dipyridamole	Planar Tl-201	15	29.4	+	Lung uptake
Abraham et al. [15]	103	3 wk	–	6–34 mo	SL bicycle or Mod Bruce	Planar Tl-201	8	7.8	No	–
Gibson et al. [16]	241	2 wk	–	30 mo	Mod Bruce	Planar Tl-201	47	19.5	+	–
Gimple et al. [17]	40	Predischarge	–	6 mo	Dipyridamole	Planar Tl-201	3	7.5	+	–
Wilson et al. [18]	97	Predischarge	–	39 mo	SL or Mod Bruce	Planar Tl-201	6	6	+	–
Younis et al. [19]	77*	9 ± 4 d	–	1 yr	Dipyridamole	Planar Tl-201	10	15	+	–
Brown et al. [20]	50	1–4 d	50%	1 yr	Dipyridamole	Planar Tl-201	12	6	+	–
Tilkemeir et al. [21]	171†	Within 3 wk	37%	1 yr	Mod Bruce	Planar Tl-201	12	7	Weak	LV cavity dilatation and lung uptake were significant predictors
Hendel et al. [22]	71	Predischarge	100%	2 yr	Dipyridamole	Planar Tl-201	10	14.1	No	–
de Cock et al. [23]	100	Within 6 wk	–	4 yr	Maximal Bruce	Planar Tl-201	20	20	+	–
Moss et al. [24]	936	1–6 mo	31%	23 mo	Maximal Bruce	Planar Tl-201	75	8.2	No	ST depression on entry, rest EKG and lung uptake of Tl-201 ($n = 5$) were significant predictors
Miller et al. [25]	210‡	9 ± 6 d	100%	21 mo	SL or Mod Bruce	SPECT Tl-201	12	5.7	No	–
Travin et al. [26]	134	14 d	40%	15 mo	SL or Mod Bruce	SPECT MIBI	6	4.5	+	–
Mahmarian et al. [27]	146§	5 d	43%‖	18 mo	Adenosine	SPECT Tl-201	20	13.6	+	Perfusion defect size the best predictor of death
Dakik et al. [28]	71	Predischarge	100%	26 mo	SL Bruce	SPECT Tl-201	7	9.8	+	LVEF, lung uptake
Basu et al. [29]	100	5–7 wk	100%	21 mo	Maximal Bruce	Planar Tl-201	8	8	+	–
Brown et al. [30]	451¶	2–4 d¶	56% (51% in exercise only arm)	2 yr	Dipyridamole¶	SPECT MIBI	37	13	+	SDS strongest predictor of events; also anterior location was predictive

Abbreviations: EF, ejection fraction; LV, left ventricle; MIBI, Tc-99m sestamibi; Mod, modified; RVG, radionuclide ventriculography; SDS, summed difference score (reversibility index); SL, symptom limited; Submax, submaximal; Tl-201, thallium 201.

*54 (58%) had unstable angina.

†64 got thrombolytic therapy.

‡36 (17%) underwent early revascularization.

§51 patients undergoing revascularization after imaging were excluded from the analysis.

‖43% of entire cohort.

¶339 randomized to early (2–4 d) dipyridamole testing followed by predischarge (6–12 d) submaximal exercise SPECT; 112 randomized to predischarge submaximal exercise SPECT only. A total of 284 out of 339 actually received dipyridamole.

Subsequent investigations delineated other useful clinical endpoints predicted by myocardial perfusion imaging following MI. Abraham and colleagues [15] examined 103 patients following uncomplicated MI who underwent coronary angiography. The sensitivity for detecting multivessel CAD was similar for exercise-induced ischemic ST depression compared to the finding of thallium-201 defects remote from the infarct zone. However, specificity and positive predictive values were higher with scintigraphic imaging. The combination of tests was superior to either alone in detecting and particularly in ruling out multivessel CAD.

In a subset of patients studied in the prethrombolytic era but relevant to the postthrombolytic era, Wilson and coworkers [18] reported on long-term outcomes in 97 patients with single-vessel CAD on angiography approximately 12 days after uncomplicated MI. Late ischemic events were associated with the extent of the reversible defect within the infarct zone, and the percentage of patients with infarct zone ischemia was greater among patients experiencing a late event. Event-free survival was not related to the presence of exercise-induced angina nor with exercise-induced ST depression on ECG, but was significantly associated with infarct zone thallium-201 redistribution.

Thus, numerous studies in the prethrombolytic era documented the importance of the presence of exercise-induced scintigraphic ischemia both within and remote from the infarct zone in identifying a cohort of patients more likely to suffer subsequent morbid and mortal cardiac events. "Low-risk" scans identified a clinically low-risk patient group who could be comfortably targeted for conservative therapy.

As data on the value of exercise perfusion scintigraphy was emerging throughout the early to mid-1980s (predominantly using planar thallium-201 techniques), a simultaneous line of investigation was being reported on the value of pharmacologic stress imaging in the same clinical setting. An important proportion of patients following an uncomplicated MI are not able to exercise even to a submaximal workload. These patients are generally at higher risk of subsequent cardiac death or MI compared to the cohort able to exercise [31]. Thus, the use of pharmacologic stress imaging in such patients is conceptually attractive and potentially clinically important.

Leppo and colleagues [14] reported on a group of 51 patients recovering from AMI who underwent dipyridamole planar thallium-201 imaging. During a mean follow-up period of 19 months, 12 patients died or had a recurrent infarction, of which 11 had demonstrated evidence of thallium-201 redistribution defects on their post-MI imaging. Among 24 patients being readmitted with unstable angina, 22 had demonstrated evidence of redistribution defects. The presence of redistribution on the dipyridamole scan was the only significant predictor of important cardiac events on multivariable analysis. The absence of redistribution defects identified a very low risk cohort. Subsequent reports by Gimple et al. [17] and Younis et al. [19] confirmed these findings.

The important data regarding the relation between stress myocardial perfusion imaging evidence of inducible ischemia within or remote from the infarct zone after an MI and subsequent outcomes have been reexamined in the more modern era of thrombolytic therapy. The results have been mixed, consistent with Bayesian predictions regarding the relation between the pretest probability of an outcome event and the predictive value of a test for that event. Two studies in which all patients underwent thrombolytic therapy for AMI have documented diminished value of perfusion imaging data for predicting events in this setting. Tilkemeier and colleagues [21] reported on 64 patients undergoing thrombolytic therapy for AMI who underwent predischarge thallium exercise testing. The reported data on the predictive value of scintigraphic testing were significantly lower than had been reported in prior studies. Similarly, Miller and colleagues [25] in a series of 210 patients with MI who had received thrombolytic therapy reported no differences at 2 years postinfarction in event-free survival for patients with high-risk compared to those with low-risk post-MI stress thallium-201 scans. In both these studies, the investigators noted that the populations in these thrombolytic therapy cohorts were quite different from populations studied in the prethrombolytic era. Patients undergoing thrombolytic therapy are younger, have more preserved left ventricular function, and have a lower prevalence of multivessel disease and a lower prevalence of subsequent outcome events. Thus, on the basis of all these factors identifying a group with a much lower pretest probability of an outcome event, Bayesian principles would dictate that the predictive value of any test would be less optimal.

However, other studies in the postthrombolytic era have reported similar favorable results regarding the relation of stress-induced scintigraphic ischemia to outcomes as those reported in the prethrombolytic era. Travin and coworkers [26] used Tc-99m sestamibi SPECT imaging after MI in 134 consecutive patients within 14 days of an uncomplicated MI. These investigators found that the extent of ischemia on the SPECT sestamibi scan was the only significant correlate of a future cardiac event on Cox regression analysis. Patients with three or more reversible defects had a 38% chance of an important cardiac event on follow-up (Fig. 9.2). Of interest, among the subgroup (40%) who had received thrombolytic therapy, the extent of sestamibi SPECT ischemia remained a strong correlate of a cardiac event.

Similarly, Mahmarian et al. [27] found that the quantitated extent of ischemia on adenosine SPECT thallium-201

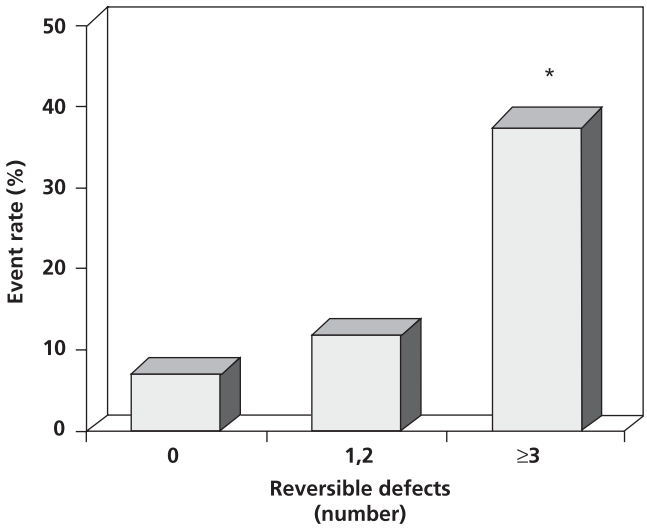

Figure 9.2 Relation between the postinfarction extent of ischemia (as determined by the number of perfusion defects by SPECT Tc-99m sestamibi) with cardiac event rate. Patients with more extensive ischemia are at progressively higher risk of unfavorable outcome. * $p = 0.017$ compared with patients with no reversible defects. (Reprinted with permission from [26].)

imaging was an important predictor of post-MI cardiac events by Cox regression analysis. Perfusion defect size on initial SPECT imaging and percent infarct zone ischemia together contained powerful predictive information, as did the combination or infarct zone ischemia and ejection fraction from a subsequent left ventricular function study.

In an elegant study reported by Brown et al. [30], 451 patients presenting with their first AMI were randomized in a 3:1 ratio to a strategy of early (2–4 days) dipyridamole Tc-99m sestamibi SPECT imaging followed by predischarge (6–12 days) submaximal exercise SPECT ($n = 339$) or predischarge submaximal exercise SPECT imaging only ($n = 112$). The treating clinicians were revealed the results of the predischarge exercise study only as part of routine care. Thus, the early dipyridamole SPECT imaging could not influence patient management. Early dipyridamole perfusion imaging was a stronger predictor of both in-hospital and late cardiac events than predischarge submaximal exercise SPECT. In the multivariable model, the extent and severity of the dipyridamole perfusion defects and the extent of reversibility were predictors for both in-hospital and late cardiac events. Importantly, this predictive model held ground irrespective of whether thrombolytic therapy had been administered – in fact, the model was more robust with those who did receive thrombolysis (Fig. 9.3).

These latter three studies were performed in cohorts of patients of whom only a subgroup received thrombolytic therapy (40% in the study of Travin et al. [26], 36% in the study of Mahmarian et al. [27], and slightly over 50% in the study by Brown et al. [30]). These data are likely representative of the contemporary management of MI in large populations and suggest that there is still an important role for scintigraphic imaging in the current era (Fig. 9.4).

The importance of the population being tested on the relation between the presence and extent of ischemia and

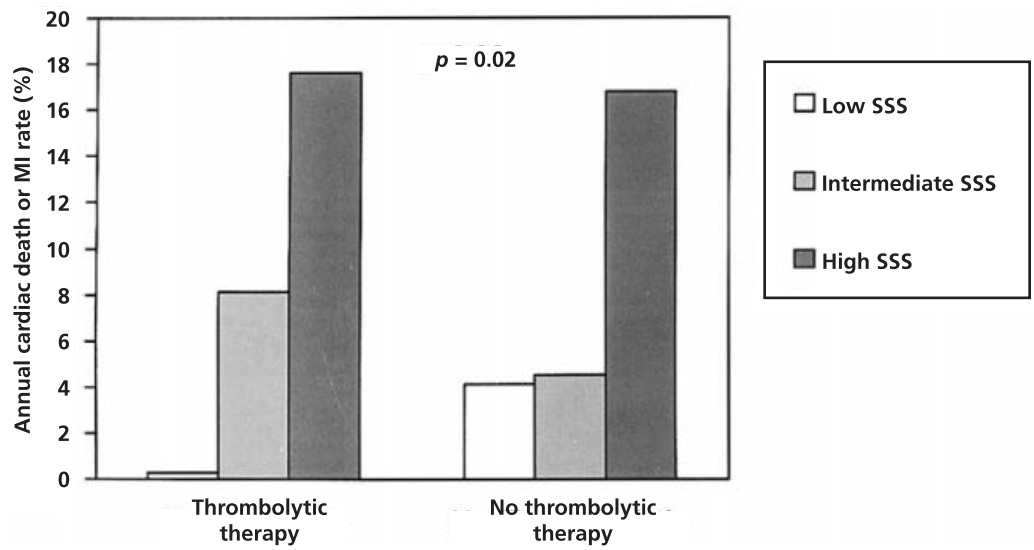

Figure 9.3 Predictive value of early dipyridamole stress perfusion imaging for cardiac death or MI in patients presenting with AMI – stratified by thrombolytic therapy. The summed stress score (SSS) had a greater discriminatory value in patients receiving thrombolysis with a sharper demarcation of high- and low-risk patients. (Reprinted with permission from [30].)

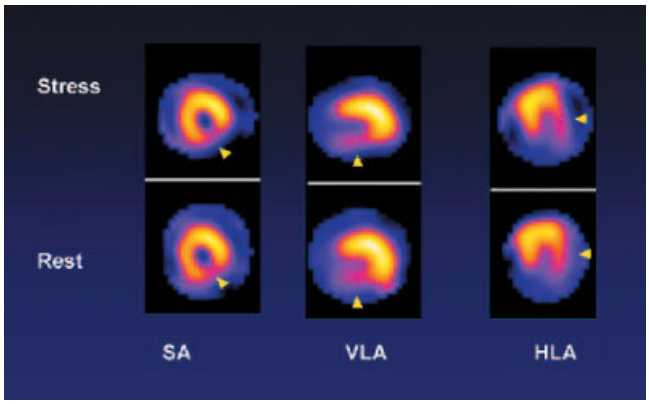

Figure 9.4 A 58-year-old woman presented with an uncomplicated acute inferior MI that was treated with thrombolytic therapy. On day 5 she underwent an exercise myocardial perfusion study. Images show a fixed inferior defect (arrows) with no inducible ischemia. The patient was treated medically and remains well 23 months after the event. Abbreviations: HLA, horizontal long axis; SA, short axis; VLA, vertical long axis.

subsequent outcome was also aptly illustrated by the results of the Multicenter Study of Myocardial Ischemia by Moss et al. [24]. In this large study, 936 patients who were clinically stable between 1 and 6 months after discharge for AMI or unstable angina underwent exercise ECG and stress thallium imaging. These investigators reported that detection of silent or symptomatic myocardial ischemia by noninvasive testing in this cohort was not useful in identifying subsequent recurrent events. In this population however, 40% of patients underwent coronary angioplasty either during the index hospitalization or prior to enrollment in the study. Thus, an important percentage of the population had been revascularized prior to testing. Moreover, the hard cardiac event rate was relatively low for a post-MI population (8.2% cardiac death or nonfatal MI during long-term follow-up), compared to many previous studies. This important study illustrates that noninvasive stress testing of any type is likely to be of most value early after MI prior to revascularization, when the risk for events is significantly higher.

The question of whether there is a differential prognostic value of peri-infarction versus remote ischemia was addressed in a recent study by Elhendy and colleagues [32]. Although performed in patients suffering from a remote MI (>1 month; mean 3.5 ± 2.2 years), and therefore different from those admitted with an acute event facing the question of risk stratification, the investigators showed that peri-infarction ischemia was independently associated with the risk of cardiac death (relative risk 2.6, 95% CI 1.1–6.1) over a mean follow-up of 5.5 years. However, remote ischemia was not. The authors speculated that perhaps ischemia superimposed on infarcted tissue was a particularly conducive substrate for lethal arrhythmias.

Clinical trials incorporating results of stress testing following MI

While the results of outcome prediction by any test following an acute ischemic event is of considerable clinical and intellectual interest, the true power of a predictive test is only demonstrated insofar as it can be used for clinical decision making to *improve* outcomes, not only *predict* outcomes. In this regard, several studies have been reported in which the presence of inducible ischemia following MI, by several techniques, is used to guide clinical decisions.

The Thrombolysis in Myocardial Infarction (TIMI) phase II trial [33] randomized 3339 patients who received intravenous tissue plasminogen activator for AMI to either an invasive strategy (cardiac catheterization at 18–48 hr after infarction with subsequent angioplasty or bypass surgery depending on anatomy) or a conservative arm in which cardiac catheterization was performed only in response to spontaneous or inducible ischemia (by stress radionuclide ventriculography). The 1-year outcome results demonstrated no difference in the primary endpoint of death or nonfatal reinfarction between the invasive or conservative strategy. The investigators concluded that among a cohort similar to those enrolled in the TIMI II trial, a noninvasive strategy with predischarge stress testing examining for the presence of inducible ischemia will be associated with similar outcome as a direct catheterization strategy. Cost-effectiveness is implied by the similar outcomes associated with fewer catheterized patients.

Whether conservative medical therapy may be appropriate for patients with inducible ischemia after MI was investigated by the Danish multicenter randomized study of patients with inducible ischemia after thrombolysis in AMI (the DANAMI trial) [34]. In this study, 503 patients who had survived an uncomplicated first AMI and who also had a positive post-MI exercise ECG for ischemia were randomized to an invasive strategy or a conservative medical treatment arm. At 2.4 years of follow-up, there was no difference in all-cause mortality between the groups; however, the invasive arm patients suffered fewer recurrent AMIs (5.6% vs. 10.5%, $p < 0.004$) and fewer subsequent admissions for unstable angina. Patients treated invasively also had less prevalence of stable angina during follow-up. These investigators concluded that invasive treatment in such patients with positive exercise ECG results in a reduction of the combined primary endpoint (death or recurrent MI) and is associated with fewer admissions for unstable angina and lower prevalence of stable angina.

The *absence* of scintigraphic ischemia has also been investigated as to its influence on clinical decision making for catheterization after MI and the relation to outcomes. Ellis and colleagues [35], in the TOPS (Treatment of

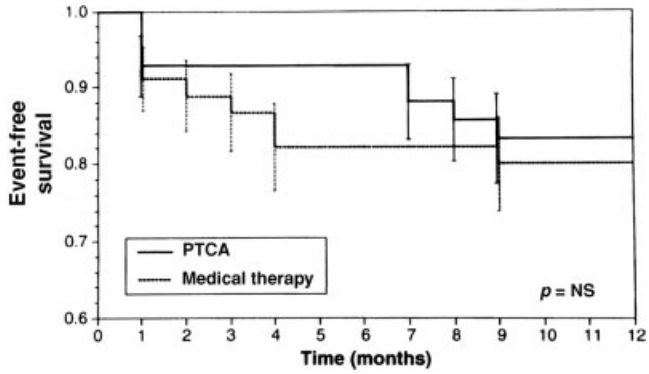

Figure 9.5 Lack of benefit of PTCA in patients receiving thrombolytics after myocardial infarct (MI) who have a residual stenosis of the infarct-related artery but no inducible ischemia. Shown is a plot of actuarial freedom from cardiac death, MI, coronary bypass surgery, or PTCA after randomization to PTCA (solid line) or medical therapy (dashed line). There is no difference in outcome between the groups. (Reprinted with permission from [35].)

Post-thrombolytic Stenoses) trial, reported on 87 patients who had received thrombolytic therapy for AMI and subsequently had a negative functional test for ischemia (predominantly thallium scintigraphy) despite a residual stenosis (though not occlusion) of the infarct-related artery. The patients were randomized to either medical therapy or angioplasty of the infarct-related artery residual stenosis. The primary endpoint was the change in left ventricular ejection fraction with exercise 6 weeks after MI. There were no differences between the study groups in the change from rest to exercise ejection fraction or in the resting ejection fraction at the 6-week endpoint. Actuarial 12-month infarct-free survival was 98% in the conservative therapy group and 91% in the group randomized to percutaneous transluminal coronary angioplasty (PTCA) ($p = 0.07$; Fig. 9.5). This trial demonstrates that patients with no evidence of scintigraphic ischemia within the infarct zone, even in the setting of a residual stenosis of the infarct-related artery, derive no benefit from angioplasty of the infarct-related artery. These data are consistent with the early results of Wilson et al. [18] in the prethrombolytic era among patients with single-vessel CAD, demonstrating that the absence of infarct zone ischemia is associated with a low-risk outcome where medical therapy alone may be sufficient. In contrast, when the presence or absence of infarct zone (or remote) ischemia is not incorporated into the decision process regarding angioplasty, and decisions are made solely on the basis of coronary anatomy, medical therapy may not produce the favorable outcomes seen in the TOPS study. In a recently published paper, Zeymer and colleagues [36] randomized 300 patients with documented single-vessel CAD following a recent (within 6 weeks) AMI to medical therapy or balloon angioplasty. The majority of patients had either no symptoms or mild angina. Although stress testing was performed prior to randomization, the results of the test (positive in 12% of medical and 15% of angioplasty group; p = NS) did not influence the decision to revascularize. At 1 year there was a trend toward an improvement in event-free survival in the angioplasty group (90% vs. 82%, $p = 0.06$) driven mainly by a reduced need for revascularization in the latter arm. There was no difference in mortality. In longer term follow-up there were fewer deaths in the angioplasty group (4% vs. 11.2%, $p = 0.02$). This study suggests that in patients who have recently suffered an AMI, coronary anatomy alone fails to define a subset of patients at low risk for adverse outcomes in whom conservative therapy would be safe and effective.

The results of trials such as TOPS and VANQWISH and the study by Zeymer suggest that scintigraphic testing for the presence and extent of myocardial ischemia in the aftermath of an AMI can indeed play an important role in clinical decision making regarding the need and utility of catheterization and invasive revascularization, and can also identify a cohort of patients whose outcome will be favorable without catheterization. With the expectation of wider application of aggressive secondary prevention strategies in the post-MI population, it might be anticipated that the "low-risk" post-MI outcome cohort will continually expand, making their identification prior to discharge even more compelling.

Dynamic assessment of prognosis after MI by serial scintigraphic studies: a new paradigm

While many studies have demonstrated an important correlation between the presence and extent of ischemia and subsequent natural history outcome events, the specificity of such determinations is often low. That is, among patients with "high-risk" scintigraphic or clinical signs, only a minority will indeed suffer an important cardiac event during follow-up, while the majority of patients categorized in this way will remain event-free. Thus, to the extent that common practice dictates most, if not all, of these "high-risk" patients should undergo catheterization and intervention, many patients are being intervened upon who would otherwise not have an event in order to presumably prevent such events in the minority.

While clinicians commonly accept this trade-off, recent intriguing data involving radionuclide perfusion imaging suggest that the *response of scintigraphic ischemia to medical therapy* may allow more precise estimates of ultimate prognosis, and more clearly identify the subgroups within the "high-risk" cohort who will and will not suffer a cardiac event.

In a population of 328 patients with single- or double-vessel CAD and a stable anginal syndrome, the

Angioplasty Compared to Medicine (ACME) investigators [37] randomized such patients to medical therapy or PTCA. Six months after randomization to either therapeutic arm, maximum symptom-limited exercise tests were performed with thallium imaging. The investigators recently reported 5-year follow-up data [38]. The 6-month postrandomization thallium data were strongly correlated with subsequent 5-year outcome events. Patients with a reversible thallium perfusion defect 6 months after either PTCA or medical therapy had a 3.6% annual mortality rate, compared to a 1.6% annual mortality rate among patients with no reversible thallium defects. The number of reversible defects was linearly related to subsequent mortality. Exercise electrocardiographic data were not predictive of late outcomes in this cohort. Of most interest, the initial randomization to either angioplasty or medical therapy did not influence this outcome analysis. That is, even if the 6-month thallium scan was performed on medical therapy alone in the absence of prior angioplasty, the outcome prediction was similar. These data suggest that follow-up scintigraphic imaging to assess the results of medical therapy on the extent of ischemia may help to more precisely define late outcomes, and subcategorize patients more precisely within outcome risk groups.

Whether this intriguing concept extends into the population of patients following an AMI was examined by Dakik and colleagues [39]. In this important pilot study, 44 stable survivors of AMI underwent adenosine SPECT thallium imaging approximately 4 days after AMI. These patients were included in the study on the basis of large total and ischemic perfusion defect size on SPECT quantitative analysis. Such patients were randomized to either aggressive and intensive medical therapy or coronary angioplasty, with a goal of suppressing myocardial ischemia as much as possible. The total stress-induced perfusion defect size was similarly reduced in the patients on medical therapy compared to the patients undergoing angioplasty (Fig. 9.6), as was the reduction in the quantitative extent of ischemia. Event-free survival was significantly related to the reduction in perfusion defect size (Fig. 9.7). Among 24 patients with 9% or more reduction in quantitative perfusion defect size, only 1 suffered a cardiac event during follow-up. In contrast, among patients with less than 9% reduction in quantitative perfusion defect size, there were six events among 17 patients. These data suggest that the response of scintigraphic SPECT ischemia to medical therapy parallel those seen with PTCA. To the extent that the change in ischemic defect size is related to outcome *independent of the intervention*, these data would suggest that even "high-risk" patients identified by stress scintigraphic imaging after MI may not all benefit from an invasive strategy, and that the relatively large proportion of patients within the high-risk cohort who are destined to remain stable might be identified on the basis of the response of scintigraphic ischemia to medical therapy. These important and encouraging pilot data are now being extrapolated to larger randomized trials. The Adenosine Sestamibi Post-Infarction Evaluation (INSPIRE) trial is an ongoing prospective, multicenter, randomized study that is examining the role of ischemia-guided optimal medical therapy in patients presenting with uncomplicated AMI. Initial risk assessment will be performed via adenosine-gated Tc-99m sestamibi imaging and therapeutic decisions will be made according to the extent of ischemia as well as left ventricular function. The effect of antiischemic therapy

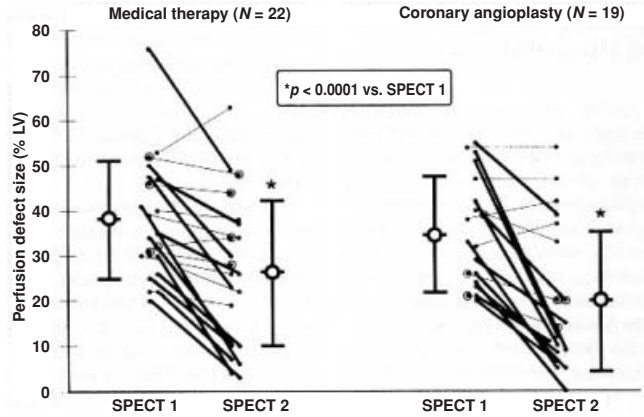

Figure 9.6 Suppression of ischemia after MI in patients with "high-risk" adenosine SPECT images early after infarction. Changes in perfusion defect size (PDS) during repeat adenosine SPECT imaging 6 weeks following randomization to medical or invasive therapy are shown. Similar diminution in PDS was achieved in both groups. Only 1 of 24 patients with a greater than 9% reduction in PDS (indicated by bold lines) had a cardiac event on follow-up. Patients who had a recurrent event are indicated by circled points. (Reprinted with permission from [39].)

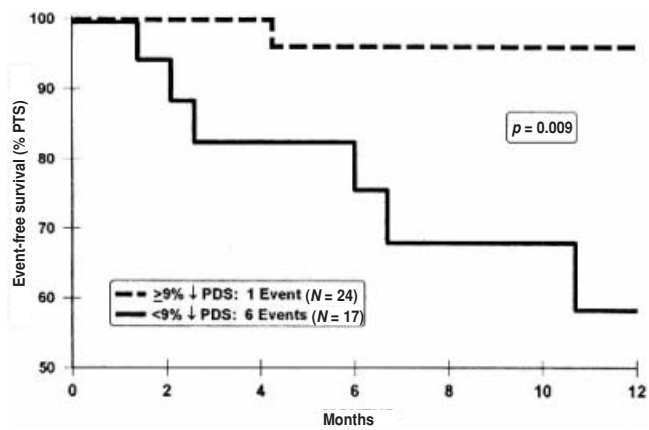

Figure 9.7 Suppression of ischemia after MI and outcome events. Kaplan–Meier curves showing that survival is favorably influenced by reduction in perfusion defect size (PDS) with either medical or invasive therapy. Patients with a greater than 9% reduction in PDS had a significantly improved event-free survival, compared to those without that magnitude of change in PDS. (Reprinted with permission from [39].)

will be prospectively followed by repeat perfusion imaging. A preliminary report [40] from this trial has shown a reduction in perfusion defect size in nearly 79% of patients enrolled so far. The Clinic Outcomes Utilizing Revascularization and Aggressive Drug Evaluation (COURAGE) trial compares aggressive medical therapy with aggressive medical therapy plus percutaneous coronary intervention (PCI) during 3–7 years of follow-up in patients with document myocardial ischemia is also underway [41]. The results of these studies may importantly affect the way patients with uncomplicated MI are treated in subsequent years.

Risk stratification by left ventricular function following MI

Few testing variables have been as powerfully and consistently associated with long-term natural history outcomes as measurement of left ventricular ejection fraction in patients with CAD. Large studies of heterogeneous CAD populations such as the Seattle Heart Watch database [42] or the Duke University database [43] have consistently demonstrated that survival decreases as the extent of left ventricular dysfunction increases. This concept also clearly applies to patients suffering from AMI. In a study of 866 patients following MI, the Multicenter Post-infarction Research Group [44] reported that left ventricular ejection fraction as measured by radionuclide angiography was an important univariate correlate of 1-year cardiac mortality after acute infarction. Radionuclide ejection fraction and the presence of ectopic depolarizations contributed independently to a survival model. As ejection fraction fell below 40%, there was a progressive increase in 1-year cardiac mortality (Fig. 9.8). In multivariate modeling, ejection fraction had a stronger relation to mortality than did the presence of ectopic depolarizations.

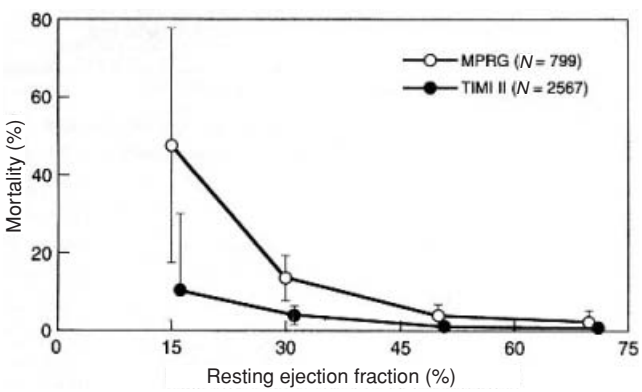

Figure 9.8 Relation of cardiovascular mortality to resting ejection fraction in the pre- and postthrombolytic era. Data from the Multicenter Post-infarction Research Group (MPRG) (upper curve) and the Thrombolysis in Myocardial Infarction Phase II (TIMI II) trial (lower curve) are shown. At any given ejection fraction, the mortality is lower in patients receiving thrombolytics, but a relation between ejection fraction and survival remains evident in the thrombolytic era. (Reprinted with permission from [45].)

Similar to the issues raised in the use of perfusion imaging among AMI patients receiving thrombolytic therapy, the different patient populations studied following thrombolytic therapy might be expected to have an effect on the relation between ejection fraction and survival. Several studies have examined this relationship. Among 618 patients randomized to conventional therapy or thrombolytic therapy with streptokinase, long-term survival remained significantly related to radionuclide ejection fraction, as reported by Cerqueira and coworkers in the Western Washington trial [46]. In a univariate analysis among a subgroup of patients with complete data, infarct size (by thallium-201 imaging), ejection fraction, age, and history of prior infarct were predictors of survival. However, in a multivariate model, only ejection fraction, age, and prior MI were strong predictors, with ejection fraction being the most powerful predictor. This study confirmed the importance of ejection fraction as a survival correlate in the thrombolytic era, and also demonstrated that once ejection fraction is taken into account, measurement of infarct size may not provide independent or incremental prognostic data, as these measurements are likely to be highly correlated.

Similar findings were reported by Zaret and coworkers in a report on the value of rest and exercise left ventricular ejection fraction among patients in the TIMI II study [45]. Compared to the prethrombolytic report of the Multicenter Post-infarction Research Group [44], 1-year mortality at any level of resting ejection fraction was lower than in the TIMI II population compared to the prethrombolytic era. However, there remained a significant relation between the extent of left ventricular dysfunction and long-term postinfarction mortality (Fig. 9.8). Among the 2567 patients studied, the majority of the predictive information was contained within the rest ejection fraction data. Once these data were used in a multivariate model to predict survival, neither peak exercise ejection fraction nor the change in ejection fraction from rest to exercise significantly improved predictive accuracy.

Large databases have also been examined in the thrombolytic era to assess predictors of short- and long-term outcomes. In the GISSI-2 database [47], 10,219 survivors of MI with available follow-up data were examined for correlates of 6-month all-cause mortality. Recovery phase left ventricular dysfunction (by echocardiography, which was determined in only 27% of patients) was an important multivariate predictor of outcome.

Thus, the data regarding the relation between ejection fraction and survival following an AMI are powerful, consistent, and appear to cross populations between the pre- and postthrombolytic era (Tables 9.2 and 9.3) [44–46,48–60].

Table 9.2 Prognostic value of assessment of left ventricular function post-MI in the prethrombolytic era.

Study	*N*	Follow-up	Method to assess LVEF	Predictors of cardiac death
De Feyter et al. [48]	179	28 mo	Contrast left ventriculography	EF <30%
Sanz et al. [49]	259	34 mo	Contrast left ventriculography	EF <20%; if three-vessel disease, EF 21–49%
MPRG [44]	866	12 mo	RVG	EF <40%
Nishimura et al. [50]	46	21 mo	2D echocardiography	Increased WMSI
Norris et al. [51]	325	3.5 yr	Cineangiocardiography	EF <40%
Ong et al. [52]	222	30 d	RVG	Killip I or II with EF <30%
White et al. [53]	605	78 mo	Contrast left ventriculography (LV volumes measured)	LV end systolic volume >130 ml
Jaarsma et al. [54]	77	In hospital	2D echocardiography	WMSI >7 predicted progression to Killip 3 or 4 (death rate not reported)
Schulman et al. [55]	143	5 yr	Contrast left ventriculography	EF <50%

Abbreviations: EF, ejection fraction; LV, Left ventricle; MPRG, Multicenter Postinfarction Research Group; RVG, radionuclide ventriculography; WMSI, wall motion score index.

Studies examining both perfusion imaging and left ventricular function following AMI

The availability of gated SPECT imaging to simultaneously evaluate myocardial perfusion and left ventricular function at little addition cost compared to perfusion imaging alone raises the important question regarding the incremental information provided by combining the analysis of perfusion and function information within one test. As the cost of adding the gated SPECT left ventricular function information is modest once perfusion imaging is performed, the increment of information required for cost-effectiveness is similarly modest.

Few studies have rigorously examined the potential complementary nature of perfusion and function information in the aftermath of AMI. Mahmarian and colleagues [27] studied 146 patients with assessment of left ventricular function (by multiple techniques) as well as adenosine SPECT thallium tomography, and related the findings to hard cardiac events over an average of 16 months of follow-up. Measurements of total perfusion defect size and the absolute extent of ischemia by quantitative analysis were univariate correlates of outcome, as was left ventricular ejection fraction in an inverse manner. The authors constructed several multivariate models for predicting late cardiac events, all of which involved either the

Table 9.3 Prognostic value of left ventricular function post-MI in the postthrombolytic era.

Study	*N*	Follow-up (mortality)	Result
Simoons et al. [56]	422	5 yr	LVEF <40%, mortality 39%; LVEF >40%, mortality 16%
Cerqueira et al. [46]	618	5 yr	LVEF <35%, survival 71%; LVEF 35–49%, survival 92%; LVEF >49%, survival 93%
GUSTO I Angiographic Investigators [57]	2431	30 d	LVEF >45%, mortality 3.9%; LVEF <45%, mortality 14.7%
Olona et al. [58]	115	5 yr	LVEF <40% by RVG or WMSI >8 by echo = risk ratio of 3.7 and 2.7 respectively for severe complications*
Zaret et al. [45]	3197 (630 no EF study)	1 yr	LVEF <30%, mortality 9.9%; LVEF >50%, mortality 1.2%
CAMI Study [59]	3178	1 yr	LVEF <30%, 9.5 times more likely to die than if LVEF >50%
Khattar et al. [60]	112	18 mo	LVEF <40%, hazard ratio 3.63

Abbreviations: CAMI, Canadian Assessment of Myocardial Infarction; GUSTO, Global Utilization of Streptokinase and t-PA for Occluded Coronary Arteries; LVEF, left ventricular ejection fraction; WMSI, wall motion score index.

*Defined as death, reinfarction, severe angina, or heart failure.

extent of quantitated ischemia or total perfusion defect size as well as left ventricular ejection fraction. Cox regression models for predicting 1-year risk in this patient cohort from both the perfusion information and the left ventricular function information are illustrated in Fig. 9.9. Knowledge of both the extent of inducible ischemia or perfusion defect size along with information on left ventricular ejection fraction allowed risk categorization superior to that provided by any of these variables alone. The incremental prognostic power of the perfusion variables and the ejection fraction information over baseline clinical data from this study are illustrated in Fig. 9.10. The same group of investigators subsequently reported very similar data with *exercise* myocardial perfusion imaging in a group of 71 stable postinfarct patients who had received thrombolytic therapy [28]. Evidence of inducible ischemia added incremental value to a prognostic model once clinical and ejection fraction had been incorporated. These data strongly suggest that measurement of perfusion abnormalities (total defect size and quantitative extent of ischemia) and left ventricular ejection fraction following MI have complementary roles, and together are powerful instruments for categorizing patient risk in this setting. Given the opportunity to derive these variables simultaneously from gated SPECT perfusion imaging should provide a powerful impetus for optimizing post-MI risk stratification.

In a study of patients late after MI (at least 3 months postinfarction) Zanco and coworkers [61] evaluated the separate and combined outcome correlations of stress sestamibi SPECT perfusion imaging and resting echocardiography over at least 4 years of follow-up. In a multivariate analysis for predicting hard (cardiac death and recurrent infarction) as well as soft (unstable angina) cardiac events during follow-up, the presence of reversible defects on the sestamibi SPECT images as well as the wall motion score index and area–length method ejection fraction by echocardiography were independently correlated with outcomes. Either the SPECT sestamibi perfusion information or the echocardiographic left ventricular function information added significant prognostic power to the clinical and baseline ECG information, while the

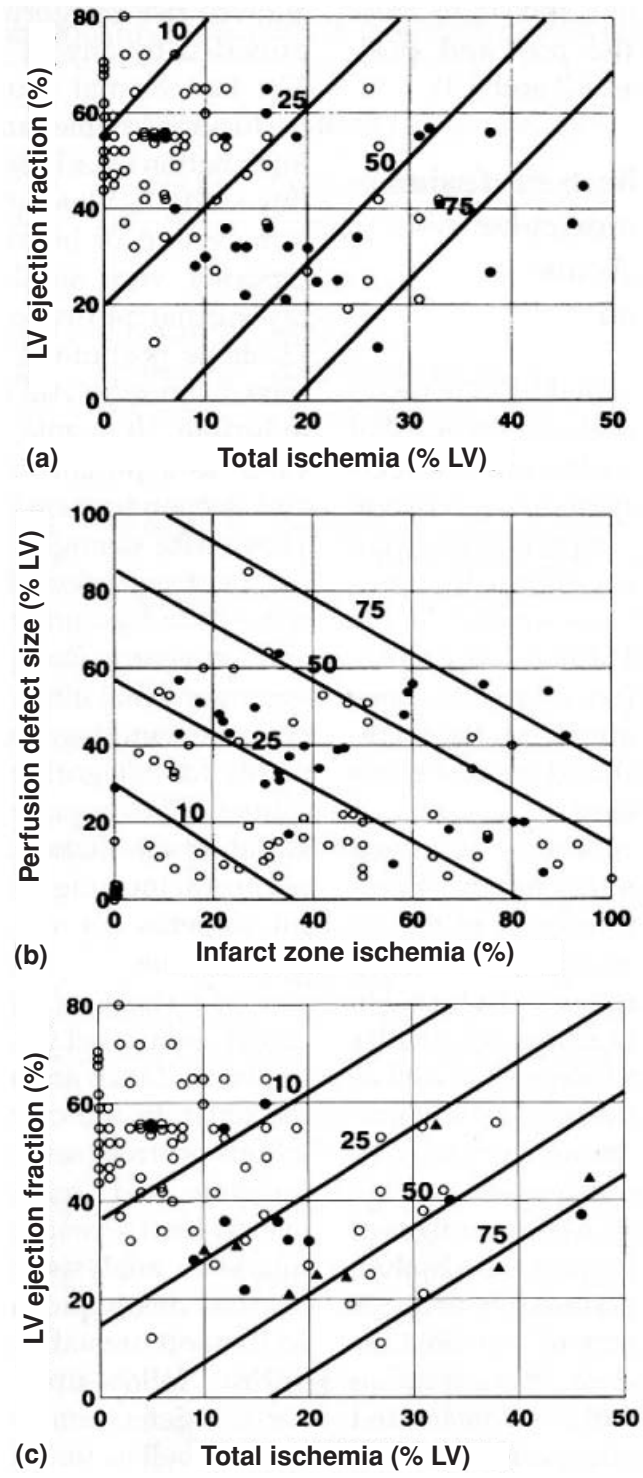

Figure 9.9 Cox regression models displaying 1-year risk for cardiac event according to left ventricular ejection fraction (LV ejection fraction) and total left ventricular ischemia (a) or scintigraphic variables (b). Regression model for predicting infarct-free survival are displayed in (c). Diagonal lines = representative isobars of percent risk of event. Patient risk for any cardiac event (a), or specifically death and nonfatal reinfarction (c), increases as total left ventricular ischemia increases and LV ejection fraction decreases, or as total perfusion defect size and percent infarct zone ischemia increase (b). For any given LV ejection fraction (a and c) or perfusion defect size (b), risk varies widely depending on the extent of ischemia. LV ejection fraction and scintigraphic results for each of 92 patients who did (solid circles) or did not (open circles) have subsequent cardiac event over entire follow-up period are plotted against calculated risk at 1 year (a and b). Patients are plotted (c) according to death (triangles), nonfatal reinfarction (solid circles), or neither of these events (open circles). (Reprinted with permission from [27].)

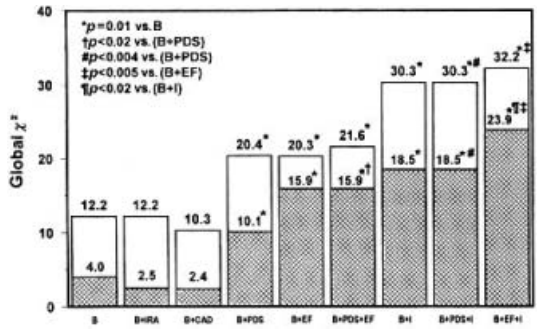

Figure 9.10 Incremental prognostic power of perfusion variables and ejection fraction information over a baseline clinical variable (B) for predicting all events (cross-hatched and open bars) or death and reinfarction (cross-hatched bar). Left ventricular ejection fraction and perfusion defect size (PDS), as well as extent of inducible ischemia (I) independently and incrementally predict risk beyond the baseline clinical model (B). Also, extent of ischemia improved the predictive power of the combined baseline clinical model and perfusion defect size (B + PDS) or baseline model and left ventricular ejection fraction (B + EF) for all events and for death and reinfarction. Left ventricular ejection fraction added significant power to the combined baseline model and PDS (B + PDS), as well as to the baseline model and extent of ischemia (B + I) for predicting death and reinfarction. Abbreviations: CAD, extent of coronary artery disease; EF, ejection fraction; IRA, infarct artery patency; χ^2, chi-square analysis. (Reprinted with permission from [27].)

combination of the perfusion and function information added more powerful prognostic information to the clinical data (Fig. 9.11). While the application of these data may be limited by the relatively late postinfarction nature of the imaging acquisition, these results nevertheless reinforce the concept that SPECT scintigraphic evidence of inducible ischemia as well as left ventricular function following MI provide complementary, additive, and incremental prognostic information in this clinical setting. In a more recent study, reflective of the contemporary practice of predischarge risk stratification, Kroll and colleagues [62] looked at 146 consecutive AMI patients who had undergone gated Tc-99m sestamibi SPECT imaging prior to discharge. Patients undergoing revascularization within 3 months of discharge were excluded. In this study, independent predictors of adverse cardiac events included a prior history of MI, diabetes, and an ejection fraction less than 40% by gated imaging (relative risk 3.13, 95% CI 1.64–5.95). Perfusion variables were *not* predictive of outcome. As the authors acknowledge in the paper, this was most likely because of the exclusion of high-risk patients (with ischemia on myocardial perfusion imaging) who underwent revascularization during the first 3 months following the index infarction. However, this study emphasizes the validity of assessment of left ventricular function by gated SPECT imaging as a marker of future risk. The strong log-linear relationship between gated SPECT measurements of ventricular function and adverse cardiac events was recently summarized by Shaw and Iskandrian [63] (Fig. 9.12). These findings are remarkably consistent with the previous findings of Zaret et al. [46] that an inverse relationship exists between left ventricular function and survival (Fig. 9.8).

End systolic volume as a predictor of cardiac events

Ejection fraction as a global measure of left ventricular function is affected not only by hypokinesis and akinesis of the infarct zone, but also by the degree of hyperkinesis in the non-infarct-related territories. Thus, a similar ejection fraction may be achieved despite differing infarct sizes, based on the presence, absence, or magnitude of hyperkinesis in the remote zones. This may be particularly relevant in studying the effects of thrombolytic therapy.

In this regard, White et al. [53] have reported that end-systolic volume (ESV) was a more powerful predictor

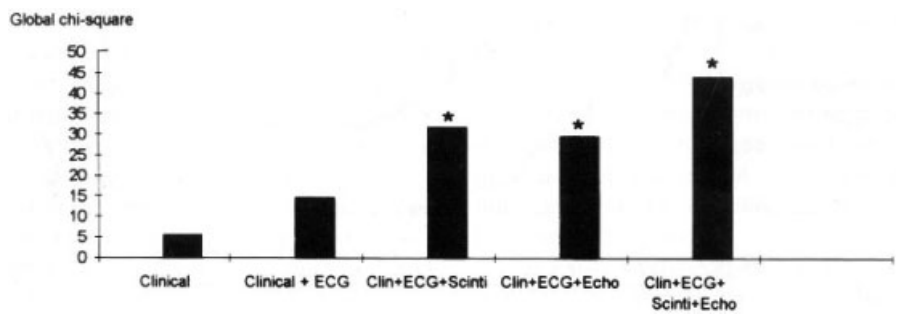

Figure 9.11 Prognostic evaluation of patients after MI: incremental predictive value of stress ECG, clinical data (Clin), SPECT sestamibi (Scinti), and echocardiography (Echo). Statistical significance (*) was reached in the following groupings: Clinical + ECG + Scinti data vs. clinical + ECG data ($p < 0.02$); clinical + ECG + Echo data vs. clinical + ECG data ($p < 0.02$); clinical + ECG + Scinti + Echo data vs. clinical + ECG + Scinti data ($p < 0.02$); clinical + ECG + Scinti + Echo data vs. clinical + ECG + Echo data ($p < 0.02$). There was a large increment in predictive value when *both* scintigraphic evidence of ischemia and left ventricular function data were considered together. (Reprinted with permission from [61].)

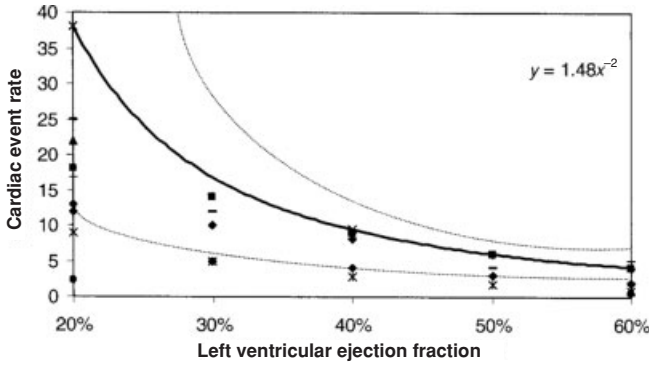

Figure 9.12 Inverse relationship between cardiac event rate and left ventricular function as assessed by gated SPECT imaging. This log-linear relationship can be summarized by the regression equation $y = 1.48x^{-2}$, where y is the cardiac event rate and x is the ejection fraction. Dotted lines mark 95% confidence intervals of predicted event rate. (Reprinted with permission from [63].)

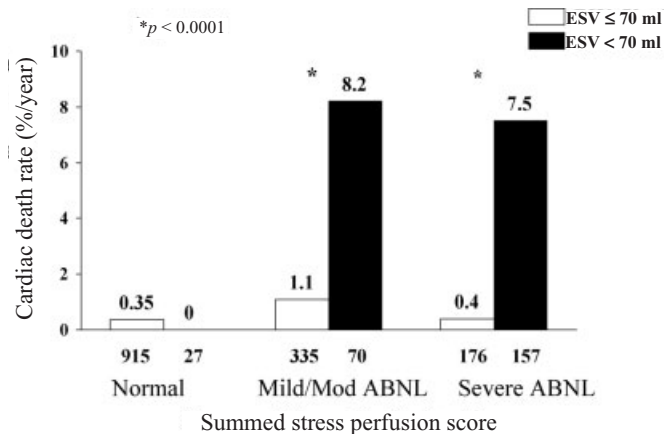

Figure 9.13 Incremental prognostic value of poststress ESV over perfusion abnormalities. See text for details. Abbreviation: ABNL, abnormal. (Reprinted with permission from [64].)

of outcome in 605 patients following MI followed for 78 months. ESV was the most powerful univariate predictor of survival, more powerful than end-diastolic volume or ejection fraction. In a multivariate analysis, once ESV was accounted for in the model, there was no additional significant predictive information gained by adding the ejection fraction data or the end-diastolic volume information. Among patients with similar degrees of left ventricular dysfunction, ESV above or below the mean within those groups significantly stratified patients into lower or higher risk for survival. More recently, Sharir and colleagues [64] studied 1690 consecutive patients undergoing gated SPECT imaging, of which 480 (25%) had a prior history of an MI. The Cox regression model showed that perfusion variables and ESV by gated SPECT imaging were independent predictors of cardiac death on follow-up. However, ESV had incremental prognostic value over the perfusion information. Patients with an ESV less than or equal to 70 ml had a very low mortality rate (0.4%/year), even in those with severe perfusion abnormalities. In contrast, those with an ESV greater than 70 ml had an approximately 8% annual mortality rate regardless of whether there were mild or severe perfusion abnormalities (Fig. 9.13). Consistent with the earlier study reported by White et al. [53], ESV was a more robust predictor of future outcomes than ejection fraction in this study. Patients with an ejection fraction less than 45% but a normal ESV (≤70 ml) had an annual death rate of only 1.7%. In contrast, those with an ejection fraction of less than 45% but dilated hearts (ESV ≥70 ml) had a mortality rate of 7.9% (Fig. 9.14). These important data suggest that more precision in outcome prediction may be obtained by incorporating information on left ventricular ESV after MI, compared to ejection fraction data.

Until recently, these compelling data on the importance of ESV analysis were difficult to apply to large general populations of postinfarction patients as the measurements (by ventricular angiography or echocardiography) were tedious and not highly reproducible. Quantitative derivation of end-systolic and end-diastolic volumes by gated SPECT imaging is reproducible [65] and has been validated against other modalities [66,67]. The studies of White [53] and Sharir [64] suggest yet another important prognostic factor that may be obtained simultaneously with the evaluation of stress and resting myocardial perfusion by gated SPECT imaging in the aftermath of AMI. The totality of information that may be obtained from gated SPECT imaging will allow the creation of powerful

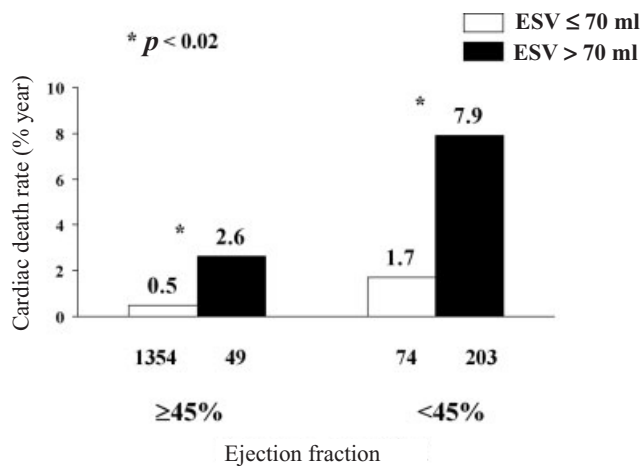

Figure 9.14 Incremental predictive value of poststress ESV over ejection fraction (EF) in patients with known or suspected coronary artery disease. An ESV of 70 ml or more predicts a low cardiac death rate regardless of EF. An ESV of less than 70 ml predicts a higher cardiac death rate, even if the EF is preserved. (Reprinted with permission from [64].)

predictive models based on information derived from large populations in this clinical setting. This prospect suggests that more refined risk categorization may be possible with the use of gated SPECT imaging, contributing significantly toward improved clinical decision making.

Assessment of infarct zone size, salvage, and viability using SPECT myocardial perfusion agents

Thallium-201

The initial distribution of thallium-201 following injection either at stress or at rest reflects myocardial blood flow. As thallium-201 is not bound intracellularly, following initial uptake, the "redistribution" phase occurs in which thallium-201 is eliminated from normally perfused zones faster than from ischemic zones, or in some cases of severe perfusion abnormality, thallium-201 accumulates into a severely ischemic zone over time [68]. Hence, thallium-201 distribution in an image taken late after initial injection will reflect regional viability, even in zones that were initially severely hypoperfused. As long as there is viable tissue with intact cell membranes capable of taking up thallium-201, the presence of thallium-201 in a myocardial region will reflect viability. Although thallium-201 uptake across the cell membrane is an energy-requiring process, it has been shown that even cells in experimental preparations of myocardial stunning are capable of maintaining normal thallium-201 uptake [69].

Because of the complex kinetics of thallium-201, the timing of injection during the occlusion/reperfusion process is an important determinant of thallium distribution in serial images, and thus impacts importantly on the assessment of viability using this agent. Several groups of investigators have demonstrated that when thallium is injected at rest in the clinical setting of an acute coronary occlusion and imaging is performed prior to thrombolytic therapy, the initial defect size represents area at risk, and the redistribution image taken several hours following thrombolytic therapy represents myocardial viability; thus, the change in defect size represents myocardial salvage [70–72]. That the redistribution image reflects regional viability in the infarct zone is suggested by clinical studies demonstrating an improvement in late ejection fraction in those patients with a significant decrease in defect size [70], as well as late improvement in thallium-201 uptake in the infarct zone on stress studies weeks after the infarct [71].

While imaging in this sequence will provide relevant data regarding coronary artery reperfusion and inference of infarct artery patency as well as myocardial salvage, there are important practical limitations to this approach. Because thallium-201 will begin to redistribute soon after initial uptake, as well as the likelihood that reperfusion will influence this process, the initial "risk area" images must be obtained *prior* to administration of thrombolytic therapy. This, of course, will delay the timing of such therapy, which would be disadvantageous to ultimate salvage.

Salvage of viable myocardium following thrombolytic therapy may also be evaluated by resting thallium-201 injection at a later time, with comparison to the pretreatment image. Using this approach, several studies have demonstrated that a change in defect size from the rest images obtained prior to thrombolysis compared to the rest images obtained 24 hours or more postthrombolysis reflects successful reperfusion and myocardial salvage [71,73,74]. That the change in defect size truly represented myocardial salvage was suggested by the improvement in regional ejection fraction in patients with the greatest reduction in defect size [73]. In both experimental models and in human studies, the ability of SPECT estimation of infarct size using rest injection of thallium-201 to accurately reflect true infarct extent has been confirmed [75,76].

Technetium-99m sestamibi

The mechanism of sestamibi uptake across myocellular membranes and subsequent kinetics following initial uptake are distinct from thallium-201. This lipophilic compound diffuses across cell membranes driven by electrochemical gradients and is retained by mitochondria [77]. There is only modest clearance out of the myocardium following initial uptake and minimal clinically relevant redistribution over time following initial injection [78]. Thus, images acquired even hours after initial injection represent a "snapshot" of blood flow conditions at the time of injection.

The uptake kinetics of both Tc-99m sestamibi and thallium-201 may be importantly affected by metabolic and cell membrane conditions, and this may have significant implications for imaging soon after MI, particularly relevant to the peri-infarct zone. In an experimental preparation involving cultured myocytes, Pinwica-Worms et al. [79] have demonstrated that with reversible cell membrane injury (as may be seen in tissue surrounding the central infarct zone), membrane hyperpolarization may lead to enhanced relative sestamibi extraction, while diminished membrane ATP stores may result in lower thallium-201 extraction. While this concept has not been directly tested in human studies, the concept that sestamibi may be somewhat preferentially accumulated in the peri-infarct zone of reversible ischemic dysfunction is suggested by human studies demonstrating smaller rest defect sizes during sestamibi imaging compared to thallium-201 redistribution images in patients with coronary disease and prior MI [80].

Like most diffusible tracers, sestamibi extraction falls off at very high flow rates; that is, uptake will underestimate

flow at high ranges of flow. These ranges of flow are not approached during routine clinical stress testing; however, there are important implications to this phenomenon regarding imaging in the early postreperfusion state. Sinusas et al. [81] have demonstrated that sestamibi activity, when injected during reperfusion soon after coronary occlusion in an animal model, is highly correlated with regional viability, as assessed by histochemical staining and autoradiography; that is, even during the hyperemic postreperfusion flow phase, sestamibi activity more closely tracks regional and cellular viability rather than flow.

As noted, the relative lack of redistribution of sestamibi following initial uptake allows imaging to be performed hours after injection, with the resulting imaging representing blood flow at the time of injection. Thus, serial imaging following separate rest injections before and after thrombolytic therapy can provide important information regarding the magnitude of the risk area, the extent of myocardial salvage, and final infarct size. When sestamibi is injected prior to thrombolytic therapy, the resulting defect, even imaged hours later after successful thrombolysis and restoration of flow, represents the risk area of the occluded artery [82–84]. Even if successful thrombolysis has been achieved, imaging may be performed hours later, and based on the relative lack of redistribution, the imaging pattern will remain stable despite restoration of flow. Numerous investigators [82–84] have confirmed the accuracy of such imaging for delineating the area at risk during coronary occlusion. A second injection of sestamibi at rest with subsequent imaging can be done at a later time, and the change in defect size will represent the magnitude of salvaged myocardium. The feasibility of this approach for detecting the results of thrombolytic therapy, not only for patency status of the vessel but for true myocardial salvage and myocardial viability in the infarct zone, has been shown for both planar and SPECT techniques [84,85]. That the change in defect size during serial imaging represents true myocardial salvage and viability is supported by the correlation of the change in defect size to predischarge and late follow-up ejection fraction [86].

Thus, serial sestamibi imaging in the course of thrombolytic therapy may provide clinically relevant information regarding myocardial viability in the infarct zone. Concepts derived in basic preparations and animal models suggest that the altered kinetics of sestamibi uptake and the "roll off" of extraction at high flow rates may actually be advantageous in assessing myocardial viability within and surrounding the infarct zone. Rest sestamibi imaging in the later postinfarct period will provide information regarding the presence, size, and location of MI. While it has been suggested that visual analysis of rest sestamibi images may underestimate viability when compared to wall motion analysis [87], it appears that quantitative analysis

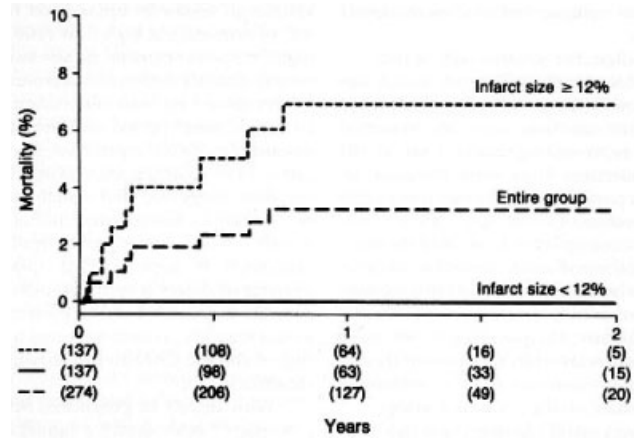

Figure 9.15 Predictive value of infarct size as determined by quantitative SPECT Tc-99m sestamibi imaging. Two hundred seventy-four patients with AMI underwent imaging on arrival *prior* to reperfusion therapy (to measure myocardium at risk) and at discharge (to measure final infarct size and myocardial salvage). Mortality curves are shown for the entire group (middle) and those with final infarct size greater than or equal to 12% (top) and less than 12% (bottom). The magnitude of infarct size was significantly associated with subsequent mortality. (Reprinted with permission from [89].)

of defect severity is important for accurate assessment of the presence of regional viability, as demonstrated in the setting of chronic CAD and hibernating myocardium [88].

With regard to prognosis, Miller and coworkers [89] have shown a significant association between infarct size assessed by predischarge SPECT sestamibi imaging using quantitative techniques and all-cause as well as cardiac mortality over long-term follow-up (Fig. 9.15). The area of myocardium at risk (by sestamibi injection just prior to thrombolytic therapy or acute angioplasty) was also associated with subsequent cardiac mortality. However, amount of myocardium salvaged (as assessed by the change in defect size on serial images) was not associated with overall or cardiac mortality [89].

Infarct size as assessed by postinfarct resting sestamibi imaging and quantitative analysis has been validated against numerous other relevant measures of infarct size [90] (Table 9.4). These powerful data, along with the demonstrated relation between infarct size measured by this technique and late outcome [89], have made this an important tool for studying adjuncts to thrombolytic therapy and primary angioplasty in AMI. Many such studies now use final infarct size by sestamibi SPECT imaging as a surrogate endpoint in early studies.

Scintigraphic techniques for assessing infarct size generally use cutpoints or thresholds established in phantom [91], animal [82,83], or human models [88] to differentiate predominantly viable from nonviable myocardium in order to determine the extent of an infarct zone. However, histologic studies of myocardial tissue following

Table 9.4 Validation of tc-99m sestamibi tomographic infarct size.

Infarct size measure	*r*	*P*
Discharge EF	−0.8	<0.0001
Six-week ejection fraction	−0.81	<0.0001
One-year ejection fraction	−0.78	<0.0001
Discharged regional wall motion	−0.75	<0.0001
Six-week regional wall motion	−0.81	<0.0001
One-year end systolic volume	0.80	<0.0001
Peak creatinine kinase levels	0.78	0.002
Tl-201 perfusion defect	0.73	0.0002
Human disease	0.91	0.0002

Source: Adapted from [90].

infarction would suggest that within an identifiable infarct zone, there exists a continuum of tissue viability. In a preliminary report, Vannan and colleagues [92] have demonstrated that *within* an infarct zone defined by standard thresholds using SPECT sestamibi imaging in patients several days after first anterior infarction, the presence of moderately preserved viability (by quantitative analysis of sestamibi activity) was associated with an attenuation of subsequent remodeling over 1 year (increasing left ventricular volumes and decreasing ejection fraction) compared to those patients with severe reduction of infarct zone viability. Thus, viability within an infarct zone should not necessarily be conceptualized as an all-or-none phenomenon; rather, a continuum exists in which physiologically relevant effects of preserved myocardial tissue may be demonstrated (Fig. 9.16).

Hence, SPECT imaging with thallium-201 or sestamibi at rest in the early postinfarct period can provide important information regarding final infarct size and infarct zone viability. The potential incremental value of such data may now be assessed carefully in the context of information regarding the extent of inducible ischemia as well as left ventricular function with the more widespread use of gated SPECT imaging in the postinfarct setting. Table 9.5 summarizes the American College of Cardiology/American Heart Association/American Society of Nuclear Cardiology (ACC/AHA/ASNC) recommendations regarding radionuclide imaging in the setting of AMI [94].

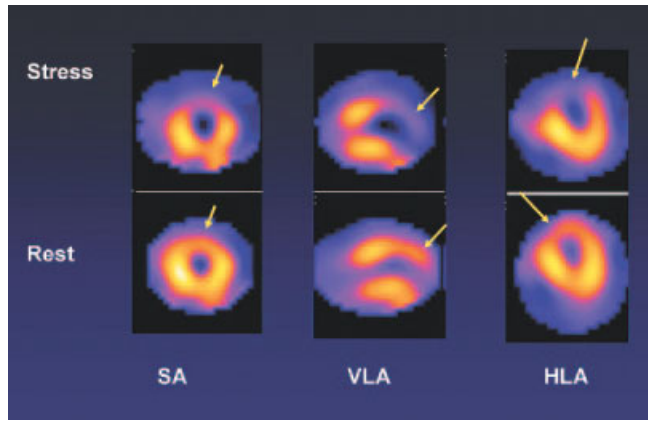

Figure 9.16 This 50-year-old woman presented 36 hours after the onset of symptoms of chest pain. ECG showed a completed anterior MI. Echocardiogram showed anterior and apical akinesis with severely reduced systolic function. Perfusion imaging 1 week later with Tl-201 reinjection shows a limited apical infarct with anterior ischemia (arrows) and significant retained viability. The patient underwent surgical revascularization with substantial recovery of left ventricular function. Abbreviations: HLA, horizontal long axis; SA, short axis; VLA, vertical long axis.

Assessment of myocardial perfusion and left ventricular function in the aftermath of unstable angina/non-ST elevation MI

The concepts derived in large populations following MI regarding the prognostic importance of the presence and extent of inducible ischemia as well as the magnitude of left ventricular dysfunction appear to be generalizable to the population of patients undergoing risk stratification following unstable angina (UA)/non-ST elevation myocardial infarction (NSTEMI). This suggests that gated SPECT imaging for simultaneous assessment of these critically important prognostic variables has a potentially very large role in this clinical setting as well.

Table 9.5 ACC/AHA/ASNC recommendations for radionuclide testing in acute STEMI.

Patient subgroups	Indication	Test	Class	Level of evidence
All	Rest left ventricular function	Rest ECG-gated SPECT	I	B
Thrombolytic therapy without catheterization	Detection of inducible ischemia and myocardium at risk	Stress MPI with ECG-gated SPECT whenever possible	I	B
Acute STEMI	Assessment of infarct size and residual viable myocardium	MPI at rest or with stress using gated SPECT	I	B

Abbreviations: MPI, myocardial perfusion imaging; SPECT, single-photon emission computed tomography; STEMI, ST-elevation myocardial infarction.
Source: From [93].

The National Center for Health Statistics reported greater than 500,000 hospital admissions for unstable angina in 1991. UA/NSTEMI as a clinical syndrome is generally conceptualized as falling midway on the risk spectrum between a stable anginal syndrome and AMI. Clinical practice guidelines for assessment and management of patients with unstable angina have been published by the Agency for Health Policy and Research (AHPR) [95]. These guidelines as well as the recently revised ACC/AHA recommendations [96] outline an approach to risk-stratify patients based on clinical and other parameters. Patients with prolonged ongoing rest ischemia, clinical or echocardiographic evidence of left ventricular dysfunction, continuing dynamic ST changes, suspected ischemic mitral regurgitation, hypotension with ischemia, ventricular arrhythmias, and elevated markers of cardiac necrosis fall into a high clinical risk category, and there is general agreement that cardiac catheterization is indicated. However, many more patients with unstable angina who have been initially stabilized with medical therapy (consisting of aspirin, intravenous or low molecular weight heparin, nitrates, HMG-CoA reductase inhibitors, and β-blockers) will have only a low or intermediate likelihood of having a recurrent event. In these patients, noninvasive risk stratification plays an important role in determining which of these low to intermediate risk patients will go on to have further adverse events.

Angiographic and pathophysiologic considerations

Among patients in whom the UA/NSTEMI syndrome is their first presentation of coronary disease, the majority has a limited extent of disease with approximately 50% of such patients demonstrating single-vessel disease at catheterization. Moreover, among patients with unstable angina in the TIMI IIIA trial [97] who underwent catheterization, 14% had no critical coronary stenosis. Such patients generally have an excellent prognosis, and it would be beneficial in terms of management if such patients could be identified by noninvasive imaging prior to catheterization in order to obviate the need for angiographic assessment and assigned to a conservative management strategy on the basis of the noninvasive data alone.

The role of active and dynamic platelet aggregation in the acute coronary syndrome is well established. In an important subset of patients, platelet thrombi will occur on coronary stenoses of initially moderate severity, which will reduce the coronary blood flow resulting in resting myocardial ischemia. With aggressive antiplatelet and antithrombic treatment, there may be resolution of the initial pathophysiologic event, and such patients are left with only moderate luminal obstruction and thus there is no need for percutaneous or surgical intervention. The advent of aggressive adjuvant antiplatelet strategies will likely increase this population of patients. Again, such patients may be best managed conservatively, and risk stratification techniques which could identify the absence of multiple critical coronary stenoses in order to diminish the need for catheterization have an important role in this population.

While there is general agreement that patients with high-risk clinical characteristics in the clinical setting of unstable angina should undergo direct and prompt catheterization, there is less clear consensus regarding patients with intermediate or low clinical risk as defined by the AHCPR guidelines [95]. Both invasive and noninvasive risk stratification strategies are defined and neither is strongly encouraged to the exclusion of the other. Factors to be taken into account in this decision include access of the patient population to interventional facilities, the skill and experience of the local interventional and surgical team, and patient preferences. In such patient groups however, noninvasive testing, particularly with myocardial perfusion imaging, has been shown to identify a very low risk outcome group which, according to principles established in the setting of outpatients with chest pain and the post-MI state, can be comfortably managed conservatively without catheterization. Indeed, the recently updated AHA/ACC/ASNC Guidelines on Cardiac Radionuclide Imaging [94] considers the use of stress myocardial perfusion imaging for detecting residual ischemia and the use of radionuclide angiography to assess left ventricular function in this syndrome as class I indications; that is, indications that are generally considered clearly appropriate.

Stress myocardial perfusion imaging in patients with UA/NSTEMI

Patients admitted to the hospital with a clinical diagnosis of acute coronary syndromes represent a heterogeneous population. While in many patients the diagnosis of underlying ischemic heart disease will be clear-cut, that is, there will have been significant and transient electrocardiographic changes of ischemia to establish the diagnosis, in other patients the diagnosis as well as prognosis will be in question in the absence of obvious ECG changes. In these latter patients, the use of stress myocardial perfusion imaging will be diagnostic as well as prognostic, as established in other large populations with chest pain syndromes [98]. Furthermore, in patients with established coronary disease (such as those who have previously undergone bypass surgery or angioplasty), perfusion imaging data will provide risk stratification information regarding the extent of ischemia and may assist in identifying the "culprit vessel" for targeted revascularization.

In the majority of patients with unstable angina who present with diagnostic ischemic ECG changes but stabilize during initial in-hospital management, the use of stress myocardial perfusion imaging can provide important data on the extent of ischemia, which relates directly to subsequent cardiac risk, with implications for the need of cardiac catheterization. Compared to the information available in the postinfarction setting, there are relatively fewer studies carefully examining the use of stress myocardial perfusion imaging in the aftermath of unstable angina. Brown and colleagues [99] reported on 52 patients who presented with unstable angina but then stabilized on medical therapy. All patients underwent stress myocardial perfusion imaging and were followed for natural history events for over 3 years. By multivariate logistic regression analysis, the presence of thallium redistribution as a sign of inducible ischemia was the only important predictor of cardiac events. Among patients with evidence of inducible ischemia, 26% suffered a cardiac event, compared to only 1 of 29 patients (3%) without evidence of inducible ischemia.

These important data have been confirmed by several other investigations (Fig. 9.17), and the concept that the presence and extent of inducible ischemia by myocardial perfusion imaging in this clinical setting is related to natural history outcomes appears to be independent of both the isotope used and the particular stress modality. Stratmann and colleagues [104] reported that exercise testing and SPECT Tc-99m sestamibi imaging performed prior to discharge in medically treated unstable angina patients was strongly predictive of future cardiac events. Among 126 such patients followed for over 1 year, the presence of a reversible sestamibi perfusion defect was associated with a relative risk of 3.8 for any cardiac event and 9.2 for MI or cardiac death on multivariate analysis. The same group of investigators later reported similar data using pharmacologic stress testing with dipyridamole [105].

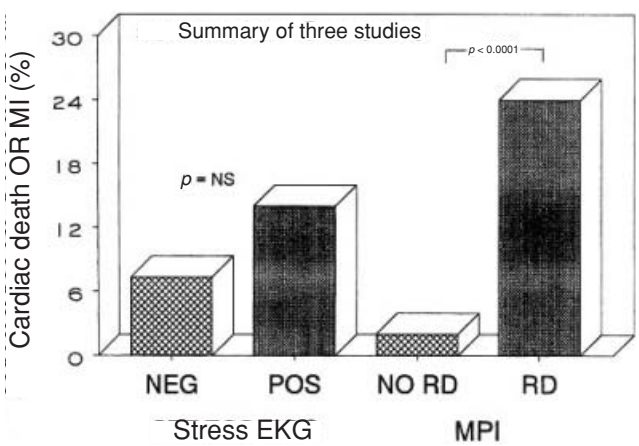

Figure 9.17 Predictive value of myocardial perfusion imaging (MPI) and stress electrocardiography (EKG) in patients studied after stabilization of unstable angina. This figure summarizes the results of three studies [100–102] in which cardiac death or nonfatal MI were endpoints. The presence of reversible perfusion defects (RD) was strongly predictive of cardiac events in this setting. Abbreviations: POS, positive; NEG, negative; NS, not significant. (Reprinted with permission from [103].)

The results of studies examining the use of stress myocardial perfusion imaging in patients with unstable angina are summarized in Table 9.6 [99–101,104–108]. There appears to be a consistent relation between the presence of inducible ischemia on noninvasive perfusion imaging and outcome events. The lack of inducible ischemia identifies a low-risk group, suggesting that such patients can be managed conservatively (Fig. 9.18).

Data are less consistent on the use of exercise electrocardiography in this setting. While the AHCPR guidelines [95] suggest that exercise ECG can be used for risk stratification in the presence of a normal resting electrocardiogram, many such patients do not have normal resting ECGs. Indeed, in several of the studies listed in Table 9.6, evidence of ischemia by ST depression on exercise testing was not as consistently predictive of outcome events as myocardial perfusion imaging information.

Clinical trials incorporating results of stress testing following UA/NSTEMI

The use of a noninvasive strategy in "stabilized" patients in the aftermath of an unstable angina presentation is supported by the results of the TIMI IIIB trial [109], in which patients were randomized to either an invasive or a conservative, ischemia-guided strategy. There was no difference in the long-term outcomes with either strategy, suggesting that a conservative approach with noninvasive risk stratification with catheterization reserved for those with evidence of higher risk characteristics on stress testing is appropriate and will diminish the need for catheterization in a subpopulation of these patients, with the expectation of a favorable outcome. In a design similar to that of the TIMI II trial, investigators in the VANQWISH (Veterans Affairs Non-Q Wave Infarction Strategies in Hospital) trial [110] randomized 953 patients with non-Q wave MI to direct catheterization during the hospital period, or to a conservative arm in which catheterization was performed only if there was recurrent rest ischemia or a certain extent of ischemia demonstrable on myocardial perfusion imaging. In contrast to the conventional wisdom in which most patients with non-Q wave MI undergo catheterization, the group randomized to the more conservative arm with stress scintigraphic imaging had outcomes similar to the invasive arm patients in terms of the primary endpoint of death or recurrent MI. Indeed, there was evidence in the early follow-up after randomization that the conservative arm population demonstrated more favorable outcomes. These important data suggest that even in settings

Table 9.6 Predictive value of myocardial perfusion imaging in unstable angina.

Study	Year	*N*	Follow-up	Patient group	Isotope	Endpoint	Result
Hillert et al. [106]	1986	19	12 wk	UA	Tl 201	MI or Class III/IV angina at 12 wk	15/19 patients with redistribution had events. 2/18 of those without redistribution had events
Freeman et al. [107]	1988	67	In hospital	UA	Tl 201	Extent of CAD	Tl-201 defect size best predictor of extent of CAD
Madsen et al. [100]	1988	158	14 mo	Chest pain syndrome, suspected UA	Tl-201	Death or MI	21% incidence of events if redistribution, 3% if not
Marmur et al. [101]	1990	54	6 mo	UA	Tl 201	Death or MI	Extent of Tl-201 reversible defects predicted cardiac events
Brown et al. [99]	1991	52	39 mo	UA	Tl 201	Death or MI	Presence of redistribution highly predictive of cardiac events
Amanullah et al. [108]	1993	40	30 mo	UA	Tl 201	Death or MI	Number of Tl-201 segments with redistribution strongly predicted cardiac events
Stratmann et al. [104]	1995	126	12 mo	UA	Tc-99m MIBI (exercise)	Death or MI	Relative risk 3.8 for cardiac event with reversible perfusion defect
Stratmann et al. [105]	1995	128	16 mo	UA	Tc-99m MIBI (dipyridamole)	Death or MI	Relative risk 2.5 for cardiac event with reversible perfusion defect, 4.3 with an abnormal scan

Abbreviations: CAD, coronary artery disease; MI, myocardial infarction; MIBI, sestamibi; Tc, technetium; Tl, thallium.

of MI in which many clinicians believe there is remaining jeopardized myocardium which should be revascularized, scintigraphic data were able to identify populations who would, and who would not, benefit from invasive therapy.

The Frisc-II study [111] suggested a significant benefit of an early invasive approach. However, this was possibly driven by an inherent disadvantage conferred upon patients randomized to the conservative arm as a result of a very stringent stress test criterion for crossover to the invasive strategy [112]. More recently, the TACTICS-TIMI 18 trial [113] randomized 2220 patients with UA/NSTEMI with high-risk characteristics (ST segment changes, elevated cardiac markers, documented CAD or all three) to an early invasive or a more selectively invasive strategy where coronary angiography would be performed in the event of failure of medical therapy or an abnormal perfusion scan. The early invasive arm had more favorable results but the overall benefit was modest and was driven mainly by benefits seen in the group with elevated troponin levels [114]. The recently reported RITA-3 study [115] sheds some light on the efficacy of modern medical therapy in treating patients with acute coronary syndromes. Conducted in the more conservative medical environment of the United Kingdom, 1810 patients with an acute coronary syndrome were randomized to a conservative versus invasive strategy. In the conservative arm, patients were treated with maximum medical therapy with coronary angiography reserved for those with recurrent symptoms despite optimal therapy. Patients were then discharged with stress testing performed as an outpatient in an unspecified number. In this relatively lower risk cohort (fewer patients had elevated cardiac markers or diabetes compared to TACTICS) there was a reduction

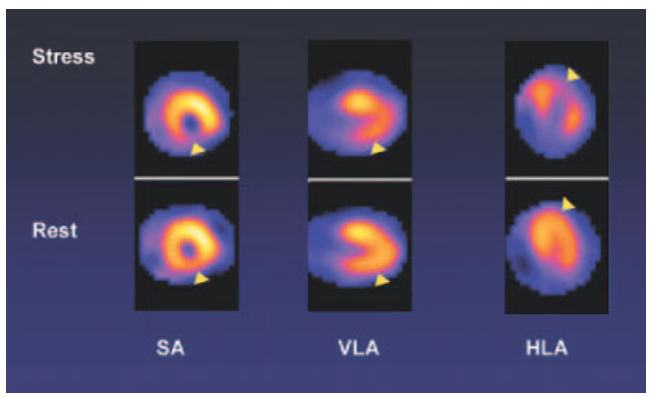

Figure 9.18 A 66-year-old man presented with unstable angina and negative serum cardiac markers. Dipyridamole myocardial perfusion imaging with tetrofosmin reveals a large area of moderate to severe inferior and inferoapical ischemia (arrows). Angiography revealed critical stenosis in the proximal right coronary artery that was treated percutaneously. Abbreviations: ; HLA, horizontal long axis; SA, short axis; VLA, vertical long axis.

in the relative risk for the combined endpoint of death, MI, and refractory angina at 4 months (14.5% vs. 9.6%, relative risk 0.66, $p = 0.001$) in the invasive arm. However, this was driven primarily by a reduction in refractory angina with no difference in reinfarction or mortality. Translating this into clinical practice in the United States, some of the 14.5% of patients destined to suffer an endpoint at 4 months would have been detected early by myocardial perfusion imaging prior to discharge and, on the basis of high-risk perfusion characteristics, would have undergone catheterization with or without revascularization. Thus, the conservatively treated patients in this trial, like in Frisc II, were at a disadvantage as predischarge risk assessment was not available to determine the high-risk subset in which medical therapy was likely to be inadequate. Importantly, the observation that over 85% of the patients in the conservative arm did not suffer an endpoint at 4 months lends support to the fact that an ischemia-guided approach rather than a "cath-for-all" strategy is more appropriate in patients without high-risk predictors. This is further confirmed by a recent retrospective analysis of the TIMI IIIB trial [116], which showed that using a rather simple score incorporating age, elevation of cardiac markers, a history of worsening angina, and ST depression on the ECG, only patients falling into the high and very high risk groups actually benefited from early cardiac catheterization.

Assessment of left ventricular function in patients with unstable angina

In patients with MI, there is, by definition, some degree of myocardial damage, resulting in a wide range of ejection fraction and degrees of left ventricular dysfunction in postinfarct populations. This has important prognostic implications. In a population of patients with UA/NSTEMI, particularly those in whom unstable angina is the initial clinical presentation of coronary disease, left ventricular function is generally preserved and would not be expected to be as powerful as an incremental discriminator of subsequent risk as the extent of residual inducible ischemia. However, a significant proportion of patients presenting with unstable angina have had prior MI and prior intervention. Among such patients, the degree of left ventricular dysfunction will play an important role in management decisions, as there are important prognostic implications to the development of unstable angina in the setting of known left ventricular dysfunction.

Besides the importance of underlying resting left ventricular function as a risk stratifier in the general population of patients with unstable angina, there are particular clinical and pathophysiologic scenarios involving transient and prolonged left ventricular dysfunction which are of considerable interest and clinical importance. In a subpopulation of patients with unstable angina, transient and severe ischemia may result in prolonged contractile dysfunction, or myocardial stunning. Gated SPECT analysis of simultaneous perfusion and function in the setting would be particularly advantageous. Echocardiography or radionuclide angiography would clearly demonstrate the presence of regional dysfunction, but gated SPECT imaging, besides demonstrating regional dysfunction, would also simultaneously evaluate the magnitude of myocardial viability within the dysfunctional territory. Thus, in one test simultaneously evaluating these parameters, important information with clear clinical decision-making implications is obtained.

Among 58 patients with unstable angina studied by Warner and colleagues [117], 58% were found to have segmental left ventricular dysfunction in the territories supplied by the culprit vessel on left ventricular contrast angiography. Such segmental dysfunction was more frequently seen if the culprit lesion was in the left anterior descending artery. Others have reported that patients with persistent wall motion abnormalities at the time of hospital discharge were more likely to have recurrent unstable angina at 12 weeks follow-up [118].

Serial investigations of left ventricular function in the setting of unstable angina have demonstrated that wall motion abnormalities seen early in the hospital course may improve with medical or revascularization therapy [119]. Whether these findings, suggestive of myocardial "stunning," translate into improved long-term outcome has not been clearly studied or established. In one study by Narahara et al. [120], of a group of 30 patients with unstable angina whose left ventricular function was studied early in the hospital course and again just prior to discharge, those with a decline in left ventricular ejection fraction across the serial studies were more likely to have severe anginal symptoms during short-term follow-up.

Similar to the large randomized trials of medical versus surgical therapy in patients with coronary disease, in which the greatest benefit of surgical therapy occurred among patients with left ventricular dysfunction, surgical revascularization therapy in the setting of unstable angina appears to be most beneficial in the subgroup of patients with diminished left ventricular function. In a VA cooperative study trial [121] in 468 patients with unstable angina, there was no overall difference in long-term survival in patients randomized to medical therapy compared to those randomized to surgical therapy. However, when the randomized patients were subgrouped according to ejection fraction, there appeared to be a clear advantage of surgical therapy among those whose baseline resting left ventricular function was less than 50% (Fig. 9.19].

Thus, assessment of left ventricular function in patients with unstable angina, though not as well studied as in the clinical syndrome of AMI, appears to have similar prognostic implications, and identifies a group of patients most

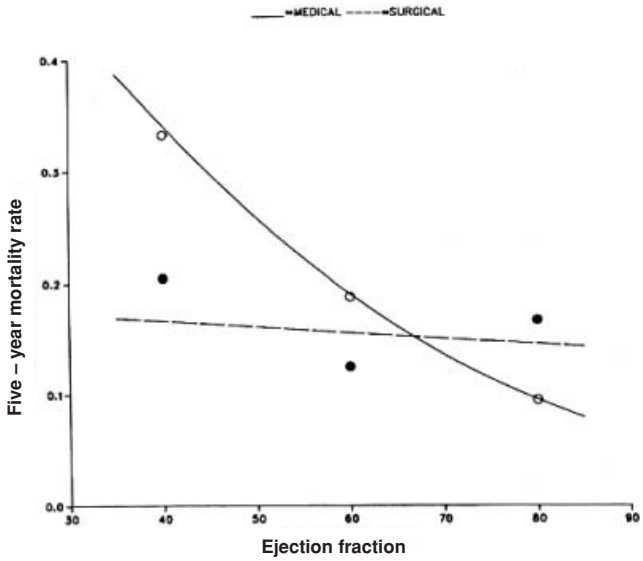

Figure 9.19 Impact of ejection fraction on 5-year mortality in patients with coronary artery disease presenting with unstable angina randomized to medical or surgical therapy. Curves were computed by logistic regression analysis with ejection fraction as a continuous variable. Mortality of medically treated patients was dependent on ejection fraction ($p = 0.004$) whereas mortality of surgically treated patients did not demonstrate such a relationship ($p = 0.76$). Patients in the lowest ejection fraction group benefited most from surgery in terms of mortality. (Reprinted with permission from [121].)

likely to benefit from surgical revascularization. Moreover, the promise of gated SPECT imaging for simultaneously evaluating perfusion and function, for better categorization of potentially reversible left ventricular dysfunction and myocardial stunning, suggests yet another role for noninvasive testing.

There are no reported data in a large population of patients with UA/NSTEMI in which information on *both* perfusion imaging evidence of inducible ischemia as well as data on left ventricular function are examined for incremental prognostic value. The separate bodies of literature on perfusion imaging as well as assessment of left ventricular function in this clinical setting would suggest, as in patients with AMI, that the simultaneous evaluation of these parameters with gated SPECT imaging would be of significant clinical value. The application of gated SPECT imaging in a large population of unstable angina patients would also allow the careful evaluation of potential incremental value in this syndrome. Table 9.7 summarizes the ACC/AHA/ASNC recommendations regarding radionuclide imaging in the setting of unstable angina [94].

Assessment of myocardial perfusion and left ventricular function in patients with chest pain in the ED

Each year in the United States, approximately 7 million patients present to EDs with symptoms suggestive of acute cardiac ischemia [104]. Two-thirds of such patients are ultimately found to have symptoms that are not cardiac in origin. Efficient and appropriate triage of these patients, as customarily based on the clinical presentation and ECG, is

Table 9.7 ACC/AHA/ASNC recommendations for radionuclide imaging in patients with unstable angina and NSTEMI.

Indication	Test	Class	Level of evidence
Identification of inducible ischemia in the distribution of the "culprit vessel" or in remote areas in patients at intermediate or low risk for major adverse cardiac events	Stress MPI with ECG gating whenever possible	I	B
Identification of the severity/extent of inducible ischemia in patients whose angina is stabilized on medical therapy or in whom the diagnosis is uncertain	Stress MPI with ECG gating whenever possible	I	A
Identification of the functional significance of coronary lesions after coronary angiography	Stress MPI	I	B
Measurement of baseline LV function	ECG gated SPECT	I	B
Identification of the severity/extent of disease in patients with ongoing suspected ischemic symptoms when ECG changes are not diagnostic	Rest MPI	IIa	B

Abbreviations: LV, left ventricular; MPI, myocardial perfusion imaging; NSTEMI, Non ST-elevation myocardial infarction; SPECT, single-photon emission computed tomography.
Source: From [93].

problematic, as the decision-making ED physicians generally operate at a high-sensitivity though low-specificity threshold for detecting acute cardiac ischemia, so as not to miss any significant cases of acute ischemic heart disease. By necessity, this approach results in many unnecessary admissions of patients without acute cardiac ischemia. Currently, over half of the patients admitted for acute cardiac ischemia prove to be "false-positive" admissions, i.e., they do not have acute cardiac ischemia [122,123], and yet about 7% of those patients with acute cardiac ischemia, including approximately 2–4% of those with AMI, are inadvertently sent home from the ED, i.e., "false-negative" discharges. Moreover, only about half of those with acute cardiac ischemia are ultimately found to rule-in for AMI. Unnecessary hospital and CCU admissions for suspected acute cardiac ischemia therefore totals in the range of 3 million per year, while approximately 60,000 patients with acute cardiac ischemia, including 20,000 with AMI, are mistakenly sent directly home from the ED. Thus, ED triage for potential acute cardiac ischemia and the associated decision-making process has important implications for individual patient morbidity and mortality, and also for overall health care costs, including those for malpractice litigation. Testing targeted to reduce both false-positive and false-negative triage decisions could potentially benefit both endpoints, and do so with substantial economic benefits. In the United States, acute cardiac ischemia is the leading cause of morbidity and mortality, and an enormous consumer of health care resources. These unnecessary CCU admissions represent a substantial waste: in this country the direct costs alone may be as high as $5 billion annually.

Although the high proportion of seemingly unnecessary admissions is not desired, it has been assumed that a more restrictive admission policy would increase the numbers of patients with AMI inappropriately sent home. Generally, about 2–4% of those who do have acute infarction are mistakenly sent home [124]. Indeed, beyond the cost and potential adverse effects of unnecessary *false-positive* CCU or hospital admissions, with the growing number of life-saving acute interventions for preventing treating arrhythmias and for preventing or reducing AMI size, there is also substantial interest in improving the historically stable *false-negative* AMI ED discharge rate.

Attempts to improve ED triage accuracy of patients with suspected acute cardiac ischemia have included the use of:

- identification of high-risk clinical indicators
- rapid determination of cardiac enzymes
- two-dimensional echocardiography
- thallium-201 scintigraphy
- Tc-99m sestamibi and tetrofosmin imaging.

In reviewing the value of each of these modalities, it is important to bear in mind the *endpoint* in any given study. While many studies focus on the endpoint of correct distinction of AMI from all other patients, the ED physician facing a triage decision (admit or not admit) is more interested in the separation of those patients with acute cardiac ischemia, that is, those with AMI *or* unstable angina, from all other patients with noncardiac chest pain. Thus, tests dependent on a degree of myocardial necrosis, such as rapid enzyme subfraction analysis, while useful to detect necrosis associated with infarction, may be less so for the ED physician, as patients with unstable angina and no necrosis may not be detected. The strength of perfusion imaging techniques in this setting is the potential identification of *both* AMI and unstable angina. As the proximate cause of any acute ischemic syndrome is an abnormality in myocardial blood flow, it is theoretically sound to examine such patients by a procedure that can identify abnormal or normal perfusion with a high degree of precision.

Observational studies of radionuclide myocardial perfusion imaging in ED patients with chest pain: diagnostic performance

Radionuclide imaging of myocardial blood flow was first studied as a means of detecting acute abnormalities in regional myocardial perfusion over 20 years ago. Thallium-201 has in the past been the most widely used agent to trace myocardial blood flow. In 1976, Wackers et al. [125] showed thallium-201 defects in 100% of patients with AMI who were studied within 6 hours of the onset of symptoms. The sensitivity was markedly diminished with increased time from the onset of symptoms after that point. In a later study involving patients with unstable angina, Wackers and coworkers [126] found planar thallium-201 scintigraphy to have a 76% sensitivity and 67% specificity for predicting MI or severe coronary disease. In the presence of an abnormal baseline ECG with transient changes, the sensitivity for a positive thallium-201 scan increased to 94% but with a specificity of only 46%. While thallium-201 scintigraphy has been widely used since that time as an indicator of myocardial perfusion in the stable patient with suspected CAD in conjunction with stress testing, its use in the ED setting is in practical terms quite limited, due to the time constraints imposed by its "redistribution" properties, requiring that imaging be completed in a relatively short time after injection. Moreover, this isotope is not readily available for acute imaging, and the count profile following resting injection is not ideally suited for gated acquisitions. These significant limitations are overcome by the use of non-redistributing Tc-99m-based compounds as the myocardial perfusion imaging agent in this setting.

More recently, Tc-99m sestamibi and Tc-99m tetrofosmin have been studied as alternative myocardial perfusion imaging agents in this clinical setting. These agents have several distinct advantages over thallium-201: their physical characteristics are better suited to gamma camera

imaging, they are less subject to tissue attenuation effects, and they may be generator produced on-site, making these agents readily available for acute imaging. In addition, there is minimal redistribution (that is, change in regional concentration) of these agents after their initial flow-related distribution in the myocardium, which allows imaging up to several hours after injection [109], with the resulting images reflecting myocardial regional blood flow at the time of injection.

The clinical basis for the use of Tc-99m agents in patients with suspected unstable angina was initially reported in a study by Bilodeau et al. [127] evaluating 45 patients already admitted to a hospital with suspected unstable angina. In this study, all patients underwent coronary angiography, revealing significant CAD in 26 patients. Tc-99m sestamibi was injected during a spontaneous episode of chest pain, and SPECT imaging demonstrated 96% sensitivity and 79% specificity for the detection of angiographic CAD, while the predictive value of a negative scan to exclude CAD was 94%. This study was performed in patients already admitted to the hospital with suspected unstable angina, and therefore does not apply to patients presenting to the ED with chest pain. However, this seminal study showed that the injection of sestamibi during an episode of chest pain was very sensitive for detecting significant coronary disease and had a strong negative predictive value for excluding significant coronary disease if the imaging was negative.

Subsequently, Christian and colleagues [128] using sestamibi imaging in ED patients found perfusion defects in 13 of 14 patients presenting with chest pain and nondiagnostic ECGs, who were ultimately found to have had an AMI. This study also demonstrated that AMI without ECG changes did not necessarily reflect a small MI, as quantitative analysis demonstrated that the sestamibi infarct size averaged 20% ± 15% (range 2–53%) of the left ventricle. Such studies demonstrated the feasibility of this technique in the ED setting, and suggested that this imaging modality may provide important incremental information beyond the clinical and electrocardiographic data to improve ED triage. Since then, several groups have conducted studies investigating the use of perfusion imaging in patients presenting with the clinical suspicion of acute cardiac ischemia in the ED (Table 9.8) [129–140].

Table 9.8 Prediction of cardiac events using resting SPECT perfusion imaging in patients with chest pain presenting to the ED.

Study	*N*	Follow-up	Abnormal scans %	Diagnostic performance		Endpoint(s)	Prognostic performance
				Sensitivity %	Specificity %		NPV %
Varetto et al. [126]	64	18 mo	47	100	92	CAD	100
				100	67	MI	100
Hilton et al. [130]*	102	In hospital	22	94	83	D/MI/Rev	99
Weissman et al. [131]	50	9–12 mo	40	ND	ND	D/MI/Rev/CHF	100
Tatum et al. [132]	442	1 yr	24	100	78	MI	100
				82	83	MI/Rev	98
Kontos et al. [133]†	532	In hospital	32	93	71	MI	99
				81	76	D/MI/Rev	95
Heller et al. [134]	357	30 d	43	90	60	D/MI/Rev	99
Kontos et al. [135]	620	6 wk	39	92	67	MI	99
				81	74	Rev	
Ducca et al. [136]	75	In hospital	36	100	73	MI	100
				73	89	CAD	81
Kosnik et al. [137]	69	1 yr	15	71	92	D/MI/Rev	97
Udelson et al. [138]	1215‡	30 d	–	–	–	MI	99.4
						D/MI/Rev	97
Dinckal et al. [139]	60	30 d	70§	97	77	MI/Rev	94
Kaul et al. [140]	163‖	In hospital	33	71	71	D/MI/Rev	91

Abbreviations: CAD, coronary artery disease on angiography; CHF, congestive heart failure; D, death; MI, myocardial infarct; ND, not deducible from study; NPV, negative predictive value; Rev, revascularization.

*At 90-d follow-up, no adverse cardiac events in patients with normal study [130].

†Some overlap with Tatum series.

‡Represents patients randomized to Tc-99m sestamibi imaging; 2475 patients in study (see text for details).

§High percentage of patients with typical chest pain.

‖203 patients in study; 163 had SPECT imaging; predictive numbers for abnormal composite assessment of function and perfusion.

Varetto et al. [129] performed resting Tc-99m sestamibi SPECT imaging in 64 patients presenting to the ED with suspected acute cardiac ischemia and nondiagnostic ECGs. Thirty-four patients had normal scans, none of whom were subsequently found to have significant CAD by coronary angiography or stress testing. All of the patients with normal scans remained free of morbid cardiac events up to 18 months after discharge. Of the 30 patients with perfusion defects, 13 were found to have had an AMI (by enzyme or electrocardiographic criteria) and 14 were found to have significant CAD by angiography, while the remaining 3 patients were considered to have false-positive findings. Overall, sensitivity and specificity for the detection of AMI or significant CAD was 100% and 92% respectively, while the predictive value of a negative scan to exclude CAD or a subsequent cardiac event was 100%. While these data strongly support the feasibility of performing acute sestamibi imaging in this population, this study was not designed to test this imaging modality in a prospective manner. The imaging results were blinded from the admitting ED physicians; thus the potential impact of sestamibi imaging in this setting on reducing unnecessary admissions (53% of the patients admitted to the CCU in this study) could not be tested. Nevertheless, this study documented for the first time that resting SPECT perfusion imaging in this setting, when normal, identified patients *without* an acute ischemic syndrome who remained free of morbid or mortal events both during the index admission as well as during follow-up.

Several other groups have reported similarly high sensitivities for detecting AMI (Table 9.8). It should be noted that the sensitivity of a resting perfusion scan is dependent on the diagnostic standard used. When more sensitive markers of myocardial necrosis like troponins are used in place of creatine kinase (or its MB fraction), the sensitivity of myocardial perfusion imaging declines to 75% according to one report [141], consistent with the notion that very small infarcts may not render a perfusion defect. In these studies, the reported specificity for detecting MI is relatively poor – on average, about 75%. This is consistent with the fact that perfusion defects can be seen in a range of ischemic syndromes including MI, unstable angina, and chronically hypoperfused myocardium. However, the utility of a screening test lies not in its specificity but in its ability to detect all subjects with the disease state in question (in other words, high sensitivity). Patients presenting to the ED with chest pain and subsequently found to have perfusion abnormalities would most likely require observation in the hospital regardless of whether the perfusion defect is due to an acute ischemic event or a prior myocardial scar. Therefore, a high specificity is of less utility to the ED physician when triage decisions (that is, admit or not) are being made.

Observational studies of radionuclide myocardial perfusion imaging in ED patients with chest pain: risk stratification and prognostic performance

The studies noted above evaluated the use of perfusion imaging against a diagnostic standard, i.e., was an AMI or unstable angina (or revascularization as its surrogate) present or not. Analogous to the general myocardial perfusion imaging literature, there is also substantial information on the *prognostic value* of perfusioin imaging in the ED setting, and its use for patient risk stratification. This is important as decision making on the part of the ED physician is more likely to be dictated by the identified *risk to the patient of a subsequent cardiac event* – in other words, the answer to the question "what is this patient's risk of death or infarction should he or she leave the ED?" Central to this decision-making process is the negative predictive value of the test, i.e., the probability of no disease (or events) if the test result is negative.

Hilton and coworkers [130] looked specifically at the prognostic significance of Tc-99m sestamibi SPECT myocardial perfusion images obtained in ED patients with chest pain. Only one cardiac event (defined as cardiac death, nonfatal MI, or need for acute coronary intervention) occurred during short-term hospital follow-up among 70 patients with normal scans. In a multivariate analysis, the presence of an abnormal sestamibi scan was the only independent variable predictive of the occurrence of a cardiac event among multiple clinical and demographic variables.

Tatum and colleagues [132] subsequently reported on a large group of 1187 patients who underwent evaluation in an ED setting in which clinical data were initially used to stratify patients into five risk groups regarding the probability of AMI or unstable angina. Patients who were initially classified into low- or intermediate-risk groups ($n = 442$) underwent SPECT sestamibi imaging with gated SPECT acquisition. The scintigraphic data contained very powerful risk stratification information: among the large number of patients with a normal resting SPECT sestamibi scan with normal gated SPECT images, no patients ruled in for an MI and only 2% underwent an angioplasty over the subsequent 12 months. In contrast, among patients with a positive or abnormal scan, approximately 35% either ruled in for MI or underwent an interventional procedure during the initial hospitalization or in follow-up.

Data have also been reported from a multicenter trial by Heller and colleagues [134], in which patients presenting to the ED with suspected acute ischemia were studied with Tc-99m tetrofosmin. This study demonstrated results consistent with the previously reported studies: patients with a normal scan in this setting had an extremely low risk of infarct, and those with a positive scan were far

more likely to rule in for an MI or undergo catheterization or revascularization. These data suggest that the concepts derived in single center studies can be generalized to a wider setting. Kontos and colleagues [135] recently showed that ED myocardial perfusion imaging in low-to-moderate-risk patients with chest pain and serial troponin testing had comparable sensitivities for detection of MI. What is important to note is that while serial troponin I estimations over 24 hours provided similar sensitivity, the *initial* troponin value, drawn at an approximately similar time point as isotope injection, was poorly sensitive (30% for MI). These data demonstrate that a major potential advantage of perfusion imaging is that of *early* diagnosis in the ED, as biomarkers take time to achieve maximum sensitivity, while perfusion imaging is abnormal as soon as a flow abnormality is present. Other studies have corroborated these findings [136,142].

Thus, the risk stratification concepts derived in populations with stable chest pain and suspected CAD, in populations with AMI, and in the setting of obvious unstable angina appear to transfer to the acute ED setting with resting SPECT imaging in patients with chest pain and nondiagnostic ECG changes.

These studies provide quite concordant data regarding the negative predictive value of a resting perfusion study in an ED patient with suspected ACS. It is important to note, however, that these studies did not *prospectively* assess the actual impact of utilizing myocardial perfusion imaging in the ED setting on the triage decision-making process. Many tests are reported to have diagnostic or prognostic value in the literature when evaluated by experts, known as the "efficacy" of a test. Whether or not that test translates in real use to favorable effects on decision making or outcomes – known as "effectiveness" – needs to be addressed by randomized trials.

Randomized trials of ED myocardial perfusion imaging to improve outcomes and decision making

There have been two reported trials in which patients have been randomly assigned to either have or *not* have imaging data influence subsequent management. These two randomized studies evaluated the benefit of using this modality on reducing health care costs, length of hospital stay, and for its ability to influence ED physicians triage decision making.

Stowers and colleagues [143] evaluated 46 patients presenting to the ED with ongoing chest pain and a nondiagnostic ECG, who underwent Tc-99m tetrofosmin imaging before being randomly assigned to a conventional arm (physicians blinded from imaging results) or perfusion imaging-guided arm (imaging results were unblinded to the physician). The study's primary analyses focused on assessing the differences in total in-hospital costs and average lengths of stay between the two study arms. They found that median hospital costs were $1843 less for patients in perfusion-guided strategy compared with costs with conventional management. In addition to these cost differences, the conventional arm had a 2 days longer median hospital stay and 1 day longer median ICU stay. This study also demonstrated that physicians provided with imaging results ordered fewer cardiac catheterizations without any difference in outcomes by hospital discharge or by 30 days of follow-up. Thus, while the study population was small, there appears to be a cost benefit and shorter lengths of stay for intermediate-risk chest pain patients admitted from the ED when myocardial perfusion imaging results are made available as part of the diagnostic strategy. Clinicians were provided a suggested management strategy per protocol based on the imaging results; thus this study did not fully evaluate how physicians would react to the myocardial perfusion imaging information on their own.

A larger prospective, randomized study – the Emergency Room Assessment of Sestamibi for the Evaluation of Chest Pain trial (ERASE Chest Pain) [138] – evaluated the role of myocardial perfusion imaging on the triage decision made by ED physicians. The investigators enrolled 2475 patients with chest pain or any other symptoms suggestive of acute cardiac ischemia and a normal or nondiagnostic ECG. Patients were randomly assigned to either the usual ED evaluation strategy or the usual strategy supplemented by information from acute resting Tc-99m sestamibi SPECT imaging. Clinicians were given the imaging information, but not specifically directed as to how to use it, beyond initial education about the literature on ED perfusion imaging prior to the start of the study. Thus, this study was the first to truly evaluate how ED clinicians would incorporate myocardial perfusion imaging information into their decision-making process.

The study found that there were no differences in the ED triage decision between the two arms for those patients with either an AMI or with unstable angina. However, for those patients without acute cardiac ischemia, hospitalization was reduced from 52% with usual care to 42% with sestamibi imaging ($p < 0.001$). In this study, the median time from ED presentation to admission or discharge home was 4.7 hours in the usual care arm and 5.3 hours in the sestamibi imaging arm, thus the imaging added an average of only approximately 30 minutes to the evaluation. On 30-day follow-up, there were no differences in outcomes between the usual care and sestamibi imaging groups. Therefore, this study showed that the incorporation of sestamibi imaging into the triage decision making

provided a clear benefit in reducing unnecessary hospital admissions in patients without ischemia, without reducing appropriate admission for patients with acute ischemia. All prospectively identified subgroups benefited in terms of reduced unnecessary admissions from SPECT perfusion imaging, including those based on gender, age, presence/absence of a formal chest pain unit, and whether or not the site had prior experience with ED myocardial perfusion imaging.

These two prospective randomized trials have shown that acute rest SPECT myocardial perfusion imaging in patients presenting to the ED with low-to-intermediate risk chest pain and nondiagnostic ECGs can significantly improve the overall clinical effectiveness of the ED triage process. Given evidence from two prospective randomized trials as well as numerous observational studies (Table 9.8), the use of rest SPECT perfusion imaging in the ED setting has attained a class I, level A indication in the 2003 ACC/AHA/ASNC Guidelines for the Clinical Use of Cardiac Radionuclide Imaging document [94], the highest indication based on strong evidence.

Methodologic issues in ED perfusion imaging studies

The goal of SPECT perfusion imaging in the ED setting is to distinguish as powerfully as possible patients with acute ischemic syndromes from those without acute ischemia. The data should contribute importantly to the ED triage decision-making process. Studies examining this technique are limited by the difficulty in independently establishing the diagnosis of unstable angina. In most therapeutic studies of unstable angina, patients are identified by transient ischemic changes on the ECG in the setting of an appropriate clinical syndrome. However, the target population in the ED setting for SPECT perfusion imaging is the group *without* obvious ischemic ECG changes, as this is the population which will benefit from further diagnostic stratification. As seen in the review of studies in Table 9.8, revascularization is often used as an outcome endpoint, as a surrogate for unstable angina. Thus, patients with unstable angina who do not undergo revascularization are not included in the endpoint analysis. This issue may explain, in part, the modest positive predictive value of acute imaging in the ED setting in most reported studies. Patients with "positive" scans (who may indeed have unstable angina) who do not undergo catheterization and revascularization are tallied as "false-positive" images. The optimal solution to this issue has not been fully explored, but may involve early follow-up stress testing to best categorize patients following presentation.

Timing of the rest injection in ED myocardial perfusion studies: effect of presence/absence of symptoms

The relationship between the timing of a test in relation to symptom onset and its diagnostic accuracy is an important consideration when evaluating the utility of a test for chest pain patients in the ED. In a substantial proportion of these patients, symptoms would have begun to resolve by the time the initial assessment has been completed and decisions regarding further testing made. While this has not been the subject of the primary analysis in any of the above mentioned trials, in the study by Wackers and colleagues [125] using Tl-201, the sensitivity for detecting ischemia diminished as time increased beyond 6 hours from the onset of symptoms. Bilodeau and colleagues [127] found perfusion abnormalities in 65% of patients injected more than 4 hours after the episode of chest pain. Similarly, Varetto et al. [129] reported that the diagnostic sensitivity of myocardial perfusion imaging was maintained even when Tc-99m sestamibi injection was delayed for up to 3–4 hours after symptom resolution. In a subgroup analysis of the ERASE Chest Pain trial, Hendel et al. [144] found no association between the presence or absence (< 3 h following resolution) of chest pain during Tc-99m sestamibi injection and the incidence of normal myocardial perfusion imaging, rate of hospitalization, death, MI, coronary angiography or revascularization, or influence on triage decisions. Similarly, in the report by Duca et al. [136] no significant difference in diagnostic accuracy was observed regardless of whether the radioisotope had been injected during (56%) or after (44%) symptoms.

Experimental support for the concept that perfusion images may remain abnormal for a substantial period of time after resolution of ischemia comes from a study of patients undergoing PCI as a model of "supply" type ischemia consistent with what occurs in an acute coronary syndrome. Fram and coworkers [145] studied patients undergoing coronary angioplasty and demonstrated perfusion defects in all patients injected with Tc-99m sestamibi during balloon inflation and in 70%, 37%, and 19% of patients reinjected 15 minutes, 1–3 hours, and 24 hours after balloon deflation, respectively.

Therefore, the available data that address this issue appear to suggest that, following an episode of transient myocardial ischemia, perfusion abnormalities may persist for several hours after symptom resolution (Fig. 9.20). Nevertheless, for practical purposes of ED triaging, tracer injection should be performed as early after the patient presents as possible, and it must be borne in mind that the sensitivity of the technique tends to diminish with time after symptom resolution.

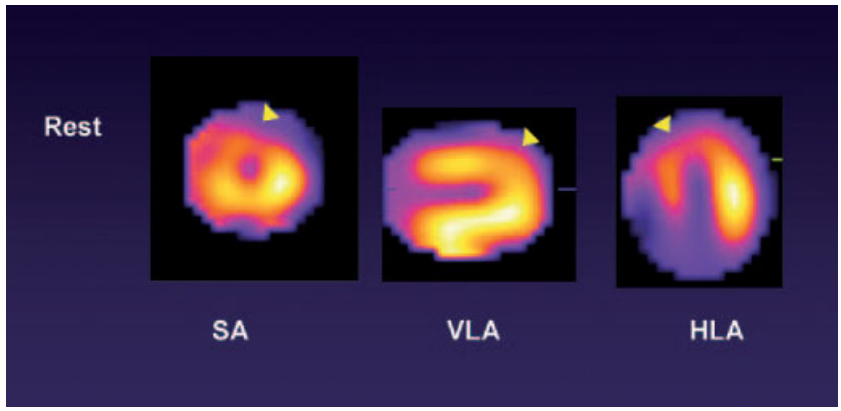

Figure 9.20 This 37-year-old premenopausal hypertensive and diabetic woman presented to the ED with atypical chest pain. ECG revealed left ventricular strain with nondiagnostic changes. The patient was injected with tetrofosmin in the ED and imaged an hour later. Myocardial perfusion image reveals an anterior and anteroseptal perfusion defect. Angiography revealed a critical lesion in the proximal left anterior descending artery that was treated percutaneously.

Value and safety of addition of stress perfusion imaging in patients with normal rest perfusion studies in the ED

Ziffer and colleagues have shown that the addition of stress imaging in patients with normal rest gated SPECT studies in the ED adds to the detection of patients with CAD, particularly when the resting perfusion tracer was injected after symptom resolution. These investigators have recommended the use of thallium-201 for the rest SPECT study in such patients, so that there would not be interference due to downscatter in scan interpretation of stress SPECT performed after peak stress injection of a Tc-99m agent. This separate acquisition dual-isotope stress procedure in the ED is the same as that described in Chapter 3 for patients under consideration for chronic CAD. Alternatively, patients can be injected with a low dose of a Tc-99m agent at rest, allowing for the performance of a higher dose stress study without major contamination from the resting study, should a stress study be indicated. Either exercise or vasodilator stress may be used in this setting. Generally, dobutamine stress is not used in these patients who may be having unstable angina. If exercise stress is chosen, appropriate caution must be taken with stress testing, being sensitive to the need to curtail exercise if signs of ischemia during stress develop in these patients with a possible acute ischemic syndrome. With these precautions, preliminary data have suggested that stress testing is both safe and effective in further stratification of patients with normal rest perfusion studies in the ED setting. It has also been noted that ED physicians have increased confidence in sending patients home if they have normal stress studies in addition to normal rest studies when the radioactive tracer is injected after resolution of symptoms.

Cost-effectiveness of perfusion imaging in the ED

Based on the technical advantages of non-redistributing Tc-99m-labeled agents over other imaging agents, their ability to delineate resting perfusion abnormalities in the acute ED setting, and the now extensive data set showing very high negative predictive value and benign prognosis associated with a normal scan in ED patients presenting with chest pain and nondiagnostic ECGs, a significant potential benefit exists for their use in the ED setting to aid in the diagnosis of acute cardiac ischemia and to improve correct triage of such patients. Given the high negative predictive value for ruling out the diagnosis of acute cardiac ischemia, its use in this setting could significantly decrease the number of unnecessary hospital admissions in patients with chest pain of noncardiac origin. In addition, with its high sensitivity, it could also potentially lower the number of patients mistakenly sent home who have active ischemia or infarction. In this regard, Ziffer and colleagues [146], in a preliminary report of 2737 patients in a chest pain evaluation unit, found that the "missed infarction" rate dropped from 1.8% to 0.1% following institution of SPECT imaging-based ED chest pain analysis protocol.

Although nuclear imaging in the ED setting for patients with suspected acute cardiac ischemia has the disadvantage of potentially adding time and cost to the ED evaluation, the potential saving to the health care system from a reduction in unnecessary hospital admissions would, at some threshold of admission reduction, more than offset the costs of such testing, resulting in overall cost savings. Given the fact that over 750,000 people with suspected acute cardiac ischemia who are admitted to CCUs each year are ultimately found *not* to have acute ischemic heart disease, a tool which would improve ED triage has the potential to save millions of dollars. Weissman et al. [131] showed that diagnostic confidence of the treating physician improved with SPECT perfusion imaging with Tc-99m sestamibi in 50 patients presenting to the ED with unexplained chest pain. Moreover, treatment strategy was altered in 34 out of 50 patients, with 29 being discharged after the imaging results were obtained. This resulted in a cost saving of approximately $786 per patient when compared to similar patients presenting to the hospital but

managed without any imaging. Radensky et al. [147] retrospectively looked at cost-effectiveness of a "scan strategy" in ED patients presenting with chest pain but nondiagnostic ECGs who underwent myocardial perfusion imaging with Tc-99m sestamibi. Compared to a "no scan" strategy where patients were admitted or discharged based on clinical and electrocardiographic characteristics, there was an approximately $900 cost saving per patient with the "scan strategy." Ziffer and colleagues [146] were able to show that by implementing a myocardial perfusion imaging-based chest pain center protocol, the length of hospital stay was reduced (12 hours vs. 1.9 days) and $1892 were saved per patient. The prospective randomized study by Stowers et al. [143] assessed differences in hospital cost between a conventional and perfusion imaging-guided strategy. They found that the median hospital costs per patient were $1843 lower in the perfusion imaging-guided arm as compared with the conventional arm. Heller and coworkers [134] estimated savings in a similar range. In contrast, an observational study by Kosnik and colleagues [137] evaluated 69 patients already being admitted to the hospital and estimated that the use of sestamibi imaging would hypothetically lead to more appropriate triage in 42% of patients but at an additional cost of $307 per patient.

Overall, the majority of studies point to a potential cost savings by incorporating the routine use of acute rest myocardial perfusion imaging in patients with low-to-moderate risk chest pain and nondiagnostic ECGs. However, the ultimate effectiveness of an ED strategy using perfusion imaging will depend on numerous factors: cooperation between ED physicians, nuclear medicine physicians, and cardiologists, as well as the ability of the decision-making physician to incorporate the strong prognostic value of the imaging data into the ED triage decision. If it is possible to significantly improve the ED decision-making process in these patients, as suggested by the growing number of studies demonstrating a very high negative predictive value for the absence of cardiac events with a normal scan in this setting, the incorporation of this test may indeed be cost-effective, potentially even cost-saving, if used to its maximum potential.

Assessment of regional and global left ventricular function in the ED chest pain patient

Hauser et al. [148] demonstrated many years ago that regional wall motion abnormalities can be visualized echocardiographically within seconds of coronary occlusion in patients undergoing percutaneous coronary angioplasty. Moreover, these changes occurred prior to the onset of electrocardiographic changes or the development of symptoms [149]. Such studies illustrate the concept of the "ischemic cascade." That is, ischemia is not an "all-or-none" phenomenon, but rather a stepwise series of events occurring as the oxygen supply and demand mismatch progressively worsens. Based on these observations, one can surmise that ischemic chest pain would be expected to often be accompanied by regional wall motion abnormalities, and also that perfusion imaging may be more sensitive to detect changes in myocardial blood flow that may not result in regional functional abnormalities.

Several authors have investigated 2D echocardiography as a tool to distinguish ischemic from nonischemic chest pain in the ED (Table 9.9) [150–155]. Specificity for acute ischemia or infarction may be modest in general populations, since the presence of regional wall motion abnormalities does not establish the diagnosis of ischemia, as regional wall motion abnormalities can result from many causes other than acute ischemia. These include prior MI, conduction abnormalities like left bundle branch block, and also non-ischemic-dilated cardiomyopathies. Using 2D echocardiography in the ED, Sasaki et al. [150] studied 46 patients with chest pain and normal ECGs. Excluded from this study were patients with prior MI, cardiomyopathy, valvular heart disease, and left bundle branch block. Eighteen patients underwent the study during chest pain, while in 28 the study was performed after resolution of symptoms. Among patients studied during chest pain, 8 of the 18 had regional wall motion abnormalities, of which 6 eventually had an infarct and 2 had significant CAD, yielding an 86% sensitivity and 82% specificity for detection of infarct. Only 1 of 10 patients with normal wall motion developed an infarct and none of the others had significant CAD. Among patients studied in the absence of chest pain, 8 of 10 patients with abnormal studies had an infarct as opposed to none of those with normal studies, yielding a sensitivity and specificity for infarct detection of 100% and 90% respectively. Eighteen of these 28 patients had no regional wall motion abnormalities, none developed an infarct but 5 had significant CAD. This relatively small study concluded that the presence of regional wall motion abnormalities both during or after chest pain correlated well with development of an infarct, and that a negative study during chest pain did not completely exclude the possibility of an infarct. Moreover, a negative study after resolution of chest pain did not miss an evolving infarct but did not detect CAD in a significant number of patients.

Peels et al. [152] studied 43 patients presenting with chest pain and nondiagnostic electrocardiography changes. Patients with prior infarcts, known CAD, and poor acoustic windows were excluded from the study. The patients were imaged in the ED as soon as possible, prior to resolution of chest pain or initiation of any medications. They found an 88% sensitivity, 78% specificity, and 82% negative predictive value for the prediction of CAD by angiography. The negative predictive value was 94% for MI alone as detected by enzymes.

Table 9.9 Studies using 2D echocardiography in assessment of patients presenting to the ED with chest pain.

Study	*N*	Number with interpretable studies	Exclusion	Time after presentation to imaging	Criteria for positive study	Endpoint	No. of events	Sensitivity %	Specificity %	NPV %	PPV %
Sasaki et al. [150]	52	46	Prior MI or CMP	1–8 hr	RWMA	MI and/or significant CAD	23	74	96	79	94
						MI alone	15	93	87	96	78
Sabia et al. [151]	180	169	None	Within 4 hr	RWMA	MI	29	93	57	98	31
Peels et al. [152]	43	Not stated	Prior MI or CAD	Not stated	RWMA	MI	12	92	53	94	46
						CAD by angiography	22	88	78	82	85
Gibler et al. [153]	901	Not stated	Prior history of CAD, hemodynamic instability	9 hr	RWMA	MI	9	47	99	99	50
Tripp et al. [154]*	173†	163	Prior MI, CHF, LV dysfunction	2.9 ± 1.8 hr	RWMA	MI, CAD by angiography, persistent typical angina	19	53*	90*	93*	42*
Kontos et al. [155]	262	260	None ("all comers")	4 hr of presentation	RWMAs or EF <40%	MI or revascularization	45	91	75	98	44

Abbreviations: CAD, coronary artery disease; EF, ejection fraction; MI, myocardial infarction; NPV, negative predictive value; PPV, positive predictive value; RWMA, regional wall motion abnormality.

*Only data for *resting* imaging presented; 24/163 patients had resting RWMAs.

†5 had difficult studies; 4 refused; 1 had recurrence of chest pain.

Sabia et al. [151] studied 180 consecutive patients presenting to the emergency room at an academic hospital with chest pain. Ninety-four percent had technically adequate ECGs. This study did not exclude patients with diagnostic ECGs, known prior infarcts, or CAD. No regional wall motion abnormalities were detected in 82 patients, of whom 60 had completely normal studies (no regional or global dysfunction) and 22 had global hypokinesis without regional wall motion abnormalities. Among these 82 patients, there were 2 (2%) who subsequently ruled in for a non-Q wave MI by cardiac enzymes, but without clinical sequelae. Of the 87 patients *with* regional wall motion abnormalities, 27 (31%) had an AMI. The initial ECG was diagnostic (ST elevation with or without Q waves) in 9 (30%) of these patients, and 8 had an ECG that was not interpretable for an AMI (due to left bundle branch block, pacing, or left ventricular hypertrophy with strain). The authors concluded that the presence of regional wall motion abnormalities in patients presenting to the ED increased the diagnostic yield and could potentially diminish unnecessary admissions. They estimated a potential 32% reduction in hospital admissions if patients with no regional wall motion abnormalities were discharged from the ED. It is important to note, however, that in this study the treating physicians were blinded to the results of the imaging and the decision to admit was based on clinical and ECG criteria only.

Trippi et al. [154] looked at the practicality and accuracy of dobutamine stress tele-echocardiography in patients presenting to the ED with chest pain. Patients underwent resting 2D echocardiography in the ED, and if a resting wall motion abnormality was not identified, the patients underwent dobutamine stress echocardiography supervised by a trained nurse. The images were transmitted by telephone to a cardiologist. Among the 24/163 patients who did have resting wall motion abnormalities, 10 had cardiac events while 14 did not. There were nine false-negative resting ECGs, of which seven were identified on subsequent dobutamine stress echocardiography. The sensitivity and specificity of resting echocardiography in this study was 53 and 90%, respectively, with a negative predictive value of 93%. These authors concluded that dobutamine stress tele-echocardiography in the ED enabled rapid triage of patients with chest pain and that pharmacologic stress echocardiography improved diagnostic accuracy over rest imaging alone.

More recently, Kontos et al. [155] performed 2D echocardiography within 4 hours of chest pain in 260 ED patients. The sensitivity of either regional wall motion abnormalities or an ejection fraction less than 40% on echocardiography for predicting cardiac events (MI or revascularization) was 91% with a negative predictive value of 98% (Table 9.9).

Thus, although the analysis of regional wall motion abnormalities by echocardiography in the ED setting is conceptually sound, the published data, particularly the important negative predictive value, are not as consistently robust as in the myocardial perfusion imaging literature (Table 9.8). There may be several potential explanations for this difference. First, the rate of technically inadequate studies is distinctly higher with echocardiography than with current SPECT imaging techniques. Approximately 8–10% of echocardiographic studies are technically inadequate for analyzing all myocardial regions. Moreover, it appears from studies in which the timing of wall motion or perfusion analysis can be assessed relative to the timing of symptoms that the analysis of regional wall motion abnormalities is far more sensitive to the presence or absence of symptoms during the time of the analysis. In one study [150], the sensitivity of regional wall motion abnormalities in patients with suspected unstable angina dropped significantly when symptoms were not present at the time of the study. The data on SPECT perfusion imaging studies on this point, while not completely consistent, suggest that there is a much large "time window" during which one may still obtain powerful stratification data, even after symptoms abate. In the study of Tatum et al. [132], sestamibi could be injected up to 6 hours after the cessation of symptoms. The negative predictive value remained strong even many hours later. This is an important point, as a large percentage of patients (up to 50% in some studies) present to the ED with symptoms having already ceased.

There are advantages to echocardiography over SPECT myocardial perfusion imaging. First, it is logistically much more convenient. Second, there is an advantage in delineation of structural abnormalities. In the setting of suspected aortic dissection, transthoracic, and particularly transesophageal echocardiography can provide critically important diagnostic data. In suspected pulmonary embolus, evaluation of right ventricular function and size is of diagnostic importance. Thus, when particular clinical syndromes in the setting of acute chest pain in the ED are suspected, echocardiography may be selected to examine these more closely. However, since the frequency of these diagnoses is quite low among large populations of ED chest pain patients, the routine application of such technology to all patients will not necessarily be of high yield.

Gated SPECT imaging in the ED

Unlike in echocardiography, gated SPECT imaging is usually delayed for 30–60 minutes after the injection of the Tc-99m-labeled tracer. Thus, the functional information obtained pertains to the resting state. Transient stress-induced abnormalities of regional left ventricular function

that have resolved prior to the beginning of image acquisition will therefore not be detected. Thus, as nonredistributing tracers are injected in the ED but imaged sometime later under a SPECT camera, the opportunity to detect blood flow abnormalities is more robust than that to detect functional abnormalities.

Furthermore, in contrast to the AMI or obvious unstable angina populations, where abnormalities of left ventricular function take on significant diagnostic and prognostic importance in the setting of known CAD, patients with chest pain in the ED make up a very heterogeneous group. In particular, patients with chest pain but nondiagnostic ECGs are, on the whole, a lower risk population with preserved left ventricular function. Thus, the prevalence of underlying abnormalities in left ventricular function is likely to be low as was shown by Tatum et al. [132] (2%).

There is limited information on the utility of incorporating information on regional or global left ventricular function in ED triaging. However, a recently published prospective multicenter study by Kaul et al. [140] examined 203 patients presenting to the ED with chest pain without ST-segment elevation who underwent contrast echocardiography and gated SPECT imaging to assess regional perfusion as well as function. SPECT imaging data were available in 163 of these 203 subjects. In this group, 36 patients had an abnormal perfusion image and 53 had an abnormal assessment of function, while a composite reading of both perfusion and function was abnormal in 60 patients. The odds ratio for adverse events as predicted by a composite reading was significantly higher than that predicted by either variable alone, suggesting that combined imaging of function and perfusion at the time of presentation in the ED provides more robust diagnostic and prognostic information. It should be noted that these were somewhat higher risk patients with 75% having a history of typical angina, 54% having a prior history of angina, and one-third undergoing prior revascularization. Whether combined assessment of perfusion and function would be as beneficial in a lower risk population remains to be determined.

Apart from its potential prognostic value, ECG gating has improved our ability to distinguish between attenuation artifacts and fixed perfusion defects (in stress/rest image pairs) since resting regional left ventricular function should be normal in the former situation. Its utility for ED triaging of chest pain patients, however, is limited because only one set of perfusion images, corresponding to the stress images in the conventional sense, is acquired, and perfusion defects with normal regional left ventricular function in this setting is consistent with a diagnosis of transient myocardial ischemia.

Attempts to distinguish true perfusion defects from artifacts have included the use of attenuation correction programs. In the context of ED triaging, Hendel and colleagues [156] examined the ERASE Chest Pain trial database in which some centers routinely used attenuation correction and gated SPECT imaging. In 319 patients, the use of both attenuation correction and gating reduced the number of equivocal scans and increased reader confidence in interpretation. Segmental scores were more normal in patients ultimately found to not have an acute ischemic syndrome, by both methods. However, attenuation correction slightly reduced the scores of patients with an acute ischemic syndrome (inappropriately). From these data it appears that either method has the potential to be useful, though gating perhaps more so. The comparative usefulness of these modalities will need to be reevaluated as attenuation correction techniques continue to evolve.

It is important to remember that the goal of perfusion scintigraphy in the ED setting is the *optimal identification of patients with acute cardiac ischemia*. Therefore, when a study appears to be equivocal, one should err on the side of interpreting it as abnormal so as to obtain a high sensitivity for the detection of cardiac ischemia. In the study by Hilton and colleagues [130], which reported the prognostic significance of resting perfusion imaging in ED patients with typical angina and a nondiagnostic ECG, patients with studies interpreted as equivocal had a prognosis that was *intermediate* between patients with a normal scan and those with an abnormal scan. While patients with a normal scan had an extremely low (1 event in 70) rate of cardiac events defined as predischarge cardiac death, nonfatal MI, or the need for immediate coronary intervention, patients with an equivocal or abnormal scan had higher event rates of 13 and 71%, respectively. In the ERASE chest pain trial, while the risk of AMI was 0.6, 0.8, and 10.3% for normal, equivocal, and abnormal Tc-99m sestamibi rest scans, respectively, the risk of the combined endpoint of AMI, death, or revascualrization was 3, 6.1, and 20.5%, respectively. Given these results, interpretation of perfusion images in this setting should optimize sensitivity for detecting acute ischemia at the cost of specificity.

While no formal analysis of the cost-effectiveness of simultaneous functional and perfusion assessment has been performed, even a small incremental yield would be considered cost-effective since the time and cost involved in performing gated SPECT imaging in conjunction with standard resting perfusion imaging is so minimal. Thus, to the extent that the limited published data such as that by Tatum and colleagues [132] are generally reflective of what would be seen in wider use, even the capture of a very small percentage of patients who have dilated cardiomyopathy with chest pain as their presentation would be of considerable importance and remain cost-effective. Table 9.10 summarizes the ACC/AHA/ASNC recommendations regarding radionuclide imaging in the ED [94].

Table 9.10 ACC/AHA/ASNC recommendations for radionuclide imaging in the ED.

Indication	Test	Class	Level of evidence
Assessment of myocardial risk in ACS patients with nondiagnostic ECG and initial serum markers (if available)	Resting MPI	I	A
Diagnosis of CAD in possible ACS patients with chest pain with nondiagnostic ECG and negative serum cardiac markers or normal resting scan	Same day rest/stress MPI	I	B
Routine imaging of patients with myocardial ischemia/necrosis already documented clinically, by ECG and/or serum markers	Rest MPI	III	C

Abbreviations: ACS, acute coronary syndrome; CAD, coronary artery disease; MPI, myocardial perfusion imaging.
Source: From [93].

Conclusions

The extensive bodies of literature that exist regarding the diagnostic and prognostic importance of SPECT perfusion imaging data as well as information on regional and global left ventricular function by many techniques suggest that the combination of the two into one test would provide a very powerful tool for patient management in the setting of acute coronary syndromes. Within one test, numerous variables of proven prognostic importance may be obtained (Table 9.11). There has been a steady increase in the number of studies that have examined the incremental role of combined assessment of ventricular function and perfusion using gated SPECT imaging and this assessment has rapidly become routine practice in most laboratories. The very modest incremental cost in terms of both time and money suggests that this practice is cost-effective. Even in the era in which the majority of patients undergo coronary angiography, there are many patient subgroups who do not, and who can, benefit from scintigraphy, either at rest alone or in combination with stress.

Table 9.11 Prognostic variables from gated SPECT perfusion imaging applicable to acute coronary syndromes.

Presence of inducible ischemia
Extent of inducible ischemia
Perfusion defect size
Final infarct size
End-systolic volume
Left ventricular ejection fraction
Extent of regional wall motion abnormality
Presence of preserved viability within dysfunctional territories

References

1. Go V, Bhatt MR, Hendel RC. The diagnostic and prognostic value of ECG-gated SPECT myocardial perfusion imaging. Journal of Nuclear Medicine 2004;45(5):912–921.
2. de Vreede JJ, Gorgels AP, Verstraaten GM, Vermeer F, Dassen WR, Wellens HJ. Did prognosis after acute myocardial infarction change during the past 30 years? A meta-analysis. Journal of the American College of Cardiology 1991;18(3):698–706.
3. Naylor CD, Chen E. Population-wide mortality trends among patients hospitalized for acute myocardial infarction: the Ontario experience, 1981 to 1991. Journal of the American College of Cardiology 1994;24(6):1431–1438.
4. Pell S, Fayerweather WE. Trends in the incidence of myocardial infarction and in associated mortality and morbidity in a large employed population, 1957–1983. New England Journal of Medicine 1985;312(16):1005–1011.
5. Ryan TJ, Anderson JL, Antman EM, et al. ACC/AHA guidelines for the management of patients with acute myocardial infarction. A report of the American College of Cardiology/American Heart Association Task Force on Practice Guidelines (Committee on Management of Acute Myocardial Infarction). Journal of the American College of Cardiology 1996;28(5):1328–1428.
6. Wackers FJT, Zaret BL. Risk stratification soon after acute infarction. Circulation 1999;100(20):2040–2042.
7. Marcus FI, Friday K, McCans J, et al. Age-related prognosis after acute myocardial infarction (the Multicenter Diltiazem Postinfarction Trial). American Journal of Cardiology 1990;65(9):559–566.
8. Stone PH, Muller JE, Hartwell T, et al., for the MILIS Study Group. The effect of diabetes mellitus on prognosis and serial left ventricular function after acute myocardial infarction: contribution of both coronary disease and diastolic left ventricular dysfunction to the adverse prognosis. Journal of the American College of Cardiology 1989;14(1):49–57.
9. Bueno H, Vidan MT, Almazan A, Lopez-Sendon JL, Delcan JL. Influence of sex on the short-term outcome of elderly patients with a first acute myocardial infarction. Circulation 1995;92(5):1133–1140.
10. DeBusk RF, Convertino VA, Hung J, Goldwater D. Exercise conditioning in middle-aged men after 10 days of bed rest. Circulation 1983;68(2):245–250.
11. Benhorin J, Moss AJ, Oakes D, et al., for the Multicenter Diltiazem Post-Infarction Research Group. The prognostic significance of first myocardial infarction type (Q wave versus non-Q wave) and Q wave location. Journal of the American College of Cardiology 1990;15(6):1201–1207.

12. Gibson RS, Watson DD, Craddock GB, et al. Prediction of cardiac events after uncomplicated myocardial infarction: a prospective study comparing predischarge exercise thallium-201 scintigraphy and coronary angiography. Circulation 1983;68(2):321–336.
13. Hung J, Goris ML, Nash E, et al. Comparative value of maximal treadmill testing, exercise thallium myocardial perfusion scintigraphy and exercise radionuclide ventriculography for distinguishing high- and low-risk patients soon after acute myocardial infarction. American Journal of Cardiology 1984;53(9):1221–1227.
14. Leppo JA, O'Brien J, Rothendler JA, Getchell JD, Lee VW. Dipyridamole-thallium-201 scintigraphy in the prediction of future cardiac events after acute myocardial infarction. New England Journal of Medicine 1984;310(16):1014–1018.
15. Abraham RD, Freedman SB, Dunn RF, et al. Prediction of multivessel coronary artery disease and prognosis early after acute myocardial infarction by exercise electrocardiography and thallium-201 myocardial perfusion scanning. American Journal of Cardiology 1986;58(6):423–427.
16. Gibson RS, Beller GA, Gheorghiade M, et al. The prevalence and clinical significance of residual myocardial ischemia 2 weeks after uncomplicated non-Q wave infarction: a prospective natural history study. Circulation 1986;73(6):1186–1198.
17. Gimple LW, Hutter AM Jr, Guiney TE, Boucher CA. Prognostic utility of predischarge dipyridamole-thallium imaging compared to predischarge submaximal exercise electrocardiography and maximal exercise thallium imaging after uncomplicated acute myocardial infarction. American Journal of Cardiology 1989;64(19):1243–1248.
18. Wilson WW, Gibson RS, Nygaard TW, et al. Acute myocardial infarction associated with single vessel coronary artery disease: an analysis of clinical outcome and the prognostic importance of vessel patency and residual ischemic myocardium. Journal of the American College of Cardiology 1988;11(2):223–234.
19. Younis LT, Byers S, Shaw L, Barth G, Goodgold H, Chaitman BR. Prognostic value of intravenous dipyridamole thallium scintigraphy after an acute myocardial ischemic event. American Journal of Cardiology 1989;64(3):161–166.
20. Brown KA, O'Meara J, Chambers CE, Plante DA. Ability of dipyridamole-thallium-201 imaging one to four days after acute myocardial infarction to predict in-hospital and late recurrent myocardial ischemic events. American Journal of Cardiology 1990;65(3):160–167.
21. Tilkemeier PL, Guiney TE, LaRaia PJ, Boucher CA. Prognostic value of predischarge low-level exercise thallium testing after thrombolytic treatment of acute myocardial infarction. American Journal of Cardiology 1990;66(17):1203–1207.
22. Hendel RC, Gore JM, Alpert JS, Leppo JA. Prognosis following interventional therapy for acute myocardial infarction: utility of dipyridamole thallium scintigraphy. Cardiology 1991;79(1):73–80.
23. de Cock CC, Visser FC, Van Eenige MJ, Bezemer PD, Roos JC, Roos JP. Prognostic value of thallium-201 exercise scintigraphy in low-risk patients after Q-wave myocardial infarction: comparison with exercise testing and catheterization. Cardiology 1992;81(6):342–350.
24. Moss AJ, Goldstein RE, Hall WJ, et al., for the Multicenter Myocardial Ischemia Research Group. Detection and significance of myocardial ischemia in stable patients after recovery from an acute coronary event. JAMA 1993;269(18):2379–2385.
25. Miller TD, Gersh BJ, Christian TF, Bailey KR, Gibbons RJ. Limited prognostic value of thallium-201 exercise treadmill testing early after myocardial infarction in patients treated with thrombolysis. American Heart Journal 1995;130(2):259–266.
26. Travin MI, Dessouki A, Cameron T, Heller GV. Use of exercise technetium-99m sestamibi SPECT imaging to detect residual ischemia and for risk stratification after acute myocardial infarction. American Journal of Cardiology 1995;75(10):665–669.
27. Mahmarian JJ, Mahmarian AC, Marks GF, Pratt CM, Verani MS. Role of adenosine thallium-201 tomography for defining long-term risk in patients after acute myocardial infarction. Journal of the American College of Cardiology 1995;25(6):1333–1340.
28. Dakik HA, Mahmarian JJ, Kimball KT, Koutelou MG, Medrano R, Verani MS. Prognostic value of exercise 201Tl tomography in patients treated with thrombolytic therapy during acute myocardial infarction. Circulation 1996;94(11):2735–2742.
29. Basu S, Senior R, Dore C, Lahiri A. Value of thallium-201 imaging in detecting adverse cardiac events after myocardial infarction and thrombolysis: a follow up of 100 consecutive patients. BMJ 1996;313(7061):844–848.
30. Brown KA, Heller GV, Landin RS, et al. Early dipyridamole (99m)Tc-sestamibi single photon emission computed tomographic imaging 2 to 4 days after acute myocardial infarction predicts in-hospital and postdischarge cardiac events: comparison with submaximal exercise imaging. Circulation 1999;100(20):2060–2066.
31. Volpi A, de Vita C, Franzosi MG, et al. Predictors of nonfatal reinfarction in survivors of myocardial infarction after thrombolysis. Results of the Gruppo Italiano per lo Studio della Sopravvivenza nell'Infarto Miocardico (GISSI-2) Data Base. Journal of the American College of Cardiology 1994;24(3):608–615.
32. Elhendy A, Schinkel AF, van Domburg RT, Bax JJ, Poldermans D. Differential prognostic significance of perinfarction versus remote myocardial ischemia on stress technetium-99m sestamibi tomography in patients with healed myocardial infarction. American Journal of Cardiology 2004;94(3):289–293.
33. The TIMI Study Group. Comparison of invasive and conservative strategies after treatment with intravenous tissue plasminogen activator in acute MI. Results of the thrombolysis in myocardial infarction (TIMI) phase II trial. New England Journal of Medicine 1989;320(10):618–627.
34. Madsen JK, Grande P, Saunamaki K, et al. Danish multicenter randomized study of invasive versus conservative treatment in patients with inducible ischemia after thrombolysis in acute myocardial infarction (DANAMI). DANish trial

in Acute Myocardial Infarction. Circulation 1997;96(3): 748–755.
35. Ellis SG, Mooney MR, George BS, et al., for the Treatment of Post-Thrombolytic Stenoses (TOPS) Study Group. Randomized trial of late elective angioplasty versus conservative management for patients with residual stenoses after thrombolytic treatment of myocardial infarction. Circulation 1992;86(5):1400–1406.
36. Zeymer U, Uebis R, Vogt A, et al. Randomized comparison of percutaneous transluminal coronary angioplasty and medical therapy in stable survivors of acute myocardial infarction with single vessel disease: a study of the Arbeitsgemeinschaft Leitende Kardiologische Krankenhausarzte. Circulation 2003;108(11):1324–1328.
37. Parisi AF, Folland ED, Hartigan P, for Veterans Affairs ACME Investigators. A comparison of angioplasty with medical therapy in the treatment of single-vessel coronary artery disease. New England Journal of Medicine 1992;326(1):10–16.
38. Folland ED, Hartigan PM, Parisi AF, for Veterans Affairs ACME Investigators. Percutaneous transluminal coronary angioplasty versus medical therapy for stable angina pectoris: outcomes for patients with double-vessel versus single-vessel coronary artery disease in a veterans affairs cooperative randomized trial. Journal of the American College of Cardiology 1997;29(7):1505–1511.
39. Dakik HA, Kleiman NS, Farmer JA, et al. Intensive medical therapy versus coronary angioplasty for suppression of myocardial ischemia in survivors of acute myocardial infarction: a prospective, randomized pilot study. Circulation 1998;98(19):2017–2023.
40. Dakik H, Filipchuk N, Pratt C. INSPIRE investigators: suppression of post-infarction myocardial ischemia with medical and revascularization therapies – results from the adenosine sestamibi post-infarction evaluation (INSPIRE) trial [abstract]. Circulation 2003;108(Suppl IV): IV-635.
41. Shaw LJ, Berman DS. Sequential single-photon emission computed tomography myocardial perfusion imaging. American Journal of Cardiology 2005;96(8A):28J–39J.
42. Hammermeister KE, DeRouen TA, Dodge HT. Variables predictive of survival in patients with coronary disease. Selection by univariate and multivariate analyses from the clinical, electrocardiographic, exercise, arteriographic, and quantitative angiographic evaluations. Circulation 1979;59(3):421–430.
43. Harris PJ, Harrell FE Jr, Lee KL, Behar VS, Rosati RA. Survival in medically treated coronary artery disease. Circulation 1979;60(6):1259–1269.
44. Multicenter Postinfarction Research Group. Risk stratification and survival after myocardial infarction. New England Journal of Medicine 1983;309(6):331–336.
45. Zaret BL, Wackers FJ, Terrin ML, et al., for the TIMI Study Group. Value of radionuclide rest and exercise left ventricular ejection fraction in assessing survival of patients after thrombolytic therapy for acute myocardial infarction: results of Thrombolysis in Myocardial Infarction (TIMI) phase II study. Journal of the American College of Cardiology 1995;26(1):73–79.
46. Cerqueira MD, Maynard C, Ritchie JL, Davis KB, Kennedy JW. Long-term survival in 618 patients from the Western Washington Streptokinase in Myocardial Infarction trials. Journal of the American College of Cardiology 1992;20(7):1452–1459.
47. Volpi A, De Vita C, Franzosi MG, et al., for the ad hoc working group of the Gruppo Italiano per lo Studio della Sopravvivenza nell'Infarto Miocardico (GISSI)-2 Data Base. Determinants of 6-month mortality in survivors of myocardial infarction after thrombolysis: results of the GISSI-2 data base. Circulation 1993;88(2):416–429.
48. De Feyter PJ, van Eenige MJ, Dighton DH, Visser FC, de Jong J, Roos JP. Prognostic value of exercise testing, coronary angiography and left ventriculography 6–8 weeks after myocardial infarction. Circulation 1982;66(3):527–536.
49. Sanz G, Castaner A, Betriu A, et al. Determinants of prognosis in survivors of myocardial infarction: a prospective clinical angiographic study. New England Journal of Medicine 1982;306(18):1065–1070.
50. Nishimura RA, Reeder GS, Miller FA Jr, et al. Prognostic value of predischarge 2-dimensional echocardiogram after acute myocardial infarction. American Journal of Cardiology 1984;53(4):429–432.
51. Norris RM, Barnaby PF, Brandt PW, et al. Prognosis after recovery from first acute myocardial infarction: determinants of reinfarction and sudden death. American Journal of Cardiology 1984;53(4):408–413.
52. Ong L, Green S, Reiser P, Morrison J. Early prediction of mortality in patients with acute myocardial infarction: a prospective study of clinical and radionuclide risk factors. American Journal of Cardiology 1986;57(1):33–38.
53. White HD, Norris RM, Brown MA, Brandt PW, Whitlock RM, Wild CJ. Left ventricular end-systolic volume as the major determinant of survival after recovery from myocardial infarction. Circulation 1987;76(1):44–51.
54. Jaarsma W, Visser CA, Eenige van MJ, Verheugt FW, Kupper AJ, Roos JP. Predictive value of two-dimensional echocardiographic and hemodynamic measurements on admission with acute myocardial infarction. Journal of the American Society of Echocardiography 1988;1(3):187–193.
55. Schulman SP, Achuff SC, Griffith LS, et al. Prognostic cardiac catheterization variables in survivors of acute myocardial infarction: a five year prospective study. Journal of the American College of Cardiology 1988;11(6):1164–1172.
56. Simoons ML, Vos J, Tijssen JG, et al. Long-term benefit of early thrombolytic therapy in patients with acute myocardial infarction: 5 year follow-up of a trial conducted by the Interuniversity Cardiology Institute of The Netherlands. Journal of the American College of Cardiology 1989;14(7):1609–1615.
57. The GUSTO Angiographic Investigators. The effects of tissue plasminogen activator, streptokinase, or both on coronary-artery patency, ventricular function, and survival after acute myocardial infarction. New England Journal of Medicine 1993;329(22):1615–1622.

58. Olona M, Candell-Riera J, Permanyer-Miralda G, et al. Strategies for prognostic assessment of uncomplicated first myocardial infarction: 5-year follow-up study. Journal of the American College of Cardiology 1995;25(4):815–822.
59. Rouleau JL, Talajic M, Sussex B, et al. Myocardial infarction patients in the 1990s – their risk factors, stratification and survival in Canada: the Canadian Assessment of Myocardial Infarction (CAMI) Study. Journal of the American College of Cardiology 1996;27(5):1119–1127.
60. Khattar RS, Basu SK, Raval U, Senior R, Lahiri A. Prognostic value of predischarge exercise testing, ejection fraction, and ventricular ectopic activity in acute myocardial infarction treated with streptokinase. American Journal of Cardiology 1996;78(2):136–141.
61. Zanco P, Zampiero A, Favero A, et al. Prognostic evaluation of patients after myocardial infarction: incremental value of sestamibi single-photon emission computed tomography and echocardiography. Journal of Nuclear Cardiology 1997;4(2, Pt 1):117–124.
62. Kroll D, Farah W, McKendall GR, Reinert SE, Johnson LL. Prognostic value of stress-gated Tc-99m sestamibi SPECT after acute myocardial infarction. American Journal of Cardiology 2001;87(4):381–386.
63. Shaw LJ, Iskandrian AE. Prognostic value of gated myocardial perfusion SPECT. Journal of Nuclear Cardiology 2004;11(2):171–185.
64. Sharir T, Germano G, Kavanagh PB, et al. Incremental prognostic value of post-stress left ventricular ejection fraction and volume by gated myocardial perfusion single photon emission computed tomography. Circulation 1999;100(10):1035–1042.
65. Vallejo E, Dione DP, Bruni WL, et al. Reproducibility and accuracy of gated SPECT for determination of left ventricular volumes and ejection fraction: experimental validation using MRI. Journal of Nuclear Medicine 2000;41(5):874–882; discussion 883–886.
66. Iskandrian AE, Germano G, VanDecker W, et al. Validation of left ventricular volume measurements by gated SPECT 99mTc-labeled sestamibi imaging. Journal of Nuclear Cardiology 1998;5(6):574–578.
67. Schaefer WM, Lipke CS, Nowak B, et al. Validation of QGS and 4D-MSPECT for quantification of left ventricular volumes and ejection fraction from gated 18F-FDG PET: comparison with cardiac MRI. Journal of Nuclear Medicine 2004;45(1):74–79.
68. Beller GA, Watson DD, Ackell P, Pohost GM. Time course of thallium-201 redistribution after transient myocardial ischemia. Circulation 1980;61(4):791–797.
69. Moore CA, Cannon J, Watson DD, Kaul S, Beller GA. Thallium 201 kinetics in stunned myocardium characterized by severe postischemic systolic dysfunction. Circulation 1990;81(5):1622–1632.
70. Reduto LA, Freund GC, Gaeta JM, Smalling RW, Lewis B, Gould KL. Coronary artery reperfusion in acute myocardial infarction: beneficial effects of intracoronary streptokinase on left ventricular salvage and performance. American Heart Journal 1981;102(6, Pt 2):1168–1177.
71. De Coster PM, Melin JA, Detry JM, Brasseur LA, Beckers C, Col J. Coronary artery reperfusion in acute myocardial infarction: assessment by pre- and postintervention thallium-201 myocardial perfusion imaging. American Journal of Cardiology 1985;55(8):889–895.
72. Simoons ML, Wijns W, Balakumaran K, et al. The effect of intracoronary thrombolysis with streptokinase on myocardial thallium distribution and left ventricular function assessed by blood-pool scintigraphy. European Heart Journal 1982;3(5):433–440.
73. Schwarz F, Schuler G, Katus H, et al. Intracoronary thrombolysis in acute myocardial infarction: duration of ischemia as a major determinant of late results after recanalization. American Journal of Cardiology 1982;50(5):933–937.
74. Schuler G, Schwarz F, Hofmann M, et al. Thrombolysis in acute myocardial infarction using intracoronary streptokinase: assessment by thallium-201 scintigraphy. Circulation 1982;66(3):658–664.
75. Tamaki S, Murakami T, Kadota K, et al. Effects of coronary artery reperfusion on relation between creatine kinase-MB release and infarct size estimated by myocardial emission tomography with thallium-201 in man. Journal of the American College of Cardiology 1983;2(6):1031–1038.
76. Prigent F, Maddahi J, Garcia EV, Satoh Y, Van Train K, Berman DS. Quantification of myocardial infarct size by thallium-201 single-photon emission computed tomography: experimental validation in the dog. Circulation 1986;74(4):852–861.
77. Piwnica-Worms D, Kronauge JF, Chiu ML. Uptake and retention of hexakis (2-methoxyisobutyl isonitrile) technetium(I) in cultured chick myocardial cells. Mitochondrial and plasma membrane potential dependence. Circulation 1990;82(5):1826–1838.
78. Okada RD, Glover D, Gaffney T, Williams S. Myocardial kinetics of technetium-99m-hexakis-2-methoxy-2-methylpropyl-isonitrile. Circulation 1988;77(2):491–498.
79. Piwnica-Worms D, Chiu ML, Kronauge JF. Divergent kinetics of 201Tl and 99mTc-SESTAMIBI in cultured chick ventricular myocytes during ATP depletion. Circulation 1992;85(4):1531–1541.
80. Narahara KA, Villanueva-Meyer J, Thompson CJ, Brizendine M, Mena I. Comparison of thallium-201 and technetium-99m hexakis 2-methoxyisobutyl isonitrile single-photon emission computed tomography for estimating the extent of myocardial ischemia and infarction in coronary artery disease. American Journal of Cardiology 1990;66(20):1438–1444.
81. Sinusas AJ, Watson DD, Cannon JM Jr, Beller GA. Effect of ischemia and postischemic dysfunction on myocardial uptake of technetium-99m-labeled methoxyisobutyl isonitrile and thallium-201. Journal of the American College of Cardiology 1989;14(7):1785–1793.
82. Verani MS, Jeroudi MO, Mahmarian JJ, et al. Quantification of myocardial infarction during coronary occlusion and myocardial salvage after reperfusion using cardiac imaging with technetium-99m hexakis 2-methoxyisobutyl isonitrile. Journal of the American College of Cardiology 1988;12(6):1573–1581.

83. Sinusas AJ, Trautman KA, Bergin JD, et al. Quantification of area at risk during coronary occlusion and degree of myocardial salvage after reperfusion with technetium-99m methoxyisobutyl isonitrile. Circulation 1990;82(4):1424–1437.
84. Gibbons RJ, Verani MS, Behrenbeck T, et al. Feasibility of tomographic 99mTc-hexakis-2-methoxy-2-methylpropyl-isonitrile imaging for the assessment of myocardial area at risk and the effect of treatment in acute myocardial infarction. Circulation 1989;80(5):1277–1286.
85. Wackers FJ, Gibbons RJ, Verani MS, et al. Serial quantitative planar technetium-99m isonitrile imaging in acute myocardial infarction: efficacy for noninvasive assessment of thrombolytic therapy. Journal of the American College of Cardiology 1989;14(4):861–873.
86. Christian TF, Behrenbeck T, Pellikka PA, Huber KC, Chesebro JH, Gibbons RJ. Mismatch of left ventricular function and infarct size demonstrated by technetium-99m isonitrile imaging after reperfusion therapy for acute myocardial infarction: identification of myocardial stunning and hyperkinesia. Journal of the American College of Cardiology 1990;16(7):1632–1638.
87. Rocco TP, Dilsizian V, Strauss HW, Boucher CA. Technetium-99m isonitrile myocardial uptake at rest, II: relation to clinical markers of potential viability. Journal of the American College of Cardiology 1989;14(7):1678–1684.
88. Udelson JE, Coleman PS, Metherall J, et al. Predicting recovery of severe regional ventricular dysfunction. Comparison of resting scintigraphy with 201Tl and 99mTc-sestamibi. Circulation 1994;89(6):2552–2561.
89. Miller TD, Christian TF, Hopfenspirger MR, Hodge DO, Gersh BJ, Gibbons RJ. Infarct size after acute myocardial infarction measured by quantitative tomographic 99mTc sestamibi imaging predicts subsequent mortality. Circulation 1995;92(3):334–341.
90. Christian TF. The use of perfusion imaging in acute myocardial infarction: applications for clinical trials and clinical care. Journal of Nuclear Cardiology 1995;2(5):423–436.
91. O'Connor MK, Hammell T, Gibbons RJ. In vitro validation of a simple tomographic technique for estimation of percentage myocardium at risk using methoxyisobutyl isonitrile technetium 99m (sestamibi). European Journal of Nuclear Medicine 1990;17(1–2):69–76.
92. Vannan M, Kettle A, Coakley A, Griffith J, Udelson JE. Influence of infarct zone viability on left ventricular remodeling in the year following anterior myocardial infarction. Circulation 1995;92(I-286).
93. Klocke FJ, et al. ACC/AHA/ASNC guidelines for the clinical use of cardiac radionuclide imaging – executive summary: a report of the American College of Cardiology/American Heart Association Task Force on Practice Guidelines (ACC/AHA/ASNC Committee to Revise the 1995 Guidelines for the Clinical Use of Cardiac Radionuclide Imaging). ACC/AHA/ASNC Guidelines for Radionuclide Imaging. Circulation 2003; (11):1404–1418.
94. Klocke FJ, Baird MG, Lorell BH, et al. ACC/AHA/ASNC guidelines for the clinical use of cardiac radionuclide imaging – executive summary: a report of the American College of Cardiology/American Heart Association Task Force on Practice Guidelines (ACC/AHA/ASNC Committee to Revise the 1995 Guidelines for the Clinical Use of Cardiac Radionuclide Imaging). Journal of the American College of Cardiology 2003;42(7):1318–1333.
95. Unstable Angina Clinical Practice Guideline Number 10. AHCPR publication No. 94-0602; March 1994.
96. Braunwald E, Antman EM, Beasley JW, et al. ACC/AHA guideline update for the management of patients with unstable angina and non-ST-segment elevation myocardial infarction – 2002: summary article. A report of the American College of Cardiology/American Heart Association Task Force on Practice Guidelines (Committee on the Management of Patients With Unstable Angina). Circulation 2002;106(14):1893–1900.
97. The TIMI IIIA Investigaters. Early effects of tissue-type plasminogen activator added to conventional therapy on the culprit coronary lesion in patients presenting with ischemic cardiac pain at rest. Results of the Thrombolysis in Myocardial Ischemia (TIMI IIIA) Trial. Circulation 1993;87(1):38–52.
98. Hachamovitch R, Berman DS, Kiat H, et al. Exercise myocardial perfusion SPECT in patients without known coronary artery disease: incremental prognostic value and use in risk stratification. Circulation 1996;93(5):905–914.
99. Brown KA, Boucher CA, Okada RD, et al. Prognostic value of exercise thallium-201 imaging in patients presenting for evaluation of chest pain. Journal of the American College of Cardiology 1983;1(4):994–1001.
100. Madsen JK, Stubgaard M, Utne HE, et al. Prognosis and thallium-201 scintigraphy in patients admitted with chest pain without confirmed acute myocardial infarction. British Heart Journal 1988;59(2):184–189.
101. Marmur JD, Freeman MR, Langer A, Armstrong PW. Prognosis in medically stabilized unstable angina: early Holter ST-segment monitoring compared with predischarge exercise thallium tomography. Annals of Internal Medicine 1990;113(8):575–579.
102. Anderson HV, Cannon CP, Stone PH, et al. One-year results of the Thrombolysis in Myocardial Infarction (TIMI) IIIB clinical trial. A randomized comparison of tissue-type plasminogen activator versus placebo and early invasive versus early conservative strategies in unstable angina and non-Q wave myocardial infarction. Journal of the American College of Cardiology 1995;26(7):1643–1650.
103. Brown KA. Management of unstable angina: the role of noninvasive risk stratification. Journal of Nuclear Cardiology 1997;4(2):S164–S168.
104. Stratmann HG, Younis LT, Wittry MD, Amato M, Miller DD. Exercise technetium-99m myocardial tomography for the risk stratification of men with medically treated unstable angina pectoris. American Journal of Cardiology 1995;76(4):236–240.
105. Stratmann HG, Tamesis BR, Younis LT, Wittry MD, Amato M, Miller DD. Prognostic value of predischarge dipyridamole technetium 99m sestamibi myocardial tomography in medically treated patients with unstable angina. American Heart Journal 1995;130(4):734–740.

106. Hillert MC Jr, Narahara KA, Smitherman TC, Burden LL, Wyatt JC, III. Thallium 201 perfusion imaging after the treatment of unstable angina pectoris – relationship to clinical outcome. Western Journal of Medicine 1986;145(3):335–340.
107. Freeman MR, Chisholm RJ, Armstrong PW. Usefulness of exercise electrocardiography and thallium scintigraphy in unstable angina pectoris in predicting the extent and severity of coronary artery disease. American Journal of Cardiology 1988;62(17):1164–1170.
108. Amanullah AM, Lindvall K, Bevegard S. Prognostic significance of exercise thallium-201 myocardial perfusion imaging compared to stress echocardiography and clinical variables in patients with unstable angina who respond to medical treatment. International Journal of Cardiology 1993;39(1):71–78.
109. Effects of tissue plasminogen activator and a comparison of early invasive and conservative strategies in unstable angina and non-Q-wave myocardial infarction. Results of the Thrombolysis in Myocardial Infarction (TIMI) IIIB Trial. Circulation 1994;89(4):1545–1556.
110. Boden WE, O'Rourke RA, Crawford MH, et al., for Veterans Affairs Non-Q-Wave Infarction Strategies in Hospital (VANQWISH) Trial Investigators. Outcomes in patients with acute non-Q-wave myocardial infarction randomly assigned to an invasive as compared with a conservative management strategy. New England Journal of Medicine 1998;338(25):1785–1792.
111. Wallentin L, Swahn E, Kontny F, et al. Invasive compared with non-invasive treatment in unstable coronary-artery disease: FRISC II prospective randomised multicentre study. 1999;354(9180):708–715.
112. Goyal A, Samaha FF, Boden WE, Wade MJ, Kimmel SE. Stress test criteria used in the conservative arm of the FRISC-II trial underdetects surgical coronary artery disease when applied to patients in the VANQWISH trial. Journal of the American College of Cardiology 2002;39(10):1601–1607.
113. Cannon CP, Weintraub WS, Demopoulos LA, et al. Comparison of early invasive and conservative strategies in patients with unstable coronary syndromes treated with the glycoprotein IIb/IIIa inhibitor tirofiban. New England Journal of Medicine 2001;344(25):1879–1887.
114. Morrow DA, Cannon CP, Rifai N, et al. Ability of minor elevations of troponins I and T to predict benefit from an early invasive strategy in patients with unstable angina and non-ST elevation myocardial infarction: results from a randomized trial. JAMA 2001;286(19):2405–2412.
115. Fox KA, Poole-Wilson PA, Henderson RA, et al. Interventional versus conservative treatment for patients with unstable angina or non-ST-elevation myocardial infarction: the British Heart Foundation Randomized Intervention Trial of unstable Angina (RITA) 3 randomised trial. Lancet 2002;360(9335):743–751.
116. Solomon DH, Stone PH, Glynn RJ, et al. Use of risk stratification to identify patients with unstable angina likeliest to benefit from an invasive versus conservative management strategy. Journal of the American College of Cardiology 2001;38(4):969–976.
117. Warner M, DiSciascio G, Kohli R, et al. Frequency and predictors of left ventricular segmental dysfunction in patients with recent rest angina. American Journal of Cardiology 1992;69(19):1521–1524.
118. Nixon JV, Brown CN, Smitherman TC. Identification of transient and persistent segmental wall motion abnormalities in patients with unstable angina by two-dimensional echocardiography. Circulation 1982;65(7):1497–1503.
119. de Zwaan C, Cheriex EC, Braat SH, Stappers JL, Wellens HJ. Improvement of systolic and diastolic left ventricular wall motion by serial echocardiograms in selected patients treated for unstable angina. American Heart Journal 1991;121(3, Pt 1):789–797.
120. Narahara KA, Hillert MC Jr, Smitherman TC, Burden LL. Alterations in left ventricular function during therapy of unstable angina pectoris: relationship to clinical outcome. American Heart Journal 1984;107(2):261–269.
121. Parisi AF, Khuri S, Deupree RH, Sharma GV, Scott SM, Luchi RJ. Medical compared with surgical management of unstable angina. 5-year mortality and morbidity in the Veterans Administration Study. Circulation 1989;80(5):1176–1189.
122. McCarthy BD, Wong JB, Selker HP. Detecting acute cardiac ischemia in the ED: a review of the literature. Journal of General Internal Medicine 1990;5(4):365–373.
123. Pozen MW, D'Agostino RB, Selker HP, Sytkowski PA, Hood WB Jr. A predictive instrument to improve coronary-care-unit admission practices in acute ischemic heart disease. A prospective multicenter clinical trial. New England Journal of Medicine 1984;310(20):1273–1278.
124. McCarthy BD, Beshansky JR, D'Agostino RB, Selker HP. Missed diagnoses of acute myocardial infarction in the ED: results from a multicenter study. Annals of Emergency Medicine 1993;22(3):579–582.
125. Wackers FJ, Sokole EB, Samson G, et al. Value and limitations of thallium-201 scintigraphy in the acute phase of myocardial infarction. New England Journal of Medicine 1976;295(1):1–5.
126. Wackers FJ, Lie KI, Liem KL, et al. Thallium-201 scintigraphy in unstable angina pectoris. Circulation 1978;57(4):738–742.
127. Bilodeau L, Theroux P, Gregoire J, Gagnon D, Arsenault A. Technetium-99m sestamibi tomography in patients with spontaneous chest pain: correlations with clinical, electrocardiographic and angiographic findings. Journal of the American College of Cardiology 1991;18(7):1684–1691.
128. Christian TF, Clements IP, Gibbons RJ. Noninvasive identification of myocardium at risk in patients with acute myocardial infarction and nondiagnostic electrocardiograms with technetium-99m-sestamibi. Circulation 1991;83(5):1615–1620.
129. Varetto T, Cantalupi D, Altieri A, Orlandi C. Emergency room technetium-99m sestamibi imaging to rule out acute myocardial ischemic events in patients with nondiagnostic electrocardiograms. Journal of the American College of Cardiology 1993;22(7):1804–1808.
130. Hilton TC, Thompson RC, Williams HJ, Saylors R, Fulmer H, Stowers SA. Technetium-99m sestamibi myocardial perfusion imaging in the emergency room evaluation of

chest pain. Journal of the American College of Cardiology 1994;23(5):1016–1022.
131. Weissman IA, Dickinson CZ, Dworkin HJ, O'Neill WW, Juni JE. Cost-effectiveness of myocardial perfusion imaging with SPECT in the ED evaluation of patients with unexplained chest pain. Radiology 1996;199(2):353–357.
132. Tatum JL, Jesse RL, Kontos MC, et al. Comprehensive strategy for the evaluation and triage of the chest pain patient. Annals of Emergency Medicine 1997;29(1):116–125.
133. Kontos MC, Jesse RL, Schmidt KL, Ornato JP, Tatum JL. Value of acute rest sestamibi perfusion imaging for evaluation of patients admitted to the ED with chest pain. Journal of the American College of Cardiology 1997;30(4):976–982.
134. Heller GV, Stowers SA, Hendel RC, et al. Clinical value of acute rest technetium-99m tetrofosmin tomographic myocardial perfusion imaging in patients with acute chest pain and nondiagnostic electrocardiograms. Journal of the American College of Cardiology 1998;31(5):1011–1017.
135. Kontos MC, Jesse RL, Anderson FP, Schmidt KL, Ornato JP, Tatum JL. Comparison of myocardial perfusion imaging and cardiac troponin I in patients admitted to the ED with chest pain. Circulation 1999;99(16):2073–2078.
136. Duca MD, Giri S, Wu AH, et al. Comparison of acute rest myocardial perfusion imaging and serum markers of myocardial injury in patients with chest pain syndromes. Journal of Nuclear Cardiology 1999;6(6):570–576.
137. Kosnik JW, Zalenski RJ, Shamsa F, et al. Resting sestamibi imaging for the prognosis of low-risk chest pain. Academic Emergency Medicine 1999;6(10):998–1004.
138. Udelson JE, Beshansky JR, Ballin DS, et al. Myocardial perfusion imaging for evaluation and triage of patients with suspected acute cardiac ischemia: a randomized controlled trial. JAMA 2002;288(21):2693–2700.
139. Dinckal MH, Aksoy N, Aksoy M, et al. Acute rest perfusion imaging in high risk unstable angina: association with troponin T and clinical endpoints. International Journal of Cardiovascular Imaging 2003;19(6):511–517.
140. Kaul S, Senior R, Firschke C, et al. Incremental value of cardiac imaging in patients presenting to the ED with chest pain and without ST-segment elevation: a multicenter study. American Heart Journal 2004;148(1):129–136.
141. Kontos MC, Fratkin MJ, Jesse RL, Anderson FP, Ornato JP, Tatum JL. Sensitivity of acute rest myocardial perfusion imaging for identifying patients with myocardial infarction based on a troponin definition. Journal of Nuclear Cardiology 2004;11(1):12–19.
142. Swinburn JM, Stubbs P, Soman P, et al. Rapid assessment of patients with non-ST-segment elevation acute chest pain: troponins, inflammatory markers, or perfusion imaging? Journal of Nuclear Cardiology 2002;9(5):491–499.
143. Stowers SA, Eisenstein EL, Th Wackers FJ, et al. An economic analysis of an aggressive diagnostic strategy with single photon emission computed tomography myocardial perfusion imaging and early exercise stress testing in ED patients who present with chest pain but nondiagnostic electrocardiograms: results from a randomized trial. Annals of Emergency Medicine 2000;35(1):17–25.
144. Hendel RC, Udelson JE, Ruthazer R, et al. Does the absence of active chest pain at the time of Tc-99m sestamibi injection affect the value of rest Tc-99m sestamibi imaging for ED patients with acute chest pain? [abstract]. Circulation 2000;102(II):543.
145. Fram DB, Azar RR, Ahlberg AW, et al. Duration of abnormal SPECT myocardial perfusion imaging following resolution of acute ischemia: an angioplasty model. Journal of the American College of Cardiology 2003;41(3):452–459.
146. Ziffer JA, Nateman DR, Janowitz WR, Williams K, Shaw L. Improved patient outcomes and cost effectiveness of utilizing nuclear cardiology protocols in an emergency department chest pain center: two year results in 6458 patients (Abstract). Journal of Nuclear Medicine 1998;39(5, Suppl):139P (Abstract).
147. Radensky PW, Hilton TC, Fulmer H, McLaughlin BA, Stowers SA. Potential cost effectiveness of initial myocardial perfusion imaging for assessment of ED patients with chest pain. American Journal of Cardiology 1997;79(5):595–599.
148. Hauser AM, Gangadharan V, Ramos RG, Gordon S, Timmis GC. Sequence of mechanical, electrocardiographic and clinical effects of repeated coronary artery occlusion in human beings: echocardiographic observations during coronary angioplasty. Journal of the American College of Cardiology 1985;5(2, Pt 1):193–197.
149. Beller GA. Myocardial perfusion imaging for detection of silent myocardial ischemia. American Journal of Cardiology 1988;61(12):22F–28F.
150. Sasaki H, Charuzi Y, Beeder C, Sugiki Y, Lew AS. Utility of echocardiography for the early assessment of patients with nondiagnostic chest pain. American Heart Journal 1986;112(3):494–497.
151. Sabia P, Afrookteh A, Touchstone DA, Keller MW, Esquivel L, Kaul S. Value of regional wall motion abnormality in the emergency room diagnosis of acute myocardial infarction. A prospective study using two-dimensional echocardiography. Circulation 1991;84(3, Suppl):I85–I92.
152. Peels CH, Visser CA, Kupper AJ, Visser FC, Roos JP. Usefulness of two-dimensional echocardiography for immediate detection of myocardial ischemia in the emergency room. American Journal of Cardiology 1990;65(11):687–691.
153. Gibler WB, Runyon JP, Levy RC, et al. A rapid diagnostic and treatment center for patients with chest pain in the ED. Annals of Emergency Medicine 1995;25(1):1–8.
154. Trippi JA, Lee KS, Kopp G, Nelson DR, Yee KG, Cordell WH. Dobutamine stress tele-echocardiography for evaluation of ED patients with chest pain. Journal of the American College of Cardiology 1997;30(3):627–632.
155. Kontos MC, Arrowood JA, Paulsen WH, Nixon JV. Early echocardiography can predict cardiac events in ED patients with chest pain. Annals of Emergency Medicine 1998;31(5):550–557.
156. Hendel RC, Selker HP, Heller GV, et al. The impact of attenuation correction and gating on SPECT perfusion imaging in patients presenting to the ED with chest pain [abstract]. Circulation 2000;102(II-543).

10 Clinical value of assessment of perfusion and function for the evaluation of myocardial viability in patients with ischemic left ventricular dysfunction

Jeroen J. Bax
Don Poldermans

Introduction

Heart failure has become one of the largest clinical problems in cardiology. Over the last years, the number of patients presenting with heart failure has increased exponentially and is projected to double in the next few years. Recent estimations have indicated that 4.7 million patients in the United States have chronic heart failure, with 400,000 new patients per year, resulting in 1 million hospitalizations [1]. From a pooled analysis of 13 randomized studies published in the *New England Journal of Medicine* on drug therapy in heart failure, it became clear that almost 70% of more than 20,000 patients had coronary artery disease as the underlying cause of heart failure [1]. This percentage may even be higher since a substantial number of patients in these studies did not undergo cardiac catheterization.

The various therapeutic options for the patients with heart failure secondary to ischemic left ventricular (LV) dysfunction are summarized in Table 10.1. *Medical therapy* forms the cornerstone of treatment in heart failure. Many improvements in medical therapy have been obtained over the past years. Angiotensin-converting enzyme (ACE) inhibitors have been demonstrated to improve survival in large heart failure studies such as the SAVE and SOLVD trials [2,3]. In patients with ischemic heart failure, the survival benefit of ACE inhibition is likely due to prevention (or reversal) of LV remodeling and hypertrophy, but a significant reduction in acute ischemic events has also been demonstrated. In addition, angiotensin-II receptor blockers have been evaluated in patients with heart failure. Data from the ELITE II trial (a direct comparison with ACE inhibitors) demonstrated that angiotensin-II receptor blockers had a comparable reduction in mortality [4]. Various trials with β-blockers have shown the benefit of these drugs in patients with heart failure [5]. Meta-analysis of 22 trials (>10,000 patients) on the use of β-blockers in heart failure have demonstrated a clinically meaningful reduction in mortality and morbidity [6]. Four major trials in ischemic heart disease have all demonstrated a reduction in overall mortality and sudden death with the use of β-blockers [7]. Also, blockade of aldosterone receptors by spironolactone has been demonstrated useful in the treatment of heart failure in the RALES study [8], and amiodarone has been demonstrated to reduce sudden death in patients with heart failure [9]. Still, the long-term prognosis remains poor when patients are treated medically. In particular, recent data from Cowie et al. [10] showed a 1-year mortality of 38%, and when these results are extrapolated to 5-year survival, the results are not that different from those obtained in the Framingham study [11].

Heart transplantation has an excellent long-term prognosis; in a recent review Kirklin et al. [12] reported that the 1-year and 7-year survival approached 90 and 75%, respectively. On the other hand, the limited amount over donor hearts does not meet the enormous demand, and is therefore no realistic option in clinical cardiology.

Cardiac resynchronization therapy is a relatively new therapeutic option for patients with heart failure [13]. Pacing of the left ventricle (in addition to right ventricular pacing) has resulted in an improvement in symptoms, quality-of-life score, exercise capacity, and LV systolic function [13]. This therapy is effective in patients with severe heart failure, dilated cardiomyopathy, and wide QRS complex (>120 ms). Still, despite these selection criteria, 30% of patients do not respond to cardiac resynchronization therapy, and it has been postulated that LV dyssynchrony is mandatory to respond to this therapy [14].

Surgery in patients with heart failure has become more popular over the recent years. In 1994, Baker et al. [15] published a meta-analysis on studies reporting on surgical revascularization in patients with depressed LV ejection

Table 10.1 Current therapeutic options for ischemic cardiomyopathy.

- Medical therapy
  - Many (new) medications: diuretics, digoxin, ACE inhibitors, AT-II receptor blockers, β-blockers, spironolactone
  - Still survival on medical therapy is poor
- Heart transplantation
  - Good long-term survival
  - Limited number of donor heart does not meet large demand
- Cardiac resynchronization therapy
  - Improvement in symptoms, exercise capacity, systolic LV function
  - Reduction in hospitalization, maybe in heart failure mortality
  - 30% of patients do not respond, due to absence of LV dyssynchrony
- Surgery
  - Revascularization if viable myocardium present, but associated risk is high
  - Additional surgery: mitral valve repair, LV aneurysmectomy, LV restoration

fraction (LVEF <40%). The results indicated that (peri-) operative mortality was high, ranging from 5 to 30% depending on the baseline LVEF and comorbidity. Moreover, based on the available studies, the benefit of patients with heart failure without concomitant angina was unclear. The observational work by Rahimtoola, however, has demonstrated that improvement in LV function can be observed after revascularization [16]. Since LV function is an important prognostic parameter, in particular in heart failure patients with severely depressed LV function, focus has shifted to preoperative identification of patients who may improve in LV function post-revascularization. To understand the improvement in LVEF post-revascularization in some patients, the concept of myocardial viability has been introduced. In some patients, dysfunctional myocardium is still alive, although resting contraction is reduced or absent and revascularization may improve function. In other patients, dysfunctional myocardium is secondary to scar tissue and revascularization will not improve LV function. This awareness has resulted in the development of techniques that are capable of detecting viable myocardium predicting improved function post-revascularization. Currently, various techniques are used and this chapter is focused on the use of perfusion and function (in particular contractile reserve) to assess viability.

Pathophysiology of dysfunctional but viable myocardium

Initially, it was thought that dysfunctional myocardium, related to coronary artery disease, was equivalent to myocardial scar formation. However, various studies demonstrated that improvement of function after revascularization was possible. In particular, Dilsizian et al. [17] studied 27 patients before and after revascularization and demonstrated an average improvement in LVEF from $55 \pm 9\%$ to $60 \pm 8\%$, with a significant improvement in 74% of patients. To evaluate the changes in LVEF in patients with depressed LVEF, Schinkel et al. [18] performed an observational study in 258 consecutive patients with ischemic cardiomyopathy (mean LVEF $29 \pm 7\%$) who were referred for surgical revascularization. The authors demonstrated that significant improvement in LVEF occurred in 39% of patients. Also, 19% showed a worsening in LVEF and 42% remained unchanged in LVEF (Fig. 10.1).

The potential improvement in LVEF is considered to be the result of revascularization of jeopardized but viable myocardium – jeopardized in terms of reduced resting flow or reduced flow reserve. Rahimtoola popularized the term *hibernation* for a process described as follows: a condition of chronic sustained abnormal contraction due to chronic underperfusion in patients with coronary artery disease in whom revascularization causes recovery of LV function [19]. Indeed, various studies have shown that resting blood flow in dysfunctional segments with improved function post-revascularization was reduced pre-revascularization as compared to remote, normal myocardium. For example, Maes and colleagues [20] evaluated 17 patients with positron emission tomography (PET) using ^{13}N-ammonia to evaluate blood flow. Blood flow in segments with reversible dysfunction was 62 ± 14 ml/(min 100 g tissue) as compared to 93 ± 11 ml/(min 100 g tissue) ($P < 0.05$). Much of the work coming from Vanoverschelde and Melin [21], however, demonstrated that resting blood flow was not significantly reduced in dysfunctional myocardium that showed improved function post-revacularization. Depre and colleagues [22] demonstrated that resting blood flow was 88 ± 23 ml/(min 100 g tissue) in dysfunctional segments with improved function post-revascularization, as compared to 100 ± 18 ml/(min 100 g tissue) in remote

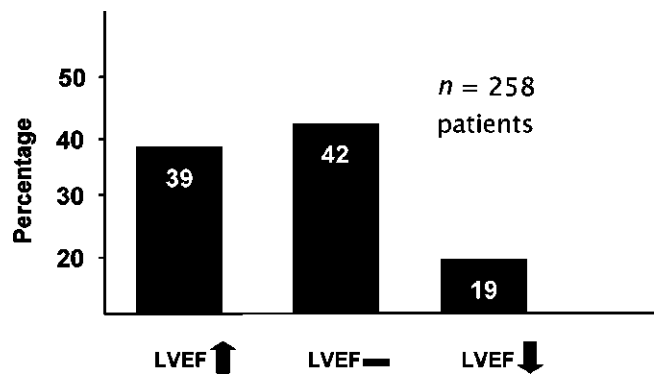

Figure 10.1 Incidence of significant improvement in LVEF post-revascularization in 258 consecutive patients with ischemic cardiomyopathy (mean LVEF 29 ± 7) undergoing surgical revascularization. (Based on [18].)

myocardium (not significant, NS). In his landmark paper, Vanoverschelde et al. [23] demonstrated that the flow reserve, however, was blunted in the dysfunctional segments that improved in LV function post-revascularization. On the basis of their observations, the authors suggested that repeated ischemic attacks may result in chronic dysfunction, with resting flow remaining normal or mildly reduced, a condition termed *repetitive stunning* [23]. In a summary of 18 PET studies [$n = 295$ patients) with quantitative flow analyses, it became evident that 7 studies had shown normal resting flow in reversible dysfunctional myocardium, whereas 11 studies had demonstrated reduced resting flow [20]. Of interest, the highest resting flow in chronic reversible dysfunctional segments was 101 ± 23 ml/(min 100 g tissue), whereas the lowest flow value was 55 ± 13 ml/(min 100 g tissue). Thus, it appears that a continuum exists in jeopardized dysfunctional myocardium from normal resting flow to severely reduced resting flow.

Over the last few years, various animal studies have been performed to better understand the issue of resting flow in chronic reversible LV dysfunction. Early work in short-term (1-week) models of coronary stenosis demonstrated preserved resting perfusion [24] in dysfunctional zones. Animal models with induction of chronic coronary artery stenosis for 6 weeks revealed the following results [25–27]: dysfunction occurred early after introduction of the coronary artery stenosis, while flow remained (near-) normal, consistent with stunning. Postmortem histopathological examination of these regions did not show evidence of necrosis. Later in time however, some dysfunctional segments developed a gradual decrease in resting flow. These later findings are consistent with hibernation, although partial infarction occurring over time may have influenced results. Fallavolita and Canty [25,26] have shown in a pig model of chronic hibernation that flow was normal at 1–2 months with a reduced flow reserve (indicative of chronic stunning), whereas resting flow became reduced at 3–4 months (indicative of hibernation). These observations support the hypothesis that a temporal progression exists from stunning, characterized by (near-) normal flow (with reduced flow reserve) to hibernation, with reduced resting flow. In the clinical setting different situations may coexist in the same patient. For these reasons, the term "jeopardized myocardium" may include the entire spectrum from (repetitive) stunning to hibernation. Indeed, Hernandez-Pampaloni et al. [28] recently evaluated 116 patients with chronic ischemic LV dysfunction; all patients underwent PET to assess perfusion and glucose utilization (to evaluate viability). In these 116 patients, 834 dysfunctional segments were identified, with 675 viable (based on preserved glucose utilization) and 159 scar segments (with reduced glucose utilization). The majority of the viable segments had normal flow (indicating stunning), whereas only 11% had reduced flow, indicating hibernation. In the clinical setting, differentiation between stunning and hibernation may be less relevant, since both conditions need revascularization with restoration of adequate flow.

Clinical relevance of myocardial viability

For many years, the clinical relevance of myocardial viability for patient management was unclear, and physicians were questioning the incidence of viable myocardium in patients with chronic LV dysfunction. Accordingly, various studies have focused on the incidence of myocardial viability. Schinkel et al. [29] evaluated 104 patients with chronic ischemic LV dysfunction (mean LVEF $25 \pm 7\%$) using perfusion/metabolic imaging with technetium-99m tetrofosmin and F18-fluorodeoxyglucose (FDG) and showed that 61% of patients had residual viability. Of interest, the number of dysfunctional segments was highest (7.2 ± 4.0) in the 23 patients with the lowest LVEF ($\leq$20%) (Fig. 10.2). Various other studies demonstrated substantial viability in a large subset of patients with chronic ischemic LV dysfunction (Table 10.2). These observations underscored that viability is not uncommon and systematic evaluation for it is necessary.

Using viability assessment, it has become possible to predict outcome after revascularization. In different studies, different endpoints after revascularization have been used (summarized in Table 10.3).

Initially, the studies aimed at prediction of improvement of regional LV function. Pooled data from 105 viability studies ($n = 3003$ patients), included 15,045 dysfunctional segments, with 7941 (53%) improving in function after revascularization [35]. Pooled analysis revealed

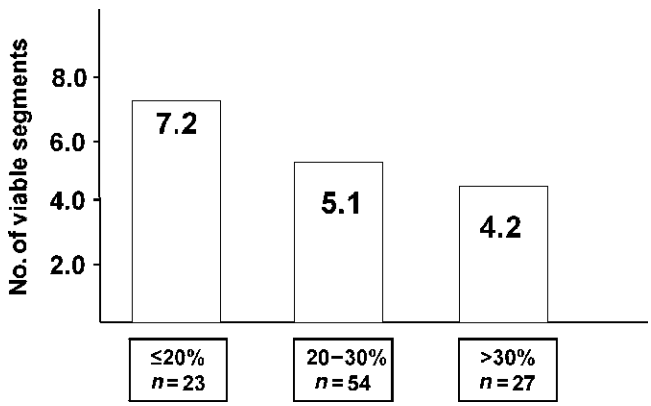

Figure 10.2 The mean number of dysfunctional but viable segments in 104 patients with ischemic cardiomyopathy, divided according to baseline LVEF. The number of dysfunctional segments was highest in patients with the lowest LVEF. (Based on [29].)

Table 10.2 Incidence of viability in patients with chronic ischemic LV dysfunction.

Author	No. of points	LVEF	Viability technique	Incidence of viability
Al-Mohammad [30]	27	19 ± 6%	PET	52%
Auerbach [31]	283	26 ± 8%	PET	55%
Schinkel [29]	104	25 ± 7%	SPECT	61%
Fox [32]	27	NA	SPECT	37%
Schinkel [33]	150	31 ± 12%	DSE	58%

Abbreviation: DSE, dobutamine stress echocardiography; LVEF, left ventricular ejection fraction; PET, positron emission tomography; SPECT, single photon emission computed tomography.

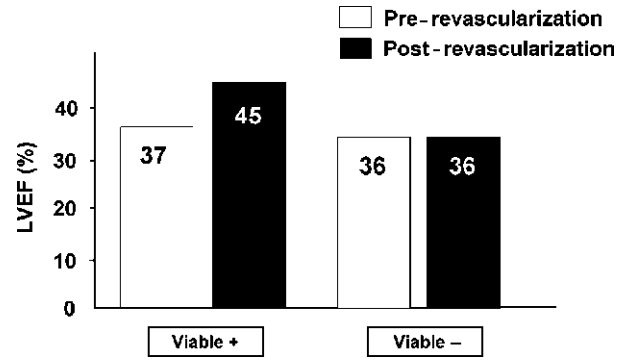

Figure 10.3 Pooling of 29 studies (with 758 patients) focusing on the prediction of LVEF after revascularization using different viability techniques demonstrated a significant improvement in LVEF post-revascularization in viable patients, while LVEF did not improve in the nonviable patients. (Based on [36].)

a sensitivity of 84% with a specificity of 69% to *predict improvement of regional LV function* [35]. From a clinical point of view, the *prediction of improvement of global LV function* (or LVEF) is more important. When data from 29 viability studies ($n = 758$ patients) on prediction of improvement in LVEF were pooled, it became evident that an improvement in LVEF was observed only in the patients with viable myocardium, whereas no improvement occurred in the patients without viable myocardium (Fig. 10.3) [36]. The precise amount of viable myocardium to predict improvement in LVEF, however, is still unclear, but it appears to be quite large. Some studies suggested that 20–30% of the left ventricle needs to be viable to result in improvement in LVEF.

While improvement in LV function has been the principal focus of most studies, whether improvement in symptoms and exercise capacity is related to viability has also been addressed. In particular, Di Carli et al. [37] evaluated 36 patients with FDG PET and demonstrated that an *increase in exercise capacity* as expressed in METS was related to the preoperative extent of viable myocardium (Fig. 10.4).

Few studies have focused on the relation between viability and *reverse LV remodeling*. These studies have shown that patients with extensive viable myocardium showed a significant reduction in LV volumes after revascularization [38,39]. Finally, various studies have evaluated the *prognostic value* of viability in relation to therapy [40]. These studies consistently showed a low event-rate in patients with viable myocardium who underwent revascularization, suggesting that revascularization stabilizes the unstable substrate of dysfunctional but viable myocardium. Pooling of 17 prognostic studies with various viability techniques showed a 7% event-rate in viable patients undergoing revascularization, as compared to a 20% event-rate in viable patients who were treated medically [36] (Fig. 10.5).

All these findings support the need and clinical relevance of viability assessment in patients with chronic LV dysfunction.

Table 10.3 Potential endpoints to measure outcome after revascularization in viability studies.

- Improvement of regional LV function
- Improvement of global LV function (LVEF)
- Improvement of symptoms
- Improvement of exercise capacity
- Reverse LV remodeling
- Long-term prognosis

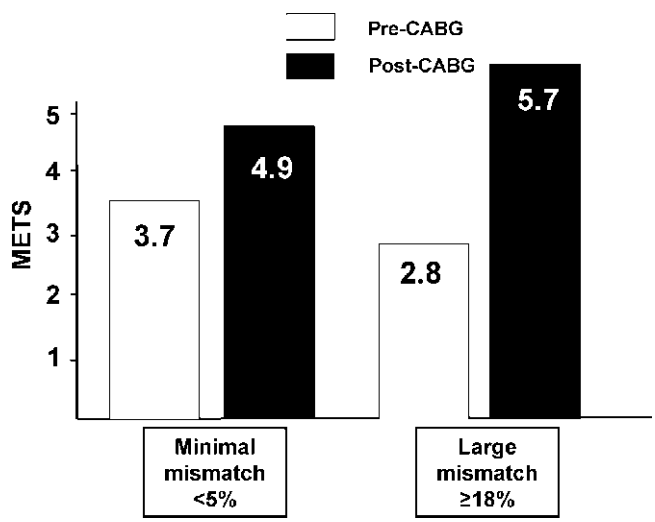

Figure 10.4 Changes in exercise capacity (METS) according to the extent of viable myocardium on FDG PET. Patients with a larger extent of viable myocardium showed a larger increase in exercise capacity post-revascularization. (Data based on [37].)

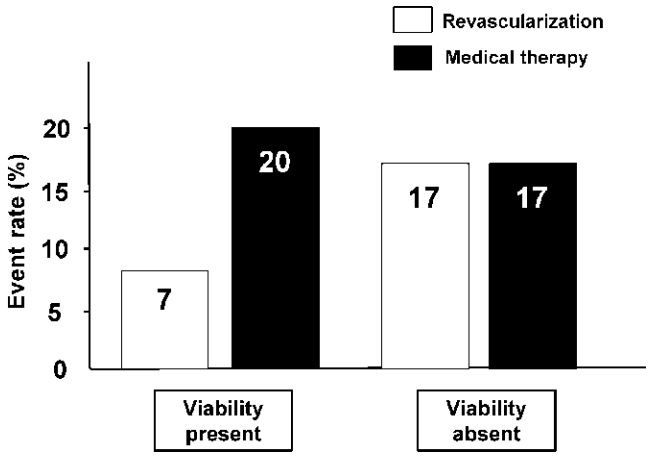

Figure 10.5 Pooling of 17 prognostic studies with various viability techniques showed a 7% event-rate in viable patients undergoing revascularization, as compared to a 20% event-rate in viable patients who were treated medically; and intermediate event-rates (17%) in nonviable patients. (Based on [36].)

Viability techniques

At present, several techniques are available for assessment of myocardial viability, focusing on various characteristics of dysfunctional but viable myocardium. These characteristics include intact perfusion, cell membrane integrity, intact mitochondria, preserved glucose and (possibly) fatty acid metabolism, and contractile reserve (Table 10.4) [36]. All of these characteristics can be evaluated by scintigraphic techniques (using PET or SPECT; see Table 10.4). Besides scintigraphy, echocardiography (using tissue Doppler imaging, dobutamine stress, or intravenous contrast) and magnetic resonance imaging (MRI) (using dobutamine stress or contrast agents) have also been used for assessment of viability (Table 10.4). In the clinical setting, assessments of function (contractile reserve) and perfusion are the most important tool for assessing viability. The available evidence with imaging of perfusion and contractile reserve (function) will be summarized in the remainder of this chapter. Applications of MRI will not be addressed here but are discussed in detail in Chapter 13.

Table 10.4 Imaging techniques versus characteristics of dysfunctional but viable myocardium.

Tracer, imaging modality	Characteristics
Thallium-201 chloride SPECT	Perfusion Intact cell membrane
Technetium-99m labeled tracers SPECT	Perfusion Intact cell membrane Intact mitochondria
F18-fluorodeoxyglucose PET or SPECT	Glucose metabolism
BMIPP SPECT	Free fatty acid metabolism
Echocardiography	
Dobutamine stress	Contractile reserve
Intravenous contrast	Perfusion
Tissue Doppler	Postsystolic thickening
Magnetic resonance imaging	
Dobutamine stress	Contractile reserve
Contrast agents	Scar tissue

Assessment of perfusion and cell membrane integrity for viability

The most frequently used nuclear imaging technique to assess viability by means of perfusion in the clinical setting is SPECT imaging with either thallium-201 chloride or technetium-99m labeled tracers (sestamibi or tetrofosmin). More recently, myocardial contrast echocardiography (MCE) has also been used for the assessment of perfusion to detect viable myocardium.

Thallium-201

Thallium-201 has been used for many years, and a variety of protocols have been employed; the two most important protocols are rest-redistribution and stress-redistribution-reinjection imaging [41]. Rest-redistribution provides information only on viability, whereas the stress-redistribution-reinjection protocol provides information on both viability and stress-induced ischemia. With rest-redistribution imaging, two sets of images are acquired: the first set of images (obtained directly following tracer injection) represents perfusion and the second set of images (obtained 3–4 h after tracer injection) allows assessment of viability. With the stress-redistribution-reinjection protocol, initial images are obtained early after stress and a second set of images is obtained 3–4 hours later (redistribution images). Subsequently, a second dose of thallium-201 chloride is injected, and 1 hour thereafter reinjection images are acquired. The stress and redistribution images allow assessment of ischemia, and the reinjection images provide further information on viability (some of the viable myocardium is already documented by the stress/redistribution images alone).

Markers of viability on thallium-201 studies are (1) normal thallium-201 uptake (normal perfusion) at stress; (2) perfusion defects on the stress or rest images with redistribution on delayed images (frequently a threshold of

20% increase in tracer uptake is used) on any of the other images (reversible defects); (3) tracer uptake greater than 50% on the redistribution or the reinjection images [41]. The first of these could apply to viable myocardium after reperfusion – such as might be seen with true stunning after successful stenting or thrombolysis. The second (reversible defects) appears to reflect adequately jeopardized but viable myocardium. The third criterion – that of 50% or more tracer uptake – is more problematic. Frequently, segments with 50% or more tracer uptake do not improve in function after revascularization. The principal reason for this observation is the presence of nontransmural infarction, rather than jeopardized, viable myocardium [42]. These segments are not capable of improving function post-revascularization and this will affect specificity of the technique to predict absence of functional recovery. Thirty-three studies (22 using rest-redistribution and 11 using a reinjection protocol) with a total of 858 patients have focused on *prediction of improvement of regional function* post-revascularization [35]. The mean sensitivity and specificity of these studies were 86 and 59% [35]. The lower specificity can be ascribed to the use of cutoff levels (usually tracer uptake >50 to 65%), which do not accurately reflect jeopardized, viable myocardium but frequently reflect subendocardial scars. To further evaluate this problem, Kitsiou et al. [42] studied 24 patients with ischemic cardiomyopathy with thallium-201 stress-redistribution-reinjection imaging prior to revascularization. Indeed, only 30% of segments with fixed defects classified viable because of thallium-201 uptake greater than 50% demonstrated recovery of function post-revascularization. However, when the fixed defects with tracer uptake greater than 50% were divided into with and without inducible ischemia (thus having jeopardized myocardium or not), it became evident that segments without inducible ischemia, but with tracer uptake greater than 50% had a low likelihood of recovery of function post-revascularization (Fig. 10.6). This approach (adding the information of ischemia) allows more accurate prediction of recovery of function post-revascularization.

Improvement of global LV function has been reported combining information from five studies with 96 patients. On average, the LVEF improved from 30 to 38% in patients with viable myocardium. In patients without viable myocardium, the LVEF remained unchanged (29% vs. 31%) [43]. Only one study has focused on the relation between *improvement in symptoms and reverse LV remodeling*. Mule and coworkers [38] evaluated 50 patients with ischemic cardiomyopathy with thallium-201 stress-redistribution-reinjection SPECT prior to revascularization. Patients with jeopardized myocardium improved in LVEF (from $35 \pm 6\%$ to $43 \pm 6\%$, $P < 0.001$) and showed reverse LV remodeling post-revascularization: LV end-systolic volume index decreased from 68 ± 16 to 52 ± 14 ml/m^2 ($P < 0.001$) and LV end-diastolic volume index decreased from 103 ± 21 to 91 ± 18 ml/m^2 ($P < 0.001$). The "viable" patients also improved in New York Heart Association (NYHA) class. In contrast, patients with scar tissue did not improve in LVEF ($34 \pm 4\%$ vs. $33 \pm 7\%$, NS), and showed further LV dilatation: LV end-systolic volume index increased from 70 ± 14 to 78 ± 23 ml/m^2($P < 0.001$) and LV end-diastolic volume index increased from 106 ± 19 to 116 ± 25 ml/m^2 ($P < 0.001$). These patients also did not improve in NYHA class.

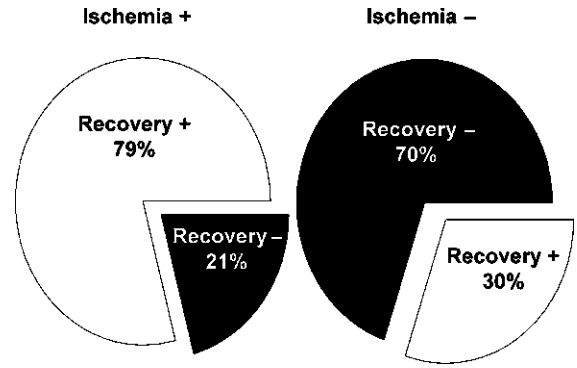

Figure 10.6 Segments with fixed defects on thallium-201 stress-redistribution-reinjection imaging with thallium-201 uptake greater than 50% may or may not improve in function post-revascularization. When inducible ischemia is present (left pie chart), the likelihood of recovery is significantly larger than when inducible ischemia is absent (right pie chart). (Based on [42].)

Long-term prognosis in patients with respect to viability has been evaluated in patients with thallium-201 imaging [44–47]. These studies were uniform in demonstrating that a superior long-term survival was present in patients with viable myocardium who underwent revascularization. The most comprehensive study was reported by Pagley et al. [46] who studied 70 patients with depressed LVEF; the patients were divided into two groups, according to the presence or absence of a substantial amount of viable myocardium. All underwent surgical revascularization; the cardiac death rate was significantly lower in patients with viable myocardium as compared to patients without viable myocardium (18% vs. 41%).

Technetium-99m sestamibi and tetrofosmin

The uptake and retention of these tracers depends on perfusion, cell membrane integrity, and mitochondrial function [48]. Most studies for assessment of viability have been performed with technetium-99m sestamibi [35], but recent studies with technetium-99m tetrofosmin have shown a comparable value of this tracer for the assessment

of viability [49]. The role of technetium-99m labeled agents for the detection of viable myocardium has been debated, since initially underestimation of viable myocardium was reported [50]. To improve the detection of viability with sestamibi, several modifications of the imaging protocol have been proposed. Early on, it was suggested that acquisition of an additional redistribution image (4 h following the initial resting image) or quantitative analysis of resting regional sestamibi activity resulted in more accurate identification of viability [51,52] compared to visual inspection of rest images alone. Several groups have performed studies with sestamibi SPECT following administration of nitrates (either orally or intravenously) [53]. It is thought that nitrates enhance blood flow (and tracer uptake) to myocardial regions that are subtended by severely stenosed arteries, i.e., hibernating myocardium. Bisi and coworkers [54] have demonstrated excellent results with nitrate-enhanced sestamibi SPECT imaging for the detection of viable myocardium. Currently, with most of the protocols used, the following criteria are used for assessment of viable myocardium with sestamibi imaging: greater than 50 to 60% tracer uptake (or a somewhat lower uptake in the inferior regions, since attenuation may falsely "lower" activity in this region [55]) or defect reversibility after nitrate administration.

Twenty studies (including seven following nitrate administration) with a total of 488 patients have focused on prediction of *improvement of regional function* post-revascularization [35]. The mean sensitivity and specificity of these studies were 81 and 66% [35]. Most of the studies used a resting image and segments were classified as viable when activity exceeded a certain threshold (frequently 50–60%). These cutoff levels however cannot differentiate between jeopardized, viable myocardium and nontransmural infarction, resulting in overestimation of recovery of function with lower specificity for prediction of functional recovery. When the nitrate-enhanced studies were analyzed separately (seven studies, 180 patients), a sensitivity of 86% and a specificity of 83% were obtained [35].

Improvement of global LV function was evaluated in four studies, with 75 patients; on average, the LVEF improved from 47 to 53% in patients with viable myocardium [43]. In patients without viable myocardium, the LVEF remained unchanged (40% vs. 39%). Of note, the LVEF was relatively preserved in the studies, whereas viability assessment is most important in patients with severely depressed LVEF.

There are no studies employing sestamibi imaging focusing at prediction of improvement of heart failure symptoms in relation to viability, and only one study with sestamibi imaging is available on *the long-term prognosis* in patients with ischemic cardiomyopathy [56]. Sciagra and coworkers [56] evaluated 105 patients with chronic coronary artery disease and LV dysfunction; all underwent nitrate-enhanced sestamibi imaging. The most important prognostic predictor of future cardiac events was the number of nonrevascularized dysfunctional regions with viable tissue on sestamibi imaging, emphasizing the value of viability but also the value of adequate revascularization.

Myocardial contrast echocardiography

The improved technical properties of the myocardial contrast agents now allow for assessment of myocardial perfusion [57]. Whereas in the early studies intracoronary injection of contrast was still needed, the more recently developed contrast agents allow intravenous administration. The recent contrast agents are composed of high-molecular-weight inert gases. The microbubbles stay in the vascular space and do not enter the extravascular space; within the vascular space, microbubbles behave like red cells in terms of rheology and can be used in combination with echocardiography to visualize directly the myocardial perfusion. Since myocardial perfusion is a prerequisite for myocardial viability, MCE has been used to assess tissue viability. Shimoni et al. [58] showed that MCE parameters of myocardial perfusion correlate positively with the microvascular density and the capillary area and inversely with the extent of fibrosis. In the clinical setting, myocardial perfusion by MCE is evaluated qualitatively, and segments are visually classified as having normal, patchy, or absent perfusion [59]. Nagueh et al. [60] performed a direct comparison between dobutamine stress echocardiography, thallium-201 imaging, and MCE in 18 patients undergoing revascularization. Both thallium-201 imaging and MCE had a high sensitivity with a lower specificity, whereas dobutamine stress echocardiography had a lower sensitivity with a relatively high specificity for the prediction of improvement after revascularization. In that study, MCE had a sensitivity of 89% and a specificity of 51% for the prediction of *improvement of regional function* post-revascularization. Additional studies using MCE confirmed this observation and consistently showed a high sensitivity with a lower specificity [61]. Similar to the problems encountered with nuclear imaging, the lower specificity is in part related to the presence of nontransmural infarction. These regions contain some (epicardial) viable myocardium with intact perfusion, but will not improve in function post-revascularization. The same authors demonstrated that patients with three or more viable segments on MCE had a high likelihood of *improvement in global LV function* post-revascularization. Currently, no MCE studies on improvement in symptoms or long-term outcome are available.

Table 10.5 Wall motion patterns during dobutamine stress.

1 *Biphasic reponse*: initial improvement followed by worsening of wall motion
2 *Worsening*: direct deterioration of wall motion without initial improvement
3 *Sustained improvement*: improvement of wall motion without subsequent deterioration
4 *No change*: no change in wall motion during the entire examination

Pattern 1 represents viability with superimposed ischemia
Pattern 2 represents ischemia, myocardium perfused by a critically stenosed vessel
Pattern 3 represents subendocardial necrosis
Pattern 4 represents transmural scar tissue

Assessment of contractile reserve for viability

Infusions of low-dose dobutamine (5–10 mcg/(kg min)) have been demonstrated to increase contractility (without a substantial increase in heart rate) in dysfunctional but viable myocardium; this phenomenon has been referred to as "contractile reserve." This contractile reserve is the hallmark of viable myocardium. In the initial studies only low-dose dobutamine was used, but more recent studies have employed a low–high dose dobutamine protocol; this protocol (with infusions up to 40 mcg/kg/min with addition of atropine if needed) permits detection of both viability and ischemia (Table 10.5). The safety of the low–high dose protocol in patients with severely depressed LVEF was demonstrated recently [62]. Visualization of wall motion during the dobutamine infusion is needed and can be performed using echocardiography or gated SPECT (or gated PET) imaging.

Dobutamine stress echocardiography

Traditionally, echocardiography has been used to evaluate wall motion during dobutamine stress. Thirty-two studies are available using dobutamine stress echocardiography with a total of 1090 patients, to predict *improvement of regional function* post-revascularization [35]. The mean sensitivity and specificity of these studies were 82 and 79% [35]. The majority of studies [28] used low-dose dobutamine echocardiography, and only four studies used a low–high dose protocol [35]. When the studies with low–high dose were analyzed separately, a mean sensitivity of 79% and a specificity of 85% were obtained [35]. Thus, a slight loss in sensitivity with a small gain in specificity was obtained when low–high dose dobutamine was compared to low-dose dobutamine echocardiography for the prediction of improvement of function post-revascularization.

Improvement of global LV function has been evaluated in seven studies, with 254 patients; on average, the LVEF improved from 35 to 43% in patients with viable myocardium [43]. Conversely, the LVEF remained unchanged (35% vs. 36%) in patients without viable myocardium. Two studies have evaluated *improvement of symptoms* after revascularization in relation to the presence of viable myocardium [62,63]. Bax et al. [63] demonstrated that the majority of patients with viable myocardium improved in NYHA class following revascularization. In particular, in viable patients the NYHA class improved from 3.2 ± 0.7 to 1.6 ± 0.5 ($P < 0.05$). Marwick and colleagues [64] however failed to demonstrate a relation between the extent of viability and the improvement of exercise capacity post-revascularization. The relation between *LV reverse remodeling* and the presence of viable myocardium on dobutamine stress echocardiography was evaluated by Rizzello et al. [39]. The authors evaluated 100 patients with ischemic cardiomyopathy and demonstrated that ongoing LV remodeling was related inversely to the number of viable segments. Patients with substantial viability exhibited reverse remodeling and patients with scar tissue showed ongoing LV dilatation.

Six studies ($n = 686$ patients) have evaluated *long-term prognosis* in relation to treatment (medical, revascularization) and viability by dobutamine echocardiography (absent/present) [43]. The patients were divided into four groups. Patients with viable myocardium who underwent revascularization had a low event-rate (6%), whereas nonviable patients who underwent revascularization had an event-rate of 16%. Patients who were treated medically had a 22% event-rate in the presence of viability, and a 28% event-rate in the absence of viability. Thus, only patients with viable myocardium who underwent revascularization had a good prognosis.

Dobutamine gated SPECT

The initial studies with nuclear imaging to evaluate contractile reserve applied dobutamine infusion during gated blood pool imaging. These studies mainly focused on the change in LVEF from rest to dobutamine stress. With the popularization of gated SPECT (and to a lesser extent gated PET), assessment of regional contractile reserve during dobutamine infusion has been more commonly performed. Everaert et al. [65] demonstrated a good agreement (83%) for assessment of segmental contractile reserve between dobutamine gated SPECT and stress echocardiography in 25 patients with LV dysfunction. A more substantial comparison was reported by Leoncini and colleagues [66] in 37 patients with ischemic LV dysfunction; contractile reserve was detected by stress echocardiography in 36% of dysfunctional segments as compared to 33% assessed by dobutamine gated SPECT,

with an overall agreement of 74% between the two techniques. Leoncini et al. demonstrated in a subsequent study that dobutamine gated SPECT was capable of predicting *improvement of regional LV function* post-revascularization [67], and a sensitivity of 64% and a specificity of 88% were reported. The same group demonstrated a sensitivity of 79% with a specificity of 78% to predict improvement in LVEF in 37 patients undergoing revascularization [68].

Assessment of contractile reserve using low-dose dobutamine gated SPECT has not yet been applied to predict improvement of symptoms or long-term outcome in patients with chronic ischemic LV dysfunction.

Contractile reserve and perfusion: agreement and disagreement

Various studies have performed a head-to-head comparison between contractile reserve and perfusion. Panza et al. [69] have evaluated 30 patients with chronic ischemic LV dysfunction (LVEF 32 ± 9%) with thallium-201 imaging and low-dose dobutamine echocardiography. Of the 311 dysfunctional segments, 56% showed contractile reserve and 84% had preserved thallium-201 uptake (intact perfusion/cell membrane integrity). The agreement between the two techniques was 68%. The disagreement was mainly related segments that were having intact perfusion/cell membrane integrity without contractile reserve. In particular, of the 262 segments considered viable by thallium-201 imaging, only 64% exhibited contractile reserve. Similar observations were reported when FDG imaging was compared to stress echocardiography. Cornel et al. [70] evaluated 40 patients with depressed LV function (LVEF 31 ± 16%) with resting echocardiography, FDG imaging, and low-dose dobutamine echocardiography. The agreement between the two techniques was 87%. Although 94% of the segments that were nonviable on FDG imaging did not show contractile reserve, the disagreement between SPECT and dobutamine echocardiography was caused mainly by the absence of contractile reserve in 27% of the segments that were viable on FDG imaging. Sloof et al. [71] further explored the relation between nuclear imaging and contractile reserve. The authors studied 14 patients with stable, chronic LV dysfunction (LVEF 34 ± 10%); all underwent perfusion imaging (with thallium-201), metabolic imaging (with FDG to assess glucose metabolism), and low-dose dobutamine echocardiography to assess contractile reserve. The comparison of the different modalities was restricted to akinetic or dyskinetic myocardium as assessed by resting two-dimensional echocardiography. Intact perfusion was found in 52% segments, glucose utilization was maintained in 59% segments, and contractile reserve was present in 33% of segments ($P < 0.01$ versus perfusion and metabolic imaging). Nearly all segments without perfusion or metabolic activity lacked contractile reserve (Fig. 10.7). In contrast, only 50% of segments with perfusion and metabolic activity also had contractile reserve (Fig. 10.7), illustrating the higher sensitivity of nuclear imaging to identify viable myocardium.

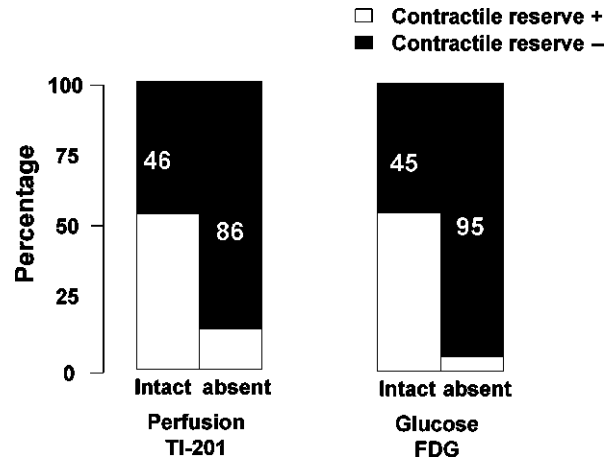

Figure 10.7 Relation between contractile reserve and viability on nuclear imaging (perfusion assessed by thallium-201, glucose metabolism assessed by FDG). Segments without perfusion or glucose metabolism virtually never had contractile reserve, but almost 50% of segments with perfusion or glucose metabolism also lacked contractile reserve. (Based on [71].)

The most comprehensive head-to-head comparison included 114 patients with ischemic cardiomyopathy (LVEF 34 ± 10%); these patients underwent perfusion imaging with resting technetium-99m tetrofosmin and assessment of contractile reserve (using low-dose dobutamine, 5–10 mcg/(kgthinsp;min)) [72]. A total of 1136 segments (77% of segments) were dysfunctional on resting 2D echocardiography. Contractile reserve was present in 412 (31% of all dysfunctional) segments. Intact perfusion was observed in 683 (51% of all dysfunctional) segments ($P < 0.05$ versus contractile reserve). Accordingly, the agreement was 72%; 92% of segments without perfusion did not have contractile reserve, but 47% of segments with perfusion also did not have contractile reserve. Thus, all the available studies indicate the higher sensitivity of perfusion imaging as compared to contractile reserve for assessment of myocardial viability. This observation can (partially) be explained when data from biopsy studies are considered. Nagueh and coworkers [73] studied 20 patients with thallium-201 imaging and dobutamine stress echocardiography before surgical revascularization and transmural biopsies were obtained during surgery. The authors demonstrated 1% fibrosis in segments with preserved thallium-201 uptake and contractile reserve (minimal damage) as compared to 28% fibrosis (extensive damage) in segments with scar tissue on thallium-201 imaging and without contractile

reserve on dobutamine stress echocardiography. Moreover, Pagano and colleagues [74] showed that segments with preserved FDG uptake without contractile reserve had more ultrastructural damage and a higher percentage of fibrosis than segments with preserved FDG uptake with contractile reserve. Borgers et al. [75] demonstrated a severe loss in contractile material in viable myocardium with recovery of function post-revascularization: the space previously occupied by myofilaments was filled with glycogen. It is thus suggested that extensive cellular damage and loss of contractile apparatus results in absence of contractile reserve whereas perfusion (and metabolic activity) may still be preserved. This hypothesis was further tested by Schinkel et al. [76] who evaluated the presence of contractile reserve in a large group of patients with stunned (less severely damaged) and hibernating (more severely damaged) myocardium; the authors demonstrated that dobutamine-induced contractile reserve was more frequently observed in stunned than in hibernating myocardium (61% vs. 51%, respectively, $P < 0.01$).

Prediction of outcome: perfusion imaging versus contractile reserve

In 114 patients with chronic ischemic LV dysfunction, both perfusion imaging with technetium-99m tetrofosmin SPECT and dobutamine stress echocardiography (to assess contractile reserve) were performed prior to revascularization [72]. Improvement of function was assessed 9–12 months after revascularization. The majority (66%) of segments with recovery of function post-revascularization had intact perfusion and contractile reserve. In contrast, the majority (58%) of segments without functional recovery lacked both perfusion and contractile reserve. Of interest, 22% of segments with functional recovery and 25% of segments without functional recovery showed intact perfusion without contractile reserve.

Perrone-Filardi et al. [77] performed a head-to-head comparison between low-dose dobutamine echocardiography and thallium-201 rest-redistribution imaging in 40 patients undergoing revascularization. The authors demonstrated a significantly higher sensitivity for thallium-201 imaging as compared to low-dose dobutamine echocardiography (100% vs. 79%, $P < 0.05$). The specificity of both techniques was comparable (78% vs. 79%). Leoncini et al. [67] performed resting and dobutamine nitrate-enhanced technetium-99m sestamibi gated SPECT before revascularization; perfusion was quantitatively assessed and contractile reserve was visually evaluated. Perfusion analysis had a sensitivity of 85% with a specificity of 55%, whereas contractile reserve had lower sensitivity (64%, $P < 0.01$) with higher specificity (88%, $P < 0.01$) to predict functional recovery. When all available studies (with a direct comparison between nuclear imaging and low-dose dobutamine echocardiography) were pooled, the higher sensitivity for nuclear imaging was confirmed. In particular, the data from 11 studies (with 325 patients) showed a sensitivity of 90% for nuclear imaging as compared to 74% for dobutamine echocardiography ($P < 0.05$) [35]. In contrast, the specificity of low-dose dobutamine echocardiography was higher (57% vs. 78%, $P < 0.05$).

This observation has led to the hypothesis that integration of information on perfusion (a very sensitive marker) with contractile reserve (a very specific marker) may further improve prediction of improvement of function. This was evaluated in 73 patients (mean LVEF $32 \pm 8\%$) who underwent dobutamine stress echocardiography and thallium-201 SPECT (resting images, obtained 4 h after tracer injection) before surgical revascularization [78]. LVEF was assessed before and 3–6 months after revascularization. Analysis of receiver operator curves showed that the optimum criteria to predict improvement in LVEF post-revascularization were six or more viable, dysfunctional segments on thallium-201 SPECT and four or more segments on dobutamine stress echocardiography. The results confirmed the higher sensitivity for thallium-201 imaging and the higher specificity for dobutamine stress echocardiography (Fig. 10.8). Changing the thallium-201 criteria to improve specificity to 78% (eight or more viable segments) yielded a low sensitivity of 44%, and changing the dobutamine stress echocardiography criteria to improve sensitivity to 84% (two or more segments) lowered

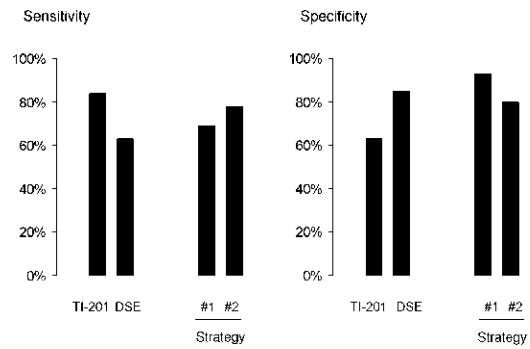

Figure 10.8 Prediction of improvement in LVEF post-revascularization by perfusion imaging (using thallium-201, Tl-201) or contractile reserve (using low-dose dobutamine echocardiography, DSE). Perfusion imaging has high sensitivity to predict improvement in LVEF, whereas contractile reserve has high specificity. Integrated imaging of perfusion and contractile reserve results in increased and balanced sensitivity and specificity to predict improvement in LVEF. Strategy 1 considered thallium-201 imaging as the first step, followed by dobutamine echocardiography in patients with an intermediate likelihood of viability on thallium-201 imaging. Strategy 2 considered dobutamine echocardiography as the first step, followed by thallium-201 imaging. (Based on [78].)

specificity to 56%. Next, two sequential testing strategies were explored to achieve optimal sensitivity and specificity. In strategy 1, 33 (45%) of 73 patients with an intermediate likelihood of viability on thallium-201 imaging (five to eight viable segments) underwent dobutamine stress echocardiography. In strategy 2, 31 (42%) of 73 patients with an intermediate likelihood of viability on dobutamine stress echocardiography (two to four viable segments) underwent thallium-201 imaging. For strategy 1, sensitivity did not change significantly (69%), whereas specificity was improved significantly (93%, $P < 0.01$ versus thallium-201 imaging). For strategy 2, sensitivity improved significantly (78%, $P < 0.05$ versus dobutamine echocardiography) and specificity remained unchanged (80%). These data clearly indicated that sequential testing with thallium-201 imaging and dobutamine stress echocardiography in a subgroup of patients with an intermediate likelihood of viability by either test significantly enhanced prediction of post-revascularization improvement of LVEF.

Sequential thallium-201 SPECT and dobutamine stress echocardiography was subsequently compared with FDG imaging to predict improvement of function post-revascularization [79]. Forty-seven patients with ischemic cardiomyopathy underwent thallium-201 SPECT at rest (4-h delayed imaging), dobutamine stress echocardiography, and FDG imaging before bypass surgery. Sensitivity, specificity, and accuracy of two sequential strategies were compared with those of FDG SPECT. Strategy 1 considered thallium-201 imaging as the first step, followed by dobutamine stress echocardiography in patients with an intermediate likelihood of viability on thallium-201 imaging. Strategy 2 considered dobutamine stress echocardiography as the first step, followed by thallium-201 imaging. LVEF was assessed before and 6 months after revascularization. Thallium-201 had a high sensitivity, whereas dobutamine stress echocardiography had a high specificity (Fig. 10.9). Both strategies 1 and 2 resulted in high sensitivities (89 and 89%, respectively) and high specificities (89 and 86%, respectively), compared with FDG SPECT (sensitivity 89%, specificity 86%). These results indicated that sequential testing by thallium-201 imaging and dobutamine stress echocardiography has a comparable accuracy to FDG imaging to predict improvement in LVEF after revascularization.

These two studies clearly demonstrated the value of integrating perfusion and contractile reserve to optimally predict improvement in function post-revascularization. From a practical point of view it would be preferred to assess perfusion and contractile reserve with one technique, to avoid misalignment between different imaging modalities instead of sequential use of techniques. Gated SPECT allows assessment of perfusion and resting (regional and global) LV function. In combination with

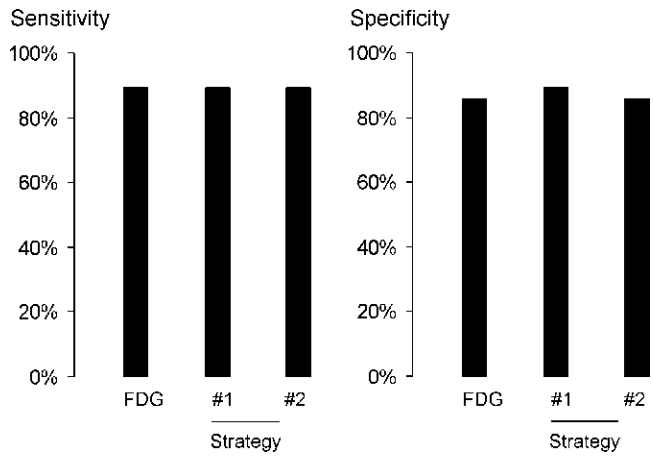

Figure 10.9 Prediction of improvement in LVEF post-revascularization by integrated imaging of perfusion (using thallium-201, Tl-201) and contractile reserve (using low-dose dobutamine echocardiography, DSE). Strategy 1 considered thallium-201 imaging as the first step, followed by dobutamine echocardiography in patients with an intermediate likelihood of viability on thallium-201 imaging. Strategy 2 considered dobutamine echocardiography as the first step, followed by thallium-201 imaging. The results of the two strategies were also compared with metabolic imaging with FDG in the same patients. (Based on [79].)

infusion of low-dose dobutamine, it is possible to also contractile reserve. Simoes et al. [80] used gated thallium-201 imaging to assess perfusion and resting function; function was also evaluated during infusion of low-dose dobutamine to assess contractile reserve. Accordingly, 32 patients underwent gated thallium-201 imaging, with gating at rest and following dobutamine infusion. This study was performed in patients after acute myocardial infarction and spontaneous improvement of function was studied by sequential rest echocardiographic studies. Intact perfusion had a sensitivity and specificity of 93 and 50% respectively. Integration with the presence of contractile reserve resulted in a sensitivity and specificity of 71 and 94% respectively. Whether these results also apply to patients with chronic LV dysfunction undergoing revascularization remains to be determined. Currently, no specific studies focusing on the integration of contractile function and perfusion (assessed from a single dobutamine gated SPECT study) to predict functional outcome post-revascularization are available.

Besides using dobutamine gated SPECT (for integrated assessment of contractile function and perfusion) dobutamine MCE could also be used for prediction of functional recovery. This approach was evaluated recently in 41 patients with ischemic LV dysfunction undergoing revascularization [81]. Before revascularization, patients underwent MCE and low-dose dobutamine echocardiography. Follow-up echocardiograms were obtained 3–6 months post-revascularization. MCE had a sensitivity of

86% with a specificity of 43% to predict functional recovery. Low-dose dobutamine echocardiography had a comparable sensitivity (83%) with a higher specificity (76%). Integration of MCE and low-dose dobutamine echocardiography resulted in a sensitivity of 96% with a specificity of 63%. Further studies are needed to fully appreciate the integration of perfusion and contractile function (using either echocardiography or SPECT) for prediction of functional recovery post-revascularization.

Conclusions

The number of patients with chronic ischemic LV dysfunction increased exponentially over the past years and evaluation for myocardial viability has become an important component to guide therapy in terms of conservative medical therapy of revascularization. Patients with viable myocardium have been demonstrated to improve in function and symptoms post-revascularization, associated with a favorable long-term prognosis.

A variety of techniques are available for assessment of viability; in clinical practice, perfusion imaging with SPECT and assessment of contractile reserve with low-dose dobutamine echocardiography are frequently performed. In general, SPECT perfusion imaging has a higher sensitivity, whereas low-dose dobutamine echocardiography has a higher specificity to predict improvement post-revascularization. Integration of contractile reserve and perfusion may thus provide optimal prediction of functional recovery. Sequential imaging with thallium-201 SPECT and low-dose dobutamine echocardiography have confirmed this hypothesis. Ideally, assessment of perfusion and contractile reserve should be performed in one session, with one imaging technique. Initial studies with dobutamine gated SPECT have shown the feasibility of integration of these parameters, but large studies in patients undergoing revascularization are still needed.

References

1. Gheorghiade M, Bonow RO. Chronic heart failure in the United States: a manifestation of coronary artery disease. Circulation 1998;97(3):282–289.
2. Pfeffer MA, Braunwald E, Moye LA, et al., for the SAVE Investigators. Effect of captopril on mortality and morbidity in patients with left ventricular dysfunction after myocardial infarction. Results of the survival and ventricular enlargement trial. [see comments]. New England Journal of Medicine 1992;327(10):669–677.
3. Yusuf S. Effect of enalapril on survival in patients with reduced left-ventricular ejection fractions and congestive-heart-failure. New England Journal of Medicine 1991;325(5):293–302.
4. Pitt B, Poole-Wilson PA, Segal R, et al. Effect of losartan compared with captopril on mortality in patients with symptomatic heart failure: randomised trial – the Losartan Heart Failure Survival Study ELITE II. Lancet 2000;355(9215):1582–1587.
5. Udelson JE. Ventricular remodeling in heart failure and the effect of beta-blockade. American Journal of Cardiology 2004;93(9A):43B–48B.
6. Brophy JM, Joseph L, Rouleau JL. Beta-blockers in congestive heart failure – a Bayesian meta-analysis. Annals of Internal Medicine 2001;134(7):550–560.
7. Braunwald E. Expanding indications for beta-blockers in heart failure. New England Journal of Medicine 2001;344(22):1711–1712.
8. Pitt B, Zannad F, Remme WJ, et al. The effect of spironolactone on morbidity and mortality in patients with severe heart failure. New England Journal of Medicine 1999;341(10):709–717.
9. Cairns JA, Connolly SJ, Roberts R, Gent M. Randomised trial of outcome after myocardial infarction in patients with frequent or repetitive ventricular premature depolarisations: CAMIAT. Lancet 1997;349(9053):675–682.
10. Cowie MR, Wood DA, Coats AJS, et al. Incidence and aetiology of heart failure – a population-based study. European Heart Journal 1999;20(6):421–428.
11. Ho KKL, Anderson KM, Kannel WB, Grossman W, Levy D. Survival after the onset of congestive-heart-failure in Framingham Heart Study subjects. Circulation 1993;88(1):107–115.
12. Kirklin J, Pambukian S, McGifiin D, Benza R. Current outcomes following heart transplantation. Seminars in Thoracic and Cardiovascular Surgery 2004;16:395–403.
13. Abraham WT, Hayes DL. Cardiac resynchronization therapy for heart failure. Circulation 2003;108(21):2596–2603.
14. Bax JJ, Ansalone G, Breithardt OA, et al. Echocardiographic evaluation of cardiac resynchronization therapy: ready for routine clinical use? A critical appraisal. Journal of the American College of Cardiology 2004;44(1):1–9.
15. Baker DW, Jones R, Hedges J, Massie BM, Konstam MA, Rose EA. Management of heart failure, 3: the role of revascularization in the treatment of patients with moderate or severe left-ventricular systolic dysfunction. JAMA 1994;272(19):1528–1534.
16. Rahimtoola SH. A perspective on the 3 large multicenter randomized clinical-trials of coronary-bypass surgery for chronic stable angina. Circulation 1985;72(6):123–135.
17. Dilsizian V, Bonow RO, Cannon ROd, et al. The effect of coronary artery bypass grafting on left ventricular systolic function at rest: evidence for preoperative subclinical myocardial ischemia. American Journal of Cardiology 1988;61(15):1248–1254.
18. Schinkel AFL, Poldermans D, Vanoverschelde JLJ, et al. Incidence of recovery of contractile function following revascularization in patients with ischemic left ventricular dysfunction. American Journal of Cardiology 2004;93(1):14–17.
19. Rahimtoola SH. The hibernating myocardium [see comments]. American Heart Journal 1989;117(1):211–221.

20. Maes A, Flameng W, Nuyts J, et al. Histological alterations in chronically hypoperfused myocardium – correlation with PET findings. Circulation 1994;90(2):735–745.
21. Vanoverschelde JLJ, Melin JA. The pathophysiology of myocardial hibernation: current controversies and future directions. Progress in Cardiovascular Diseases 2001;43(5):387–398.
22. Depre C, Vanoverschelde JLJ, Gerber B, Borgers M, Melin JA, Dion R. Correlation of functional recovery with myocardial blood flow, glucose uptake, and morphologic features in patients with chronic left ventricular ischemic dysfunction undergoing coronary artery bypass grafting. Journal of Thoracic and Cardiovascular Surgery 1997;113(2):371–378.
23. Vanoverschelde JLJ, Wijns W, Depre C, et al. Mechanisms of chronic regional postischemic dysfunction in humans – new insights from the study of noninfarcted collateral-dependent myocardium. Circulation 1993;87(5):1513–1523.
24. Bolukoglu H, Liedtke AJ, Nellis SH, Eggleston AM, Subramanian R, Renstrom B. An animal-model of chronic coronary stenosis resulting in hibernating myocardium. American Journal of Physiology 1992;263(1):H20–H29.
25. Fallavollita JA, Canty JM. Differential F-18-2-deoxyglucose uptake in viable dysfunctional myocardium with normal resting perfusion – evidence for chronic stunning in pigs. Circulation 1999;99(21):2798–2805.
26. Fallavollita JA, Perry BJ, Canty JM. F-18-2-deoxyglucose deposition and regional flow in pigs with chronically dysfunctional myocardium – evidence for transmural variations in chronic hibernating myocardium. Circulation 1997;95(7):1900–1909.
27. Firoozan S, Wei K, Linka A, Skyba D, Goodman NC, Kaul S. A canine model of chronic ischemic cardiomyopathy: characterization of regional flow-function relations. American Journal of Physiology. Heart and Circulatory Physiology 1999;276(2):H446–H455.
28. Hernandez-Pampaloni M, Bax JJ, Morita K, Dutka DP, Camici PG. Incidence of stunned, hibernating and scarred myocardium in ischaemic cardiomyopathy. European Journal of Nuclear Medicine and Molecular Imaging 2005;32(3):314–321.
29. Schinkel AFL, Bax JJ, Sozzi FB, et al. Prevalence of myocardial viability assessed by single photon emission computed tomography in patients with chronic ischaemic left ventricular dysfunction. Heart 2002;88(2):125–130.
30. Al-Mohammad A, Mahy IR, Norton MY, Prevalence of hibernating myocardium in patients with severely impaired ischaemic left ventricles. Heart 1998;80(6):559–564.
31. Auerbach MA, Schoder H, Hoh C, et al. Prevalence of myocardial viability as detected by positron emission tomography in patients with ischemic cardiomyopathy. Circulation 1999;99(22):2921–2926.
32. Fox KF, Cowie MR, Wood DA, et al. Coronary artery disease as the cause of incident heart failure in the population. European Heart Journal 2001;22(3):228–236.
33. Schinkel AFL, Bax JJ, Boersma E, et al. Assessment of residual myocardial viability in regions with chronic electrocardiographic Q-wave infarction. American Heart Journal 2002;144(5):865–869.
34. Bax JJ, Poldermans D, Elhendy A, Boersma E, Van der Wall EE. Assessment of myocardial viability by nuclear imaging techniques. Current cardiology Report 2005;7:124–129.
35. Bax J, Poldermans D, Elhendy A, Boersma E, Rahimtoola S. Sensitivity, specificity, and predictive accuracies of various noninvasive techniques for detecting hibernating myocardium. Current Problems in Cardiology 2001;26:142–186.
36. Bax JJ, van der Wall EE, Harbinson M. Radionuclide techniques for the assessment of myocardial viability and hibernation. Heart 2004;90:V26–V33.
37. Di Carli MF, Asgarzadie F, Schelbert HR, et al. Quantitative relation between myocardial viability and improvement in heart failure symptoms after revascularization in patients with ischemic cardiomyopathy. Circulation 1995;92(12):3436–3444.
38. Mule JD, Bax JJ, Zingone B, et al. The beneficial effect of revascularization on jeopardized myocardium: reverse remodeling and improved long-term prognosis. European Journal of Cardio-Thoracic Surgery 2002;22(3):426–430.
39. Rizzello V, Poldermans D, Boersma E, et al. Opposite patterns of left ventricular remodeling after coronary revascularization in patients with ischemic cardiomyopathy – role of myocardial viability. Circulation 2004;110(16):2383–2388.
40. Allman KC, Shaw LJ, Hachamovitch R, Udelson JE. Myocardial viability testing and impact of revascularization on prognosis in patients with coronary artery disease and left ventricular dysfunction: a meta-analysis. Journal of the American College of Cardiology 2002;39(7):1151–1158.
41. Bonow RO, Dilsizian V. Thallium 201 for assessment of myocardial viability [see comments]. Seminars in Nuclear Medicine 1991;21(3):230–241.
42. Kitsiou AN, Srinivasan G, Quyyumi AA, Summers RM, Bacharach SL, Dilsizian V. Stress-induced reversible and mild-to-moderate irreversible thallium defects – are they equally accurate for predicting recovery of regional left ventricular function after revascularization? Circulation 1998;98(6):501–508.
43. Bax J, Wahba F, Van der Wall E. Myocardial viability/hibernation. In Iskandrian AE, Verani MS, eds. Nuclear Cardiac Imaging: Principles and Applications. 3rd edn. New York: Oxford University Press; 2003:386–398.
44. Cuocolo A, Petretta M, Nicolai E, et al. Successful coronary revascularization improves prognosis in patients with previous myocardial infarction and evidence of viable myocardium at thallium-201 imaging. European Journal of Nuclear Medicine 1998;25(1):60–68.
45. Gioia G, Powers J, Heo JY, Iskandrian AS. Prognostic value of rest-redistribution tomographic Tl-201 imaging in ischemic cardiomyopathy. American Journal of Cardiology 1995;75(12):759–762.
46. Pagley PR, Beller GA, Watson DD, Gimple LW, Ragosta M. Improved outcome after coronary bypass surgery in patients with ischemic cardiomyopathy and residual myocardial viability. Circulation 1997;96(3):793–800.
47. Zafrir N, Leppo JA, Reinhardt CP, Dahlberg ST. Thallium reinjection versus standard stress/delay redistribution imaging for prediction of cardiac events [see comments]. Journal of the American College of Cardiology 1998;31:1280–1285

48. Piwnica-Worms D, Kronauge JF, Chiu ML. Uptake and retention of hexakis (2-methoxyisobutyl isonitrile) technetium(I) in cultured chick myocardial cells. Mitochondrial and plasma membrane potential dependence. Circulation 1990;82(5):1826–1838.
49. Matsunari I, Böning G, Ziegler SI, et al. Attenuation-corrected 99mTc-tetrofosmin single-photon emission computed tomography in the detection of viable myocardium: comparison with positron emission tomography using 18F-fluorodeoxyglucose. Journal of the American College of Cardiology 1998;32(4):927–935.
50. Soufer R, Dey HM, Ng CK, Zaret BL. Comparison of sestamibi single-photon emission computed-tomography with positron emission tomography for estimating left-ventricular myocardial viability. American Journal of Cardiology 1995;75(17):1214–1219.
51. Bonow RO, Dilsizian V. Thallium-201 and technetium-99m-sestamibi for assessing viable myocardium [editorial; comment]. Journal of Nuclear Medicine 1992;33(5):815–818.
52. Maurea S, Cuocolo A, Soricelli A, et al. Myocardial viability index in chronic coronary artery disease: technetium-99m-methoxy isobutyl isonitrile redistribution. Journal of Nuclear Medicine 1995;36(11):1953–1960.
53. Sciagra R. Nitrates and viability: a durable affair. Journal of Nuclear Medicine 2003;44(5):752–755.
54. Bisi G, Sciagrà R, Santoro GM, Fazzini PF. Rest technetium-99m sestamibi tomography in combination with short-term administration of nitrates: feasibility and reliability for prediction of postrevascularization outcome of asynergic territories. Journal of the American College of Cardiology 1994;24(5):1282–1289.
55. Schneider CA, Voth E, Gawlich S, et al. Significance of rest technetium-99m sestamibi imaging for the prediction of improvement of left ventricular dysfunction after Q wave myocardial infarction: importance of infarct location adjusted thresholds. Journal of the American College of Cardiology 1998;32(3):648–654.
56. Sciagra R, Pellegri M, Pupi A, et al. Prognostic implications of Tc-99m sestamibi viability imaging and subsequent therapeutic strategy in patients with chronic coronary artery disease and left ventricular dysfunction. 2000;36(3):739–745.
57. Lepper W, Belcik T, Wei K, Lindner JR, Sklenar J, Kaul S. Myocardial contrast echocardiography. Circulation 2004;109(25): 3132–3135.
58. Shimoni S, Frangogiannis NG, Aggeli CJ, et al. Microvascular structural correlates of myocardial contrast echocardiography in patients with coronary artery disease and left ventricular dysfunction – implications for the assessment of myocardial hibernation. Circulation 2002;106(8):950–956.
59. Shimoni S, Frangogiannis NG, Aggeli CJ, et al. Identification of hibernating myocardium with quantitative intravenous myocardial contrast echocardiography – comparison with dobutamine echocardiography and thallium-201 scintigraphy. Circulation 2003;107(4):538–544.
60. Nagueh SF, Vaduganathan P, Ali N, et al. Identification of hibernating myocardium: comparative accuracy of myocardial contrast echocardiography, rest-redistribution thallium-201 tomography and dobutamine echocardiography. Journal of the American College of Cardiology 1997;29(5):985–993.
61. Zoghbi WA. Evaluation of myocardial viability with contrast echocardiography. American Journal of Cardiology 2002;90(10A):65J–71J.
62. Poldermans D, Rambaldi R, Bax JJ, et al. Safety and utility of atropine addition during dobutamine stress echocardiography for the assessment of viable myocardium in patients with severe left ventricular dysfunction. European Heart Journal 1998;19(11):1712–1718.
63. Bax JJ, Poldermans D, Elhendy A, et al. Improvement of left ventricular ejection fraction, heart failure symptoms and prognosis after revascularization in patients with chronic coronary artery disease and viable myocardium detected by dobutamine stress echocardiography. Journal of the American College of Cardiology 1999;34(1):163–169.
64. Marwick TH, Zuchowski C, Lauer MS, Secknus MA, Williams MJ, Lytle BW. Functional status and quality of life in patients with heart failure undergoing coronary bypass surgery after assessment of myocardial viability. Journal of the American College of Cardiology 1999;33(3):750–758.
65. Everaert H, Vanhove C, Franken PR. Low-dose dobutamine gated single-photon emission tomography: comparison with stress echocardiography. European Journal of Nuclear Medicine 2000;27(4):413–418.
66. Leoncini M, Marcucci G, Sciagrà R, et al. Nitrate-enhanced gated technetium 99m sestamibi SPECT for evaluating regional wall motion at baseline and during low-dose dobutamine infusion in patients with chronic coronary artery disease and left ventricular dysfunction: comparison with two-dimensional echocardiography. Journal of Nuclear Cardiology 2000;7(5):426–431.
67. Leoncini M, Marcucci G, Sciagra R, et al. Prediction of functional recovery in patients with chronic coronary artery disease and left ventricular dysfunction combining the evaluation of myocardial perfusion and of contractile reserve using nitrate-enhanced technetium-99m sestamibi gated single-photon emission computed tomography and dobutamine stress. American Journal of Cardiology 2001;87(12): 1346–1350.
68. Leoncini M, Sciagra R, Maioli M, et al. Usefulness of dobutamine Tc-99m sestamibi-gated single-photon emission computed tomography for prediction of left ventricular ejection fraction outcome after coronary revascularization for ischemic cardiomyopathy. American Journal of cardiology 2002;89(7):817–821
69. Panza JA, Dilsizian V, Laurienzo JM, Curiel RV, Katsiyiannis PT. Relation between thallium uptake and contractile response to dobutamine – implications regarding myocardial viability in patients with chronic coronary-artery disease and left-ventricular dysfunction. Circulation 1995;91(4):990–998.
70. Cornel JH, Bax JJ, Elhendy A, et al. Agreement and disagreement between "metabolic viability" and "contractile reserve" in akinetic myocardium [see comments]. Journal of Nuclear Cardiology 1999;6(4):383–388.
71. Sloof GW, Knapp FF, van Lingen A, Eersels J, Poldermans D, Bax JJ. Nuclear imaging is more sensitive for the detection of viable myocardium than dobutamine echocardiog-

raphy. Nuclear Medicine Communications 2003;24(4):375–381.
72. Bax JJ, Poldermans D, Schinkel AFL, et al. Perfusion and contractile reserve in chronic dysfunctional myocardium: relation to functional outcome after surgical revascularization. Circulation 2002;106(13):I14–I18.
73. Nagueh SF, Mikati I, Weilbaecher D, et al. Relation of the contractile reserve of hibernating myocardium to myocardial structure in humans. Circulation 1999;100(5):490–496.
74. Pagano D, Townend JN, Parums DV, Bonser RS, Camici PG. Hibernating myocardium: morphological correlates of inotropic stimulation and glucose uptake. Heart 2000;83(4):456–461.
75. Borgers M, Thone F, Wouters L, Ausma J, Shivalkar B, Flameng W. Structural correlates of regional myocardial dysfunction in patients with critical coronary-artery stenosis – chronic hibernation. Cardiovascular Pathology 1993;2(4):237–245.
76. Schinkel AFL, Bax JJ, van Domburg R, et al. Dobutamine-induced contractile reserve in stunned, hibernating, and scarred myocardium in patients with ischemic cardiomyopathy. Journal of Nuclear Medicine 2003;44(2):127–133.
77. Perrone-Filardi P, Pace L, Prastaro M, et al. Assessment of myocardial viability in patients with chronic coronary artery disease. Rest-4-hour-24-hour 201Tl tomography versus dobutamine echocardiography [see comments]. Circulation 1996; 94(11):2712–2719.
78. Bax JJ, Maddahi J, Poldermans D, et al. Sequential Tl-201 imaging and dobutamine echocardiography to enhance accuracy of predicting improved left ventricular ejection fraction after revascularization. Journal of Nuclear Medicine 2002;43(6):795–802.
79. Bax JJ, Maddahi J, Poldermans DE, et al. Preoperative comparison of different noninvasive strategies for predicting improvement in left ventricular function after coronary artery bypass grafting. American Journal of Cardiology 2003;92(1):1–4.
80. Simoes MV, de Almeida OC, Pintya AO, et al. Prediction of left ventricular wall motion recovery after acute myocardial infarction by Tl-201 gated SPECT: incremental value of integrated contractile reserve assessment. Journal of Nuclear Cardiology 2002;9(3):294–303.
81. Korosoglou G, Hansen A, Hoffend J, et al. Comparison of real-time myocardial contrast echocardiography for the assessment of myocardial viability with fluorodeoxyglucosom-18 positron emission tomography and dobutamine stress echocardiography. American Journal of Cardiology 2004; 94(5):570–576.

11 Quantitative gated blood pool SPECT

Serge D. Van Kriekinge
Daniel S. Berman
Guido Germano

Introduction

Gating of nuclear cardiology studies had originally been applied to planar blood pool imaging using ^{99m}Tc-albumin [1] and ^{99m}Tc-labeled red blood cells [2], and was successfully extended to blood pool SPECT following the gain in popularity of perfusion SPECT over perfusion planar imaging [3–5]. The rationale for the use of gated blood pool SPECT was that a more accurate determination of left-ventricular function could be obtained if the overlap of cardiac chambers could be avoided, background correction were not necessary, and geometric assumptions for volume estimation not needed. In addition, the separation of left ventricle (LV) and right ventricle (RV) conceptually allows gated blood pool SPECT to measure right-ventricular function parameters. All these advantages initially had to be weighed against the increase in processing and analysis time (a major problem in the early days of gating), the decrease in the number of cardiac intervals acquired compared to planar imaging (with consequent reduced ability to measure diastolic function), and the absence of fast and reliable quantitative algorithms for the measurement of function.

With the enormous increase in the use of echocardiography procedures and the widespread acceptance of gated myocardial perfusion SPECT, gated planar blood pool imaging has decreased to less than 5% of all nuclear cardiac studies in the United States, although the percentage may be substantially higher in other countries. On the other hand, the case for gated blood pool SPECT imaging has considerably strengthened, due to the increase in computer speed, the greater diffusion of multidetector cameras, and the general acceptance of state-of-the-art three-dimensional analysis and display techniques. While it is likely that blood pool imaging will never regain its role as *the* nuclear technique for the measurement of cardiac function, we believe that "upgrading" it to SPECT can well serve nuclear cardiology's search for new and effective techniques and protocols vis-à-vis competitive modalities. In fact, due to the larger dimension of the left-ventricular blood pool compared to the myocardial thickness, partial volume effects [6] would be expected to be less of a problem, and the measurements of volume (especially end-diastolic) potentially more accurate with gated blood pool SPECT than with gated myocardial perfusion SPECT. In addition, gated blood pool SPECT may be better suited to specific applications such as wall motion phase analysis.

Acquisition

Most of the technical issues examined in Chapter 2 with respect to gated perfusion SPECT imaging also apply to gated blood pool SPECT imaging. In particular, a gated blood pool SPECT acquisition is usually accomplished with 8-frame or 16-frame temporal resolution. Higher frame-count SPECT acquisitions are technically feasible (as demonstrated with myocardial perfusion SPECT [7–9], though the length of the acquisition may have to be increased to maintain adequate count statistics. Acquisition follows an injection of ^{99m}Tc-labeled red blood cells in dosages similar to those described in Tables 2.2 and 2.3 for gated ^{99m}Tc-based stress perfusion imaging. Acquisition is generally performed with the patient in the resting state, although acquisitions after nitroglycerin [10] or during low-dose dobutamine, to assess myocardial contractile reserve, are clearly feasible. Since it would be difficult to maintain stress conditions throughout the duration of the SPECT acquisition for function measurement purposes, acquisition during exercise has been considered technically too demanding. While technically feasible, the issue of poststress myocardial stunning and its associated decrease in regional and global function has not been studied with gated blood pool SPECT.

Although the injected dose and the specific patient's attenuation characteristics may be the same in perfusion

and blood pool imaging, the number of cardiac counts collected per millicurie of injected radioactivity is higher for the latter, because a lesser amount of activity is taken up by the myocardium in perfusion studies than is present in the blood pool with blood pool radiopharmaceuticals. To verify this expected result, we analyzed 40 patients studies acquired using 8-frame gated blood pool SPECT. For each study, the eight projection sets corresponding to the different phases of the cardiac cycle were first summed together to generate an "ungated" or summed set. Then, the projection image corresponding to LAO (left anterior oblique) 45° was automatically extracted from each ungated set, based on the information contained in the image file header. Three projection images from either side of LAO 45° were summed to LAO 45° (total = 7 of 60 or 64 images, over a 21° arc) to improve image statistics, resulting in an LAO 45° ± 10.5° image. The heart was automatically isolated using a segmentation algorithm, and the maximum and average myocardial pixel counts in the heart calculated for each patient and averaged across the 40 patients studied. The average value of the maximum cardiac pixel count in the 40 patients was 2120 ± 916, while the average value of the average cardiac pixel count was 1603 ± 702, pixel size being 6.4 × 6.4 mm^2. These values are about twice those previously calculated for 8-frame gated ^{99m}Tc-sestamibi SPECT imaging in 121 patients [11]. We feel that the acquisition durations reported in Table 2.2 for gated ^{99m}Tc-based imaging still constitute a good guideline for blood pool imaging, and we now routinely use 16-frame acquisitions for gated blood pool SPECT. It has recently been reported that quantitative gated blood pool SPECT measurements may be more sensitive to the length of the acquisition arc (i.e., 360° vs. 180°) than gated perfusion SPECT measurements [12,13]. However, these findings await further investigation, and we currently employ 180° acquisitions.

Detector rotation and collimator considerations described in Chapter 2 also apply to gated blood pool SPECT. While it is still sensible to use as large an acquisition zoom as practical, gated blood pool SPECT images must allow for visualization of both the LV and the RV and atria, and consequently a smaller zoom factor than used in perfusion SPECT could be preferred. Nonetheless, for purposes of reducing complexity we employ the same zoom as used in perfusion. Based on the published literature, there has been a tendency to favor 16-frame over 8-frame acquisitions in gated blood pool SPECT imaging [14–18], since this number of frames has been documented to permit more accurate assessment of left-ventricular ejection fraction using planar blood pool imaging [19]. Although the use of either general-purpose collimators [14,16,20–22] and high-resolution collimators [15,18,23] has been reported, we feel that the latter best complement the high-count, high-photon-energy characteristics of ^{99m}Tc, and may help reduce partial volume effects in the systolic images, especially with regard to the RV.

Framing options are virtually the same as for gated perfusion SPECT; however, in blood pool imaging no perfusion information is acquired, and therefore it is advisable to always set the cardiac beat length acceptance window to 20–30% in order to minimize the effects of arrhythmia. This contrasts with gated perfusion SPECT imaging, where the use of a wide window is advocated in the absence of a mechanism to "save" rejected beat counts (see Chapter 2). With the use of 10% acceptance windows and 16-frame studies, assessment of diastolic function could be both feasible and accurate.

Processing

Dataset processing (reconstruction and reorientation) is somewhat more challenging for blood pool studies than it is for myocardial perfusion SPECT, largely because of the lack of automated software to perform the common tasks of selecting the reconstruction limits, reorienting the transaxial data and cropping the resulting short-axis dataset, thereby introducing inter- and intraobserver variability. Automated quantitative algorithms may also have additional requirements that impact the processing of raw data, as detailed in the Reconstruction and Reorientation sections below.

Reconstruction

At our institution, we presently use two-dimensional Butterworth filters of order 2.5 and cutoff frequency 0.3 out of a 0–0.5 range, as explained in Table 2.4 for ^{99m}Tc-based gated perfusion SPECT. The only published study concerning the effect of pre- or postreconstruction filtering on quantitative results of an automatic gated blood pool SPECT algorithm [24] indicates that below a certain filter cutoff quantitative volumes and ejection fractions are affected, though there was no assessment of which filter parameters provide more accurate values. Moreover, the effect of filtering and other reconstruction parameters may vary between algorithms. Reconstruction has traditionally been reported based on filtered backprojection, although iterative reconstruction techniques could possibly improve image quality. The degree to which gated blood pool SPECT would benefit from attenuation correction is currently not clear, since it is likely that attenuation affects perfusion ("cold spot" detection technique) more than function; indeed, the presence of attenuation was found to have no measurable effect on ejection fraction in the only reported study on the subject [25], though a recent phantom study indicates that attenuation may be

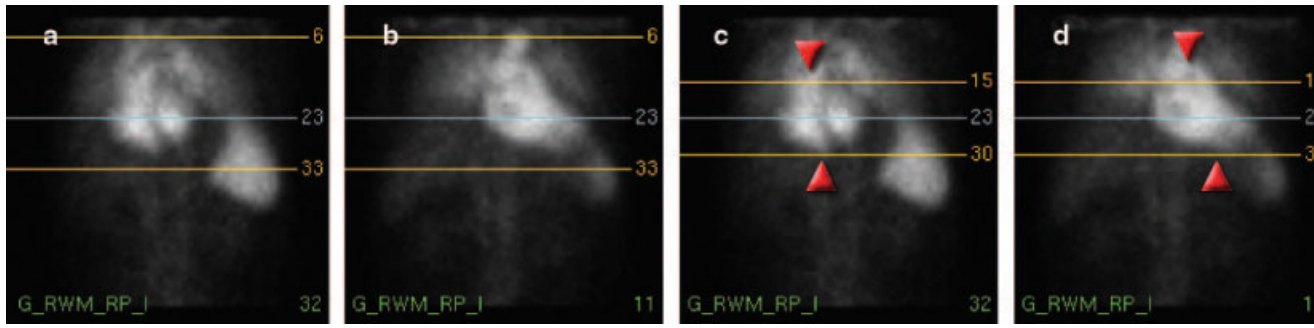

Figure 11.1 Reconstruction limits. Correct limits are shown in LAO (a) and RAO views (b), while incorrect limits that truncate the inferoapical portion of the RV as well as the pulmonary conus are shown in LAO (c) and RAO (d) views. Red triangular markers in images (c) and (d) indicate areas that will be incorrectly truncated after reconstruction. A summed dataset is used for clarity.

more detrimental to volume calculations from blood pool images acquired using a shorter scan arc [26].

Reorientation

Reorientation of the reconstructed transaxial image data is routinely done, but currently must rely on manual implementation because automatic reorientation algorithms are not available. Because of the lack of automation this step introduces operator-dependent variability that may affect quantification. In addition, optimal performance of subsequent quantification steps requires that all necessary information be included in the resulting short-axis dataset. Specifically, it is recommended that the reconstruction limits fully include the LV and RV, including the pulmonary outflow tract and that they include the atria in the image to allow automated programs to properly delineate the various cardiac structures. It may be detrimental to subsequent quantification to tighten the reconstruction limits around the LV alone (Fig. 11.1).

As in gated perfusion SPECT, manual reorientation consists in tracing projections of the left-ventricular long axis in two mid-ventricular planes, and should result in long-axis images in which the LV and the RV are either parallel (horizontal long-axis image) or perpendicular (vertical long-axis image) to the north-south (vertical) direction (Fig. 11.2). The LV and RV should be aligned along the east-west (horizontal) direction in short-axis images. Application software that gives immediate feedback on the effect of a particular angle selection on the reoriented image prior to actual reorientation may greatly help in quickly determining the appropriate reorientation angles. As a general rule, the reorientation axis can be drawn [1] as a line parallel to the long axis of the LV/atrium complex, which in turn can be assimilated to an ellipsoid having major axis equal to that long axis, or [2] as a line that bisects the "dark" septal space between the LV and RV. The former may often be easier as the corresponding sagittal view will bisect the LV, thereby making any adjustments needed to the elevation angle more obvious (see Fig. 11.2).

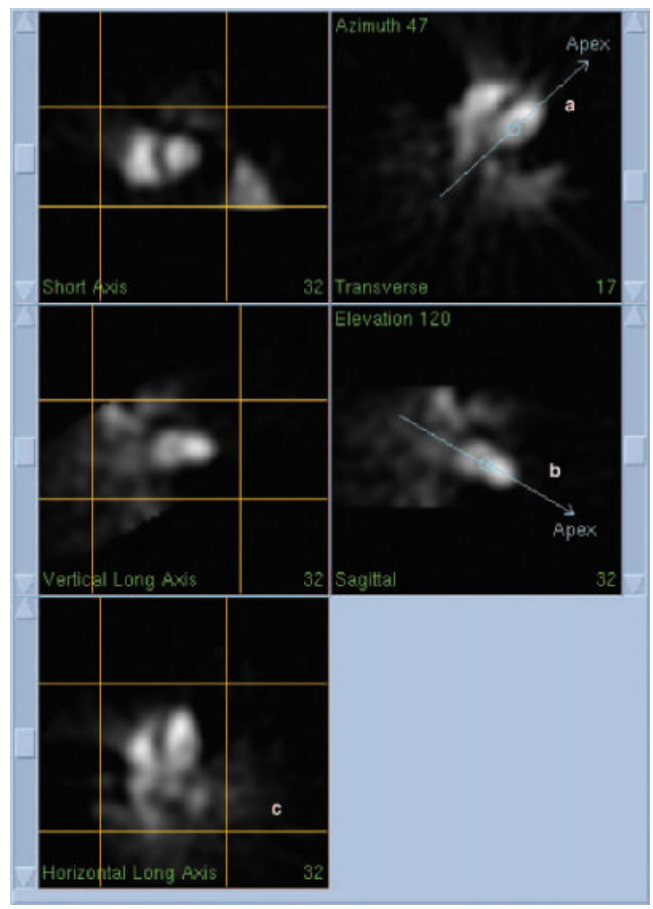

Figure 11.2 Reorientation and cropping. Note the correct alignment of the blue arrow with the long axis of the LV (a, b) and the basal cropping limit (c) that includes the atria in the resulting short-axis dataset. A summed dataset is used for clarity.

Analysis and quantification

Gated blood pool SPECT's key advantage of virtually eliminating the overlap of different cardiac chambers translates in the elimination of the need for background subtraction, a requirement of gated blood pool planar imaging. Moreover, the three-dimensional nature of the tomographic data lends itself naturally to space-based as well as count-based analysis instead of being limited to count-based methods alone.

Algorithms

Five different categories of algorithms for the quantification of gated blood pool SPECT have been described. While some methods could easily be classified as belonging to several of these categories, for purposes of presentation we have arbitrarily placed them in a single category.

Manual ROIs

Contours are manually drawn around the blood pool in a number of long-axis [27] or short-axis images [20,25], the total number of voxels bound by the various contours is counted, and the blood pool volume derived as the number of voxels multiplied by an individual voxel's volume. Count density within images can be used to scale individual slice volumes so as to account for partial volume effects [27] or to separate ventricles from atria [20], but is generally not solely responsible for the quantitative measurements of function.

Thresholding

In this very popular approach [14–16,18,21–23,28,29], only the volumes of voxels with a count value greater than a certain threshold are summed for the purpose of blood pool volume (and, consequently, endocardial borders) derivation. Threshold values vary from 30% [21] to 70% [16] of the maximum voxel count value within the ventricular cavity, the average being around 45%, though recently a 35% threshold has been favored [29,30] for volumetric measurements. Thresholding is usually combined with manual masking to separate the LV from the RV [15,22,28] and with either masking [14] or phase analysis [18,21–23,31] to separate the ventricles from the atria. In the "variable threshold" implementation of the thresholding approach, the threshold varies along the manually selected long axis of the ventricle, and ventricle–atrium separation is achieved by increasing the threshold in the basal portion of the ventricle [17]. In another implementation [32] a threshold is iteratively computed by the algorithm to best fit the dataset's count distribution gradient.

As described for manual ROI methods, once voxels have been selected there are still two alternatives for the calculation of ejection fractions: ejection fractions can be derived from the ratio of the number of selected voxels at end-diastole and end-systole (equivalent to a ratio of volumes), or from the ratio of the summed counts for the selected voxels. These two approaches provide different results, chiefly because of partial volume effects [33].

Relaxation labeling

In this method [34] an initial estimate of the three-dimensional endocardial surface is obtained by thresholding. Distances along radial directions are then computed from the manually defined long axis of the ventricle, and constrained iterations are used to compute a final set of distances representing the endocardium.

Reprojection

In this approach [35] tomographic data are reprojected either to a standard LAO planar view or (preferably) to a true long-axis planar view, which provides a reduction in background activity due to the absence of overlap of the other cardiac and noncardiac structures. Standard planar processing can then be performed using a planar quantification algorithm [36].

Gradient operators

The remaining implementation [37] is an adaptation of an algorithm developed for myocardial perfusion SPECT [38] that uses a combination of gradient information and morphological operators to generate spline-based surfaces for each interval. This method provides quantification of LV parameters only and may require user intervention to modify the LV valve plane.

Comparisons and validations

All the above algorithms require some degree of manual operation with respect to "masking," setting axes, setting one or several threshold values, or setting limits for the boundary search (for example, at the valve plane level), except for algorithms described in [32] and [37]. A totally automatic quantitative approach based on the three-dimensional, knowledge-directed analysis of count gradients in space and time, developed by our group, has been clinically available for several years [39] and validations have been reported by several groups with respect to the LV and RV [29,30,40–50]. Figure 11.3 shows how applying the algorithm to a short-axis dataset results in the contouring of the LV and the RV, as well as their separation from the respective atria. The left- and right-ventricular

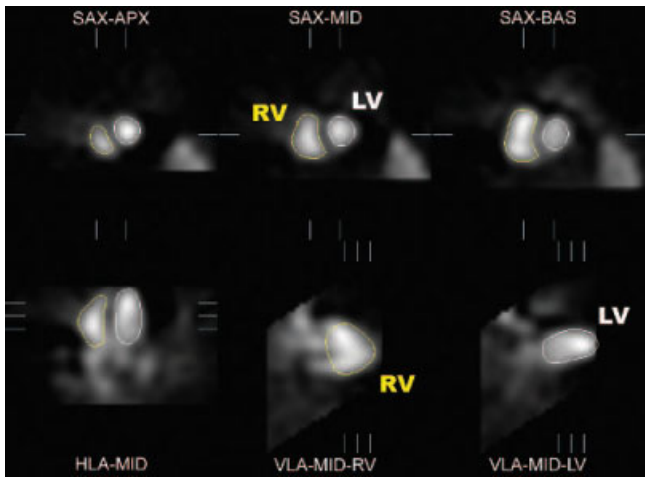

Figure 11.3 Reconstructed and reoriented short-axis (top row, left to right = apex to base), mid-ventricular horizontal (bottom left), and vertical (bottom center and right, respectively, through the RV and LV) long-axis images for a gated blood pool SPECT study, at end-diastole. Automatically determined and overlaid contours are displayed for both ventricles (white = LV, yellow = RV).

endocardia are generated as three-dimensional surfaces, which can be displayed in a manner similar to that employed for gated myocardial perfusion SPECT imaging (Fig. 11.4). More recently, a new segmentation algorithm with a more tightly coupled LV/RV model was developed at Cedars-Sinai [51]. Although this method has not yet undergone widespread clinical validation, it offers previously unavailable count-based calculations using the automatically generated three-dimensional ROIs and will soon include regional phase measurement capabilities. It is possible that count-based methods are inherently more robust because they do not rely on the exact delineation of endocardial borders but rather will only consider activity above a certain threshold within an ROI [27,52]. Small errors in the localization of the endocardium lead to large volume variations, which may account for less than ideal repeatability and reproducibility [53]. Our experience with inter- and intraobserver variability through repeated reconstruction and reorientation indicates reduced variability for LV end-diastolic volume (EDV) measurements using a count-based technique [51].

Table 11.1 presents a synopsis of published human validation studies of quantitative gated blood pool SPECT algorithms, including the standard used for comparison and the parameters quantified. While the agreement between gated SPECT and gold standard measurements of global ventricular function is generally very good to excellent, it is apparent from Table 11.1 that right-ventricular function or regional function in general is rarely validated, and may be more sensitive to the acquisition protocol used

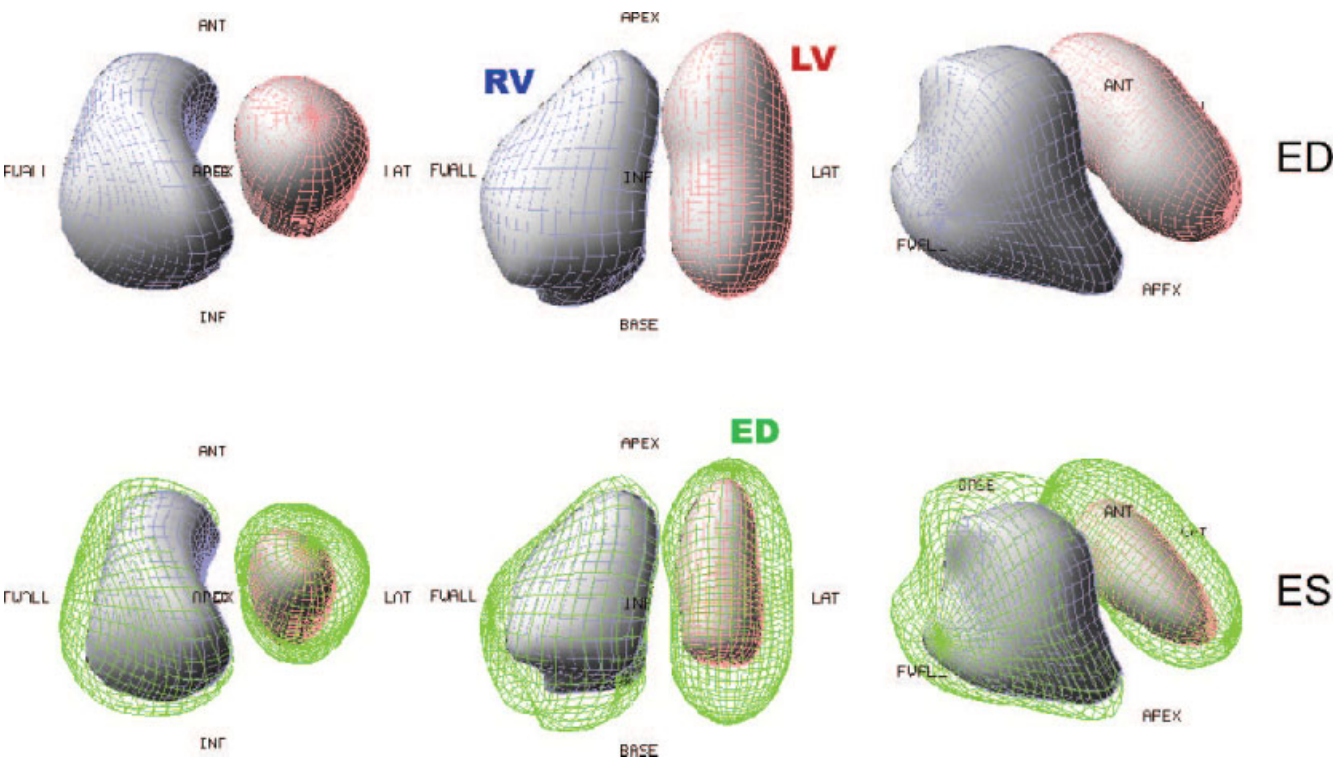

Figure 11.4 Three-dimensional representation of the LV and RV displayed in three standard orientations at end-diastole (top row) and end-systole (bottom row). Shaded gray surfaces = endocardia (red grid = LV, blue grid = RV); green grid = reference endocardial location at end-diastole.

Table 11.1 Validation of quantitative gated blood pool SPECT measurements.

Method	"Gold standard"	Parameter	Agreement	No. of patients	Reference
Manual ROI	CVG	EDV	$r = 0.97$, SEE = 23 ml	25	(27)
Threshold	CVG	Regional EF	$r = 0.45–0.78$	61	(21)
Threshold	MUGA	LVEF	$r = 0.94$	25	(28)
Threshold	MUGA	LVEDV	$r = 0.85$	25	(28)
Threshold	MUGA	LVESV	$R = 0.88$	25	(28)
Threshold	CVG	LVEF	$r = 0.85$, SEE = 6%	36	(23)
Threshold	CVG	LVEDV	$r = 0.81$, SEE = 27 ml	36	(23)
Threshold	CVG	LVESV	$r = 0.96$, SEE = 12 ml	36	(23)
Threshold	MUGA	LVEF	$r = 0.88–0.92$	30	(14)
Threshold	CVG	LVEDV	$r = 0.90–0.91$	30	(14)
Threshold	CVG	LVESV	$r = 0.91–0.93$	30	(14)
Threshold	CVG	LVEF	$r = 0.75–0.79$	30	(14)
Threshold	MUGA	LVEF	$r = 0.92$, SEE = 8%	12	(15)
Threshold	CVG	LVEF	$r = 0.92$, SEE = 8%	12	(15)
Threshold	CVG	LVEDV	$r = 0.94$, SEE = 20 ml	12	(15)
Threshold	CVG	LVESV	$r = 0.93$, SEE = 24 ml	12	(15)
Threshold	MRI	LVEF	$r = 0.94$, SEE = 9%	10	(18)
Threshold	MRI	RVEF	$r = 0.88$, SEE = 6%	10	(18)
Threshold	MRI	LVV	$r = 0.96$, SEE = 18 ml	20	(18)
Threshold	MRI	RVV	$r = 0.91$, SEE = 16 ml	20	(18)
Threshold	MUGA	LVEF	$r = 0.96$, SEE = 7%	18	(18)
Threshold	MUGA	RVEF	$r = 0.86$, SEE = 8%	10	(18)
Threshold	MUGA	LVEF	$R = 0.80$	45	(54)
Threshold	MUGA	LVEF	$r = 0.78$, SD = 8.8%	53	(32)
Threshold	MUGA	LVEF	$r = 0.82$, SD = 8.8%	92	(42)
Threshold	MUGA	LVEF	$R = 0.90$	59	(31)
Threshold	Echo	LVEDV	$R = 0.69$	59	(31)
Threshold	Gated SPECT	LVEDV	$r = 0.93$, SEE = 25 ml, SD = 36 ml	37	(55)
Threshold	Gated SPECT	LVESV	$r = 0.95$, SEE = 19 ml, SD = 32 ml	37	(55)
Threshold	Gated SPECT	LVEF	$r = 0.91$, SEE = 6.8%, SD = 6.9%	37	(55)
Gradients	MUGA	LVEF	$R = 0.89$	76	(56)
Gradients	MUGA	LVEF	$R = 0.87$	63	(57)
Gradients	MUGA	RVEF	$R = 0.76$	63	(57)
Gradients	MUGA	LVEF	$r = 0.77$, SEE = 10%	90	(40)
Gradients	MUGA	LVEF	$r = 0.99$, SD = 0.2 ± 7.2	30	(58)
Gradients	MUGA	LVEF	$r = 0.80$, SD = 9.4%	92	(42)
Gradients	MUGA	LVEF	$R = 0.92$	70	(45)
Gradients	MUGA	LVEDV	$R = 0.78$	70	(45)
Gradients	MUGA	LVESV	$R = 0.91$	70	(45)
Gradients	MUGA	LVEF/RVEF	$R = 0.99$	12	(59)
Gradients	MUGA	LVEF	$R = 0.97$	56	(37)
Gradients	MUGA	LVEF	$R = 0.81$	422	(30)
Gradients	MUGA	LVEF (PET)	$R = 0.91$	60	(49)
Gradients	First pass	LVEF	$R = 0.89$	14	(57)
Gradients	First pass	RVEF	$R = 0.82$	14	(57)
Gradients	First pass	LVEF	$r = 0.64$, SEE = 16%	90	(40)
Gradients	First pass	RVEF	$r = 0.68$, SEE = 8.6%	64	(48)
Gradients	First pass	RVEF	$r = 0.82$	65	(50)
Gradients	Gated SPECT	LVEF	$r = 0.88$	15	(41)
Gradients	Gated SPECT	LVEDV	$r = 0.92$, SEE = 38 ml	15	(41)
Gradients	Gated SPECT	LVESV	$r = 0.93$, SEE = 36 ml	15	(41)
Gradients	Gated SPECT	LVEDV	$r = 0.98$	16	(60)
Gradients	Gated SPECT	LVESV	$r = 0.93$	16	(60)
Gradients	Gated SPECT	LVEF	$r = 0.98$	56	(37)

Table 11.1 (*Continued*)

Method	"Gold standard"	Parameter	Agreement	No. of patients	Reference
Gradients	Gated SPECT	LVEF	$r = 0.98$	45	(61)
Gradients	CVG	(EDV+ESV)	$r = 0.84$, SD $= -0.2 \pm 37$	30	(58)
Gradients	CVG	RVEDV	$r = 0.98$	16	(60)
Gradients	CVG	RVESV	$r = 0.83$	16	(60)
Gradients	MRI	LVEF	$r = 0.86$	31	(44)
Gradients	MRI	LVEDV	$r = 0.93$	31	(44)
Gradients	MRI	LVESV	$r = 0.95$	31	(44)
Gradients	MRI	RVEF	$r = 0.60$	31	(44)
Gradients	MRI	LVEDV	$r = 0.71$	31	(44)
Gradients	MRI	LVESV	$r = 0.75$	31	(44)
Relaxation labeling	MRI	LVV	$r = 0.96$, SEE = 11 ml	8	(34)
Count analysis	MUGA	LVEF	$r = 0.91$	82	(62)
Count analysis	MUGA	LVEF	$r = 0.90$	40	(63)
Count analysis	MUGA	LVEF	$r = 0.93$	104	(64)
Count analysis	MUGA	LVEF	$r = 0.95$	60	(65)
Count analysis	MUGA	LVEDV	$r = 0.67$	60	(65)
Count analysis	MUGA	LVESV	$r = 0.83$	60	(65)
Count analysis	MUGA	LVEF	$r = 0.90$	201	(66)
Count analysis	MUGA	LVEF	$r = 0.83$	422	(30)
Count analysis	First pass	RVEF	$r = 0.70$, SEE = 8.4%	64	(48)
Count analysis	MRI	LVEF	$r = 0.88$, SEE = 8%	26	(67)
Count analysis	MRI	RVEF	$r = 0.80$, SEE = 9%	26	(67)
Count analysis	MRI	LVV	$r = 0.84$, SEE = 16ml	26	(67)
Count analysis	MRI	RVV	$r = 0.95$, SEE = 16 ml	26	(67)
Count analysis	MRI	RVEF	$r = 0.85$, SEE = 6%	28	(68)
Count analysis	MRI	RVEDV	$r = 0.94$, SEE = 24 ml	28	(68)
Reprojection	MUGA	LVEF	$r = 0.89$, SEE = 8%	23	(35)

Abbreviations: CVG, contrast ventriculography; LVEDV, left-ventricular end-diastolic volume; LVEF, left-ventricular ejection fraction; LVESV, left end-systolic volume; LVV, left-ventricular volumes (end-diastolic and end-systolic); MRI, magnetic resonance imaging; MUGA, planar blood pool; *r*, Spearman's correlation coefficient; RVEDV, right-ventricular end-diastolic volume; RVEF, right-ventricular ejection fraction; RVESV, right end-systolic volume; RVV, right-ventricular volumes (end-diastolic and end-systolic); SD, random error (standard deviation of the difference between gated blood pool SPECT and gold standard); SEE, standard error of the estimate; WM, wall motion.

than LV function measurements [13]. This may be related to the limited ability of gated planar blood pool to accurately quantify right-ventricular function [69], as well as to the limitations of planar techniques in the assessment of regional function. Indeed, it has been stressed [70] that two-dimensional gold standards may be intrinsically less accurate than gated SPECT algorithms operating in the three-dimensional space, because of the geometric assumptions required by the former. More recent interest in right-ventricular validation work has shown good correlation between a semiautomatic count-based SPECT method and manual delineation of the RV cavity using MRI images [68], and better correlation between SPECT-based methods and first-pass imaging than between planar planar blood pool and first-pass imaging [48]. This may be caused largely by the difficulty in accurately locating RV valves in SPECT images, which may in turn lead fully automated methods to perform less adequately for the RV than for the LV, as may be evidenced by a recent dynamic phantom study [47] showing that manual adjustment of the tricuspid and pulmonary valve limits may be needed to achieve good correlation with other measurement techniques. The anisotropic nature of MRI datasets, combined with the irregular geometry of the RV, requires that RV volume measurements be computed with care in order to avoid large volume errors that may decrease the usefulness of MRI as a "gold standard."

Comparisons between various SPECT algorithms (automated and semiautomated) and the algorithm developed at Cedars-Sinai have also been published [29,30,42,47,48,58]. Measurements derived from SPECT methods often correlate better with each other than they do with measurements obtained from other modalities, with the exception of some RV measurements [30]. The Cedars-Sinai algorithm was also applied to CO-15 PET studies [49], and excellent correlation was reported both between

PET and planar blood pool as well as between PET and SPECT (though in the latter case the same program was used for both types of images).

Clinical applications of gated blood pool SPECT

Because of the ease of SPECT acquisition and processing, and given the growing widespread use of gated SPECT in myocardial perfusion scintigraphy, we believe that gated blood pool SPECT will become the most commonly utilized nuclear cardiology method for blood pool scintigraphy.

Current applications

Until automatic algorithms for assessment of left-ventricular ejection fraction are widely available, it will be common for laboratories to employ a planar left anterior view for measurement of ejection fraction, and the SPECT data for regional function assessment. Should automatic methods for measurement of left-ventricular ejection fraction become widely accepted, however, it is likely that blood pool SPECT without planar imaging would become the routine for cardiac gated blood pool studies. The clinical circumstances in which this procedure is likely to become effective are the same as those in which resting blood pool scintigraphy is currently applied. Chief among these is the assessment of doxorubicin cardiotoxicity [71]. While global ejection fraction is the mainstay of this assessment, it has been shown that regional dysfunction, often of the apex, may allow the detection of early doxorubicin cardiotoxicity at a time in which the ejection fraction is still normal. In our experience, gated blood pool SPECT, by eliminating the overlap of cardiac structures inherent in planar imaging, appears to be more reliable for detecting this early abnormality. Serial quantitative assessments by gated blood pool SPECT can also be employed in serial assessment of patients with asymptomatic aortic insufficiency or with congestive heart failure.

Areas of potential increased application of cardiac blood pool SPECT

The potential to accurately assess diastolic function by gated cardiac blood pool SPECT could be an area of future growth of the application of the method. Additionally, the method may be well suited to the evaluation of the effects of nitroglycerin or low-dose dobutamine on myocardial contractile reserve. Although gated myocardial perfusion SPECT can assess these parameters, gated cardiac blood pool SPECT has the advantage of an increased cardiac count rate per millicurie injected, with resultant potential to diminish acquisition time (for better assessment of interventions such as nitroglycerin or dobutamine) or increase the number of frames per cardiac cycle (to improve assessment of systolic and potentially diastolic function). These new applications of blood pool SPECT may become more widely explored and clinically utilized as accurate, automated methods for global and regional biventricular function measurement become widely available.

Cardiac resynchronization therapy

It has also been recently suggested [72] that using phase analysis of gated blood pool SPECT may be valuable in selecting patients who might benefit from cardiac resynchronization therapy (CRT). While echocardiography is the current modality of choice in this setting, the three-dimensional nature of SPECT provides unique theoretical advantages that have not yet been adequately explored clinically. Gated blood pool SPECT may be better suited than gated myocardial perfusion SPECT for phase analysis of contraction patterns, since in the presence of a large perfusion defect, myocardial perfusion SPECT contour detection may be less accurate as it relies on interpolation and myocardial mass constraints to delineate the myocardial edges, which in turn may lead to decreased accuracy in computing regional wall motion. Blood pool SPECT, however, offers high count statistics even in highly dysfunctional hearts and unlike perfusion SPECT is not hampered by the presence of extensive ventricular scarring, which might have little, if any, uptake of a perfusion tracer. Thus, with gated blood pool SPECT, reliable contraction phase information can be extracted in all cases. Regional wall motion phase and amplitude measurements [73–75] have recently been added by our group to the existing automated segmentation algorithm in order to provide tools for the assessment of ventricular contraction abnormalities [76,77] and to enable the analysis of differences between phase measurements obtained before and after CRT [78]. These phase measurements are based either on Fourier transforms (FT) [79] of voxel time–activity curves or on FT of wall displacements. From each FT two measurements are commonly derived, the amplitude and the phase of the first harmonic, though multiharmonic measures are also used [80]. The phase values for all points considered (voxels or surface points) can be mapped into a histogram that graphically depicts the frequency with which a given phase value is present in the data [81]. Figure 11.5 shows phase histograms and phase-mapped parametric ventricular surfaces for an 81-year-old male patient. The two datasets were acquired pre- and postimplantation of a cardiac resynchronization device (i.e., biventricular pacemaker). A narrow histogram indicates synchronous contraction while a wider histogram indicates delays in the contraction process within a given region, and differences

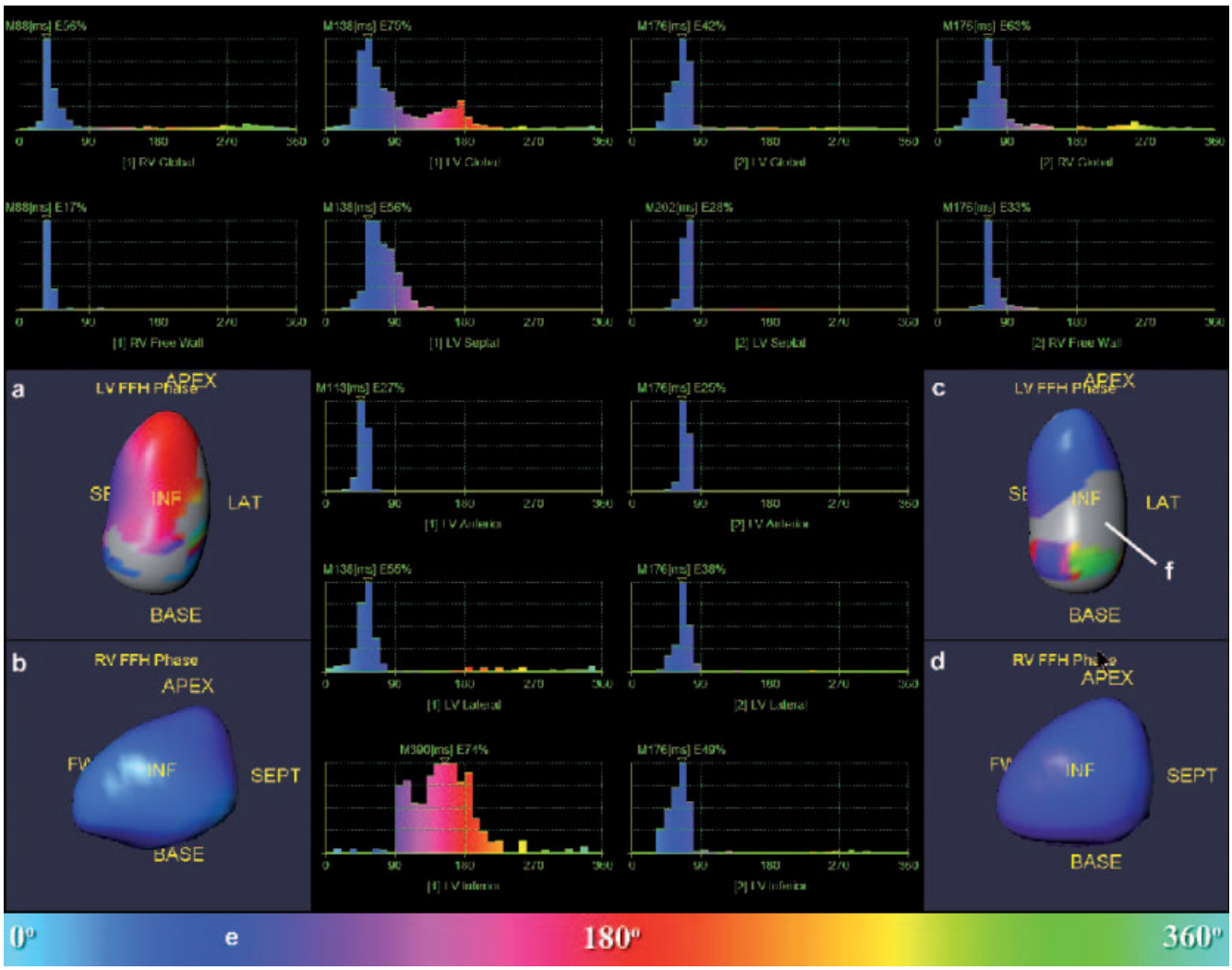

Figure 11.5 Pre- (left) and post-CRT (right) phase information. Pre-CRT LV and RV surfaces (a, b) are shown, as well as post-CRT LV and RV surfaces (c, d). Phase information is displayed onto the surfaces using color mapping (e), with phase information not displayed (i.e., grayed out) wherever the amplitude is lower than 5**%** of the maximum wall motion amplitude (f). This figure also shows global and regional phase histograms (regional histograms are computed for the anterior, lateral, inferior, and septal walls of the LV, and for the RV free wall). For each histogram the mode (Mxxx[ms]) and entropy (Eyy**%**) are displayed (see text for explanation). Pre-CRT, note the wide histograms for the LV septal and inferior walls, as well as the delay (shift) between the modes of the LV regional histograms. Post-CRT, note the narrow histograms and synchronized modes. In the software this view can be gated, which simplifies the observation of wall motion phase changes: pre-CRT the inferior wall and apex can be seen contracting out of phase, while post-CRT all walls contract synchronously.

in the location of histogram peaks indicate delays between regions. The mean and mode of a histogram are two common measures of peak location, while standard deviation from the mean [82], full width at half or 10% of the maximum intensity (FWHM, FW10M), and other entropy or synchrony measures [83] can be used to quantify histogram dispersion. This type of assessment, especially if combined with a measure of myocardial viability, could help in identifying patients that may respond well to CRT, and in locating the optimal sites for pacemaker lead placement.

References

1. Strauss HW, Zaret BL, Hurley PJ, Natarajan TK, Pitt B. A scintiphotographic method for measuring left ventricular ejection fraction in man without cardiac catheterization. American Journal of Cardiology 1971;28(5):575–580.
2. Berman DS, Salel AF, DeNardo GL, Bogren HG, Mason DT. Clinical assessment of left ventricular regional contraction patterns and ejection fraction by high-resolution gated scintigraphy. Journal of Nuclear Medicine 1975;16(10):865–874.

3. Moore ML, Murphy PH, Burdine JA. ECG-gated emission computed tomography of the cardiac blood pool. Radiology 1980;134(1):233–235.
4. Tamaki N, Mukai T, Ishii Y, et al. Multiaxial tomography of heart chambers by gated blood-pool emission computed tomography using a rotating gamma camera. Radiology 1983;147(2):547–554.
5. Maublant J, Bailly P, Mestas D, et al. Feasibility of gated single-photon emission transaxial tomography of the cardiac blood pool. Radiology 1983;146(3):837–839.
6. Hoffman EJ, Huang SC, Phelps ME. Quantitation in positron emission computed tomography, 1: Effect of object size. Journal of Computer Assisted Tomography 1979;3(3):299–308.
7. Kikkawa M, Nakamura T, Sakamoto K, et al. Assessment of left ventricular diastolic function from quantitative electrocardiographic-gated (99)mTc-tetrofosmin myocardial SPET. European Journal of Nuclear Medicine 2001; 28(5):593–601. [errata in European Journal of Nuclear Medicine 2001;28:1579).
8. Kumita S, Cho K, Nakajo H, et al. Assessment of left ventricular diastolic function with electrocardiography-gated myocardial perfusion SPECT: comparison with multigated equilibrium radionuclide angiography. Journal of Nuclear Cardiology 2001;8(5):568–574.
9. Sakamoto K, Nakamura T, Zen K, et al. Identification of exercise-induced left ventricular systolic and diastolic dysfunction using gated SPECT in patients with coronary artery disease. Journal of Nuclear Cardiology 2004;11(2):152–158.
10. Salel AF, Berman DS, DeNardo GL, Mason DT. Radionuclide assessment of nitroglycerin influence on abnormal left ventricular segmental contraction in patients with coronary heart disease. Circulation 1976;53(6):975–982
11. Germano G, Erel J, Kiat H, Kavanagh PB, Berman DS. Quantitative LVEF and qualitative regional function from gated thallium-201 perfusion SPECT. Journal of Nuclear Medicine 1997;38(5):749–754.
12. Vanhove C, Franken PR, Defrise M, Bossuyt A. Comparison of 180 and 360 degree data acquisition for determination of left ventricular function from gated myocardial perfusion tomography and gated blood pool tomography. European Journal of Nuclear Medicine 2003;30(11):1498–1504.
13. Adachi L, Akagi H, Umeda T, et al. Differential effect of 180 degree and 360 degree acquisition orbits on the accuracy of quantitative blood pool SPECT imaging [abstract]. Journal of Nuclear Cardiology 2003;10(1):S26.
14. Corbett JR, Jansen DE, Lewis SE, et al. Tomographic gated blood pool radionuclide ventriculography: analysis of wall motion and left ventricular volumes in patients with coronary artery disease. Journal of the American College of Cardiology 1985;6(2):349–358.
15. Gill JB, Moore RH, Tamaki N, et al. Multigated blood-pool tomography: new method for the assessment of left ventricular function. Journal of Nuclear Medicine 1986;27(12):1916–1924.
16. Yamashita K, Tanaka M, Asada N, et al. A new method of three dimensional analysis of left ventricular wall motion. European Journal of Nuclear Medicine 1988;14(3):113–119.
17. Faber TL, Stokely EM, Templeton GH, Akers MS, Parkey RW, Corbett JR. Quantification of three-dimensional left ventricular segmental wall motion and volumes from gated tomographic radionuclide ventriculograms. Journal of Nuclear Medicine 1989;30(5):638–649.
18. Chin BB, Bloomgarden DC, Xia W, et al. Right and left ventricular volume and ejection fraction by tomographic gated blood-pool scintigraphy. Journal of Nuclear Medicine 1997;38(6):942–948.
19. Hamilton G, Williams D, Caldwell J. Frame-rate requirements for recording time–activity curves by radionuclide angiocardiography. In Nuclear Cardiology: Selected Computer Aspects. 1978 Symposium sponsored by the Computer Council of the Society of Nuclear Medicine; 1978; Atlanta, GA; 1978:75–83.
20. Ohtake T, Nishikawa J, Machida K, et al. Evaluation of regurgitant fraction of the left ventricle by gated cardiac blood-pool scanning using SPECT. Journal of Nuclear Medicine 1987;28(1):19–24.
21. Barat JL, Brendel AJ, Colle JP, et al. Quantitative analysis of left-ventricular function using gated single photon emission tomography. Journal of Nuclear Medicine 1984;25(11):1167–1174.
22. Cerqueira MD, Harp GD, Ritchie JL. Quantitative gated blood pool tomographic assessment of regional ejection fraction: definition of normal limits. Journal of the American College of Cardiology1992;20(4):934–941.
23. Stadius ML, Williams DL, Harp G, et al. Left ventricular volume determination using single-photon emission computed tomography. American Journal of Cardiology 1985;55(9):1185–1191.
24. Daou D, Coaguila C, Rouzet F, Slama M, Le Guludec D. ECG-gated SPECT radionuclide angiography (RNA SPECT) and QBS processing software: influence of different SPECT processing parameters [abstract]. European Journal of Nuclear Medicine 2003;30(Suppl 2):S212.
25. Bartlett ML, Bacharach SL, Barker C, et al. SPECT gated blood pool imaging-potentials and problems. In Computers in Cardiology, 1994, Bethesda, MD, USA: IEEE, 197–200.
26. Seierstad T, Bogsrud T, Skretting A. Effects of photon attenuation on the determination of cardiac volumes from reconstructed counts in gated blood pool SPET. European Journal of Nuclear Medicine and Molecular Imaging 2004;31(3):399–402.
27. Bunker SR, Hartshorne MF, Schmidt WP, et al. Left ventricular volume determination from single-photon emission computed tomography. American Journal of Roentgenology 1985;144(2):295–298.
28. Underwood SR, Walton S, Ell PJ, Jarritt PH, Emanuel RW, Swanton RH. Gated blood-pool emission tomography: a new technique for the investigation of cardiac structure and function. European Journal of Nuclear Medicine 1985;10(7–8):332–337.
29. Daou D, Harel F, Helal BO, et al. Electrocardiographically gated blood-pool SPECT and left ventricular function: comparative value of 3 methods for ejection fraction and volume estimation. Journal of Nuclear Medicine 2001;42(7):1043–1049.

30. Nichols K, Humayun N, De Bondt P, Vandenberghe S, Akinboboye OO, Bergmann SR. Model dependence of gated blood pool SPECT ventricular function measurements. Journal of Nuclear Cardiology 2004;11(3):282–292.
31. Eder V, Bernis F, Drumm M, Diarra MI, Baulieu F, Leger C. Three-dimensional analysis of left ventricle regional wall motion by using gated blood pool tomography. Nuclear Medicine Communications 2004;25(9):971–978.
32. Vanhove C, Franken PR, Defrise M, Momen A, Everaert H, Bossuyt A. Automatic determination of left ventricular ejection fraction from gated blood-pool tomography. Journal of Nuclear Medicine 2001;42(3):401–407.
33. Daou D, Vilain D, Coaguila C, Helal BO, Fourme T, Slama M. Left ventricular ejection fraction calculation with ECG-gated blood pool tomography: is activity ratio better than volume ratio [abstract]? Journal of Nuclear Medicine 2001;42(5): 136P.
34. Faber TL, Stokely EM, Peshock RM, Corbett JR. A model-based four-dimensional left ventricular surface detector. IEEE Transactions on Medical Imaging 1991;10(3):321–329.
35. Bartlett ML, Srinivasan G, Barker WC, Kitsiou AN, Dilsizian V, Bacharach SL. Left ventricular ejection fraction: comparison of results from planar and SPECT gated blood-pool studies. Journal of Nuclear Medicine 1996;37(11):1795–1799.
36. Reiber JH. Quantitative analysis of left ventricular function from equilibrium gated blood pool scintigrams: an overview of computer methods. European Journal of Nuclear Medicine 1985;10(3–4):97–110.
37. Ficaro EP, Quaife RF, Kritzman JN, Corbett JR. Validation of a new fully automatic algorithm for quantification of gated blood pool SPECT: correlations with planar gated blood pool and perfusion SPECT [abstract]. Journal of Nuclear Medicine 2002;43(5):97P.
38. Chugh A, Ficaro EP, Moscucci M, Kritzman JN, Corbett JR. Quantification of left ventricular function by gated perfusion tomography: testing of a new fully automatic algorithm [abstract]. Journal of the American College of Cardiology 2001;37(2):394A.
39. Van Kriekinge S, Berman D, Germano G. Automatic quantification of left ventricular ejection fraction from gated blood pool SPECT [abstract]. Circulation 1997;96(8):I-309.
40. Schwartz R, Le Guludec D, Holder L, et al. Blood pool gated SPECT: validation of left ventricular volumes and ejection fraction with planar radionuclide angiography [abstract]. Journal of Nuclear Cardiology 2000;7(4):S2.
41. Van Kriekinge S, Paul AK, Hasegawa S, Nishimura T, Berman DS, Germano G. Validation of quantitative left-ventricular end-diastolic and end-systolic volumes from gated blood pool SPECT [abstract]. Journal of the American College of Cardiology 2001;37(2):500A.
42. Vanhove C, Franken PR. Left ventricular ejection fraction and volumes from gated blood pool tomography: comparison between two automatic algorithms that work in three-dimensional space. Journal of Nuclear Cardiology 2001;8(4):466–471.
43. Higuchi T, Taki J, Nakajima K, Kinuya S, Tonami N. Accuracy and reproducibility of left and right ventricular ejection fraction assessed by automatic evaluation of ECG-gated blood pool SPECT [abstract]. Journal of Nuclear Medicine 2002;43(5):97P.
44. Keng F, Tan R, Chua T, Koh T. Quantitative blood pool single photon emission computed tomography (QBS) program: comparison to cardiac magnetic resonance imaging (CMR) [abstract]. Journal of Nuclear Cardiology 2003;10(1):S5.
45. Keng F, Chua T, Koh T. Quantitative blood pool single-photon emission computed tomography (QBS) program: comparison with conventional planar equilibrium blood pool imaging (MUGA) [abstract]. Journal of Nuclear Cardiology 2003;10(1):S25.
46. Wright GA, Thackray S, Howey S, Cleland JG. Left ventricular ejection fraction and volumes from gated blood-pool SPECT: comparison with planar gated blood-pool imaging and assessment of repeatability in patients with heart failure. Journal of Nuclear Medicine 2003;44(4):494–498.
47. De Bondt P, Claessens T, Rys B, et al. Accuracy of 4 different algorithms for the analysis of tomographic radionuclide ventriculography using a physical, dynamic 4-chamber cardiac phantom. Journal of Nuclear Medicine 2005;46(1):165–171.
48. Daou D, Van Kriekinge SD, Coaguila C, et al. Automatic quantification of right ventricular function with gated blood pool SPECT. Journal of Nuclear Cardiology 2004;11(3):293–304.
49. Higuchi T, Taki J, Nakajima K, Ikeda M, Namura M, Tonami N. Measurement of LVEF with CO-15 gated blood-pool 3D mode PET using automatic edge-detection program [abstract]. Journal of Nuclear Medicine 2004;45(5):223P.
50. Higuchi T, Taki J, Nakajima K, Ikeda M, Namura M, Tonami N. Automatic analysis of right ventricular ejection fraction using ECG-gated blood SPECT: comparison with first-pass angiography [abstract]. Journal of Nuclear Medicine 2004;45(5):178P.
51. Van Kriekinge S. Ventricular function analysis from gated blood pool single photon emission computed tomography images [PhD dissertation]. Los Angeles: University of California; 2003.
52. Caputo GR, Graham MM, Brust KD, Kennedy JW, Nelp WB. Measurement of left ventricular volume using single-photon emission computed tomography. American Journal of Cardiology 1985;56(12):781–786.
53. Daou D, Gharzeddine L, Haider M, et al. Limits of repeatability of a completely automatic ECG gated blood pool SPECT processing software for left ventricular function measurement [abstract]. European Journal of Nuclear Medicine and Molecular Imaging 2002;29(Suppl 1):S146.
54. Vanhove C, Everaert H, Bossuyt A, Franken P. Automatic determination of LV ejection fraction and volumes by gated blood pool SPECT [abstract]. Journal of Nuclear Medicine 2000;41(5):187P.
55. Vanhove C, Walgraeve N, De Geeter F, Franken PR. Gated myocardial perfusion tomography versus gated blood pool tomography for the calculation of left ventricular volumes and ejection fraction. European Journal of Nuclear Medicine and Molecular Imaging 2002;29(6):735–741.
56. Van Kriekinge SD, Berman DS, Germano G. Automatic quantification of left ventricular ejection fraction from gated blood pool SPECT. Journal of Nuclear Cardiology 1999;6(5):498–506.

57. Van Kriekinge S, Berman D, Germano G. Automatic quantification of left and right ventricular ejection fractions from gated blood pool SPECT [abstract]. Circulation 1999;100(18):I-26.
58. Daou D, Harel F, Mariano-Goulart D, et al. Left ventricular function estimated with ECG-gated blood pool spect: comparison of two different processing softwares [abstract]. Journal of Nuclear Medicine 2001;42(5):137P.
59. Alexanderson E, Espinola N, Meavel A, Victoria D. Assessment of ventricular perfusion and function with nuclear scan and echocardiography in patients with corrected transposition of great arteries [abstract]. Journal of Nuclear Cardiology 2003;10(1):S66.
60. Nakajima K, Higuchi T, Taki J, et al. Quantitative gated SPECT with myocardial perfusion and blood-pool studies to determine ventricular volumes and stroke volume ratio in congenital heart diseases [abstract]. Journal of Nuclear Cardiology 2003;10(1):S11.
61. Ficaro EP, Kritzman' JN, Corbett JR. Normal LV ejection fraction limits using 4D MSPECT: comparisons of gated perfusion and gated blood pool SPECT data with planar blood pool imaging [abstract]. Journal of Nuclear Cardiology 2003;10(1):S9.
62. Groch M, Belzberg A, DePuey E, et al. Evaluation of ventricular performance using gated blood pool SPECT: a multicenter study [abstract]. Journal of Nuclear Medicine 2000;41(5):5P.
63. Groch M, Marshall R, Erwin W, Spies S, Barnett C. Left ventricular ejection fraction computed from gated SPECT blood pool imaging correlates with conventional planar imaging [abstract]. Journal of Nuclear Medicine 2000);41(5):98P.
64. Groch M, Depuey E, Belzberg A, et al. Assessment of left ventricular performance by gated blood pool SPECT: a multicenter study [abstract]. Circulation 2000;102(18):II-725.
65. Keng F, Tan H, Chua T. Gated SPECT blood pool imaging: a comparison with equilibrium blood pool imaging [abstract]. Journal of Nuclear Cardiology 2000;7(4):S3.
66. Groch MW, Erwin WD, DePuey EG, et al. Multicenter clinical evaluation of gated blood pool SPET for the assessment of ventricular function [abstract]. European Journal of Nuclear Medicine 2001;28(8):PS85.
67. Nichols K, Ababneh A, Rheem J, et al. Accuracy of gated blood pool SPECT ventricular function parameters: validation by MRI [abstract]. Journal of the American College of Cardiology 2001;37(2):393A.
68. Nichols K, Saouaf R, Ababneh AA, et al. Validation of SPECT equilibrium radionuclide angiographic right ventricular parameters by cardiac magnetic resonance imaging. Journal of Nuclear Cardiology 2002;9(2):153–160.
69. Rezai K, Weiss R, Stanford W, Preslar J, Marcus M, Kirchner P. Relative accuracy of three scintigraphic methods for determination of right ventricular ejection fraction: a correlative study with ultrafast computed tomography. Journal of Nuclear Medicine 1991;32(3):429–435.
70. Germano G, Kiat H, Kavanagh PB, et al. Automatic quantification of ejection fraction from gated myocardial perfusion SPECT. Journal of Nuclear Medicine 1995;36(11):2138–2147.
71. Wittry MD, Juni JE, Royal HD, Heller GV, Port SC. Procedure guideline for equilibrium radionuclide ventriculography. Journal of Nuclear Medicine 1997;38(10):1658–1661.
72. Botvinick EH. Scintigraphic blood pool and phase image analysis: the optimal tool for the evaluation of resynchronization therapy. Journal of Nuclear Cardiology 2003;10(4):424–428.
73. Adachi I, Akagi H, Umeda T, et al. Gated blood pool SPECT improves reproducibility of right and left ventricular Fourier phase analysis in radionuclide angiography. Annals of Nuclear Medicine 2003;17(8):711–716.
74. Casset-Senon D, Babuty D, Philippe L, et al. Fourier phase analysis of SPECT equilibrium radionuclide angiography in symptomatic patients with mitral valve prolapse without significant mitral regurgitation: assessment of biventricular functional abnormalities suggesting a cardiomyopathy. Journal of Nuclear Cardiology 2000;7(5):471–477.
75. Casset-Senon D, Philippe L, Babuty D, et al. Diagnosis of arrhythmogenic right ventricular cardiomyopathy by Fourier analysis of gated blood pool single-photon emission tomography. American Journal of Cardiology 1998;82(11):1399–1404.
76. Machac J, Horowitz SF, Miceli K, et al. Quantification of cardiac conduction abnormalities using segmental vector Fourier analysis of radionuclide gated blood pool scans. Journal of the American College of Cardiology 1983;2(6):1099–1106.
77. Fauchier L, Marie O, Casset-Senon D, Babuty D, Cosnay P, Fauchier JP. Interventricular and intraventricular dyssynchrony in idiopathic dilated cardiomyopathy – a prognostic study with Fourier phase analysis of radionuclide angioscintigraphy. Journal of the American College of Cardiology 2002;40(11):2022–2030.
78. Kerwin WF, Botvinick EH, O'Connell JW, et al. Ventricular contraction abnormalities in dilated cardiomyopathy: effect of biventricular pacing to correct interventricular dyssynchrony. Journal of the American College of Cardiology 2000;35(5):1221–1227.
79. Harris J, Stocker H. Handbook of Mathematics and Computational Science. New York: Springer; 1998.
80. Daou D, Lebtahi R, Faraggi M, Petegnief Y, Le Guludec D. Cardiac gated equilibrium radionuclide angiography and multiharmonic Fourier phase analysis: optimal acquisition parameters in arrhythmogenic right ventricular cardiomyopathy. Journal of Nuclear Cardiology 1999;6(4):429–437.
81. Cardot JC, Berthout P, Verdenet J, et al. Temporal Fourier analysis applied to equilibrium radionuclide cineangiography. Importance in the study of global and regional left ventricular wall motion. European Journal of Nuclear Medicine 1982;7(8):353–358.
82. Ratib O, Henze E, Schon H, Schelbert HR. Phase analysis of radionuclide ventriculograms for the detection of coronary artery disease. American Heart Journal 1982;104(1):1–12.
83. O'Connell W, Schreck CE, Moles MP, Botvinick EH. A unique method to quantitate ventricular synchrony with gated equilibrium blood pool (MUGA) imaging. Journal of Nuclear Medicine 2004;45(5):175P.

12 Gated positron emission tomography for the assessment of myocardial perfusion and function

Josef Machac

The owl of Minerva spreads its wings only with the setting of dusk

G.W.F. Hegel

Why do cardiac PET?

Strengths and limitations of SPECT imaging

In spite of the impressive overall performance of gated myocardial perfusion SPECT imaging, there are significant limitations with the approach. Diffuse coronary artery disease (CAD) without segmental stenosis is frequently the substrate for plaque rupture and coronary events [1–3]. Furthermore, the identification of early atherosclerosis potentially provides a target for early intervention through diet, glycemic control, lifestyle changes, and pharmacologic therapy [4–9]. The detection of coronary disease by SPECT relies on a significant decrease in the ability of regional coronary blood flow to respond to exercise or pharmacologic stress. Early disease may not cause a hemodynamically significant obstruction to blood flow. Sensitivity of disease detection is also limited by incomplete extraction of tracer by the myocardium during first passage and its further decrease with hyperemia, more so for Tc-99m sestamibi or Tc-99m tetrofosmine [10–12], compared to thallium-201. Despite a high sensitivity of 90–94% for multivessel coronary disease, conventional SPECT myocardial perfusion imaging has a limited sensitivity of 60–76% for detecting single-vessel disease [13,14] and frequently underestimates CAD extent. The presence of diffuse disease in all three coronary vessels may decrease the sensitivity for each individual vessel, and fortunately infrequently "balanced ischemia" may mask the presence of disease altogether [15–19].

The hemodynamic response to exercise performed with myocardial perfusion imaging contains information about the adequacy of the stress test. In contrast, the hemodynamic response to the vasodilator stress agents dipyridamole or adenosine, used in about 40% of all stress imaging procedures, does not contain independent information about the adequacy of the stress. Despite an overall high success rate, the surreptitious use of caffeinated beverages may contribute to decreased negative prognostic predictive value of pharmacologic myocardial perfusion imaging as compared to exercise. In one notable study, patients with a high clinical likelihood of CAD but normal adenosine dual-isotope SPECT imaging still suffered a 4.2% rate of hard cardiac events over an average of 27.5 months [20]. The occasional failure to diagnose extensive disease stems also, in part, from our reliance on detecting relative deficiencies in regional perfusion, which may mask a uniformly poor response to vasodilator stimulation. This type of perfusion abnormality could, in theory, be detected with quantification of coronary flow reserve – a potential that has been explored in several studies with positron emission tomography (PET) but only in a limited manner with SPECT.

SPECT myocardial perfusion imaging is also subject to imaging artifacts stemming from nonuniform attenuation, scatter, and resolution. In spite of the ability to recognize the presence of attenuation artifacts through intensive training, experience, and the use of gated SPECT imaging [21], there is frequent uncertainty about the status of possible underlying CAD in the presence of overlying imaging artifact [22,23]. The need for separate rest and stress imaging sessions can result in changes in positioning, resulting in altered attenuation artifact, leading to possible false-positive or false-negative results.

Another limitation to SPECT imaging is the relative low efficiency of collimation and low geometric efficiency of conventional gamma cameras. Coupled with a limit on the maximal dose of radiotracer due to radiation dosimetry considerations, there is a limit on the shortest amount of time required for image acquisition with current SPECT cameras. The use of multiheaded gamma cameras compensates for the latter factor to some degree. From the patient's point of view, standard acquisition protocols

characteristically take at least a few hours to complete, offering an area of potential improvement. The half-lives of currently used radioisotopes limit the number of repeat tracer injections that can be administered.

Improvement in SPECT gamma camera capability, including multiple heads, external line source or CT attenuation correction, and sophisticated software, has come with increasing cost. Thus, a full-fledged multiheaded gamma camera with attenuation correction and all necessary software approaches the cost of some PET cameras.

Evolution in the status of PET imaging

Despite the fact that the clinical value of cardiac PET imaging was demonstrated more than 20 years ago [24–26], its clinical utilization has until recently been very low. The impracticality of clinical PET included limitation to a few large research centers with a PET camera and a cyclotron, the great expense of PET imaging, and the lack of reimbursement for clinical studies. Another disincentive was lack of availability of standardized software for cardiac PET image processing, display, or regional quantification on most PET systems.

All that has changed. With more than 1000 installed PET cameras in North America (M. Emmons, GE Health Care, personal communication, 2004), there is an extensive infrastructure in PET imaging. With an average utilization of only four oncological studies being performed per PET scanner per day (M. Emmons, GE Health Care, personal communication, 2004), there is room for part-time availability of most PET scanners for cardiac imaging. With widespread upgrading of dedicated PET systems to PET/CT systems for oncology, there is a market for used dedicated PET systems suitable for cardiac imaging.

Myocardial PET perfusion imaging with rubidium-82 (Rb-82), reimbursed by Centers for Medicare and Medicaid Services (CMS) since 1995, is possible with a commercially available generator on a 24-hour basis, obviating the need for a cyclotron. More recently, shared mobile Rb-82 generators have become available in some localities for centers that are not financially able to subscribe to 7 days a week Rb-82 service and choose to offer PET myocardial perfusion imaging only one to several times a week. All metropolitan areas in North America now have at least one commercial F-18 fluorodeoxyglucose (FDG) supplier. FDG PET imaging is now reimbursed for myocardial viability. More recently, CMS reimbursement became available for myocardial perfusion imaging with N-13 ammonia.

The widespread installation of PET/CT cameras represents another leap forward. The use of CT for attenuation correction substantially shortens the acquisition time for a clinical study. The combination of PET scanners with 16 or more slice multidetector CT scanners offers the tantalizing possibilities of PET perfusion and viability imaging in concert with coronary calcium scoring and coronary CT angiography, representing potential one-stop service.

The power of PET

PET utilizes a class of radioactive tracers, which decay with the emission of a positron particle, which has the same mass as an electron, but with a positive charge. The positron travels a variable distance through the surrounding tissues, depending on the positron's energy and tissue density, varying from a fraction of a millimeter to a few millimeters, until it interacts with an electron. The two undergo mutual annihilation, resulting in the transformation of their combined mass into energy ($E = mc^2$) in the form of two gamma photons directed 180° apart from each other. If these gamma photons are detected in coincidence by an array of detectors surrounding the patient, one is able to, on the basis of a large number of such events, assemble an image of the distribution of the radiotracer.

An important property of PET is its high image uniformity as a result of the integration in all commercial PET systems of nonuniform attenuation correction. Since this can be performed with high accuracy and relative ease, this effectively compensates for tissue attenuation. It also allows one to calibrate the PET imaging system, which allows quantification of absolute tissue activity. This in turn allows the quantification of actual myocardial flow and glucose utilization rate, using appropriate mathematical models. It should be noted, however, that the misregistration of transmission and emission maps in the implementation of the attenuation correction also is a source of artifact of PET, one that is becoming increasingly apparent with the use of CT scans from PET/CT systems for this purpose.

PET offers a potentially high resolution of 4–6 mm, compared to 15 mm with SPECT [27], although this resolution is degraded by the distance the positron travels before undergoing annihilation to produce the two gamma photons in coincidence [28–31], noise, particularly for the short-lived Rb-82, the need for filtering, and the added noise from transmission scans for attenuation correction. In cardiac PET, resolution is further degraded by respiratory and cardiac wall movement. This can be compensated by cardiac or respiratory gating, but at the cost of higher noise under conditions of limited imaging time. Thus, cardiac PET currently offers some, albeit not all, of the potential improved resolution of PET compared to SPECT.

The ability of PET to image radioactive decay events in coincidence with electronic rather than physical collimation, and the geometrical efficiency of the ring detector design, leads to high acquisition efficiency. This results in high image quality acquired in a short time. The short half-life of Rb-82 also allows multiple short imaging sessions with multiple interventions. The short half-lives of

Table 12.1 Cardiac PET tracers.

Agent	Physical half-life [32]	Mean positron range (mm) [28–30]	Production	Extraction
N-13 NH_3	10.0 min	0.7	Cyclotron	80% [33]
Rb-82	78 s	2.6	Generator	50–60% [34]
O-15 H_2O	2.0 min	1.1	Cyclotron	Diffusible
F-18 FDG	110 min	0.2	Cyclotron	1–3% [35]

Rb-82 or N-13 ammonia (Table 12.1) result in acceptable radiation exposure for the patient, even with multiple injections (Table 12.2). This allows one to perform multiple intervention studies in one session. The short half-life of Rb-82 or N-13 ammonia also allows a patient to have other radionuclide imaging studies on the same day, including FDG viability imaging. On the other hand, SPECT has the potential of imaging more than one tracer at a time, but PET does not, since all PET agents have the same photon energy.

Myocardial PET perfusion tracers and imaging protocols

Nitrogen-13 ammonia

The principal cardiac radiotracers are described in Tables 12.1 and 12.2. N-13 ammonia has been used for most of the scientific investigations in cardiac PET imaging over the past two decades. Its 10-minute half-life (Table 12.1) requires an on-site cyclotron and radiochemistry synthesis capability. A sample imaging protocol is given in Table 12.3. A dose injected at rest is followed by imaging. The process is repeated, usually with pharmacologic stress, after the initial activity has been allowed to decay, by staggering patients, or using differential doses for rest and stress. N-13 ammonia stress imaging can be performed with exercise stress. Both rest and stress images can be gated. For quantification of blood flow, a dynamic acquisition is acquired. This can be accomplished by performing separate dynamic and gated acquisitions with the same injection, or through list-mode acquisition. One may add a third injection during cold-pressor stress testing.

Table 12.2 Cardiac PET tracer dosimetry.

Agent	Activity (mCi)	EDE (rem)	Critical organ	Organ dose (rem)
N-13 NH_3	20	0.148 [216]	Bladder	0.60 [217]
Rb-82	60	0.096 [218]	Kidneys	1.92 [218]
		0.78 [216]	Thyroid	8.4 [217]
O-15 H_2O	60	0.252 [37]	Heart	0.49 [37]
F-18 FDG	10	0.70 [217]	Bladder	5.9 [217]

Table 12.3 Imaging protocol for N-13 ammonia PET imaging.

Procedure	Time (min)
Positioning (scout)	5
Transmission imaging	10
Injection and blood clearance	5
Rest gated perfusion imaging	10–20
N-13 decay waiting time	45
Pharmacologic stress	7
Injection and blood clearance	5
Stress imaging	10–20
Total duration	100–120

N-13 ammonia imaging requires coordinating the activities of at least four individuals: the cyclotron operator, the radiochemist, the PET technologist, and the supervising PET physician. It can be a daunting task to coordinate a large number of rest and stress N-13 ammonia studies in the same day.

In the blood stream, N-13 ammonia consists of neutral NH_3 in equilibrium with its charged ammonium (NH_4^+) ion. The neutral NH_3 molecule readily diffuses in the plasma and across cell membranes. Inside the myocyte, it reequilibrates with its ammonium form, which is trapped in glutamine via the enzyme glutamine synthase [32,38]. Despite back diffusion, the first-pass trapping of N-13 ammonia at rest is high (Table 12.1), although it decreases at higher blood flow rates.

N-13 ammonia allows excellent quality (Fig. 12.1) ungated and gated images, taking full advantage of the superior resolution of PET relative to SPECT imaging, stemming from a sufficiently long half-life and the very short length of travel before annihilation of the N-13

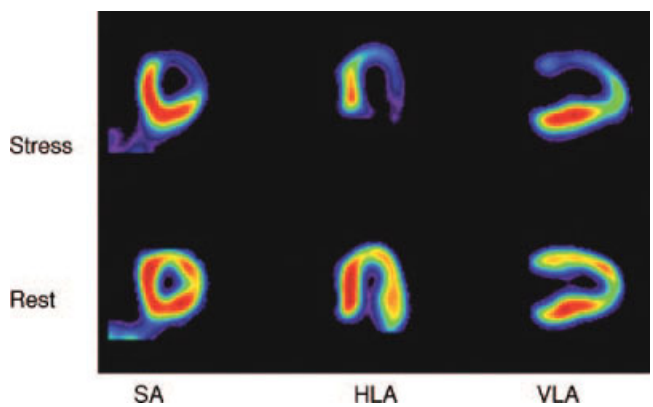

Figure 12.1 N-13 ammonia PET images demonstrating anterior and lateral defects during pharmacologic stress and significant improvement at rest, consistent with ischemia. Abbreviations: HLA, horizontal long axis; SA, short axis; VLA, vertical long axis. (Courtesy of Dr. H Schelbert, UCLA School of Medicine, CA, reproduced with permission from [214].)

positrons (Table 12.1). N-13 ammonia PET produces accurate assessment of regional and global cardiac function [39]. Interestingly, normal volunteers show heterogeneity or mild defects of N-13 ammonia retention in the lateral wall of the left ventricle, being decreased by about 10% compared to the other segments. The mechanism of this finding is not known [40]. This peculiarity must be taken into account for both visual and quantitative analysis. N-13 ammonia images also may be degraded by occasional intense liver activity, which can interfere with the evaluation of the inferior wall. Increased lung activity can interfere in patients with lung congestion [41].

N-13 ammonia allows absolute quantification of myocardial blood flow, and coronary flow reserve, although this requires special acquisition and processing methods (see further below). While N-13 ammonia is considered overall the best PET myocardial perfusion tracer, the need for a cyclotron imposes a profound limitation on its widespread clinical use.

Oxygen-15 water

Oxygen-15 (O-15) water is another important myocardial perfusion tracer (Table 12.1). Unlike N-13 ammonia or rubidium-82, O-15 water is neither an approved tracer nor reimbursed for clinical imaging in the United States, but is included in this discussion as an important tracer for investigations with quantification of myocardial blood flow. Its main attraction is the ability of water to diffuse freely across plasma membranes. This property allows the quantification of myocardial blood flow with the help of a simple one-compartment model [42], making this tracer a favorite for quantitation of myocardial blood flow: it is the only tracer that is extracted virtually 100% across the full range of myocardial blood flow. However, this very property leads to poor contrast between the myocardium and cardiac blood, requiring the subtraction of a separately acquired blood pool image after inhalation of O-15 carbon monoxide, or the subtraction of the earliest blood pool phase right after injection of O-15 water (Fig. 12.2). This in turn results in poor image quality compared to N-13 ammonia.

Rubidium-82

Rubidium-82 (Rb-82) is produced in a commercially available generator by decay from strontium-82 attached to an elution column. Rb-82 is eluted with 25–50 cm^3 normal saline by a computer-controlled elution pump, connected by IV tubing to the patient. With a half-life of 25 days, the strontium-82 containing generator is replaced every 4 weeks. Rb-82 decays by positron emission with a short half-life of Rb-82 of 75 seconds (Table 12.1). While the generator is fully replenished every 10 minutes, our experiments have shown that 90% of maximal available activity can be obtained within 5 minutes since the last elution [44]. While the short half-life of Rb-82 taxes the performance limits of PET scanners, it facilitates the rapid completion of a series of resting and stress myocardial perfusion studies. Thus, Rb-82 is a very efficient imaging agent for routine clinical usage. Acquisition protocols for different representative scanners are shown in Tables 12.4–12.7. Because of the short half-life of Rb-82 and the need for the patient to lie still in the camera during the study, stress imaging of this agent is generally limited to pharmacologic stress.

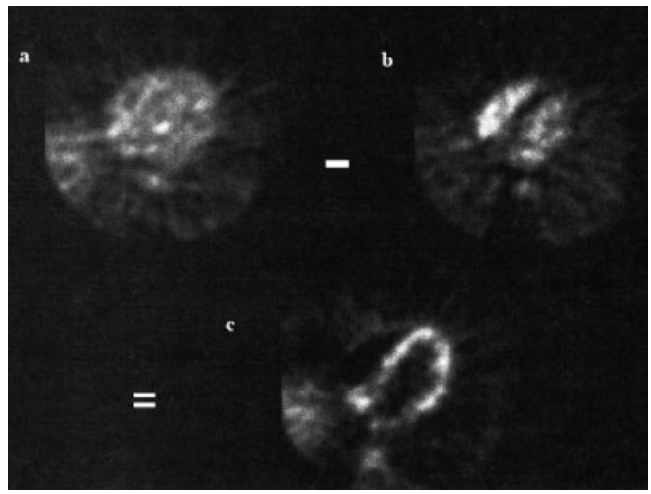

Figure 12.2 Late (a) and early blood pool (b) phases of O-15 H_2O images. Rapid equilibration between blood pool and myocardium prevents visualization of the myocardium, which can be achieved (c) by subtracting (b) from (a). Image (c) can then be used to draw the region of interests to use with the original images to generate regional time–activity curves for quantitative analysis. (Reproduced with permission from [43].)

Rb-82, like thallium-201, is a cation and an analogue of potassium. It is extracted from plasma with high efficiency by myocardial cells via the Na^+/K^+ ATPase pump. Myocardial extraction of Rb-82 is similar to thallium-201 [46,47] slightly less than N-13 ammonia (Table 12.1). Extraction decreases with increasing blood flow [48,49]. Rb-

Table 12.4 Imaging protocol for Rb-82 PET imaging with a BGO PET scanner (the Mount Sinai Medical Center, NY)*.

Procedure	Time (min)
Positioning (Scout)	5
Rest gated imaging	8
Rest perfusion imaging	8
Transmission imaging	8
Pharmacologic stress	7
Stress imaging	8
Total duration	44

*A 50–60 mCi dose is used routinely with 2D imaging.

Table 12.5 Imaging protocol for Rb-82 PET imaging with an LSO PET scanner [45]*.

Procedure	Time (min)
Rest transmission imaging	4
Rest perfusion 2D imaging	5
Rest gated 3D imaging	3
Pharmacologic stress	7
Stress transmission imaging	4
Stress perfusion 2D imaging	5
Stress gated 3D imaging	3
Total duration	31

*A 50–60 mCi Rb-82 dose is used.

82 extraction can also be altered by severe acidosis, hypoxia, and ischemia [50–52]. Thus, uptake of Rb-82 is a function of both blood flow and myocardial cell integrity.

Patient preparation and stress testing

Patient preparation for stress and rest myocardial perfusion PET is identical to pharmacologic SPECT perfusion imaging. Myocardial PET perfusion imaging is usually performed with pharmacologic stress, primarily with dipyridamole or adenosine. N-13 ammonia imaging can be performed successfully with treadmill stress testing. Satisfactory results have been obtained with supine bicycle exercise using O-15 water [53], or even with treadmill exercise with Rb-82 [54].

Imaging of Rb-82

In spite of the short half-life of Rb-82, modern PET gamma cameras are able to obtain good quality images (Figs. 12.3 and 12.4). Imaging with Rb-82 is not able to take full advantage of the superior resolution of PET, due to the relatively long mean path (2.6 mm) (Table 12.1) of the energetic Rb-82 positrons and due to the need for filtering required to obtain optimal images with the short-lived tracer. The total body dosimetry from a 50–60 mCi dose of the short-lived Rb-82 varies among different calculated estimates, but is sufficiently low to allow multiple injections with an acceptable dosimetry to the patient (Table 12.2).

Table 12.6 Imaging protocol for Rb-82 PET imaging with a GSO PET scanner (O. Almeida, personal communication, August 2004).

Procedure	Time (min)
Positioning (scout)	5
Transmission imaging	3
Rest perfusion imaging	5
Pharmacologic stress	7
Stress imaging	5
Total duration	25

Table 12.7 Imaging protocol for Rb-82 PET imaging with a PET/CT scanner (M. DiCarli, personal communication, August 2004)*.

Procedure	Time (min)
Positioning (scout)	1
CT transmission scan #1	15 s
Rest gated imaging	8
Rest perfusion imaging	8
Pharmacologic stress	7
CT transmission scan #2	
Stress imaging	8
CT transmission scan #3	15 s
Total duration	33

*A 50–60 mCi dose was used for all injections.

Our protocol for a dedicated BGO PET scanner (Table 12.4) begins with a low-dose (20 mCi) injection of Rb-82 at rest, a short 3-minute scout acquisition, and quick reconstruction that allows proper positioning. The patient then receives a full (50–60 mCi) dose of Rb-82 at rest, acquired in two-dimensional eight-frame gated mode for 6 minutes, beginning at 2 minutes after the onset of injection. This is followed by another 50–60 mCi injection, at rest, using a phasic (dynamic), 8-minute acquisition, for perfusion imaging. The dynamic acquisition allows a retrospective choice of selecting the onset of the myocardial phase (which is delayed in heart failure and low cardiac output states, or poor bolus quality), and allows blood

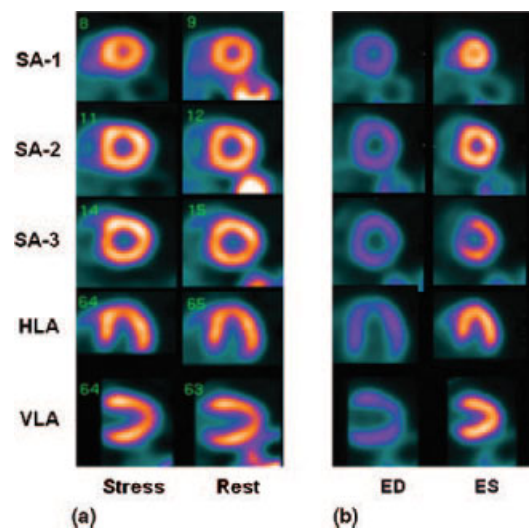

Figure 12.3 (a) Normal stress and rest Rb-82 PET images. (b) Resting end-diastolic (ED) and end-systolic (ES) gated images, showing uniformly good contractility. (Reproduced with permission from [214].)

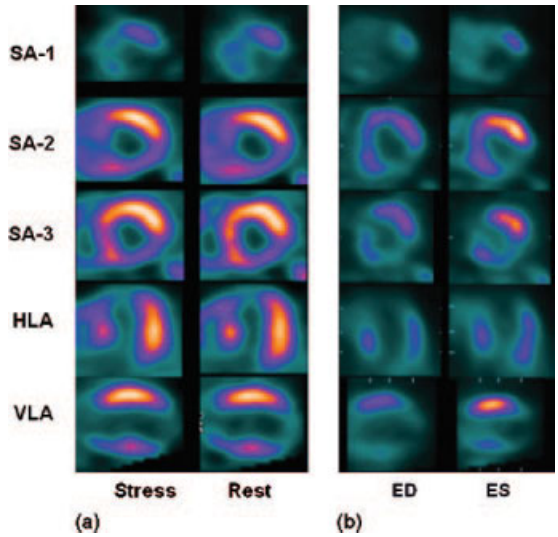

Figure 12.4 (a). Stress and rest of Rb-82 PET images demonstrating severe extensive apical, septal, and inferior scarring and only minimal basal septal ischemia. (b) Resting end-diastolic (ED) and end-systolic (ES) gated images, showing poor or absent contractility in the scarred regions, and poor overall left ventricular function. (Reproduced with permission from [214].)

flow quantification. This is followed by an 8-minute transmission scan with a germanium-68 pin source. The patient then undergoes pharmacologic stress with dipyridamole, adenosine, or, in patients with asthma, dobutamine. At peak stress, the patient is injected with the final 50–60 mCi Rb-82 dose, for the last 8-minute dynamic (phasic) acquisition. The camera acquisition time for the entire study is about 45 minutes. Any need to reposition the patient or repeat an acquisition, or need for patient observation, may lengthen the required time.

For the rest and stress perfusion image reconstruction, we use filtered backprojection with a Hanning filter. We have found that best myocardial uniformity is obtained with filtered backprojection and measured attenuation correction. Iterative reconstruction with either measured or segmented attenuation correction is satisfactory too, but in our experiments, led in normal controls to less uniformity among regions [55]. These results should be considered specific to our dedicated PET scanner (ADVANCE-GE Medical Systems) and should be verified for the other scanners by their respective users. We reconstruct the gated wall motion images with iterative reconstruction with segmented attenuation correction, in order to more effectively suppress the higher level of noise.

The resulting transaxial resting and stress static images undergo oblique reslicing to produce oblique short-axis, horizontal long-axis, and vertical long-axis cuts, using any one of standard display software packages developed for SPECT images and adapted for PET.

An important decision for any laboratory is the choice of two-dimensional (2D) vs. three-dimensional (3D) PET imaging, a decision specific for each type of PET scanner. In studies with our BGO scanner (ADVANCE-GE Medical Systems), acquisition in 3D mode with high-injected doses (50–60 mCi) of Rb-82 and immediate acquisition did not yield good results, due to dead time and excessive randoms. We did obtain good results, similar to our routine 2D high-dose imaging, by waiting for 5 minutes after Rb-82 injection. The delay would seem to defeat the purpose of imaging early after injection in trying to maximize counts. However, similar image quality could be obtained with low-dose (20 mCi) Rb-82 3D imaging as with high-dose (50–60 mCi) 2D imaging [56,57]. Our experiments with phantoms showed similar resolution for 3D and 2D images. Thus, we found no advantage in 3D imaging with high-dose Rb-82 injections. Three-dimensional imaging requires longer reconstruction time, and fills much more computer disk space. In lean individuals, the resolution and quality of 2D and 3D images were identical. In obese individuals, both contrast and image quality were better with 2D imaging. Quantification with 3D imaging should be done with caution, since 3D imaging produces significant axial nonuniformity without proper correction [32]. The benefit of 3D imaging in our scanner would be realized if a lower dose, less expensive Rb-82 generator were offered. Thus, one could obtain similar results with 3D low-dose imaging as with high-dose 2D imaging, at lower cost.

LSO detector PET scanners (CTI, Knoxville, TN) offer the ability to function in 3D mode even at high activities. The cardiac PET laboratory at the Mid America Heart Institute of Kansas City, MO, acquires in quick succession, 2D perfusion and 3D gated imaging at rest and with stress (Table 12.5), resulting in faster throughput and enhanced efficiency. Moser et al. [58] performed a quantitative comparison between 2D and 3D Rb-82 perfusion acquisitions on their system. They found that resting images were identical. Initial results showed that dipyridamole stress images showed significant differences in perfusion defect detection between 2D and 3D images. Subsequent studies showed that these differences were eliminated with modifications in methodology. Thus, the investigators confirmed that 2D and 3D imaging could be used with equal confidence [36], but three-dimensional imaging would save time.

Another laboratory that compared a BGO 2D system with an LSO 3D system observed with a slightly reduced Rb-82 dose of 30–50 mCi reduced noise levels with the 3D LSO system, albeit with increased background levels [59], presumably due to a higher random events level.

Satisfactory results in myocardial perfusion imaging with Rb-82 have also been reported with a GSO PET system (O. Almeida, personal communication, August 2004). Recently, gated and dynamic imaging have also been

achieved with this system (D. Berman, personal communication, 2004; V. Dilsizian, personal communication, 2004). A sample protocol for a GSO PET imaging system is shown in Table 12.6.

Combined PET and CT imaging in a single combined PET/CT unit has become the preferred approach for PET imaging in oncology. Approximately 80% new units installed in 2003 were PET/CT units (M. Emmons, GE Health Care, personal communication, August 2004). Table 12.7 shows a sample imaging protocol with a PET/CT scanner. First, the scout CT scan can, in a few seconds, reveal proper positioning of the patient. CT scanning reduces the time for transmission scan. Since 30–35 minutes are projected for the entire study, 45 minutes for the more difficult patients [60], throughput is enhanced. One group reported saving 12 minutes for the complete study, after switching from a dedicated PET system to a PET/CT system [59]. We have verified these results with a BGO PET/CT system using the protocol in Table 12.7.

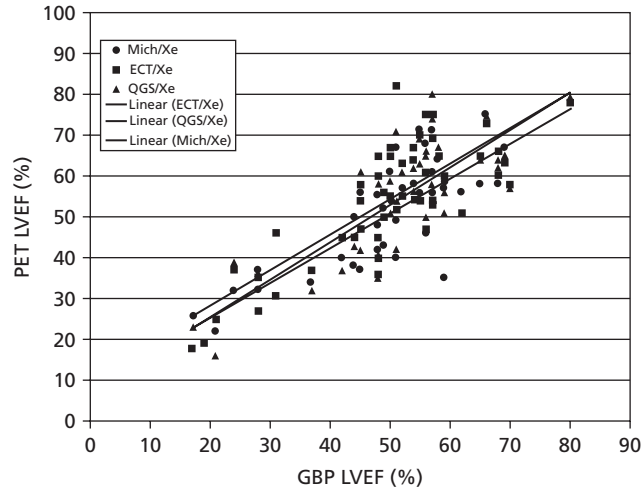

Figure 12.5 Left ventricular ejection fractions obtained from gated Rb-82 PET imaging and QGS, Emory toolbox (ECT), and Michigan 4D (MICH) software, correlated with planar gated blood pool imaging. (Reproduced with permission from [214].)

Gated imaging with Rb-82

In our Rb-82 acquisition protocol (Tables 12.4 and 12.7), we include a separate resting injection to obtain a gated PET acquisition in 2D mode. If one does not need to acquire the perfusion images using a dynamic (phasic) acquisition (a case in most clinical settings), the perfusion and gated images can be obtained at the same time, both at rest and at stress. Ideally, one would like to obtain both gated and dynamic acquisitions at the same time. This would be possible with a list-mode acquisition, but this capability is not readily available with most commercial PET scanners.

As already noted above, we compared 2D vs. 3D imaging. On our BGO PET imaging system, we could obtain similar results with high-dose (50–60 mCi of Rb-82) 3D imaging as with high-dose 2D imaging, provided that we waited 5 minutes between injection and the onset of 3D imaging, so that dead time and randoms fell to acceptable levels. Likewise, we could obtain similar results with low-dose (20 mCi Rb-82) 3D acquisition as with high-dose 2D acquisition, provided that patients were not obese, where image quality was worse. Overall 3D imaging could equal, but not exceed, 2D image quality [56].

With proper image processing, good quality Rb-82 PET gated images can be obtained in the vast majority of patients (Figs. 12.3 and 12.4). Iterative reconstruction and proper choice of filter will result in good results with most patients. Patients with frequent ectopy or irregular heart rhythms may yield gated images of inferior quality. Poor gated image quality may also result from a slow or fragmented Rb-82 injection.

After reconstruction, the gated images can be processed and viewed with one of a number of different commercially available display software packages originally developed for SPECT imaging.

We compared visually assessed regional and global left ventricular (LV) function from 67 gated Rb-82 PET studies to either gated SPECT images (17), gated blood pool images (11), echocardiography (25), or contrast ventriculography (23) performed within 3 months of each other. We demonstrated an 81–92% close agreement in segmental wall motion scores [61], with best agreement (92%) between PET and either gated SPECT perfusion or gated planar blood pool imaging.

More recently, we compared the ability of three commercial software packages to calculate the left ventricular ejection fraction (LVEF) from gated Rb-82 PET images. In 52 patients, gated resting Rb-82 PET images were processed with either the QGS (Cedars Sinai) software, the ECT Toolbox (Emory) software, or the 4D (Michigan) software and the resulting ejection fractions were compared with those obtained from planar gated blood pool images acquired within 24 hours. The results showed all three methods to perform satisfactorily, with correlation coefficients of 0.81–0.83 [62] (Fig. 12.5).

Successful results with 3D gated Rb-82 PET imaging were also obtained with an LSO system in 35 patients and compared with gated Tc-99m sestamibi SPECT. The authors found a good correlation ($r = 0.91$) for the LVEFs between the two methods [63]. Thus, both regional as well as global LV function can be successfully evaluated with either BGO or LSO PET imaging systems using Rb-82.

Regional wall motion as well as LVEFs obtained with N-13 ammonia gated PET images also yielded excellent agreement with other wall motion modalities [39].

The value of PET for clinical myocardial perfusion imaging

Image uniformity in PET imaging

A major challenge for cardiac radionuclide perfusion imaging is the varying distribution of the disparate densities of the tissues surrounding the heart, including bone, water density, fat, and air. Their respective proportions vary markedly between men and women, and among individuals within each gender, leading to a wide range of normal limits to the distribution of apparent myocardial perfusion due to attenuation artifact. Image uniformity is the most important property of cardiac PET perfusion imaging. Due to the requirement of coincidence detection, the probability of attenuation or scatter for the two gamma photons is the same anywhere along the line between any two detectors. The attenuation between any two detectors can be measured and easily corrected. By contrast, with a conventional collimated gamma camera, resolution deteriorates with distance from the face of the gamma camera, along with increasing attenuation and scatter with increasing depth of the source in the subject, which is difficult to correct reliably [32]. The result is that while normal maps for regional quantification of SPECT images are nonuniform and different for men and women, the maps with Rb-82 PET are uniform and identical for both genders [64].

The problem is illustrated by the example of a 53-year-old male with diabetes, end-stage renal disease, and left-ventricular hypertrophy (LVH), referred for dipyridamole Tc-99m sestamibi SPECT imaging for preoperative risk evaluation (Fig. 12.6). The stress SPECT images show a severe inferior defect, moderate apical defect, and a possible mild anterior defect. The resting images show no improvement in the inferior wall, mild improvement in the apex, and in the anterior wall. The gated SPECT images showed global hypokinesis. Even though attenuation artifact was suspected, the study could not exclude inferior wall scarring, and mild apical and possibly anterior wall ischemia. Obtained within a short time afterward, the stress and rest PET images showed uniform distribution. This patient nonetheless underwent coronary angiography, which showed normal coronary arteries with mild diffuse LV dysfunction, confirming the diagnosis of mild cardiomyopathy, probably due to chronic hypertension.

SPECT images frequently show attenuation artifact in women due to attenuation from overlying breast tissue, illustrated in Fig. 12.7 for a 72-year female studied for evaluation of development of CAD several years following a heart transplant. The SPECT images showed a moderate anterior wall defect, with a suggestion of improvement at rest. Even though attenuation artifact was likely on the basis of an obvious breast shadow on the raw images, disease could not be ruled out in this patient at risk of coronary

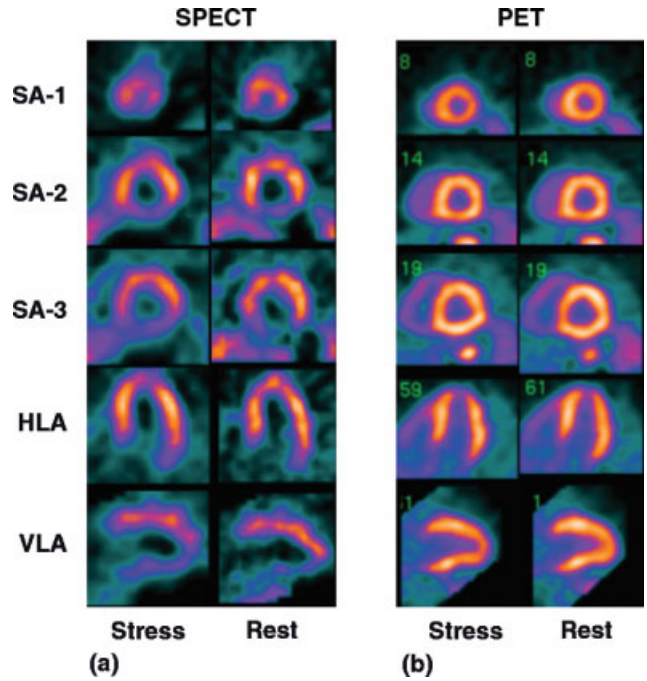

Figure 12.6 (a) Dipyridamole stress and rest Tc-99m sestamibi SPECT images of a 53-year-old male show a moderate inferior defect and possible mild anterior defect during stress with mild improvement in the anterior wall and apex at rest. (b) The stress and rest PET images for the same patient showed uniform distribution. (Reproduced with permission from [214].)

disease. The PET imaging study showed a normal distribution.

Table 12.8 lists studies that compared PET myocardial perfusion imaging in the detection of CAD. Representing a

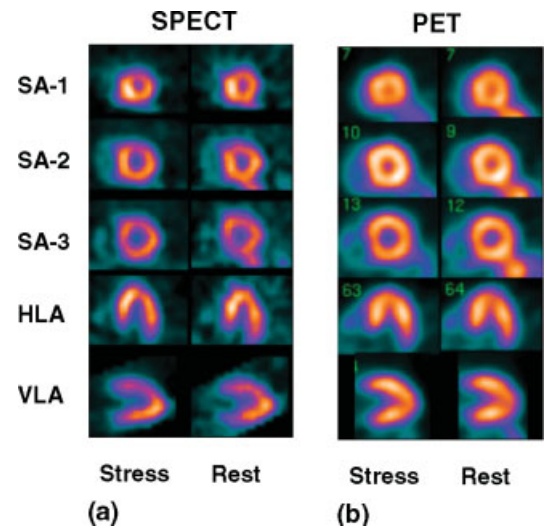

Figure 12.7 (a) Tc-99m sestamibi dipyridamole stress and rest SPECT images of a 72-year-old female show a mild to moderate anterior wall defect at stress, with a suggestion of partial improvement at rest. (b) The Rb-82 PET imaging study shows normal images. (Reproduced with permission from [214].)

Table 12.8 Diagnostic accuracy of PET myocardial perfusion imaging for CAD.

Sensitivity (%)	Specificity (%)	No. of points	Agent	Author
95	100	50	NH_3, Rb-82	Gould et al. [65]
94	95	193	Rb-82	Demer et al. [66]
93	78	202	Rb-82	Go et al. [67]
97	100	45	NH_3	Schelbert et al. [25]
93	100	49	NH_3	Yonekura et al. [68]
98	93	146	Rb-82	Williams et al. .[69]
84	88	81	Rb-82	Stewart et al. [70]
95	95	25	NH_3	Tamaki et al. [71]
93	92	791		*Average*

total of 791 patients, eight studies – some performed with N-13 ammonia, others with Rb-82 PET – showed in aggregate a mean of 93% sensitivity and 92% specificity for CAD. Table 12.9 lists studies that compared PET myocardial perfusion imaging with thallium-201 SPECT imaging in the same patients. These studies showed higher overall sensitivity, specificity, and accuracy for PET compared to SPECT imaging.

In 2748 patients, Patterson et al. [72] found a reduction in the number of interpretations classified by two experienced physicians as "probably" normal or abnormal, from 37% with Tl-201 SPECT to 21% with Rb-82 PET. These results indicate that PET can produce unequivocal result in the great majority of patients. Nondiagnostic or uncertain interpretation of a noninvasive test is one of the factors prompting physicians to recommend more costly invasive diagnostic studies.

Regional quantification has been shown to further improve the accuracy of PET perfusion imaging. Churchwell et al. [73,74] compared quantitative PET Rb-82 myocardial perfusion imaging studies with clinical follow-up in 52 patients and coronary angiography in 91 patients. They found a 99% sensitivity, 83% specificity, and 100% normalcy rate for CAD, and a high interobserver agreement of 94% among three physicians interpreting the images independently [75,76].

Over the last 10–15 years, both SPECT and PET imaging have undergone significant improvements, with the addition of gated SPECT imaging, Tc-99m agents [21,77–79], and SPECT attenuation [80,81]. The current literature lacks a direct comparison of the accuracy of PET in comparison with SPECT imaging, complete with gating and attenuation correction, but as more centers are now involved with PET perfusion imaging, these data are rapidly being collected. A recent study presented by Bateman et al. [82] showed a higher interpretive certainty (definitely normal or abnormal) for PET (87% vs. 71% for SPECT imaging, $p < 0.05$) in 112 patients studied with gated Tc-99m sestamibi SPECT, and matched with 112 patients studied with gated Rb-82 PET. PET myocardial perfusion imaging showed a higher diagnostic accuracy of 86% for CAD vs. 68% for SPECT imaging ($p < 0.05$). For individual coronary vessels, PET imaging showed both higher sensitivity (78% vs. 61%, $p < 0.05$) and higher specificity (94% vs. 86%, $p < 0.05$).

Despite improvements in the accuracy of SPECT imaging, uncertainty remains in many patients. Studies have shown that significant problems of SPECT nonuniformity remain even after attenuation correction, with significant differences in the ability of commercial attenuation correction systems to reduce artifacts due to attenuation and scatter [23].

SPECT imaging in women is challenged by a high incidence of breast attenuation artifact, a greater and growing prevalence of obesity (Table 12.10), as well as smaller heart size [21,77,83]. The higher resolution of PET imaging and the greater ease in dealing with attenuation artifact are expected to yield high accuracy in women. Williams et al. [85] studied 57 female patients with stress PET imaging and observed a high specificity compared to coronary angiography. In women who had undergone both stress SPECT and stress PET imaging within a period of 3 months, the

Table 12.9 Comparison of PET and SPECT myocardial perfusion imaging for detection of CAD in the same patients.

Author	Tracer	Accuracy (%)	Sensitivity (%)	Specificity (%)
Go et al. [67]				
($n = 132$)	Rb-82	92	95	82
	Tl-201	78	79	76
Stewart et al. [70]				
($n = 81$)	Rb-82	85	87	82
	Tl-201	78	87	52
Tamaki et al. [71]				
($n = 51$)	NH3	98	98	100
	Tl-201	98	96	100
Total				
($n = 264$)	PET	91	93	82
	SPECT	81	85	67

Table 12.10 Prevalence of obesity (BMI > 30) in adults [84].

Year	Men	Women
1960	10.7%	15.8%
1972	12.1%	16.6%
1978	12.7%	17%
1990	20.6%	25.9%
2000	27.7%	34%

SPECT and PET imaging tests had similar high sensitivity, but the specificity for PET was significantly higher than for SPECT. In a population of men and women studied with coronary angiography, Patterson et al. [86] showed that both sensitivity and specificity of CAD detection with PET myocardial perfusion imaging were similarly high for men and women.

An increasing challenge to noninvasive diagnostic imaging is posed by the growing prevalence of moderate and severe obesity in the general population (Table 12.10). The prevalence of obesity is greater in women than in men, in older individuals compared to the young, and among African-Americans and Hispanic-Americans [84]. Obese patients nearly always exhibit some degree of attenuation artifacts on myocardial SPECT perfusion imaging, which can be recognized in many cases, but in others cause incorrect, or at least equivocal results.

Figure 12.8 shows attenuation-corrected SPECT and PET images of a 290-lb, 51-year-old male with risk factors for CAD. The non-attenuation corrected images showed a moderate to severe inferior wall defect. Even after attenuation correction, the SPECT images (Fig. 12.8a) show mild to moderate inferior and apical defects which slightly improved on the resting images, accompanied by 1 mm ST depression with nearly maximal exercise. Rest and dipyridamole stress Rb-82 PET images obtained a short time afterward (Fig. 12.8b) showed a normal distribution. The defects seen on SPECT images even after attenuation correction were attributable to attenuation artifact. Our experience and that of others has shown that in the obese

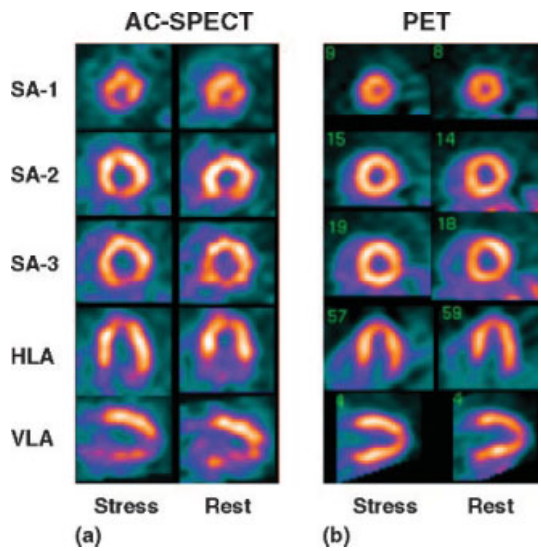

Figure 12.8 (a) Stress and rest attenuation-corrected (AC) Tc-99m sestamibi SPECT images of a 290-lb, 51-year-old male. The SPECT image show mild to moderate inferior and apical ischemia and partial scarring. (b) The stress and rest PET images showed normal distribution. (Reproduced with permission from [214].)

population and in women, routine gated SPECT imaging, even with attenuation correction, frequently results in a high level of uncertainty [45,72]. It is in these populations that PET is most helpful.

There are limitations to the ability of PET to image very obese individuals. The weight-bearing ability of most imaging tables is limited to 400–450 lb. Frequently, patients are limited more by the size of the scanner opening, so that while a tall, 450-lb patient can be accommodated, a short, 350-lb patient may not be able to fit in the PET scanner opening if it is 60–63 cm in diameter. Several of the currently marketed PET scanners have a larger opening of 70 cm, which is less limiting on the size of the patient that can be accommodated [87]. This should be determined individually for each type of PET camera. It is these larger patients who are frequently denied accurate diagnostic imaging because of their size.

Imaging in the pediatric population

The pediatric population is a challenge for diagnostic SPECT imaging. Infants and children can derive benefit from myocardial perfusion imaging to assess coronary vessel patency following switch operations, correction of anomalous coronary arteries, or in patients with Kawasaki's disease or myocardial injuries. Image quality is limited by resolution and the activity of thallium-201 that can be delivered to the heart in infants or small children is limited by dosimetry, thus resulting in poor quality images. Tc-99m sestamibi and Tc-99m tetrofosmine images are compromised by high liver activity in close proximity to the small heart, virtually obliterating the inferior wall of the heart. We have found the performance of PET Rb-82 myocardial perfusion imaging in infants and in small children to be excellent. The short half-life of PET allows sufficiently high doses of Rb-82 to be delivered to achieve good quality images with low dosimetry to the child. Figure 12.9 illustrates a stress and rest study in a 4-year-old child who had sustained severe trauma to the chest, requiring surgical repair and patching of myocardial rupture, followed by symptoms suggestive of ischemia. The Rb-82 PET study documented significant ischemia at the margins of the defect. Studies involving small children require careful preparation, since sedation and/or anesthesia are required to achieve good results.

Prognostic value of myocardial PET imaging

Given the proven value of PET myocardial perfusion imaging in the diagnosis of CAD, it is expected that the prognostic value of gated PET is at least as valuable as for gated SPECT imaging. In a study of 153 consecutive patients studied with Rb-82 PET imaging, Yoshinaga et al. showed 94% event-free survival over a 3-year period

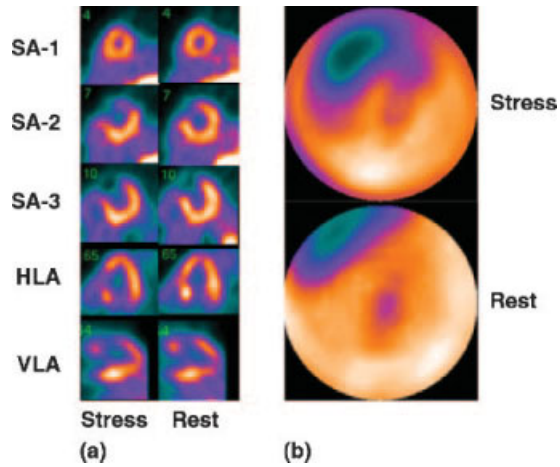

Figure 12.9 Stress and rest study Rb-82 imaging study of a 4-year-old child who had sustained severe trauma to the chest, requiring surgical repair of the anterior and septal walls, with subsequent symptoms suggestive of ischemia. The images demonstrate absent perfusion in the anteroseptal wall in the region of the patch, and significant ischemia at its edges, confirming insufficient blood supply around the margins of the defect.

in patients with normal PET scans, compared with 62% event-free survival in patients with mild defects, 58% survival in patients with moderate defects, and 45% survival with severe defects [88]. Van Tosh et al. [89] showed that a normal stress PET study predicts a very low cardiac event rate in women with chest pain and significant cardiac risk factors. Nevertheless, documented literature on the proven value of myocardial PET perfusion imaging, as has been shown for SPECT imaging, still remains to be written.

Gating of LV function during pharmacologic stress, and quantification of coronary flow reserve (see below), is expected to improve the detection of patients with balanced ischemia, thus enhancing the prognostic accuracy. Parkash et al. have shown improved ability to diagnose three-vessel disease, as opposed to single-vessel disease, with quantification of myocardial Rb-82 retention [90].

The evaluation of LV function, which is acquired as part of gated myocardial perfusion imaging, plays an important role in the assessment of clinical risk. Decreased LV function, the resultant thinning, and myocardial elongation in both infarcted and noninfarcted tissue contribute to further dilatation, heart failure, and decreased survival [91,92]. Increased LV volume is a predictor of poor outcome in patients undergoing coronary bypass surgery [93,94].

Combined perfusion and metabolic PET imaging offers the additional prognostic value of prediction of myocardial functional recovery of dysfunctional, viable myocardium, and identifies patients at high risk of cardiac events while managed with medical therapy compared to revascularization.

Imaging of myocardial viability

F-18 fluorodeoxyglucose

Preserved metabolism for the production of ATP is one of the critical features of myocardial viability. FDG is fluorine-18 labeled 2-deoxyglucose, an analogue of glucose. It is the principal workhorse in clinical PET viability imaging. Like D-glucose, FDG is transported into the myocardium by specific transporters by facilitated diffusion (Fig. 12.10). Inside the cell, FDG undergoes phosphorylation by the enzyme hexokinase. The phosphorylated product FDG-6-phosphate is not metabolized any further. Because of very low levels of the enzyme glucose-6-phosphatase catalyzing the reverse reaction, FDG is essentially trapped in the cell [95]. It has been demonstrated that in a metabolic steady state, FDG uptake in the myocardium correlates linearly with uptake and utilization of exogenous glucose [96].

Following injection, FDG is slowly taken up by body tissues, including the myocardium. Imaging is performed about 45–90 minutes after injection. As a result, the 110-minute physical half-life of F-18 FDG is well-suited for viability imaging (Table 12.1). The dietary state of the patient, as well as the metabolic integrity, determines the rate of glucose utilization. In the fasting state, normal myocardium preferentially utilizes free fatty acids. The uptake of glucose and FDG is generally low, although fairly variable. In the fasting state, inhomogeneity in uptake frequently occurs [97]. Subsequent to glucose loading, glucose and insulin plasma levels are elevated, and glucose is the preferred substrate for energy metabolism [98].

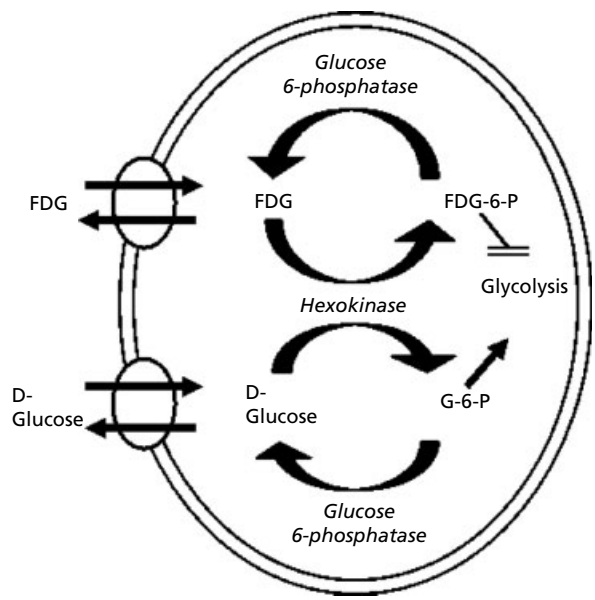

Figure 12.10 Schema of cellular uptake and retention of FDG.

Following transient ischemia, or in chronic state of hibernation, viability and the ability of injured myocardium to recover function depends on the recovery of oxidative metabolism [99,100].

Myocardial glucose utilization, and therefore metabolism, can be evaluated with imaging of FDG uptake. This is done most often in combination with myocardial perfusion imaging and wall motion imaging. This can be done with resting myocardial perfusion and function imaging followed by FDG metabolic imaging, which itself can be gated for functional imaging. When possible, one performs rest and stress myocardial perfusion imaging, followed by FDG metabolic imaging.

Wall motion imaging defines hypofunctional regions of the left ventricle. Resting perfusion defines hypoperfused or well-perfused hypofunctional regions. Stress perfusion imaging adds power by allowing one to assess jeopardized myocardium in addition to dysfunctional, hypoperfused regions. Perfusion imaging can be done separately with thallium-201, Tc-99m sestamibi, or Tc-99m tetrafosmine SPECT imaging. Perfusion imaging performed with Rb-82 or N-13 ammonia, together with FDG metabolic PET imaging, offers the advantage of being done at nearly the same time, easy coregistration of images for perfusion and metabolism, and having most closely matched image resolution and correction for attenuation.

In our protocol, the patient undergoes resting perfusion imaging with Rb-82, and whenever possible, pharmacologic stress Rb-82 perfusion imaging. Usually on the same day, this is followed by FDG PET imaging. The latter portion begins with glucose loading with supplementary insulin, as necessary [101]. In the course of early studies with perfusion/metabolic imaging, FDG metabolic imaging was performed during fasting. This approach amplifies the presence of ischemia or hibernation, and may overestimate the degree of perfusion–metabolism mismatch but image quality may be poor, which makes image coregistration with perfusion imaging more difficult. Subsequently, most centers have switched to imaging with glucose loading. A number of methods of glucose loading exist. These include oral glucose loading, IV glucose loading, or continuous insulin–glucose infusion, in order of difficulty. The patient is injected with FDG. After a 45–60-minute rest, the patient then undergoes emission PET imaging, along with a transmission scan.

Three distinct perfusion–metabolism patterns can be observed in dysfunctional myocardium. The first pattern is normal blood flow in association with normal FDG uptake. The second pattern is that of a matched, proportional reduction in blood flow and glucose utilization (Fig. 12.11). The third pattern is that of a mismatched pattern, with a regional decrease in perfusion and relatively preserved glucose utilization, as shown by preserved FDG uptake,

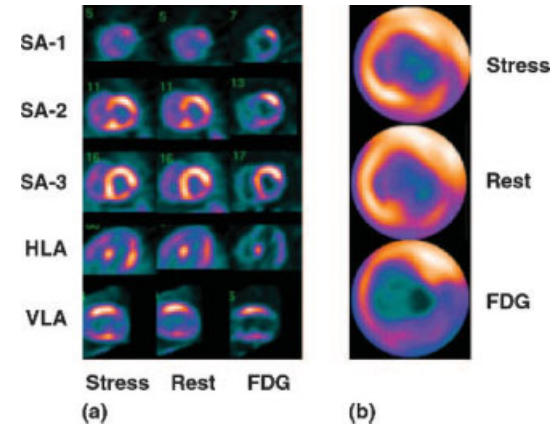

Figure 12.11 Rest and stress Rb-82 perfusion and FDG metabolic images (a) and polar maps (b) in a patient with a dilated left ventricle with a large area of fixed stress and rest perfusion defect. The FDG metabolic images show a matching large defect, consistent with permanent scarring.

or FDG uptake significantly better than uptake of the perfusion tracer (Fig. 12.12).

The mismatch pattern has been found to predict reversible dysfunction, while a matched pattern predicts scarring [26]. Preserved perfusion at rest but decreased perfusion at stress in a dysfunctional segment indicates stress-inducible ischemia, and suggests that the contractile dysfunction is due to repetitive ischemia and stunning,

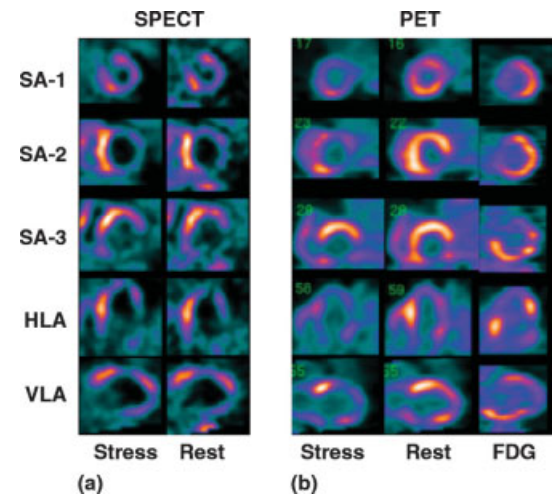

Figure 12.12 (a) Tc-99m sestamibi (MIBI) exercise stress and rest images in a 49-year-old male with known CAD and congestive heart failure. The MIBI images show severe apical, anterior, lateral, and inferior defects with no improvement on the resting images. (b) The dipyridamole stress Rb-82 images show severe apical, anterior, lateral, and inferior-basal defects, and a moderate to severe septal defect. The resting Rb-82 images show marked anterior, septal, and anterolateral improvement, and mid-inferior improvement. The FDG PET images showed preserved or increased activity in the anterolateral, lateral, inferior, and inferior-basal walls, demonstrating a classical mismatch pattern in these regions. (Reproduced with permission from [214].)

which may be remedied by coronary revascularization. Extensive LV dysfunction and dilatation associated with preserved flow and FDG uptake suggest remodeling or diffuse myopathy, not likely to respond to revascularization [102].

FDG PET imaging frequently shows additional viability in patients with fixed stress and rest perfusion defects, or in patients with only partial stress-inducible reversibility. An example is shown in images of Fig. 12.12, obtained in a 49-year-old male with history of myocardial infarction, very poor LV function, and congestive heart failure. Exercise stress Tc-99m sestamibi (MIBI) images showed severe apical, anterior, lateral, and inferior defects, with no improvement on the rest MIBI images. The dipyridamole stress Rb-82 images showed severe apical, anterior, lateral and posterior defects, and a moderate to severe septal defect, similar to the MIBI SPECT images. The resting images, however, showed marked anterior, septal, and anterolateral improvement, and mid-inferior improvement. The extent of stress-inducible ischemia was at least 50% of the myocardium. The FDG PET images showed preserved or increased activity in the anterolateral, lateral inferior, and based-inferior walls, demonstrating a classical mismatch pattern in these regions, occupying at least 50% of the myocardium. The end result is that about 75% of the myocardial mass shows either stress-inducible ischemia, or hibernation, including most of the regions considered scarred by MIBI SPECT imaging.

In some instances, it is not necessary to proceed with FDG PET viability imaging, if the stress and rest Rb-82 PET imaging provides evidence of ischemia, rather than scarring. Conversely, many patients do not show viability with FDG PET imaging in hypoperfused dysfunctional myocardium. An example in Fig. 12.11 shows a dilated left ventricle with a large area of fixed stress and rest perfusion defect. The FDG metabolic images show a matching large defect, consistent with permanent scarring.

Why viability imaging matters

The consideration of myocardial viability is important in a patient with significantly impaired LV function due to CAD being evaluated for revascularization. Severe reduction in resting flow in these dysfunctional regions by SPECT and PET perfusion imaging identifies predominantly nonviable myocardium that is unlikely to improve function after revascularization. Dysfunctional myocardium with mild to moderate and moderate to severe flow reduction contains variable amounts of viable tissue. Flow measurements by themselves do not distinguish between regions with potentially reversible dysfunction and regions with irreversible dysfunction [103].

The clinical value of cardiac metabolic PET imaging in the assessment of myocardial viability in combination with perfusion imaging was demonstrated more than 18 years ago [26]. Since then, 17 published studies with 462 patients using FDG PET imaging along with PET myocardial perfusion imaging or SPECT perfusion imaging have shown a 76% positive predictive value for improved regional function following revascularization and a 82% negative predictive value [104]. Bax et al., on the basis of pooled data from multiple studies involving 332 patients, determined a 88% sensitivity and 73% specificity of FDG PET for myocardial viability [105].

The magnitude of LV ejection fraction improvement has been shown to be proportional to the size and extent of viable dysfunctional myocardium, demonstrating the perfusion–metabolism mismatch pattern by PET [106,107]. An improvement in LV ejection fraction after revascularization is, in turn, associated with an improvement in prognosis [108]. The extent of viable myocardium also predicts improvement in heart failure symptoms after revascularization [109] and improvement in exercise parameters. This improvement was only in patients with significant extent of viability on FDG PET studies [110].

Not only does PET perfusion/metabolic imaging identify patients who benefit from revascularization, but also identify a group of patients at high risk when treated medically alone, while event-free survival in patients without viable myocardium is similar with medical therapy or revascularization [111–113]. Studies have shown, however, that this window of opportunity for a given patient does not last. Beanlands et al. showed that while preoperative FDG PET can be used to identify a high-risk group of patients who may benefit from early revascularization, a long waiting time for revascularization is associated with a high mortality rate and suggests that early revascularization is desirable after the identification of hibernating viable myocardium [114].

Where does FDG PET imaging predictive value stand in comparison with conventional SPECT imaging? A pooled analysis of multiple studies shows that FDP PET imaging offers slightly increased accuracy, arguably of marginal significance, compared to thallium-201 or Tc-99m sestamibi imaging [105]. These studies were not performed in the same subjects. A direct comparison between thallium-201 SPECT, with FDG SPECT and FDG PET in the same patients with very poor LV function, FDG PET imaging showed significant incremental benefit above thalium-201 stress-redistribution/reinjection imaging in predicting functional recovery, while in patients with relatively preserved LV function, the predictive value was similar [115]. Likewise, in patients with LVEF greater than 25%, Tc-99m sestamibi SPECT imaging showed close agreement with FDG PET, while in patients with LVEF less than 25%, Tc-99m sestamibi SPECT underestimated viability in segments that showed perfusion–metabolism mismatch with FDG PET [116]. This is illustrated in the example of

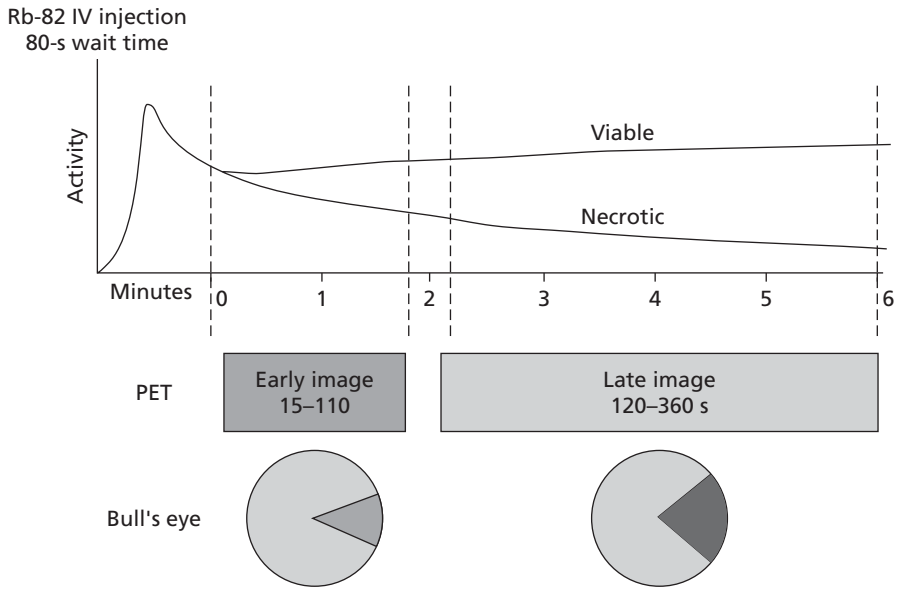

Figure 12.13 Schematic of the imaging protocol utilizing washout or retention of Rb-82 for assessing myocardial viability. (Reproduced with permission from [121].)

Fig. 12.12. These studies demonstrate that in patients with very poor LV function, FDG PET imaging adds significant value in viability imaging. PET viability imaging has also been successfully applied in infants and children with high accuracy, similar to that seen in adults [117].

Studies of PET perfusion tracer kinetics for viability

One of the principal applications of PET is in the assessment of myocardial viability with FDG in conjunction with a perfusion tracer. Kinetic tracer analysis provides another means of making this assessment. It is well known that the pharmacokinetics of thallium-201 in stress and redistribution imaging provide useful information for distinguishing ischemia from scarring and the demonstration of myocardial viability [118]. Since Rb-82 is an analogue of thallium-201, albeit a very short-lived one, Rb-82 sometimes shows reversible stress–rest defect, where Tc-99m sestamibi or Tc-99m tetrofosmine SPECT studies show extensive fixed defects [119]. An attempt was made to analyze myocardial kinetics with Rb-82. Despite the short half-life of Rb-82, animal studies showed that acutely injured, postischemic myocardium that eventually proved to be viable showed retention of Rb-82, while myocardium, which proved to be necrotic, showed washout of Rb-82 [120]. Clinical studies by the same group seemed to bear this out, when measuring the washout rate between 1 and 2 minutes after injection vs. 4 and 6 minutes afterward (Fig. 12.13) and compared uptake and retention of Rb-82 in comparison to FDG PET imaging studies [121]. We have tried to duplicate this experiment and have been unable to replicate the results. We found that Rb-82 washout rate was greater in segments with poor initial uptake of Rb-82, and retention was better in segments with only mild initial defects, regardless of the FDG uptake, illustrated in Fig. 12.14 [122]. Thus, in our approach, patients who undergo Rb-82 stress and rest imaging still need FDG PET imaging for viability, if they do not demonstrate significant stress-inducible ischemia.

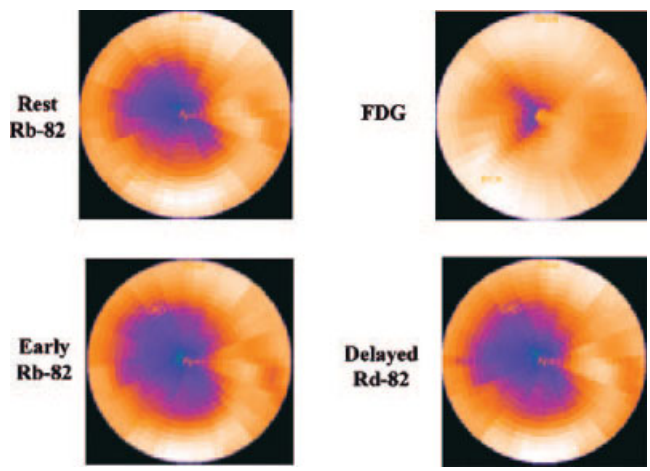

Figure 12.14 Polar rest Rb-82 and FDG metabolic images in a patient who suffered a myocardial infarction several months earlier. The resting perfusion image shows a large, severe perfusion defect. The FDG image shows preserved uptake in much of the region with impaired perfusion, demonstrating a classical perfusion–metabolism mismatch pattern. The early resting Rb-82 images and late Rb-82 images (obtained as in Fig. 12.13) do not show retention of Rb-82, thus failing to predict preserved FDG uptake.

Beanlands et al. [123] studied the ability of N-13 ammonia kinetic modeling to express viability through a mathematical separation of the metabolic component of tracer uptake expressed as the volume of distribution (VD) from the effect of blood flow, and compared the results to F-18 FDG uptake. Flow and VD were both reduced in the hypoperfused regions of patients with scar, while partially preserved flow and VD were seen in regions with viability. The sensitivity and specificity of this combination were 100 and 90%, respectively. These interesting results deserve further studies.

Detection and follow-up of diffuse and early disease

Myocardial PET perfusion imaging has been used to follow the progression or regression of disease, in response to long-term and short-term control of elevated cholesterol and other risk factors [4,5]. Merhige et al. [124] recently reported results on 128 patients with CAD using stress and rest Rb-82 PET. After aggressive lipid-lowering therapy at a mean follow-up of 1.5 years, 80 patients demonstrated improvement in myocardial perfusion, 64 patients showed no change, and 34 showed progression of CAD despite treatment. Coronary events had occurred in 3.3, 10.9, and 17.7% of patients, respectively, 7.5 months after the second scan. Thus, PET perfusion imaging identified 26% of patients with progressive CAD, despite lipid-lowering therapy, at a high risk of subsequent hard coronary events. This application of PET perfusion imaging, similar to SPECT perfusion imaging, relies on the traditional evaluation of relative changes in perfusion during stress and at rest.

PET imaging also appears to be useful in the diagnosis and prognostication at a very early stage in disease, when disease is either diffuse or only minimal, and measuring the response to dietary and lifestyle changes and antilipid drug therapy [125,126]. This involves the use of novel approaches, including base to apex flow gradient quantification, quantification of coronary flow reserve, and the use of cold-pressor testing (CPT).

Base to apex flow gradient quantification

Once attenuation correction has been successfully applied, PET myocardial perfusion imaging is able to assess the gradient in blood flow between the base and the apex. Invasive studies with Doppler flow probes and pressure probes in coronary arteries with diffuse, though nonobstructive, disease have demonstrated a continuous gradient between the proximal and distal vessel, resulting in a longitudinal gradient in flow reserve [127]. In patients with mild diffuse coronary narrowing documented by quantitative arteriography, Gould et al. found a graded, longitudinal, base-to-apex myocardial perfusion gradient significantly different from normal control subjects (Fig. 12.15) [128]. This observation was confirmed by Pampaloni et al. [129]. Hence, an abnormal base-to-apex perfusion gradient observed during vasodilator stress associated with coronary risk factors suggests the presence of early or preclinical CAD, prompting and allowing early secondary preventive intervention in patients at higher risk of progression to clinical disease [9].

Quantification of myocardial blood flow

The noninvasive quantification of myocardial blood flow and coronary flow reserve is one of the most potentially useful, but as yet clinically unexplored, applications of myocardial PET imaging. Myocardial uptake of a perfusion tracer is the result of a complex interaction of blood flow, capillary and cellular membrane permeability, the transport or trapping of the tracer, and back-diffusion. Formal quantification of blood flow requires compartmental analysis in order to take these factors into account. It usually requires a multiframe (50 frames or so) dynamic PET acquisition. Myocardial and blood pool time–activity curves are generated and corrected for decay, partial volume effect, tissue cross-talk, and dead time. A compartmental model is then applied to solve for blood flow.

The rapid equilibration of O-15 water between plasma, interstitial space, and intracellular water allows the use of a simple one-compartment model [42], making this tracer a favorite in scientific studies of quantitative myocardial perfusion. Unfortunately, the very same property prevents O-15 water from being a very useful clinical perfusion imaging agent, since blood pool and myocardium are blurred together. Its use is further limited to sites with a cyclotron.

N-13 ammonia has been successfully used for blood flow measurements in many pioneering scientific studies of myocardial vascular pathophysiology [103], with the use of a two-compartmental model. Satisfactory reproducibility and accuracy are obtainable [130,131]. Muzik et al. found a high diagnostic accuracy and sensitivity using absolute N-13 ammonia blood flow for detection of coronary disease. In patients with a low probability of CAD, the specificity was also high, while an abnormal flow reserve in regions with angiographically normal territories in patients with CAD in other territories was postulated to represent early functional vascular abnormality [132]. PET imaging with N-13 ammonia thus combines excellent image quality with excellent quantification ability. Its use is limited, however, to laboratories with an on-site cyclotron.

Quantification of blood flow with Rb-82 has been shown to be possible as well. The major challenge is its 75-second half-life, resulting in noisy myocardial and blood pool

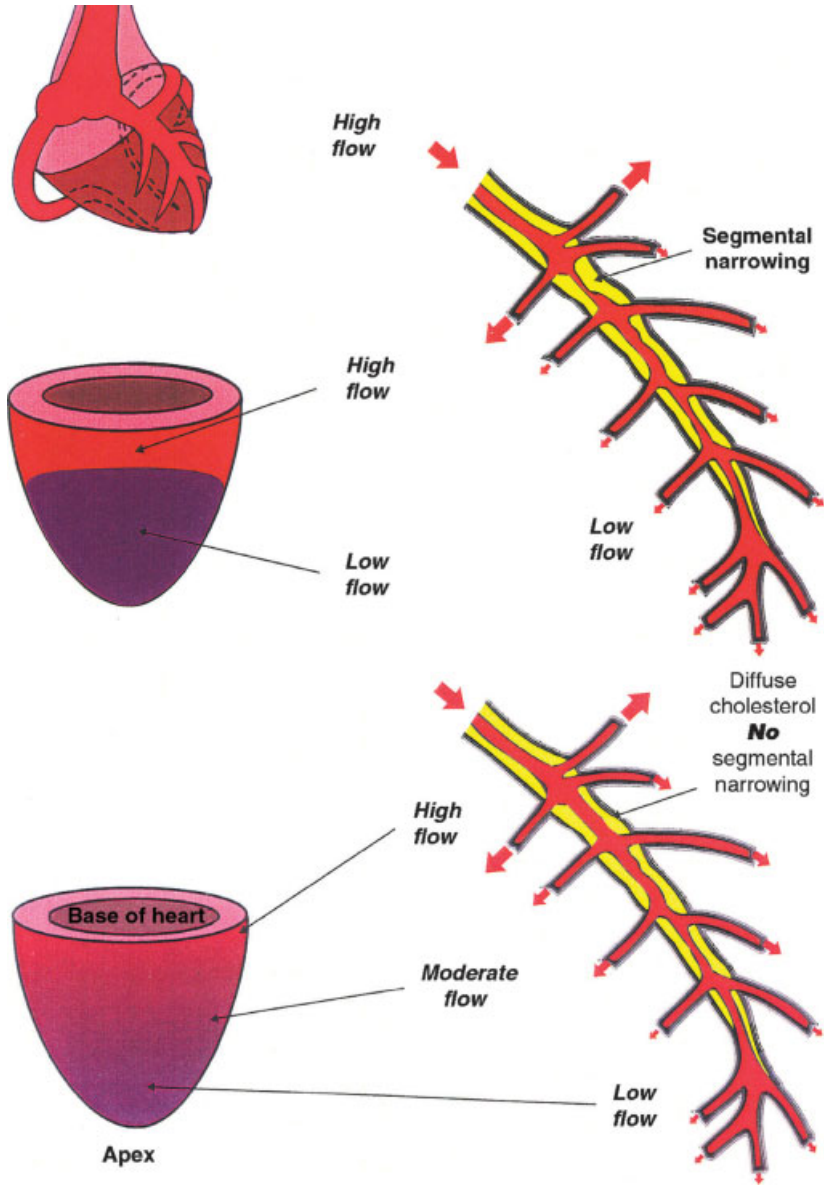

Figure 12.15 Schema of a longitudinal base-to-apex myocardial perfusion abnormality caused by diffuse coronary artery narrowing compared with segmental perfusion defects caused by localized stenosis. (Reproduced with permission from [128].)

time–activity curves. Compartmental analysis of Rb-82 in humans has yielded a reproducibility correlation coefficient of 0.83 in our laboratory [133], and a correlation coefficient of 0.79 against O-15 water by Lin et al., who demonstrated that with specialized wavelet-based noise reduction methods, the correlation with O-15 water measurements improved ($r = 0.94$) [134].

Limitations of the compartmental modeling approach to blood flow quantification include the need for a multiframe dynamic acquisition, requirement for high expertise, and its being a time-consuming process, which makes it impractical for routine clinical use. It is very likely that the standardization of acquisition protocols and the development, standardization, and commercial availability of automatic analysis software will make this important PET capability user-friendly and accessible for routine use in the near future, similarly to the impact of regional quantification, wall motion, and ejection fraction analysis in the past.

In the meantime, it is possible to estimate coronary flow reserve using methods, which, while lacking the rigor of compartmental analysis, offer greater simplicity and ease of use in laboratories using Rb-82 PET for clinical perfusion imaging. The simplest approach utilizes a ratio of Rb-82 uptake during stress and during rest, after normalization for injected activity. The uptake ratio reflects the true coronary flow reserve, although it ignores the effects of changing cardiac output on the plasma tracer activity

and decreasing extraction fraction of Rb-82 during hyperemia. Thus, the normal uptake ratio is closer to 1.5, rather than actual coronary flow reserve, which is usually greater than 2.0 in normal subjects. The stress/rest Rb-82 uptake ratio has been used successfully as an index of blood flow response to stress in the presence of LVH, and in the detection of coronary steal syndrome [135–137].

A compromise alternative proposed by Yoshida et al. [138] corrects the uptake of Rb-82 or N-13 ammonia by the summed blood pool activity and by the relation between the extraction fraction of the tracer and blood flow obtained from animal experiments [34,51]. This approach (simple model) was validated in animal experiments against standard compartmental analysis and against electromagnetic flow probe measurements. We have adapted this method for human studies. A comparison of the simple model with the compartmental model yielded a fair correlation ($r = 0.72$, $p < 0.001$), and an excellent reproducibility ($r = 0.97$) less susceptible to noise than the compartmental method [133]. Using a similar method of Rb-82 myocardial uptake corrected by blood pool activity, DeKemp et al. showed a good correlation with microsphere flow measurements ($r = 0.74$, $p = 0.001$) in animal studies, with a sensitivity and specificity of 85–90% for retention differences of 20% over baseline obtained through comparisons of repeated Rb-82 scans [139].

Clinical applications of myocardial blood flow and coronary flow reserve quantification

A number of clinical applications of coronary flow reserve are given in Table 12.11. The first application is quality control to verify the global response to vasodilator stress. Some patients fail to follow instructions and ingest some caffeine prior to their pharmacologic stress test. A normal flow reserve (greater than 2.0 in our normal population) provides assurance that the stress test was adequate. Some patients may have small-vessel disease due to hypertension, hyperlipidemia, or diabetes [7,8].

Patients with end-stage liver disease appear to have decreased vasodilatory capacity during dipyridamole stress, even after excluding patients with LVH, hypertension, or diabetes [140,141]. This too may limit the sensitivity to detect epicardial coronary disease. In the absence of flow reserve quantification, the adequacy of response to pharmacologic stress is unknown. Mishra et al. [142] demonstrated that cardiac hemodynamics, i.e., blood pressure and heart rate, during intravenous adenosine infusion are poor predictors of changes in the coronary blood flow during peak hyperemia. Quantification of the hyperemic response is also a useful indicator of the potency of any new hyperemic agent [143].

Table 12.11 Clinical applications of coronary flow reserve quantification.

1	Verification of efficacy of pharmacologic vasodilation
2	Detection of global/diffuse disease
3	Evaluation of extent of multivessel disease
4	Evaluation of significance of individual vessel lesions
5	Detection of coronary steal syndrome-collaterals
6	Evaluation of endothelial function
7	Monitoring therapy

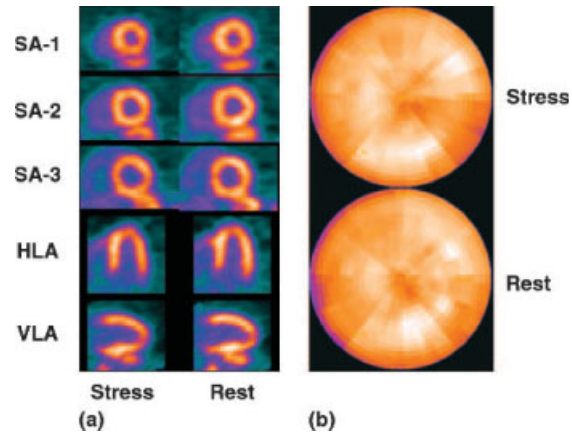

Figure 12.16 Tomographic slices (a) and polar maps (b) of stress and rest Rb-82 PET images of a 70-year-old male with multiple risk factors for CAD and mild chest pain. The images suggest only minimal apical and inferolateral ischemia. The CFR was 1.3, indicating severe diffuse disease. (Reproduced with permission from [214].)

Another important application is to help exclude extensive epicardial disease in a high-risk patient with normal or minimally abnormal stress and rest images due to "balanced ischemia". Figure 12.16 shows stress and rest images of a 70-year-old male with multiple risk factors for CAD and mild chest pain. During dipyridamole stress, the ECG response was negative and the stress Rb-82 PET images showed only minimal, apical, and inferolateral ischemia. This would not be a patient for invasive evaluation, were it not for the fact that the global coronary flow reserve (CFR) was only 1.3 (normal CFR > 2.0). The patient's angiogram showed three-vessel disease, most severe in the OM1 branch of the circumflex artery.

A similar problem comes up when a patient with risk factors for CAD undergoes SPECT imaging with treadmill exercise, and while the ECG response is positive and the SPECT study is normal, as shown in Fig. 12.17. With a suspicion for balanced ischemia, a pharmacologic Rb-82 PET imaging study was then performed, which showed anterior wall ischemia, plus a diffusely decreased coronary flow reserve of 1.5 (normal CFR > 2.0). The patient's subsequent coronary angiogram showed three-vessel disease.

Flow reserve quantification helps define the full extent of multivessel disease, thus potentially impacting on

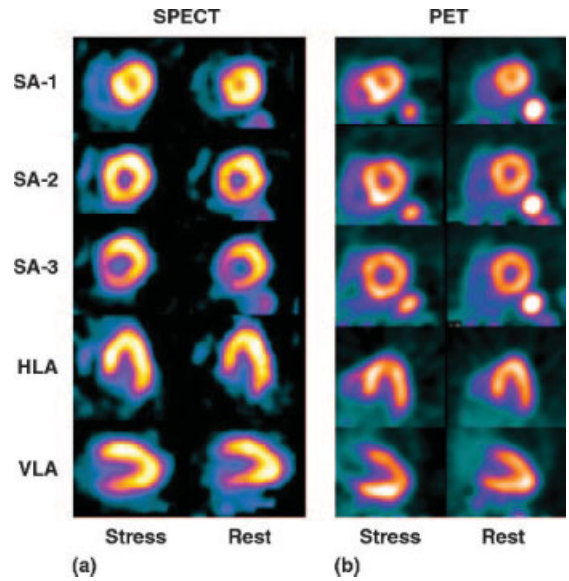

Figure 12.17 (a) Exercise stress and rest Tc-99m sestamibi imaging study in a patient with multiple risk factors for CAD, and a positive ECG response. (b) Pharmacologic stress and rest Rb-82 PET imaging study showed anterior wall ischemia, plus a diffusely decreased coronary flow reserve of 1.5 (normal CFR > 2.0). The patient's subsequent coronary angiogram showed three-vessel disease.

estimation of prognosis. Parkash et al. [90] compared the ability of standard display and interpretation to quantification of absolute perfusion reserve with Rb-82 PET to detect abnormalities in patients with three-vessel disease vs. only single-vessel disease. With standard display, three-vessel disease showed a mean 42% of LV area abnormal. With absolute quantification, 65% of LV area was abnormal, thus increasing sensitivity for all three vessels. Flow reserve quantification helps assess disease severity in the "normal" segments, when others are abnormal, since these "normal segments" are used for normalization of stress and rest images.

Coronary arteriography is considered the "gold standard" for evaluating the severity of coronary stenosis. Because the resistance to blood flow through a stenotic lesion depends on a number of lesion characteristics, the physiological significance of coronary lesions of intermediate severity is often difficult to determine from angiography alone. DiCarli et al. have showed in humans that myocardial blood flow and flow reserve by PET are inversely and nonlinearly related to stenosis severity. CFR measured with N-13 ammonia could differentiate coronary lesions of 50–70% stenosis from lesions with 70–90% stenosis on coronary angiography [103], previously demonstrated in an animal model [144–146]. However, a number of factors other than lesion diameter influence the measured coronary flow reserve, including the heart rate, resting blood flow, the LV end-diastolic pressure, contractility, and the magnitude of dipyridamole-induced hyperemia [147–150]. Nevertheless, there is a role for the accurate assessment of the physiological severity of coronary stenoses as a more objective determination of medical versus mechanical treatment of coronary artery stenosis and for monitoring of the results of their treatment, since clinical tools, such as chest pain, are poorly related to stenosis severity. The estimation of severity of vessel stenosis by relative myocardial perfusion indices depends on the presence of normally perfused myocardium. In patients with multivessel disease, such normally perfused myocardium may not be available, as seen in our examples in Figs. 12.16 and 12.17.

Another application of potential usefulness in intervention is the assessment of the presence of collaterals to diseased regions. It is axiomatic that blood flow to myocardium supplied by diseased arteries does not increase to the same degree as in normal regions. In multivessel disease in the presence of collaterals, blood flow to the most diseased region may actually decrease with stress, demonstrating "coronary steal" (Fig. 12.18), which can be detected by quantification of regional blood flow [135,136,151]. Knowledge of the presence of such collaterals, which cannot always be seen angiographically, can help in the planning of intervention procedures.

Another application is the monitoring of the progression or possible regression of diffuse disease in atherosclerosis, hypertension, diabetes, hyperlipidemia, and post-transplant vasculopathy [7,152,153]. The patient shown in Fig. 12.16 declined coronary bypass surgery, and allowed only revascularization of the OM1, the most severely

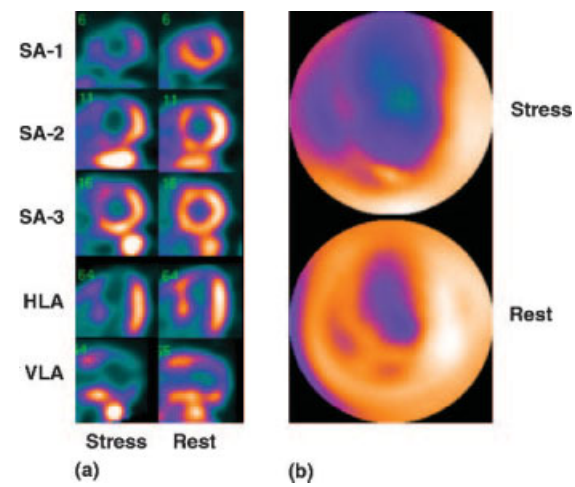

Figure 12.18 Stress and rest Rb-82 PET myocardial perfusion images (a) and polar maps (b) in a patient with severe apical, anterior, and septal perfusion defects during stress, with nearly normal perfusion at rest. Flow quantification revealed a severely reduced flow reserve of less than 1.0 in the apex and anterior and septal walls, demonstrating evidence of coronary steal.

diseased vessel, to be stented. The patient was placed on a rigorous antilipid regimen with diet and medication. One year later, the PET study was repeated. This time the inferolateral wall did not show any focal abnormality, and the global CFR was 2.2 (normal), and at 2 years after the first study, the CFR was 2.9, demonstrating reversibility of the hemodynamic effects of CAD with diet and antilipid medication alone, a phenomenon well documented in the literature [5,7,154].

Detection of early disease

Decreased CFR has been found even in the absence of visible coronary stenoses, including, for example, in normal-appearing vessels in patients with coronary disease in other vessels [155–157]. The presence of even mild, nonobstructive coronary disease was found to be predictive of progression to clinically significant disease in 6 years [9]. Quantitative PET offers a sensitive tool to detect early disease in high-risk patients, such as asymptomatic individuals who are relatives of patients with CAD [158]. Helle et al. [159] showed that cholesterol-lowering therapy can improve coronary vasodilator capacity even in young and middle-aged men with no signs of CAD and fairly low cholesterol levels.

The presence of reduced coronary flow reserve needs to be interpreted with great caution, since its causes are numerous. This includes balanced ischemia, inadequate pharmacologic stimulation, early subclinical CAD, hypertrophic disease states [160], in poorly controlled diabetes, and hyperlipidemia [7,8,161]. Glycemic control as well as reduction of serum lipids through low-fat diet and exercise and antilipid drugs have been shown to lead to an improvement in coronary flow reserve [6]. This is not true of all interventions. McMahon et al. [162], for example, found in insulin-treated patients with type 2 diabetes no demonstrable effect of pioglitazone, an insulin sensitizer, for 3 months on coronary flow reserve, despite improvement in glycemic and lipid control.

Cold-pressor stress testing

The vascular endothelium plays an important role in the regulation of circulatory function and in the structural and functional integrity of the vascular wall, including its antithrombotic and antiatherosclerotic effect [163]. Abnormal endothelium-dependent coronary vasomotion has been found to be an independent predictor of CAD and of coronary events [164–166]. Invasive methods of evaluating endothelial function include quantitative angiography and intracoronary flow velocity measurements of response to acetylcholine-stimulated endothelial release of nitric oxide. Intracoronary acetylcholine normally causes vasodilation. In the presence of endothelial disease, with and without observed coronary disease, acetylcholine produces a lack of vasodilation or even vasoconstriction. A normal response has been restored after cholesterol-lowering and antioxidant therapy [167]. Endothelial function can also be studied with flow-dependent vasodilation in response to sympathetic stimulation with Cold pressor testing (CPT) [168]. CPT consists of immersing one hand in ice or ice water during coronary angiography or 60 seconds before injection of a flow tracer and for 60 seconds after injection during noninvasive PET imaging. CPT results in sympathetic stimulation [169] and α-adrenergic-mediated vasoconstriction of the vascular smooth muscle, which is, under normal conditions, offset by flow-mediated vasodilation and by a possible direct adrenergic-induced endothelium-dependent vasodilator response [170]. In the presence of endothelial disease or atherosclerosis, the vasoconstrictor component is left unopposed [171]. The balance of vasodilation and vasoconstriction represents an index of the integrity of the vascular wall [172]. Changes in luminal area of the epicardial vessels during CPT correlate with changes in coronary blood flow, demonstrating that flow-dependent vasodilation can be studied with measurements of coronary blood flow [173,174].

A 30–40% increase in blood flow is considered a normal response to CPT. Despite angiographically normal coronary arteries, diminished or even paradoxically decreased endotholium-dependent myocardial flow response may result in a mismatch between an increase in demand and supply that has been related to myocardial ischemia during daily life [175–177)]. Abnormal responses to CPT have been found in early CAD [178], hyperlipidemia [173,179], insulin resistance [180], diabetes [181,182], elevated CRP levels [183)], the metabolic syndrome [184], elevated leptin levels in obese individuals [185], and smoking [186,187]. Endothelial dysfunction is reversible with insulin-sensitizing drugs in the case of insulin resistance, improved glycemic control, or angiotensin I-converting enzyme inhibitors in diabetes, L-arginine, citric acid or smoking cessation in smokers, and antilipid therapy in patients with elevated serum lipids [188–190]. Abnormal CPT results have been associated with menopause [191]. They can be reversed by long-term hormone replacement therapy (in the absence of other risk factors for CAD) using estrogens with or without progesterone [192].

The changes in response to CPT as a result of therapy are more dramatic compared to the minimal changes in angiographic lesion characteristics or lumen diameter [193]. The response to CPT tends to be more sensitive than changes in response to hyperemia (dipyridamole or adenosine) [194].

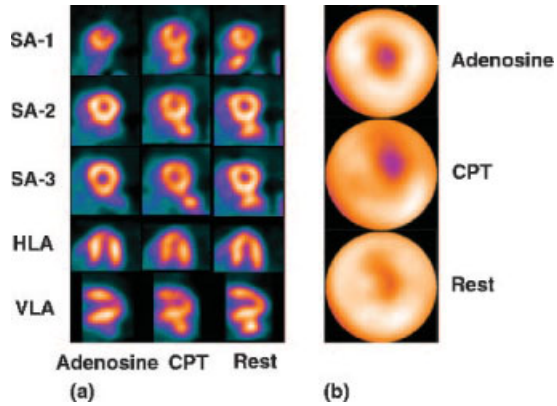

Figure 12.19 Rb-82 PET tomographic images (a) and polar maps (b) of adenosine stress, CPT, and resting images of a 58-year-old female, with atypical chest pains at night and in cold weather, but no obstructive coronary disease. Resting perfusion is normal. The adenosine stress images show mild anteroapical hypoperfusion. The cold pressor perfusion images show moderate anteroapical and extensive mild anterior, anterolateral, and septal hypopoperfusion. (Reproduced with permission from [214].)

The fact that some patients with risk factors have a normal response to CPT while other patients have an abnormal response or that "normal" subjects have an abnormal response [195] attests to the variability of the susceptibility of the individual to these environmental factors. Of relevance is the observation that only 50% of the total attributable risk burden for CAD can be related to conventional risk factors [196,197], warranting an alternative determination of risk such as CPT, for the development of atherosclerosis. Thus, noninvasive CPT can serve as an early marker of endothelial dysfunction, and as an early warning of development of atherosclerosis, that is susceptible to reversibility with diet and medication [164].

While most studies with CPT have been performed with N-13 ammonia, or O-15 water, the short half-life and low dosimetry of Rb-82 allow for multiple sequential stress interventions, including adenosine, CPT, or mental stress in the same session, to elucidate troubling symptoms. An example is given by a 58-year-old female, with hyperlipidemia and chest pain, who was initially diagnosed with a distal left anterior descending occlusion, which was treated with a stent. After several years of doing well, the patient presented with atypical chest pains at night and in cold weather. An angiogram showed no obstructive disease. The patient underwent serial imaging at rest, CPT, and adenosine stress testing with Rb-82 PET imaging. The results are shown in Fig. 12.19. The resting perfusion polar map is normal. The adenosine stress polar map shows mild periapical hypoperfusion, suggesting a mild basal-to-apical gradient. The cold-pressor perfusion polar map shows moderate periapical and extensive mild anterior and anterolateral and septal hypopoperfusion accompanied by her usual chest pain. The patient was treated with a calcium-channel blocker and stricter antilipid therapy, with complete relief of symptoms.

Is cardiac PET imaging cost-effective?

In spite of increased cost of an individual PET study, the use of PET perfusion imaging has been shown to be cost-effective, through its enhanced diagnostic power. These analyses do not even take into account the extra-added information of blood flow quantification in response to vasodilator or CPT stimulation.

The results of an analysis by Gould et al. [198–200] are shown in Fig. 12.20. They investigated the cost of angiography in all cases, vs. Tl-201 SPECT or Rb-82 PET, followed by coronary angiography only in patients with abnormal perfusion studies. The most expensive diagnostic approach is that of coronary angiography in all patients with a pretest probability of less than 70%. In patients with more than 70% likelihood of disease, angiography is more cost-effective for diagnosis. This analysis does not include benefit of prognostication. Both SPECT and PET achieved a savings compared to performing angiography, due to decreased referral for unnecessary coronary catheterization. PET achieved a savings compared to SPECT imaging for patients with a probability of disease between 0 and 60%, due to the more effective avoidance of angiography in patients who did not need it. If only half of all patients with an abnormal noninvasive test underwent angiography (a more realistic scenario), then the cost savings of PET was even greater. A cost analysis by Patterson et al. [201] came to similar conclusions.

Merhige [202] studied what actually happens when PET imaging is introduced into clinical practice. One hundred

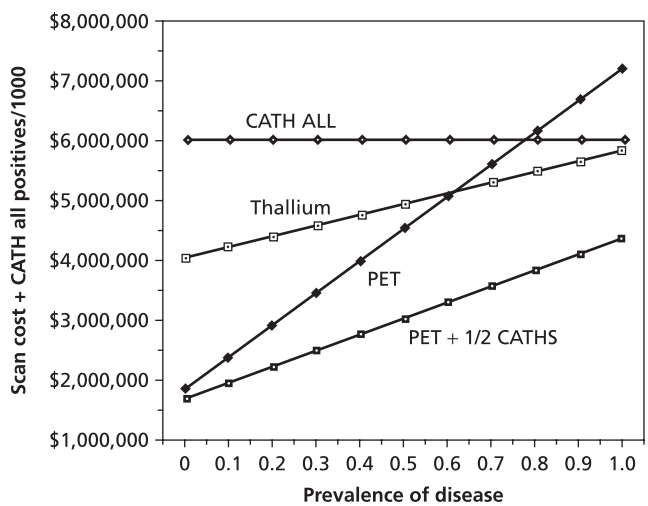

Figure 12.20 Comparative costs of Tl-201 SPECT, Rb-82 PET, and coronary angiography as a function of disease prevalence. (Reproduced with permission from [198].)

two patients studied with stress and rest Rb-82 PET imaging were identified, with a mean pretest probability of 37% for CAD. Another 102 patients selected with matching pretest probability of CAD were studied with SPECT prior to the installation of the PET scanner. Both sets of patients were followed for a mean of 12 months. The use of PET led to a reduction in the false-positive rate, leading in turn to a reduction in angiographies. The diagnostic cost per patient was similar for SPECT and PET, in spite of higher cost of PET per study, due to lower referral for further diagnostic studies. While there was no significant change in the rate of angioplasties in their study group, there was a reduction in the number of bypass operations. The therapeutic cost per patient was lower with PET, mainly due to a reduction in the number of bypass operations. Although the mortality for the two groups did not significantly differ, the mortality from cardiac causes and/or an acute myocardial infarction was lower for the group initially imaged with PET, mainly due to lower complications at the time of bypass surgery. This clinical field study supported the predictions of cost-effectiveness from the model of Patterson et al. [201].

Along similar lines, the usage of FDG for the determination of myocardial viability in patients with poor LV function due to CAD has been demonstrated to be cost-effective by selection of patients for revascularization who are likely to benefit, and by sparing patients not likely to benefit further costs and morbidity from additional testing and revascularization attempts in vain [203].

From the viewpoint of the imaging laboratory, a disadvantage for the beginning user or low-level user of Rb-82 is the high fixed cost of its generator. While at a low volume of one patient a day, the cost is approximately $1400 per patient, the cost decreases to $230 per patient with a volume of six patients a day, and becomes only $140 per patient with 10 studies per day. The cost of radiotracer thus becomes quite competitive compared to thallium-201 or a Tc-99m labeled perfusion agent. The usage of N-13 ammonia for perfusion imaging also carries a high fixed cost of the overhead and operations budget, although a multiuser cyclotron facility may dispense the tracer on a unit-dose basis. Likewise, FDG is purchased on a unit-dose basis, with a low overhead, and for a center with a high utilization rate of FDG for all combined purposes, the cost per dose is competitive.

Technical problems encountered with cardiac PET imaging

The vast majority of patients tolerate PET imaging well. Occasional patients do feel claustrophobic. One should offer sedation in that event. Frequently, a thorough explanation of the procedure, providing reassurance, soothing or favorite music, and close supervision can overcome this difficulty without medication.

Myocardial PET imaging, as all other imaging modalities, is subject to artifacts. A faulty detector block or a poorly maintained PET scanner can cause a major streak and defect artifact. Recognition and checking the PET blank study, the equivalent to a flood source in a conventional camera, aids in diagnosing the problem. The PET camera needs to be properly calibrated in order to achieve accurate quantification.

An important source of image artifact is the movement of the heart out of position between the transmission scan and either of the emission scans. The patient may hyperventilate during stress, or have a change in the respiratory pattern. The assumption of successful PET attenuation correction is that the transmission scan reflects the true position of the heart, diaphragm, and adjacent structures. Significant displacement of the average position up or down will violate that assumption and lead to artifact.

Our recent work with 178 patients studied with dipyridamole stress and rest Rb-82 PET imaging [204] showed that prevalence of noticeable vertical heart drop of more than 10 mm was 6% in an unselected group of 100 patients, although it was 17% in a subset of 78 asymptomatic patients, and 14% in a subset of 27 patients at low risk of CAD. In spite of a relatively high frequency of vertical heart displacement, there was no significant increase in frequency of PET scan defects with large or small heart drop in any of patient subgroups, notably in the group with low probability of CAD. Fortunately, some displacement does not necessarily lead to artifactual findings, but should be suspected in cases of inferior "hot spots," or basal anterolateral, anteroseptal, or lateral defects. Figure 12.21 shows such an artifact, and its resolution after a second transmission scan was obtained.

A systematic analysis of artifacts in PET myocardial perfusion images due to attenuation–emission misregistration was recently published by Loghin et al. [205]. They performed 1177 studies with either Rb-82 or N-13 ammonia while varying the order of the transmission and emission scans. They found that 21% of subjects had artifactual defects due to attenuation–emission misregistration. The frequency of artifact varied, depending on the specific protocol used. Misregistration defects were predicted by horizontal plane misregistration between the emission and transmission scans. Horizontal misregistration in turn was predicted by diaphragm displacement between rest and dipyridamole stress images, a greater body mass index, and small heart size. Misregistration was greatest with attenuation scans performed at the very beginning of the imaging protocol. It was predictably greater in obese individuals, suggesting possible delayed displacement of the diaphragm after positioning due to pressure from abdominal contents. By shifting the emission images to match the

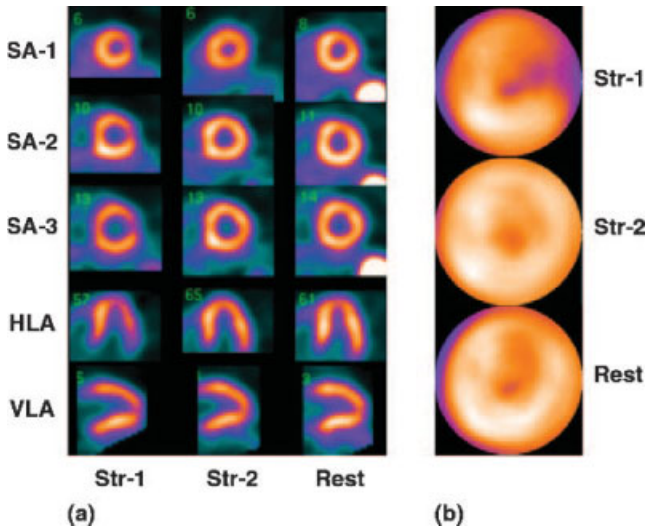

Figure 12.21 Stress and rest Rb-82 PET tomographic images (a) and polar maps (b) of a patient that shows a perfusion defect during stress (Str-1), coincident with a significant displacement of the heart from the resting position. A repeat transmission scan resulted in absence of a perfusion defect on the new stress (Str-2) study.

transmission scan, the quantitative severity and size of defects were significantly decreased.

The recognition of this problem in any given patient needs appropriate software to display the matched emission and transmission maps, both in the transaxial plane and in the axial plane. Remedies include repeating the stress study when recognized. Thus, an optimal image sequence, where the transmission scan is close in time to the emission scan, particularly the stress study, minimizes artifact frequency. This is likely specific to PET camera manufacture. When feasible, a separate transmission scan with each of the resting and stress studies is used routinely in some laboratories (Table 12.5). In our protocol with a dedicated PET scanner (Table 12.4), we perform the transmission scan after the resting scans, just before the pharmacologic stress, thus close in time to both rest and stress imaging. This may account for the relatively lesser frequency of displacement misregistration artifact in our studies [204].

Potential benefit of PET/CT imaging

Combined PET and CT imaging in a single combined PET/CT unit has become the preferred approach for PET imaging in oncology. Approximately 80% new units installed in 2003 were PET/CT units (M. Emmons, GE Health Care, personal communication, 2004). Table 12.12 summarizes the known or potential benefits of PET/CT imaging of the heart.

Table 12.12 Value of PET/CT.

1	Positioning
2	Attenuation correction
3	Calcium scoring
4	Coronary angiography
5	Contrast ventriculography

Transmission scan

Table 12.6 shows a typical acquisition protocol with a BGO PET/CT scanner. First, the scout CT used to position the patient in the PET scanner can be obtained in just a few seconds. CT scanning markedly reduces the time for the transmission scan. The shortening of time is not only in cutting the time by 8–10 minutes used for the transmission scan, but since the transmission scan is relatively noise free, it reduces the amount of noise in the attenuation-corrected emission scan, thus reducing the length of time required for the emission scan itself. Since 30–35 minutes are projected for the entire study, throughput is enhanced. One group reported saving 12 minutes for the complete study, after switching from a dedicated PET system to a PET/CT system [59].

PET/CT imaging holds both challenges and solutions for the attenuation correction problem. The transmission scan is markedly shortened. It is possible to repeat the transmission scan separately for both rest and stress images, and a separate CT transmission scan before and after the stress study, in order to ensure correct registration [60]. In addition, the CT transmission and PET emission scans can be easily displayed and superimposed using existing display software for easier detection of misalignment. The CT transmission map can be potentially moved on some PET/CT systems. Using appropriate 3D pattern fitting algorithms, the CT transmission map could conceivably be automatically repositioned to provide more reliable attenuation correction.

On the other hand, CT attenuation correction is more susceptible to artifacts produced by metallic implants or pacemakers than pin-source-produced attenuation maps, due to the lower energy (80–130 keV) of the CT x-rays. A short scanning time for the CT attenuation map (less than 15 s) raises an entirely new challenge, due to potential undersampling of the position of the heart and diaphragm, due to the motion of the heart during contraction, and due to respiratory movement. Thus, a very rapid attenuation scan is likely to result in even greater artifact than with a 8–10-minute pin-source transmission scan [206], as is seen frequently in whole-body PET imaging for oncology purposes [207]. The attenuation map needs to be obtained over a sufficient number of respiratory and cardiac cycles, in order to match the average position of the heart during the

emission scan at rest and again during stress, confirmed by superior results from a "slow" CT attenuation map, obtained over 42 seconds during free breathing, vs. a "fast" CT map obtained over 5 seconds at either end-inspiration or end-respiration [208]. The x-ray tube current used for the transmission scan can be set low, in order to allow a prolonged scan time, while minimizing radiation exposure. At this time, the most optimal protocol for PET/CT transmission imaging has not yet been determined, due to the limited experience with PET/CT imaging of the heart.

Respiratory gating of the CT as well as of the PET images offers the potential for a closer emission–transmission match, coupled with an appropriate display of the emission and transmission scans, along with the means to correct for any mismatch [209–211]. It is hoped that PET camera manufacturers will address this important need in the future.

Coronary calcium scoring

Another potential application of PET/CT is the possibility of obtaining coronary calcium scores at the time of PET perfusion imaging. This subject is discussed in Chapter 14.

CT coronary angiography

An intriguing possibility is the potential value of CT coronary angiography performed together with the PET rest and stress and/or viability imaging in selected patients. CT angiography requires IV contrast, which in turn requires careful screening for a history of allergy to contrast dye, and the status of renal function and diabetes. Multislice (16 slices or greater) CT scans have been found to have up to 95% accuracy in the detection of occlusive CAD when compared with invasive coronary angiography. Limitations exist in visualizing the small distal vessels, in the presence of heavy calcifications, or some stents. The latter limitations can be overcome with the aid of the PET perfusion results [212].

The combination of PET myocardial perfusion imaging, coronary calcium scoring, and CT angiography offers a comprehensive set of information about a patient. However, it is doubtful that the complete set would prove to be cost-effective, or worth the radiation exposure, for routine screening. Nonetheless, in selected patients, this combination of complementary imaging techniques could help solve difficult diagnostic problems. PET myocardial perfusion imaging would evaluate the significance of borderline stenoses or densely calcified vessels or stents, difficult to evaluate by CT angiography presently. CT angiography, on the other hand, would help evaluate the anatomical correlates of perfusion abnormalities. Patients with known or suspected multivessel disease and anticipated intervention could be studied with sequential stress–rest perfusion imaging and followed by CT angiography, together with CT ventriculography for LV and RV function. Thus, patients could need to go to the invasive catheterization laboratory mainly for intervention.

Reimbursement requirements would probably call for such patients to be chosen in advance. With the patient in the same position, allowing acquisitions of easily superimposable images, one would like to reconstruct superimposable displays of both coronary anatomy as well as maps of rest and stress perfusion, wall motion, and viability. Faber et al. [213] demonstrated that their software allows accurate alignment of the coronary artery tree and LV myocardial surfaces acquired from a single PET/CT exam of perfusion and metabolism. This complete set of information, through spatially matched physiological significance of disease with coronary anatomy and lesion calcium content, could add interpretation power and ease to decision making for interventions in multivessel disease intervention planning. This proposition still needs to be tested in clinical studies.

Future prospects

Clinical PET perfusion and viability imaging has had a long incubation period. With the recent widespread availability of PET scanners, the commercial availability of tracers for perfusion imaging and viability imaging, and reimbursement, the setting is ripe for widespread adoption of PET for indications that have been shown to benefit from PET imaging. In the meantime, there have been several major paradigm shifts in the understanding and management of coronary disease, in which PET imaging of the heart is a strong contender to affect diagnosis and therapy. One is the shift in emphasis from the assessment of structural to functional alterations. With quantification of myocardial blood flow, the function of the coronary circulation can be evaluated noninvasively. PET can detect early endothelial disease in the absence of obstructive disease, which is related to risk factors, is predictive of future development of disease, and can be reversed by lifestyle, dietary, and pharmacologic interventions. Moreover, early disease can be detected even in patients that lack classical risk factors. Thus, the study of endothelial dysfunction is suggested to be a key to the early diagnosis and control of early coronary disease. Another major paradigm shift is offered by the intriguing potential of combined multimodality imaging, represented by PET/CT imaging.

Another unique feature of PET imaging is the ability to image tracers labeled with isotopes like F-18, C-11, and N-13. The growing PET infrastructure will allow PET imaging to become a tool in the noninvasive assessment of in vivo cellular metabolism, receptor function, and gene

expression, which hold great potential in applications beyond perfusion and glucose metabolism.

References

1. Falk E, Shah PK, Fuster V. Coronary plaque disruption. Circulation 1995;92(3):657–671.
2. Libby P. Molecular-bases of the acute coronary syndromes. Circulation 1995;91(11):2844–2850.
3. Farb A, Tang AL, Burke AP, Sessums L, Liang YH, Virmani R. Sudden coronary death – frequency of active coronary lesions, inactive coronary lesions, and myocardial-infarction. Circulation 1995;92(7):1701–1709.
4. Gould KL, Martucci JP, Goldberg DI, et al. Short-term cholesterol-lowering decreases size and severity of perfusion abnormalities by positron emission tomography after dipyridamole in patients with coronary-artery disease – a potential noninvasive marker of healing coronary endothelium. Circulation 1994;89(4):1530–1538.
5. Gould KL, Ornish D, Scherwitz L, et al. Changes in myocardial perfusion abnormalities by positron emission tomography after long-term, intense risk factor modification. JAMA 1995;274(11):894–901.
6. Czernin J, Barnard J, Sun KT, et al. Effect of short-term cardiovascular conditioning and low-fat diet on myocardial blood-flow and flow reserve. Circulation 1995;92(2):197–204.
7. Yokoyama I, Momomura S, Ohtake T, et al. Improvement of impaired myocardial vasodilatation due to diffuse coronary atherosclerosis in hypercholesterolemics after lipid-lowering therapy. Circulation 1999;100(2):117–122.
8. Huggins GS, Pasternak RC, Alpert NM, Fischman AJ, Gewirtz H. Effects of short-term treatment of hyperlipidemia on coronary vasodilator function and myocardial perfusion in regions having substantial impairment of baseline dilator reverse. Circulation 1998;98(13):1291–1296.
9. Brunel P, Bourassa MG, Wiseman A. Different rates of coronary-artery disease progression in patients with normal and mildly diseased coronary-arteries. Coronary Artery Disease 1991;2(4):449–454.
10. Glover DK, Ruiz M, Edwards NC, et al. Comparison between Tl-201 and Tc-99m sestamibi uptake during adenosine-induced vasodilation as a function of coronary stenosis severity. Circulation 1995;91(3):813–820.
11. Glover DK, Okada RD. Myocardial kinetics of Tc-MIBI in canine myocardium after dipyridamole. Circulation 1990;81(2):628–637.
12. Sinusas AJ, Shi Q, Saltzberg MT, et al. Technetium-99m-tetrofosmin to assess myocardial blood flow: experimental validation in an intact canine model of ischemia. Journal of Nuclear Medicine 1994;35(4):664–671.
13. Kong BA, Shaw L, Miller DD, Chaitman BR. Comparison of accuracy for detecting coronary-artery disease and side-effect profile of dipyridamole Tl-201 myocardial perfusion imaging in women versus men. American Journal of Cardiology 1992;70(2):168–173.
14. Nishimura S, Mahmarian JJ, Boyce TM, Verani MS. Quantitative Tl-201 single-photon emission computed-tomography during maximal pharmacological coronary vasodilation with adenosine for assessing coronary-artery disease. Journal of the American College of Cardiology 1991;18(3):736–745.
15. Bateman TM, Maddahi J, Gray RJ, et al. Diffuse slow washout of myocardial thallium-201: a new scintigraphic indicator of extensive coronary artery disease. Journal of the American College of Cardiology 1984;4(1):55–64.
16. Aarnoudse W, Botman K, Pijls N. False-negative myocardial scintigraphy in balanced three-vessel disease, revealed by coronary pressure measurement. International Journal of Cardiovascular Intervention 2003;5:67–71.
17. Stolzenberg J. Dilatation of left ventricular cavity on stress thallium scan as an indicator of ischemic disease. Clinical Nuclear Medicine 1980;5(7):289–291.
18. Kumar SP, Movahed A. Importance of wall motion analysis in the diagnosis of left main disease using stress nuclear myocardial perfusion imaging. International Journal of Cardiovascular Imaging 2003;19(3):219–224.
19. Martin W, Tweddel AC, Hutton I. Balanced triple-vessel disease – enhanced detection by estimated myocardial thallium uptake. Nuclear Medicine Communications 1992; 13(3):149–153.
20. Hachamovitch R, Berman DS, Kiat H, et al. Incremental prognostic value of adenosine stress myocardial perfusion single-photon emission computed tomography and impact on subsequent management in patients with or suspected of having myocardial ischemia. American Journal of Cardiology 1997;80(4):426–433.
21. DePuey EG, Rozanski A. Using gated technetium-99m-sestamibi SPECT to characterize fixed myocardial defects as infarct or artifact. Journal of Nuclear Medicine 1995;36(6):952–955.
22. Rigo P, Van Boxem P, Foulon J, Safi M, Engdahl J, Links J. Quantitative evaluation of a comprehensive motion, resolution, and attenuation correction program: initial experience. Journal of Nuclear Cardiology 1998;5(5):458–468.
23. O'Connor MK, Kemp B, Anstett F, et al. A multicenter evaluation of commercial attenuation compensation techniques in cardiac SPECT using phantom models. Journal of Nuclear Cardiology 2002;9(4):361–376.
24. Gould K, Schelbert H, Phelps M. Noninvasive assessment of coronary stenoses with myocardial perfusion imaging during pharmacologic coronary vasodilation. American Journal of Cardiology 1979;43(2):200–208.
25. Schelbert HR, Wisenberg G, Phelps ME, et al. Non-invasive assessment of coronary stenoses by myocardial imaging during pharmacologic coronary vasodilation, 6: detection of coronary-artery disease in human-beings with intravenous N-13 ammonia and positron computed-tomography. American Journal of Cardiology 1982;49(5):1197–1207.
26. Tillisch J, Brunken R, Marshall R, et al. Reversibility of cardiac wall-motion abnormalities predicted by positron tomography. New England Journal of Medicine 1986;314(14):884–888.

27. Phelps M, Cherry S. The changing design of positron imaging systems. Clinical Positron Imaging 1998;1(1):31–45.
28. Cho ZH, Chan JK, Ericksson L, et al. Positron ranges obtained from biomedically important positron-emitting radionuclides. Journal of Nuclear Medicine 1975;16(12):1174–1176.
29. Phelps ME, Hoffman EJ, Huang SC, Ter-Pogossian MM. Effect of positron range on spatial resolution. Journal of Nuclear Medicine 1975;16(7):649–652.
30. Derenzo SE, Budinger TF. Resolution limit for positron-imaging devices. Journal of Nuclear Medicine 1977;18(5):491.
31. Debenedetti S, Cowan CE, Konneker WR, Primakoff H. On the angular distribution of 2-photon annihilation radiation. Physical Review 1950;77(2):205–212.
32. Cherry S, Sorenson J, Phelps M, eds. Physics in Nuclear Medicine. 3rd edn. Philadelphia: Saunders; 2003.
33. Schelbert HR, Phelps ME, Huang SC, Macdonald NS, Hansen H, Kuhl DE. N-13 ammonia as an indicator of myocardial blood-flow. Circulation 1981;63(6):1259–1272.
34. Mullani NA, Goldstein RA, Gould KL, et al. Myocardial perfusion with rubidium-82, 1: measurement of extraction fraction and flow with external detectors. Journal of Nuclear Medicine 1983;24(10):898–906.
35. Schelbert H, Schwaiger M. PET studies of the heart. In Phelps ME, Mazziotta JC, Schelbert HR, eds. Positron Emission Tomography and Autoradiography: Principles and Applications for the Brain and Heart. New York: Raven Press; 1986:581–661.
36. Moser K, Cullom S, Hsu B. 2D vs. 3D Rb-82 myocardial perfusion PET using an LSO scanner: segmental quantification in normal and fixed defect populations [abstract]. Journal of Nuclear Cardiology 2004;11(4):S30.
37. Stabin M, Stubbs J, Toohey R, Howe D. Radiation Dose Estimates for Radiopharmaceuticals (CR-6345). Oak Ridge, TN: Oak Ridge Institute for Science and Education; 1996.
38. Schelbert HR, Phelps ME, Hoffman EJ, Huang SC, Selin CE, Kuhl DE. Regional myocardial perfusion assessed with N-13 labeled ammonia and positron emission computerized axial tomography. American Journal of Cardiology 1979;43(2):209–218.
39. Hickey KT, Sciacca RR, Bokhari S, et al. Assessment of cardiac wall motion and ejection fraction with gated PET using N-13 ammonia. Clinical Nuclear Medicine 2004;29(4):243–248.
40. Beanlands RSB, Muzik O, Hutchins GD, Wolfe ER, Schwaiger M. Heterogeneity of regional nitrogen 13-labeled ammonia tracer distribution in the normal human heart – comparison with rubidium-82 and copper-62-labeled PTSM Journal of Nuclear Cardiology 1994;1(3):225–235.
41. Tamaki N, Ruddy T, Dekemp R. Myocardial perfusion. In Wahl R, Buchanan J, eds. Principles and Practice of Positron Emission Tomography. Philadelphia, PA: Lippincott, Williams & Wilkins; 2002:320–333.
42. Bergmann SR, Fox KAA, Rand AL, et al. Quantification of regional myocardial blood-flow in vivo with (H_2O)-O-15. Circulation 1984;70(4):724–733.
43. Bacharach S. Introduction to tracer kinetics. In Dilsizian V, ed. Myocardial Viability: A Clinical and Scientific Treatise. Armonk, NY: Futura Publishing Co.; 2000:251–264.
44. Kim S, Machac J, Almeida O. Optimization of rubidium-82 generator performance [abstract]. Clinical Nuclear Medicine 2004;29:135P.
45. Bateman T. PET myocardial perfusion imaging: making the transition to a clinical routine. Applied Imaging 2002;3(1):1–6.
46. Meerdink DJ, Leppo JA. Experimental studies of the physiological-properties of Tc-99m agents – myocardial transport of perfusion imaging agents. American Journal of Cardiology 1990;66(13):E9–E15.
47. Leppo JA, Meerdink DJ. Comparison of the myocardial uptake of a technetium-labeled isonitrile analogue and thallium. Circulation Research 1989;65(3):632–639.
48. Mack RE, Nolting DD, Hogancamp CE, Bing RJ. Myocardial extraction of Rb-86 in the rabbit. American Journal of Physiology 1959;197(6):1175–1177.
49. Becker L, Ferreira R, Thomas M. Comparison of Rb-86 and microsphere estimates of left-ventricular bloodflow distribution. Journal of Nuclear Medicine 1974;15(11):969–973.
50. Selwyn AP, Allan RM, Labbate A, et al. Relation between regional myocardial uptake of rubidium-82 and perfusion – absolute reduction of cation uptake in ischemia. American Journal of Cardiology 1982;50(1):112–121.
51. Goldstein RA, Mullani NA, Marani SK, Fisher DJ, Gould KL, Obrien HA. Myocardial perfusion with rubidium-82, 2: effects of metabolic and pharmacologic interventions. Journal of Nuclear Medicine 1983;24(10):907–915.
52. Schelbert H, Ashburn WL, Chauncey DM, Halpern SE. Comparative myocardial uptake of intravenously administered radionuclides. Journal of Nuclear Medicine 1974;15(12):1092–1100.
53. Wyss CA, Koepfli P, Mikolajczyk K, Burger C, von Schulthess GK, Kaufmann PA. Bicycle exercise stress in PET for assessment of coronary flow reserve: repeatability and comparison with adenosine stress. Journal of Nuclear Medicine 2003;44(2):146–154.
54. Chow BJW, Ananthasubramaniam K, deKemp RA, Dalipaj MM, Beanlands RSB, Ruddy TD. Comparison of treadmill exercise versus dipyridamole stress with myocardial perfusion imaging using rubidium-82 positron emission tomography. Journal of the American College of Cardiology 2005;45(8):1227–1234.
55. Machac J, Chen H, Almeida O, et al. Comparison of filtered back projection vs iterative reconstruction of rubidium-82 cardiac PET perfusion images. Journal of Nuclear Medicine 2003;44(5):270P.
56. Machac J, Chen H, Almeida OD, Krynyckyi BR, Kim CK, Knesaurek K. Comparison of 2D and high dose and low dose 3D gated myocardial Rb-82 PET imaging. Journal of Nuclear Medicine 2002;43(5):188P.
57. Knesaurek K, Machac J, Krynyckyi BR, Almeida OD. Comparison of 2-dimensional and 3-dimensional Rb-82 myocardial perfusion PET imaging. Journal of Nuclear Medicine 2003;44(8):1350–1356.

58. Moser K, Case J, Bateman T. A quantitative comparison of 2D and 3D acquisition of Rb-82 myocardial perfusion PET studies on an LSO scanner [abstract]. Journal of Nuclear Medicine 2004;45(5):222P.
59. DiFilippo F, Brunken R, Neumann D. Initial clinical experience with Rb-82 cardiac PET imaging on a PET/CT system [abstract]. Journal of Nuclear Medicine 2004;45(5):117P.
60. DiCarli M, Dorbala S, Mishra R. Clinical myocardial perfusion PET/CT imaging with rubidium-82: initial experience in 94 patients [abstract]. Journal of Nuclear Medicine 2004;45(5):117P.
61. Machac J, Mosci K, Almeida OD, et al. Gated rubidium-82 cardiac PET imaging: evaluation of left ventricular wall motion. Journal of the American College of Cardiology 2002;39(5):393A.
62. Almeida O, Machac J, Travis J, et al. Measurement of left ventricular ejection fraction with gated cardiac rubidium-82 positron emission tomography [abstract]. Journal of Nuclear Medicine 2004;45(5):224P.
63. Case J, Bateman T, Moser K, Cullom S, Herstenstein G. Comparison of LVEF measurements from ECG-gated Rb-82 myocardial perfusion PET and Tc-99m sestamibi myocardial perfusion SPECT [abstract]. Journal of Nuclear Cardiology 2003;10(4):S13.
64. Eisner R, Patterson R. Differences between women and men in the heterogeneity of myocardial perfusion images: SPECT Tl-201, Tc-99m sestamibi, and PET Rb-82 [abstract]. Journal of Nuclear Cardiology 1997;4(1 (Suppl), Pt. 2):S104.
65. Gould KL, Goldstein RA, Mullani NA, et al. Noninvasive assessment of coronary stenoses by myocardial perfusion imaging during pharmacological coronary vasodilation, 8: clinical feasibility of positron cardiac imaging without a cyclotron using generator-produced Rb-82. Journal of the American College of Cardiology 1986;7(4):775–789.
66. Demer LL, Gould KL, Goldstein RA, et al. Assessment of coronary-artery disease severity by positron emission tomography – comparison with quantitative arteriography in 193 patients. Circulation 1989;79(4):825–835.
67. Go RT, Marwick TH, Macintyre WJ, et al. A prospective comparison of Rb-82 Pet and Tl-201 spect myocardial perfusion imaging utilizing a single dipyridamole stress in the diagnosis of coronary-artery disease. Journal of Nuclear Medicine 1990;31(12):1899–1905.
68. Yonekura Y, Tamaki N, Senda M, et al. Detection of coronary-artery disease with N-13 ammonia and high-resolution positron-emission computed-tomography. American Heart Journal 1987;113(3):645–654.
69. Williams B, Jansen D, Wong L. Positron emission tomography for the diagnosis of coronary artery disease: a non-university experience and correlation with coronary angiography. Journal of Nuclear Medicine 1989;30(5):845P.
70. Stewart RE, Schwaiger M, Molina E, et al. Comparison of Rb-82 positron emission tomography and Tl-201 spect imaging for detection of coronary-artery disease. American Journal of Cardiology 1991;67(16):1303–1310.
71. Tamaki N, Yonekura Y, Senda M, et al. Value and limitation of stress Tl-201 single photon-emission computed-tomography – comparison with N-13 ammonia positron tomography. Journal of Nuclear Medicine 1988;29(7):1181–1188.
72. Patterson R, Cloninger K, Churchwell K. Special problems with cardiovascular imaging in women. In Julian D, Wenger N, eds. Women and Heart Disease. London: Martin Dunitz Ltd.; 1997:91–115.
73. Churchwell KB, Pilcher WC, Eisner RL, et al. Accuracy of Pet Rb-82 myocardial perfusion imaging to diagnose disease – new software for objective quantitative-analysis. Journal of Nuclear Medicine 1994;35(5):P23.
74. Churchwell K, Pilcher W, Eisner R. Quantitative analysis of PET: the women's test for coronary disease [abstract]. Journal of Nuclear Medicine 1995;36(5):76P.
75. Eisner RL, Tamas MJ, Cloninger K, et al. Normal spect Tl-201 bull-eye display – gender differences. Journal of Nuclear Medicine 1988;29(12):1901–1909.
76. Shonkoff D, Eisner R, Gober A. What quantitative criteria should be used to read defects on the SPECT Tl-201 bullseye display in men? ROC analysis [abstract]. Journal of Nuclear Medicine 1987;28(5):674P–675P.
77. Taillefer R, DePuey EG, Udelson JE, Beller GA, Latour Y, Reeves F. Comparative diagnostic accuracy of Tl-201 and Tc-99m sestamibi SPECT imaging (perfusion and ECG-gated SPECT) in detecting coronary artery disease in women. Journal of the American College of Cardiology 1997;29(1):69–77.
78. Choi JY, Lee KH, Kim SJ, et al. Gating provides improved accuracy for differentiating artifacts from true lesions in equivocal fixed defects on technetium 99m tetrofosmin perfusion SPECT. Journal of Nuclear Cardiology 1998;5(4):395–401.
79. Smanio PEP, Watson DD, Segalla DL, Vinson EL, Smith WH, Beller GA. Value of gating of technetium-99m sestamibi single-photon emission computed tomographic imaging. Journal of the American College of Cardiology 1997;30(7):1687–1692.
80. Ficaro EP, Fessler JA, Shreve PD, Kritzman JN, Rose PA, Corbett JR. Simultaneous transmission/emission myocardial perfusion tomography. Diagnostic accuracy of attenuation-corrected 99mTc-sestamibi single-photon emission computed tomography. Circulation 1996;93(3):463–473.
81. Hendel RC, Corbett JR, Cullom SJ, DePuey EG, Garcia EV, Bateman TM. The value and practice of attenuation correction for myocardial perfusion SPECT imaging: a joint position statement from the American Society of Nuclear Cardiology and the Society of Nuclear Medicine. Journal of Nuclear Cardiology 2002;9(1):135–143.
82. Bateman TM, Heller GV, McGhie AI, et al. Diagnostic accuracy of rest/stress ECG-gated Rb-82 myocardial perfusion PET: comparison with ECG-gated Tc-99m sestamibi SPECT. Journal of Nuclear Cardiology 2006;13:24–33.
83. Hansen CL, Crabbe D, Rubin S. Lower diagnostic accuracy of thallium-201 SPECT myocardial perfusion imaging in women: an effect of smaller chamber size. Journal of the American College of Cardiology 1996;28(5):1214–1219.
84. Flegal KM, Carroll MD, Ogden CL, Johnson CL. Prevalence and trends in obesity among US adults, 1999–2000. JAMA 2002;288(14):1723–1727.
85. Williams B. Women and coronary disease: is PET rubidium-82 imaging the preferred noninvasive diagnostic test?

Applied Imaging Applications Nuclear Cardiology 2000;1(2):1–4.
86. Patterson R, Churchwell K, Eisner R. Diagnosis of coronary artery disease in women: roles of three-dimensional imaging with magnetic resonance imaging or positron emission tomography. American Journal of Cardiac Imaging 1996;10:78–88.
87. McCann C, Alasti H. Comparative evaluation of image quality from three CT simulation scanners. Journal of Applied Clinical Medicine Physics 2004; 5:55–70.
88. Yoshinaga K, Chow B, deKemp R, et al. Prognostic value of rubidium-82 perfusion positron emission tomography: preliminary results from the consecutive 153 patients. Journal of the American College of Cardiology 2004;43(5):338A.
89. Van Tosh A, Supino PG, Smulever RP, et al. Normal PET myocardial perfusion imaging in women with chest pain predicts a low cardiovascular event rate and favorable long term clinical outcome. Journal of the American College of Cardiology 2001;37(2):381A.
90. Parkash R, DeKemp RA, Ruddy TD, et al. Potential utility of rubidium 82 PET quantification in patients with 3-vessel coronary artery disease. Journal of Nuclear Cardiology 2004;11(4):440–449.
91. Pfeffer M. Left ventricular remodeling following myocardial infarction. Cardiologia 1994;39:25–26.
92. White HD, Norris RM, Brown MA, Brandt PW, Whitlock RM, Wild CJ. Left ventricular end-systolic volume as the major determinant of survival after recovery from myocardial infarction. Circulation 1987;76(1):44–51.
93. Louie HW, Laks H, Milgalter E, et al. Ischemic cardiomyopathy – criteria for coronary revascularization and cardiac transplantation. Circulation 1991;84(5):290–295.
94. Yamaguchi A, Ino T, Adachi H, et al. Left ventricular volume predicts postoperative course in patients with ischemic cardiomyopathy. Annals of Thoracic Surgery 1998;65(2):434–438.
95. Gallagher BM, Ansari A, Atkins H, et al. Radiopharmaceuticals, 27: F-18-labeled 2-deoxy-2-fluoro-D-glucose as a radiopharmaceutical for measuring regional myocardial glucose-metabolism in vivo – tissue distribution and imaging studies in animals. Journal of Nuclear Medicine 1977; 18(10):990–996.
96. Ratib O, Phelps ME, Huang SC, Henze E, Selin CE, Schelbert HR. Positron tomography with deoxyglucose for estimating local myocardial glucose-metabolism. Journal of Nuclear Medicine 1982;23(7):577–586.
97. Gropler RJ, Siegel BA, Lee KJ, et al. Nonuniformity in myocardial accumulation of fluorine-18-fluorodeoxyglucose in normal fasted humans. Journal of Nuclear Medicine 1990;31(11):1749–1756.
98. Choi Y, Brunken RC, Hawkins RA, et al. Factors affecting myocardial, 2: F-18 fluoro-2-deoxy-D-glucose uptake in positron emission tomography studies of normal humans. European Journal of Nuclear Medicine 1993;20(4):308–318.
99. Buxton DB, Mody FV, Krivokapich J, Phelps ME, Schelbert HR. Quantitative assessment of prolonged metabolic abnormalities in reperfused canine myocardium. Circulation 1992;85(5):1842–1856.
100. Weinheimer CJ, Brown MA, Nohara R, Perez JE, Bergmann SR. Functional recovery after reperfusion ss predicated on recovery of myocardial oxidative-metabolism. American Heart Journal 1993;125(4):939–949.
101. Bacharach SL, Bax JJ, Case J, et al. PET myocardial glucose metabolism and perfusion imaging, Part I: guidelines for patient preparation and data acquisition. Journal of Nuclear Cardiology 2003;10(5):545–556.
102. Pfeffer MA, Braunwald E. Ventricular remodeling after myocardial infarction – experimental observations and clinical implications. Circulation 1990;81(4):1161–1172.
103. DiCarli M, Czernin J, Hoh CK, et al. Relation among stenosis severity, myocardial blood-flow, and flow reserve in patients with coronary-artery disease. Circulation 1995;91(7):1944–1951.
104. Di Carli MF, Maddahi J, Rokhsar S, et al. Long-term survival of patients with coronary artery disease and left ventricular dysfunction: implications for the role of myocardial viability assessment in management decisions. Journal of Thoracic and Cardiovascular Surgery 1998;116(6):997–1004.
105. Bax JJ, Wijns W, Cornel JH, Visser FC, Boersma E, Fioretti PM. Accuracy of currently available techniques for prediction of functional recovery after revascularization in patients with left ventricular dysfunction due to chronic coronary artery disease: comparison of pooled data. Journal of the American College of Cardiology 1997;30(6):1451–1460.
106. Schoder H, Campisi R, Auerbach M, Phelps ME, Schelbert HR. Extent of PET blood flow metabolism mismatches can predict the magnitude of post-revascularization improvements in global left ventricular function. Journal of Nuclear Medicine 1998;39(5):162P.
107. Bax JJ, Visser FC, Poldermans D, et al. Relationship between preoperative viability and postoperative improvement in LVEF and heart failure symptoms [comment: Journal of Nuclear Medicine Jan 2001;42(1):87–90]. Journal of Nuclear Medicine 2001;42(1):79–86.
108. Alderman EL, Fisher LD, Litwin P, et al. Results of coronary-artery surgery in patients with poor left-ventricular function (CASS). Circulation 1983;68(4):785–795.
109. Di Carli MF, Asgarzadie F, Schelbert HR, et al. Quantitative relation between myocardial viability and improvement in heart failure symptoms after revascularization in patients with ischemic cardiomyopathy. Circulation 1995;92(12):3436–3444.
110. Marwick TH, Nemec JJ, Lafont A, Salcedo EE, Macintyre WJ. Prediction by postexercise fluoro-18 deoxyglucose positron emission tomography of improvement in exercise capacity after revascularization. American Journal of Cardiology 1992;69(9):854–859.
111. Di Carli MF, Davidson M, Little R, et al. Value of metabolic imaging with positron emission tomography for evaluating prognosis in patients with coronary artery disease and left ventricular dysfunction. American Journal of Cardiology 1994;73(8):527–533.
112. Eitzman D, Al-Aouar Z, Kanter H. Clinical outcome of patients with advanced coronary artery disease after viability studies with positron emission tomography. Journal of the American College of Cardiology 1992;20:559–565.

113. Lee KS, Marwick TH, Cook SA, et al. Prognosis of patients with left-ventricular dysfunction, with and without viable myocardium after myocardial-infarction – relative efficacy of medical therapy and revascularization. Circulation 1994;90(6):2687–2694.
114. Beanlands RSB, Hendry PJ, Masters RG, deKemp RA, Woodend K, Ruddy TD. Delay in revascularization is associated with increased mortality rate in patients with severe left ventricular dysfunction and viable myocardium on fluorine 18-fuorodeoxyglucose positron emission tomography imaging. Circulation 1998;98(19):II51–II56.
115. Srinivasan G, Kitsiou AN, Bacharach SL, Bartlett ML, Miller-Davis C, Dilsizian V. [18F]fluorodeoxyglucose single photon emission computed tomography: can it replace PET and thallium SPECT for the assessment of myocardial viability? [see comments]. Circulation; 1998;97:843–850.
116. Arrighi JA, Ng CK, Dey HM, Wackers FJT, Soufer R. Effect of left ventricular function on the assessment of myocardial viability by technetium-99m sestamibi and correlation with positron emission tomography in patients with healed myocardial infarcts or stable angina pectoris, or both. American Journal of Cardiology 1997;80(8):1007–1013.
117. Hernandez-Pampaloni M, Allada V, Fishbein MC, Schelbert HR. Myocardial perfusion and viability by positron emission tomography in infants and children with coronary abnormalities - correlation with echocardiography, coronary angiography, and histopathology. Journal of the American College of Cardiology 2003;41(4):618–626.
118. Dilsizian V, Bonow RO. Current diagnostic techniques of assessing myocardial viability in patients with hibernating and stunned myocardium [erratum: Circulation Jun 1993;87(6):2070]. Circulation 1993;87(1):1–20.
119. Dilsizian V, Arrighi JA, Diodati JG, et al. Myocardial viability in patients with chronic coronary artery disease. Comparison of 99mTc-sestamibi with thallium reinjection and [18F]fluorodeoxyglucose [erratum: Circulation Jun 15, 1995;91(12):3026]. Circulation 1994;89(2):578–587.
120. Goldstein RA. Kinetics of rubidium-82 after coronary-occlusion and reperfusion – assessment of patency and viability in open-chested dogs. Journal of Clinical Investigation 1985;75(4):1131–1137.
121. Gould KL, Yoshida K, Hess MJ, Haynie M, Mullani N, Smalling RW. Myocardial-metabolism of fluorodeoxyglucose compared to cell-membrane integrity for the potassium analog Rb-82 for assessing infarct size in man by PET. Journal of Nuclear Medicine 1991;32(1):1–9.
122. Almeida O, Machac J, Knesaurek K, Krynyckyi B, Kim CK. The predictive value of rest and stress rubidium-82 washout for the determination of myocardial viability. Journal of Nuclear Medicine 2003;44(5):7P.
123. Beanlands RSB, deKemp R, Scheffel A, et al. Can nitrogen-13 ammonia kinetic modeling define myocardial viability independent of fluorine-18 fluorodeoxyglucose? Journal of the American College of Cardiology 1997;29(3):537–543.
124. Merhige ME, Watson GM, Oliverio JG, Shelton V, Frank SN, Perna AF. Efficacy of lipid lowering therapy in inducing arrest or reversal of coronary disease as assessed with positron emission tomography. Journal of the American College of Cardiology 2004;43(5):332A.
125. Nitenberg A, Valensi P, Sachs R, Cosson E, Attali JR, Antony I. Prognostic value of epicardial coronary artery constriction to the cold pressor test in type 2 diabetic patients with angiographically normal coronary arteries and no other major coronary risk factors. Diabetes Care 2004;27(1):208–215.
126. Dorbala S, Mishra R, Logsetty G. PET measurements of coronary flow reserve identify individuals at high risk of developing clinically apparent coronary artery disease (CAD) [abstract]. Journal of Nuclear Medicine 2004;45(5):236P.
127. Kern MJ, Anderson HV. A symposium: the clinical applications of the intracoronary doppler guidewire flow velocity in patients – understanding blood-flow beyond the coronary stenosis – introduction. American Journal of Cardiology 1993;71(14):D1–D2.
128. Gould KL, Nakagawa Y, Nakagawa K, et al. Frequency and clinical implications of fluid dynamically significant diffuse coronary artery disease manifest as graded, longitudinal, base-to-apex myocardial perfusion abnormalities by noninvasive positron emission tomography. Circulation 2000;101(16):1931–1939.
129. Hernandez-Pampaloni M, Keng FYJ, Kudo T, Sayre JS, Schelbert HR. Abnormal longitudinal, base-to-apex myocardial perfusion gradient by quantitative blood flow measurements in patients with coronary risk factors. Circulation 2001;104(5):527–532.
130. Nagamachi S, Czernin J, Kim AS, et al. Reproducibility of measurements of regional resting and hyperemic myocardial blood flow assessed with PET. Journal of Nuclear Medicine 1996;37(10):1626–1631.
131. Sawada S, Muzik O, Beanlands RSB, Wolfe E, Hutchins GD, Schwaiger M. Interobserver and interstudy variability of myocardial blood-flow and flow-reserve measurements with nitrogen 13 ammonia-labeled positron emission tomography. Journal of Nuclear Cardiology 1995;2(5):413–422.
132. Muzik O, Beanlands RSB, Hutchins GD, Mangner TJ, Nguyen N, Schwaiger M. Validation of nitrogen-13-ammonia tracer kinetic-model for quantification of myocardial blood-flow using PET. Journal of Nuclear Medicine 1993;34(1):83–91.
133. Machac J, Knesaurek K, Chen H, Almeida O, Krynyckyi B, Kim CK. Validation of a practical method of coronary flow reserve quantification with rubidium-82 myocardial PET perfusion imaging. Journal of Nuclear Medicine 2003;44(5):90P.
134. Lin JW, Sciacca RR, Chou RL, Laine AF, Bergmann SR. Quantification of myocardial perfusion in human subjects using Rb-82 and wavelet-based noise reduction. Journal of Nuclear Medicine 2001;42(2):201–208.
135. Demer LL, Gould KL, Goldstein RA, Kirkeeide RL. Noninvasive assessment of coronary collaterals in man by pet perfusion imaging. Journal of Nuclear Medicine 1990;31(3):259–270.
136. Garza D, VanTosh A, Roberti R, et al. Detection of coronary collaterals using dipyridamole PET myocardial perfusion imaging with rubidium-82. Journal of Nuclear Medicine 1997;38(1):39–43.

137. Goldstein RA, Haynie M. Limited myocardial perfusion reserve in patients with left-ventricular hypertrophy. Journal of Nuclear Medicine 1990;31(3):255–258.
138. Yoshida K, Mullani N, Gould KL. Coronary flow and flow reserve by PET simplified for clinical applications using rubidium-82 or nitrogen-13-ammonia. Journal of Nuclear Medicine 1996;37(10):1701–1712.
139. deKemp RA, Ruddy TD, Hewitt T, Dalipaj MM, Beanlands RSB. Detection of serial changes in absolute myocardial perfusion with Rb-82 PET. Journal of Nuclear Medicine 2000;41(8):1426–1435.
140. Henzlova M, Machac J, Squire A. Screening for the presence of coronary artery disease in patients with end stage liver disease using SPECT and PET imaging: is dipyridamole a good stressor? [abstract]. Journal of Nuclear Cardiology 2003;10(1):S5.
141. Machac J, Travis A, Almeida O. Is coronary flow reserve decreased in patients with end-stage liver disease? [abstract]. Journal of Nuclear Medicine 2004;45(5):238P.
142. Mishra R, Sciammarella M, Dorbala S. Do changes in hemodynamics during intravenous adenosine infusion predict the magnitude of coronary hyperemia? [abstract]. Journal of Nuclear Medicine 2004;45(5):4P.
143. Mamede M, Tadamura S, Kubo S, Toyoda M. Comparison of myocardial blood flow induced by adenosine triphosphate and dipyridamole in patients with coronary artery disease [abstract]. Journal of Nuclear Medicine 2004;45(5):238P.
144. Gould KL, Lipscomb K, Hamilton GW. Physiologic basis for assessing critical coronary stenosis. Instantaneous flow response and regional distribution during coronary hyperemia as measures of coronary flow reserve. American Journal of Cardiology 1974;33(1):87–94.
145. Khouri EM, Gregg DE, LowensohnHS. Flow in major branches of left coronary artery during experimental coronary insufficiency in unanesthetized dog. Circulation Research 1968;23(1):99–109.
146. Uren NG, Melin JA, Debruyne B, Wijns W, Baudhuin T, Camici PG. Relation between myocardial blood-flow and the severity of coronary-artery stenosis. New England Journal of Medicine 1994;330(25):1782–1788.
147. Bache RJ, Cobb FR. Effect of maximal coronary vasodilation on transmural myocardial perfusion during tachycardia in awake dog. Circulation Research 1977;41(5):648–653.
148. McGinn AL, White CW, Wilson RF. Interstudy variability of coronary flow reserve – influence of heart-rate, arterial-pressure, and ventricular preload. Circulation 1990;81(4):1319–1330.
149. Rossen JD, Winniford MD. Effect of increases in heart-rate and arterial-pressure on coronary flow reserve in humans. Journal of the American College of Cardiology 1993;21(2):343–348.
150. Hoffman JIE. Maximal coronary flow and the concept of coronary vascular reserve. Circulation 1984;70(2):153–159.
151. Akinboboye OO, Idris O, Chou RL, Sciacca RR, Cannon PJ, Bergmann SR. Absolute quantitation of coronary steal induced by intravenous dipyridamole. Journal of the American College of Cardiology 2001;37(1):109–116.
152. Pethig K, Heublein B, Meliss RR, Haverich A. Volumetric remodeling of the proximal left coronary artery: early versus late after heart transplantation. Journal of the American College of Cardiology 1999;34(1):197–203.
153. Zanco P, Gambino A, Livi U, et al. Chances in myocardial blood flow (MBF) and coronary reserve (CR) evaluated by PET in early and late heart transplant (HT). Journal of Nuclear Medicine 2000;41(5):3P.
154. Sdringola S, Nakagawa K, Nakagawa Y, et al. Combined intense lifestyle and pharmacologic lipid treatment further reduce coronary events and myocardial perfusion abnormalities compared with usual-care cholesterol-lowering drugs in coronary artery disease. Journal of the American College of Cardiology 2003;41(2):263–272.
155. Uren NG, Marraccini P, Gistri R, Desilva R, Camici PG. Altered coronary vasodilator reserve and metabolism in myocardium subtended by normal arteries in patients with coronary-artery disease. Journal of the American College of Cardiology 1993;22(3):650–658.
156. Zeiher AM, Drexler H, Wollschlager H, Just H. Endothelial dysfunction of the coronary microvasculature is associated with impaired coronary blood-flow regulation in patients with early atherosclerosis. Circulation 1991;84(5):1984–1992.
157. Yoshinaga K, Katoh C, Noriyasu K, et al. Reduction of coronary flow reserve in areas with and without ischemia on stress perfusion imaging in patients with coronary artery disease: a study using oxygen 15-labeled water PET. Journal of Nuclear Cardiology 2003;10(3):275–283.
158. Sdringola S, Patel D, Gould KL. High prevalence of myocardial perfusion abnormalities on positron emission tomography in asymptomatic persons with a parent or sibling with coronary artery disease. Circulation 2001;103(4):496–501.
159. Helle T, Laaksonen R, Vesalainen R, et al. The effect of pravastatin on myocardial blood flow in young healthy adults. Journal of the American College of Cardiology 2000;35(2):418A.
160. Rajappan K, Rimoldi O, Schafers KP, Pennell DJ, Sheridan DJ, Camici PG. Evidence of stress-induced subendocardial hypoperfusion in patients with aortic stenosis demonstrated by positron emission tomography. Journal of the American College of Cardiology 2001;37(2):419A–420A.
161. Yokoyama I. Improvement of myocardial flow reserve after successful improvement of hyperglycemia in non-insulin dependent diabetics (NIDDM) was more prominent in NIDDM with coronary artery disease rather than in NIDDM with chest pain syndrome. Journal of Nuclear Medicine 1999;40(5):168P.
162. McMahon G, DiCarli M. Effect of insuline resistance on myocardial blood flow in vivo: a randomized controlled clinical trial [abstract]. Journal of Nuclear Medicine 2004;45(5):236P.
163. Drexler H. Endothelial dysfunction: clinical implications. Progress in Cardiovascular Diseases 1997;39(4):287–324.
164. Schachinger V, Britten MB, Zeiher AM. Prognostic impact of coronary vasodilator dysfunction on adverse long-term outcome of coronary heart disease. Circulation 2000;101(16):1899–1906.

165. Halcox JPJ, Schenke WH, Zalos G, et al. Prognostic value of coronary vascular endothelial dysfunction. Circulation 2002;106(6):653–658.
166. Schindler TH, Hornig B, Buser PT, et al. Prognostic value of abnormal vasoreactivity of epicardial coronary arteries to sympathetic stimulation in patients with normal coronary angiograms. Arteriosclerosis Thrombosis and Vascular Biology 2003;23(3):495–501.
167. Anderson TJ, Meredith IT, Yeung AC, Frei B, Selwyn AP, Ganz P. The effect of cholesterol-lowering and antioxidant therapy on endothelium-dependent coronary vasomotion. New England Journal of Medicine 1995;332(8):488–493.
168. Zeiher AM, Drexler H, Wollschlager H, Just H. Modulation of coronary vasomotor tone in humans – progressive endothelial dysfunction with different early stages of coronary atherosclerosis. Circulation 1991;83(2):391–401.
169. Sendowski I, Savourey G, Launay JC, et al. Sympathetic stimulation induced by hand cooling alters cold-induced vasodilatation in humans. European Journal of Applied Physiology 2000;81(4):303–309.
170. Heusch G, Baumgart D, Camici P, et al. Alpha-adrenergic coronary vasoconstriction and myocardial ischemia in humans. Circulation 2000;101(6):689–694.
171. Baumgart D, Naber C, Haude M, et al. G protein beta 3 subunit 825T allele and enhanced coronary vasoconstriction on alpha(2)-adrenoceptor activation. Circulation Research 1999;85(10):965–969.
172. Zeiher AM, Drexler H, Wollschlaeger H, Saurbier B, Just H. Coronary vasomotion in response to sympathetic-stimulation in humans – importance of the functional integrity of the endothelium. Journal of the American College of Cardiology 1989;14(5):1181–1190.
173. Schindler TH, Nitzsche EU, Olschewski M, et al. PET-measured responses of MBF to cold pressor testing correlate with indices of coronary vasomotion on quantitative coronary angiography. Journal of Nuclear Medicine 2004;45(3):419–428.
174. Schindler T, NItzche E, Dacta A. Abnormal longitudinal base-to-apex myocardial perfusion gradient in response to cold-pressure test as assessed by PET correlates with indices of epicardial vasomotion on quantitative angiography [abstract]. Journal of Nuclear Medicine 2004;45(5):2P.
175. Lanza GA, Manzoli A, Pasceri V, et al. Ischemic-like ST-segment changes during Holter monitoring in patients with angina pectoris and normal coronary arteries but negative exercise testing. American Journal of Cardiology 1997;79(1):1–6.
176. Schindler TH, Nitzsche E, Magosaki N, et al. Regional myocardial perfusion defects during exercise, as assessed by three dimensional integration of morphology and function, in relation to abnormal endothelium dependent vasoreactivity of the coronary microcirculation. Heart 2003;89(5):517–526.
177. Zeiher AM, Krause T, Schachinger V, Minners J, Moser E. Impaired endothelium-dependent vasodilation of coronary resistance vessels is associated with exercise-induced myocardial-ischemia. Circulation 1995;91(9):2345–2352.
178. Nabel EG, Ganz P, Gordon JB, Alexander RW, Selwyn AP. Dilation of normal and constriction of atherosclerotic coronary-arteries caused by the cold pressor test. Circulation 1988;77(1):43–52.
179. Zeiher AM, Drexler H, Saurbier B, Just H. Endothelium-mediated coronary blood-flow modulation in humans – effects of age, atherosclerosis, hypercholesterolemia, and hypertension. Journal of Clinical Investigation 1993;92(2):652–662.
180. Quinones MJ, Hernandez-Pampaloni M, Schelbert H, et al. Coronary vasomotor abnormalities in insulin-resistant individuals. Annals of Internal Medicine 2004;140(9):700–708.
181. Nitenberg A, Ledoux S, Valensi P, Sachs R, Attali JR, Antony I. Impairment of coronary microvascular dilation in response to cold presser-induced sympathetic stimulation in type 2 diabetic patients with abnormal stress thallium imaging. Diabetes 2001;50(5):1180–1185.
182. Momose M, Abletshauser C, Neverve J, et al. Dysregulation of coronary microvascular reactivity in asymptomatic patients with type 2 diabetes mellitus. European Journal of Nuclear Medicine and Molecular Imaging 2002;29(12):1675–1679.
183. Schindler TH, Nitzsche EU, Olschewski M, et al. Chronic inflammation and impaired coronary vasoreactivity in patients with coronary risk factors. Circulation 2004;110(9):1069–1075.
184. Schindler T, Facta A, Quinones M. Metabolic syndrome is associated with abnormal coronary circulatory functions as measured by N-13 ammonia and PET [abstract]. Journal of Nuclear Medicine 2004;45(5):65P.
185. Schindler T, Facta A, Prior J. Association of serum leptin levels and coronary vasomotor function in obesity [abstract]. Journal of Nuclear Medicine 2004;45(5):64P.
186. Campisi R, Czernin J, Schoder H, Sayre JW, Schelbert HR. L-arginine normalizes coronary vasomotion in long-term smokers. Circulation 1999;99(4):491–497.
187. Schindler TH, Magosaki N, Jeserich M, et al. Effect of ascorbic acid on endothelial dysfunction of epicardial coronary arteries in chronic smokers assessed by cold pressor testing. Cardiology 2000;94(4):239–246.
188. Schindler TH, Nitzsche EU, Munzel T, et al. Coronary vasoregulation in patients with various risk factors in response to cold pressor testing – contrasting myocardial blood flow responses to short- and long-term vitamin C administration. Journal of the American College of Cardiology 2003;42(5):814–822.
189. Morita K, Noriyasu K, Tasukamoto T. Reversible endothelial dysfunction after one month smoking cessation in healthy young smokers [abstract]. Journal of Nuclear Medicine 2004;45(5):3P.
190. Facta A, Schinder T, Prior J. Noninvasively measured myocardial blood flow responses to sympathetic stimulation may allow assessment of glucose control in type 2 diabetes [abstract]. Journal of Nuclear Medicine 2004;45(5):236P.
191. Di Carli MF, Afonso L, Campisi R, et al. Coronary vascular dysfunction in premenopausal women with diabetes mellitus. American Heart Journal 2002;144(4):711–718.

192. Campisi R, Nathan L, Pampaloni MH, et al. Noninvasive assessment of coronary microcirculatory function in postmenopausal women and effects of short-term and long-term estrogen administration. Circulation 2002;105(4):425–430.
193. Jensen LO, Thayssen P, Pedersen KE, Stender S, Haghfelt T. Regression of coronary atherosclerosis by simvastatin – a serial intravascular ultrasound study. Circulation 2004;110(3):265–270.
194. Prior J, Facta A, Schindler T. Effect of the number of criteria of the metabolic syndrome on coronary circulatory function as measured by N-13 ammonia and PET [abstract]. Journal of Nuclear Medicine 2004;45(5):237P.
195. Kjaer A, Meyer C, Nielsen FS, Parving HH, Hesse B. Dipyridamole, cold pressor test, and demonstration of endothelial dysfunction: a PET study of myocardial perfusion in diabetes. Journal of Nuclear Medicine 2003;44(1):19–23.
196. Bonetti PO, Lerman LO, Lerman A. Endothelial dysfunction – a marker of atherosclerotic risk. Arteriosclerosis Thrombosis and Vascular Biology 2003;23(2):168–175.
197. Loscalzo J. Functional polymorphisms in a candidate gene for atherothrombosis – unraveling the complex fabric of a polygenic phenotype. Journal of the American College of Cardiology 2003;41(6):946–948.
198. Gould KL, Goldstein RA, Mullani NA. Economic-analysis of clinical positron emission tomography of the heart with rubidium-82. Journal of Nuclear Medicine 1989;30(5):707–717.
199. Gould KL. Goals, gold standards, and accuracy of noninvasive myocardial perfusion imaging for identifying and assessing severity of coronary-artery disease. Current Opinion in Cardiology 1989;4(6):834–844.
200. Gould KL, Mullani N, Williams B. PET, PTCA, and economic priorities. Clinical Cardiology 1990;13(3):153–164.
201. Patterson RE, Eisner RL, Horowitz SF. Comparison of cost-effectiveness and utility of exercise ECG, single photon emission computed tomography, positron emission tomography, and coronary angiography for diagnosis of coronary artery disease [see comments]. Circulation 1995;91(1):54–65.
202. Merhige M. PET myocardial perfusion imaging: a new standard for the management of coronary artery disease. Applied Imaging: Applications in Nuclear Cardiology 2001;1(1):1–4.
203. Besocci M, Lalagona P, Hunter K. Clinical Applications and Economic Implications of PET in the Assessment of Myocardial Viability: A Retrospective Study. Fairfax, VA: Institute for Clinical PET; 1994.
204. Chan P, Machac J, Almeida O, Krynyckyi B, Kim CK. The prevalence and impact of vertical heart movement during rest–stress rubidium-82 cardiac PET imaging. Journal of Nuclear Medicine 2003;44(5):210P–211P.
205. Loghin C, Sdringola S, Gould KL. Common artifacts in PET myocardial perfusion images due to attenuation-emission misregistration: clinical significance, causes, and solutions. Journal of Nuclear Medicine 2004;45(6):1029–1039.
206. Wassenaar R, Wells R, Dekemp R. Clinical evaluation of CT versus Ge-68 attenuation correction in cardiac PET imaging [abstract]. Journal of Nuclear Medicine 2004;45(5):188P.
207. Stanger R, Jana S, Mistein D. Accuracy of CT transmission maps in PET imaging studies [abstract]. Journal of Nuclear Medicine 2004;45(5):41P.
208. Brunken R, DiFilippo F, Bybel B. Clinical evaluation of cardiac PET attenuation correction using "fast" and "slow" CT images [abstract]. Journal of Nuclear Medicine 2004;45(5):120P.
209. Erdi Y, Pevsner K, Rosenzweig E. 4D-PET/CT acquisition in the thorax [abstract]. Journal of Nuclear Medicine 2004;45(5):48P.
210. Kim J, Czernin J, Auerbach M. Mutual information software fusion of PET and CT improves image coregistration of in-line PET/CT images [abstract]. Journal of Nuclear Medicine 2004;45(5):48P.
211. Nehmeh S, Erdi Y, Pan T, et al. Quantitation of respiratory motion during 4D PET/CT acquisition [abstract]. Journal of Nuclear Medicine 2004;45(5):49P.
212. Namdar M, Hany T, Siegrist P. Improved CAD assessment using a combined PET/CT scanner [abstract]. Journal of Nuclear Medicine 2004;45(5):117P.
213. Faber T, Garcia E, Hertel S. Evaluation of automatic fusion of coronary arteries onto left ventricular surfaces from PET/CT [abstract]. Journal of Nuclear Medicine 2004;45(5):399P.
214. Machac J. Cardiac positron emission tomographic imaging. Seminars in Nuclear Medicine 2005;35:17–36.
215. CDE, Inc. Dosimetry Services. ACRP-35. URL http://www.internaldosimetry.com [accessed in August 2005].
216. International Commission on Radiological Protection. (ICRP) Publication 80: radiation dose to patients from radiopharmaceuticals, 80. 2000;28(3):p113, p116.
217. International Commission on Radiological Protection. ICRP Publication 53: radiation dose to patients from radiopharmaceuticals, 53. 1998;18(1–4):p62, p162.
218. Cardiogen Package Insert. Oak Ridge, TN: Radiation Internal Dose Information Center, Oak Ridge Institute for Science and Education.

13 Comparison of function, viability, and perfusion assessed by myocardial perfusion SPECT and CMR

Louise E.J. Thomson
David S. Fieno

Introduction

The enormous societal impact of heart disease provides motivation for exploration of newer, potentially improved imaging techniques for assessment of ventricular function, viability, and perfusion. While current methods of diagnosis and treatment in cardiology are successful in preventing adverse events in a large number of patients, it has been suggested that up to 50% of patients with acute and chronic coronary syndromes are either not identified or fail suggested treatment [1]. A possible strategy for improving this medical dilemma is to improve diagnosis through faster, more accurate, and more reliable imaging techniques.

Cardiac magnetic resonance (CMR) imaging is an established modality for the assessment of cardiac function, an emerging modality for routine assessment of viability, and has potential for myocardial perfusion imaging. CMR imaging is considered a gold standard for assessment of cardiac mass, volumes, and ventricular ejection fraction (EF). In addition, a growing body of literature suggests that CMR may be a new gold standard for high-resolution identification of irreversibly injured myocardial territories, i.e., noninvasive determination of myocardial viability. In addition, data from a limited number of centers have emerged that suggest utility of CMR in identification of ischemic but viable myocardium during pharmacologic stress testing.

Although CMR imaging has been available for more than 20 years, advances in hardware and software in the last decade have led to its increasing clinical use for a variety of cardiac conditions. There are new guidelines for training and specialization in cardiac MR imaging for cardiologists, radiologists, and nuclear physicians, and training programs are being offered throughout the United States and worldwide [2]. Overall, there is recognition of the potential for CMR to impact on current cardiology practice. Nuclear cardiologists need to be aware of the potential indications for CMR, the scope of the evidence supporting a role for this new modality, and how it compares with established techniques. The purpose of this chapter is to critically appraise the data directly comparing CMR and myocardial perfusion SPECT (MPS) for assessment of myocardial function, viability, and perfusion.

Functional assessment by CMR

The assessment of cardiac function is important for determining the state of the myocardium, for predicting of patient outcome, and for monitoring response to therapeutic interventions. Historically, planar gated blood pool (GBP) and first pass radionuclide angiography were considered gold standard techniques for assessment of biventricular volumes and function. The advent of GBP SPECT improved accuracy of blood pool imaging for assessment of volumes and EF. GBP SPECT also allows visualization of segmental function and permits detection of the relationships between right and left ventricular systolic contraction in patients with heart failure and biventricular pacing (as detailed in Chapter 11). In addition to GBP SPECT, gated perfusion SPECT provides assessment of left ventricular volumes and function. Literature comparing CMR and nuclear techniques has focused on the validation of the GBP SPECT in comparison to older GBP techniques. CMR has been assumed to be the gold standard in these papers for noninvasive determination of EF, volumes, and segmental function because of high reproducibility, high resolution, and the ability of CMR to image in any arbitrary anatomic plane.

The standard cardiac MR method for assessment of ventricular volumes is to obtain multiple contiguous planar cine images covering the entire ventricular volume and to use these images to contour ventricular systolic and diastolic dimensions. Volumes are derived from added area

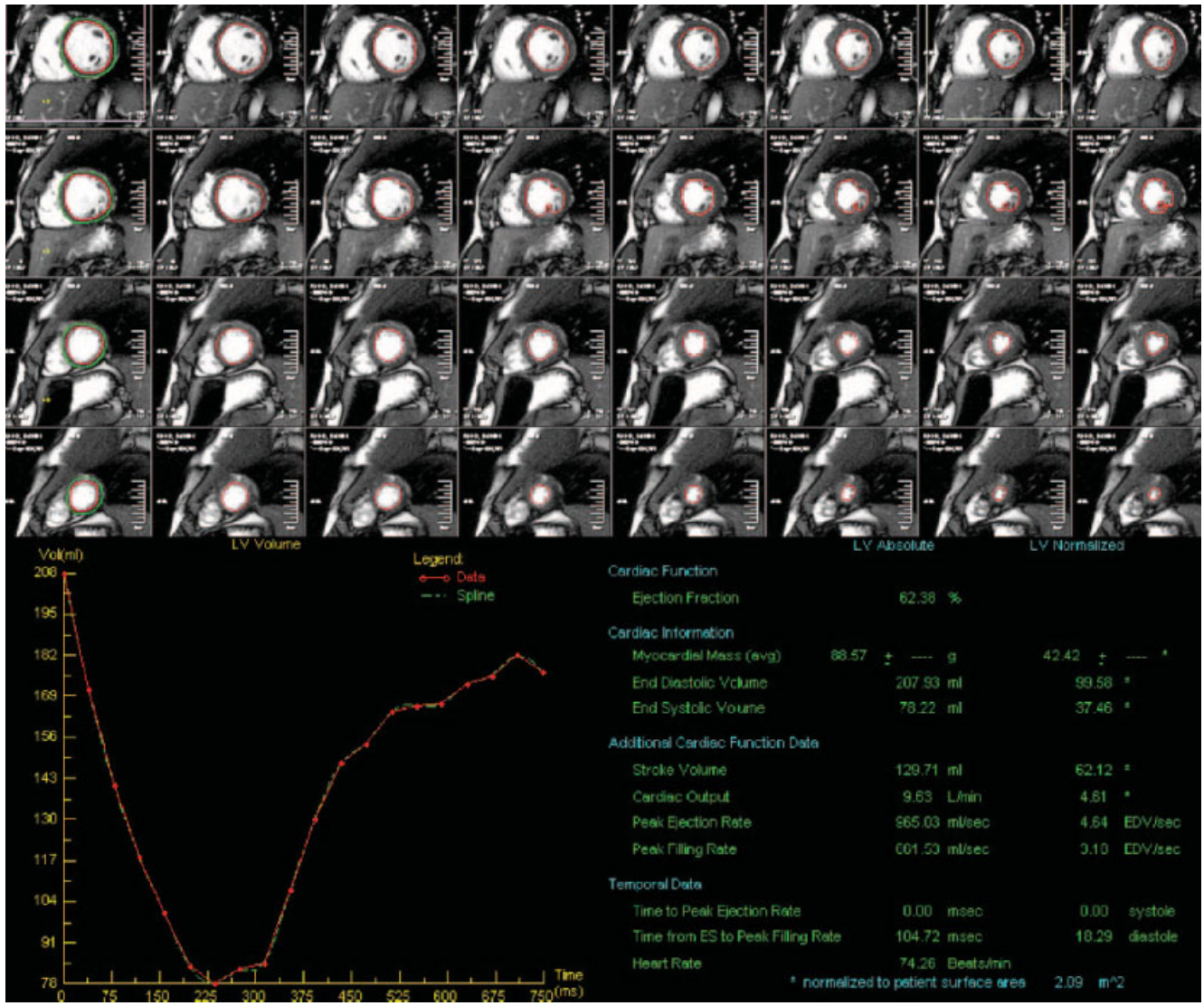

Figure 13.1 Analysis of typical CMR functional data set displayed from base to apex (left to right) with endocardial contours (red outlines) at diastole (rows 1 and 3) and at systole (rows 2 and 4) to compute left ventricular volumes. This data set allows computation of ventricular volume versus time (lower left panel) and parameters related to the left ventricular function (lower right panel).

measurements multiplied by slice thickness and taking into account any interslice gap (see Fig. 13.1).

Planar and SPECT gated blood pool versus CMR

Comparisons between radionuclide and CMR methods using a standard phantom model as the gold standard are rare. Debatin et al. [3] compared planar GBP, ventricular angiography, and cine CMR methods using a biventricular compliant model with three measurements at each of the three different EFs. The average relative error for EF by GBP was 7.1–22.0% but by cine CMR was only 4.4–8.5%. Both CMR and GBP measurements were significantly more reproducible than angiography. De Bondt et al. [4] described validation of GBP SPECT measurement of ventricular volumes and EF, using a biventricular dynamic phantom. They performed 20 experiments at varying ventricular volumes and noted significant overestimation of ventricular volumes and right ventricular EF by SPECT GBP as compared to the true phantom values.

Comparisons between planar GBP, SPECT GBP, first-pass radionuclide imaging, and echocardiography techniques have referenced the calculated volumes to CMR. For example, an initial comparison of planar and first-pass radionuclide angiography compared to echocardiography and CMR suggested superiority of first-pass radionuclide angiography to planar two-dimensional radionuclide angiography or two-dimensional echocardiographic

assessment of absolute volumes [5]. Chin et al. [6] compared planar and tomographic GBP assessments of ventricular volumes with CMR in 18 patients and demonstrated very close correlation for right and left ventricular volumes ($r = 0.91$ and $r = 0.96$ respectively). In their study, tomographic and planar methods for assessment of left venrticular ejection fraction (LVEF) correlated equally well with CMR. Lethimonnier et al. [7] also found a good correlation between LVEF by radionuclide angiography and magnetic resonance imaging (MRI) in a group of 35 patients and 15 volunteers ($r = 0.77$). Nichols et al. [8] demonstrated a similar relationship for assessment of right ventricular volumes comparing GBP SPECT to cine CMR.

Turning to gated perfusion SPECT for assessment of cardiac volumes and EF, CMR again provides a standard for comparison. Faber et al. [9,10] assessed performance of different software packages (QGS and Emory Toolbox) as compared to cine CMR. They found a close correlation between SPECT and CMR volumes and EF with the observation that SPECT volumes were on average 30% higher than CMR volumes. In this study, performance of QGS and Emory Toolbox software programs was similar with a trend toward better correlation of QGS measured LVEF.

A recently published meta-analysis by Ioannidis et al. [11] summarized gated SPECT perfusion and CMR data pooled from several studies [9,10,12–19]. These authors specifically compared gated perfusion SPECT assessment of left ventricular volume and function with CMR in a pooled group of 164 patients. Although there was an excellent correlation between the modalities for all measures of volume and EF, there were frequent individual discrepancies of at least 30 ml for end diastolic volume (37% of cases), 20 ml for end systolic volume (35%), and 5 or 10% for LVEF (52% and 23% respectively). These discrepancies resulted in misclassification by SPECT of patients with LVEF less than 40% in 11% of cases. The authors suggested that gated SPECT offers useful functional information but that CMR should be used when an accurate result is required.

Segmental function

The detection of segmental function abnormalities by radionuclide methods in patients with coronary artery disease (CAD) has been improved by the use of tomographic as compared to planar blood pool methods [20,21]. CMR is a highly accurate method for assessment of regional wall function (thickness and thickening) as a consequence of excellent spatial and temporal resolution. Cardiac MR is the technique of choice for evaluation of segmental function and change in segmental function, following revascularization procedures or other interventions. The relevance of this application of CMR is in the ability to monitor surrogate endpoints for cardiac recovery in patients being assessed for response to therapy who have impaired systolic function. Global improvement in EF and volumes is undoubtedly important; however, the changes in regional function in response to a targeted revascularization, following myocardial infarction, in response to a treatment such as alcohol septal ablation may also be important for assessment of therapy. From a statistical perspective, ability to divide a ventricle into multiple segments increases power for detection of small improvements in function. Whether these improvements will impact on overall patient well-being is the subject of ongoing CMR research.

Velocity-encoded imaging

Velocity-encoded imaging is an alternative CMR technique for assessment of cardiac function that derives an accurate measure of cardiac output by measuring flow in the proximal ascending aorta (see Fig. 13.2) [22]. This technique utilizes the ability to observe a phase shift in moving objects (CMR voxels) within a magnetic field when equal and opposite magnetic gradients are applied. Stationary voxels within the imaging plane gain a zero net phase shift with the application of such gradient pulses while moving voxels gain a net phase shift, the magnitude of which is proportional to the velocity of flow. The subsequent relationship between voxel net phase shift and time allows for calculation of peak and mean blood flow velocity, stroke volume, and cardiac output based on a single assessment of flow in the proximal ascending aorta. This technique has been validated in phantoms, normal volunteers, and patients [23–25] as an accurate method for assessment of aortic flow. Note that, although stroke volume can be derived from velocity-encoded images in this manner, the technique does not give information regarding ventricular end diastolic or end systolic volume or regional function.

Applications for velocity-encoded imaging include valvular and congenital disease. In the setting of aortic valvular disease, velocity-encoded imaging can be used to accurately grade severity of aortic stenosis and correlates well with echocardiographic measures of valvular stenosis [26]. In congenital heart disease, the technique has application in the assessment of cardiac shunt when combined with measurement of pulmonary flow and vascular stenosis, and in confirming the patency of surgically implanted shunts. The accuracy of velocity-encoded imaging is influenced by image acquisition parameters as well as the quality of imaging [27]. For example, severely turbulent flow may decrease the accuracy of velocity-encoded imaging.

Advantages and limitations of CMR assessment of volumes and EF

There are theoretical reasons why CMR evaluation of left ventricular function and volume is accurate when

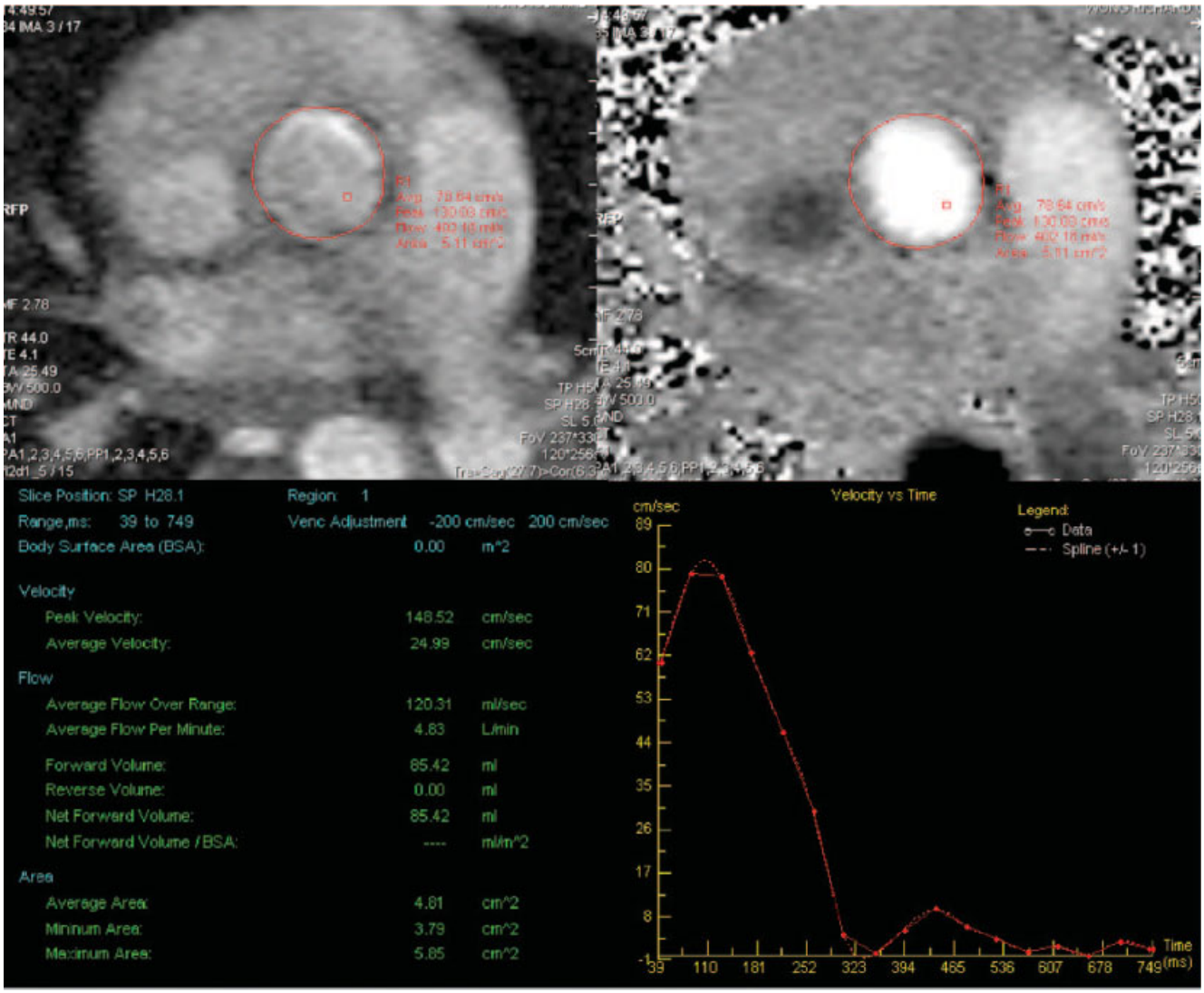

Figure 13.2 Analysis of typical CMR velocity-encoded data set. A cross section through the proximal ascending aorta is shown as a magnitude image (left upper panel) and as a phase image (right upper panel) during aortic ejection. The regions of interest (red outline) are used to quantify absolute blood flow based on the net phase of voxels, resolution, and heart rate.

carefully performed. The use of multiple cine image slices through the true short axis of the left ventricle from the base to the apex allows high spatial and temporal resolution imaging for identification of the endocardial border throughout systole and diastole. CMR permits full coverage of the heart without acoustic window restrictions encountered in echocardiography and geometric assumptions are not required for calculation of end systolic and end diastolic volumes.

Data have demonstrated that cine CMR is highly reproducible in patients with normal and abnormal left ventricular function [28]. Moreover, as emphasized by Bellenger et al., improvements in measurement reproducibility has major implications in power and sample size calculations for study designs, and accordingly, more accurate techniques reduce associated costs for research studies, making the use of CMR for assessment of interval ventricular volumes and EF desirable [29].

In addition, CMR is considered a standard for evaluation of the right ventricle. Higher resolution, independence from geometric assumptions, and ability to anatomically segment the right ventricle from adjacent structures are inherent advantages of CMR over echo and radionuclide techniques. Perhaps more importantly, CMR may permit detection of both structural changes of and fibrous or fatty infiltration within the right ventricular myocardium and has been proposed as a useful diagnostic tool in patients with right ventricular dysplasia [30].

As more data emerge, new intricacies of CMR are being realized. For example, the reproducibility of CMR for right ventricular volumes and EF appears to be slightly less than the reproducibility of left ventricular measures, most probably as a result of differences in accuracy of endocardial border detection in the highly trabeculated right ventricle [31].

There exist potential limitations of CMR for assessment of ventricular volumes. Full coverage of the ventricle is required, and often individual slices are acquired one at a time on different breathholds. This implies that 10–15 separate breathhold images are acquired to arrive at ventricular volumes. Changes in diaphragmatic position during breathholding potentially alters the position of the heart on sequential images and may affect ventricular volumes [32]. Other artifacts from image acquisition include electrocardiographic gating errors, cardiac motion, and field inhomogeneity (e.g., sternal wires), all of which can significantly reduce image quality. In addition, off-line image processing is a semiautomated process that requires skill on the part of the technologist or physician. Decisions regarding inclusion or exclusion of the papillary muscles, selection of the basal and apical slices in diastole and systole, and separation of myocardium from other tissues can all significantly impact calculation of ventricular volumes. In addition, because there are many vendors and techniques are not at present standardized across platforms, assessment of serial changes in a given patient can be challenging, especially if different hardware or software are used for scanning/analysis on different scan dates.

Summary for cardiac function assessment by CMR

- Highly accurate
- Highly reproducible
- Ideal technique for repeated assessments when very accurate assessment of LVEF is required
- It has definite advantages for following segmental changes in systolic function-spatial resolution and unequalled definition of endocardial/epicardial borders and myocardial anatomy
- Can be formed either as multiple two-dimensional images and/or using velocity-encoded imaging for stroke volume only.

Cardiac viability assessment by CMR

Recent advances in CMR technology have improved image quality and have resulted in growing interest in the use of CMR for assessment of viability, a relatively new application of the technology. Identification of viable myocardium (converse infarction), especially in the setting of left ventricular dysfunction, is important for identification of patients with the potential for improved ventricular function. There are growing data suggesting that the revascularization of patients without presence of viability may actually be associated with increased morbidity and mortality compared to medical therapy [33,34].

CMR offers three distinct methods for assessment of myocardial viability: spectroscopy for direct interrogation of cellular components, dobutamine stress MR for evaluation of contractile response, and delayed contrast-enhanced imaging for direct visualization of nonviable myocardium. To variable degrees, these methods have been compared to MPS and PET (positron emission tomography).

Approaches to myocardial viability assessment

There are several different definitions of myocardial viability. Ideally, myocardial viability is defined as the presence of intact cell membranes with the converse, absence of living myocytes being the case for myocardial infarction. In practice, this is a useful definition for animal studies but it is impractical for clinical cardiology, except in the infrequent circumstance of cardiac transplantation. Imaging methods have accordingly been developed for the noninvasive definition of viability, with viability defined as dependent upon the information provided by each technique. These include radionuclide techniques, echocardiography, and more recently CMR. Echocardiography examines contractile reserve, MPS demonstrates perfusion and intact cell membrane transport, and PET examines metabolism fluorine-18-deoxyglucose (FDG) in myocytes. CMR techniques can be used to examine cellular composition, contractile reserve, or presence of cell membrane integrity, dependent upon the CMR approach chosen. Whichever imaging modality is used, the accepted clinical gold standard for viability is global recovery or segmental recovery of myocardial contractile function in a dysfunctional segment following a revascularization procedure.

CMR spectroscopy

The first of three distinctly different CMR techniques available for the assessment of viability is magnetic resonance spectroscopy (MRS). This technique assesses components of myocytes such as phosphocreatine, sodium, or potassium and can be used to noninvasively observe changes in the relative chemical compositions of myocardial tissue in ischemia and infarction. This is a largely experimental technique to date and is performed in a small number of expert centers.

While conventional magnetic resonance images are created by receiving radio-frequency signals based on the magnetic moment of water protons (^{1}H) within the

magnetic field, the magnetic moment of other nuclei such as sodium-23, potassium-39, and phosphorus-31 can also be measured by adjusting the transmit and receive frequencies that are employed. MRS allows observation of the phosphate-31 concentrations, including important cellular metabolites such as adenosine triphosphate (ATP), phosphocreatine, phosphodiester, and inorganic phosphate. Further, one can attempt to observe differences in phosphate concentrations between viable, ischemic, and infarcted myocardium. One example of a comparison between CMR phosphate MRS and MPS was a study performed by Yabe et al. [35], who compared CMR phosphate-31 spectra in patients with CAD versus reversible or irreversible anterior perfusion defects on exercise redistribution thallium SPECT; these comparisons were also made in control subjects. This group observed a reduction in phosphocreatine content of the anterior wall in patients but not controls. Additionally, ATP peak levels differentiated patients with viable myocardium (redistribution positive) from those without viability (redistribution negative). This study was performed at 1.5 T, with imaging of the anterior wall only using MRS techniques.

Currently, although preliminary data appear encouraging, there is no established routine clinical role for CMR MRS.

Dobutamine CMR

There is established evidence demonstrating the value of dobutamine echo for detection of viable myocardium in dysfunctional segments that possess contractile reserve [36]. Interest in dobutamine CMR has been based, in part, on the established role for dobutamine echocardiography in patient care. An advantage of CMR over echo is in visualization of all myocardial regions (no acoustic window limitation) and recent advances in hardware and software allow rapid, near real-time cine imaging. Thus, dobutamine CMR is now performed in several specialized centers in the United States and Europe.

Although reported protocols have varied, the common approach to dobutamine CMR is to assess segmental wall motion responses to a low dose (5–10 mcg/(kg min)) infusion of dobutamine. Recruitment of contractile elements in viable myocardium permits differentiation of nonviable from viable myocardium. Several preliminary reports have suggested that it is relatively safe to administer dobutamine in the CMR environment; however, this experience has been limited to a small number of centers with highly controlled clinical protocols. Issues of concern include the inability to monitor electrocardiograms in a high magnetic field, the possibility of inducing ischemia and/or arrhythmias even at low dobutamine levels, and the difficulty associated with resuscitative efforts in the CMR environment.

Comparisons of dobutamine CMR and nuclear techniques have emerged. Baer and colleagues [37] performed FDG-PET and dobutamine (10 mcg/(kg min)) CMR in 35 patients with known myocardial infarction. End-diastolic wall thickness and systolic wall thickening by CMR were compared to FDG uptake in short-axis slices. Two CMR-based definitions of viability were considered: first, end-diastolic wall thickness of 5.5 mm, and second, dobutamine-induced systolic wall thickening greater than or equal to 1 mm. Dysfunctional segments were defined as viable by FDG-PET if FDG uptake was greater than or equal to 50% of the maximal uptake in a normal region. CMR viability was defined as either dobutamine-induced wall thickening and/or end-diastolic wall thickness of at least 5.5 mm. Taking FDG-PET as the standard for comparison, the sensitivity and specificity of CMR for segmental detection of viability was 88 and 87%, respectively. Gunning et al. [38] studied 30 patients with three-vessel CAD scheduled for coronary artery bypass grafting (CABG) by four techniques prior to surgery. Rest/dobutamine stress (5–10 mcg/(kg min)) cine CMR, adenosine/rest tetrofosmin MPS, and adenosine/redistribution and separate-day rest/redistribution thallium MPS. Results of these studies were compared findings to stress/redistribution thallium MPS and resting cine CMR after surgery. Of 207 myocardial segments analyzed, 145 had significantly abnormal wall motion before surgery, and 82 of these improved function after revascularization. Comparing imaging modalities for prediction of post-revascularization improvement in function, radionuclide uptake was a sensitive but nonspecific predictor of myocardial functional recovery, while response to dobutamine visualized by CMR was specific but relatively insensitive.

More recently, there is a growing interest in the potential additive role that dobutamine CMR may play in conjunction with delayed gadolinium-enhanced CMR. This will be discussed in the next section.

Delayed contrast-enhanced CMR

The most important advance in CMR viability assessment in the last decade is the development and validation of techniques to demonstrate gadolinium-contrast enhancement of nonviable myocardium. Although altered tissue signal characteristics in myocardial infarction was noted as early as the mid-1980s, the recent use of gadolinium paramagnetic contrast agents and pulse sequence developments have led to marked improvement in image quality and thus accuracy of delineation of nonviable myocardium. New developments in contrast-enhanced CMR (ceCMR) imaging have naturally led to comparisons with existing modalities and literature comparing MPS, PET, and CMR viability imaging is the focus of this section.

The development of "inversion recovery" (IR) CMR pulse sequences has led to improved image quality in viability images and has led to increased clinical interest in application of CMR for viability imaging. Originally described by Edelman et al. [39] and compared systematically to other sequences by Simonetti et al. [40], segmented inversion recovery imaging permits improved signal to noise and increased relative signal intensity difference between normal and infarcted myocardium compared to all prior CMR techniques. In brief, inversion recovery results in a T1-weighted image acquisition that makes use of an inversion prepulse prior to standard image acquisition. Typically, image data are acquired in diastole, with slice positions corresponding to precontrast cine images to permit comparison between segmental systolic function and extent of infarction.

As validated in animal models of myocardial infarction, gadolinium injected intravenously washes out more slowly from nonviable myocardium in both acute and chronic infarction [41–43]. Increased relative gadolinium concentration in infarcted myocardium results in an increased signal intensity on T1-weighted images, especially apparent in infrared imaging performed such that normal myocardium is nulled (black) and abnormal myocardium has up to 500% increased signal intensity (bright) [40]. Hence the basis for viability imaging by delayed ceCMR is the observation that infarcted myocardium is bright ("bright is dead") and viable myocardium is not bright, whether injured or not. Clinical validation in acute and chronic infarction has confirmed the observations in animal models and strongly suggests that this technique is both robust and clinically useful for detection of infarction, quantification of viable tissue, and prediction of post-revascularization recovery of function [40,44,45].

Over the last 15 years there have been several comparisons of SPECT, PET, and CMR imaging for the detection of infarction, and the prediction of recovery of function in patients with ischemic heart disease. Prior to the advent of gadolinium enhancement for assessment of irreversibly injured myocardium, investigators examined other indices of anatomy and function by CMR in an effort to characterize myocardial viability. In one such study by Lawson and colleagues [46], 24 patients underwent stress, redistribution, and reinjection ^{201}Tl SPECT and cine CMR for myocardial function assessment. The authors found that reduced end-systolic wall thickness by CMR was only seen in segments with reduced thallium uptake, suggesting that reduced wall thickness might be a marker for the presence of myocardial scar (see Fig. 13.3). Kitsiou and colleagues [47] studied 24 patients with ischemic heart disease prior to revascularization using an exercise–redistribution–reinjection ^{201}Tl SPECT protocol, CMR, and radionuclide angiography followed by post-revascularization CMR. Their aim was to explore

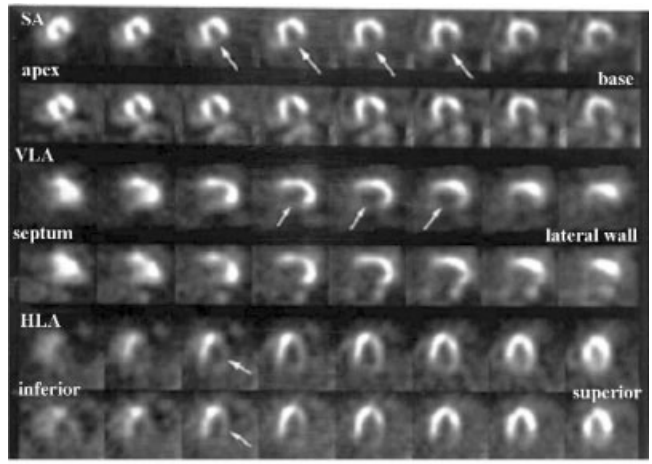

(a)

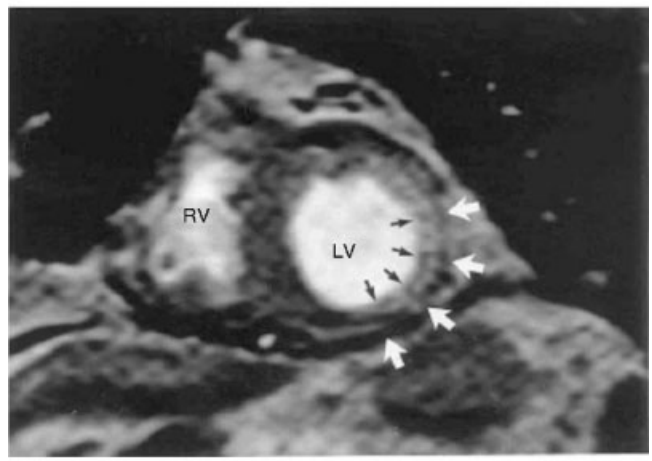

(b)

Figure 13.3 (a) Myocardial perfusion imaging with thallium-201 in a patient with a severe fixed perfusion defect involving the inferior and inferolateral segments of the left ventricle (arrows). Images are displayed in the short-axis (SA), horizontal long-axis (HLA), and vertical long-axis (VLA) orientations. (b) An end-systolic, short-axis, gradient echo CMR image in the same patient, demonstrating wall thinning in the same myocardial segments (arrows) corresponding to the perfusion images in part (a). Abbreviations: LV, left ventricle; RV, right ventricle. (Reproduced with permission from [46].)

the relationship between thallium SPECT patterns and subsequent functional recovery, comparing the relative predictive value of either a stress-induced reversible defect or a mild-to-moderate irreversible defect for segmental recovery of function as measured by CMR (see Fig. 13.4). They noted that for segments with akinesis or dyskinesis, functional recovery was observed in 83% of segments with reversible defects compared with 33% of segments with mild-to-moderate irreversible defects. In summary, the presence of inducible ischemia in a dyskinetic or akinetic segment was predictive of recovery following revascularization. This paper showed the utility of CMR for demonstration of segmental functional recovery.

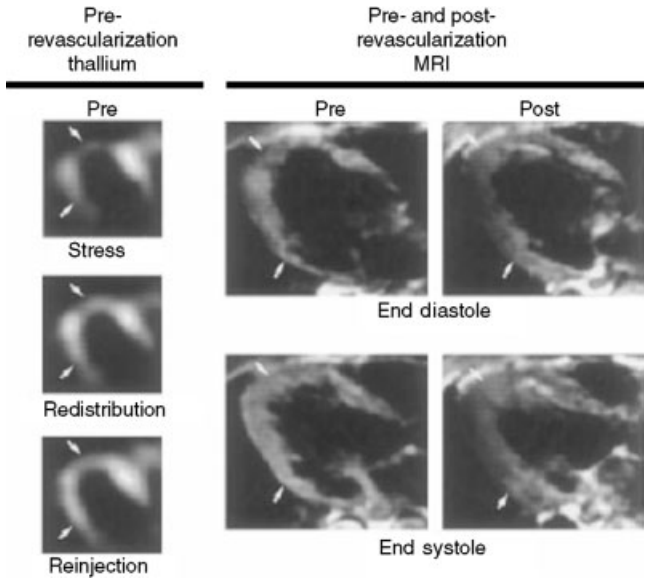

Figure 13.4 Improved post-revascularization systolic wall thickening is shown in a patient with pre-revascularization stress-induced reversible thallium defects. Matched transaxial tomograms are displayed for thallium stress, redistribution, and reinjection (left), with corresponding end-diastolic and end-systolic CMR tomograms before and after revascularization (right). There are extensive thallium abnormalities in apical and posterolateral regions during stress (arrows) that improve on redistribution and reinjection images (reversible defects). Corresponding CMR tomograms demonstrate abnormal systolic wall thickening in apical and posterolateral regions before revascularization that improve after revascularization. (Reproduced with permission from [47].)

Early investigation of the patterns of CMR gadolinium-contrast enhancement prior to the development of inversion recovery pulse sequences suggested interesting relationships between enhancement patterns by CMR and perfusion defects by MPS in patients with ischemic heart disease. Lima and colleagues studied 12 patients who underwent both ceCMR and ^{201}Tl MPS [48]. They found that regions with hypoperfusion on exercise scintigraphy tended to be hyperenhanced by ceCMR. Further, in patients with an occluded infarct-related artery, hyperenhanced regions frequently had a central hypoenhanced core, the location of which corresponded to perfusion defects seen by MPS (see Fig. 13.5). Judd et al. reported further on the nature of these hypoenhanced regions using thioflavin staining in animal models and demonstrated hypoenhancement corresponded to microvascular obstruction [49]. A subsequent study by Wu et al. showed that presence of hyper- and hypoenhancement by gadolinium CMR had prognostic value in patients with myocardial infarction [50]. Patients with a large amount of gadolinium hyperenhancement and/or a significant region of microvascular obstruction had poorer 5-year survival. Ramani and colleagues [51] conducted a study in

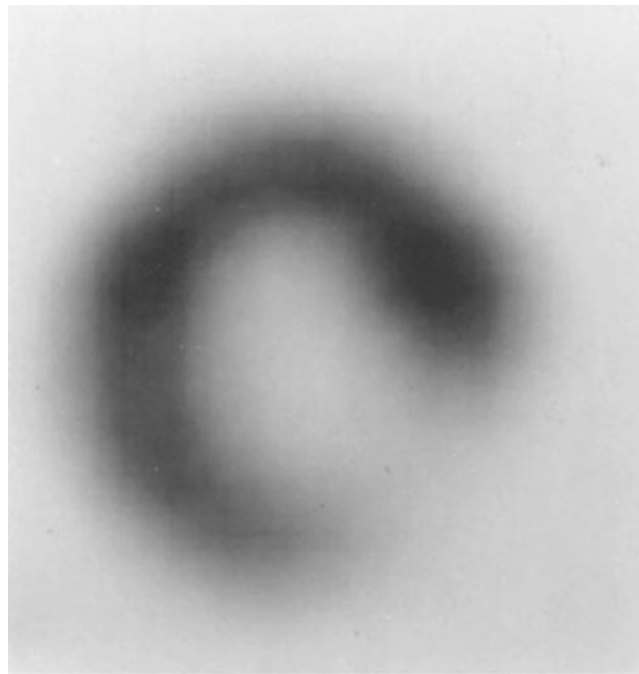

(a)

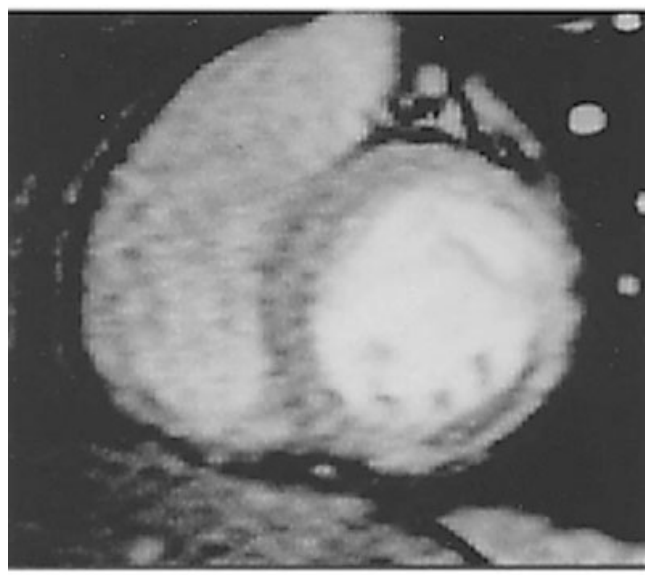

(b)

Figure 13.5 (a), Left ventricular short-axis SPECT thallium scan obtained during tracer redistribution from a patient with left circumflex occlusion who failed thrombolysis but was treated with rescue percutaneous transluminal coronary angioplasty within 6 hours of the onset of chest pain. Inferolateral fixed thallium defect is seen 5 days after infarction. (b) Left ventricular CMR short-axis image matched by location to the thallium scan shown in part (a). The central zone of reduced signal enhancement seen in the subendocardial half of the left ventricular wall is surrounded by a region of hyperenhanced signal that corresponds in location and extent to the fixed thallium defect obtained the day before the CMR study. (Reproduced with permission from [48].)

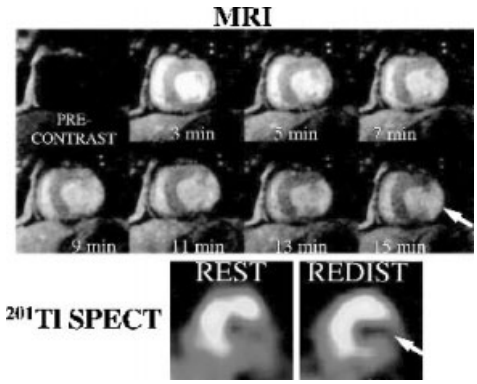

Figure 13.6 Short-axis CMR images obtained after contrast administration compared with corresponding short-axis ^{201}Tl tomograms at rest and after redistribution (REDIST). Persistent CMR hyperenhancement develops in inferolateral wall, corresponding to severe irreversible ^{201}Tl defect in the same region. Inferior wall also demonstrates substantial perfusion defect at rest but shows redistribution, indicating myocardial viability; CMR images in this area show lesser degree of hyperenhancement than in area of irreversible injury. (Reproduced with permission from [51].)

24 patients with known stable CAD and compared cine and ceCMR images to rest-redistribution ^{201}Tl SPECT and dobutamine echocardiography. Their data suggested that delayed enhancement was associated with nonviability as defined by MPS, especially for regions exhibiting akinesis or dyskinesis. Conversely, segments without delayed enhancement on ceCMR were associated with radionuclide viability, irrespective of presence of any underlying wall motion abnormality (see Fig. 13.6). These studies collectively led to recognition that gadolinium enhancement probably related in a specific way to presence of myocardial infarction and, likely, to infarct patterns seen by MPS.

Inversion recovery pulse sequences improved the contrast between viable and infarcted myocardium on CMR images such that it became possible to clearly delineate small regions of subendocardial enhancement and to define the transmural extent of infarction (TME) [52,53]. This improved infarct imaging has led to a new wave of clinical studies comparing ceCMR to radionuclide techniques for detection of myocardial infarction. Ansari and colleagues [54] compared delayed enhancement on ceCMR to rest-redistribution ^{201}Tl SPECT in 15 patients with mean EF 35 $\pm$ 11%. Short-axis ceCMR and SPECT images were divided into six sectors, with transmural extent of CMR hyperenhancement judged using a semiquantitative score. Presence of normalized thallium uptake of less than 50% at rest or redistribution was considered nonviable. These authors found an inverse relationship between the transmural extent of ceCMR hyperenhancement and thallium uptake ($r = 0.51$). On an individual sector basis, the inferior-septal segment showed the poorest correlation ($r = 0.38$), suggested by the authors to be possibly related to attenuation. Lund and colleagues studied 60 patients early after first myocardial infarction by ceCMR and rest-redistribution ^{201}Tl SPECT. This group noted that infarct size by ceCMR correlated to defect size on ^{201}Tl SPECT, but SPECT failed to depict six areas of hyperenhancement located in the inferior myocardium [55] (see Fig. 13.7). Wagner et al. [56] published a study in 91 patients comparing rest ^{201}Tl SPECT and ceCMR for detection of myocardial infarction. Results indicated that all segments with nearly transmural infarction, as defined by ceCMR, were also detected by SPECT. However, 85/181 segments with subendocardial infarction were not detected by SPECT and on a per-patient basis this represented six (13%) individuals with subendocardial infarcts by ceCMR who had no evidence of infarction by SPECT (see Fig. 13.8). In addition to SPECT, FDG-PET has been compared to ceCMR for detection of viable myocardium. Klein et al. [44] studied 31 patients with ischemic cardiomyopathy by both FDG-PET and delayed enhancement by ceCMR using the PET perfusion–metabolism mismatch as the gold standard for scar tissue. In 1023 segments analyzed, sensitivity and specificity of ceCMR were 96 and 86%, respectively. The investigators noted that 11% of segments defined as viable by PET had some degree of hyperenhancement on ceCMR and suggested that ceCMR, due to its higher resolution, was able to identify infarcts missed by PET (see Fig. 13.9).

This series of papers comparing ceCMR and radionuclide imaging has suggested that very small foci of infarction or infarction that is subendocardial as depicted by ceCMR might not be evident by MPS or PET. Reasons for this observation may include that, firstly, ceCMR is not influenced by soft tissue attenuation and, secondly, that CMR image resolution is superior to SPECT and PET.[In general, voxel sizes by ceCMR are approximately $1.5 \times 1.5 \times 8$ mm^3 = 18 mm^3 while those by SPECT are approximately $10 \times 10 \times 10$ mm^3 = 1000 mm^3 and those by PET are approximately $5 \times 5 \times 5$ mm^3 = 125 mm^3, resulting in an approximately 50-fold higher and approximately 10-fold higher spatial resolution for ceCMR versus SPECT and PET, respectively.] One of the few papers to directly explore the relationship between thallium activity and transmural extent of contrast enhancement by ceCMR is by Nelson et al. [57]. This study compared rest-redistribution ^{201}Tl SPECT, with the transmural extent of infarction by ceCMR in 60 patients post-infarct (see Fig. 13.10). The authors demonstrated that as the transmural extent of scar on CMR increases mean ^{201}Tl uptake decreases (see Figs. 13.11 and 13.12). Thus, inversion recovery ceCMR techniques show that the extent of thallium activity in segments with infarction is inversely related to the transmural extent of infarction and radionuclide counts, assuming normal wall thickness. The choice of imaging

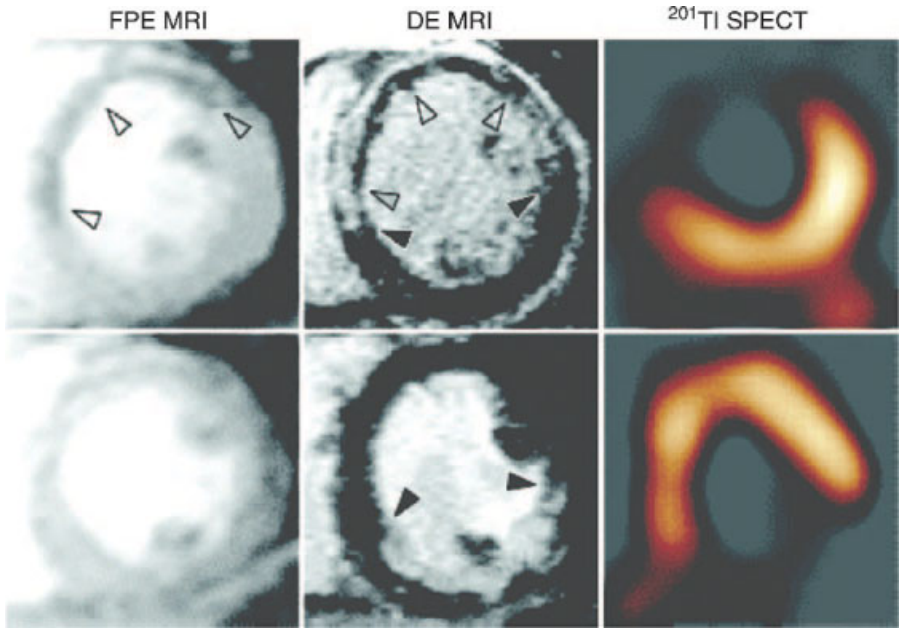

Figure 13.7 Midventricular short-axis images in a patient with microvascular obstruction (top row) and a patient without microvascular obstruction (bottom row). An inversion recovery T1-weighted turbo fast low-angle shot sequence was used for first-pass and delayed enhancement (FPE and DE) CMR imaging. In the patient with microvascular obstruction, the perfusion defect is depicted as a subendocardial hypoenhanced region on the first-pass CMR image (arrowheads). DE CMR image shows a persistent hypoenhanced zone (open arrowheads) surrounded by a larger hyperenhanced area (solid arrowheads). In the patient without microvascular obstruction on the first-pass CMR image, homogeneous enhancement of the area affected by infarction (arrowheads) is seen on the DE MR image. In both patients, the uptake defect on the ^{201}Tl SPECT image corresponds to the enhanced zone on the DE CMR image. (Reproduced with permission from [55].)

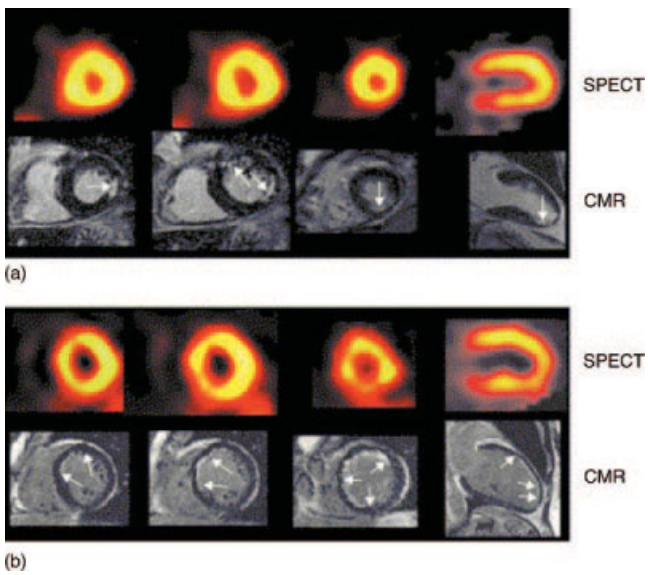

Figure 13.8 Short-axis views of rest thallium SPECT and ceCMR in two patients with subendocardial infarcts. (a) Patient with a creatine kinase concentration of 513 IU/l, occluded left circumflex coronary artery, and history of an older anteroseptal infarct with angioplasty and stent-implantation in the left anterior descending coronary artery. (b) Patient's infarct not recognized in the acute event, 90% stenosis of the left anterior descending coronary artery. (Reproduced with permission from [56].)

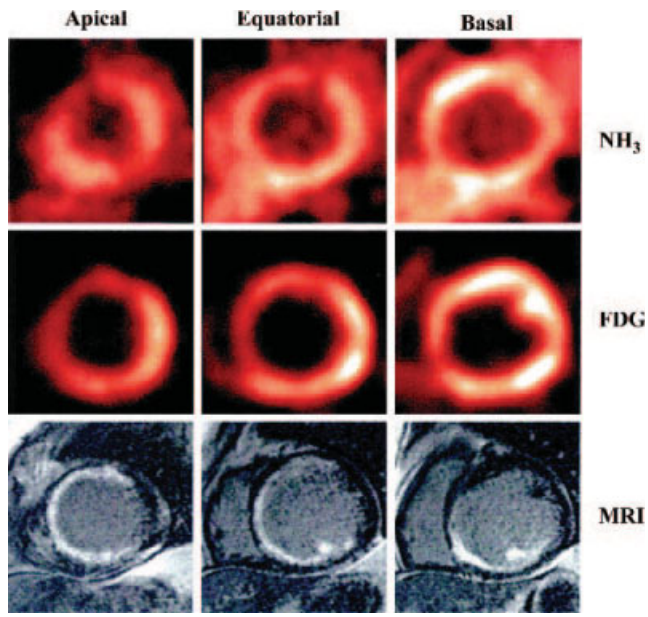

Figure 13.9 (Top) Three short-axis views (apical, equatorial, and basal) of a PET viability study with assessment of rest perfusion (NH_3) and glucose metabolism (FDG). (Below) MRI images in corresponding slices showing hyperenhancement. Note that in segments with reduced perfusion and metabolism, there is an increased signal in MRI. Because of better spatial resolution in MRI, distinction between transmural, subendocardial, and papillary defects can be made. The border between enhanced and normal areas is distinct. (Reproduced with permission from [44].)

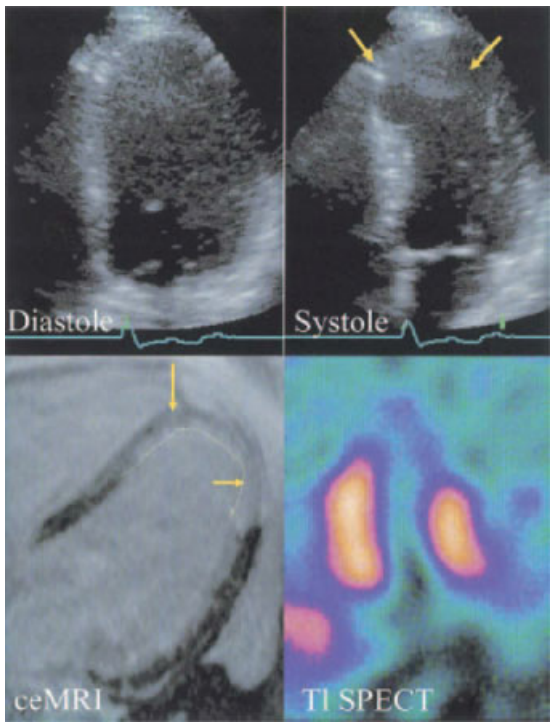

Figure 13.10 Correlation between dobutamine echocardiography and ^{201}Tl SPECT in a patient demonstrating nontransmural infarction in the apical septum (long arrow) and transmural infarction of the apical lateral segment (short arrow) by contrast-enhanced MRI. The resting echocardiogram shows akinesia of both segments, and ^{201}Tl SPECT shows a severe perfusion defect. (Reproduced with permission from [57].)

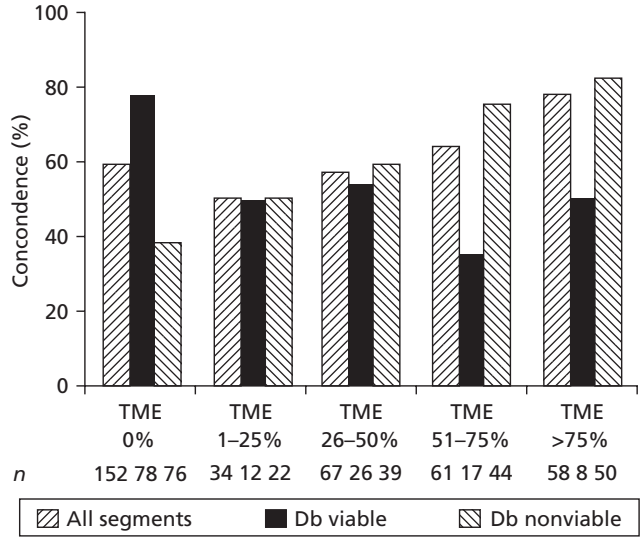

Figure 13.12 Proportion of segments in which the results of ^{201}Tl SPECT and dobutamine echocardiography (Db) were concordant (viable by both tests or nonviable by both tests) in each category of transmural extent of scar (TME). The overall concordance between ^{201}Tl SPECT and Db is similar in each category of TME, increasing with TME greater than 75%. Most segments that are viable by Db are viable by ^{201}Tl SPECT when there is no scar (i.e., TME 0%), with more discrepancies as TME increases ($p < 0.03$). Segments that are nonviable by Db show increasing concordance with increasing TME ($p < 0.0001$). (Reproduced with permission from [57].)

modality for assessing the size of infarction was addressed literature on quantification of infarct size by serum markers, technetium-99m SPECT, and MRI. Emphasis was given to infarct size as an endpoint in evaluation of therapies designed to limit myocardial necrosis. Thus, determining which imaging modality is appropriate and suitable for multicenter trials is important. Gibbons et al. concluded that while serum markers had limitations, MPS has multiple separate lines of evidence supporting validity and has been used successfully in multicenter trials. They concluded that while CMR has great promise, its application and validation in large numbers of patients has not, to date, been documented and it has no multicenter

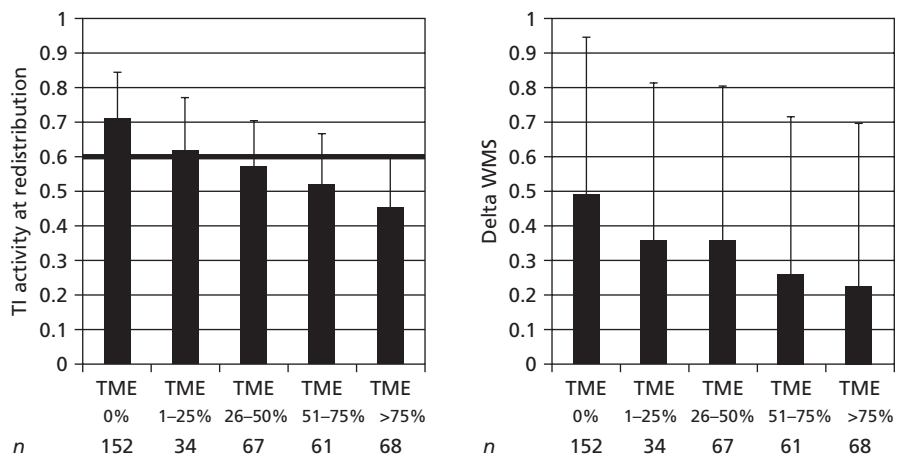

Figure 13.11 Relationship between transmural extent of scar (TME) and thallium (Tl) activity at late redistribution (left) and increase in wall motion score (WMS) with low-dose dobutamine (right). Thallium activity at redistribution and the degree of low-dose augmentation both decrease significantly with increasing TME ($p < 0.001$), with no significant difference between dobutamine echocardiography and Tl SPECT. The 60% Tl activity cutoff for viability is shown. (Reproduced with permission from [57].)

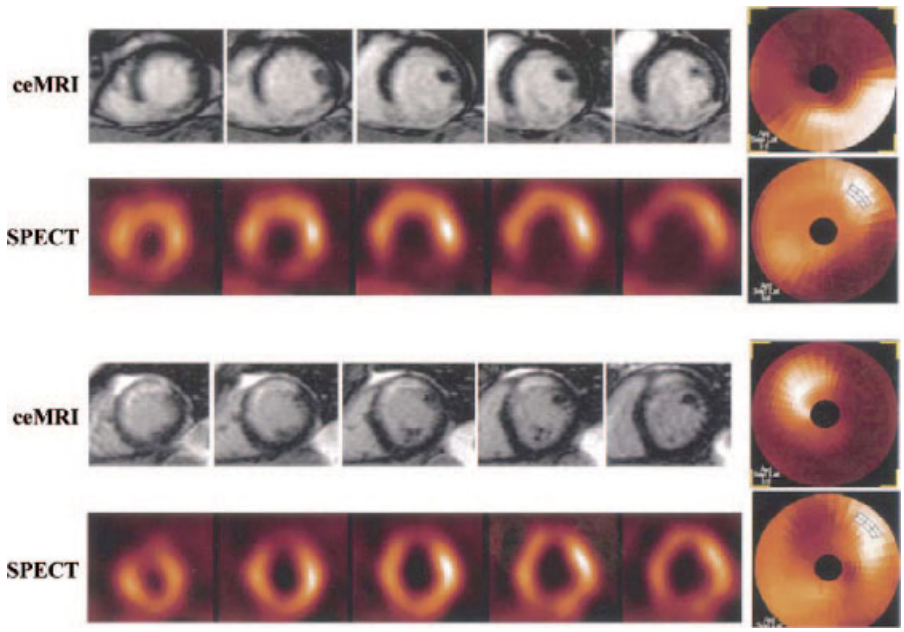

Figure 13.13 Comparison of contrast-enhanced MRI (ceMRI) at 28 minutes after contrast and single-photon emission computed tomography perfusion defect with corresponding polar maps. Short-axis slices are orientated from apical (left) to basal (right). (Top 2 rows) Myocardial infarction of the inferior wall (day 6) with transmural contrast enhancement. (Bottom 2 rows) Anterior infarction (day 8) with subendocardial enhancement. (Reproduced with permission from [59].)

experience. Accordingly, the authors suggested that MPS is the best currently available technique for quantitation of infarct size and evaluation of novel therapies in acute myocardial infarction. One study that directly compares inversion recovery ceCMR infarct size with defect size by using technetium-99m SPECT was recently reported by Ibrahim et al. who studied the kinetics of gadolinium washout in 33 patients after acute myocardial infarction and sought to define the optimal protocol for visualization of infarct size by ceCMR [59]. Infarcts were demonstrated by ceCMR in all patients and the relative intensity of infarcts compared to remote myocardium was 478%. Importantly, the infarct size by ceCMR was stable over time and correlated closely with MPS infarct size ($r = 0.86$), with an average difference of 3% of the left ventricular myocardium (see Fig. 13.13).

Further studies comparing ceCMR to radionuclide methods have focused on the prediction of functional recovery. In the study mentioned above by Nelson et al., patients underwent dobutamine echocardiography in addition to MPS and CMR. In addition to observing the relationship between transmurality of infarction and thallium activity, the authors also demonstrated that contractile reserve decreased as transmurality of infarction increased. More than 50% of segments with 25–75% transmural scar showed contractile improvement during dobutamine stress. Consistent with the notion that thallium SPECT is highly sensitive and dobutamine echocardiography is specific for identification of viable myocardium, ^{201}Tl SPECT identified more segments as viable than dobutamine stress echo for all degrees of infarct transmurality. Knuesel and colleagues [60] studied 10 patients with ischemic chronic left ventricular dysfunction before and after CABG and assessed the relative predictive value of delayed enhancement by ceCMR and presence of glucose metabolism on FDG-PET for prediction of segmental recovery (see Fig. 13.14). Authors noted that viability by ceCMR correlated with preserved FDG activity. They also noted that 85% of segments with a greater than or equal to 4.5-mm rim of viable epicardium (subendocardial scar) on ceCMR improved function after revascularization. Conversely, only 36% of dysfunctional segments that were viable by PET but had a very thin viable rim (<4.5 mm) by ceCMR recovered function. Kitagawa et al. studied 22 patients within 10 days of acute myocardial infarction by both rest ^{201}Tl SPECT and delayed ceCMR. Cine images were acquired using CMR both early and 8 weeks post-myocardial infarction [61] (see Fig. 13.15). Both transmural extent of infarction on ceCMR and the severity of thallium abnormality at rest were predictive of late regional thickening. Sensitivity and specificity of CMR for predicting recovery were 98 and 75%, respectively, while corresponding values for ^{201}Tl SPECT were 90 and 54%, respectively. These studies indicate a close relationship between nuclear and CMR techniques for identification of viable myocardium and suggest utility of ceCMR for prediction of functional recovery in both acute and chronic ischemic heart disease, with a possible advantage of ceCMR for the detection of small and subendocardial infarctions. Whether differences between thallium SPECT, FDG-PET, and ceCMR translate into altered and/or improved patient management is less clear.

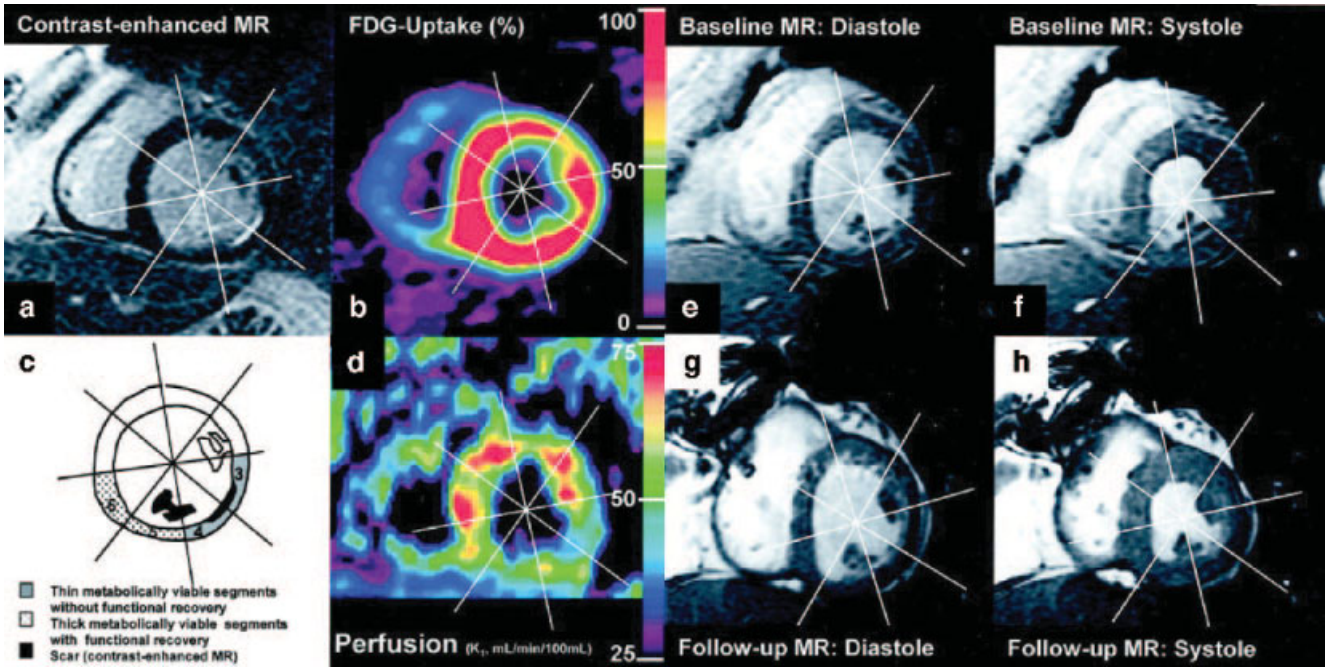

Figure 13.14 In this 48-year-old female patient, 3 years after a lateral myocardial infarction, a small subendocardial scar in the lateral segments 3 and 4 is demonstrated (a) with a thin rim of viable tissue. These segments show preserved FDG uptake (b) with a reduced perfusion (d), thus exhibiting the pattern predictive for recovery of function (see also schematic c). Although these segments were hypocontractile at baseline (e and f), 11 months after bypass surgery these segments did not improve function (g and h). Conversely, segments 5 and 6 were not infarcted (a), had a thick rim of viable tissue (a), and fulfilled metabolic viability criteria (b and d). Follow-up CMR demonstrates substantial improvement of contractile function (g and h) compared with baseline function in these segments (e and f). (Reproduced with permission from [60].)

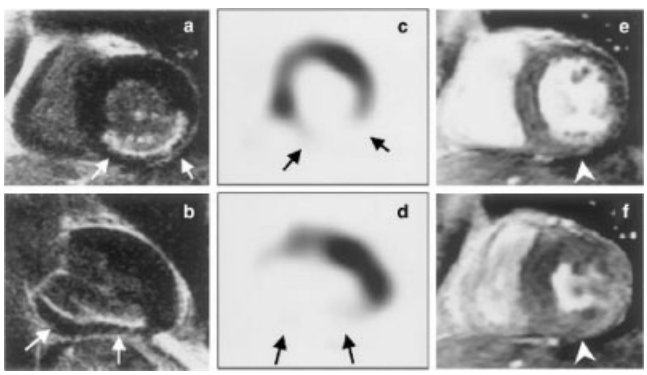

Figure 13.15 Contrast-enhanced MR images obtained with a segmented inversion-recovery fast low-angle shot sequence in (a) short-axis and (b) long-axis imaging planes and resting ^{201}Tl SPECT images obtained in (c) short-axis and (d) long-axis imaging planes in a 59-year-old man with inferior myocardial infarction. Transmural extent of hyperenhancement in the inferior wall (white arrows) was less than 50% of wall thickness, which indicates preserved regional viability. The ^{201}Tl SPECT images show reduced uptake of less than 60% of peak, which indicates nonviable myocardium (black arrows). Follow-up short-axis cine CMR images obtained with a segmented fast low-angle shot sequence at (e) the end of diastole and (f) the end of systole demonstrate preserved regional contractile function in the inferior wall (arrowheads). (Reproduced with permission from [61].)

Combined approaches to viability by CMR

The comparative data presented above confirms a correlation between SPECT, PET, and CMR for detection of infarction and, to some extent, for prediction of functional recovery in patients with ischemic heart disease. Interestingly, all studies presented show some degree of discordance between modalities. There is ongoing work examining the reasons for disagreement between modalities.

Recently, there has been interest in comparing whether low-dose dobutamine CMR in place of or in conjunction with ceCMR is more accurate for prediction of wall motion improvement after revascularization. Motivation for this comes, in part, from a study by Kim et al., who examined patients by ceCMR before and after coronary revascularization [45]. Overall, the authors found ceCMR was predictive of functional recovery; dysfunctional segments with 0–25% transmural extent of infarction had a high probability of recovery and segments with greater than 75% transmural infarction were unlikely to recover function. However, the likelihood of functional recovery was intermediate for segments with 26–75% transmural infarction. The underlying reason(s) that accounts for intermediate likelihood of recovery for this group of

segments with intermediate transmuralities of infarction is unclear.

There are multiple clinical factors that could influence the likelihood of functional recovery in the setting of intermediate grade subendocardial scar. Cardiac factors include wall thickness, contractile reserve, volume loading, presence of ischemia, and the duration of dysfunction. It is possible that contractile reserve may be a better marker of functional recovery after revascularization than just the extent of infarction alone. Wellnhofer et al. studied a series of patients by both ceCMR and low-dose dobutamine CMR [62]. Data were analyzed by receiver operator curve (ROC) analysis for prediction of segmental functional recovery. When all segments were considered, the logistic model demonstrated that the combination of dobutamine and ceCMR data was superior to either approach alone. This interest in using a combined approach, especially for segments with intermediate transmural extent of infarction, may lead to improved predictive accuracy of CMR. Whether such methods are feasible, add clinical value, and are cost-effective remains to be seen.

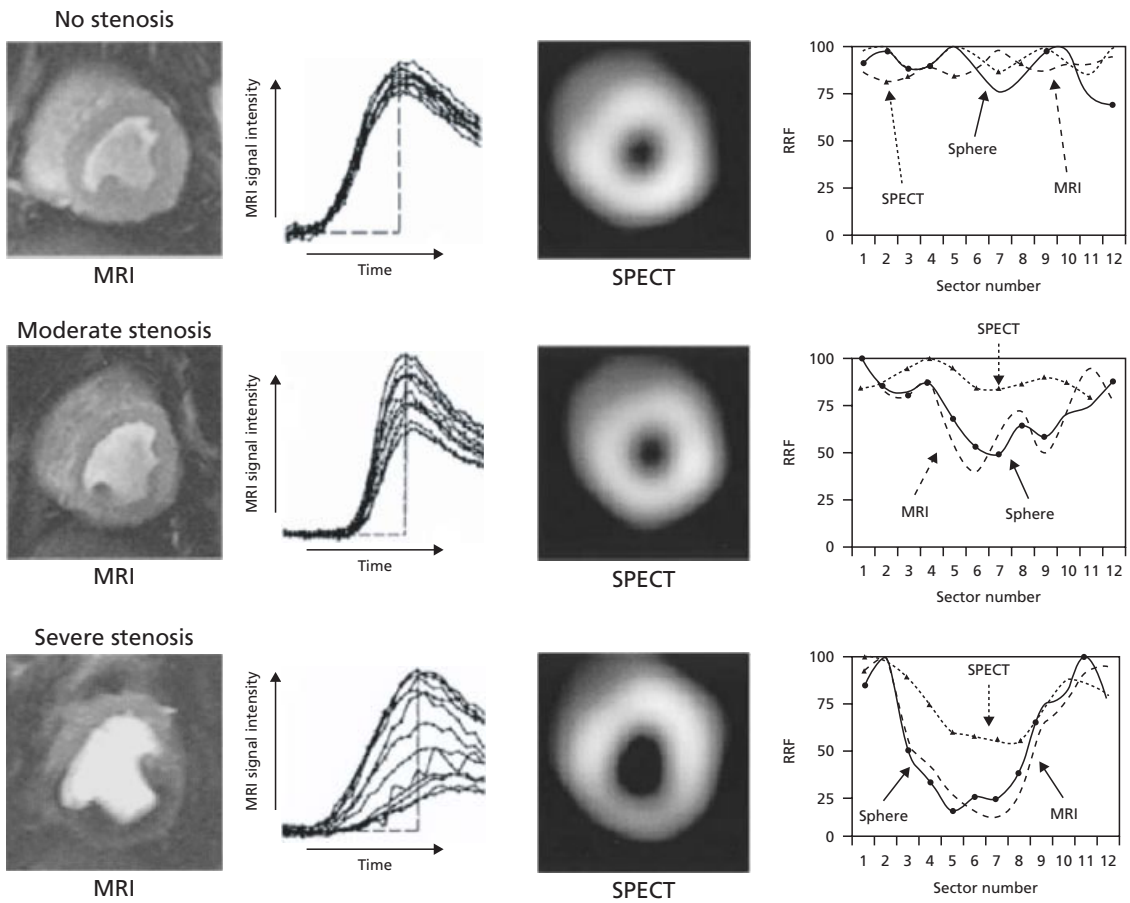

Figure 13.16 Magnetic resonance first-pass (MRFP), ^{99m}Tc-sestamibi SPECT, and microsphere data during pharmacologic vasodilation in animals with no (top), moderate (middle), and severe (bottom) reductions in microsphere flow in the circumflex bed. Shown from left to right are (1) a single frame from the MRFP image stack; (2) MRFP signal-intensity curves for 12 30° sectors (beginning at the most cranial image point and proceeding clockwise); (3) the corresponding ^{99m}Tc-sestamibi SPECT image; and (4) relative MRFP curve areas, ^{99m}Tc-sestamibi count rates, and microsphere concentrations in each 30° sector. Peak flow reductions indicated by microspheres are 50% or more and 85%, respectively (lower two panels). MRFP images show homogeneous myocardial contrast enhancement in the absence of stenosis, moderately reduced enhancement in the circumflex bed with moderate flow reduction, and markedly reduced enhancement with severe flow reduction. A transmural gradient in flow is visually apparent in both cases of flow reduction. MRFP signal intensity curves have nearly identical initial areas in the absence of stenosis. Areas in the circumflex distribution are reduced moderately and markedly with moderate and severe flow reductions, respectively. ^{99m}Tc-sestamibi SPECT images show a uniform signal intensity in the absence of flow reduction and in the presence of moderate flow reduction. A prominent perfusion defect is apparent with severe flow reduction. Relative MRFP curve areas and microsphere concentrations correspond closely in all cases. ^{99m}Tc-sestamibi count rates are homogeneous at rest and remain so with moderate flow reduction but show an approximately 50% peak reduction with severe flow reduction. (Reproduced with permission from [65].)

Summary for viability assessment by CMR

The choice of CMR or SPECT for determination of myocardial viability is a subject of ongoing debate. While CMR provides images with higher resolution, may provide improved detection of small or subendocardial infarcts, and does not suffer from attenuation, SPECT is more widely available and can be performed in a broader patient population (i.e., patients with contraindications to MRI). From evidence available, the following can be stated regarding CMR assessment of viability:

- Correlates with SPECT and FDG-PET
- Can be assessed using spectroscopy, dobutamine CMR, or delayed ceCMR
- High resolution and excellent contrast between normal and infarcted myocardium
- Can be used to predict functional recovery after revascularization or post-myocardial infarction.

Cardiac MR perfusion imaging

In addition to imaging of myocardial function, volumes, mass, and scarring within the heart, there is evidence that MR may also be useful in imaging blood flow within the heart and, further, able to identify regions of reduced blood flow secondary to CAD. One of the more recent advances in CMR imaging is the development of techniques designed to image blood flow within the myocardium at rest and during pharmacologic vasodilation. While several studies have reported feasibility of absolute blood flow quantification at rest in animal models [63,64], these techniques are challenging in clinical practice and require assumptions that may break down in patients with CAD. In addition, because coronary disease can result in a reduced myocardial flow reserve without a significant decrease in resting blood flow, the assessment of the relative difference between blood flow at rest versus during vasodilation is likely of greater clinical importance than absolute blood flow computed at rest.

The technique most commonly employed for assessment of myocardial blood flow using CMR is rapid multislice imaging of certain slices of the heart during transit of a bolus of gadolinium contrast agent, the so-called first-pass perfusion imaging. To assess coronary disease, such first-pass data sets may be acquired at rest and compared to exercise or pharmacologic stress to gauge whether a difference in flow within the myocardium can be observed. There is currently no consensus regarding the ideal methodology for this cardiac MR technique and no data to demonstrate whether a certain MR pulse sequence, contrast dose, or slice selection improves diagnosis. For detection of CAD, CMR first-pass perfusion imaging is most commonly performed at rest and during some form of pharmacologic stress within the magnet setting, often dipyridamole or adenosine. Adenosine stress testing in the magnet most commonly utilizes a 3–5-minute infusion of adenosine (140 mcg/(kg min)) with rapid bolus injection of gadolinium-based contrast during rapid multislice image acquisition. Dependent upon the pulse sequence used and the heart rate of the patient, three to five slices can be acquired during every heartbeat while gadolinium is injected into a peripheral or central venous catheter. This process requires coordination of effort by CMR operators and results in an image sequence for each slice where gadolinium traces blood flow through the heart for each R–R interval. Dynamic rest and stress CMR first-pass images are frequently viewed side by side to visualize and compare blood flow through the myocardium.

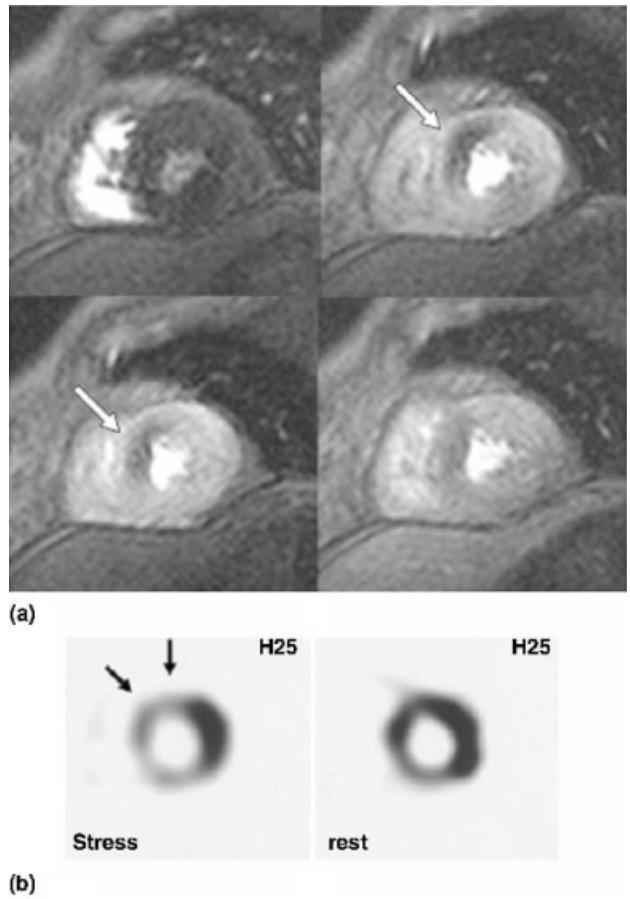

Figure 13.17 (a) First-pass contrast-enhanced multishot echo-planar stress MR images (6.7/1.4/180 repetition time ms/echo time ms/saturation recovery time ms) and (b) Tl SPECT images obtained during stress and at rest in a patient with 70% or greater diameter stenosis of the left anterior descending artery. The hypoperfused region (arrows) in the anteroseptal wall is depicted as a region of lower enhancement in (a) and as an apparent perfusion abnormality in (b). (Reproduced with permission from [69].)

Data in animal models with direct comparison to SPECT have come from a study by Lee and colleagues who imaged 18 chronically instrumented dogs using first-pass perfusion CMR and compared results to stress/rest SPECT for coronary stenoses of varying severity [65]. The gold standard for assessment of myocardial perfusion in this study was obtained by postmortem microsphere quantification. Although data in this study were limited to the animal model, perfusion across the transmural myocardial extent was visually and quantitatively apparent for reductions in flow of greater than or equal to 50%. Further, reductions in flow of greater than or equal to 50% that were not identified by dual isotope SPECT were apparent in first-pass CMR (see Fig. 13.16).

Two studies in patients examined first-pass CMR at rest and during pharmacologic stress with comparison to cardiac catheterization. Al-Saadi and colleagues studied 34 patients with CAD and compared signal time–intensity curves on first-pass MR perfusion images acquired before and after dipyridamole infusion to results at coronary angiography [66]. Sensitivity and specificity in this patient population were 90 and 83%, respectively, with low intraobserver variability. Nagel and colleagues [67] studied 84 patients referred for primary diagnostic coronary angiography with rest-adenosine first-pass MRI. Sensitivity and specificity using a quantitative analysis of signal intensity curves for multiple slices were 88 and 90%, respectively, while the corresponding values were 70 and 78% for visual assessment. In an additional study by this group [68], 79 patients were studied by dobutamine stress cine MRI and by adenosine stress first-pass perfusion and results were compared to coronary angiography. In their study, 53/79 patients had coronary artery stenoses greater than or equal to 50% and data revealed that the sensitivity and specificity for detection by dobutamine wall motion were 89 and 80%, while the corresponding values for adenosine first-pass perfusion were 91 and 62%, respectively.

In addition, a few studies have compared first-pass CMR perfusion imaging to radionuclide methods and to invasive angiography. Ishida and colleagues studied 104 patients using first-pass CMR during dipyridamole and isometric handgrip exercise and compared stress/rest ^{201}Tl SPECT (69/104 patients) and invasive coronary angiography (104/104 patients) [69] (see Fig. 13.17). Overall, the sensitivity of first-pass CMR for detection of CAD was 90%, with sensitivities for one-, two-, and three-vessel coronary disease of 85, 96, and 100%, respectively. ROC analyses suggested that stress/rest first-pass CMR was more accurate than stress/rest thallium imaging for detection of significant coronary lesion. Schwitter et al. studied 48 patients using a multislice first-pass CMR approach during dipyridamole versus ^{13}N-ammonia PET and quantitative coronary angiography [70] (see Fig. 13.18). ROCs for CMR and PET suggested that PET had sensitivity and specificity of 91 and 94%, respectively, for detection of CAD, while the corresponding values for the CMR approach employed were 87 and 85% (see Fig. 13.19). These preliminary studies are important work to begin understanding whether perfusion CMR may be additive to information provided by established radionuclide techniques.

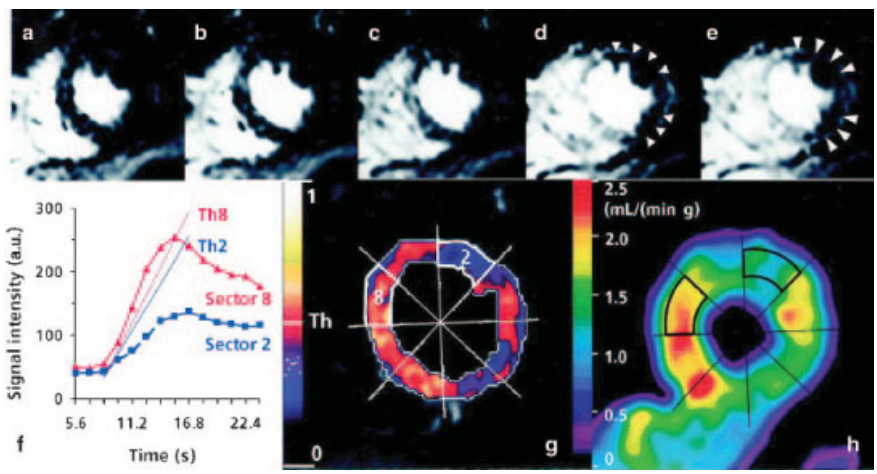

Figure 13.18 In this patient with stenoses in the left anterior descending coronary artery and the right coronary artery, the transit of CM through the left ventricular myocardium during hyperemia demonstrates delayed wash-in in both the subendocardial and subepicardial layers of both arteries (a through e, arrowheads). (f) Representative signal intensity–time curves are shown for normal myocardium (red curve, sector 8) and hypoperfused myocardium (blue curve, sector 2). Th2 and Th8 indicate thresholds for full-wall thickness data in corresponding sectors derived from the ROC analyses (Fig. 13.2). On the parametric slope map (g), pixels below/above the threshold (Th) are encoded in shades of blue/red, respectively. On the PET image (h), reduced hyperemic flow is demonstrated in corresponding sectors. (Reproduced with permission from [70].)

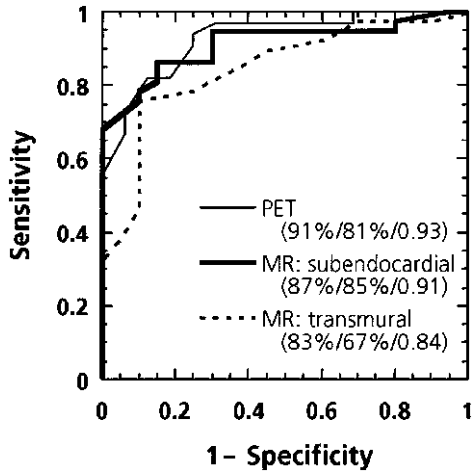

Figure 13.19 ROC of CMR upslope data is shown for the detection of CAD defined by quantitative coronary analysis (one or more artery with ≥50% diameter stenosis). The diagnostic performances of MR and PET are comparable. Numbers in parentheses represent sensitivity, specificity, and area under the ROC, respectively. (Reproduced with permission from [70].)

The clinical utility of CMR for detection of myocardial ischemia is presently under intense investigation by multiple groups. Whether CMR will be useful in this regard is at present unclear.

Summary

CMR techniques for assessment of ventricular volumes, regional and global function, and cardiac viability are established in clinical practice and arguably represent a standard by which other noninvasive imaging modalities can be compared. The image resolution and reproducibility of CMR cine imaging permit very accurate and reproducible assessment of biventricular volume and function. Although GBP and gated perfusion SPECT correlate well, accuracy and reproducibility of CMR mean this modality is currently regarded as the gold standard for measurement of biventricular volume and function.

There is evidence that the delayed gadolinium-contrast enhancement CMR technique for assessment of myocardial viability is a precise and reproducible method that compares favorably to echocardiographic, SPECT, and PET assessments of viability. The place of ceCMR in comparison to current clinical techniques for assessment of myocardial viability is not yet well defined. However, it is possible that superior spatial resolution of ceCMR viability imaging may lead to altered clinical management and improvement in detection of viability in selected patient populations.

CMR first-pass perfusion imaging is a promising technique that currently presents practical challenges and is the subject of ongoing clinical research.

References

1. Myerburg RJ, Kessler KM, Castellanos A. Sudden cardiac death. Structure, function, and time-dependence of risk. Circulation 1992;85(1, Suppl):I2–I10.
2. Taylor AJ, Udelson JE, Fuster V. Training cardiovascular fellows in cardiovascular magnetic resonance and vascular imaging: current status following the core cardiovascular training symposium (COCATS-2) guidelines. Journal of the American College of Cardiology 2004;43(11):2108–2112.
3. Debatin JF, Nadel SN, Paolini JF, et al. Cardiac ejection fraction: phantom study comparing cine MR imaging, radionuclide blood pool imaging, and ventriculography. Journal of Magnetic Reasonance Imaging 1992;2(2):135–142.
4. De Bondt P, Nichols K, Vandenberghe S, et al. Validation of gated blood-pool SPECT cardiac measurements tested using a biventricular dynamic physical phantom. Journal of Nuclear Medicine 2003;44(6):967–972.
5. Mogelvang J, Stokholm KH, Saunamaki K, et al. Assessment of left ventricular volumes by magnetic resonance in comparison with radionuclide angiography, contrast angiography and echocardiography. European Heart Journal 1992;13(12):1677–1683.
6. Chin BB, Bloomgarden DC, Xia W, et al. Right and left ventricular volume and ejection fraction by tomographic gated blood-pool scintigraphy. Journal of Nuclear Medicine 1997;38(6):942–948.
7. Lethimonnier F, Furber A, Balzer P, et al. Global left ventricular cardiac function: comparison between magnetic resonance imaging, radionuclide angiography, and contrast angiography. Investigative Radiology 1999;34(3):199–203.
8. Nichols K, Saouaf R, Ababneh AA, et al. Validation of SPECT equilibrium radionuclide angiographic right ventricular parameters by cardiac magnetic resonance imaging. Journal of Nuclear Cardiology 2002;9(2):153–160.
9. Faber TL, Cooke CD, Folks RD, et al. Left ventricular function and perfusion from gated SPECT perfusion images: an integrated method. Journal of Nuclear Medicine 1999;40(4):650–659.
10. Faber TL, Vansant JP, Pettigrew RI, et al. Evaluation of left ventricular endocardial volumes and ejection fractions computed from gated perfusion SPECT with magnetic resonance imaging: comparison of two methods. Journal of Nuclear Cardiology 2001;8(6):645–651.
11. Ioannidis JP, Trikalinos TA, Danias PG. Electrocardiogram-gated single-photon emission computed tomography versus cardiac magnetic resonance imaging for the assessment of left ventricular volumes and ejection fraction: a meta-analysis. Journal of the American College of Cardiology 2002;39(12):2059–2068.
12. Stollfuss JC, Haas F, Matsunari I, et al. 99mTc-tetrofosmin SPECT for prediction of functional recovery defined by MRI in patients with severe left ventricular dysfunction: additional value of gated SPECT. Journal of Nuclear Medicine 1999;40(11):1824–1831.

13. Mochizuki T, Murase K, Tanaka H, Kondoh T, Hamamoto K, Tauxe WN. Assessment of left ventricular volume using ECG-gated SPECT with technetium-99m-MIBI and technetium-99m-tetrofosmin. Journal of Nuclear Medicine 1997;38(1):53–57.
14. Vaduganathan P, He ZX, Vick GW III, Mahmarian JJ, Verani MS. Evaluation of left ventricular wall motion, volumes, and ejection fraction by gated myocardial tomography with technetium 99m-labeled tetrofosmin: a comparison with cine magnetic resonance imaging. Journal of Nuclear Cardiology 1999;6(1, Pt 1):3–10.
15. Stollfuss JC, Haas F, Matsunari I, et al. Regional myocardial wall thickening and global ejection fraction in patients with low angiographic left ventricular ejection fraction assessed by visual and quantitative resting ECG-gated 99mTc-tetrofosmin single-photon emission tomography and magnetic resonance imaging. European Journal of Nuclear Medicine 1998;25(5):522–530.
16. Tadamura E, Kudoh T, Motooka M, et al. Assessment of regional and global left ventricular function by reinjection T1-201 and rest Tc-99m sestamibi ECG-gated SPECT: comparison with three-dimensional magnetic resonance imaging. Journal of the American College of Cardiology 1999;33(4):991–997.
17. Tadamura E, Kudoh T, Motooka M, et al. Use of technetium-99m sestamibi ECG-gated single-photon emission tomography for the evaluation of left ventricular function following coronary artery bypass graft: comparison with three-dimensional magnetic resonance imaging. European Journal of Nuclear Medicine 1999;26(7):705–712.
18. Bax JJ, Lamb H, Dibbets P, et al. Comparison of gated single-photon emission computed tomography with magnetic resonance imaging for evaluation of left ventricular function in ischemic cardiomyopathy. American Journal of Cardiology 2000;86(12):1299–1305.
19. Bavelaar-Croon CD, Kayser HW, van der Wall EE, et al. Left ventricular function: correlation of quantitative gated SPECT and MR imaging over a wide range of values. Radiology 2000;217(2):572–575.
20. Lee HS, Cross S, Norton M, Walton S. Comparison between planar and tomographic radionuclide ventriculography for detecting inferior wall motion abnormalities. Clinical Radiology 1998;53(4):264–267.
21. Metcalfe MJ, Norton MY, Jennings K, Walton S. Improved detection of abnormal left ventricular wall motion using tomographic radionuclide ventriculography compared with planar radionuclide and single plane contrast ventriculography. British Journal of Radiology 1993;66(791):986–993.
22. Hundley WG, Li HF, Hillis LD, et al. Quantitation of cardiac output with velocity-encoded, phase-difference magnetic resonance imaging. American Journal of Cardiology 1995;75(17):1250–1255.
23. Lee VS, Spritzer CE, Carroll BA, et al. Flow quantification using fast cine phase-contrast MR imaging, conventional cine phase-contrast MR imaging, and Doppler sonography: in vitro and in vivo validation. AJR American Journal of Roentgenology 1997;169(4):1125–1131.
24. Kondo C, Caputo GR, Semelka R, Foster E, Shimakawa A, Higgins CB. Right and left ventricular stroke volume measurements with velocity-encoded cine MR imaging: in vitro and in vivo validation. AJR American Journal of Roentgenology 1991;157(1):9–16.
25. Debatin JF, Leung DA, Wildermuth S, Botnar R, Felblinger J, McKinnon GC. Flow quantitation with echo-planar phase-contrast velocity mapping: in vitro and in vivo evaluation. Journal of Magnetic Resonance Imaging 1995;5(6):656–662.
26. Caruthers SD, Lin SJ, Brown P, et al. Practical value of cardiac magnetic resonance imaging for clinical quantification of aortic valve stenosis: comparison with echocardiography. Circulation 2003;108(18):2236–2243.
27. Greil G, Geva T, Maier SE, Powell AJ. Effect of acquisition parameters on the accuracy of velocity encoded cine magnetic resonance imaging blood flow measurements. Journal of Magnetic Resonance Imaging 2002;15(1):47–54.
28. Semelka RC, Tomei E, Wagner S, et al. Normal left ventricular dimensions and function: interstudy reproducibility of measurements with cine MR imaging. Radiology 1990;174(3, Pt 1):763–768.
29. Bellenger NG, Davies LC, Francis JM, Coats AJ, Pennell DJ. Reduction in sample size for studies of remodeling in heart failure by the use of cardiovascular magnetic resonance. Journal of Cardiovascular Magnetic Resonance 2000;2(4):271–278.
30. Blake LM, Scheinman MM, Higgins CB. MR features of arrhythmogenic right ventricular dysplasia. AJR American Journal of Roentgenology 1994;162(4):809–812.
31. Grothues F, Moon JC, Bellenger NG, Smith GS, Klein HU, Pennell DJ. Interstudy reproducibility of right ventricular volumes, function, and mass with cardiovascular magnetic resonance. American Heart Journal 2004;147(2):218–223.
32. Shea SM, Kroeker RM, Deshpande V, et al. Coronary artery imaging: 3D segmented k-space data acquisition with multiple breath-holds and real-time slab following. Journal of Magnetic Resonance Imaging 2001;13(2):301–307.
33. Hachamovitch R, Hayes SW, Friedman JD, Cohen I, Berman DS. Comparison of the short-term survival benefit associated with revascularization compared with medical therapy in patients with no prior coronary artery disease undergoing stress myocardial perfusion single photon emission computed tomography. Circulation 2003;107(23):2900–2907.
34. Allman KC, Shaw LJ, Hachamovitch R, Udelson JE. Myocardial viability testing and impact of revascularization on prognosis in patients with coronary artery disease and left ventricular dysfunction: a meta-analysis. Journal of the American College of Cardiology 2002;39(7):1151–1158.
35. Yabe T, Mitsunami K, Okada M, Morikawa S, Inubushi T, Kinoshita M. Detection of myocardial ischemia by 31P magnetic resonance spectroscopy during handgrip exercise. Circulation 1994;89(4):1709–1716.
36. Chen C, Li L, Chen LL, et al. Incremental doses of dobutamine induce a biphasic response in dysfunctional left ventricular regions subtending coronary stenoses. Circulation 1995;92(4):756–766.
37. Baer FM, Voth E, Schneider CA, Theissen P, Schicha H, Sechtem U. Comparison of low-dose dobutamine-gradient-echo magnetic resonance imaging and positron emission tomography with [^{18}F]fluorodeoxyglucose in patients with

chronic coronary artery disease. A functional and morphological approach to the detection of residual myocardial viability. Circulation 1995;91(4):1006–1015.
38. Gunning MG, Anagnostopoulos C, Knight CJ, et al. Comparison of ^{201}Tl, ^{99m}Tc-tetrofosmin, and dobutamine magnetic resonance imaging for identifying hibernating myocardium. Circulation 1998;98(18):1869–1874.
39. Edelman RR, Wallner B, Singer A, Atkinson DJ, Saini S. Segmented turboFLASH: method for breath-hold MR imaging of the liver with flexible contrast. Radiology 1990;177(2):515–521.
40. Simonetti OP, Kim RJ, Fieno DS, et al. An improved MR imaging technique for the visualization of myocardial infarction. Radiology 2001;218(1):215–223.
41. Rehwald WG, Fieno DS, Chen EL, Kim RJ, Judd RM. Myocardial magnetic resonance imaging contrast agent concentrations after reversible and irreversible ischemic injury. Circulation 2002;105(2):224–229.
42. Fieno DS, Kim RJ, Chen EL, Lomasney JW, Klocke FJ, Judd RM. Contrast-enhanced magnetic resonance imaging of myocardium at risk: distinction between reversible and irreversible injury throughout infarct healing. Journal of the American College of Cardiology 2000;36(6):1985–1991.
43. Kim RJ, Fieno DS, Parrish TB, et al. Relationship of MRI delayed contrast enhancement to irreversible injury, infarct age, and contractile function. Circulation 1999;100(19):1992–2002.
44. Klein C, Nekolla SG, Bengel FM, et al. Assessment of myocardial viability with contrast-enhanced magnetic resonance imaging: comparison with positron emission tomography. Circulation 2002;105(2):162–167.
45. Kim RJ, Wu E, Rafael A, et al. The use of contrast-enhanced magnetic resonance imaging to identify reversible myocardial dysfunction. New England Journal of Medicine 2000;343(20):1445–1453.
46. Lawson MA, Johnson LL, Coghlan L, et al. Correlation of thallium uptake with left ventricular wall thickness by cine magnetic resonance imaging in patients with acute and healed myocardial infarcts. American Journal of Cardiology 1997;80(4):434–441.
47. Kitsiou AN, Srinivasan G, Quyyumi AA, Summers RM, Bacharach SL, Dilsizian V. Stress-induced reversible and mild-to-moderate irreversible thallium defects: are they equally accurate for predicting recovery of regional left ventricular function after revascularization? Circulation 1998;98(6):501–508.
48. Lima JA, Judd RM, Bazille A, Schulman SP, Atalar E, Zerhouni EA. Regional heterogeneity of human myocardial infarcts demonstrated by contrast-enhanced MRI. Potential mechanisms. Circulation 1995;92(5):1117–1125.
49. Judd RM, Lugo-Olivieri CH, Arai M, et al. Physiological basis of myocardial contrast enhancement in fast magnetic resonance images of 2-day-old reperfused canine infarcts. Circulation 1995;92(7):1902–1910.
50. Wu KC, Zerhouni EA, Judd RM, et al. Prognostic significance of microvascular obstruction by magnetic resonance imaging in patients with acute myocardial infarction. Circulation 1998;97(8):765–772.
51. Ramani K, Judd RM, Holly TA, et al. Contrast magnetic resonance imaging in the assessment of myocardial viability in patients with stable coronary artery disease and left ventricular dysfunction. Circulation 1998;98(24):2687–2694.
52. Mahrholdt H, Wagner A, Parker M, et al. Relationship of contractile function to transmural extent of infarction in patients with chronic coronary artery disease. Journal of the American College of Cardiology 2003;42(3):505–512.
53. Ricciardi MJ, Wu E, Davidson CJ, et al. Visualization of discrete microinfarction after percutaneous coronary intervention associated with mild creatine kinase-MB elevation. Circulation 2001;103(23):2780–2783.
54. Ansari M, Araoz PA, Gerard SK, et al. Comparison of late enhancement cardiovascular magnetic resonance and thallium SPECT in patients with coronary disease and left ventricular dysfunction. Journal of Cardiovascular Magnetic Resonance 2004;6(2):549–556.
55. Lund GK, Stork A, Saeed M, et al. Acute myocardial infarction: evaluation with first-pass enhancement and delayed enhancement MR imaging compared with 201Tl SPECT imaging. Radiology 2004;232(1):49–57.
56. Wagner A, Mahrholdt H, Holly TA, et al. Contrast-enhanced MRI and routine single photon emission computed tomography (SPECT) perfusion imaging for detection of subendocardial myocardial infarcts: an imaging study. Lancet 2003;361(9355):374–379.
57. Nelson C, McCrohon J, Khafagi F, Rose S, Leano R, Marwick TH. Impact of scar thickness on the assessment of viability using dobutamine echocardiography and thallium single-photon emission computed tomography: a comparison with contrast-enhanced magnetic resonance imaging. Journal of the American College of Cardiology 2004;43(7):1248–1256.
58. Gibbons RJ, Valeti US, Araoz PA, Jaffe AS. The quantification of infarct size. Journal of the American College of Cardiology 2004;44(8):1533–1542.
59. Ibrahim T, Nekolla SG, Hornke M, et al. Quantitative measurement of infarct size by contrast-enhanced magnetic resonance imaging early after acute myocardial infarction: comparison with single-photon emission tomography using Tc99m-sestamibi. Journal of the American College of Cardiology 2005;45(4):544–552.
60. Knuesel PR, Nanz D, Wyss C, et al. Characterization of dysfunctional myocardium by positron emission tomography and magnetic resonance: relation to functional outcome after revascularization. Circulation 2003;108(9):1095–1100.
61. Kitagawa K, Sakuma H, Hirano T, Okamoto S, Makino K, Takeda K. Acute myocardial infarction: myocardial viability assessment in patients early thereafter comparison of contrast-enhanced MR imaging with resting (201)Tl SPECT. Single photon emission computed tomography. Radiology 2003;226(1):138–144.
62. Wellnhofer E, Olariu A, Klein C, et al. Magnetic resonance low-dose dobutamine test is superior to SCAR quantification for the prediction of functional recovery. Circulation 2004;109(18):2172–2174.
63. Wilke N, Simm C, Zhang J, et al. Contrast-enhanced first pass myocardial perfusion imaging: correlation between

myocardial blood flow in dogs at rest and during hyperemia. Magnetic Resonance in Medicine 1993;29(4):485–497.
64. Wilke N, Kroll K, Merkle H, et al. Regional myocardial blood volume and flow: first-pass MR imaging with polylysine-Gd-DTPA. Journal of Magnetic Resonance Imaging 1995;5(2):227–237.
65. Lee DC, Simonetti OP, Harris KR, et al. Magnetic resonance versus radionuclide pharmacological stress perfusion imaging for flow-limiting stenoses of varying severity. Circulation 2004;110(1):58–65.
66. Al-Saadi N, Nagel E, Gross M, et al. Noninvasive detection of myocardial ischemia from perfusion reserve based on cardiovascular magnetic resonance. Circulation 2000;101(12):1379–1383.
67. Nagel E, Klein C, Paetsch I, et al. Magnetic resonance perfusion measurements for the noninvasive detection of coronary artery disease. Circulation 2003;108(4):432–437.
68. Paetsch I, Jahnke C, Wahl A, et al. Comparison of dobutamine stress magnetic resonance, adenosine stress magnetic resonance, and adenosine stress magnetic resonance perfusion. Circulation 2004;110(7):835–842.
69. Ishida N, Sakuma H, Motoyasu M, et al. Noninfarcted myocardium: correlation between dynamic first-pass contrast-enhanced myocardial MR imaging and quantitative coronary angiography. Radiology 2003;229(1):209–216.
70. Schwitter J, Nanz D, Kneifel S, et al. Assessment of myocardial perfusion in coronary artery disease by magnetic resonance: a comparison with positron emission tomography and coronary angiography. Circulation 2001;103(18):2230–2235.

14 Complementary roles of cardiac CT and gated myocardial perfusion SPECT or PET in patients with known or suspected CAD

Daniel S. Berman
Leslee J. Shaw
Alan Rozanski
Guido Germano

Introduction

Noninvasive cardiac imaging is now central to the diagnosis and management of patients with known or suspected chronic coronary artery disease (CAD). While rest echocardiography has become the most common of the techniques, nuclear cardiology, and more recently cardiac computed tomography (CCT), and cardiac magnetic resonance (CMR) play important roles in this regard. CMR has been reviewed in Chapter 13. This chapter examines the current applications of CCT and the interactions between CT and nuclear cardiology procedures.

Which of these methods is most appropriate as the initial test depends on the clinical question being asked. Among asymptomatic patients, the clinical question frequently revolves around the presence of subclinical coronary atherosclerosis for delineation of *long-term* risk for developing clinical CAD. Here CT coronary calcium testing can help determine who needs aggressive medical management. But in symptomatic patients, as the a priori risk for CAD increases, a second question becomes increasingly important: "What is the *shorter-term* risk of myocardial infarction (MI) or cardiac death?" – a question that appears to be best answered by determining the extent and severity of inducible ischemia, often using gated myocardial perfusion SPECT. In patients with advanced disease and extensive ventricular dysfunction, the question frequently becomes "Is improvement in ventricular function, survival or symptoms likely with revascularization or should surgical reshaping of the left ventricle be performed?" Here the answer may depend on the extent of viable and nonviable myocardium – possibly best addressed by positron emission tomography (PET) or magnetic resonance imaging (MRI).

Cardiac CT scanning for assessment of subclinical atherosclerosis

Vascular calcification has been associated with atherosclerosis since the 1920s [1]. In 1959, Blankenhorn and Stern described the importance of coronary artery calcium (CAC) as a marker of coronary atherosclerosis [2]. For many years, the assessment of CAC using fluoroscopy was recognized as providing clinically useful information. In fact, Diamond et al. incorporated a subjective fluoroscopic assessment of CAC into their original algorithm for assessing the likelihood of angiographically significant CAD by Bayesian analysis [3]. The advent of CT scanning provided a technique which was potentially quantifiable, avoiding the subjectivity of fluoroscopy. While CAC measurements were first described using electron beam CT (EBT), increasingly investigators are recognizing that recent generation multislice CT (MSCT) and EBT provide comparable measurements for practical clinical purposes [4,5]. In standard practice, the presence and extent of coronary calcium is expressed by the Agatston *coronary calcium score* (CCS), related to the extent and the density of calcification in the coronary tree. Examples of coronary calcium scans obtained with EBT are shown in Fig. 14.1.

Acquisition of the CT coronary calcium scan and measurement of coronary calcium

Whether using EBT or MSCT, the acquisition of the CCS is performed in a single breathhold. There is no need for patient preparation. With either approach the amount of radiation is small, estimated to be approximately 0.8 rad,

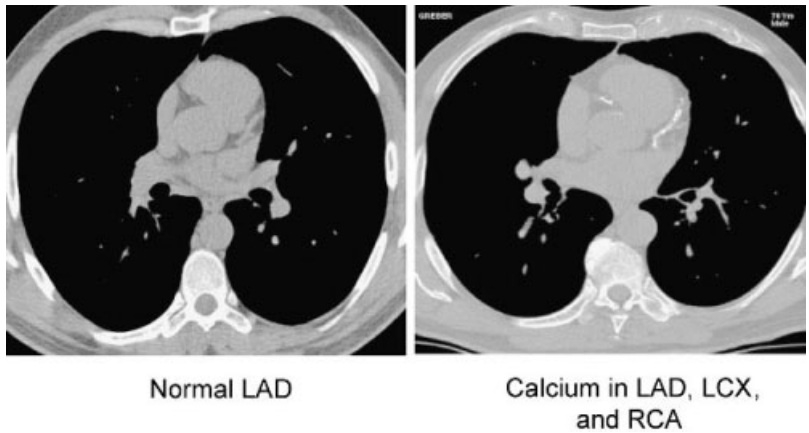

Figure 14.1 Examples of normal and abnormal coronary calcium scans obtained by electron beam tomography. Abbreviations: LAD, left anterior descending artery; LCX, left circumflex artery; RCA, right coronary artery.

somewhat lower with EBT than with MSCT [6]. No special patient preparation is required, except in patients with heart rate over about 80 beats per minute who are having MSCT, in whom β-blockers may be needed. The scoring of these scans typically involves a reproducible semiautomatic computer method as exemplified in Fig. 14.2. The CCS is defined for each focus of calcium in the coronary tree, with areas containing calcium being defined by having Hounsfield units (HU) greater than 130. The software generally calculates lesion-specific scores as the product of the area of each calcified focus and peak CT number (scored as 1 if 131–199 HU, 2 if 200–299 HU, 3 if 300–399 HU, and 4 if 400 HU or greater) according to the Agatston method [7]. These are summed across all lesions identified in the coronary arteries to provide the total CCS.

In common practice, this score is often also expressed as a coronary calcium percentile score based on age and gender using one of many available databases [8–10]. While initially developed for EBT, methods for approximating the density-weighted Agatston score using MSCT have been developed and validated. Most of the available software programs also often provide a *calcified volume score* developed by Callister [11], which has been reported as more useful for monitoring the progression (or regression) of calcification over time, in particular following intercurrent treatment with statin therapy [12]. With the use of calcium phantoms as standards, the mass of calcium in the coronary tree can also be accurately measured by EBT or MSCT; however, whether calcified coronary mass will become the standard assessment of the future is not yet clear, and given the large body of evidence developed with the CCS, it is likely that the CCS will remain the standard for clinical coronary calcium measurement for some time.

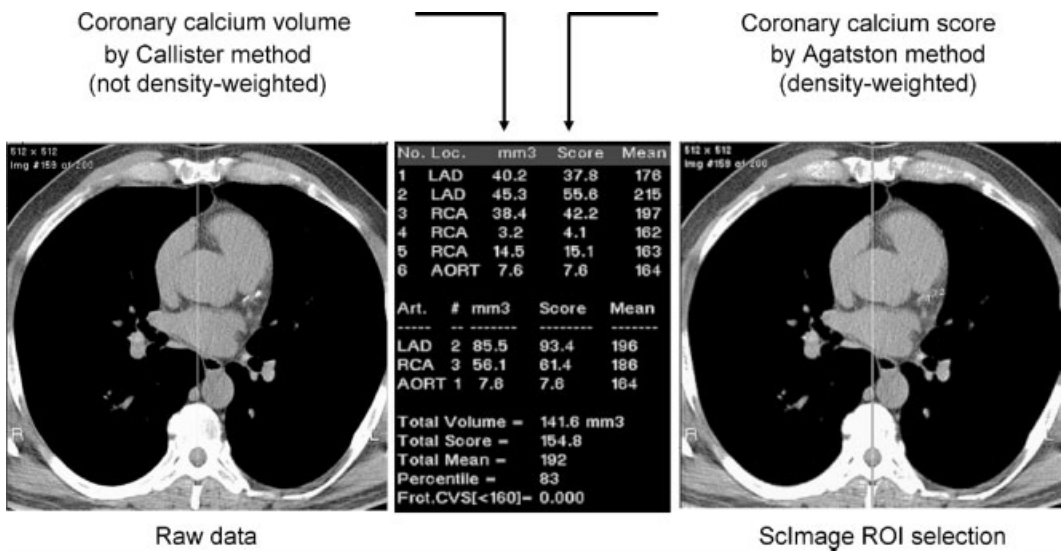

Figure 14.2 Illustration of measurement of the coronary calcium volume (Callister method) and the coronary calcium score (Agatston method). Scoring is determined semiquantitatively by Netra MD™ (ScImage, Inc.).

Angiographic and pathologic correlates of CT coronary calcium

It became clear from early coronary calcium scanning experience that the presence of CAC had low specificity for angiographically significant CAD (≥50% stenosis); i.e., calcification implies atherosclerosis but not necessarily the presence of a stenosis. This phenomenon is explained by a process referred to as the Glagov phenomenon ([13] (Fig. 14.3). Characteristically, in the early stages of coronary atherosclerosis, and often in the more advanced stages, plaque accumulation produces an outward remodeling (expansion) of the external elastic membrane. During this phase, there is little or no encroachment of the plaque on the vascular lumen. In simplistic terms, in most circumstances, only after maximal outward remodeling does a narrowing of the lumen develop. Due to this process, there is only a weak relationship between the plaque burden and the percent of the coronary artery tree supplied by vessels with greater than 50% stenosis. However, if more mild luminal narrowing is considered, for example, the number of segments demonstrating greater than or equal to 20% stenosis by coronary angiography, the total CCS as determined from EBT has been shown to correlate strongly with the angiographic extent of atherosclerosis ($r = 0.77$) [14]. Thus, assessment of coronary calcium allows detection of atherosclerotic lesions often long before they become hemodynamically significant.

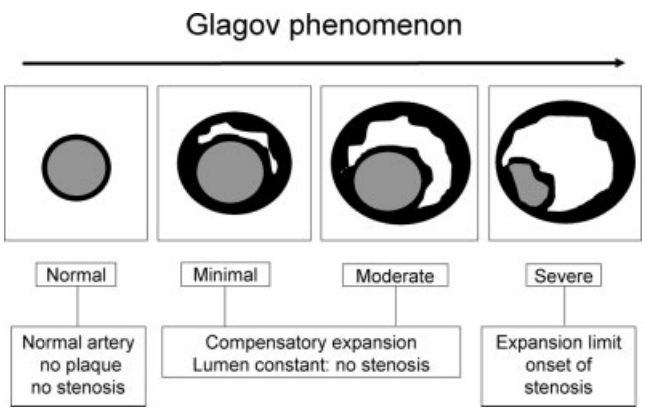

Figure 14.3 Diagrammatic representation of progression of atherosclerosis as described by Glagov. The white area indicates the presence of plaque, without consideration of the distinction of calcified and noncalcified plaque. Positive remodeling during the minimal and moderate phases of plaque buildup can occur without compromise of the lumen. However, as the plaque volume becomes large, the artery no longer enlarges at a rate sufficient to prevent narrowing of the lumen. While this is a highly simplified illustration of a complex and variable process, this phenomenon is the likely explanation for the observation that vast majority of coronary plaques are not associated with coronary stenosis. (Adapted with permission from [13].)

Table 14.1 Early detection and quantification of atherosclerosis.

- Most accurate noninvasive test for early detection: abnormal study implies coronary atherosclerosis
- Strong quantitative relationship between coronary calcium score and plaque burden
- High sensitivity for ≥50% angiographic stenosis (but low specificity)
- Independent and incremental information over risk factors for predicting extent of angiographic CAD and prognosis

In contrast, stress nuclear cardiology techniques (as with all stress imaging methods) require the presence of a hemodynamically significant lesion, either fixed or dynamic, before an abnormality becomes evident. In the study noted above, without the CCS [14], stress myocardial perfusion SPECT (MPS) provided significant information for the prediction of the number of segments with 20% or greater maximal coronary stenosis at angiography, along with age, male gender, and cholesterol measurements in a multivariable model. However, once the CCS was known, the radionuclide perfusion score and conventional risk factors were no longer a significant predictor. While this study represents only one of a number of studies that have demonstrated that the CCS provides independent and incremental information over risk factors for predicting the extent of angiographic CAD, it gives insight into the perceived discordance between angiographic and CAC results, and is illustrative of the concept that the presence of CAC is expected to be more sensitive than MPS or even the angiographic "gold standard" in the detection of early coronary atherosclerosis. Table 14.1 summarizes the implications of coronary calcium measurements by EBT/MSCT for early detection and quantification of coronary atherosclerosis. Currently, third-party payers generally do not reimburse for CCS measurements, although we expect this to change within a few years.

Limitations of CCS

Although considered virtually pathognomonic of coronary atherosclerosis, the site of CCS is not site specific for coronary stenosis as noted above. Furthermore, macroscopic calcification – the amount necessary to be visualized by CT – is a relatively late phenomenon in atherosclerosis, considered to be a response of the body to wall off coronary inflammation (i.e., provide plaque stability). In some patients (estimated to be approximately 5% of those with acute coronary syndrome), vulnerable plaques may rupture causing coronary thrombosis at a time in which there is no coronary calcification. Furthermore, CCS requires at least a four-slice scanner with rotation time of 500 milliseconds or less [5].

CT coronary angiography

Beyond its use in assessment of coronary calcium, cardiac CT scanning is increasingly being used for noninvasive coronary CT angiography (CTA), which has been demonstrated to have high sensitivity and specificity for detecting coronary stenosis[15–17]. While virtually all EBT scanners and most recent generation MSCT scanners are capable of the CCS measurements, coronary CTA is technically more demanding. At the present time, further development of the EBT scanners are not being pursued by industry. Current EBT scanners are limited in their *z*-axis resolution (1.5 mm), diminishing their value for coronary CTA. On the other hand, with 16-slice or greater MSCT scanners operating with rotation times of 420 milliseconds or less, clinically useful results have been reported with coronary CTA. Since tomography with CT requires approximately 210° acquisition (slightly greater than with SPECT), the fastest of the currently available scanners, operating at a 330-millisecond rotation time, has a single beat acquisition time of approximately 180 milliseconds. This limitation of temporal resolution limits the approach to heart rates of 65 beats per minute or less for single beat acquisitions, generally necessitating the use of β-blockers prior to acquisition. The most recent generation of scanners produces images with as low as 0.4-mm isotropic spatial resolution. Manuscripts showing approximately 90% sensitivity and 90% specificity for greater than 50% coronary stenosis have consistently been reported with 16-slice scanners [18–21]. Several manuscripts in press have documented that the 64-slice approach also results in very high sensitivity and specificity for CAD and it appears to be associated with a smaller number of uninterpretable segments due to motion or the presence of coronary calcium [22–30]. With the 64-slice scanners, covering between 20 and 40 mm with each rotation, fewer heartbeats are required for acquisition, and contrast volumes of less than 100 cm^3 are routine. The low contrast dose reduces problems associated with higher contrast loads in terms of potential nephrotoxicity, of particular concern if the CT findings result in diagnosis of a condition that requires urgent contrast coronary angiography.

The most common protocol involves the administration of 100 mg atenolol 1 hour before scanning to slow the heart rate (unless the baseline heart rate is less than 60 beats per minute), and the insertion of an 18–20 gauge IV for the power injection of contrast. After placement of electrodes for R-wave markers, the patient lies on the CT table, and a scout film is obtained to localize the heart. As with the CCS acquisition, imaging is performed in a single breathhold, beginning shortly when sufficient contrast reaches the aorta. With some systems a small timing bolus (~10 cm^3) is required, while with others the arrival of the bolus can be accurately timed automatically during the contrast injection of the CTA study itself. The entire coronary CTA procedure can be performed in approximately 10 minutes, and rapid reconstruction possible with new computer systems makes the study available for final interpretation within a few minutes.

Interpretation of coronary CTA

Currently, interpretation relies on visual assessment of the CTA data on a three-dimensional workstation. While the axial images provide perhaps the most useful information for this purpose, it is routine to take advantage of the three-dimensional data sets, which, due to the isotropic voxels of the recent generation systems, can be viewed in any orientation without significant reduction in image resolution. Despite early developments of software intended to objectify the assessment of stenosis, these software programs are not yet validated for routine clinical use. Thus, there is a great deal of subjectivity at the present time in the assessment of coronary stenosis.

Of additional note, coronary CTA can visualize not only the vessel lumen but also the wall, potentially allowing the noninvasive assessment of the presence and the size of noncalcified coronary plaque [31], but this assessment is even more difficult at the present time than the assessment of coronary stenosis. Potentially, this approach can also become of value in the emergency department setting, and has the potential to provide assessments of pulmonary embolism, acute coronary syndrome, and aortic dissection in a single study (i.e., "triple rule out"). Figure 14.4 shows an example of a normal 16-slice coronary CTA from our

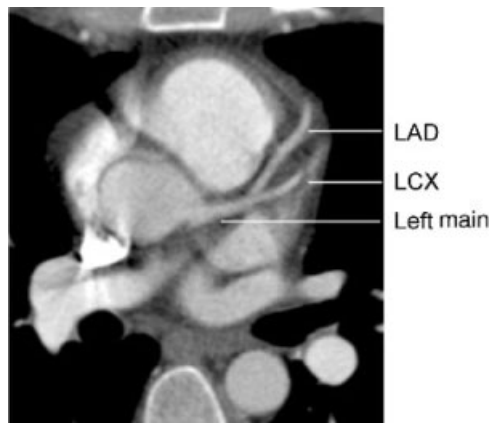

Figure 14.4 Example from our laboratory of a normal coronary CTA using a 16-slice MSCT scanner (Philips).

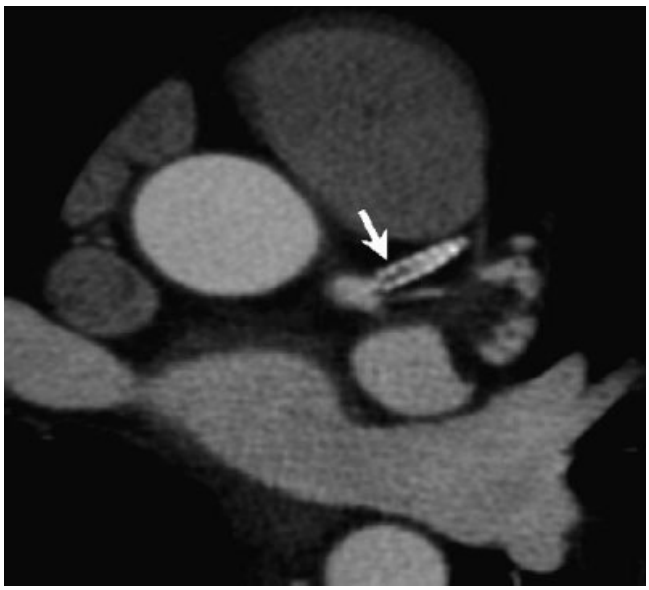

Figure 14.5 An example of a 64-slice CTA (Siemens) in a 33-year-old male with chest pain who had PCI with stent to LAD nearly three years ago. CTA revealed a nearly obstructive lesion (arrow) within the proximal portion of the stent of LAD. Conventional coronary angiography after the showed subtotal stenosis of proximal LAD following by restenosis in the stent.

laboratory, and Fig. 14.5 illustrates a published 16-slice example of coronary stenosis [20].

While reimbursement for coronary CTA has not yet been broadly established, it is likely that reimbursing will be accepted for coronary CTA very shortly. Currently, the Centers for Medicare and Medicaid Services (CMS) have implemented procedural codes for tracking utilization of CTA.

Limitations of coronary CTA

The principal limitation of coronary CTA, given the most recent generation scanners, is the presence of dense calcification of the coronary arteries. While modest amounts of calcification do not pose a problem for these scanners, with dense calcification it is not possible to assess the degree of luminal obstruction within the calcified zone. Other limitations include the need for a regular heart rhythm and a relatively low heart rate (usually considered less than 65 as noted above). To date, it is not possible to perform adequate CTA in patients with atrial fibrillation. Additionally, a tendency of the coronary CTA to overestimate the degree of stenosis has been described, resulting in a frequent need for a confirmatory functional test after the anatomic CTA reveals a borderline stenosis [32]. Of course, coronary CTA also involves radiation exposure to the patient. However, with beam modulation, involving full beam x-ray exposure only during the portion of the cardiac cycle with the least coronary motion – now standard on most systems, the amount of radiation associated with these procedures becomes similar to that received with the standard nuclear cardiology procedures.

SPECT/CT and PET/CT

The availability of PET/CT and SPECT/CT will add further complexity to the concepts regarding appropriate selection of tests, with their ability to provide both detection of coronary stenosis and assessment of functional significance [33]. With the development of cardiac dedicated CT/PET and CT/SPECT systems, it may be that a large body of data will be available in the future providing information regarding coronary calcium, coronary stenoses, and stress-induced ischemia. Such databases would be a source of evidence regarding which test or combination of tests is the most appropriate in a given setting. Since rest/stress PET or SPECT studies could be performed as a routine in conjunction with coronary CTA, the possibility of taking "all comers" regardless of the amount of coronary calcium that they have would enhance the usefulness of the noninvasive coronary angiography. One of the main potential advantages of SPECT/CT and PET/CT in cardiology may be that of assessing plaque vulnerability – through the combination of CT for the plaque volume and PET or SPECT assessment of an aspect of plaque activity (see below).

Contrast CT for assessment of left ventricular volumes, ejection fraction, and mass

The data sets that are used for coronary CTA contain the information that can be used to reconstruct the ventricular data to assess left ventricular volumes, ejection fraction, and mass. With most current systems, these reconstructions can be performed obtaining 8–10 frames per cardiac cycle. From these reconstructions, it has been demonstrated that left ventricular volumes and left ventricular ejection fraction measurements can be obtained [34]. Currently, these measurements generally require manual assignment of regions of interest. There is a slight underestimation of left ventricular ejection fraction due to the limited number of reconstructed frames, as has been reported with eight-frame gated SPECT.

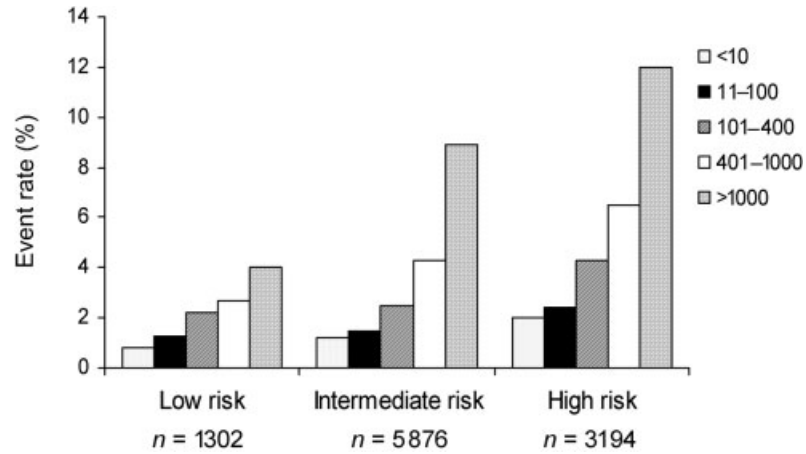

Figure 14.6 Risk stratification for each category of Framingham risk (from low to high) according to calcium score ($p < 0.001$ across risk groups). Event rate is predicted mortality at 5 years. (Adapted with permission from [37].)

Contrast CT for assessment of myocardial scar or necrosis

Recently, it has been shown that a second CT scan with lower x-ray dose, obtained a few minutes after the contrast injection, provides an opportunity to visualize areas of infarcted myocardium as regions of increased myocardial concentration of contrast, directly analogous to the delayed enhancement imaging with CMR described in Chapter 13. Unlike CMR, this application of CT could be applied in patients with pacemakers or metallic implants, but it would increase the radiation burden of the examination (though at reduced dose compared with the CT angiogram).

Prognostic applications of cardiac CT: CCS

The prognostic applications of gated MPS are the subject of the entirety of Chapter 8. There has not yet been sufficient time to gain experience with the prognostic implications of coronary CTA. The coronary CTA and the CCS also have potentially wide prognostic applications. In contrast to MPS, however, which provides useful information across the spectrum of patients with *known* as well as suspected CAD, it is not considered likely that the assessment of CCS will provide incremental prognostic discrimination in patients with known CAD. In such patients prognosis is governed more by functional parameters such as ischemia and left ventricular function than by measurements of atherosclerotic disease burden. Rather, the principal prognostic value of CCS is likely to reside in asymptomatic patients with a low to intermediate likelihood of CAD (e.g., 15–50% range) based on age, gender, and risk factors, which is basically another way of expressing a group with intermediate long-term risk by Framingham Risk Score (FRS) [30,35,36].

Prognostic significance of CCS

A large number of studies have demonstrated that CCS provides incremental prognostic information over conventional risk factors in assessing the risk of hard cardiac events. For example, a publication of results in over 10,000 asymptomatic patients followed over 5 years for all-cause mortality demonstrated that in both men and women the previously described categories for degrees of CCS abnormality were strongly predictive of all-cause mortality and that CCS provided significant incremental information over that provided by conventional risk factor analysis alone (Fig. 14.6) [37]. Similarly, Kondos et al. [38] demonstrated in 37-month follow-up of 5635 initially asymptomatic low- to intermediate-risk adults (1484 women) that cardiac events (death, MI, or revascularization) were predicted by the CCS in both genders using multivariable analysis. Similarly, Greenland et al. [35] demonstrated that the CCS adds to the FRS in prediction of nonfatal MI or cardiac death in asymptomatic individuals. Their conclusion from their data is consistent with the recommendations from the Bethesda conference supporting the concept that the CCS is useful for risk assessment in patients with an intermediate risk category. Regarding the definition of the intermediate risk category, while the consensus document of the Bethesda conference suggested this category should be expanded to 6–20% rate of hard cardiac event over 10 years (which would detect more women than the more commonly used 10–20% range), others still consider that this range should be 10–20%, since even with the relatively narrow range, there is a large proportion of the adult population of the United States (11.9%) that would be in need of testing [39,40].

Most recently, two prospective, population-based trials have demonstrated the incremental prognostic value of CCS over the traditional Framingham risk assessment.

The St. Francis Heart Study [41] determined relationship of CCS by EBT to standard coronary disease risk factors and C-reactive protein in the prediction of atherosclerotic cardiovascular disease events in 4613 asymptomatic persons aged 50–70 who underwent electron beam computed tomographic scanning of the coronary arteries and were followed up at a mean of 4.3 years. One hundred nineteen had sustained at least one atherosclerotic cardiovascular disease event. For CCS threshold greater than 100 vs. less than 100, relative risk was 9.6 (6.7–13.9 95% CI) for all atherosclerotic cardiovascular disease events, 11.1 (7.3–16.7 95% CI) for all coronary events, 3 and 9.2 (4.9–17.3 95% CI) for nonfatal MI and death. The CCS predicted coronary disease events independently of standard risk factors, and C-reactive protein ($p = 0.004$), was superior to the Framingham risk index in the prediction of events (area under the receiver operating characteristic curve of $0.79 + 0.03$ vs. $0.69 + 0.03$, $p = 0.0006$), and enhanced stratification of those falling into the Framingham categories of low, intermediate, and high risk ($p < 0.0001$) [41]. In a second prospective study, Taylor et al. reported a prognostic population-based study of a younger, male cohort [42]. Of a cohort of 2000 nonreferred, asymptomatic, healthy men and women aged 40–50 years, incident MI, acute coronary syndromes, and sudden cardiac death were ascertained via annual telephonic contacts, with follow-up (mean 3.0 ± 1.4 years, range 1–6 years) in 99.2% of the cohort.

A total of nine acute events occurred in men at a mean age of 46 years, including 7 of 364 men with coronary calcium (1.95%) and 2 of 1263 men without coronary calcium (0.16%; $p < 0.0001$ by log-rank). No events occurred in women. In young men, the presence of any coronary calcium was associated with an 11.8-fold increased risk for incident coronary heart disease ($p = 0.002$) in a Cox model controlling for the FRS. Among those with CAC present, the risk of coronary events increased incrementally across tertiles of coronary calcium severity (hazard ratio 4.3 per tertile). In this study of relatively young individuals, the authors concluded that the presence of coronary artery calcification provides substantial, cost-effective, independent prognostic value in predicting incident coronary heart disease that is incremental to measured coronary risk factors [42].

The evidence is now strong that CCS is valuable for purposes of risk assessment of asymptomatic patients with intermediate clinical risk. There is now, therefore, widespread support that third-party carriers should pay for testing in this patient group, rather than having it be a test only for patients who can afford to pay for it.

The CCS may be *limited* in ruling out disease in *symptomatic* patients. While several reports have shown that approximately 95% of patients suffering a first MI have an abnormal CCS within days of the MI, implying that it is unusual for coronary atherosclerosis to result in acute MI before the development of any coronary calcification [8,43–45], the increasing experience with CT coronary angiography suggests that the latter, rather than the CCS, will become the most commonly used CT method of choice to triage these patients, due to the observation that approximately 5% of patients with documented acute infarction have no coronary calcium. The images illustrated in Figs. 14.7 and 14.8 illustrate this potential drawback of relying on the CCS to rule out an acute coronary syndrome.

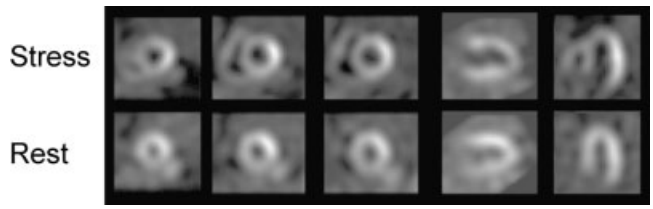

Figure 14.7 Exercise stress sestamibi/rest thallium-201 MPS images in a 64-year-old male with recent onset angina raising suggesting unstable CAD. The clinical and ECG responses to stress were ischemic. Large reversible defects are seen in the anterior, septal, inferior, and apical walls consistent with a critical LAD stenosis.

Guiding patient management decisions by CCS

One of the important applications of noninvasive testing is in determining the appropriate therapy in an individual patient. In asymptomatic patients with coronary risk factors, the CCS may be of particular use in this regard. For

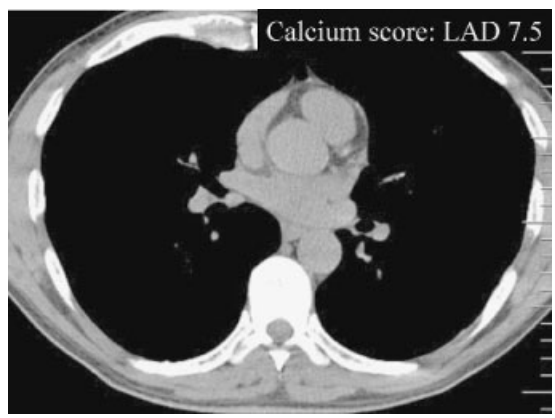

Figure 14.8 EBT for CCS performed as part of a research study after MPS of the patient in Fig. 11.7 shows minimal calcification in LAD – an almost imperceptible small calcified area was seen (CCS 7.5). Subsequent coronary angiography revealed 80% stenosis in proximal LAD and subtotal occlusion of first diagonal branch. This case example illustrates how an acute coronary syndrome might be misclassified by noncontrast CT alone.

example, in patients with borderline cholesterol elevations or borderline hypertension, the CCS can help the primary care physician decide whether or not to treat aggressively to prevent the development of clinical atherosclerotic disease. On the basis of available data, the CCS may be used to determine the appropriateness and aggressiveness of medical therapies, such as statin use, or need for stress testing, among patients presenting with an intermediate 10-year risk of MI or cardiac death by the FRS.

One group of patients affected in this manner are those with the metabolic syndrome – characterized by varying combinations of abdominal obesity, insulin resistance, lipid abnormalities, and hypertension, many of whom are at intermediate risk. Approximately, one-fourth of these patients have a CCS greater than or equal to 75th percentile, which has been designated by the National Cholesterol Educational Program as a criterion to stratify the patient into more intensive risk factor management [46]. The use of the CCS to guide management is one of the most common reasons that the test is currently ordered by physicians.

Part of guiding management decisions is the manner in which a test result affects the choice of subsequent testing. From the above discussion, it would seem clear that asymptomatic patients with extensive coronary atherosclerosis by CCS would benefit from additional testing for ischemia. This concept fits with recommendations made years ago by Rumberger [47]. For purposes of cost-effectiveness, it would not be appropriate for all patients with atherosclerosis who had undergone EBT to be referred for further testing.

There are now several published manuscripts that have been helpful in determining the CCS threshold above which asymptomatic patients merit referring for stress imaging. He et al. [48] evaluated the frequency of stress-induced ischemia by MPS in patients who had undergone EBT scanning. These investigators evaluated 370 patients undergoing both MPS and EBT for coronary calcification. They divided their patients into the traditional categories of no (CCS 0), minimal (CCS 1–10), mild (CCS 11–100), moderate (CCS 101–399), and extensive coronary calcium (CCS >400) [47]. Only 1 patient of more than 100 with CCS less than or equal to 100 had abnormal MPS. Twelve percent of patients with moderate CCS had abnormal MPS and 47% of patients with extensive CCS had abnormal MPS. Moser et al. [49] recently reported results of combined SPECT and CCS testing in 102 patients, with these investigators employing MSCT for CCS. In this smaller group, none of 19 patients with a CCS less than 100, 6 of 51 (12%) patients with CCS 100–400, and 13 of 32 (41%) patients with CCS greater than or equal to 400 had an abnormal SPECT study. They concluded that a CCS threshold of greater than 400 was useful in determining the need for subsequent MPS.

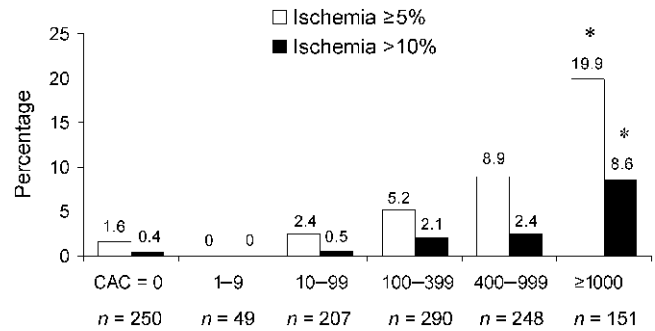

Figure 14.9 The frequency of an ischemic MPS (≥5% ischemic) and of a moderate to severe ischemia (>10% ischemic) for patients divided into six CAC score groupings. *$p < 0.0001$ for trend. (Adapted with permission from [50].)

Data from our institution have confirmed the findings of previous studies with respect to the patients with CCS greater than or equal to 400 [50]. In 1195 consecutive patients with no history of CAD who had undergone EBT and MPS, among the patients with a CCS less than 100, MPS ischemia was rare, occurring in less than 2% of such patients [50]. This low frequency of ischemia with a CCS less than 100 was present in patients with and without clinical symptoms, although a trend toward more ischemia in symptomatic patients with scores 10–99 was observed. As the CCS increased in magnitude above 100, the frequency of myocardial ischemia on MPS increased progressively (Fig. 14.9). Among patients with CCS exceeding 1000, 20% manifested an ischemia by MPS. Our results further indicate that the likelihood of myocardial ischemia by MPS is more tightly related to the absolute CCS rather than age-gender-stratified CCS percentile. These three studies were concordant that the CCS greater than 400 threshold generally appeared appropriate for guiding the decision to refer for stress MPS.

Another aspect of our study was of particular importance in documenting the insensitivity of MPS for detecting coronary atherosclerosis (in contrast to detecting patients with hemodynamically significant CAD). Of 1119 patients with normal MPS, a large proportion had high enough CCS that there would be consensus that aggressive medical management is warranted: 56% had CCS greater than 100 and 31% had CCS greater than 400 (Fig. 14.10). These findings suggest that if testing begins with MPS in a given patient, further assessment of atherosclerotic burden by CAC testing may be useful in assessment of the need for aggressive attempts to prevent coronary events.

In a more recent study, we further examined the relationships between CCS and MPS according to the presence of the metabolic syndrome [51]. In patients with the metabolic syndrome and CCS 100–400, the frequency of abnormal MPS was as high as in patients with no

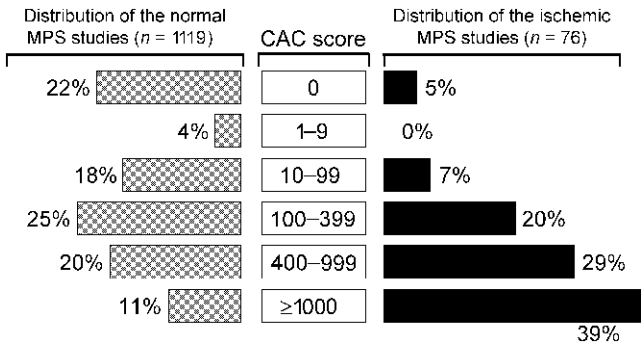

Figure 14.10 Distribution of CAC scores for the 1119 patients manifesting a normal MPS (left) and the 76 patients with an ischemic MPS (right). (Adapted with permission from [50].)

metabolic abnormality with CCS greater than or equal to 400 (15.0% vs. 14.8%, respectively). Thus, in this group of patients a lower threshold for determining the need for assessment of stress ischemia may be indicated; i.e., additional testing with MPS might be appropriate in patients with the metabolic syndrome and CCS greater than or equal to 100. Similarly, Anand et al. [52] reported that there was an intermediate to high frequency of abnormal MPS studies in diabetic patients with CCS greater than or equal to 100.

The data from these studies suggest an important distinction between short- and long-term risk. Whereas a low CCS with a high percentile ranking in young patients may be indicative of *long-term* risk for developing cardiac events [53–55], this same score is probably not predictive of *short-term* risk, given the finding that such patients rarely have evidence of ischemia on MPS. Thus, further testing by MPS of patients found to have high CCS percentile but a CCS less than 100 would not appear to be needed in most patients. In contrast, MPS appears excellent for determining short-term risk, but due to the insensitivity of the method for detecting subclinical atherosclerosis, MPS may not be as effective as atherosclerosis imaging in determining long-term risk.

Based on the available data, the following three summary statements might be made regarding combined MPS and CCS testing: (1) It appears that the referral of patients for MPS is generally not needed when the CCS is less than 100 due to the very low likelihood of observing inducible myocardial ischemia in such patients. Conversely, when the CCS is greater than or equal to 400, stress imaging would appear to be generally beneficial, because the frequency of inducible ischemia is substantial, even in asymptomatic patients. (2) CCS of 100–400 constitutes a "gray zone" relative to the issue of who may require stress test referral following CAC imaging. For CAC scores in this range, clinical factors, such as gender, concomitant chest pain, or specific combinations of coronary risk factors, are likely to determine whether ischemia testing is needed, but prospective studies are needed in this regard. (3) The wide range of CCS in patients with normal MPS studies exposes an important limitation relevant to all forms of stress testing: they do not effectively screen for subclinical atherosclerosis [50]. However, there are no available data to compare the relative short- and long-term risk for cardiac events among patients with various combinations of MPS results and CAC scores, such as those presenting with the combination of very high CAC scores but normal MPS results. It is reasonable to hypothesize that such patients might be at low *short-term* risk but high *long-term* risk for cardiac events, as supported by a preliminary analysis [56]. If born out by further study, CAC could then be unmasking a subgroup of patients who would receive more aggressive anti-atherosclerotic intervention than would have been indicated based on the results of MPS testing alone. Accordingly, future study that incorporates the prognostic follow-up data from patients undergoing both studies would now be of interest, to determine which patients with normal stress imaging tests are best suited for undergoing *subsequent* CAC scanning.

Prognostic applications of coronary CTA

To date, the majority of published reports dealing with coronary CTA using MSCT have described the diagnostic accuracy of this test. As discussed extensively in the first part of this review [57], many published manuscripts have reported high sensitivity and specificity of 16-slice MSCT for detection of CAD [58], and manuscripts are beginning to be reported with the 64-slice scanners [25–30,59]. One of the key advantages of coronary CTA over nuclear testing is that the method is very unlikely to be normal in patients in whom revascularization would be warranted, in contrast to MPS in which balanced reduction in flow can occasionally result in a normal study despite the presence of severe and extensive CAD.

It should be noted that whether CCS should also be measured in patients undergoing coronary CTA is a matter of controversy, due to the added radiation burden – approximately 25% as much as the coronary CTA. While the CCS cannot be accurately measured during the contrast infusion acquisition of the CTA itself, many investigators consider the ability to assess the presence and extent of coronary calcium adequate to provide sufficient information regarding early atherosclerosis to guide management decisions without the additional radiation exposure. This visual estimate of the coronary calcium is routinely reported with coronary CTA. The current clinical applications of coronary CTA are listed in Table 14.2.

Table 14.2 Clinical applications of CTA.

- Screening: no application
- Diagnosis of CAD
  - Intermediate likelihood of disease
  - After equivocal/discordant stress imaging
  - Coronary anomalies
  - Prior to valvular surgery
  - Nonischemic vs. ischemic cardiomyopathy
  - Acute chest pain
  - Bypass graft patency/location
- Risk stratification (known CAD)
  - After equivocal/dicordant stress imaging

While the diagnostic use of CTA as the first test in symptomatic patients with a low to intermediate likelihood of CAD is increasingly being accepted, there is no data yet regarding the use of CTA for risk stratification of patients with known or suspected CAD. There has not yet been adequate time for the collection of the prognostic data needed to fully investigate this potential of CTA with MSCT. Nonetheless, since the extent and severity of coronary obstructive lesions on selective coronary angiography has been known to be a potent predictor of outcome and to identify subgroups of patients likely to benefit from revascularization [60], it is likely that coronary CTA will also have strong prognostic power. In some patients, sufficiently high risk may be defined by the location of severity of CT defined coronary stenosis, leading directly to selective coronary angiography after the CT procedure. However, the ability of selective coronary angiography to predict benefit from revascularization in randomized trials has been shown to be dependent on the presence of inducible ischemia [61,62]. Furthermore, in these previous trials, inducible ischemia was evaluated only by traditional ECG stress testing [60,61]. We consider it likely that in a large proportion of patients found to have coronary lesions by CTA, further assessment of the extent and severity of ischemia by SPECT or PET will prove useful in effective identification of patients who are likely to derive a survival benefit from coronary revascularization.

Conceptual framework for the use of cardiac CT and gated myocardial perfusion SPECT or PET in patients with known or suspected CAD

Screening for coronary atherosclerosis: *asymptomatic* patients

Figure 14.11 illustrates our conceptual approach to the use of atherosclerosis imaging, coronary CTA, and nuclear testing in CAD diagnosis and risk stratification with respect to *screening of asymptomatic patients*. While screening for CAD with imaging is not yet widely reimbursed, the approach is gaining acceptance. In the asymptomatic patient, the initial assessment involves estimation of the 10-year risk of developing MI or cardiac death, based on measures such as the FRS, as recommended by standard ATP III guidelines with addition of family history of early CAD and assessment of the metabolic syndrome. Then, patients are assigned to groups corresponding to less than 10%, 10–20%, and greater than 20% 10-year risk of MI or cardiac death categories recently advocated as low, intermediate, and high risk [63]. Patients with a very low risk would only need counseling regarding diet and exercise. Patients with a high 10-year risk (>20%) are considered to have a CAD risk equivalent, meriting treatment using secondary prevention guidelines. In these patients, atherosclerosis testing is not generally recommended, although it might be appropriate in order to determine the need for ischemia testing. In this regard, on the basis of data from the Detection of Ischemia in Asymptomatic Diabetics (DIAD) study [64], in conjunction with data from Anand et al. regarding the relationship between CCS and ischemia in diabetics [52], it has been suggested that CCS might be routinely performed in asymptomatic diabetic adults. Given the high frequency of silent ischemia in diabetics, atherosclerosis imaging may be useful to identify those with advanced coronary atherosclerosis in whom stress MPS would be appropriate. The remaining large group of patients with an intermediate 10-year risk (10–20%) are excellent candidates for atherosclerosis

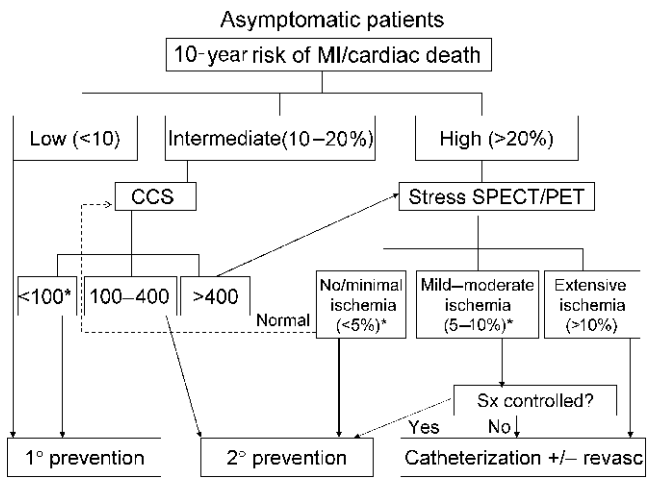

Figure 14.11 Approach to the use of coronary calcium scanning and nuclear testing in screening for CAD in asymptomatic patients (see text). *Beware ancillary markers. Abbreviations: CCS, coronary calcium score by electron beam tomography or multislice spiral computed tomography; revasc: revascularization.

screening, currently using the CCS or the carotid intimal-medial thickness (IMT).

Patients would then have the intensiveness of their medical therapy guided by the degree of CCS or IMT abnormality. As shown in Fig. 14.11, scores less than 100 are generally considered low enough that aggressive medical therapy may not be needed. Scores greater than 100 are generally accepted as the cut-off for recommending aggressive medical therapy with target low-density lipoprotein less than 70 and the target blood pressure 120/80 mm Hg [63]. Patients with scores greater than or equal to 10 but less than 100 might be considered as appropriate for aggressive medical therapy when CCS is greater than or equal to 90th percentile for age and gender [50], although the exact thresholds remain controversial. Regarding further testing, patients with CCS greater than 400 would be candidates for further testing with MPS for purposes of risk–benefit assessment with respect to the possible need to consider revascularization. The specific cut-points for CCS shown in Fig. 14.11 are somewhat arbitrary. In this regard, an increasing proportion of cardiologists interested in prevention are treating aggressively at cutoffs lower than 100. The exact cutoff above which patients should be referred for stress imaging is also unclear; however, as noted above, in asymptomatic patients, the threshold of 400 for this referral may be appropriate. In the CCS category 100–400, it would not be cost-effective to refer all patients for myocardial perfusion scanning; however, if tailoring this referral to the individual patient, based on age, sex, and risk factors, selective referral for stress imaging might be appropriate. In this regard, recent manuscripts have suggested that the category of 100–400 would deserve testing if the patient is diabetic [52] or has the metabolic syndrome [51].

A modification of this approach has recently been adopted by the Association for the Eradication of Heart Attacks (AEHA) in developing a National Screening for Heart Attack Prevention and Education (SHAPE) program, as shown in Fig. 14.12 [65]. In an attempt to *eradicate* heart attacks rather than to simply reduce their frequency, this group recommends screening of all men over age 45 and women over age 55, since a substantial proportion of heart attacks occur in patients with low Framingham risk. After atherosclerosis imaging, the intensity of therapy and the need for ischemia testing is governed by the post-atherosclerosis imaging assessment of risk. In general, the use of coronary CTA or MPS would not be recommended for initial testing, as reflected for the latter in recent guidelines [66]. However, in some high-risk asymptomatic individuals, particularly those with high-risk occupations, MPS or coronary CTA might be appropriate.

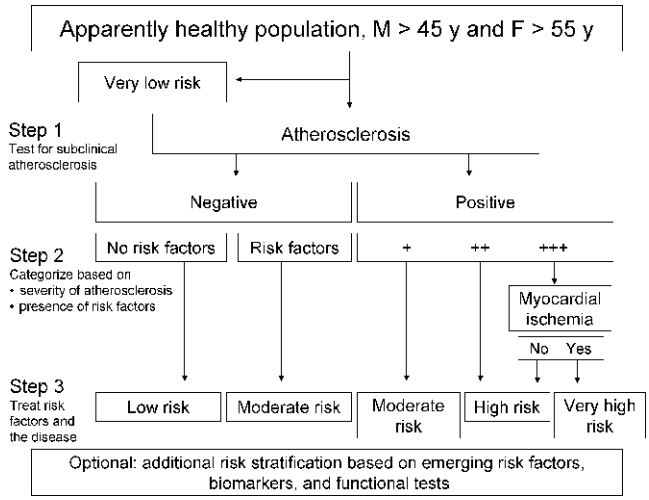

Figure 14.12 An approach to screening for atherosclerosis proposed in the SHAPE program [65].

Detection and management of CAD: *symptomatic* patients

Figure 14.13 illustrates our approach to *patients with symptoms* of possible ischemic origin in the setting where 16-slice or greater coronary CTA is available. In symptomatic patients, the pretest likelihood of angiographically significant CAD, employing age, gender, risk factors, and symptoms, as initially suggested by Diamond et al. [3,67], becomes the starting point for the clinician – rather than the 10-year risk used for screening. While

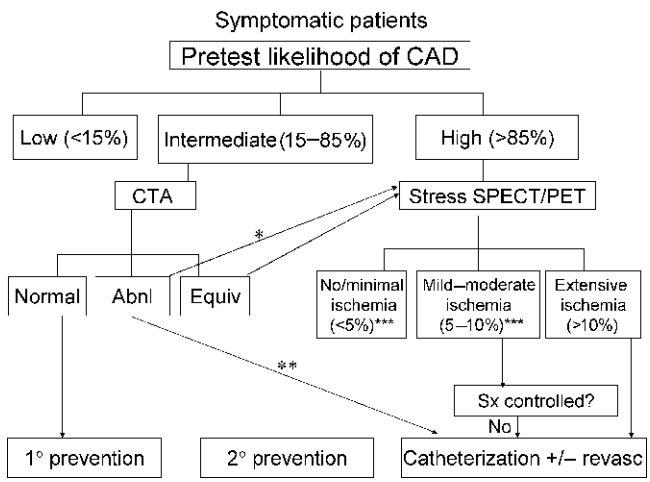

Figure 14.13 Approach to Diagnosis and Management of CAD in symptomatic patients using CTA and stress SPECT or PET. *No critical stenosis: (>90%); **critical stenosis (>90% proximal lesion); ***beware of ancillary markers (e.g., transient dilation, lung uptake, stunning). Abbreviations: Abnl, abnormal; CT angiography; CTA, coronary; Equiv, equivocal.

various pretest likelihood cut-points have been recommended, we have adopted the cut-points of 15 and 85% based on our prognostic observations [68], resulting in three likelihood groups: low (<15%), intermediate (15–85%), and high (>85%). In general, patients with chest pain symptoms or shortness of breath have at least a 15% likelihood of CAD. Since the value of diagnostic testing is greatest in patients with an intermediate likelihood of disease, patients with an intermediate likelihood of CAD (15–85%) become excellent candidates for the CT coronary angiogram – the test with the highest accuracy, combining sensitivity and specificity. This patient group in general has an intermediate risk of developing a clinical cardiovascular event over 10 years (10–20%) [63], as described for the asymptomatic patients above. While existing guidelines recommend exercise testing *without* imaging for these patients [69], since coronary CTA provides a far more sensitive test for CAD in this population, we consider it more useful than the exercise ECG in selecting patients for aggressive medical management and for additional testing. After the coronary CTA, further testing and therapy would be guided by the posttest likelihood of CAD and the extent and severity of the observed disease. If the coronary CTA (including the estimated or measured CCS) is normal, primary prevention would be appropriate. It is likely that the definitive ability to rule out CAD will become a principal driving force in the application of coronary CTA. If critical proximal stenoses are observed (e.g., >90%), direct referral to selective coronary angiography would appear to be recommended. If the results of the coronary CTA are equivocal for a proximal coronary stenosis or if the CTA is clearly abnormal but the anatomy is not "compelling" regarding the need for revascularization, referral for ischemia testing with MPS would appear appropriate to determine the need to consider coronary revascularization. In older men and very elderly women with an intermediate likelihood of CAD, the frequency of a CCS of greater than 400 is quite high. In these patients, it may be more appropriate to begin with the CCS and MPS, since in the presence of dense coronary calcium, coronary CTA is nondiagnostic for the presence of CAD [20].

Patients deemed to have a high (>85%) likelihood of CAD or those with known CAD are often directly catheterized, particularly if they have symptoms that persist after maximal medical therapy. In those without limiting symptoms, it may be most effective to start with MPS for purposes of determining the need for consideration of revascularization. Since these patients in general have a greater than 20% 10-year risk of CAD, they would usually already be suited for secondary prevention treatment. The likelihood of disease is sufficiently high that it is generally assumed that their symptoms are from the disease. We have recently reported data supporting the effectiveness and cost-effectiveness of this approach [70]. Similar findings have also been reported by the Mayo Clinic group [71], who showed that even in patients with a normal resting ECG, if the clinical risk of CAD is high, a low-risk treadmill test alone is insufficient to result in a low risk of cardiac events. If the resting ECG is abnormal or otherwise uninterpretable (e.g., digoxin or left bundle branch block) or the patient cannot exercise adequately, there is concordance of opinion that direct referral to a stress imaging procedure is appropriate [66,69].

If stress imaging is performed, patients with extensive ischemia by nuclear testing (or those who are for other reasons considered to be at high risk by clinical assessment after stress imaging) would be candidates for coronary angiography. As discussed in Chapter 8, patients with ischemia of lesser magnitude might be candidates for angiography depending on the clinical presentation. In this regard, we have described that there are a number of clinical and nonperfusion MPS indicators of risk that should be considered in making the decision regarding the need for coronary angiography (Table 14.3). Patients considered to be at high risk despite having only 5–10% ischemia include low left ventricular ejection fraction [72], transient ischemic dilation [73], lung uptake [74], diabetes [75,76], atrial fibrillation [77]. In patients with equivocal MPS or those with marked discordance in between the clinical or ECG responses to stress and the MPS results, coronary CTA *after* MPS might be useful.

Figure 14.14 illustrates our approach to the symptomatic patient in settings where the coronary CTA is not available, contraindicated (e.g., allergy to contrast, renal failure), or cannot be accurately performed (e.g., atrial fibrillation). While not yet shown to be cost-effective in the lower range of intermediate likelihood of CAD (15–50%), most investigators would agree that MPS would appear to be the initial test of choice in patients with a high intermediate likelihood (≥50–85%) or high likelihood of CAD. In

Table 14.3 Clinical (nonnuclear) and nuclear factors useful in guiding the decision to proceed with selective coronary angiography after stress MPS.

Nonnuclear factors	Nuclear factors
Symptoms/clinical presentation	Extent and severity of perfusion defects
Comorbidities (e.g., diabetes, metabolic syndrome)	Stress, rest, late
Exercise duration	Lung uptake
Exercise hypotension	Transient ischemic dilation
Heart rate reserve and recovery	Left ventricular function
Duke treadmill score	Left ventricular ejection fraction
Type of stress	
Hemodynamic response to pharmacologic stress	Left ventricular volume
ECG evidence of ischemia	

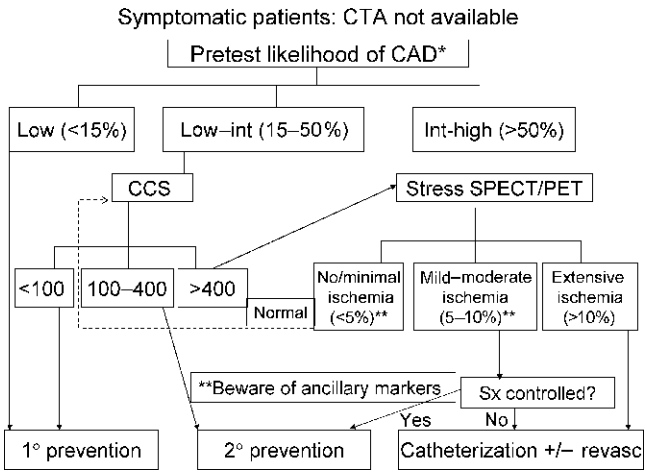

Figure 14.14 Approach to Diagnosis and Management of CAD in symptomatic patients using CCS, stress SPECT or PET, in situations where coronary CTA is unavailable. This approach is the same as that employed for screening, except that the starting point becomes the likelihood of CAD rather than 10-year risk of events. *Based on age, sex, symptoms, and risk factors; **beware ancillary markers.

those within the lower intermediate range, it may be sufficient to perform atherosclerosis imaging as the initial step (Fig. 14.14). In those sent directly to MPS, the management after MPS would be as described in the previous paragraph. An important distinction, however, is worthy of mention. In selected patients with normal or nearly normal nuclear scans, CCS might be appropriate after MPS in order to evaluate the extent of atherosclerosis and help guide medical management decisions [78], and to avoid missing extensive atherosclerosis simply because there is no stress-induced ischemia. While atherosclerosis imaging may not be needed in patients who are already following an aggressive medical management approach using secondary prevention guidelines, a CCS in this setting may help motivate patients to follow medical approaches to the control of CAD, as well as to guide the intensity of medical management in settings in which the need for secondary prevention is not clear. We have also found that CCS after MPS is very effective in defining further management in patients with equivocal MPS results, occasionally helping recognize patients in whom the MPS severely underestimates the ischemic burden.

In patients with poor ventricular function, the approach to testing often includes the assessment of myocardial viability as discussed in Chapter 10 (and with CMR in Chapter 13). While the cardiac CT with contrast may have some potential in this regard, at present the assessment of these patients most commonly involves scintigraphic assessment of ischemia and viability with PET or SPECT, or the assessment of scar and contractile reserve with CMR (Chapter 13), or dobutamine echocardiography.

Conclusion

The extent of CAC in asymptomatic patients provides incremental information over traditional risk factor assessment in the identification of patients with subclinical atherosclerosis who may benefit from aggressive medical therapeutic options. Coronary CTA, with its very high sensitivity, high specificity, and its characteristic of being highly unlikely to miss the presence of high-risk angiographic disease, is likely to become a first-line diagnostic test in symptomatic patients with an intermediate likelihood of CAD. However, in patients with a high likelihood of CAD or known CAD, there is greater information gained and far more outcome data with assessment of the extent and severity of ischemia using myocardial perfusion SPECT. The anatomic (CT) and functional imaging (SPECT/PET) methods are complementary, each playing a role in particular patient settings, and at times being useful in the same patient. CMR offers the opportunity to assess both anatomic and functional conditions effectively, although CT is superior to CMR for noninvasive coronary angiography at the present time. We consider it likely that with an increased emphasis on prevention and a concomitant aging of the population, many forms of noninvasive cardiac imaging will continue to grow, with nuclear cardiology continuing to grow but at a slower rate than observed over the last 20 years, partly related to growth in the application of cardiac CT and to a lesser extent CMR.

Acknowledgments

Funded in part by grants from The Eisner Foundation, BMS Medical Imaging, and Astellas Healthcare.

References

1. Holes GW, Ruggles HE. Roentgen interpretation. 3rd edn. Philadelphia: Lea & Febiger; 1926:21–27.
2. Blankenhorn DH, Stern D. Calcification of the coronary arteries. American Journal of Roentgenology, Radium Therapy and Nuclear Medicine 1959;81(5):772–777.
3. Diamond GA, Staniloff HM, Forrester JS, Pollock BH, Swan HJ. Computer-assisted diagnosis in the noninvasive evaluation of patients with suspected coronary artery disease. Journal of the American College of Cardiology 1983;1(2, Pt. 1):444–455.
4. Becker CR, Kleffel T, Crispin A, et al. Coronary artery calcium measurement: agreement of multirow detector and electron beam CT. American Journal of Roentgenology 2001;176(5):1295–1298.
5. Daniell AL, Wong ND, Friedman JD, et al. Concordance of coronary artery calcium estimates between MDCT and

electron beam tomography. American Journal of Roentgenology, in press.
6. Gerber TC, Kuzo RS, Morin RL. Techniques and parameters for estimating radiation exposure and dose in cardiac computed tomography. International Journal of Cardiovascular Imaging 2005;21(1):165–176.
7. Agatston AS, Janowitz WR, Hildner FJ, Zusmer NR, Viamonte M Jr, Detrano R. Quantification of coronary artery calcium using ultrafast computed tomography. Journal of the American College of Cardiology 1990;15(4):827–832.
8. Raggi P, Callister TQ, Cooil B, et al. Identification of patients at increased risk of first unheralded acute myocardial infarction by electron-beam computed tomography. Circulation 2000;101(8):850–855.
9. Cheng YJ, Church TS, Kimball TE, et al. Comparison of coronary artery calcium detected by electron beam tomography in patients with to those without symptomatic coronary heart disease. American Journal of Cardiology 2003;92(5):498–503.
10. Hoff JA, Chomka EV, Krainik AJ, Daviglus M, Rich S, Kondos GT. Age and gender distributions of coronary artery calcium detected by electron beam tomography in 35,246 adults. American Journal of Cardiology 2001;87(12):1335–1339.
11. Callister TQ, Cooil B, Raya SP, Lippolis NJ, Russo DJ, Raggi P. Coronary artery disease: improved reproducibility of calcium scoring with an electron-beam CT volumetric method. Radiology 1998;208(3):807–814.
12. Callister TQ, Raggi P, Cooil B, Lippolis NJ, Russo DJ. Effect of HMG-CoA reductase inhibitors on coronary artery disease as assessed by electron-beam computed tomography. New England Journal of Medicine 1998;339(27):1972–1978.
13. Glagov S, Weisenberg E, Zarins CK, Stankunavicius R, Kolettis GJ. Compensatory enlargement of human atherosclerotic coronary arteries. New England Journal of Medicine 1987;316(22):1371–1375.
14. Schmermund A, Denktas AE, Rumberger JA, et al. Independent and incremental value of coronary artery calcium for predicting the extent of angiographic coronary artery disease: comparison with cardiac risk factors and radionuclide perfusion imaging. Journal of the American College of Cardiology 1999;34(3):777–786.
15. Budoff MJ, Achenbach S, Duerinckx A. Clinical utility of computed tomography and magnetic resonance techniques for noninvasive coronary angiography. Journal of the American College of Cardiology 2003;42(11):1867–1878.
16. Ropers D, Baum U, Pohle K, et al. Detection of coronary artery stenoses with thin-slice multi-detector row spiral computed tomography and multiplanar reconstruction. Circulation 2003;107(5):664–666.
17. Nieman K, Cademartiri F, Lemos PA, Raaijmakers R, Pattynama PM, de Feyter PJ. Reliable noninvasive coronary angiography with fast submillimeter multislice spiral computed tomography. Circulation 2002;106(16):2051–2054.
18. Achenbach S, Giesler T, Ropers D, et al. Detection of coronary artery stenoses by contrast-enhanced, retrospectively electrocardiographically-gated, multislice spiral computed tomography. Circulation 2001;103(21):2535–2538.
19. Rensing BJ, Bongaerts A, van Geuns RJ, van Ooijen P, Oudkerk M, de Feyter PJ. Intravenous coronary angiography by electron beam computed tomography: a clinical evaluation. Circulation 1998;98(23):2509–2512.
20. Kuettner A, Beck T, Drosch T, et al. Diagnostic accuracy of noninvasive coronary imaging using 16-detector slice spiral computed tomography with 188 ms temporal resolution. Journal of the American College of Cardiology 2005;45(1):123–127.
21. Mollet NR, Cademartiri F, Krestin GP, et al. Improved diagnostic accuracy with 16-row multi-slice computed tomography coronary angiography. Journal of the American College of Cardiology 2005;45(1):128–132.
22. Leber A, Knez A, Ziegler FV, et al. Quantification of obstructive and nonobstructive coronary lesions by 64-slice CT: a comparative study with quantitative coronary angiography and intravascular ultrasound. Journal of the American College of Cardiology, in press.
23. Ropers D, Anders K, Lell M, et al. Noninvasive coronary artery imaging using 64-slice spiral computed tomography: initial experiences [abstract]. Circulation 2004;110:III–522.
24. Ropers D, Anders K, Baum U, Bautz W, Daniel WG, Achenbach S. Noninvasive coronary angiography by retrospectively ECG-gated 64-slice spiral computed tomography: initial clinical experiences [abstract]. Journal of the American College of Cardiology 2005;45:311A.
25. Ropers D, Rixe J, Anders K, Kuttner A, Baum U, Bautz W, Daniel WG, Achenbach S. Usefulness of multidetector row spiral computed tomography with 64- × 0.6-mm collimation and 330-ms rotation for the noninvasive detection of significant coronary artery stenoses. American Journal of Cardiology 2006 (Feb 1);97(3):343–348. (Epub 2005 Dec. 1.)
26. Fine JJ, Hopkins CB, Ruff N, Newton FC. Comparison of accuracy of 64-slice cardiovascular computed tomography with coronary angiography in patients with suspected coronary artery disease. American Journal of Cardiology 2006 (Jan 15);97(2):173–174. (Epub 2005 Nov 17.)
27. Leshchka S, Alkadhi H, Plass A, Desbiolles L, Grunenfedler J, Marincek B, Wildermuth S. Accuracy of MSCT coronary angiography with 64-slice technology: first experience. European Heart Journal 2005;25(15):1482–1487.
28. Raff GL, Gallagher MJ, ONeill WW, Goldstein JA. Diagnostic accuracy of noninvasive coronary angiography using 64-slice spiral computed tomography. Journal of the American College of Cardiology 2005;46:552–557.
29. Leber AW, Knez A, von Ziegler F, Becker A, Nikolaou K, Paul S, Wintersperger B, Reiser M, Becker CR, Steinbeck G, Boekstegers P. Quantification of obstructive and nonobstructive coronary lesions by 64-slice computed tomography a comparative study with quantitative coronary angiography and intravascular ultrasound. Journal of the American College of Cardiology 2005;46:147–154.
30. Mollet NR, Cademartiri F, Van Mieghem CAG, Runza G, McFadden EP, Baks T, Serruys PW, Krestin GP, de Feyter PJ. High-resolution spiral computed tomography coronary angiography in patients referred for diagnostic conventional coronary angiography. Circulation 2005;112:2318–2323.
31. Schoepf UJ, Becker CR, Ohnesorge BM, Yucel EK. CT of coronary artery disease. Radiology 2004;232(1):18–37.

32. Raff GL, Gallagher MJ, O'Neill WW, Goldstein JA. Diagnostic accuracy of noninvasive coronary angiography using 64-slice spiral computed tomography. Journal of the American College of Cardiology 2005;46(3):552–557.
33. Shaw LJ, Berman DS, Bax JJ, et al. Computed tomographic imaging within nuclear cardiology. Journal of Nuclear Cardiology 2005;12:131–142.
34. Schlosser T, Pagonidis K, Herborn CU, et al. Assessment of left ventricular parameters using 16-MDCT and new software for endocardial and epicardial border delineation. AJR American Journal of Roentgenology 2005;184(3):765–773.
35. Greenland P, LaBree L, Azen SP, Doherty TM, Detrano RC. Coronary artery calcium score combined with Framingham score for risk prediction in asymptomatic individuals. JAMA 2004;291(2):210–215.
36. Mosca L, Linfante AH, Benjamin EJ, et al. National study of physician awareness and adherence to cardiovascular disease prevention guidelines. Circulation 2005;111(4):499–510.
37. Shaw LJ, Raggi P, Schisterman E, Berman DS, Callister TQ. Prognostic value of cardiac risk factors and coronary artery calcium screening for all-cause mortality. Radiology 2003;228(3):826–833.
38. Kondos GT, Hoff JA, Sevrukov A, et al. Electron-beam tomography coronary artery calcium and cardiac events: a 37-month follow-up of 5635 initially asymptomatic low- to intermediate-risk adults. Circulation 2003;107(20):2571–2576.
39. Wilson PW, Smith SC Jr, Blumenthal RS, Burke GL, Wong ND. 34th Bethesda Conference: Task force #4 – how do we select patients for atherosclerosis imaging? Journal of the American College of Cardiology 2003;41(11):1898–1906.
40. Berman DS, Wong ND. Implications of estimating coronary heart disease risk in the United States population. Journal of the American College of Cardiology 2004;43:1797–1798.
41. Arad Y, Goodman KJ, Roth M, Newstein D, Guerci AD. Coronary calcification, coronary disease risk factors, C-reactive protein, and atherosclerotic disease events: the St. Francis Heart Study. Journal of the American College of Cardiology 2005;46:158–165.
42. Taylor AJ, Bindeman J, Feuerstein I, Cao F, Brazaitis M, O'Malley PG. Coronary calcium independently predicts incident premature coronary heart disease over measured cardiovascular risk factors: mean 3-year outcomes in the prospective army coronary calcium project. Journal of the American College of Cardiology 2005;46:807–814.
43. Schmermund A, Baumgart D, Gorge G, et al. Coronary artery calcium in acute coronary syndromes: a comparative study of electron-beam computed tomography, coronary angiography, and intracoronary ultrasound in survivors of acute myocardial infarction and unstable angina. Circulation 1997;96(5):1461–1469.
44. Schmermund A, Schwartz RS, Adamzik M, et al. Coronary atherosclerosis in unheralded sudden coronary death under age 50: histo-pathologic comparison with "healthy" subjects dying out of hospital. Atherosclerosis 2001;155(2):499–508.
45. Pohle K, Ropers D, Maffert R, et al. Coronary calcifications in young patients with first, unheralded myocardial infarction: a risk factor matched analysis by electron beam tomography. Heart 2003;89(6):625–628.
46. Wong ND, Sciammarella MG, Polk D, et al. The metabolic syndrome, diabetes, and subclinical atherosclerosis assessed by coronary calcium. Journal of the American College of Cardiology 2003;41(9):1547–1553.
47. Rumberger JA, Brundage BH, Rader DJ, Kondos G. Electron beam computed tomographic coronary calcium scanning: a review and guidelines for use in asymptomatic persons. Mayo Clinic Proceedings 1999;74(3):243–252.
48. He ZX, Hedrick TD, Pratt CM, et al. Severity of coronary artery calcification by electron beam computed tomography predicts silent myocardial ischemia. Circulation 2000;101(3):244–251.
49. Moser KW, O'Keefe JH, Bateman TM, McGhie IA. Coronary calcium screening in asymptomatic patients as a guide to risk factor modification and stress myocardial perfusion imaging. Journal of Nuclear Cardiology 2003;10:590–598.
50. Berman DS, Wong ND, Gransar H, et al. Relationship between stress-induced myocardial ischemia and atherosclerosis measured by coronary calcium tomography. Journal of the American College of Cardiology 2004;44:923–930.
51. Wong ND, Rozanski A, Gransar H, et al. Metabolic syndrome and diabetes are associated with an increased likelihood of inducible myocardial ischemia among patients with subclinical atherosclerosis. Diabetes Care 2005;28:1445–1450.
52. Anand DV, Lim E, Raval U, Lipkin D, Lahiri A. Prevalence of silent myocardial ischemia in asymptomatic individuals with subclinical atherosclerosis detected by electron beam tomography. Journal of Nuclear Cardiology 2004;11(4):450–457.
53. Taylor AJ, Merz CN, Udelson JE. 34th Bethesda Conference: Executive Summary – can atherosclerosis imaging techniques improve the detection of patients at risk for ischemic heart disease? Journal of the American College of Cardiology 2003;41(11):1860–1862.
54. Budoff MJ, Raggi P. Coronary artery disease progression assessed by electron-beam computed tomography. American Journal of Cardiology 2001;88(2A):46E–50E.
55. Raggi P, Cooil B, Shaw LJ, et al. Progression of coronary calcium on serial electron beam tomographic scanning is greater in patients with future myocardial infarction. American Journal of Cardiology 2003;92(7):827–829.
56. Berman DS, Gransar H, Rozanski A, et al. Does coronary calcium add incremental value for predicting cardiac events when myocardial perfusion SPECT is normal? [abstract]. Circulation 2004;110:III-561–III-562.
57. Berman DS, Hachamovitch R, Shaw LJ, et al. Roles of nuclear cardiology, cardiac computed tomography, and cardiac magnetic resonance, Part I: assessment of patients with suspected coronary artery disease. Journal of Nuclear Medicine, in press.
58. Hoffmann MH, Shi H, Schmitz BL, et al. Noninvasive coronary angiography with multislice computed tomography. JAMA 2005;293(20):2471–2478.
59. Leschka S, Alkadhi H, Plass A, et al. Accuracy of MSCT coronary angiography with 64-slice technology: first experience. European Heart Journal 2005.

60. Yusuf S, Zucker D, Peduzzi P, et al. Effect of coronary artery bypass graft surgery on survival: overview of 10-year results from randomised trials by the Coronary Artery Bypass Graft Surgery Trialists Collaboration. Lancet 1994;344:563–570.
61. Solomon AJ, Gersh BJ. Management of chronic stable angina: medical therapy, percutaneous transluminal coronary angioplasty, and coronary artery bypass graft surgery. Lessons from the randomized trials. Annals of Internal Medicine 1998;128(3):216–223.
62. Weiner DA, Ryan TJ, McCabe CH, et al. The role of exercise testing in identifying patients with improved survival after coronary artery bypass surgery. Journal of the American College of Cardiology 1986;8(4):741–748.
63. Grundy SM, Cleeman JI, Merz CN, et al. Implications of recent clinical trials for the National Cholesterol Education Program Adult Treatment Panel III guidelines. Circulation 2004;110(2):227–239.
64. Wackers FJ, Young LH, Inzucchi SE, et al. Detection of silent myocardial ischemia in asymptomatic diabetic subjects: the DIAD study. Diabetes Care 2004;27(8):1954–1961.
65. Naghavi M, Falk E, Hecht H, et al. From vulnerable plaque to vulnerable patient – Part III introducing a new paradigm for the prevention of heart attack; identification and treatment of the asymptomatic vulnerable patient. A screening for Heart Attack Prevention and Education (SHAPE) Task Force Report. Journal of the American College of Cardiology 2006:(In press).
66. Klocke FJ, Baird MG, Lorell BH, et al. ACC/AHA/ASNC guidelines for the clinical use of cardiac radionuclide imaging: Executive Summary. A report of the American College of Cardiology/American Heart Association Task Force on Practice Guidelines (ACC/AHA/ASNC Committee to Revise the 1995 Guidelines for the Clinical Use of Cardiac Radionuclide Imaging). Circulation 2003;108:1404–1418.
67. Diamond GA, Forrester JS. Analysis of probability as an aid in the clinical diagnosis of coronary-artery disease. New England Journal of Medicine 1979;300(24):1350–1358.
68. Berman DS, Hachamovitch R, Kiat H, et al. Incremental value of prognostic testing in patients with known or suspected ischemic heart disease: a basis for optimal utilization of exercise technetium-99m sestamibi myocardial perfusion single-photon emission computed tomography. Journal of the American College of Cardiology 1995;26(3):639–647.
69. Gibbons RJ, Balady GJ, Bricker JT, et al. ACC/AHA 2002 guideline update for exercise testing: summary article. A report of the American College of Cardiology/American Heart Association Task Force on Practice Guidelines (Committee to Update the 1997 Exercise Testing Guidelines). Circulation 2002;106(14):1883–1892.
70. Hachamovitch R, Hayes SW, Friedman JD, Cohen I, DS. B. Stress myocardial perfusion SPECT is clinically effective and cost-effective in risk-stratification of patients with a high likelihood of CAD but no known CAD. Journal of the American College of Cardiology 2004;43:200–208.
71. Gibbons RJ, Hodge DO, Berman DS, et al. Long-term outcome of patients with intermediate-risk exercise electrocardiograms who do not have myocardial perfusion defects on radionuclide imaging. Circulation 1999;100(21):2140–2145.
72. Sharir T, Germano G, Kang X, et al. Prediction of myocardial infarction versus cardiac death by gated myocardial perfusion SPECT: risk stratification by the amount of stress-induced ischemia and the poststress ejection fraction. Journal of Nuclear Medicine 2001;42(6):831–837.
73. Abidov A, Bax JJ, Hayes SW, et al. Transient ischemic dilation ratio of the left ventricle is a significant predictor of future cardiac events in patients with otherwise normal myocardial perfusion SPECT. Journal of the American College of Cardiology2003;42:1818–1825.
74. Kaminek M, Myslivecek M, Skvarilova M, et al. Increased prognostic value of combined myocardial perfusion SPECT imaging and the quantification of lung Tl-201 uptake. Clinical Nuclear Medicine 2002;27(4):255–260.
75. Kang X, Berman DS, Lewin HC, et al. Incremental prognostic value of myocardial perfusion single photon emission computed tomography in patients with diabetes mellitus. American Heart Journal 1999;138(6, Pt 1):1025–1032.
76. Berman DS, Kang X, Hayes SW, et al. Adenosine myocardial perfusion single-photon emission computed tomography in women compared with men. Impact of diabetes mellitus on incremental prognostic value and effect on patient management. Journal of the American College of Cardiology 2003;41(7):1125–1133.
77. Abidov A, Hachamovitch R, Rozanski A, et al. Prognostic implications of atrial fibrillation in patients undergoing myocardial perfusion single-photon emission computed tomography. Journal of the American College of Cardiology 2004;44(5):1062–1070.
78. Berman DS, Hayes S, Friedman J, et al. Normal myocardial perfusion SPECT does not imply the absence of significant atherosclerosis [abstract]. Circulation 2003;108:IV-562.

Index